



THE APPLICATION OF ARTIFICIAL THERMOLUMINESCENCE TO URANIUM

EXPLORATION AND URANIUM ORE GENESIS STUDIES

By

Mark Brett McEwen Hochman

B.Sc.(Hons) Adelaide

Accepted 16.8.89

Department of Geology and Geophysics

University of Adelaide

May, 1989

STATEMENT OF ORIGINALITY

This thesis contains no material which has been accepted for the award of any other degree or diploma in any University; nor does it contain to the best of my knowledge and belief, any material previously published or written by any other person, except where due reference and acknowledgement is made in the text.

M.B.M. Hochman

ACKNOWLEDGEMENTS

This project was initiated and supervised by Professor Peter Ypma, to whom I am grateful for his interest, helpful advice and continual enthusiasm.

During the term of this study I have appreciated the friendship of many colleagues including Dr. Y. Bone, Dr. A. Gabell, Dr. R. Lawrence, Dr. R. Akber and Dr. G. Mortimer. I also benefited from discussions with Urangesellschaft Aust. geologists, particularly Bruce Penny, Rod Evans and Lindsay Curtis. Appreciation is also expressed to Dr. John Foden for critiquing the geochemical interpretations contained in Appendix 4.

Gratitude is expressed to C.R.A. Exploration and Urangesellschaft Aust. for permission to sample the Bremer River and Westmoreland areas respectively.

Many technical staff assisted in sample preparation and equipment operation methods including Messrs. John Willoughby, Event Bleys, Wayne Mussared, Phil McDuie, John Stanley, Geoff Trevellyan and Mrs. Sharon Proferes. Miss Argyro Magoulianos is especially thanked for her speedy and cheerful work in the typing of this thesis.

Constructive criticism of an earlier version of this thesis by two reviewers is also gratefully acknowledged. This contributed to professional and personal development more than they will probably ever realize.

Finally, yet pre-eminently, the assistance of my wife Rosemary and our children is sincerely appreciated. Their sacrifices, encouragement and challenge to keep things in perspective contributed much to this thesis.

Financial assistance was provided by a University of Adelaide URG Scholarship for part of the study period.

ABSTRACT

Artificial thermoluminescence (TL) studies have been undertaken on three uranium deposits or prospects to examine their use in uranium exploration and ore genesis.

TL is the light emitted by a substance when it is heated and which results from previous exposure to ionizing radiation. The emitted light can be recorded as a number of glow peaks which form a glow curve. Quartz from the three areas studied contained three major glow peaks which were classified as: 1) The low temperature peak (LT) occurring at temperatures less than 200°C; 2) The middle temperature peak (MT) occurring at temperatures between 201°C and 300°C; and 3) The high temperature peak (HT) at temperatures greater than 301°C.

Studies on the TL dosimeter TLD LiF-100 by Fairchild et al (1975) had indicated that in the dose range 800 rad - 3×10^7 rad the intensity of individual glow peaks and the overall glow curve shape changed. At lower doses there was an initial increase in LT peak intensity. As the radiation dose increased the LT peak intensity decreased and the MT peaks progressively increased in intensity. At still larger doses the MT peak intensities also decreased, till, at the conclusion of the experiment, (at 3×10^7 rad), HT glow peaks were dominant.

Literature reports on the TL of quartz after large artificial irradiations also suggest that at doses greater than 5×10^5 rad the LT peak(s) are sensitized and increase in intensity such that they overshadow other peaks. At doses greater than 10^8 rad the LT peak begins to decrease in intensity whilst the middle temperature (MT) peak continues to increase. As radiation continues, the MT peak reaches a maximum and then also begins to decrease such that only the HT peak remains. When combined with the work of Levy (1979), who found that quartz "remembers" prior exposure to radiation doses greater than 5×10^5 rad, then, artificial TL (ATL) could be expected to be useful in uranium exploration.

The importance of this thesis is that it has shown that the progressive decrease of LT and MT glow peaks and increase of HT glow peaks, observed previously in laboratory studies on LiF and postulated to occur with quartz, has actually been observed in a natural geological radiative environment. This progressive change in glow curve shapes remains a permanent feature of the quartz TL and therefore TL should be useful in uranium exploration.

An ATL study on quartz extracted from 100 samples from the Tertiary sandstone-hosted Beverley uranium deposit in the Lake Frome embayment, South Australia, showed:

- 1) A decrease in the LT peak intensity of two orders of magnitude and an increase in the HT peak percentage, over a distance of eight kilometres eastward from the granitic Mount Painter basement towards the present ore location. This trend of increasing radiation effects is consistent with the theory of an eastwardly moving mobile ore front.
- 2) An ATL halo of marginal radiation effects around the ore body much larger than the corresponding subsurface radiometric halo.

- 3) A zone of ore type ATL glow curves (i.e. HT peak being the dominant peak) immediately surrounding the ore deposit and four to five times larger than the ore deposit.
- 4) A rapid increase in the LT peak intensity (i.e. a sharp decrease in radiation effects) in samples taken beyond (down-plunge of) the orebody.

The increase in cumulative radiation effects towards the orebody, and rapid return to background levels beyond the orebody, show that the radiation effects observed are not simply due to proximity to mineralization, but are suggestive of an accreting uranium front similar to the western U.S.A. roll-front deposits.

ATL has also been used during a uranium exploration program at Bremer River, South Australia, to determine the presence or absence of a mobile ore front. ATL analyses of 100 samples from 12 drill holes extending away from Cambrian and Precambrian metamorphic basement showed no trend of increasing radiation effects as had been found at the Beverley deposit. The LT peak intensity was at a minimum and HT/LT ratio at a maximum in two drill holes adjacent to the basement. The LT peak intensity increased irregularly in holes away from the basement and HT/LT ratio decreased. The lack of a consistent trend of increasing radiation effects in this series of drill holes, enabled a recommendation to be made to the company concerning further exploration in the area.

The third area studied was the Westmoreland uranium deposit in north-west Queensland. Uranium mineralization occurs in Middle Proterozoic sandstones in reducing environments provided beneath flat lying basaltic volcanics and at dolerite dyke margins. Because the mineralization is much older than at Beverley interpretation of TL results at Westmoreland is more complicated.

Approximately 700 samples from within and around the Westmoreland orebodies (up to 10 kilometres away from known mineralisation) have been measured by ATL. All samples have a reduced intensity such that glow curves are similar to those encountered only in, or near, the ore zone at Beverley. Considering the age of the Westmoreland Conglomerate (1.6×10^9 years), and its uranium content (still 4-6ppm), the total radiation dose incident upon the sandstone should have been in the order of 10^9 to 10^{10} rad. Such a dose has also been previously found by laboratory studies to cause a decrease in quartz TL intensity and sensitivity. Because of the decreased TL intensity, the variations in TL parameters approaching uranium mineralization were not as clearcut as at the Beverley deposit.

A series of traverses across mineralization at the Junnagunna prospect examined variations in LT and HT peak intensities and the HT/LT ratio. Both LT and HT peak intensities vary irregularly approaching mineralization though generally the HT peak intensity is at a maximum within the orebody. The HT/LT peak ratios are better indicators of proximity to uranium mineralization, increasing towards the orebody. Similar variations detected nearby, in areas devoid of known mineralization, are consistent with the idea of increasing proximity to further uranium occurrences. The temperature of the HT glow peak varies irregularly towards the orebody, though is consistently at a minimum within the ore zones.

Variation diagrams incorporating changes in glow peak ratios and the HT peak percentage have been used at other prospects in the Westmoreland region to suggest further prospective areas for uranium mineralization.

The ATL studies are also useful in determining a genetic model for the Westmoreland deposits. ATL measurements at Junnagunna show:

- 1) A radiation sensitization along the sandstone-basalt contact regardless of the presence or absence of mineralization;
- 2) A vertical homogenisation of radiation effects within drill holes.

The fact that all of the Westmoreland Conglomerate has been affected by radiation (as evidenced by all samples having glow curves that at Beverley were only found in, or near, ore), is interpreted to indicate a high initial uranium concentration within the sandstone. The present background uranium content is 4-6 ppm which compared to average sandstones (1ppm uranium) is very high.

These observations, and local geological considerations, lead to a genetic model as follows:

- 1) Derivation of the Westmoreland Conglomerate from a uraniferous hinterland (such as the Middle Proterozoic Clifdale Volcanics) leading to a high inherited uranium content, perhaps higher than 10 ppm;
- 2) Remobilization of the precontained uranium by convective cell systems, possibly related to dolerite dyke intrusion;
- 3) Precipitation and concentration of uranium from the convective cells, where suitable reducing conditions existed at the margins of altered dolerite dykes, or at the base of the basaltic Siegal Volcanics.

Other Middle Proterozoic sandstones in South Australia (the Corunna Conglomerate, Pandurra Formation) do not show the same widespread radiation effects as the Westmoreland Conglomerate, indicating a low inherent uranium content which may be related to their provenance. Thus, a two-fold classification of Middle Proterozoic sandstones may be possible into:

- 1) Those derived from uranium-rich source rocks, with a high inherent uranium content and widespread radiation effects; and
- 2) Those derived from uranium-poor source rocks, with a resultant low inherent uranium content and lack of widespread radiation effects.

The former are considered most suitable for remobilization of syngenetic uranium into epigenetic concentrations.

TABLE OF CONTENTS

	Page numbers
STATEMENT OF ORIGINALITY	
ACKNOWLEDGEMENTS	
ABSTRACT	
<u>PART 1: PRINCIPLES OF THERMOLUMINESCENCE AND USE IN</u>	
<u>EXPLORATION FOR TERTIARY SANDSTONE HOSTED URANIUM</u>	
<u>DEPOSITS</u>	
<u>CHAPTER 1: INTRODUCTION</u>	
1.1	2
1.2	3-4
1.3	5
<u>CHAPTER 2: PRINCIPLES OF THERMOLUMINESCENCE</u>	
Summary of Chapter	6
2.1	7
2.1.1	8
2.2	9
2.2.1	10
2.2.2	10
2.2.3	11
2.3	12
2.3.1	13-14
2.3.2	15
2.3.3	16-19
2.4	19
2.4.1	20-22
2.4.2	22-24
2.4.3	24-27
2.4.4	28-29
2.4.4.1	30-33
2.5	34
2.5.1	34-39
2.5.1.1	39-40
2.5.1.2	41
2.5.1.3	42-47
2.5.2	47-52
2.5.2.1	52-57
2.5.2.2	57-61
2.6	62
2.6.1	62-63

	Page Numbers	
2.6.2	Sample Preparation	63-66
2.6.2.1	Thermal Bleaching or Pre-annealing	66
2.6.2.2	The Lack of Hydrofluoric (HF) Acid Etching	66-69
2.6.2.3	The ATL Test Dose	69
2.6.3	Apparatus Used	70
2.6.3.1	Radiation Sources	70
2.6.3.2	Thermoluminescence Apparatus	70
2.6.4	Measurement Procedure	71-72
2.6.5	Data Analysis	72-73
<u>CHAPTER 3:</u>	<u>THE APPLICATION OF THERMOLUMINESCENCE TO EXPLORATION FOR URANIUM IN TERTIARY SANDSTONES</u>	
	Summary of Chapter	74
3.1	Previous Geological Uses of Thermoluminescence	75-77
3.1.1	Previous Uranium Case Histories Utilizing Thermoluminescence	77
3.1.1.1	A South Texas Roll-Front Type Uranium Deposit	77-78
3.1.1.2	The "Blaton" Anomaly, Mons, Belgium	78
3.1.1.3	Ambrosia Lake, U.S.A.	79-80
3.1.1.4	Narlaby Palaeochannel, Eyre Peninsula, South Australia	80
3.1.1.5	Other Studies	81
3.2	The Beverley Uranium Deposit, Frome Embayment, South Australia	81
3.2.1	Introduction to the Geology and Genesis of Tertiary "Roll-Front" Uranium Deposits	81-82
3.2.2	Geology of the Beverley Uranium Deposit	83
3.2.3	Results	84-86
3.2.4	Uranium Exploration Implications of Thermoluminescence from the Beverley Results	86-87
3.2.5	Genesis of the Beverley Deposit - Source of the Uranium	88
3.2.6	Genesis of the Beverley Deposit - The Accretionary Movement of Uranium	89
3.3	Bremer River Prospect, South Australia	90
3.3.1	Geological Setting of the Bremer River Exploration Lease	91
3.3.2	Results	92
3.3.3	Discussion	93
3.4	Conclusions on the use of Thermoluminescence for Tertiary Sandstone Hosted Uranium Deposits	93-94
<u>CHAPTER 4:</u>	<u>A PROPOSED MODEL FOR THE GAMMA RAY INDUCED VARIATION OF QUARTZ THERMOLUMINESCENCE GLOW CURVES</u>	
	Summary of Chapter	95
4.1	Introduction	96-98
4.2	The Model	98-104
<u>PART 2:</u>	<u>USE OF THERMOLUMINESCENCE IN URANIUM EXPLORATION FOR PROTEROZOIC URANIUM DEPOSITS: THE CASE OF THE WESTMORELAND URANIUM DEPOSIT, NORTHWEST QUEENSLAND</u>	

CHAPTER 5: GEOLOGY OF THE WESTMORELAND REGION

5.1	Introduction	105
5.1.1	Location and Access	105
5.1.2	Previous Investigations	106
5.2	Regional Geology of the Westmoreland Area	106-109
5.2.1	Uranium Mineralization of the Murphy Tectonic Ridge	109-110
5.3	Local Geology of the Westmoreland Area	110
5.3.1	The Westmoreland Conglomerate	111-112
5.3.1.1	Environment of Deposition of the Westmoreland Conglomerate	113
5.3.2	The Siegal Volcanics	113-114
5.3.3	Dolerite Dykes	115
5.3.4	Geochemistry of the Siegal Volcanics, Dykes and Tuffs	115
5.3.5	Structure and Metamorphism	116
5.3.6	Uranium Mineralization at Westmoreland	117-120
5.3.6.1	Geology of Individual Prospects at Westmoreland Where Thermoluminescence Studies Were Undertaken	120-122

CHAPTER 6: THE USE OF THERMOLUMINESCENCE IN URANIUM EXPLORATION AT WESTMORELAND

	Summary of Chapter	123
6.1	Westmoreland - Introduction to Data	124-125
6.2	Junnagunna Area	126
6.2.1	Interpretive Methods Used	126
6.2.2	Variations in Glow Peak Intensities	126-127
6.2.2.1	Discussion	127-129
6.2.3	Variations in Glow Peak Ratios	129
6.2.3.1	Discussion	130
6.2.4	Further Prospective Areas for Uranium Exploration	131
6.2.5	Glow Peak Temperature Traverses	131
6.2.5.1	Discussion	132
6.2.6	A Vertical Profile Study Through Westmoreland Conglomerate, Unit 4	132-133
6.2.6.1	Hole UMD 78/60	133-134
6.2.6.2	Hole UMD 78/77	134-135
6.2.7	Vertical Homogenization of Thermoluminescence Within Drill holes	135-136
6.2.8	Distribution of Sensitization: Contour Maps	136-139
6.2.8.1	Discussion	139
6.3	Variation Diagrams: 190°C Peak (LT)/260°C Peak (MT) vs 350°C Peak (HT) Percentage	140-141
6.3.1	Jack-Garee-Langi Uranium Deposits (Redtree Lenses)	141-146
6.3.2	Junnagunna Area	146-149
6.3.3	Junnagunna North	149
6.3.4	Huarabagoo	150
6.4	Further Usage of Variation Diagrams in Non- Mineralized Areas and Areas Distant from the Redtree Joint Zone	151
6.4.1	Jinjaree Valley	151-153
6.4.2	Longpocket	153-154
6.4.3	Flying Fox Anticline	154-155
6.4.4	Lilypond	155
6.4.5	Others	156

	Page Numbers	
6.5	Surface Traverse Results	156-158
6.6	Conclusions on the Use of Thermoluminescence in Exploration for Uranium in the Proterozoic Sandstone Hosted Deposits at Westmoreland	158-161
<u>PART 3:</u>	<u>IMPLICATIONS OF THE WESTMORELAND THERMOLUMINESCENCE RESULTS IN DETERMINING GENETIC MODELS FOR THE WESTMORELAND URANIUM DEPOSITS AND OTHER PROTEROZOIC SANDSTONE HOSTED URANIUM DEPOSITS</u>	
<u>CHAPTER 7:</u>	<u>GENESIS OF THE WESTMORELAND URANIUM DEPOSITS</u>	
	Summary of Chapter	162-163
7.1	Previous Genetic Theories for the Westmoreland Uranium Deposits	163-168
7.2	Characteristics of the Westmoreland Deposits	169
7.2.1	Thermoluminescence Characteristics	169-170
7.2.2	Geochemical and Mineralogical Characteristics	170-173
7.2.3	Location and Structural Characteristics	173
7.3	Genetic Model	173-174
7.3.1	Source of Uranium	174-179
7.3.2	The Mechanism to Hold Uranium Within the Westmoreland Conglomerate	179-180
7.3.3	Transport and Precipitation	180-183
7.3.4	Preservation	183-185
7.4	Summary of the Genetic Model	185-187
<u>CHAPTER 8:</u>	<u>PROTEROZOIC SANDSTONE HOSTED URANIUM DEPOSITS - A BIMODAL CLASSIFICATION?</u>	
	Summary of Chapter	188-190
8.1	Comparison of the Westmoreland Uranium Deposits With Other Similarity Aged Uranium Deposits	190
8.1.1	The Athabasca Formation and its Uranium Deposits, Saskatchewan, Canada	190-192
8.1.2	The Oklo Deposit, Gabon, West Africa	192-193
8.1.3	Deposits of the Dubawnt Group, Keewatin, North West Territories, Canada	193-194
8.1.4	The Kombolgie Sandstone in the East Alligator Uranium Field, Northern Territory, Australia	194-197
8.2	Discussion	197
8.2.1	A Comparison of the Westmoreland and Oklo Deposits	198-199
8.2.2	A Comparison of the Westmoreland and Oklo Deposits with those of the Athabasca, Keewatin and East Alligator Regions	199-201
8.3	The Corunna Conglomerate, South Australia	202
8.4	A Possible Bimodal Classification of Proterozoic Sandstones and Implications for Uranium Exploration	203-205

CHAPTER 9: CONCLUSIONS AND RECOMMENDATIONS FOR FURTHER RESEARCH

9.1	Introduction	206
9.2	Conclusions Regarding the Use of Artificial Thermoluminescence in Uranium Exploration	207-209
9.3	Conclusions Regarding the Use of Thermoluminescence in Ore Genesis Studies	209
9.3.1	The Beverley Uranium Deposit, South Australia	209
9.3.2	The Westmoreland Uranium Deposit, Queensland	210-212
9.4	Recommendations for Further Research	212-213

BIBLIOGRAPHY

LIST OF APPENDICES

- Appendix 1: Tabulated binocular microscope descriptions for Westmoreland samples.
- Appendix 2: Tabulated thermoluminescence glow peak intensities and glow peak temperatures for Westmoreland samples.
- Appendix 3: Microscope descriptions of selected thin and polished sections.
- Appendix 4: Major and trace element geochemical tables for the Siegal Volcanics, dykes and tuffs at Westmoreland with a discussion of their geochemistry and comparison to other simlairly aged basaltic rock suites in Northern Australia.

ATTACHED PUBLICATIONS

- Hochman, M.B.M. and Ypma, P.J.M. 1984: Thermoluminescence as a tool in uranium exploration. *Journal of Geochemical Exploration*, 22, 1-3, p. 315-333.
- Hochman, M.B.M. and Ypma, P.J.M. 1984: Thermoluminescence applied to uranium exploration and genesis of the Westmoreland uranium deposits; - Implications for the Northern Territory. *Aust. Inst. of Mining and Metallurgy, Conference Volume, 1984, Darwin*, p. 215-224.
- Hochman, M.B.M. and Ypma, P.J.M. 1987: The accretionary migration of uranium in Tertiary sandstones - Thermoluminescence evidence from the Beverley Deposit, South Australia, *Uranium*, 3, p. 245-259.
- Hochman, M.B.M. and Ypma, P.J.M. 1988: Changes in the artificial thermoluminescence glow curves of quartz associated with uranium deposits. *Nuclear Tracks and Radiation Measurements* 14, $\frac{1}{2}$, p. 105-111.

Ypma, P.J.M. and Hochman, M.B.M. 1987: A thermoluminescence study of the role of a Middle Proterozoic unconformity in controlling uranium mineralization as shown at Eyre Peninsula, South Australia. *Bulletin Francais Mineralogie*, 110, p. 173-186.

LIST OF TABLES

- Table 2.1 The effect of Al, Na and Li on quartz TL, (summarized after Ichikawa, 1968).
- Table 2.2 Effective temperature ranges for various diffusion-limited anneal mechanisms (after Griscom 1985).
- Table 2.3 Increase in E_1' centre signal in response to gamma doses from 3.2×10^8 rad to 1.2×10^{10} rad. Increase in E_1' centre signal with alpha and neutron irradiation is also observed (after Chatagnon, 1986).
- Table 4.1 The change in E_1' centre signal in quartz samples from positions of variable palaeoradiation dose in the Beverley uranium region. Location of samples is given in figure 4.2.
- Table 7.1 Mineral associations with uranium at the Junnagunna prospect, Westmoreland.
- Table 8.1 A comparison of worldwide Proterozoic sandstones and their uranium deposits (where present).
- Table 8.2 A more detailed comparison of the geology of the Westmoreland and Oklo uranium deposits.

LIST OF FIGURES

- Figure 1.1 Location of major Australian uranium deposits.
- Figure 2.1 Energy band model for an insulator or semi conductor. E_v represents the lowest energy band (valence band), E_c the highest energy band (conduction band) and E_g the energy gap, (after McKeever, 1985).
- Figure 2.2 The location, or relative energy states, of electron and hole traps within the forbidden energy band, (after McKeever, 1985).
- Figure 2.3 The location, or relative energy states, of electron and hole traps and recombination centres within the forbidden energy band, (after McKeever, 1985).
- Figure 2.4 The relationship between untrapping probability, luminescent intensity and trapped charge population, (after Levy, 1974).
- Figure 2.5 An example of a glow curve obtained from a material with four different types of charge traps (after Levy, 1974).

- Figure 2.6 First order (top diagram) and second order (lower diagram) glow peaks computed for the same $s(10^{10}/\text{sec})$ and $E(1.0\text{eV})$ values but with different initial trapped charge concentrations, (after Levy 1982).
- Figure 2.7 First and second order glow curves computed for different recombination to retrapping ratios (after Levy 1982).
- Figure 2.8 First and second order glow curves computed for cross-section ratios near one (after Levy 1982).
- Figure 2.9 First and second order glow curves computed for different trapped hole concentrations (after Levy 1982).
- Figure 2.10 The change in computed glow curve shape for trapped hole - electron ratios near one (after Levy 1982).
- Figure 2.11 First order, second order and interactive kinetics glow curves obtained with varying the cross-section ratio (after Levy 1984b).
- Figure 2.12 First order, second order and interactive kinetics glow curves obtained when the trapped charge is varied in one trap only and kept constant in other traps (after Levy 1984b).
- Figure 2.13 First order, second order and interactive kinetics glow curves where the trapped charge is varied similarly in each of the three traps (after Levy, 1984b).
- Figure 2.14 Peak height vs n_0 , or dose, curves for glow peaks shown in the preceding figure and showing supralinear behaviour, especially in the lower temperature peaks (after Levy 1985b).
- Figure 2.15 Model for the E_1' centre (after McKeever, 1985).
- Figure 2.16 Quartz emission spectra (after David et al 1977).
- Figure 2.17 Quartz emission spectra (after Medlin 1963).
- Figure 2.18 Quartz emission spectra (after Durrani et al 1977a).
- Figure 2.19 Increase in quartz 110°C glow peak intensity with temperature of annealing (after Ichikawa 1968) (after test dose).
- Figure 2.20 Effect on TL of quenching quartz from an elevated temperature (after David et al 1977).
- Figure 2.21 Increased TL intensity in quartz after a test dose of 10^5 rad as a function of temperature of annealing (after David et al 1977).
- Figure 2.22 The effect of thermal sensitization and radiation dose on the TL of quartz (after Durrani et al 1977).
- Figure 2.23 The effect of annealing temperature on glow peak intensities of quartz (after Kaul et al 1972).

- Figure 2.24 Model for the pre-dose mechanism in quartz (after Zimmerman 1971).
- Figure 2.25 The change in glow peak intensity and glow curve shape in quartz as a function of radiation (after Ichikawa 1968).
- Figure 2.26 The change in area under the glow curve in quartz as a function of radiation (after Ichikawa 1968).
- Figure 2.27 Change in TL intensity and sensitivity in Brazilian quartz as a function of radiation dose (after Durrani et al 1977a).
- Figure 2.28 Change in TL response (area under glow curve from 240°C to 480°C) and TL sensitivity in quartz as a function of proton irradiation dose (after Durrani et al 1977a).
- Figure 2.29 (a) TL glow curve for quartz slice irradiated with a dose of 10^7 rad 10 MeV protons, and
(b) 2×10^{10} rad 10 MeV protons (after Durrani et al 1977a).
- Figure 2.30 A comparison of the TL sensitivity in quartz induced by gamma and proton irradiation (after Durrani et al 1977a).
- Figure 2.31 TL response in quartz following
(a) a test dose of 2×10^5 rad,
(b) a variable sensitization dose and
(c) a second test dose of 2×10^5 rad (after Levy 1979).
- Figure 2.32 Change in optical absorption in quartz with radiation (after Mattern et al 1975).
- Figure 2.33 Change in LiF glow curve shape with gamma radiation from 800 rad to 3×10^7 rad (after Fairchild et al, 1975).
- Figure 2.34 Expected change in generalized quartz glow curve shape with radiation.
- Figure 2.35 Glow curves for quartz where
(a) NTL was drained and ATL induced with a standard test dose and
(b) NTL was not drained prior to the standard test dose.
- Figure 2.36 Effect of HF on quartz from the Westmoreland area (high radiation flux) showing very little change in TL intensity with etching time. Test dose was 5×10^5 rad.
- Figure 2.37 Effect of HF on quartz from the background Beverley host rock (low radiation flux) showing a large decrease in TL intensity of the low temperature glow peak. Test dose was 5×10^5 rad.
- Figure 2.38 Effect of air abrasion on the TL of quartz from the background Beverley host rock showing little change in TL intensity. The time of abrasion was between 0 and 5 minutes. Test dose was 5×10^5 rad.

- Figure 2.39 Effect of air abrasion on the TL of quartz from the background Beverley host rock showing a small change in TL intensity with abrasion. The time of abrasion was between 0 and 137 minutes. Test dose was 5×10^5 rad.
- Figure 3.1 Change in LT glow peak intensity and LT/HT ratio approaching a South Texas roll front uranium deposit, after Spirakis et al (1977).
- Figure 3.2 Location of the Beverley uranium deposit, South Australia (after Haynes, 1975).
- Figure 3.3 Beverley drill hole locations showing zones of background, marginal and ore-type quartz TL glow curves.
- Figure 3.4 The change in quartz LT peak intensity and HT peak percentage in samples from the ore transport horizon in the Beverley region.
- Figure 3.5 Change in quartz TL for samples from the Beverley region taken 10 metres stratigraphically above the ore transport horizon.
- Figure 3.6 Change in quartz TL for samples from the Beverley region taken 10 metres stratigraphically below the ore transport horizon.
- Figure 3.7 Typical TL glow curve for quartz from the background zone at Beverley.
- Figure 3.8 Typical TL glow curve for quartz from the marginal TL zone at Beverley.
- Figure 3.9 Typical TL glow curve for quartz from the ore-type TL zone at Beverley.
- Figure 3.10 Location of the Bremer River prospect, South Australia.
- Figure 3.11 Bremer River data examining variations in quartz glow peak intensities and ratios for different stratigraphic levels within the "Continental Group".
- Figure 4.1 TL glow curves for quartz samples from the Beverley region representing
- (a) the background TL zone (low radiation),
 - (b) the marginal TL zone (intermediate radiation) and
 - (c) the "ore-type" TL zone (high radiation).
- Figure 4.2 Location of EPR samples taken from the Beverley region.
- Figure 4.3 A computed glow curve where the initial trapped charge is distributed such that $n_{10} > n_{20}$ and n_{30} (after Levy 1983b). The LT peak dominates. Note the similarity to the sample in figure 4.1 from the Beverley background TL zone.
- Figure 5.1 Location of Westmoreland.

- Figure 5.2 Local geology of the Westmoreland region.
- Figure 5.3 Location of uranium deposits on the Murphy Tectonic Ridge.
- Figure 5.4 Location of individual uranium deposits and prospects in the Westmoreland region.
- Figure 5.5 Vertical and horizontal mineralization styles at Westmoreland.
- Figure 6.1 Location of Junnagunna drill holes used in TL traverses.
- Figure 6.2 Variation in TL glow peak intensities and ratios across the Junnagunna orebody.
- Figure 6.3 Variation in the HT glow peak (350°C) temperature across the Junnagunna orebody.
- Figure 6.4 Vertical profiles through Unit 4 of the Westmoreland Conglomerate showing variations in glow peak intensity (peak 3 is the HT peak) peak percentages, ratios and temperatures for
(a) hole UMD 78/60 and
(b) hole UMD 78/77.
The sample interval is one metre.
- Figure 6.5 Detailed drill hole location map of the Junnagunna region.
- Figure 6.6 Examples of the vertical homogenization of ATL quartz glow curves in drill holes at Junnagunna:
(a) Holes showing an approximate uniform sensitization,
(b) Holes showing an approximate uniform lack of sensitization.
- Figure 6.7 Contour maps showing the distribution of sensitization at Junnagunna in slices of sediment
(a) 10 metres below the Siegal Volcanic/Westmoreland Conglomerate contact
(b) 10-30 metres below the contact and
(c) 30-50 metres below the contact.
- Figure 6.8 The distribution of mineralization at Junnagunna.
- Figure 6.9 A blank variation diagram showing the expected trends of increasing radiation effects on quartz. As radiation effects increase the LT/MT ratio should decrease and the HT percentage should increase.
- Figure 6.10 Location of drill holes sampled at the Redtree Lenses and Huarabagoo prospect.
- Figure 6.11 Variation diagram for the Redtree area.
- Figure 6.12 Variation diagram for the Junnagunna area.
- Figure 6.13 Variation diagram for mineralized samples from the Junnagunna area.
- Figure 6.14 Variation diagram for samples from the Siegal Volcanics/Westmoreland Conglomerate Contact.

- Figure 6.15 Variation diagram for samples from the Junnagunna North prospect.
- Figure 6.16 Variation diagram for samples from Huarabagoo.
- Figure 6.17 Location of the Jinjaree Valley.
- Figure 6.18 Variation diagram for samples from Jinjaree Valley.
- Figure 6.19 Location of holes sampled in the Jinjaree Valley.
- Figure 6.20 Location of holes sampled at Longpocket and Red Hill.
- Figure 6.21 Variation diagram for samples from Longpocket.
- Figure 6.22 Variation diagram for samples from Red Hill.
- Figure 6.23 Location of the Flying Fox Anticline with holes sampled. SWC = South West Corner, BC = Battle Creek and LC = Lagoon Creek.
- Figure 6.24 Variation diagram for the Flying Fox Anticline samples.
- Figure 6.25 Variation diagram for samples from the Lilydale area.
- Figure 6.26 Variation diagram for samples from minor localities.
- Figure 6.27 Variation in TL intensity and ratios for quartz samples taken along a surface traverse over the Redtree dyke.
- Figure 6.28 Variation diagram for samples on a surface traverse over the Redtree dyke.
- Figure 7.1 TL glow curve of quartz from tuffs within Unit 4 of the Westmoreland Conglomerate.
- Figure 7.2 TL glow curve of quartz from the Westmoreland Conglomerate, Unit 3.
- Figure 7.3 Cartoon sketch of the genetic model for the Westmoreland uranium deposits.
- Figure 7.4 Eh-pH stability fields of pitchblende and carnotite (after Langmuir, 1978).
- Figure 8.1 (a) TL glow curve of a sample outside the reactor core at the Oklo uranium deposit, Gabon (after Durrani et al 1975).
(b) TL glow curve of quartz from within the Jack Lens deposit at Westmoreland.
- Figure 8.2 Stratigraphic position of uranium mineralization in the Westmoreland deposits, the Athabasca deposits (after Hoeve et al 1980) and the Oklo deposit (after Pfiffelmann, 1975).

PART 1

PRINCIPLES OF THERMOLUMINESCENCE AND USE IN EXPLORATION
FOR TERTIARTY SANDSTONE HOSTED URANIUM DEPOSITS

CHAPTER 1

INTRODUCTION



1.1 Introduction

Throughout the late 1960's, 1970's and into the early 1980's uranium was a much sought after metal, with exploration in Australia having a high profile. This exploration had resulted in the discovery of a number of new uranium orebodies and ore types. These included the Ranger, Jabiluka, Nabarlek and Koongarra deposits of the unconformity or vein type association in the East Alligator River, Northern Territory; the Yelirree deposit of the calcrete association in Western Australia; the Olympic Dam copper-uranium-gold deposit on the Stuart Shelf in South Australia, and a number of Tertiary sandstone type deposits in the Lake Frome Embayment, South Australia, including the Beverley and Honeymoon deposits. These were in addition to a number of older deposits which had been known and studied, continued to be sought and in some cases mined, such as the Rum Jungle deposits in the Northern Territory, those of Mount Painter and Radium Ridge in South Australia and the Mary Kathleen and Westmoreland deposits of Queensland. Locations of these and other prospects are contained in figure 1.1.

At the same time, a number of new techniques in uranium exploration were being investigated and developed. These included lead isotope studies, uranium series disequilibria, hydrogeochemical techniques, remote sensing and various other geochemical, radiometric and geostatistical methods. These and others are described in Bailey and Childers (1977) and the I.A.E.A. publication "Exploration for uranium ore deposits" (1976).

An exciting new application emerged when physicists researching the applications of thermoluminescence at Brookhaven National Laboratories, New York, found that quartz "remembered" exposure to prior large radiation doses (Levy, 1978). This was a quite different concept to many of the then current lines of research, which were working on detecting

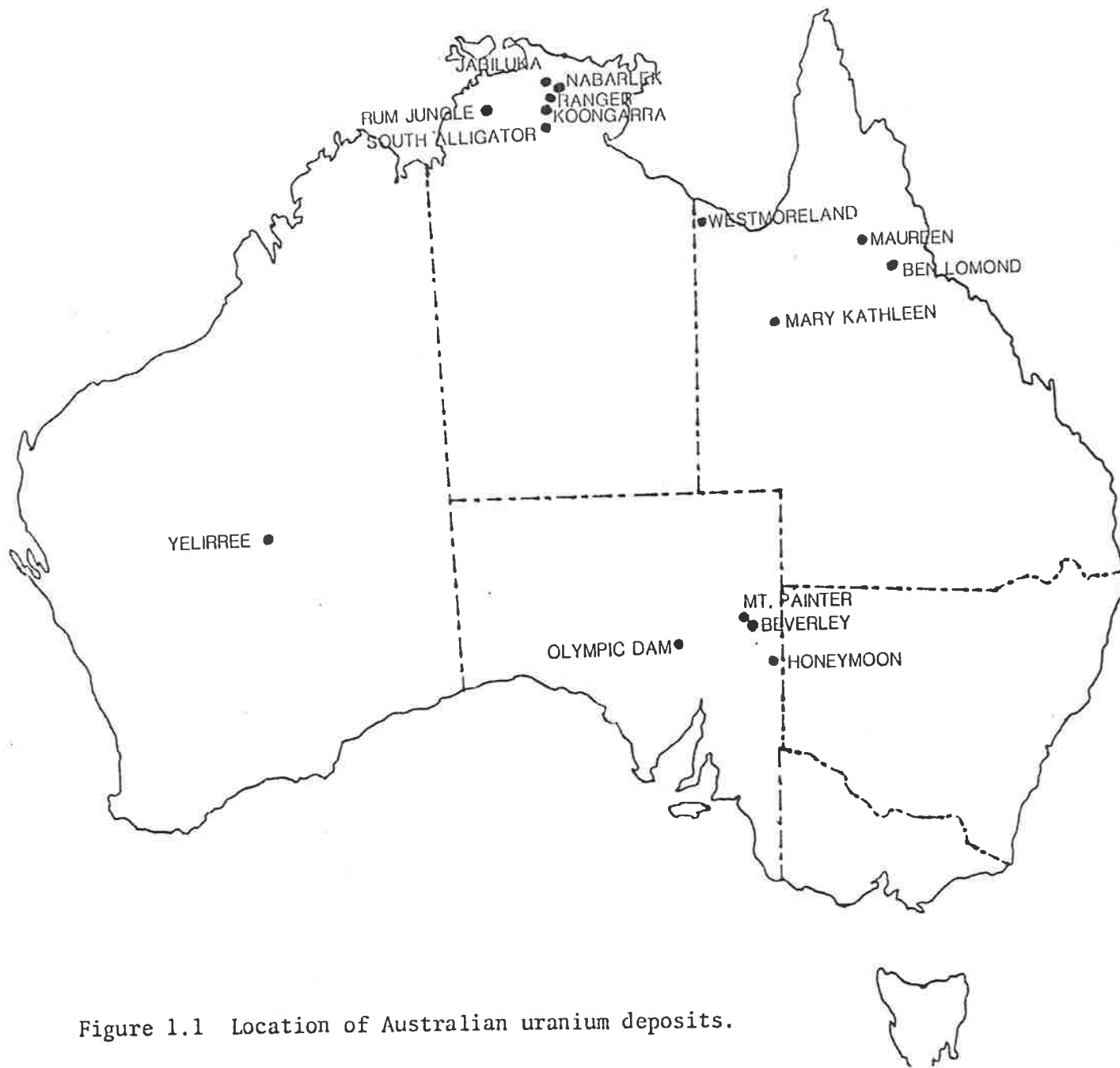


Figure 1.1 Location of Australian uranium deposits.

the actual presence of uranium and daughter products associated with uranium orebodies. Thermoluminescence, in contrast, was a means of also detecting the effects of the past presence of uranium, i.e. by determining the radiation damage to host mineral lattices, even after the uranium had migrated or had been leached from that position. The potential thus existed to detect past areas of uranium accumulation and to track protore movement.

1.2 Aims of Thesis

This study was undertaken with the general aim of testing the application of thermoluminescence (TL) to uranium exploration and problems of uranium ore genesis and where possible, to use the technique in further exploration.

The thesis is therefore separated into three parts: Part 1 deals with the principles of TL and its application in exploration for Tertiary sandstone hosted uranium deposits. These are genetically perhaps the simplest of uranium deposits, and if TL is to be of use in uranium exploration then it should be usable for such deposits.

Two Tertiary sandstone environments were studied, one an actual uranium deposit (Beverley) and one during an active uranium exploration program (Bremer River). Results at Beverley showed that TL was of direct use in exploration for Tertiary deposits and could be expected to reduce exploration costs.

Part 1 then concludes with an attempt to explain TL results obtained on Tertiary uranium deposits and prospects in terms of presently accepted kinetic and physical principles.

Part 2 deals with uranium exploration applications of TL at a Proterozoic sandstone hosted uranium deposit - the Westmoreland Uranium Deposit in Northwestern Queensland, Australia. Proterozoic uranium deposits could be expected to be much more complex than their Tertiary

counterparts because of their greater age, complicating TL applications accordingly.

For this reason, and because most drilling in the Westmoreland area was concentrated around known uranium mineralization, more closely spaced studies across deposits were made, to assess whether TL could thus be used to detect extensions to, or repetitions of, known orebodies. TL results in uranium exploration at Westmoreland were not as spectacularly successful as at Beverley, nevertheless were still interesting and indicate some localized use for TL in such deposits.

Part 3 takes TL results from Westmoreland and integrates them with other geological and geochemical results and formulates a genetic model for the formation of the Westmoreland Uranium Deposits - a much vexed question at which many attempts have been made and opinions proffered since their discovery in the late 1950's. Because of the importance of Proterozoic sandstone hosted uranium deposits as a source of mineable uranium, and since fresh insights were made using TL at Westmoreland, this thesis then concludes with a chapter on similarities and differences between such deposits, speculations on how their genesis may have occurred and suggestions as to how TL may be used in exploration for such types of uranium deposit.

Finally a word concerning the presentation of this study. Since this thesis aims to apply what is currently considered a "physics technique" to solve real problems in geology, and since this thesis may be at least partially read by both geologists and physicists, then, in order to assist readability for both groups, a short summary of conclusions is presented at the beginning of each major chapter.

1.3 Definition of Terms

All geological terminology in this thesis concerning igneous rocks is adopted from Joplin (1971). Similarly, sedimentary rock terminology is from Folk (1974). Terms concerning TL are following explanations and definitions given in McKeever (1985), with the exception of the term sensitization, which in this study simply refers to any trend of increasing radiation effects. Following Griscom (1985), the terms radiation damage or radiation effects, refer to ".....the existence of past irradiation local structures (either atomic or electronic) which differ from the structures present before irradiation.....".

CHAPTER 2

PRINCIPLES OF THERMOLUMINESCENCE

CHAPTER 2: PRINCIPLES OF THERMOLUMINESCENCE

- Summary of Chapter

This chapter summarizes principles of thermoluminescence (TL) beginning with the role of crystal defects that may function as electron traps, hole traps or recombination centres. The TL process is then described in terms of the absorption of ionizing radiation by a crystal, the trapping of ionization charges, their subsequent thermal untrapping, possible recombination and production of luminescent radiation. Kinetic models for the TL process are then presented.

Quartz is the mineral on which all future TL work is conducted and therefore this chapter continues with an examination of the defect structure of quartz and factors affecting quartz TL. It is shown that for quartz in a natural geological radiative environment, radiation effects on quartz TL far outweigh any other influences. A literature survey of other studies on the effect of radiation on quartz TL and LiF TL is then used to suggest variations in quartz TL glow curve shapes as a function of radiation.

Chapter 2 concludes with a presentation of experimental techniques used in TL measurements presented in following chapters.

*

*

*

2.1 Introduction

Thermoluminescence (abbreviated TL) is the light emitted by a substance when it is heated and which results from previous exposure to ionizing radiation.

Thermoluminescence is merely one type of luminescent occurrence in the much larger field of luminescence phenomena. The fundamental principles governing production of the many different luminescence processes are very similar and the names given to each process reflect the type of radiation used to excite the emission. Therefore, photoluminescence is caused by excitation by optical or ultra-violet rays, radioluminescence by nuclear radiations and cathodoluminescence by electron beams. Other types of luminescence are described by McKeever (1985).

Thermoluminescence is used today in a wide range of applications. The most common usages are in the field of radiation dosimetry and age determination of both archaeological and geological samples. TL is also used in conjunction with other techniques, e.g. electron spin resonance, to develop an understanding of the nature of crystal defects. Geological applications of TL include use in ore prospecting (McDougall 1968), determination of meteorite orbits (Sears and McKeever 1980), geothermometry (McDiarmid 1963), sediment provenance studies (Charlet 1971) and others summarized in McDougall (1968) and McKeever (1985).

TL properties of solids, as utilized in the above applications, are dependant on many factors, the primary one being the concentration and type of crystal imperfections.

2.1.1 Defects and Colour Centres

A crystal defect is any abnormality causing a variation in the normal crystal lattice. All crystals, including those grown artificially, in laboratory environments, contain imperfections or defects which may affect physical processes occurring in the crystal.

Defects occur as point, line or structural defects. Point defects considered to be influential in the TL process include substitutional impurities, lattice vacancies or interstitial atoms. An example of an interstitial point defect is the Frenkel defect, which occurs where an atom or ion which is normally located on a lattice site occurs in one of the interstices of the crystal lattice. A Schottky defect is an example of a vacancy and is caused by the diffusion of an ion from the lattice to the surface of the crystal. Both Frenkel and Schottky defects occur regularly in ionic crystals though in molecular crystals there is a predominance of Schottky defects owing to the difficulty of forming interstitials with large molecules.

Chemical impurities occur when a normal atom in the lattice is replaced by a different atom which may have the same or different valency eg. Al^{3+} or Ge^{4+} substituting for Si^{4+} in quartz.

Under favourable conditions, point defects may trap electrons and holes created by ionizing radiation. If a defect centre containing an electron absorbs visible light then it is called a colour centre. Levy (1977) states that many colour centres are due to impurity defects within the crystal lattice, or to alteration of the valence state of imperfections (often by exposure to ionizing radiation). Examples of solids that appear coloured because of the presence of colour centres include ruby (Al_2O_3 with Cr^{3+} impurities substituting for Al^{3+}), smoky quartz (SiO_2 with Al^{3+} /alkali substitutions for Si^{4+} , and requiring

exposure to ionizing radiation to form the smoky colour), citrine (SiO_2 with Fe^{3+} substituting for Si^{4+}) and emerald ($\text{Be}_3\text{Al}_2\text{Si}_6\text{O}_{18}$ with Cr^{3+} substitution in Al^{3+} sites).

Colour centres are important in the thermoluminescence process because they may act as trapping centres or recombination centres and contribute to luminescent emission.

2.2 The Role of Defects in the Thermoluminescence Process

The TL process is best understood by utilizing the energy band theory of solids from which an explanation of observed luminescent properties of various materials can be obtained. An energy band model for an insulator or semiconductor is shown in figure 2.1. E_v represents the lowest full energy band, the valence band, and E_c represents the next highest empty energy band, the conduction band.

In such an ideal insulator, electronic conduction will only occur when valence electrons are given enough energy to traverse the energy gap (E_g) to the conduction band. Such energy may result from ionizing radiation.

When structural defects occur in a crystal, or if there are impurities in the lattice, there is a local perturbation in the periodic potential. The defects are then said to possess localized energy levels, in contrast to the valence and conduction bands which extend through the crystal. The presence of defects with localized energy levels thus makes it possible for electrons to possess energies within the forbidden energy band.

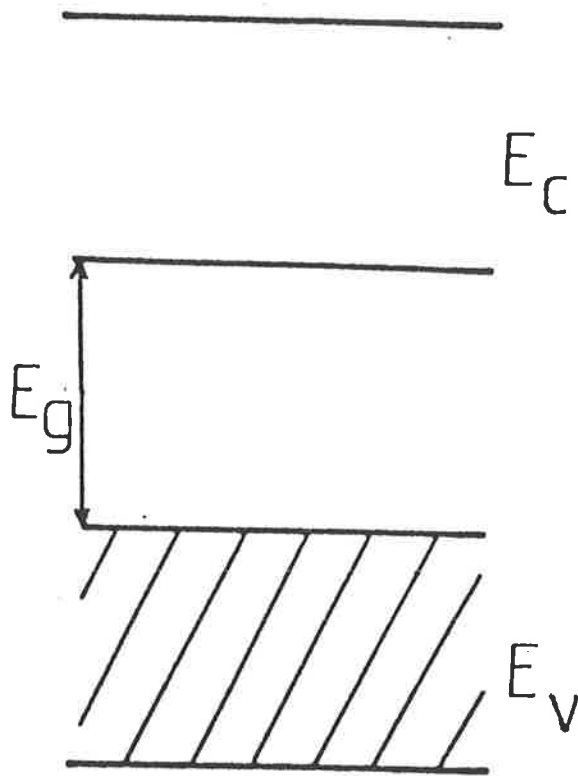


Figure 2.1 Pictorial representation of the energy band model for insulators and semiconductors (after M^CKeever 1985). E_C is the conduction band, E_V the valence band and E_g the energy gap.

2.2.1 Defects that Function as Electron and Hole Traps

Defect states in the forbidden energy band may act as electron traps, hole traps, or in some cases as both, depending on the properties of each centre. Figure 2.2 (after McKeever 1985) illustrates the positions, or relative energy states of electron and hole traps within the forbidden energy band in relation to the valence and conduction bands. E_f is the Fermi level.

Electron traps (sites which can trap an electron) are usually located between the Fermi level and the bottom of the conduction band. The energy required to release any electron from a trap is always less than the energy required to transfer a valence electron to the conduction band. Hole traps are any defect which can trap a hole. Often they are sites with a negative charge which must capture a positive charge to restore local charge neutrality. They are usually located between the top of the valence band and Fermi level.

2.2.2 Defects that Function as Recombination Centres

Defects and their associated trapped charges, (if any) and their localized energy levels may function as either charge traps or as recombination centres. Within the energy band model the distinction between the two is based on the relative probabilities of recombination or thermal excitation.

The mean time (τ) that a charge will remain in a single individual trap, at temperature T , is given by the equation $\tau = s^{-1} \exp (E/kT)$ where s (t^{-1}) is a constant for the trap, E (eV) is the energy difference between the trap and the edge of the corresponding delocalized energy band (also called trap depth) and k is Boltzmann's constant.

(Boltzmann's constant gives the relationship between energy and absolute

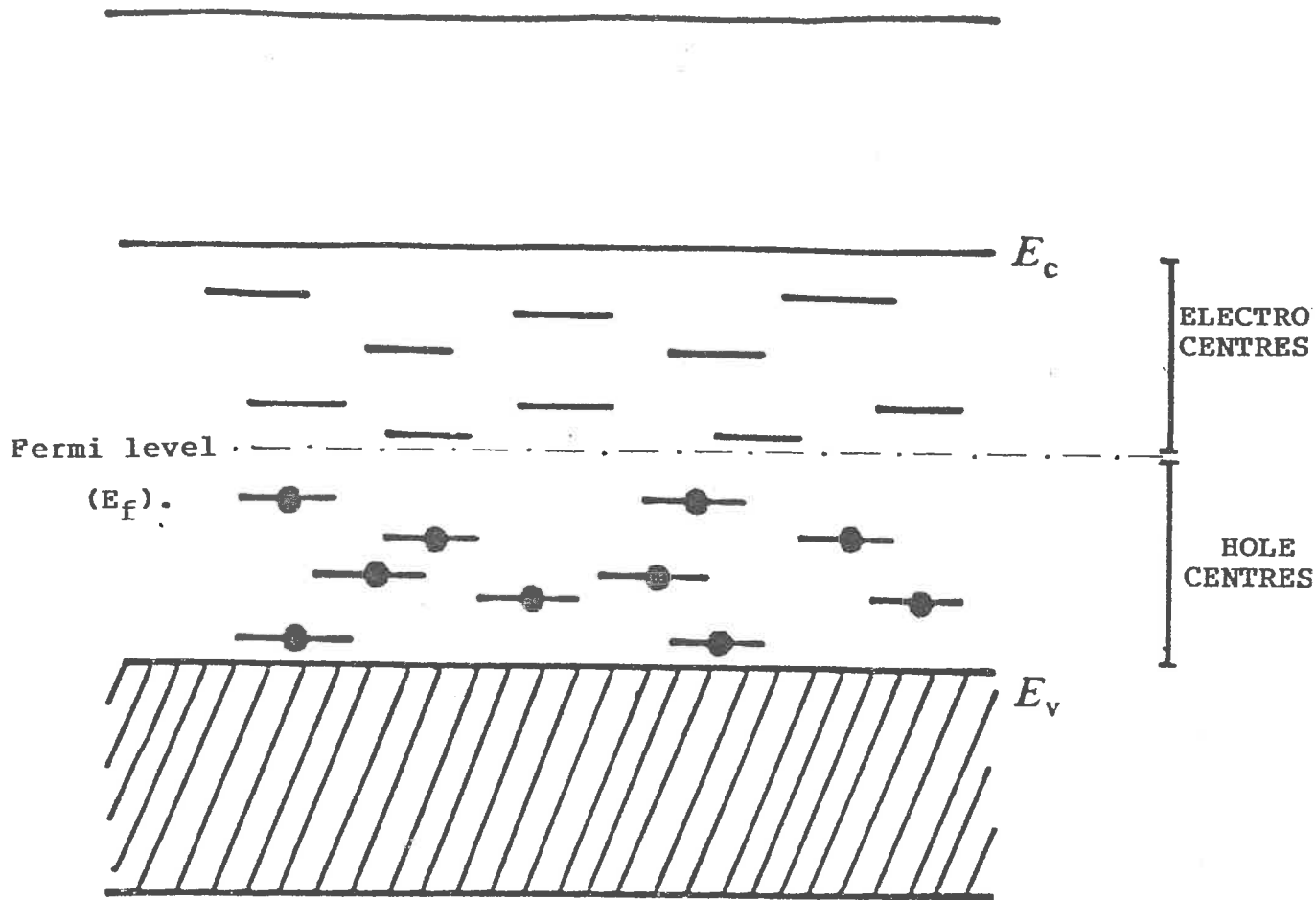


Figure 2.2 The location, or relative energy states, of electron and hole traps within the forbidden energy band, or energy band gap, (after McKeever, 1985).

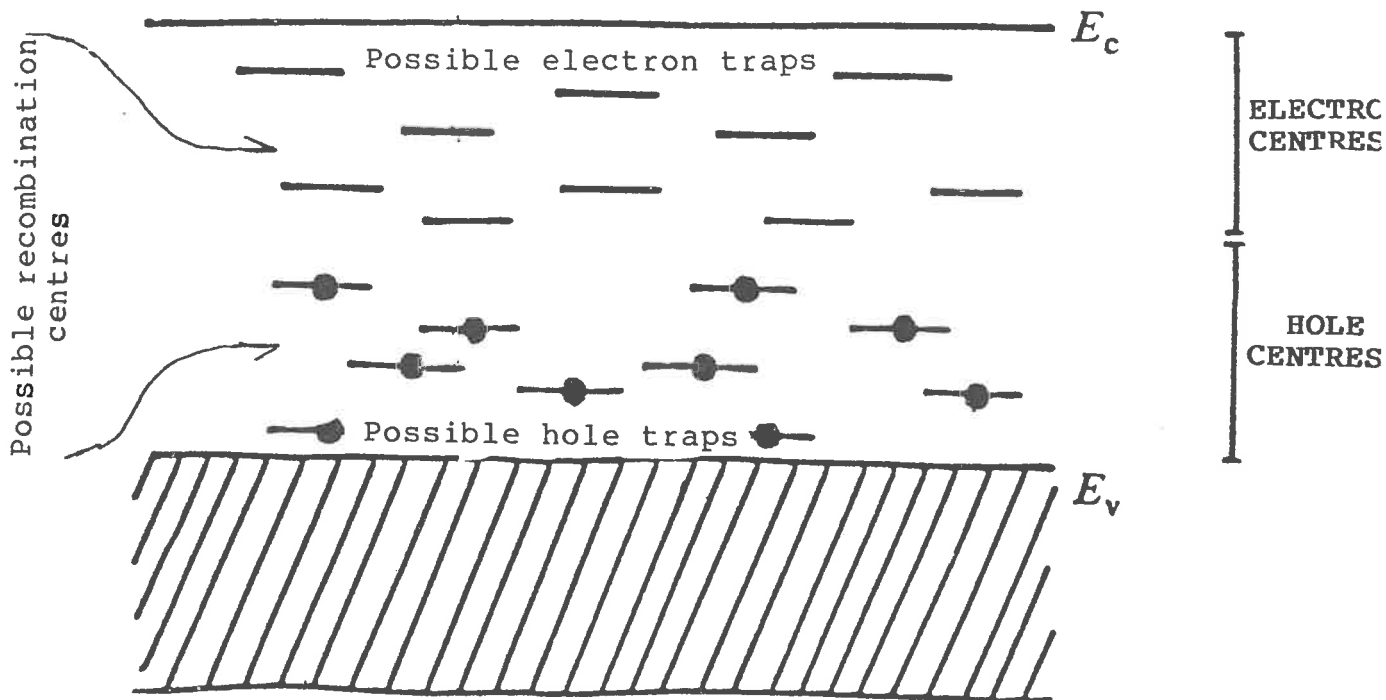


Figure 2.3 The location, or relative energy states, of electron and hole traps and recombination centres within the forbidden energy band (after McKeever, 1985).

temperature). Because the probability of a trapped charge being thermally released is exponentially related to $-E/kT$, then, for a given temperature those centres of small E are less likely to retain charges than centres of large E . This is represented in figure 2.3 (after McKeever, 1985) where electron traps have localized energy levels, not only above the Fermi level, but also near to the conduction band. Conversely, usually, hole traps are situated below the Fermi level and near to the valence band.

The position of a trap in the forbidden band depends on the details of the (quantum mechanical) interaction between the defect and the surrounding lattice. Depending on its "charge" state and other details, a defect may be an electron trap, or a hole trap, or in some instances may be both a hole and an electron trap. Electron traps tend to lie near the conduction band, hole traps near the valence band and traps near the centre of the gap tend to be the most likely recombination centres. The interaction between a conduction band electron (valence band hole) and a trap is expressed as a trapping probability or cross section. This probability (as given by quantum mechanical transition theory) contains a factor inversely dependent on the energy between the electron trap (hole trap) and the conduction band (valence band) and thus, the trapping probability for each type of trap tends to increase as these energy differences decrease.

2.2.3 Non-radiative Recombination Centres

In order for luminescence to occur electron-hole recombination must be accompanied by emission of a photon. However, recombination can also occur without light emission in which case non-radiative recombination is said to occur. The nature of these centres is well known (Mott and Gurney, 1948) and has been summarized in McKeever (1985 p.34-40). In

cases where all emission is quenched, such as produced by numerous metallic impurities these centres are known as "killer centres".

2.3 The Thermoluminescence Process

Thermoluminescence, as stated previously, is the emission of light from a substance as it is heated, and which results from previous exposure to ionizing radiation. The ionizing radiation includes alpha particles, beta particles, gamma rays, x-rays, protons, neutrons and fission fragments. Many common rock-forming minerals exhibit TL including quartz, feldspar, calcite, dolomite, zircon, apatite and others.

In the natural geological environment most rocks and minerals will either contain radioactive impurities such as uranium, thorium and potassium, or will be in close proximity to these radioactive elements in their environment. Over time the radiation from these impurities will cause ionization and charge trapping in the host mineral. When the mineral is removed from its natural environment and subjected to a thermal cycle the TL emitted is called the natural TL, (NTL) i.e. that which occurs from exposure to radiation in the mineral's natural environment. No further TL occurs after one thermal cycle unless the mineral is exposed to further radiation. The TL that is induced by exposure to laboratory radiation is called artificial TL (ATL).

The processes occurring in NTL and ATL are the same and both give information about defects and impurities in minerals. Usually only NTL can provide information about the naturally accumulated radiation dose, such as the dose levels applicable to archaeological dating.

The TL process can be most conveniently described in three stages: (a) absorption of ionizing radiation, (b) trapping of charges and (c) thermal untrapping and TL emission.

2.3.1 Absorption of Ionizing Radiation

When radiation, be it alpha, beta or gamma radiation, enters a crystal lattice it will cause ionization. A 1 MeV beta particle (electron) penetrating a crystal will give up its energy in two main ways: (a) it causes electrons to be removed from atoms resulting in formation of electron-hole ionization pairs and (b) it dissipates energy by heating the lattice. (Another way in which an electron entering a crystal may lose energy is by atom displacement though this depends on its initial energy, and the energy transferred). Levy (1974) states that "very roughly" half of the energy of the incident electron is used up in each of the above processes.

The distance travelled by the electron in this process is called the range. In a silicate lattice the range is approximately 1mm for each MeV of energy possessed by the incident electron.

An alpha particle entering a crystal will produce very similar effects to a beta particle. The major differences are in the range and the ionization rate per unit path length of the alpha particle. The alpha particle has a range of approximately 5 microns for each MeV of energy possessed.

A 1 MeV beta particle will cause approximately 5×10^4 ionization events per millimetre whereas a 1 MeV alpha particle will cause approximately 5×10^7 ionization events per millimetre (of extrapolated path length). The implications of this difference in range and ionization rate are that for a grain (say quartz) with a one millimetre diameter, the ionization events caused by the beta particles will be evenly distributed through the grain, whereas those caused by the alpha particle will be concentrated in the outer 5-25 micron "skin" of the quartz grain (Levy 1974).

Gamma rays are much more penetrative than either alpha or beta particles. When 1 MeV gamma rays enter a typical silicate crystal roughly one half of them will traverse (statistically) approximately 10-15 centimetres of the crystal before undergoing an interaction. This distance is called the half distance. The interaction of gamma rays with the solid results in a transfer of roughly two-thirds of the energy of the gamma ray to one of the electrons in the crystal. This interaction may occur by the photoelectric effect, the Compton effect or by pair production. The Compton effect refers to an elastic collision between the gamma ray and an electron. The "struck" electron is ejected from its atomic position and traverses the lattice with an initial high velocity. It interacts with the lattice in the same manner as any other electron such as the energetic beta particle discussed earlier. These energetic electrons transfer their energy to the lattice either by atom displacement (if the energy is large enough), creation of electron-hole ionization pairs or heat. Because of the more penetrative nature of gamma rays they produce ionization pairs through the crystal that are more uniformly distributed than those created by alpha and beta particles.

Ionization causes creation of electron-hole pairs where an electron is excited from the valence band to the conduction band leaving an electronic hole (or hole) in the valence band. Both the electron and hole are mobile in their respective energy bands and may migrate through the crystal until they recombine or become trapped at defect centres. Holes produced during ionization are very quickly trapped on hole traps. Electrons may either recombine with holes trapped on hole traps or may be trapped on electron traps. Levy (op.cit) suggests that less than 1% of ionization electrons are trapped whereas 99% undergo recombination. Those electrons and holes which are trapped are important in the TL process.

2.3.2 Trapping of charges by defects

As discussed in section 2.1.1 and 2.2.1 traps that are important for TL are crystal lattice imperfections, of which there are many in solids. The majority of traps are either impurity ions, which are substitutions for regular atoms in the crystal, or vacancies. An impurity concentration of 1 or 2ppm leads to a defect concentration of $10^{16}/\text{cm}^3$ - a very large number, which can give rise to an easily detectable TL signal, (Levy 1974).

The most common electron trap is any defect in a crystal where a negatively charged ion is missing from the lattice or where an impurity ion is present containing fewer valence electrons than the atom normally occupying its position in the lattice. Consequently this site will tend to attract electrons to preserve the electrical neutrality of the lattice immediately surrounding the trap. Similarly, defect centres possessing fewer positive charges than usually associated with the atom occupying that lattice position will function as hole traps. The greater the difference between the valence state of the defect centre and the atom normally occupying the particular site, the more strongly or tightly a charge will be trapped. If a defect centre has the same valence state as associated with the normal atom in the lattice position then the centre may under some conditions function as either an electron or hole trap, depending on its electron affinity. In this case the trapped charges will usually be only weakly bound.

Conceptually, in quartz (the mineral with which this thesis is concerned), a well known hole trap is an Al^{3+} ion substituting for Si^{4+} (O'Brien 1955). Electrons may be trapped on vacant oxygen sites where an O^{2-} charge is missing and thus electrons on these sites will be tightly bound. The role of OH^- groups as possible traps has also been investigated by Griscom (1978, 1985) who suggests that holes may be

trapped on OH groups which themselves may have formed "from hydrogen decoration" of silicon vacancies formed during crystal growth. Bernhardt (1982) also suggests that OH groups may play a prominent role as traps in production of quartz TL at high temperatures.

Other defects in quartz which may function as charge traps include substitutional impurities such as Ti^{4+} in rose quartz (Wright et al 1963) and Ge^{4+} in smoky quartz (Schlesinger 1964). McKeever et al (1984) suggest that the Ge^{4+} centres function as electron traps for the quartz 110°C glow peak. Ichikawa (1968) suggests that interstitial alkali ions (Li^+ and Na^+) also act as electron traps (possibly for the quartz 230°C and 270°C glow peaks).

Griscom (1978) contains a comprehensive review of these and other impurities and defects in quartz. Griscom (1985) also reviews defects in amorphous silica and suggests where these results may be applicable to quartz. In these articles, and in addition to the above mentioned defects, Griscom (op.cit) also considers other defects which may act as charge traps in quartz including: atomic hydrogen (at temperatures below 100K); gallium centres, which perform the same role as Al centres; Fe^{3+} centres, which he considers may be interstitial rather than substitutional and finally, stable multi-alkali centres ($[Ge, e^-/Na^+, M, N]$ where $M, N = Na^+$ or Li^+). These latter centres are considered to be the principal stable electron traps in heavily x-irradiated α quartz with low Ge/Al ratios.

2.3.3 Thermal Untrapping and Luminescent Recombination

Once charges are trapped they will remain trapped for periods ranging from fractions of seconds to thousands of years depending on the half life of the trap. The charges must be released by subsequent heating in order for TL to be produced by recombination at luminescent centres.

Charges may be trapped on defect centres of different energy. The more tightly a charge is bound (or the deeper the trap) the more the thermal energy required to release it. Therefore as the temperature is raised the least tightly bound charges will be released first. Each type of trap, usually formed by similar defect centres, will release their trapped charges at approximately the same temperature.

This process is illustrated in figure 2.4 (after Levy 1974). The uppermost curve shows the untrapping probability as a function of crystal temperature. At low temperatures all charges remain trapped as the probability of escape is insignificant - in this stage the input of thermal energy is less than the activation energy of the trap. The probability of the charge escaping from the trap increases as the temperature increases since there is an increased probability of the bound electron gaining the energy required to escape the trap. Therefore in the uppermost curve of figure 2.4 the probability of escape increases with the temperature. As the probability of untrapping increases, the trapped charge concentration will begin to decrease.

The trapped charge concentration is shown in the middle curve of figure 2.4 and decreases with increasing temperature. At some temperature sufficient thermal energy will have been provided to allow all trapped charges to escape. The temperature range over which the trapped charge population decreases from 100% to 0% is 10°C-50°C (in case of single stage untrapping).

During the depopulation process a fraction of charges will undergo recombination at luminescent centres in the crystal lattice, with resultant radiative emission. This results in a curve of TL light intensity vs temperature with an intensity maximum at a particular temperature as illustrated in the lowermost curve.

A single heating is sufficient to release all trapped charges and no further light will be emitted within the same temperature range upon subsequent reheating. Exposure to further radiation is required to repopulate traps and then upon subsequent reheating TL will again usually be observed.

A curve as portrayed in the lowermost portion of figure 2.4 which describes the light emission from a single trap is referred to as a glow peak. Over a wider range of temperature a number of superposed glow peaks may occur which constitute a glow curve. Each glow peak in a glow curve is characterized by a particular temperature of maximum emission (T), a trap depth or activation (E) and a pre-exponential factor or "attempt to escape" frequency (s). This is illustrated in figure 2.5 after Levy (1974). Thus a glow curve, which is the basic data in TL studies, represents a number of specific activation energies for charge release from various traps.

Once the trapped charges are released they can undergo a number of different processes. Electrons may interact with trapped holes, recombination centres or other electron traps. Recombination may be either luminescent or non-luminescent depending on the nature of the recombination centre.

An important luminescent centre is a recombination luminescent centre. This centre is often a hole trap that emits a quantum of light upon recombining with a mobile electron. As part of the trapping and recombination process an electron becomes trapped in one of the higher energy levels of the centre for a very short time (eg. 10^{-12} seconds). The electron then makes a transition to the ground state with the emission of a light quanta. Once the electron enters the ground state recombination occurs almost instantaneously (Levy op.cit).

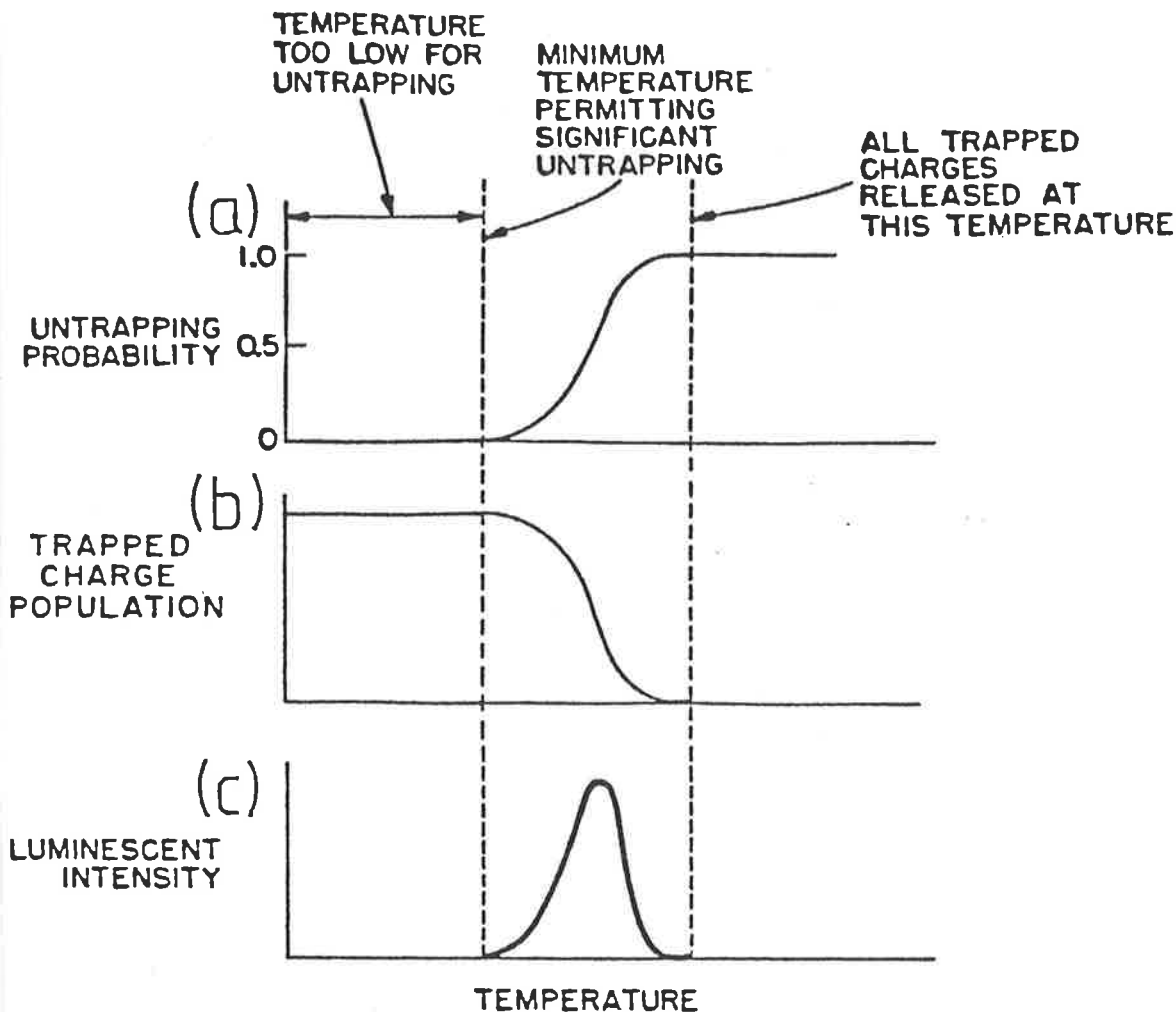


Figure 2.4 The relationship between (a) untrapping probability, (b) trapped charge population and (c) luminescent intensity. As temperature increases more and more charges are released and the trapped charge population decreases. This corresponds to luminescence. As the trapped charge population continues to decrease the luminescent signal passes through a maximum and then decreases also (Levy 1974)

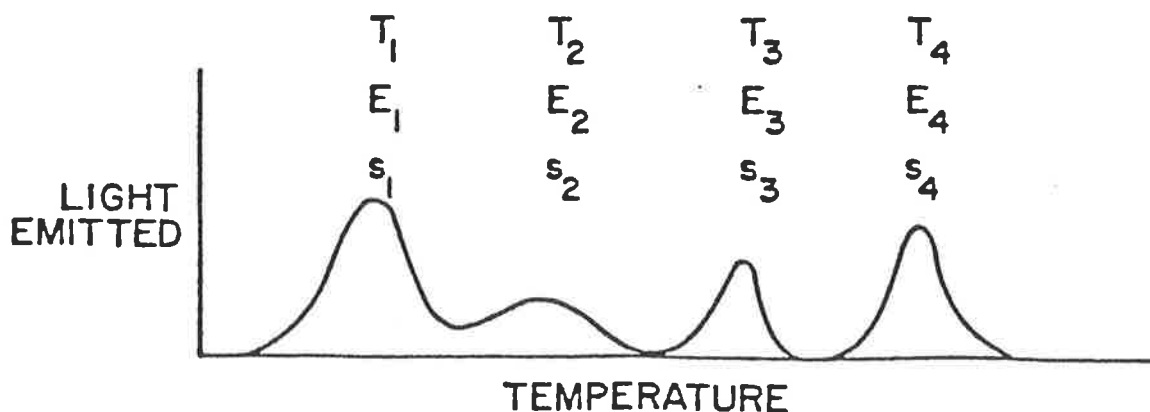


Figure 2.5 An example of a glow curve from a material with four different types of charge traps. Each trap type is characterized by a particular "attempt to escape frequency", s and activation energy for thermal detrapping E . The temperature T will vary with the heating rate (Levy 1974).

A second type of luminescent centre is a transition-emission luminescent centre which is usually an impurity ion in the crystal lattice. This type of centre does not often function as a charge trapping centre, therefore when a thermally released charge encounters this type of centre it is momentarily trapped in one of the upper energy levels before making one or more transitions to lower energy levels, with the emission of one or more quanta of light. The charge might then remain in the lowest energy level long enough for the centre to be classified as a trap or a recombination centre. Usually, however, the transition-emission luminescent centre releases its trapped charge which migrates through the crystal until it is stably trapped or undergoes recombination.

Not all thermally released electrons will undergo recombination and some may be retrapped, either on similar electron traps to those from which they have been released, or by different types of electron traps with higher activation energy. The probability of retrapping vs recombination depends on a number of factors though principally on the relative numbers of available electron traps and recombination centres and the capture cross sections for each centre. Mathematical models have been developed which consider retrapping processes. These are called kinetic models of TL.

2.4 Kinetic Models For Thermoluminescence

A number of mathematical theories have been developed to describe some aspects of TL glow peaks. These theories are referred to as kinetic models and can be used to provide information about parameters associated with charge trapping sites responsible for TL emission. Kinetic models can also be used to explain variations in glow peak intensities, shapes, areas and temperatures of maximum emission. Methods of kinetic analysis

of glow peaks are contained in Chen and Kirsh (1981) and a useful summary in McKeever (1985).

Although no kinetic analyses of activation energies or pre-exponential factors have been carried out in this thesis, it is still considered useful to include a discussion of kinetic models as these may help explain variations in glow curves in a qualitative fashion in future chapters. As will be seen in chapter 2.5.2 and chapters 3, 6 and 7 there is a systematic variation in some glow curve parameters (eg. temperature of maximum emission, intensities and glow peak ratios) as a function of proximity to uranium mineralization. Chapter 4 will contain an attempt to explain such variations in terms of the kinetic models explained in this section.

Almost all of the following discussion on kinetic models for TL has been taken from numerous publications by Levy and co-workers ie. Levy (1981,1982,1983,1984a,1984b,1985a,1985b), Schwartzman et al (1983) and Hornyak et al (1985).

2.4.1 First Order Kinetics

The original theoretical treatment of first order kinetics was given by Randall and Wilkins (1945). Among other assumptions, first order kinetics assume that when a trapped electron is thermally released it will recombine with a trapped hole with the possibility of a resultant photon emission. Retrapping is assumed to be negligible in their model. Under such conditions the intensity of the light emitted is proportional to the number of charges untrapped per unit time. The number of charges released per unit time is equal to the trapped charge population multiplied by the probability that each charge will escape. The probability that an electron will escape from a trap, per unit time, is given by:

$$p = se^{-E/kT} \quad (1)$$

where

p = the probability of escape

s = the "attempt to escape" frequency or pre-exponential factor

E = the thermal activation energy for charge untrapping (in eV)

k = Boltzmann constant

T = absolute temperature in Kelvin

If retrapping is negligible then the intensity I , at any time T , is given by:

$$I = - \frac{dn}{dt} = nse^{-E/kT} \quad (2)$$

where n is the trapped charge concentration time t , and dn/dt is the number of charges released per unit time.

In the usual TL measurement the sample is irradiated at a temperature low enough to ensure that the term $e^{-E/kT}$ is negligible and light emission is undetectable. During the TL measurement the sample temperature is usually increased linearly with time since: (a) a precise and reproducible linear temperature increase is the easiest to achieve experimentally, and (b) a linear temperature program enables a simple solution of equation (2).

For a linear temperature rise, time and temperature are related by the equation:

$$T = T_0 + \beta t \text{ or } dT = \beta dt \quad (3)$$

where: β is the heating rate in degrees per unit time and T_0 is the temperature at which the TL measurement begins.

Integration of (2) after substitution of (3) results in the following expression for luminescent emission as a function of time or temperature, for a single type of trapping centre:

$$I = n_0 s e^{-E/kt} \exp \left(- \int_0^T \frac{s}{\beta} e^{-E/kT} dT \right) \quad (4)$$

where n_0 is the number of initial trapped charges.

Equation (4) is known as the first order glow curve expression and shows that the total emission is dependent on n_0 , number of trapped charges which is a function of the pre-measurement dose. This is illustrated in figure 2.6 (after Levy 1982). Both peak intensity and peak area vary linearly with the pre-measurement dose. Other properties of the first order expression are that the shape of the glow peak, and the glow peak temperature depend on heating rate. For a fixed heating rate the glow peak shape and peak temperature are independent of n_0 .

The physical situation leading to first order kinetics, i.e. negligible retrapping, occurs when the concentration of luminescent centres is much larger than the number of traps. If concentrations are approximately equal then first order kinetics will still occur if the charge-capture cross section (Levy 1982) of the luminescent centre is much larger than the corresponding cross section of the trapping centre. In cases where the glow curve consists of more than one glow peak, in applying first order kinetics it is assumed there is no interaction between different types of traps.

2.4.2 Second Order Kinetics

When the number of traps is large compared with the number of luminescent centres there is a possibility of retrapping. The retrapping concept and the original second order kinetic expressions were introduced by Garlick and Gibson (1948). Equation (2) must therefore be replaced by one that includes retrapping. In this case the emission after thermal untrapping is controlled by competition between retrapping and recombination. The assumptions made in deriving the appropriate equation

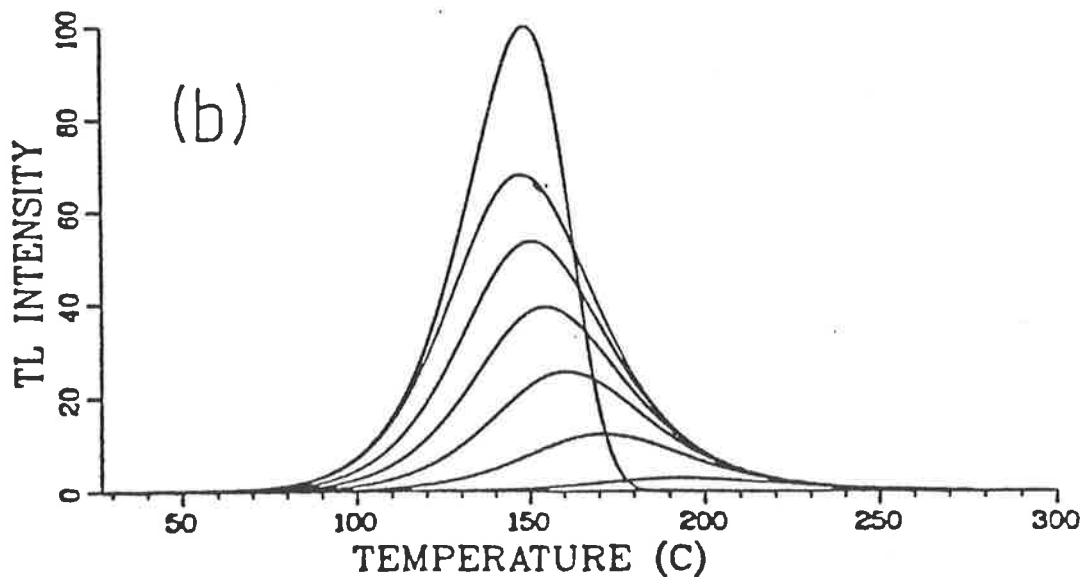
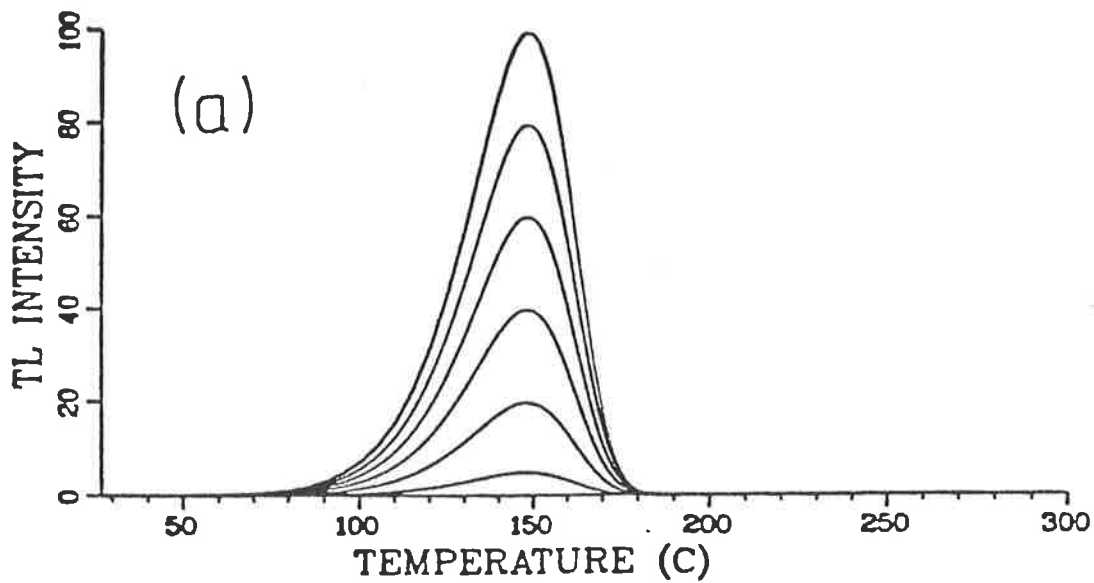


Figure 2.6 First order (a) and second order (b) glow peaks computed for the same s and E values ($s=10^{10}/\text{sec}$, $E=1.0$ eV) but different initial trapped charge concentrations. The peak temperature of first order curves remains constant whereas the peak temperature and curve shape of the second order curves changes (Levy 1982).

are that for each charge trapped in a trapping centre there is an opposite-sign charge trapped in a recombination or luminescent centre and that light is emitted when thermally released electrons recombine with trapped holes (after having been retrapped one or more times) or when thermally released holes interact with trapped electrons.

The probability that a conduction band electron will be retrapped is proportional to $\sigma_t (N_1 - n_1)$ where σ_t is the cross-section for retrapping, N_1 is the concentration of available electron traps and n_1 the concentration of trapped electrons (Levy 1982). $N_1 - n_1$ is therefore the concentration of empty electron traps. The probability that a conduction band electron will undergo recombination is $\sigma_r n_r$ where σ_r is the cross section for recombination and n_r is the trapped hole concentration. The fraction of electrons being retrapped is thus given by:

$$f_t = \frac{\sigma_t (N_1 - n_1)}{\sigma_t (N_1 - n_1) + \sigma_r n_r} \quad (5)$$

The fraction undergoing recombination is given by

$$1 - f_t = 1 - \frac{\sigma_t (N_1 - n_1)}{\sigma_t (N_1 - n_1) + \sigma_r n_r} \quad (6)$$

Assuming that the cross section for retrapping and recombination are equal (ie. $\sigma_r = \sigma_t$) and the number of trapped electrons equals the number of trapped holes (ie. $n_1 = n_r$) then equation (6) becomes:

$$1 - f_t = \frac{n_1}{N_1} \quad (7)$$

The intensity of emission $I = \frac{-dn_1}{dt}$ thus becomes:

$$\begin{aligned} I &= \frac{-dn}{dt} = \left(\frac{n_1}{N_1} \right) n_1 s_1 e^{-E_1/kT} \\ &= \frac{n_1^2}{N_1} s_1 e^{-E_1/kT} \end{aligned} \quad (8)$$

Intensity of equation (8) after substitution of equation (3) yields

$$I(t) = \frac{n_{01}^2 s_1 \exp(-E_1/kT)}{N_1 \left[1 + \frac{n_{01}}{N_1} \int_0^T \frac{s_1 \exp(-E/kT) dt}{\beta} \right]^2} \quad (9)$$

Equation (9) is referred to as the second order glow curve expression. Plots of second order glow curves are also contained in figure 2.6. The principal properties of second order glow curves are: (a) that for other parameters kept constant, the glow peak shape and peak temperature depend on heating rate. (b) For a fixed heating rate the glow peak temperature and shape are dependent on n_{01} -the initial trapped charge concentration, or more importantly: $\frac{n_{01}}{N_1}$ -the fraction of traps filled. This is an important observation as $\frac{n_{01}}{N_1}$ changes in glow peak temperature were observed approaching uranium mineralization at the Westmoreland orebodies. This is noted in chapter 5 and discussed in chapter (4). (c) The second order glow curves coincide as they approach low intensity on the high temperature side of the glow peak. Both (b) and (c), when observed in TL measurements, can be regarded as indicating that retrapping is occurring when different test doses are applied.

In second order kinetics, if more than one type of electron trap is present, i.e. if more than one glow peak present in the glow curve, then it is assumed that the interactions between different trap types is negligible.

2.4.3 Thermoluminescence in Systems Not Subject to the Usual Approximations for First and Second Order Kinetics

First and second order kinetic expressions for TL glow curves are based on the following assumptions:

- (1) Retrapping is negligible in first order kinetics and non-negligible in second order kinetics.

- (2) In second order kinetics $\sigma_r = \sigma_{t1}$ and $n_r = n_1$, whereas in first order kinetics $\sigma_r \gg \sigma_{t1}$.
- (3) Interactions between different types of traps are negligible, ie. when charges are retrapped, retrapping occurs on the same type of trap, and there is no transfer of charges between traps.

Levy (1982,1983,1984a) has developed expressions to describe glow curves where the above assumptions do not apply. Solutions to these expressions show that glow peak intensity, shape and temperature vary with recombination and retrapping cross sections, trap concentration and initial trapped charge concentration.

Using the definitions given previously, the differential equation for trapped electron concentration as a function of time is:

$$\frac{dn}{dt} = (-1) [n_1 s_1 \exp(-E_1/kT)] \left[\frac{1 - \sigma_{t1}(N_1 - n_1)}{\sigma_{t1}(N_1 - n_1) + \sigma_r n_r} \right] \quad (10)$$

This equation is described as the General One Trap (GOT) TL equation (Levy 1984a). The (-1) factor occurs because the trapped electron concentration is decreasing. The second factor is the concentration of trapped electrons released to the conduction band per unit time. The third factor is the fraction of thermally released electrons not retrapped ie. those undergoing recombination.

Note that if the probability for recombination is very much larger than the probability for retrapping, ie. $\sigma_r n_r \gg \sigma_{t1}(N_1 - n_1)$ then

equation (10) reduces to $I(t) = \frac{-dn_1}{dt} = n_1 s_1 \exp(-E_1/kT)$ which upon substitution of the linearly increasing temperature equation yields the normal first order kinetics glow curve expression ie. equation (4).

Similarly the second order kinetic glow curve equation can be derived from equation (10) when the two approximations for second order kinetics are made ie. $n_1 = n_r$ and $\sigma_{t1} = \sigma_r$, and the appropriate integration after substitution of linearly increasing temperature equation.

When the trapping and recombination cross sections are not equal ie. $\sigma_{t1} \neq \sigma_r$ then equation (10) will not yield the normal first or second order glow curves. This is illustrated in figures 2.7 and 2.8 (after Levy 1982).

Figure 2.7 shows the case where first and second order glow curves were computed when all parameters were fixed except for the recombination to retrapping cross-section ratio. The first order glow peak is marked with the symbol +, the second order glow peak with the symbol *. The following points are discernible:

- (1) As σ_r/σ_{t1} increases the glow peaks more closely resemble first order glow peaks.
- (2) The second order glow peak is fitted when $\sigma_r/\sigma_{t1} = 1$. This is also indicated by a closer spacing of σ_r/σ_{t1} ratios in figure 2.8.
- (3) The glow peak intensity, shape and temperature vary with the σ_r/σ_{t1} ratio, ie. the intensity decreases and the temperature increases as σ_r/σ_{t1} decreases.
- (4) Although the intensity and shape of each glow peak change, the area under each peak is constant, or independent of the σ_r/σ_{t1} ratio in the one trap model.

Levy (1982) also demonstrated that glow peak shape, intensity and temperature also vary with the trapped hole concentration. This is evident from figures 2.9 and 2.10 where glow curves were computed with all parameters constant except n_{r0} . The following points arise:

- (1) First order kinetics is approached as n_r/n_1 increases (ie. >10)
- (2) Second order kinetics occur when $n_r = n_1$.
- (3) The glow peak temperature increases and glow peak height decreases with decreasing n_r/n_1 .

Levy (op.cit) considers that it is likely that the condition $n_{01} \neq n_{r0}$ or $n_1 \neq n_r$ applies to most materials exhibiting second order kinetics that contain more than one glow peak. For example a material which

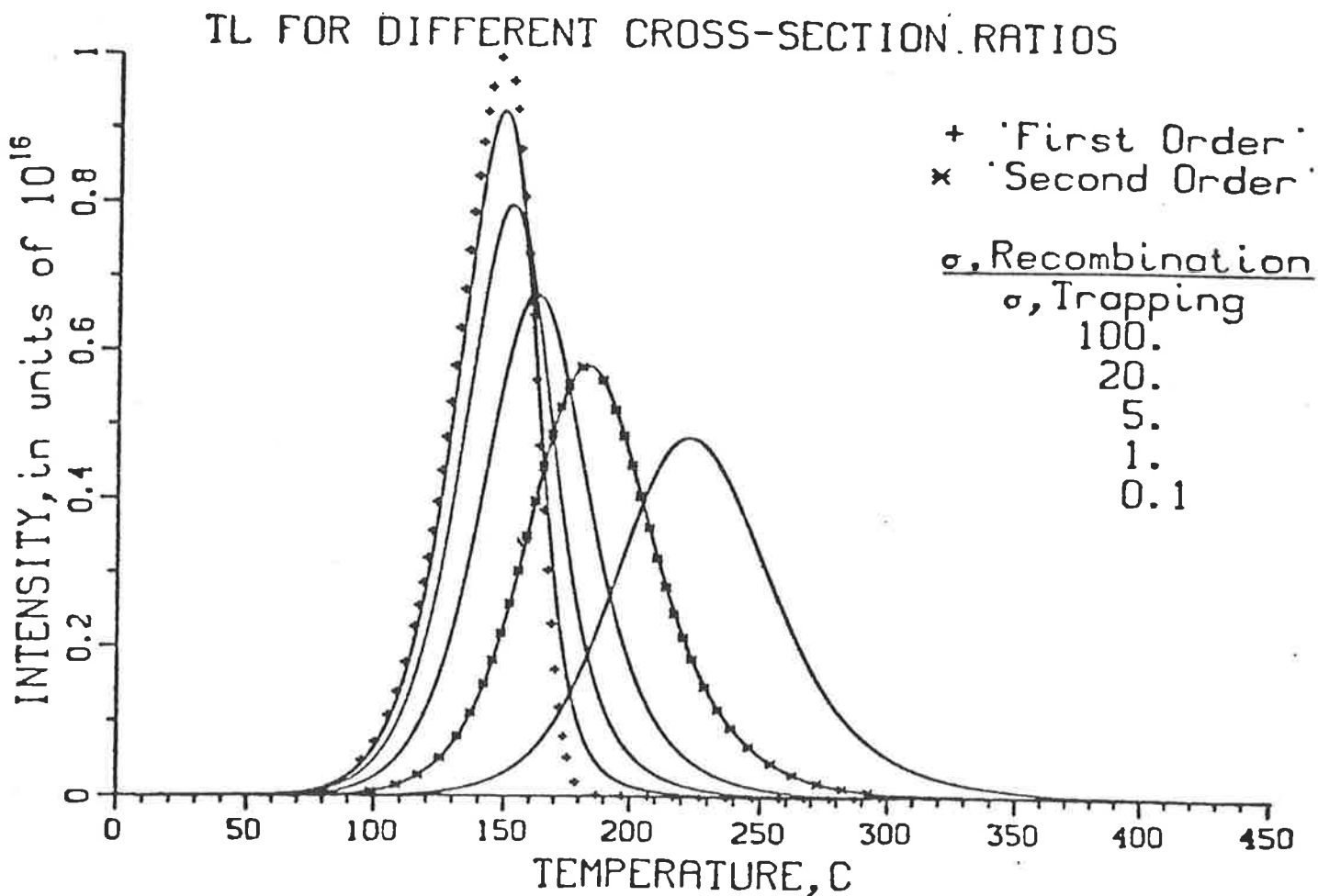


Figure 2.7 First order (all untrapped charges leading to recombination) and second order (some untrapped charges being retrapped) glow curves computed for different recombination to retrapping ratios. First order kinetics is approached only when the cross section ratio is very large (Levy 1982).

TL FOR DIFFERENT CROSS-SECTION RATIOS NEAR 1

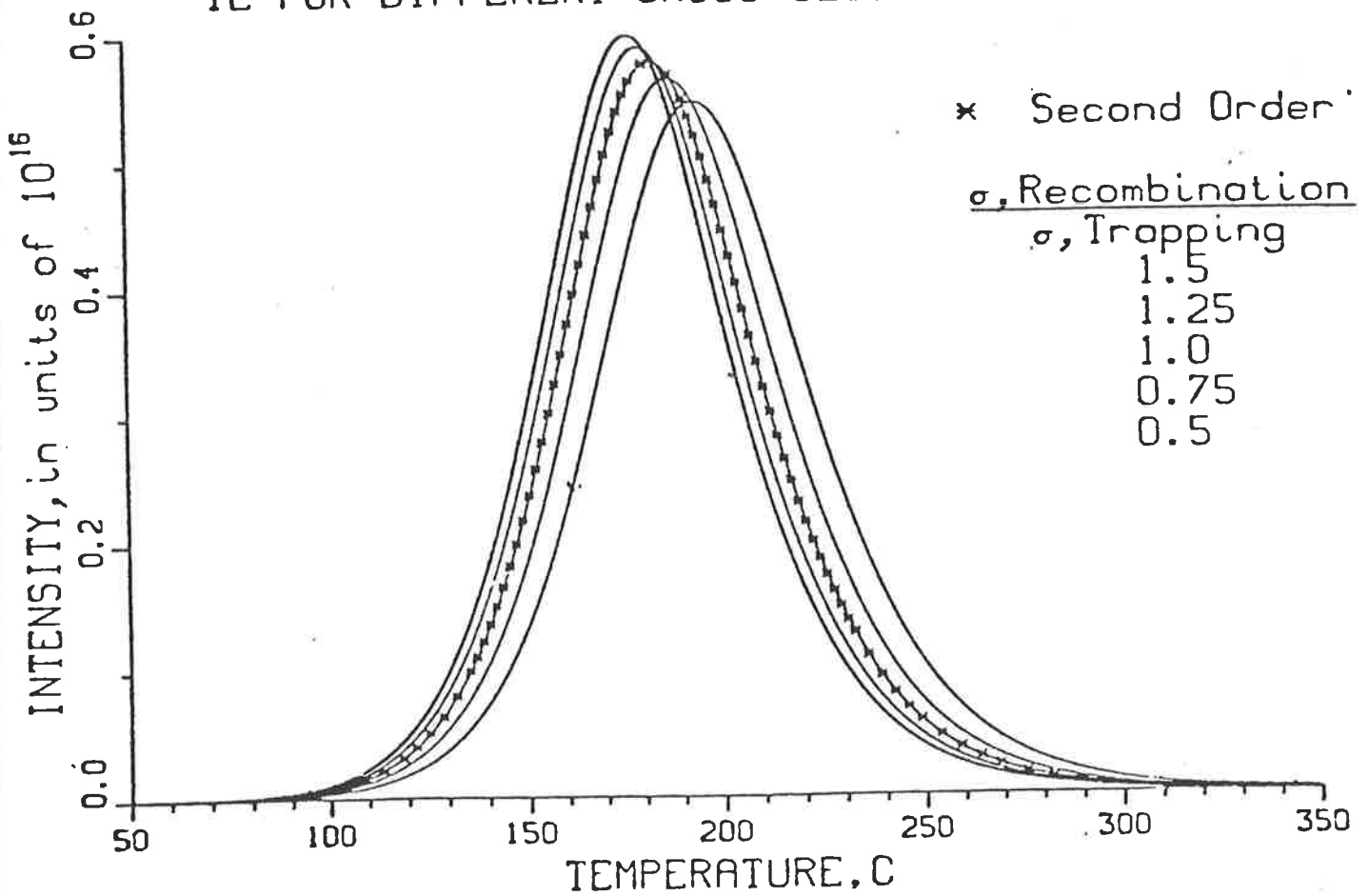


Figure 2.8 Glow curves computed for cross section ratios near one. Second order kinetics is obeyed only when the cross section ratio equals one (Levy 1982).

TL FOR DIFFERENT HOLE-ELECTRON RATIOS

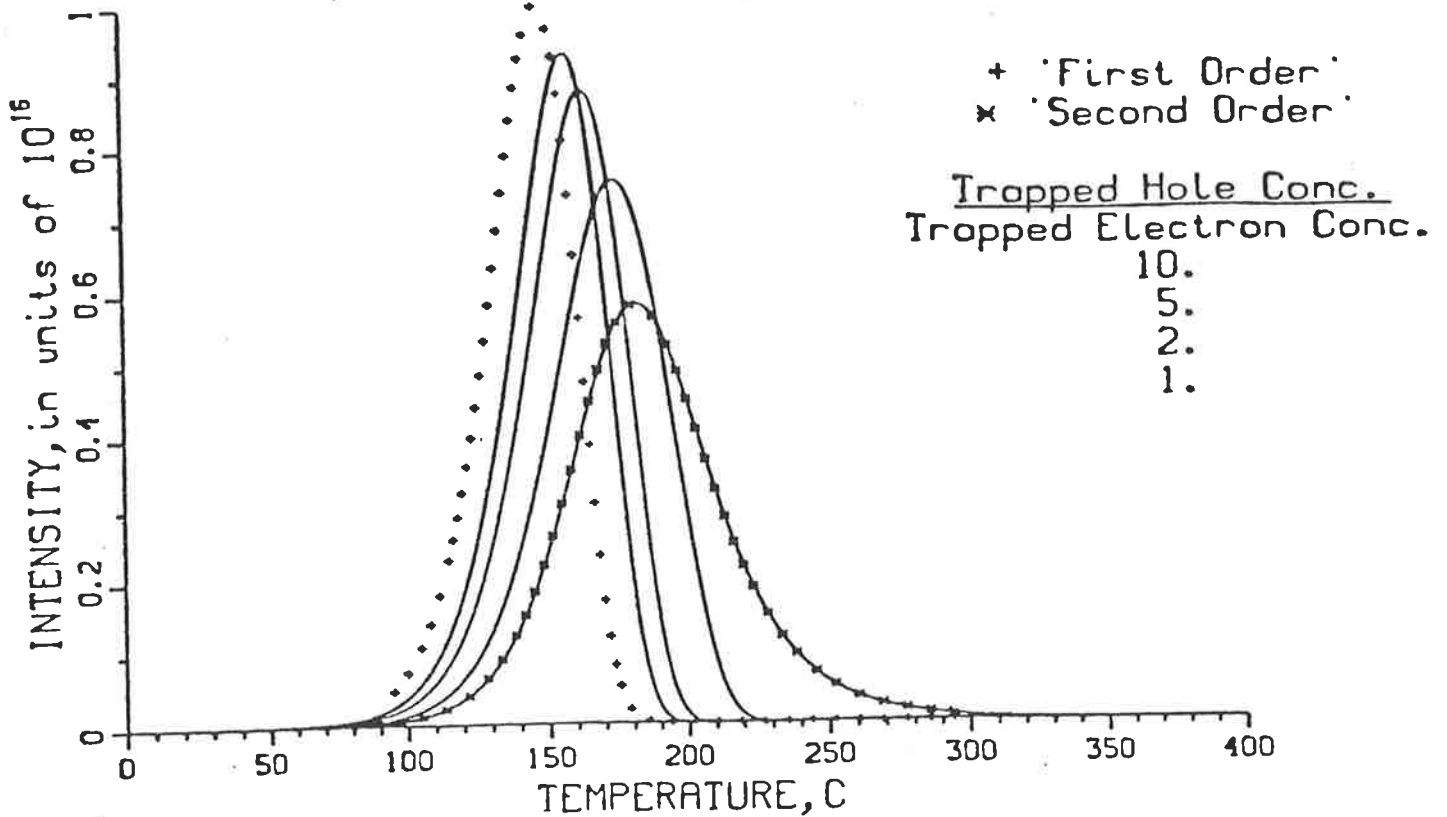


Figure 2.9 First and second order glow curves computed for different trapped hole to electron ratios. First order kinetics is approached only when the ratio is very large. The temperature of the glow peak varies with the trapped hole to electron ratio (Levy 1982).

TL FOR DIFFERENT HOLE-ELECTRON RATIOS NEAR 1

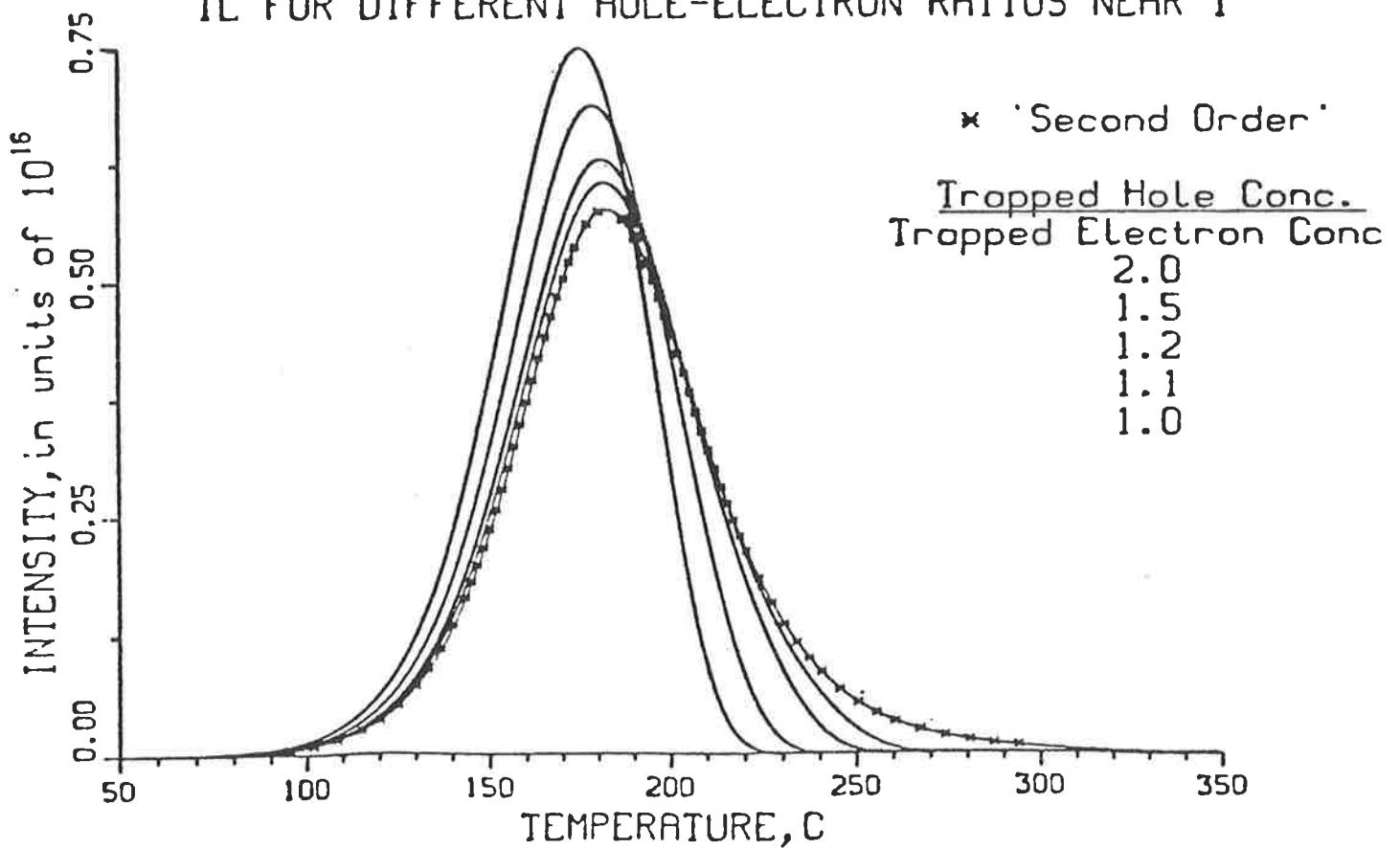


Figure 2.10 Glow curves computed for trapped hole to electron ratios near one. Second order kinetics is obeyed only when the ratio is one (Levy 1982).

exhibits two or more glow peaks may have two or more different types of electron traps and only one type of hole trap. Ionizing irradiation will cause electrons to be trapped in the two types of electron traps whereas holes will only be trapped on the one type of hole trap. Naturally, after irradiation the total number of trapped holes will be very nearly equal to the total number of trapped electrons in order to maintain the charge balance. During heating, thermally released electrons from the lowest energy electron trap can combine with a trapped hole population equal to the sum of all trapped electrons, ie. the total number of electrons in the lowest energy traps can recombine with a much larger population of trapped holes.

In this regard one might expect that lower temperature peaks would approach first order kinetics. In fact the trapped electron and hole populations will only be equal for the highest temperature peaks. Therefore, the highest temperature peak is likely to conform to second order kinetics. However, this would only occur if there was no interaction between different types of traps. Levy (1985a,b) also considers the possibility proposed by Chen and Kirsh (1981) that single glow peaks are described by "partial order kinetics", ie. that single glow peaks are described by the equation:

$$I(t) = - \frac{dn}{dt} = sn^p e^{-E/kT} \quad \text{where } p \neq 1, 2 \quad (11)$$

For partial order kinetics to be consistent with the GOT equation it would be necessary that,

$$n \left(1 - \frac{\sigma_t (N-n)}{\sigma_t (N-n) + \sigma_r n_r} \right) = n^p, \quad \text{where } p \neq 1 \text{ or } 2.$$

By expanding the fraction it is seen that this is not possible, thus partial order kinetics is not consistent with GOT kinetics and is an empirical concept without a physical basis.

2.4.4 General Thermoluminescence Glow Curve Kinetics For Systems Having More Than One Glow Peak - Interactive Kinetics

The general one-trap first and second order kinetics all require the assumption that charges released from one type of trap do not interact with other types of traps. Interactions between different types of traps can be described by very general equations as developed by Levy (1984b, 1985a,b).

Consider a system of j different types of electron traps and a single type of hole trap. Let N_i be the concentration of the i th type of electron trap and N_r the concentration of the hole traps. Assume $N_r \geq N_1 + N_2 + N_3 + \dots$. Let n_i be the trapped electron concentrations and n_r the trapped hole concentration at time t , n_{01} and n_{r0} the corresponding concentrations at $t=0$. σ_{ti} is the cross section for electron retrapping on the $(N_i - n_i)$ empty electron traps of the i th type, and σ_r the cross section for TL light emitting electron-hole recombination. The final σ_{ti} is the cross section for electron retrapping on the $(N_i - n_i)$ empty electron traps of the i th type and σ_r the cross section for TL light emitting electron-hole recombination. The final assumption is that the substance is irradiated at a temperature low enough to consider the thermal untrapping processes to be negligible.

After irradiation and before heating the initial trapped electron concentrations are $n_{01}, n_{02}, n_{03}, \dots$, and $n_{01} + n_{02} + n_{03} + \dots = n_{r0}$ (the trapped hole concentration). The equations for the trapped electron and hole concentrations during heating are: Levy 1984(b)

$$\frac{dn_i}{dt} = -n_i s_i e^{-E_i/kT} + \left(\sum_{i=1}^j n_i s_i e^{-E_i/kT} \right) \left(\frac{\sigma_i (N_i - n_i)}{n_r + \sum_{i=1}^j \sigma_i (N_i - n_i)} \right) \quad (12)$$

$$I(t) = \frac{-dn_r}{dt} = - \sum_{i=1}^j \frac{dn_i}{dt} \quad (13)$$

$$\sigma_i = \sigma_{ti} / \sigma_r$$

This is essentially an extension of Levy's GOT equation (1984(a)) to multitrapping systems.

In equation (12), the first term describes the thermal untrapping from the i th type of trap, the first bracket gives the total charge concentration in the conduction at time t and the second bracket is the function of conduction band electrons retrapped on the i th type of electron traps. The conduction band electrons that are not retrapped will recombine with holes to produce TL light $I(t)$, as described by equation (13). In all calculations $\sigma_i = \sigma_{ti}/\sigma_r$ and thus only the retrapping-recombination cross section ratios appear, not the actual cross sections themselves.

These equations describe a TL system in which charges released from one type of electron trap may be retrapped on all of the empty electron traps present - not just on the same type of trap from which they have been released. The lifetime of electrons in low temperature traps may be very short and may even fail to produce a TL signal at all (Hornyak and Levy, 1985), however the dominant effect is the retrapping of charges released at low temperatures by traps operative at higher temperatures. This process, where released charges may be retrapped on any available trap, is termed interactive kinetics, as opposed to non-interactive kinetics where it is assumed that interactions between different types of traps do not occur.

Note that in equation (12) when

$$\sigma_r n_r \gg \sum_{i=1}^j \sigma_{ti} (N_i - n_i),$$

then these equations reduce to a set of j independent first order kinetic equations.

2.4.4.1 Properties of Thermoluminescence Systems Described By Interactive Kinetics

Levy (op.cit) has studied the properties of interactive TL systems by obtaining computerized numerical solutions of equations (12) - (14) and varying one parameter whilst others are kept fixed. For the purposes of this thesis the three trap interactive system will be shown as this is most similar to results obtained in future chapters.

Consider firstly the effect on the TL glow curves of varying the σ_{ti}/σ_r cross section ratios. This is illustrated in figure 2.11 for the following parameters:

$$N_1 = N_2 = N_3 = 10^{16}$$

$$n_{01} = n_{02} = n_{03} = 5 \times 10^{15}$$

$$n_{r0} = 1.5 \times 10^{16}$$

$$s_1 = s_2 = s_3 = 10^{10}$$

$$E_1 = 1.0\text{eV}, E_2 = 1.25\text{eV}, E_3 = 1.50\text{eV}$$

$$\sigma_{ti}/\sigma_r = \text{as shown.}$$

Typical first order (+) and second order (*) glow curves are also shown which were computed from the appropriate parameters above. These show the expected glow curves assuming non-interactive TL systems.

Figure 2.11 indicates large differences between interactive and non-interactive systems. It is only as the σ_{ti}/σ_r ratios decrease (ie. recombination much more probable than retrapping) that the glow curves begin to approach the usual first order glow curves.

Recall that one of the assumptions made in deriving second order kinetic expressions was that $\sigma_{ti} = \sigma_r$. One might therefore expect that satisfying this condition ($\sigma_{ti}/\sigma_r=1$) in interactive

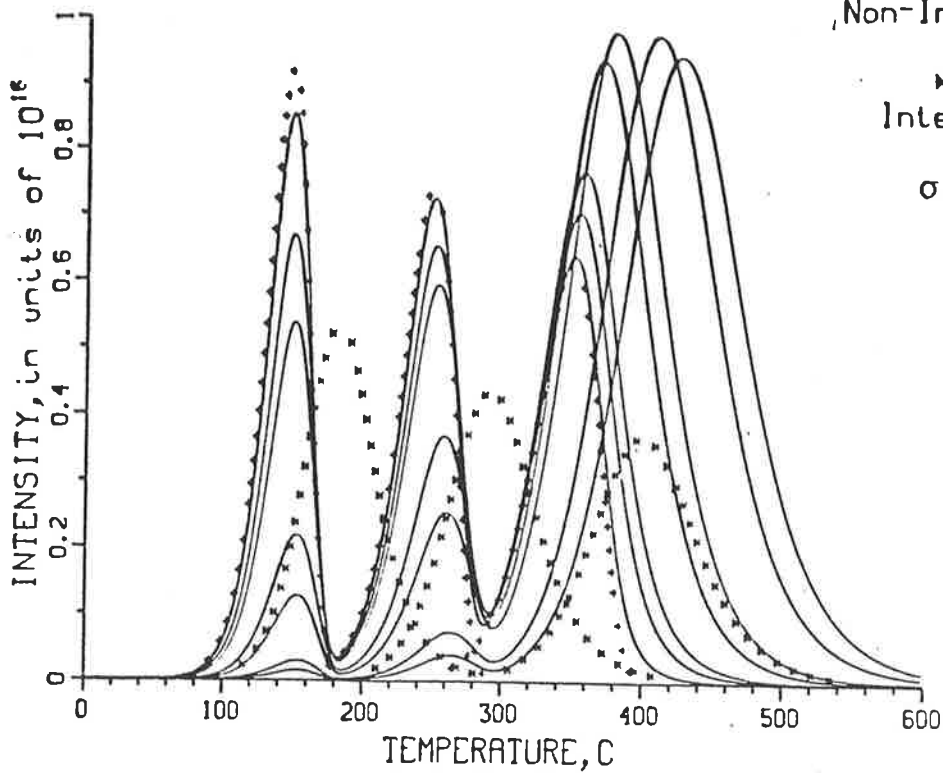


Figure 2.11 First order, second order and interactive kinetics glow curves computed for different cross section ratios showing both changes in glow peak temperature and glow curve shape (Levy 1984).

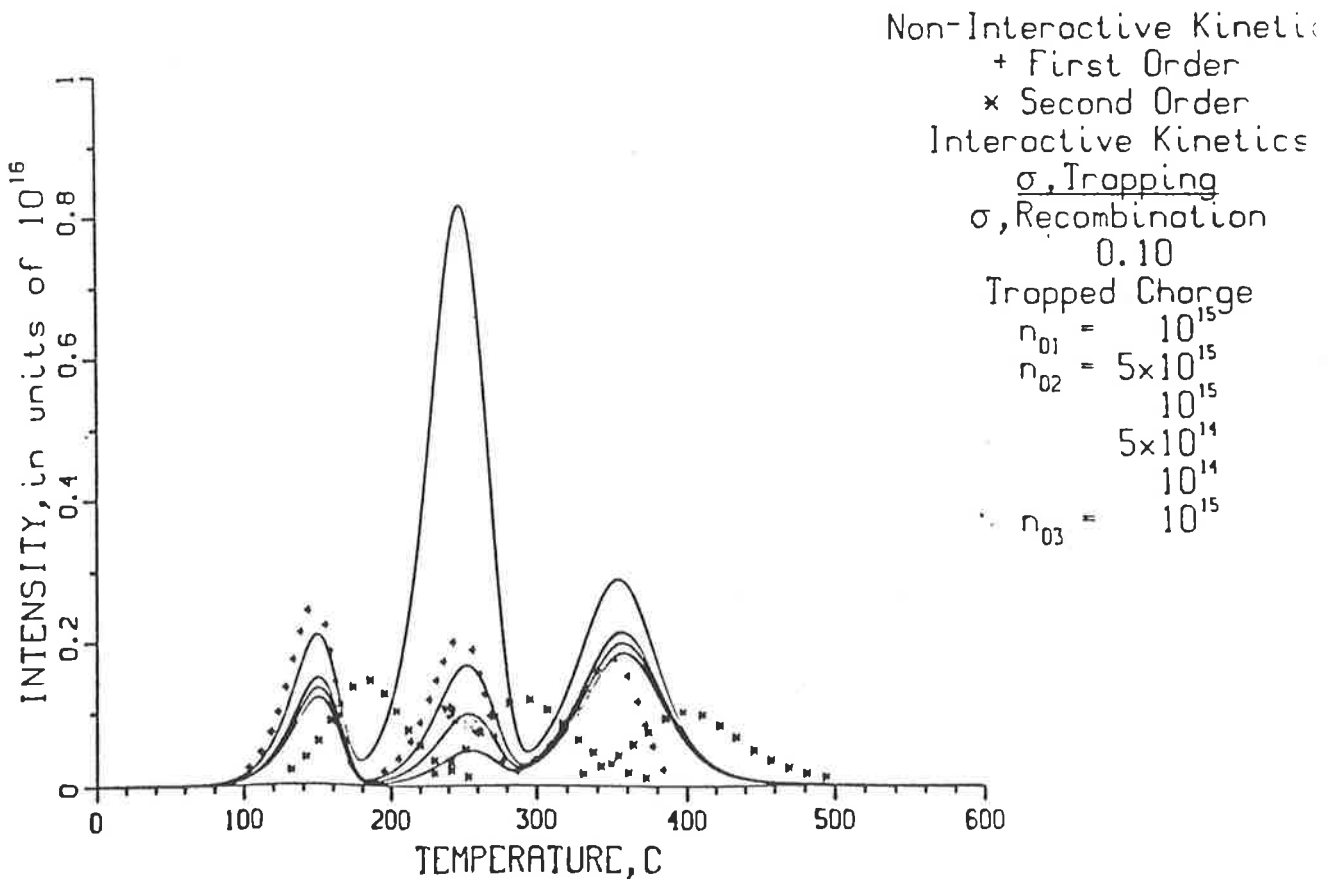


Figure 2.12 Change in glow curve shape and glow peak intensities when the trapped charge concentration is varied in one trap and interactive kinetics is obeyed (Levy 1984).

kinetics systems would produce a glow curve resembling that of the computed non-interactive second order one. Figure 2.11 indicates that this is not the case and that the glow curve when $\sigma_{ti}/\sigma_r=1$ more closely resembles first order than second order non-interactive kinetics.

As the σ_{ti}/σ_r ratio increases the glow peak temperature of the highest temperature peak increases. The intensities of the low and middle temperature peaks become smaller whilst the intensity of the high temperature peak initially increases (for σ_{ti}/σ_r ratios from 0.01 - 1.0) then slightly decreases (for σ_{ti}/σ_r ratios of 5.0 and 10.0).

Figure 2.12 shows the change in glow curve characteristics when the concentration of trapped charges vary in one trap for a fixed number of traps (N), and interactive kinetics apply. The major observation is that the shape and position of the glow peaks depend on the distribution of initial trapped charge concentration, ie. in this case on the n_{02} values.

Of particular importance is the way in which the glow curve properties depend on the pre-TL measurement dose, or on the magnitude of the initial trapped charge concentration. Levy (op.cit) computed glow curves demonstrating this dependence under the following conditions:

3 types of electron traps, N_1, N_2, N_3 such that $N_1 + N_2 + N_3 <$

N_r (concentration of hole traps)

$\sigma_{ti}/\sigma_r = 0.1$

E_i and s_i values as given previously

$n_{01} = n_{02} = n_{03}$ - values are shown on figure 2.13.

The resultant glow curves (computed from equations (12)-(14)) are shown in figure 2.13 for n_{0i} values ranging from 10^{10} to 5×10^{15} .

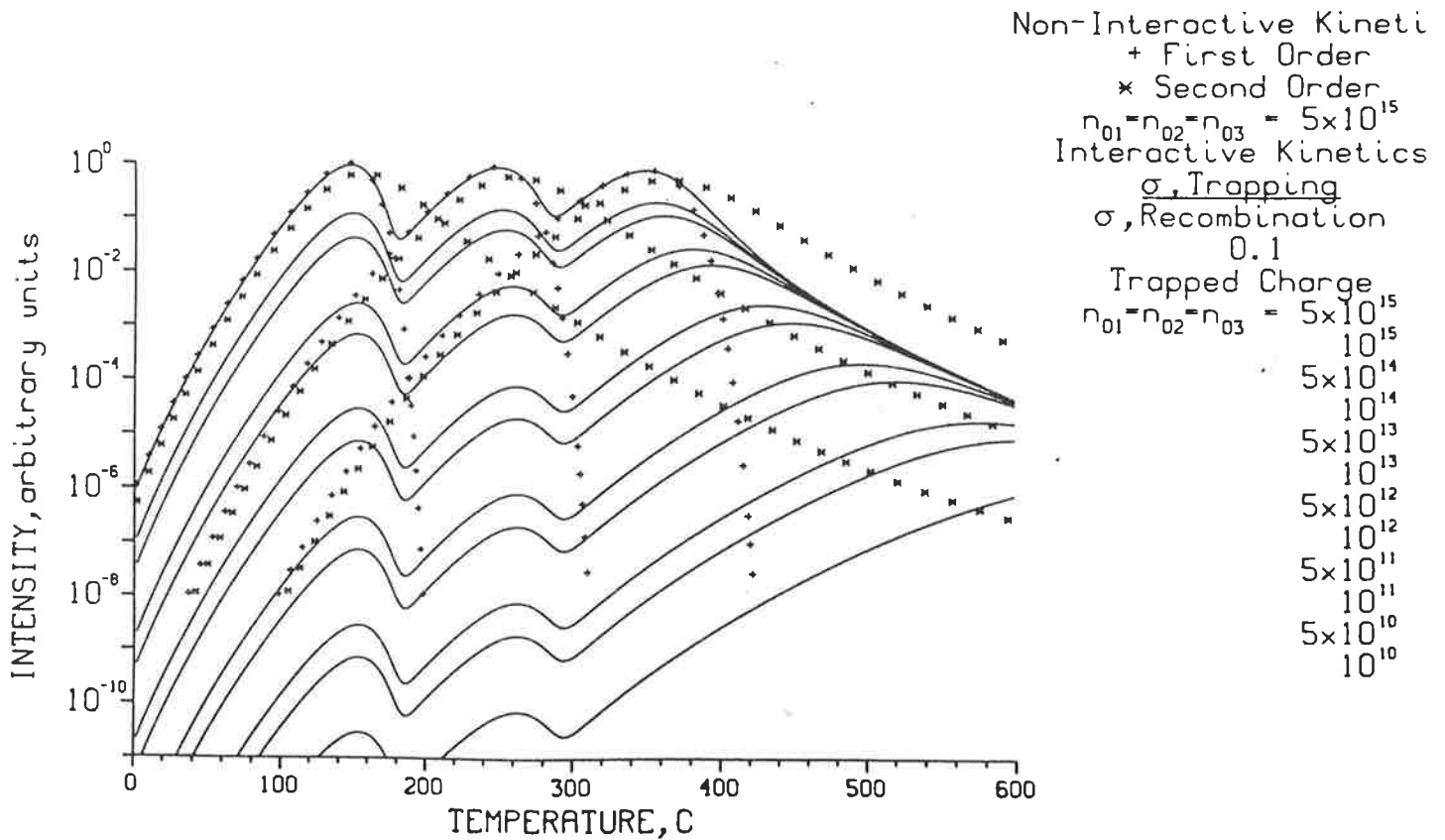


Figure 2.13 First order, second order and interactive kinetics glow curves computed where the trapped charge concentration is varied similarly in each of the three electron traps. An increase in the high temperature glow peak intensity and position of the high temperature peak are observed (Levy 1984).

Also shown are the usual first and second order glow curves ($n_{01} = n_{02} = n_{03} = 5 \times 10^{15}$). Although the shape of the first order glow curves do not depend on initial trapped charge level, the second order glow curves become broader and the peak temperature shift to higher temperatures as the initial trapped charge level decrease. Levy (op.cit) from computed interactive glow curves made the following observations.

- (1) The glow peak shapes depend on the initial trapped charge concentration.
- (2) As the n_{0i} values decrease the relative heights of the peaks change drastically. At low n_{0i} values the height of the highest temperature peak is so large that one would not expect to detect the two lower temperature peaks on the usual plot with the high temperature peak at normal intensity.
- (3) At low doses, ie. low values of n_{0i} , curves of either dose vs intensity or dose vs glow peak area will not be linear. This has particularly important implications for archaeometry where doses are frequently low.
- (4) At high n_{0i} values (ie. large pre-measurement dose and more traps filled) the computed glow curves most closely resemble non-interactive first order peaks.
- (5) The peak temperatures change with n_{0i} values. This is most noticeable in the temperature of the high temperature peak.
- (6) Glow peak shape also changes with n_{0i} values ie. the high temperature peak becomes much broader at low n_{0i} values. The shape of the two lower peak temperatures remains more constant.
- (7) The high temperature sides of the highest temperature peak superimpose as the temperature increases. As mentioned in a previous section this is a property of single glow peaks described by usual second order kinetics.

Levy (1984b, 1985a) also includes some quantitative analysis and features of the glow curves contained in figure 2.13. As no quantitative kinetic analysis of glow curves has been undertaken in this study, not all of Levy's (op.cit) conclusions are immediately applicable. Two conclusions, however, are worth mentioning.

(1) Low dose curves in which the lower temperature peaks have negligible intensity can be fitted as a single glow peak (although the resultant E and s values obtained will differ appreciably from those used to compute the theoretical curves). The significance of this conclusion is that a plot of peak area vs dose will be linear, and that peaks described by first order kinetics will also provide linear peak height vs dose curves. Peaks described by GOT or second order kinetics may appear to be linear in certain dose ranges.

(2) A most important conclusion is that interactive kinetics appears to explain the phenomena of supralinearity. This is illustrated in figure 2.14 after Levy (1985a,b) which is a plot of peak height vs dose for the computed glow curves.

The two lower temperature peaks both exhibit supralinear characteristics, whereas the high temperature peak does not (because its width increases rapidly with dose). The significance of this conclusion is that supralinearity is a natural feature of interactive kinetics.

A discussion of kinetics as applied qualitatively to this study occurs after presentation of data ie. chapter 4.

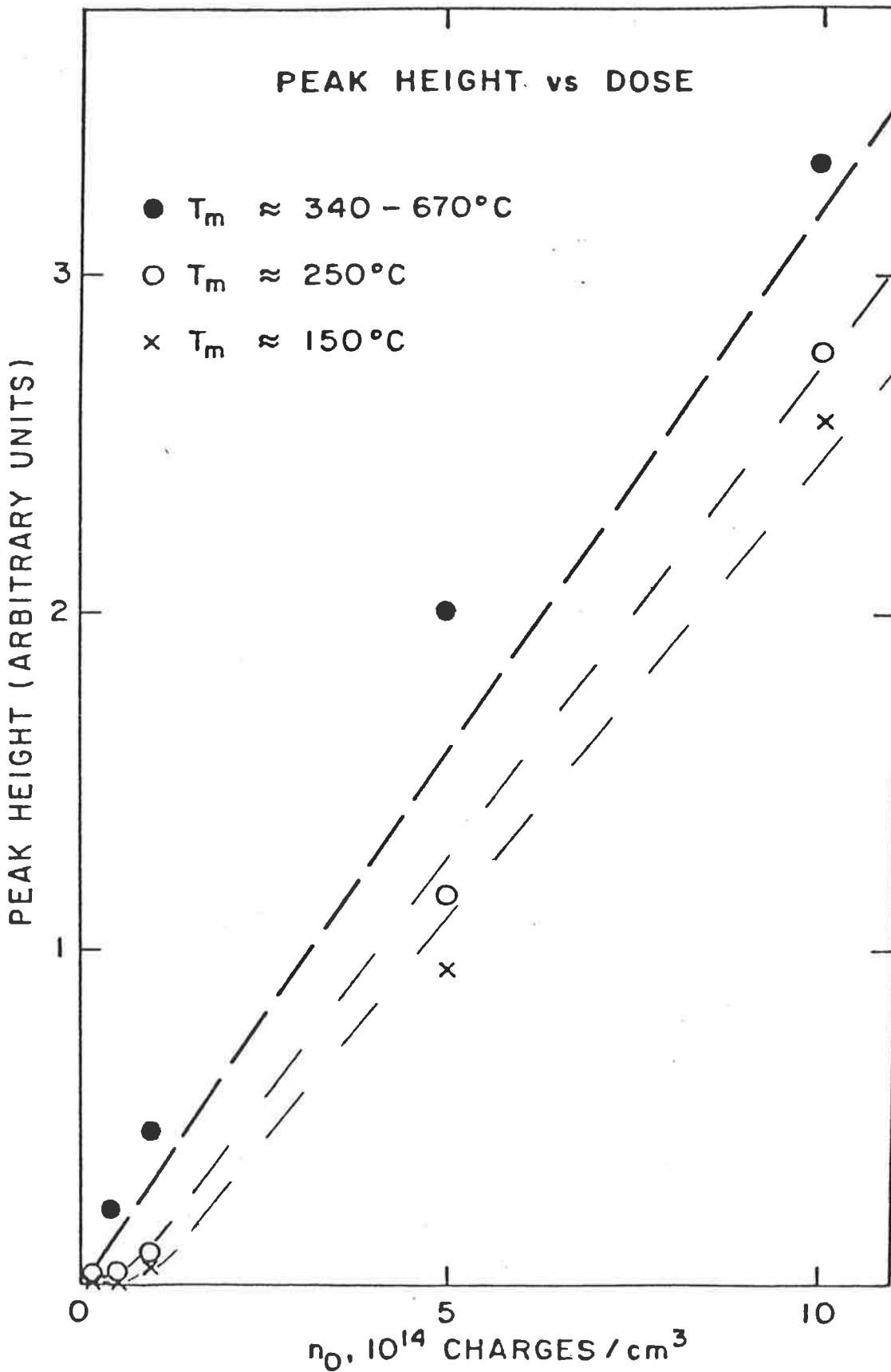


Figure 2.14 Peak height vs n_0 , or dose, curves for glow peaks shown in the preceding figure and showing supralinear behaviour, especially in the lower temperature peaks (after Levy 1985b).

2.5 Natural Processes Affecting The Thermoluminescence Of Quartz

2.5.1 Quartz Before Irradiation - Introduction

This thesis is concerned with the use of TL in uranium exploration and ore genesis studies. Therefore one could expect that ionizing radiation will be the dominant influence on the TL of quartz in such environments. It is still useful however, even necessary, to consider the influence of other parameters on the TL of quartz, particularly under the physio-chemical conditions encountered in sedimentary rocks which often host uranium mineralization. The nature and intensity of individual glow peaks in quartz depends on a number of factors of which many are poorly understood. This section (2.5.1) gives a brief summary of some factors, section 2.5.2 considers the effect of ionizing radiation in more detail. More extensive discussions of the factors influencing TL of quartz are found in Ichikawa (1968), McDougall (1968), Kaul et al (1972), Sankaran et al (1983), David et al I-IX (1977-82), McKeever (1984) and McKeever (1985).

Natural quartz is stable at temperatures up to 870°C at 0.1 MPa. It has two forms; the alpha form (α), which is stable to 573°C, and the beta (β) form which is stable between 573°C and 870°C. The α - β transition involves slight adjustments in atomic positions without bond rupture, and is a reversible change. The α form is trigonal and the β form has a hexagonal structure. In both forms, oxygen atoms are tetrahedrally shared between those of silicon. The nature of the Si - O bond in SiO_2 is between 40% ionic/60% covalent (Evans, 1966) and 50% ionic/50% covalent Dana (1968).

The role of defects is particularly important in controlling various physical properties of quartz. Many defects even those caused by radiation appear to be located at pre-existing imperfections - predominantly impurity ions.

Defects in SiO_2 associated with oxygen vacancies are called E' centres. The model for the E_1' centre is that of an oxygen vacancy with an unpaired electron located on one of two non-equivalent Si atoms. This is illustrated in figure 2.15 after McKeever 1985.

The E_2' centre also consists of an oxygen vacancy, but with an associated proton on the Si(II) site. A third E' centre, the E_4' centre, is identified as an oxygen vacancy with a hydride ion bonded to the Si(I) atom. As well as oxygen vacancies, oxygen interstitials are also important defects in SiO_2 . Oxygen vacancies are potential electron traps whereas oxygen interstitials are potential hole traps. Broken Si-O bonds are also viewed by McKeever (op.cit) as important defects where non-bridging oxygen gives rise to oxygen dangling bonds (potential hole traps) and empty Si orbitals (potential electron traps). Chatagnon (1986) records another oxygen vacancy defect which function as double electron traps (called E'p centres). Griscom (1985) and Weil (1984) also record OH groups acting as hole traps in quartz.

One of the major defects in quartz is the Al^{3+} ion substituting for an Si^{4+} ion, often with accompanying charge compensating alkali ions or H^+ ions. The Al^{3+} is thought to substitute for Si^{4+} and thus needs an accompanying positively charge ion to maintain charge conservation. This model proposed by O'Brien (1955) which has gained widespread acceptance, views the compensatory ion being located near to the Al^{3+} ion and within the open c-axis channelway of quartz. Several different Al centres exist depending upon the nature of the compensatory ion and its exact location. The Al^{3+} centre also has an

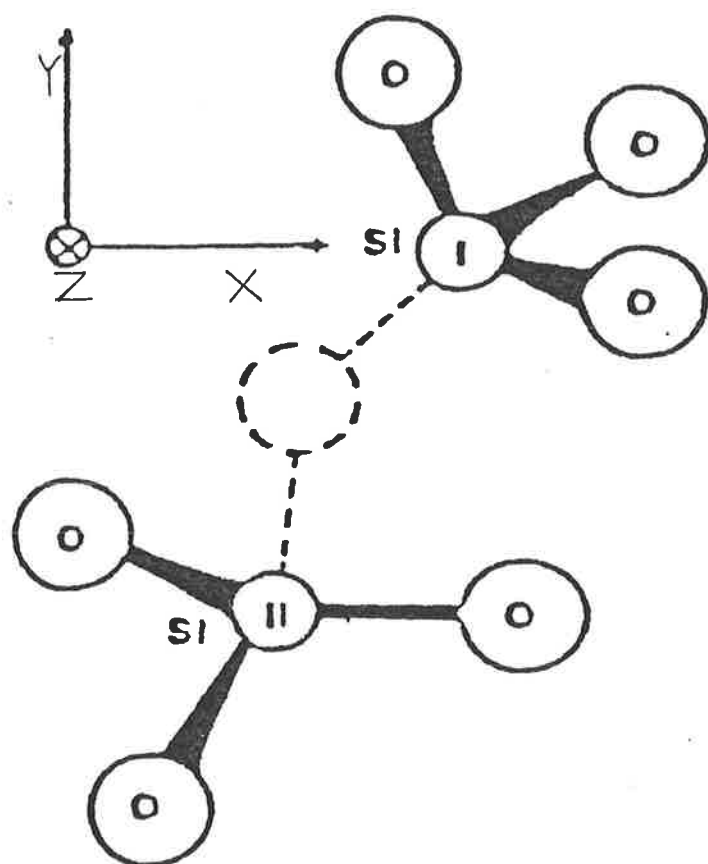


Figure 2.15 Model for the E_1' centre (after McKeevor, 1985).

important function in acting as a hole trap and recombination centre. McKeever (op.cit) considers optical absorption measurements to show that the A-bands give rise to irradiated quartz's smoky colour. ESR and dielectric relaxation measurements show these bands to be related to an Al^{3+} hole centre.

Evidence used to support the role of the Al-alkali centre as a recombination centre includes the enhancement of TL intensity with increasing temperature of irradiation (Malik et al (1981, Durrani et al 1977a). The interpretation of these results is that at high enough temperatures of irradiation, the alkali ion is able to diffuse away from the Al site during the irradiation, which results in the formation of an Al^{3+} hole centre. Electrons which are thermally freed can then recombine with trapped holes at the Al^{3+} site with resultant luminescent emission. Aspects of such a model have been used to explain some features of the TL of quartz, eg. sensitization, and will be discussed in section 2.5.2.

Further evidence used to support the above interpretations have come from the work of Kitt and Martin (1983) and Jani et al (1983). Kitt and Martin (op.cit) have measured the change in the Al-OH centre with temperature of irradiation which is an indirect measurement of the mobility of the alkali ion in quartz. (The relationship is such that if an M^+ ion moves away from an Al^{3+} it may be replaced by a proton on an adjacent non-bonding oxygen orbital thus giving rise to an Al-OH centre). Their results show an increase in the optical absorption band related to the Al-OH centre with increasing temperature of irradiation, thereby implying that M^+ ions are being moved from Al^{3+} sites in relation to temperature of irradiation. Kitt and Martin (op.cit) also found that the Li^+ ion was released from the Al^{3+} site temperatures 10-15K lower than Na^+ .

Jani et al (1983) present evidence to support the role of an $[Al O_4]^\circ$ centre as a recombination centre - at least for glow peaks above 200°C. They point to the identical spectral responses for two glow peaks at 245°C and 280°C and the $[AlO_4]^\circ$ centre decay in the same temperature region. This they suggest, indicates at least two different electron trapping centres having different decay temperatures which use the same recombination site, namely the $[AlO_4]^\circ$ centre. They further suggest that the two different electron trapping centres are related to alkali ions which have been previously liberated from $Al^{3+} M^+$ sites as a result of irradiation.

Evidences used against the role of the Al-alkali centre in recombination are:

- (a) That no clearcut correlation exists between the Al content and the A-band absorption and ESR signals. McKeever (1985) suggests that this may be because aluminium has to be in a silicon substitutional position in order to give rise to these signals, and that measurement of bulk aluminium content will also include non-substitutional aluminium, i.e. interstitial aluminium or in inclusions. This suggestion is supported by the work of Cohen (1960) who found that aluminium may be incorporated into alpha quartz either interstitially or substitutionally and that visible colour centre phenomena in quartz was related to substitutional aluminium but not interstitial aluminium.
- (b) If the smoky colour of quartz is related to A-band absorption which is related to Al^{3+} - hole centres which in turn function as TL recombination centres, then if the smoky colouration is bleached the TL signal should also be affected. Yet, in some cases (McMorris 1971), bleaching of the smoky colour of quartz does not affect the TL. McKeever (op.cit) explains this

feature as being related to non-radiative pathways in the TL process, ie. Fe^{3+} acting in similar fashion to Al^{3+} and contributing to the smoky colouration, yet also acting as a "killer" centre in the TL process.

In contrast, Cohen and Makar (1982) support the idea of A-band absorption being related to Al^{3+} - hole centres. They draw an analogy to soda-silica glass absorption bands and propose a model for colour centres in smoky quartz with the A_3 band related to a trapped hole on an oxygen attached to a substantial aluminium impurity. The A_1 and A_2 bands are related to centres consisting of three (A_1) and two (A_2) non-bonding oxygens attached to the aluminium ion with related trapped hole.

Other impurities important in the TL process are Ge^{4+} and Ti^{4+} , both of which are thought to function as electron traps though Marfunin (1979), also suggests that electrons trapped at Ge^{4+} or Ti^{4+} centres act as recombination sites though are activated in a different temperature range to the Al^{3+} - hole recombination centre.

Thermoluminescence is observed in quartz at temperatures both below and above room temperature. As this thesis is concerned with TL measurements at temperatures above room temperature, only a brief summary will be given of TL below room temperature. McKeever (1985), who summarizes studies of TL below room temperature, contains the following results:

- (a) Following X irradiation, Medlin (1963) found a prominent glow peak at 165K related to the presence of Ti^{4+} , with a maximum spectral emission at 380nm.
- (b) Mattern et al (1975) observed a single Gaussian emission peak at 380nm for a glow peak at 180K, following gamma irradiation.

They also showed that the low temperature glow peaks were perfectly described by first order kinetics.

- (c) Malik et al (1981) note 380nm emission for several glow peaks between 145 and 270K, and 450nm emission for a glow peak between 115 and 145K.
- (d) Schlesinger (1965) suggests that all peaks below room temperature are due electron traps and recombination at Al^{3+} centres except for a peak at 257K which he considers a hole trap.

Malik et al (op.cit) suggest that glow peaks between 185K and 270K are related to an Al-alkali centre. Therefore, combined with the results of Schlesinger (op.cit) this suggests that the TL glow peaks in this temperature range, emitting at 380nm, are due to the recombination of electrons with holes at Al-alkali centres. Malik et al (op.cit) also suggest that emission at 450nm is also due to recombination of an electron (released from a hydrogen interstitial) with a nearby Al^{3+} - hole centre.

All further sections will be concerned with TL above room temperature.

2.5.1.1 Quartz Emission Spectra

Numerous workers have examined the emission spectra of various crystalline quartzes which have been found to vary considerably between samples. David et al (1977) portray emission spectra for 11 quartz samples (figure 2.16) which show two major regions of emission at about 350 and 470nm. In some cases emission occurred at 425nm rather than 470nm. Generally the 470nm emission was stronger than that at 350nm.

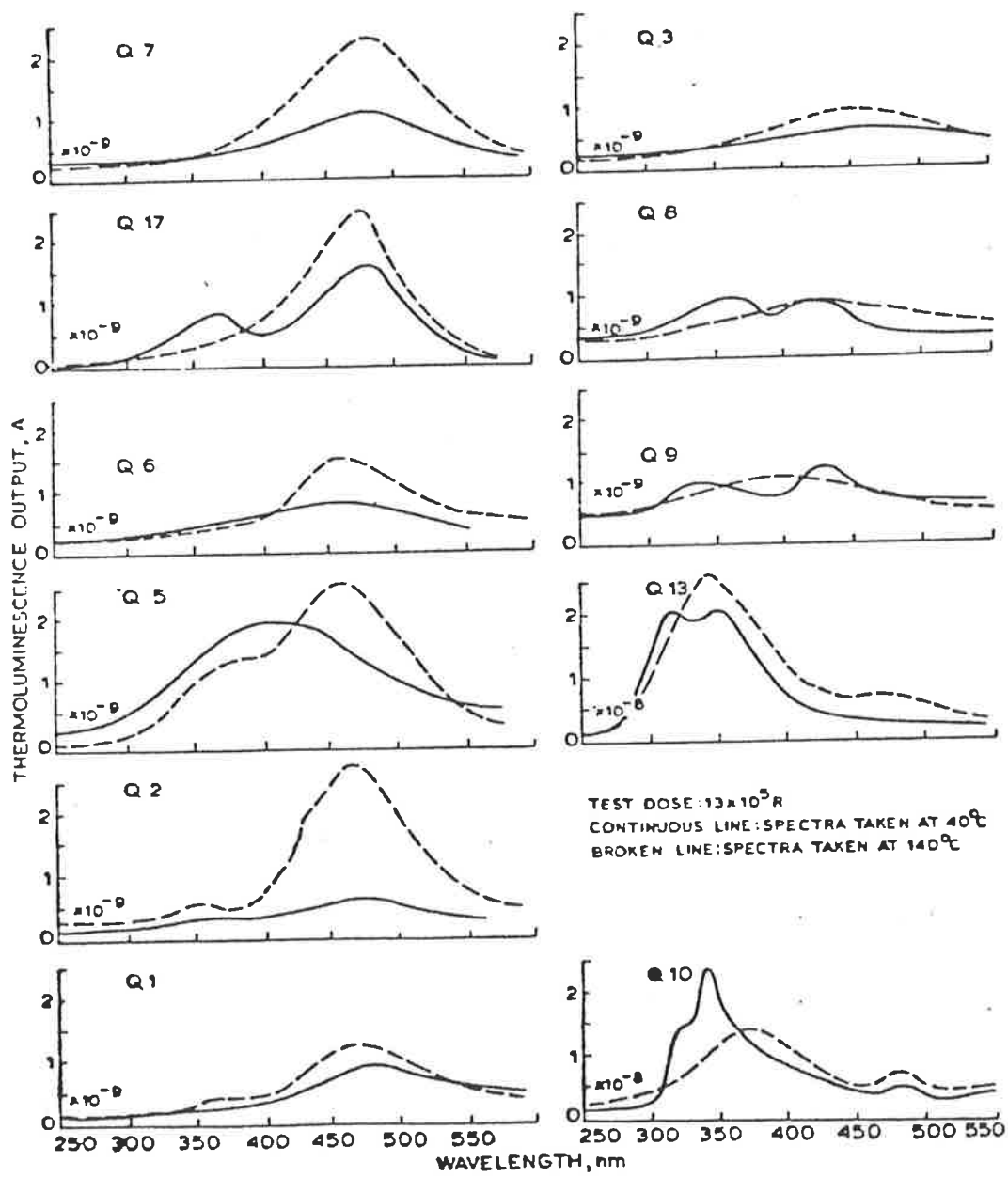


Figure 2.16 Quartz emission spectra (after David et al 1977).

Fuller and Levy (1977) report an emission at 490nm for the 316°C glow peak from Arizona natural quartz.

Medlin's paper of 1963 contains emission spectra for two glow peaks below room temperature and two above room temperature (280K and 330K). His data is shown in figure 2.17 and indicates a maximum emission spectra at 380nm for the 280K and 330K glow peaks.

Durrani et al's (1977a) emission spectra data is shown in figure 2.18 for glow peaks at 200°C, 255°C, 275°C and 355°C. All four glow peaks have an emission spectra maximum at 450-460nm. Durrani et al (op.cit) interpret these results as indicating that four different electron traps, responsible for the observed glow peaks, are using the same recombination centre. They consider the recombination centre to be the Al-alkali centre.

Zimmermann (1971) working on the 110°C TL peak found that both radioluminescence (RL) and TL emission maxima occurred at 380nm with a weaker emission at 470nm. In contrast, Jani et al (1984) found that higher temperature glow peaks (>250°C) in quartz emitted at a maximum of 470nm. Jani et al (1984) concluded that TL in higher temperature regions is due to the recombination of electrons with holes at Al^{3+} - hole centres. The recombination centre responsible for emission at 380nm has not yet been identified. Medlin (1963) attributes it to an unidentified lattice defect, McKeever et al (1984) call it an unidentified hole centre and later (McKeever 1987) tentatively describes it as a H_3O_4 centre.

McKeever (1985) contains other emission spectra studies in his review of the TL of quartz. He concludes that most of the TL glow peaks above room temperature emit in the range 450-470nm and that the source of this emission may be the recombination of electrons with Al^{3+} - hole centres, though at this stage it is unwise to be too categorical about the TL emission process.

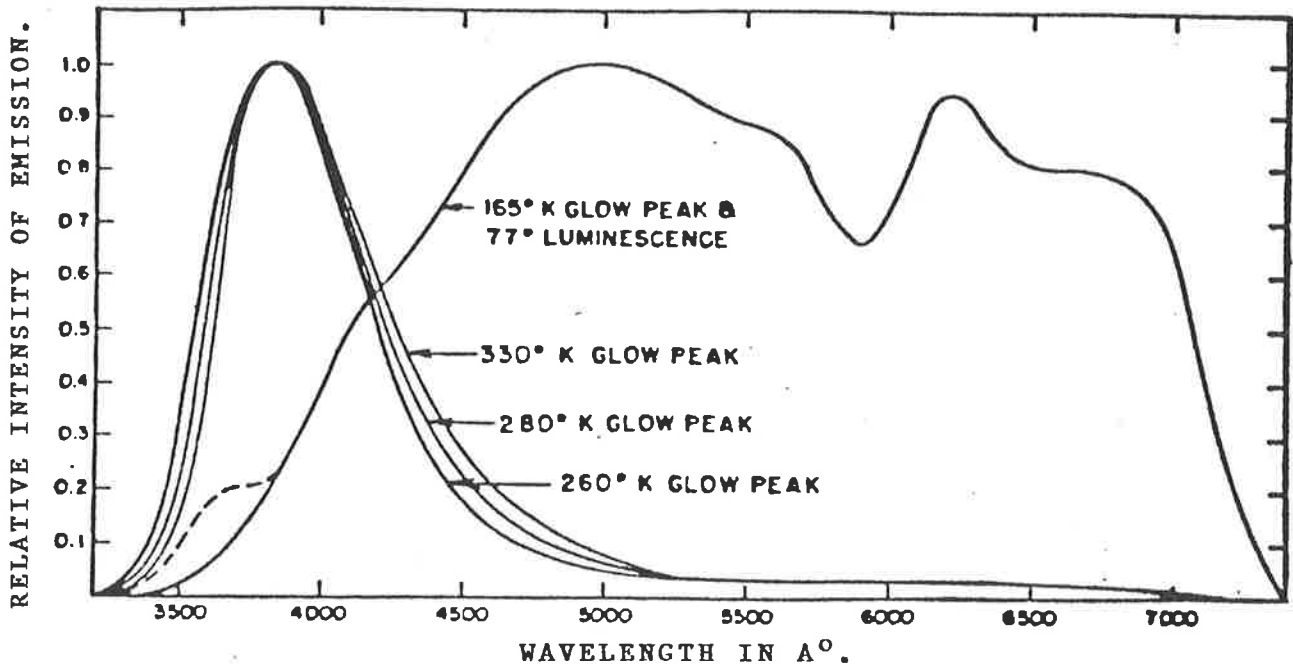


Figure 2.17 Quartz emission spectra (after Medlin 1963).

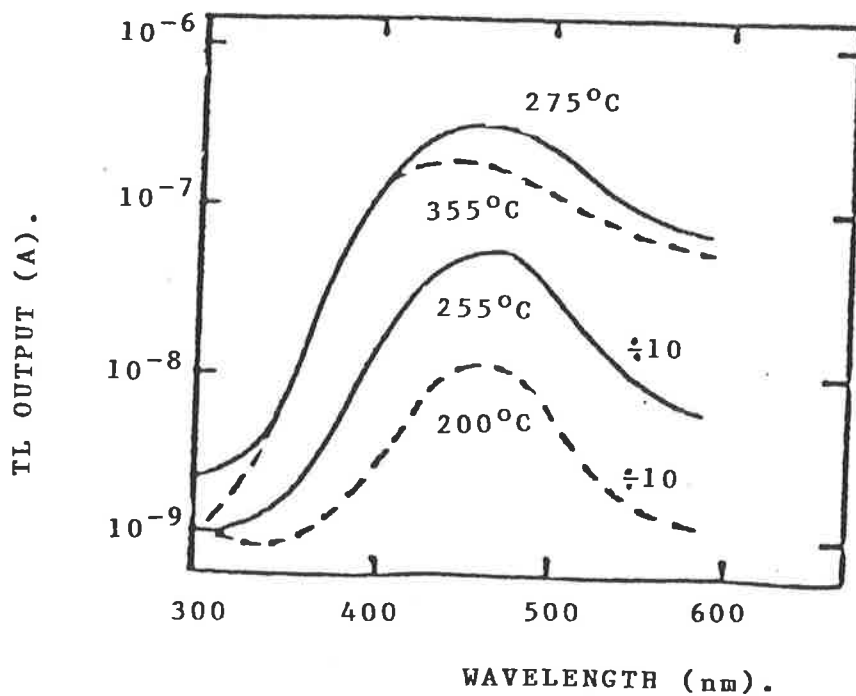


Figure 2.18 Quartz emission spectra (after Durrani et al 1977a).

2.5.1.2 Role of Trace Elements on Quartz Thermoluminescence

The effect of impurities on the TL of quartz is not yet fully understood. Medlin (1963) investigated the effects of impurity cations added in solution to an amorphous silica suspension from which quartz samples were crystallized. From Al^{3+} , Bi^{3+} , Sb^{3+} , As^{3+} , P^{5+} , Ag^+ , B^{3+} , Pb^{4+} , Mn^{4+} , Ti^{4+} , Li^+ , Fe^{2+} , Sn^{4+} , Zn^{2+} , Ge^{4+} , Ga^{3+} , In^{2+} , Co^{2+} , V^{5+} , Ni^{2+} , Cd^{2+} , Hg^{2+} , Cr^{3+} and Cr^{6+} he found that only the addition of Ti^{4+} affected the glow curves of these synthetic samples. The presence of Ti resulted in an intense glow peak at 165°K with an optimum concentration near 4000ppm. Medlin's (op.cit) results seem to contradict those of later workers, notably the lack of effect of Al^{3+} , Ge^{4+} and Li^+ on quartz TL. Possibly his method of trying to incorporate impurities into the quartz lattice was not as successful as the vacuum evaporation or electrolytic sweeping employed by other workers.

The effects of Al^{3+} , Li^+ and Na^+ on the TL of quartz were studied by Ichikawa (1968). He diffused these impurities into the sample grains followed by vacuum evaporation heat treatment at 1000°C . His results are contained in table 2.1. Ichikawa (op.cit) concluded that sodium concentration was an influencing factor on 280°C peak intensity and lithium on the 245°C peak intensity. It is also noteworthy that aluminium, either singly or in combination with the monovalent ions, has an effect (to varying degrees) on four of the five peaks considered. The similarity of Ichikawa's (op.cit) results to those quoted earlier of Jani et al (1983) is worthy of mention. Recall that Jani et al (op.cit) (using sweeping techniques on three different types of quartz) also correlated TL peaks in quartz at 245°C and 280°C with alkali ions which acted as electron traps and which had been previously liberated from Al^{3+} M^+

Element	Peak temperature				
	150°C	185°C	245°C	280°C	400°C
Al	small				large
Li		✓	✓		
Na				✓	
Al + Li		✓		small	
Al + Na				✓	
Al + Li + Na		✓		✓	

Table 2.1 The effect of Al, Na and Li on quartz TL, (summarized after Ichikawa, 1968).

sites by ionizing radiation. Martini et al (1986) using similar techniques to those of Jani et al (op.cit) also attribute peaks between 200°C and 300°C to alkali ions and suggest that a peak in quartz at 380°C is related to a Cu impurity.

Ichikawa (op.cit) considered that the 400°C glow peak was related to oxygen vacancies rather than any specific trace element.

McMorris (1969, 1971) suggests that Ge^{4+} is an important electron trap in the TL of the 300°C glow peak whereas McKeever et al (1984) consider that Ge^{4+} acts as an electron trap in the TL of the 110°C glow peak. McKeever (1987) also suggests that a hydrogen impurity may be important in production of the 110°C peak. Jani et al (1983) considers that hydrogen impurities may play a role in quartz TL in peaks from 60°C–180°C.

From these, and other works summarized in McKeever (1985), no firm conclusions regarding the effect of impurities on the TL of quartz can be drawn, though the presence of alkali ions does seem to be connected with glow peaks in the range of 200°C–300°C, specifically peaks at 245°C and 280°C.

2.5.1.3 Thermal Effects on the Thermoluminescence of Quartz

The effect on TL properties of preheating quartz before irradiation and TL measurement has been studied by several workers.

Ichikawa (1968) found that after heating, samples of single crystal Brazilian quartz showed a prominent glow peak at 110°C and a less prominent peak at 170°C. The intensity of the 110°C glow peak continued to increase (for a given test dose of 10^3 Rad) with

increasing temperature of annealing, as shown in figure 2.19, and increased at a faster rate after passing the α - β quartz transition at 573°C.

David et al (1977) studied the effect of temperature of annealing, time of annealing and time of cooling on TL intensity and emission spectra of a natural pink quartz. Their major conclusions were:

- (a) Sudden quenching of quartz from an elevated temperature caused a large enhancement in TL sensitivity. This is indicated in figure 2.20 where glow curves for natural and three different cooling rates are shown.
- (b) The shape of the glow curve remains the same despite the cooling rate.
- (c) The emission spectra maximum was independent of cooling rate.
- (d) Increasing temperature of annealing (time of annealing 90 minutes) resulted in increased TL intensity (following exposure to a test dose of 10^5 rads). This is shown in figure 2.21 where the area under the glow curve continues to increase with temperature of annealing with inversions at approximately 600°C and 800°C.

David et al (op.cit) interpret these results as indicating that at higher temperatures of annealing more vacancies are formed either by themselves or in association with impurities. Rapid quenching after heat treatment freezes these vacancies into the quartz lattice. The increased number of vacancies result in higher intensity TL as more charges may initially be trapped. Although the same test dose was applied the unaltered shape of the glow

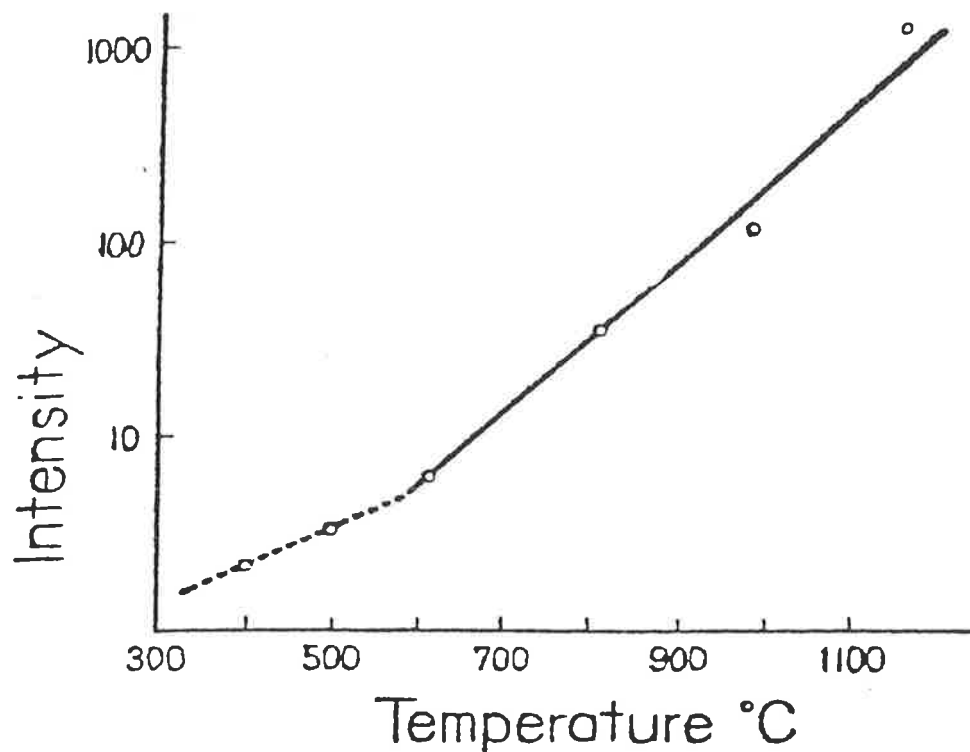


Figure 2.19 Increase in quartz 110°C glow peak intensity with temperature of annealing, after a given test dose, (after Ichikawa 1968).

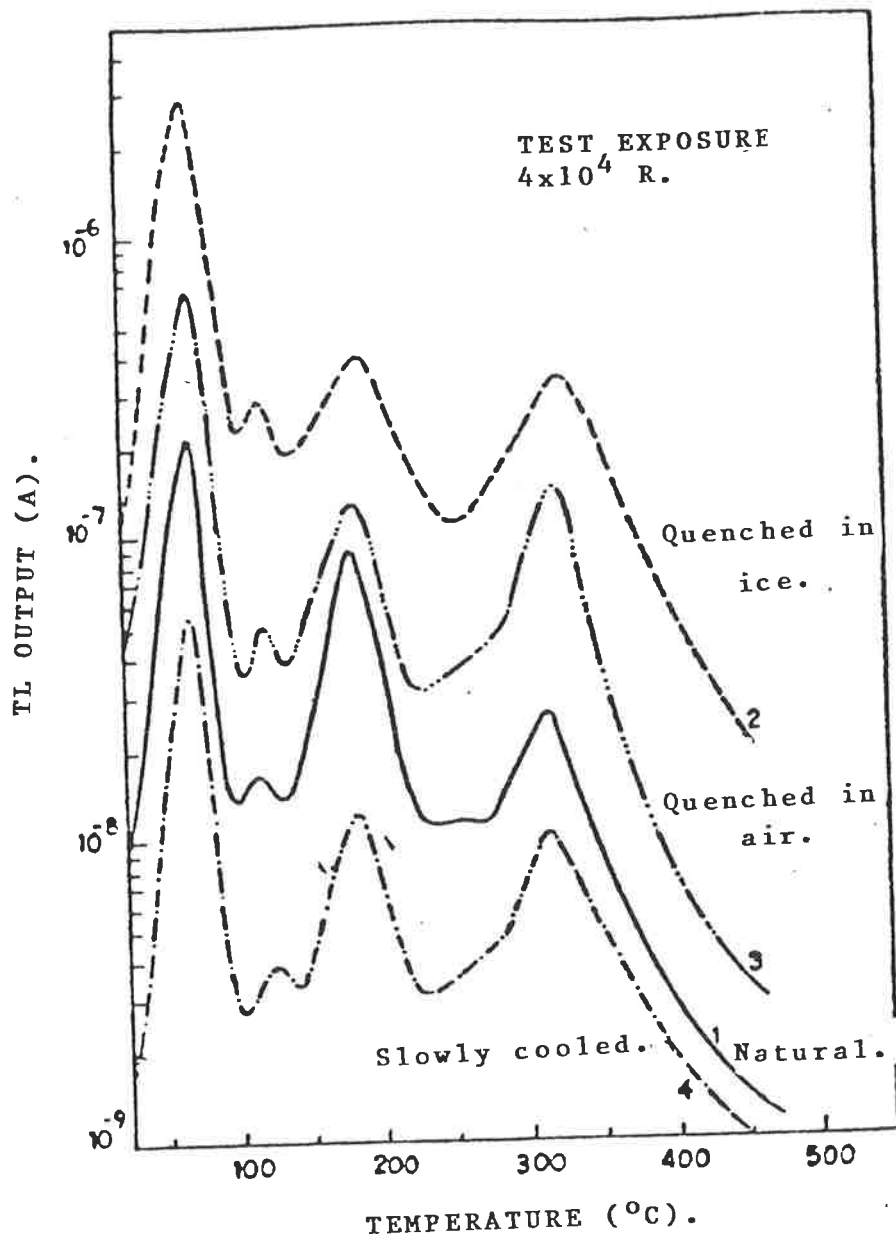


Figure 2.20 Effect on TL of quenching quartz from an elevated temperature (after David et al 1977).

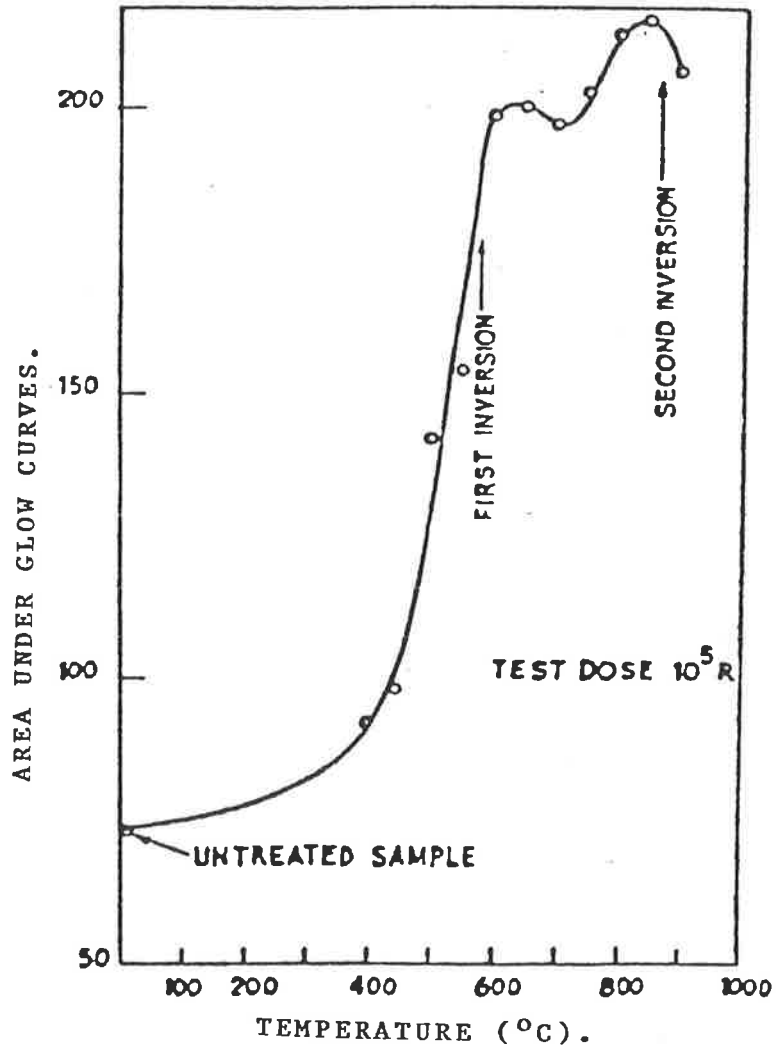


Figure 2.21 Increased TL intensity in quartz after a test dose of 10^5 rad as a function of temperature of annealing (after David et al 1977).

curves is interpreted as showing that the newly created defects are the same as pre-existing ones. The decrease in TL intensity in slowly cooled samples is explained by the annealing out of some of the pre-existing defects along with all of the temperature generated defects.

A particularly important observation for the use of TL in uranium exploration is that high-irradiation caused sensitization superimposes over the thermal sensitization effect. This is illustrated in figure 2.22 for the dose range 10^3 rads to 10^7 rads where a sharp rise in intensity for all samples is observed at approximately 4×10^4 rads. Ultimately saturation occurs for all samples at approximately 10^6 rads. The predominance of radiation sensitization is greatest in the slowly cooled samples.

Kaul et al (1972) studied the effect of annealing at different temperatures on the TL of Jadugudah quartz. The time of annealing was five hours and the test dose 1.75×10^5 rads. Their data is contained in figure 2.23 and shows a complicated variation in the TL intensity of each glow peak with temperature TL. Intensity usually decreases initially, then increases then decreases again. Kaul et al (op.cit) interpret their data as indicating that increasing temperature of annealing results in an initial production of new traps followed by a destruction of traps.

Although not considering TL specifically, Griscom (1985) summarizes the behaviour of defects in fused silica as a function of annealing temperature. His data are reproduced in table 2.2. These indicate that in the temperature range with which this thesis is concerned (quartz from sedimentary rocks having been exposed to temperatures no higher than 150°C) that annealing processes would be limited to H_2 and O_2 diffusion. Hobbs (pers. comm. 1989) suggests that at temperatures less than 150°C oxygen diffusion in

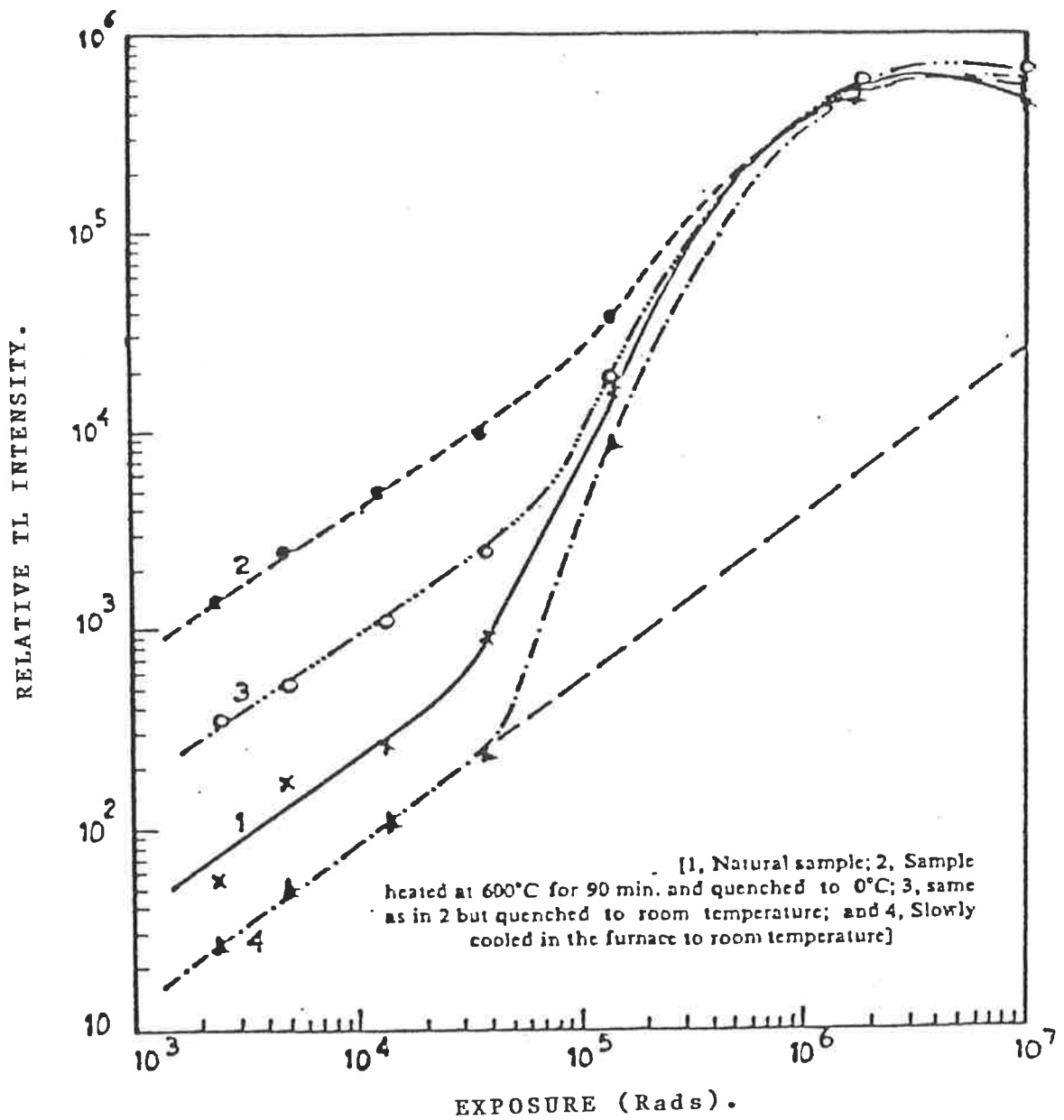


Figure 2.22 TL intensity vs radiation dose for samples with different thermal histories (after David et al 1977). Note that all samples reach saturation at the same radiation dose despite the differing thermal histories.

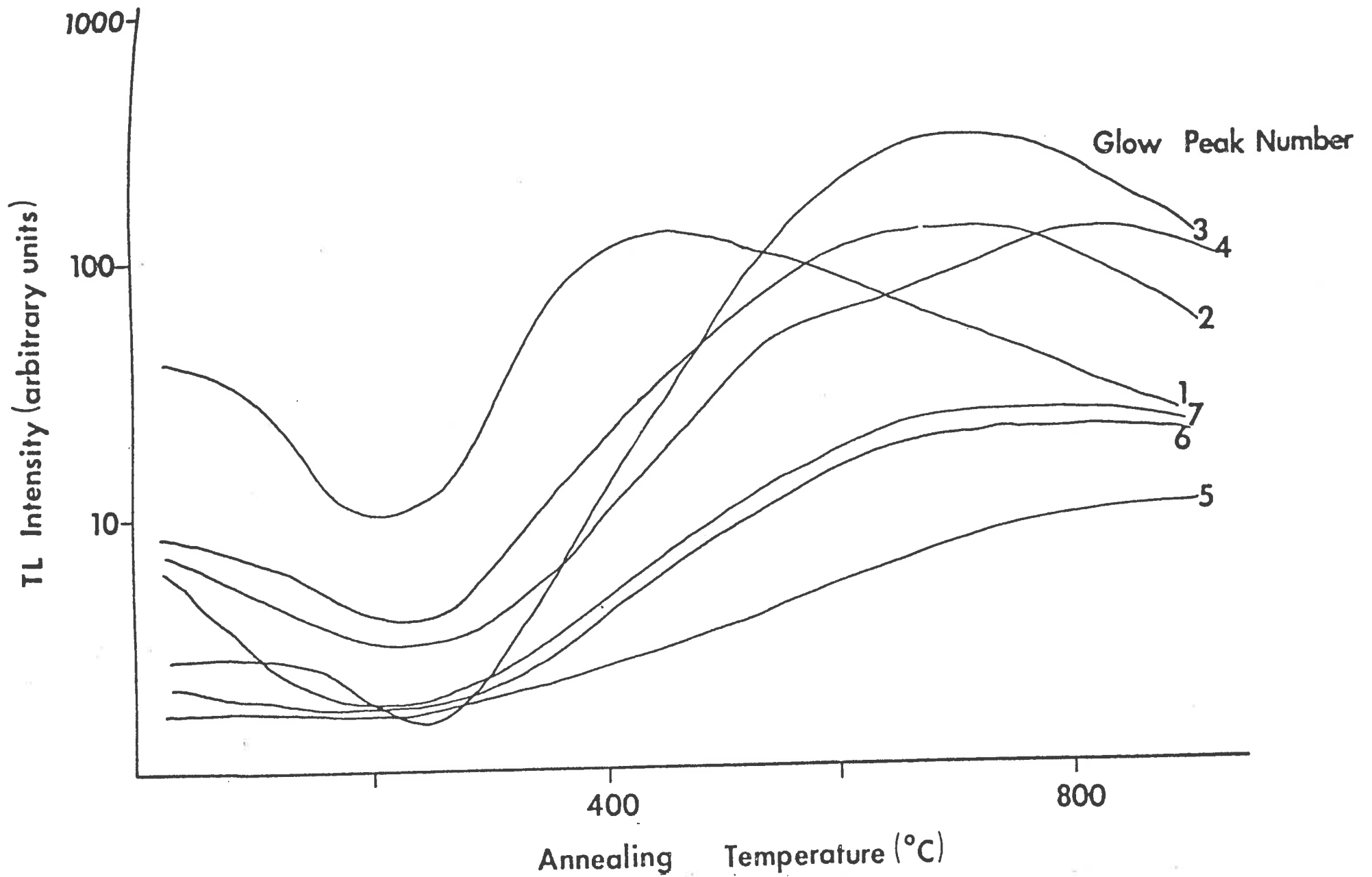


Figure 2.23 The effect of annealing temperature on the intensities of seven identifiable glow peaks in quartz, (after Kaul et al 1972). Peaks 1-7 correspond to temperatures of approximately 110, 180, 230, 280, 320, 370 and 430°C for a heating rate of 20°C per second.

		Anneal Temperature (K)									
		200	300	400	500	600	700	800	900	1000	
100											Vacancy Diffusion (?)
											H ₂ O Diffusion
											O ₂ Diffusion
											H ₂ Diffusion
											H ⁰ Diffusion

Table 2.2 Effective temperature ranges for various diffusion-limited anneal mechanisms (after Griscom 1985).

dry quartz is too slow to be considered important. It is not certain however, whether these results on fused silica can be correlated with effects in α -quartz and furthermore H_2 and O_2 contents of quartz are likely to be extremely low. If H_2 diffusion does occur in α -quartz then by analogy to fused silica some E' centres would be converted to OH^- centres. Similarly O_2 diffusion would be expected to lead to annealing of E' centres and a growth in the concentration of superoxide radicals. How any of these processes would affect the TL of quartz is unknown as the role of E' centres, OH^- centres and superoxide radicals themselves in the TL of quartz is only poorly known.

A more complete knowledge of the effect of thermal annealing on the TL of quartz must wait until the nature of defects responsible for production of TL itself is more precisely known. Without such knowledge any hypothesis on the effect of annealing on quartz TL remain speculative. At this stage McKeever (1985) perhaps presents the most accurate summary of the effect of thermal treatment on the TL sensitivity of quartz. He states "...measurements on the effect of thermal treatments of TL sensitivity of quartz cannot as yet be properly interpreted and the measurements themselves add little to an understanding of the quartz defect structure".

One point that was worthy of more attention concerned the observation by David et al (1977 - reported above) concerning the increased TL sensitivity of quartz as a result of pre-irradiation annealing. McKeever et al (1984) found similar increases with pre-irradiation annealing. They concluded that TL sensitivity changes up to approximately $450^\circ C$ are the result of an increase in the recombination centre concentration. Beyond the α - β quartz transition at $573^\circ C$ however, increase in TL sensitivity is related

to the formation of a metastable defect cluster. Although at variance with David et al's (op.cit) interpretation of thermally generated vacancy - impurity ion defects, both models could explain increased TL sensitivity following high temperature annealing.

The effect of both irradiation and heat treatment was studied by Zimmermann (1971) to explain the "pre-dose effect" property of the 110°C glow peak in quartz. This refers to the increase in sensitivity of the 110°C glow peak following both pre-irradiation and heating.

The model proposed by Zimmermann (op.cit) is shown in figure 2.24. She explained the increased TL sensitivity in terms of an increased number of luminescent centres. The model contains two electron traps - T and Z. Electron trap T corresponds to the 110°C glow peak whereas electron trap Z is a much deeper trap. There are also two hole traps R and L. L acts as the luminescent centre for the 110°C glow peak whereas R is a non-radiative site with a larger capture cross section than L. During pre-dose irradiation, electrons are trapped in Z and holes in R. Electron trap T is too shallow to retain appreciable trapped charges.

If a small test dose is given to this sample in the laboratory then some electrons are trapped in T and some holes in L. Heating to beyond 110°C releases electrons from T, some of which recombine with holes at L, with resultant TL (intensity S_0). Increasing the temperature to 500°C or beyond has the effect of transferring some trapped holes from R to L though electrons in Z remain trapped. After the sample has been cooled to room temperature there are now more holes in L than prior to heating. Therefore after a test irradiation and TL measurement a TL intensity S_N is produced such that $S_N > S_0$. S_N is thus

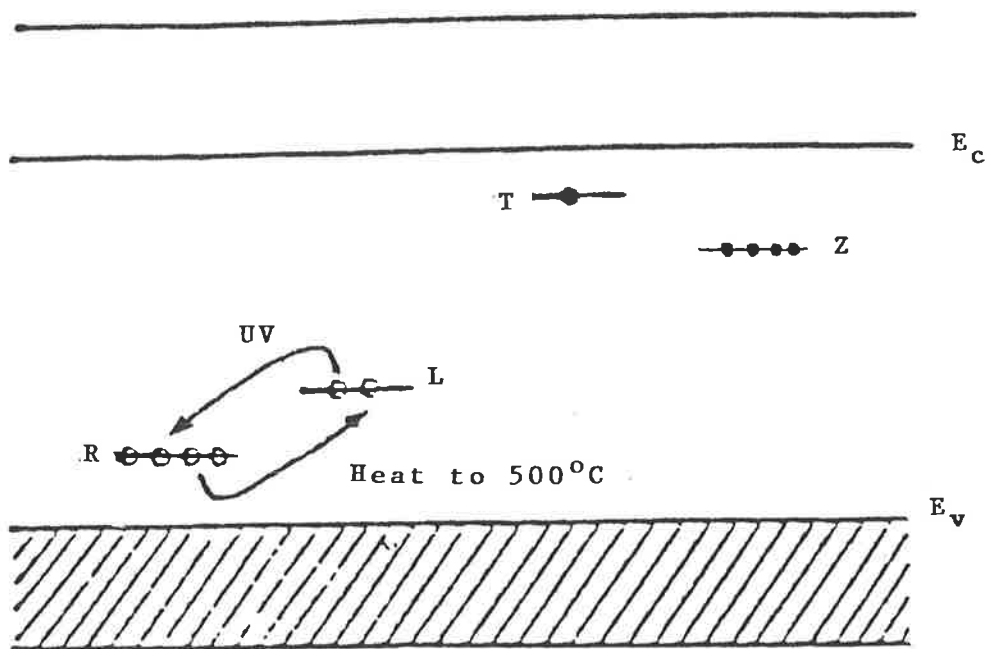


Figure 2.24 Zimmerman's (1971) model for the pre-dose effect in quartz. Heating to 500°C transfers trapped holes from R to L (L acts as a luminescence centre, R does not). A subsequent TL cycle thus results in an enhanced TL intensity proportional to the number of holes transferred from R (which itself depends on the number of holes trapped in R during antiquity). UV illumination reverses the process by transferring holes from L to R.

proportional to the number of holes initially in R, which in turn is dependent on the pre-dose or dose in antiquity.

Although this model has been proposed to explain only the increased sensitivity of the 110°C glow peak, it is possible that aspects of the model could also be useful in explaining increased TL sensitivity of other glow peaks as a result of irradiation and annealing.

2.5.2 Radiation Induced Changes in Quartz

By far the largest factor influencing the TL of quartz, particularly for uranium exploration, is ionizing radiation. The effect of gamma radiation of the TL of quartz has been studied by several authors.

Ichikawa (1968) exposed samples of clear crystal Brazilian quartz to varying amounts gamma radiation up to 9.2×10^6 rads. His data are shown in figure 2.25 - the change in intensity and shape of glow curves as a function of radiation and figure 2.26 - the change in total area under the glow curve. The significant points about these data are that TL intensity and integrated area under the glow curve continue to increase with increasing radiation, but, at higher doses (figure 2.25C) the low temperature glow peak (the B1 peak) begins to decrease. Ichikawa's (op.cit) B1 glow peak (180°C) reaches maximum intensity after exposure to 5.7×10^6 rads. Similarly the C peak (260°C) reaches maximum intensity at 8×10^6 rads and then decreases after exposure to higher doses. The higher temperature D peak (350°C) continues to increase throughout the experiment. Although the area under the glow curve continues to increase with increasing radiation (up to 8×10^6 rads when intensity levels off (saturation occurs)), the significant

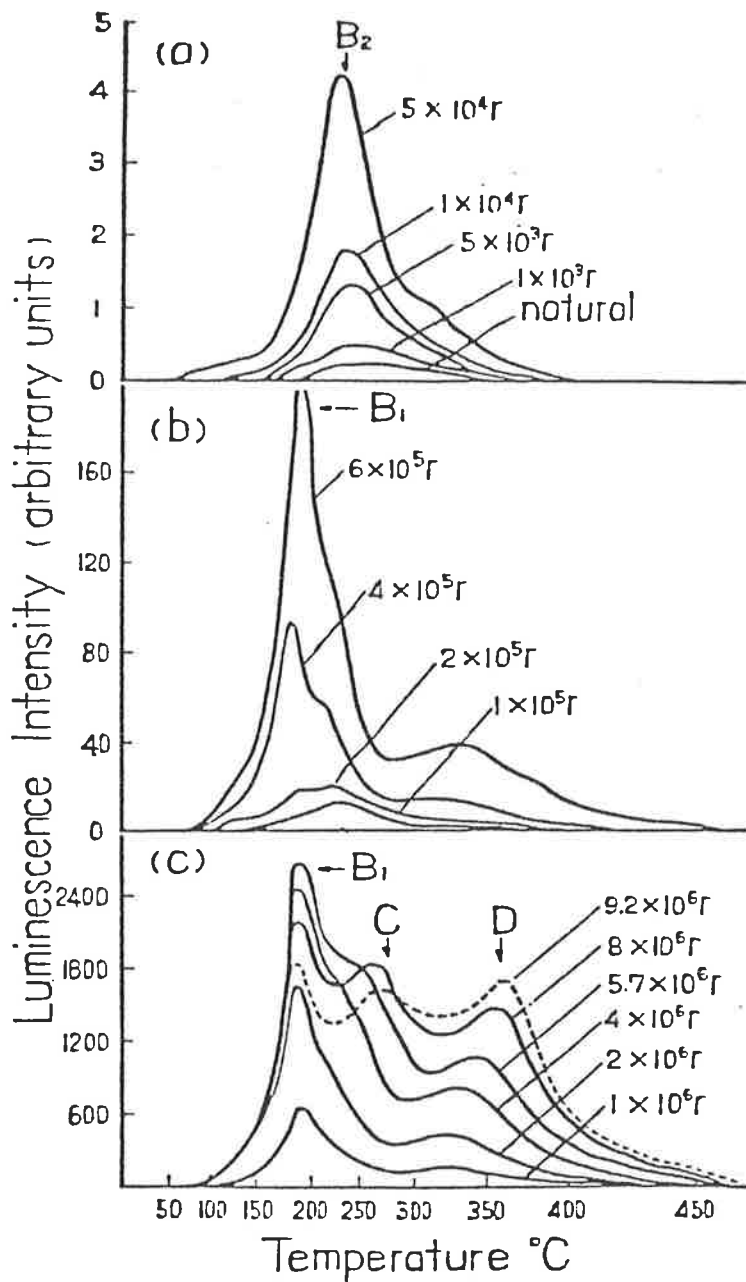


Figure 2.25 The change in glow peak intensity and glow curve shape in quartz as a function of radiation (after Ichikawa, 1968). Peaks B₁, B₂, C and D correspond to temperatures of approximately 180, 230, 260 and 350°C at a heating rate of 75°C per minute.

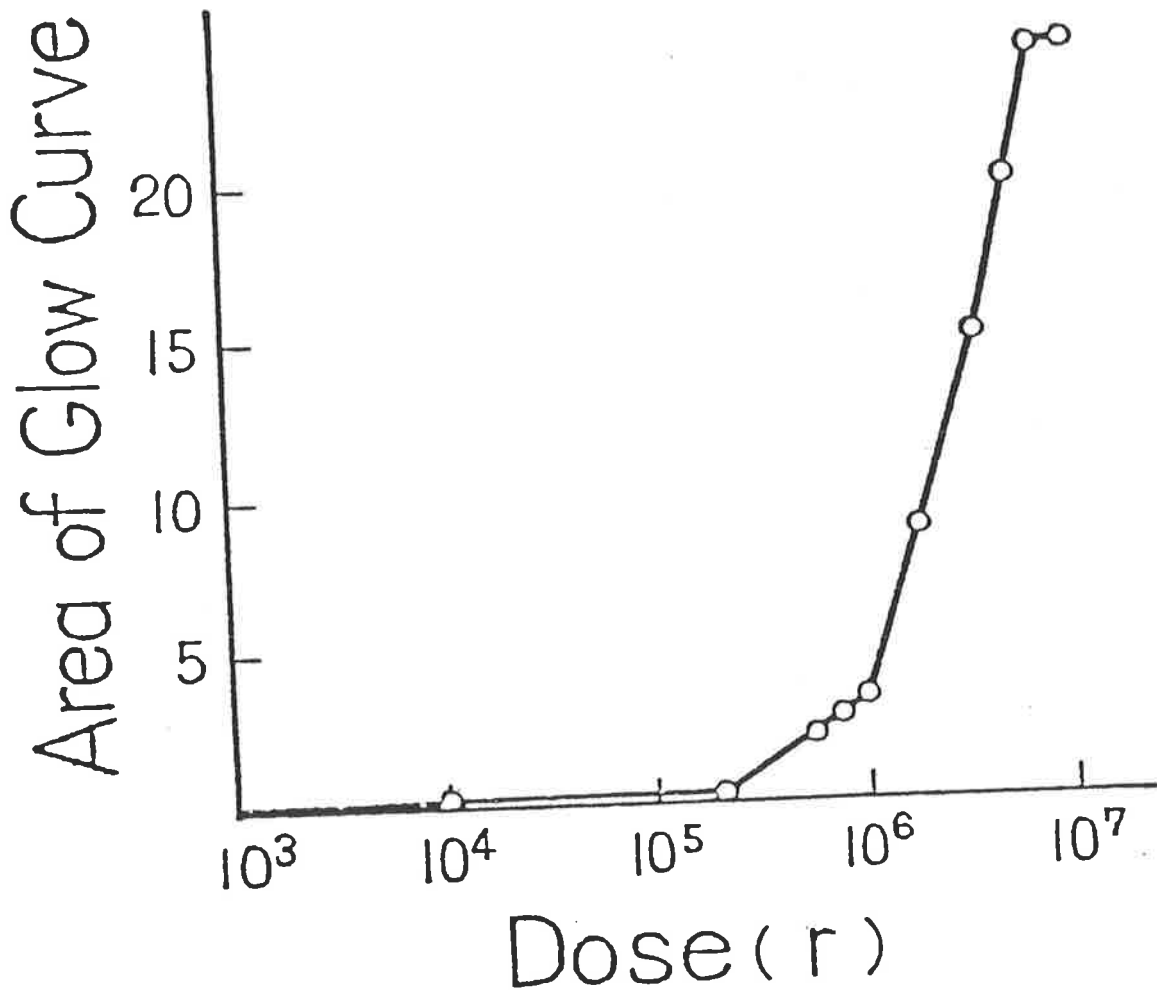


Figure 2.26 The change in area under the glow curve of quartz as a function of radiation (after Ichikawa, 1968). Quartz is of the same type used to generate the glow curves in figure 2.25.

point is illustrated in figure 2.25(C), ie. that the shape of the glow curve changes with increasing radiation. For geological purposes the shape of the glow curve may therefore be just as important or useful, as peak intensities or the area under the glow curve.

Similar results have been found by Durrani et al (1977) who found that both TL intensity and sensitivity increased over three orders of magnitude in natural clear Brazilian quartz exposed to gamma radiation doses between 10^5 and 10^7 rad. These data are shown in figure 2.27.

In order to examine the effect of even larger radiation doses on the TL of quartz, Durrani et al (op.cit) used proton irradiation to obtain doses up to 5×10^{11} rads. These data are shown in figure 2.28 where normalized TL response (the area under the glow curve from 240°C to 480°C) and TL sensitivity are plotted against proton dose. This figure shows that there is an initial growth of TL up to doses of approximately 10^7 rad, at which it levels off followed by a sharp decrease in both TL response and TL sensitivity at doses greater than 10^9 rad. A further decrease in TL occurs at doses greater than 10^{11} rad. This response to radiation indicates that one has to be cautious with the interpretation of integrated or total TL intensities. For example, the TL response is the same at 10^6 rad as at approximately 10^{10} rad, yet the shape of the glow curves changes drastically in this range. This is illustrated in figure 2.29 where (a) is the glow curve for a quartz slice irradiated with a dose of 10^7 rad 10 MeV protons. This sample has four glow peaks with the two lowest temperature peaks having largest intensity. Figure 2.29(b) shows a quartz slice irradiated at 2×10^{10} rad 10 MeV protons. Only one peak is obvious at

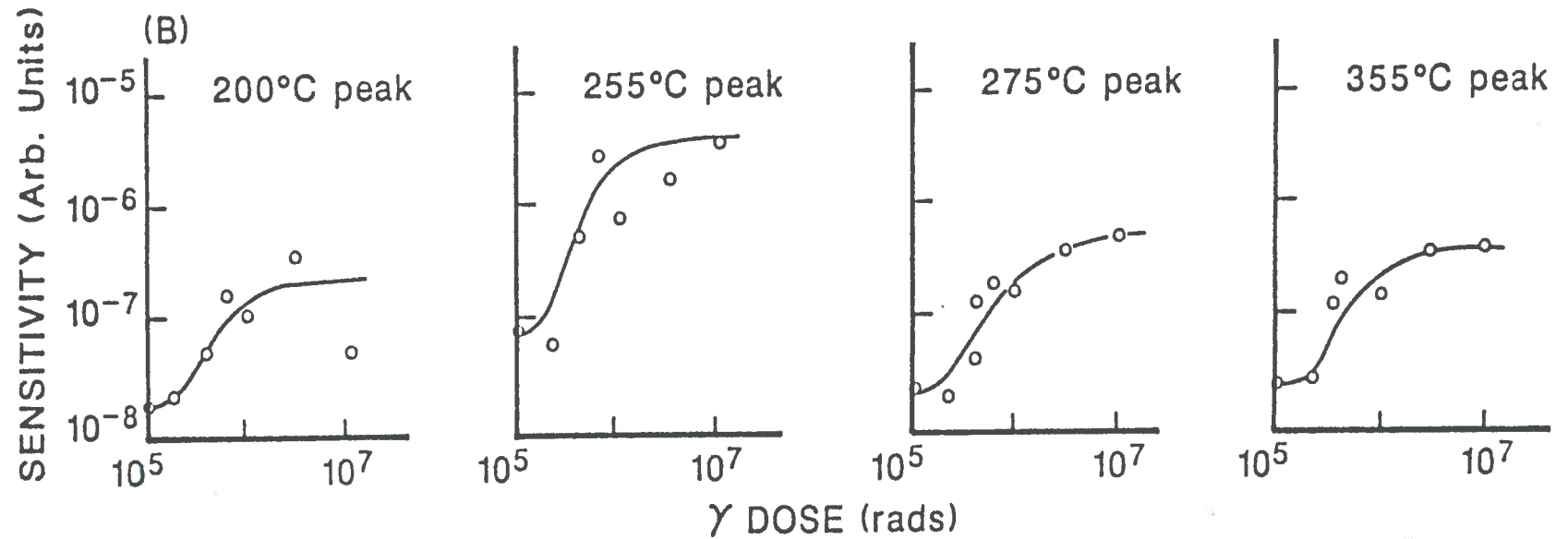
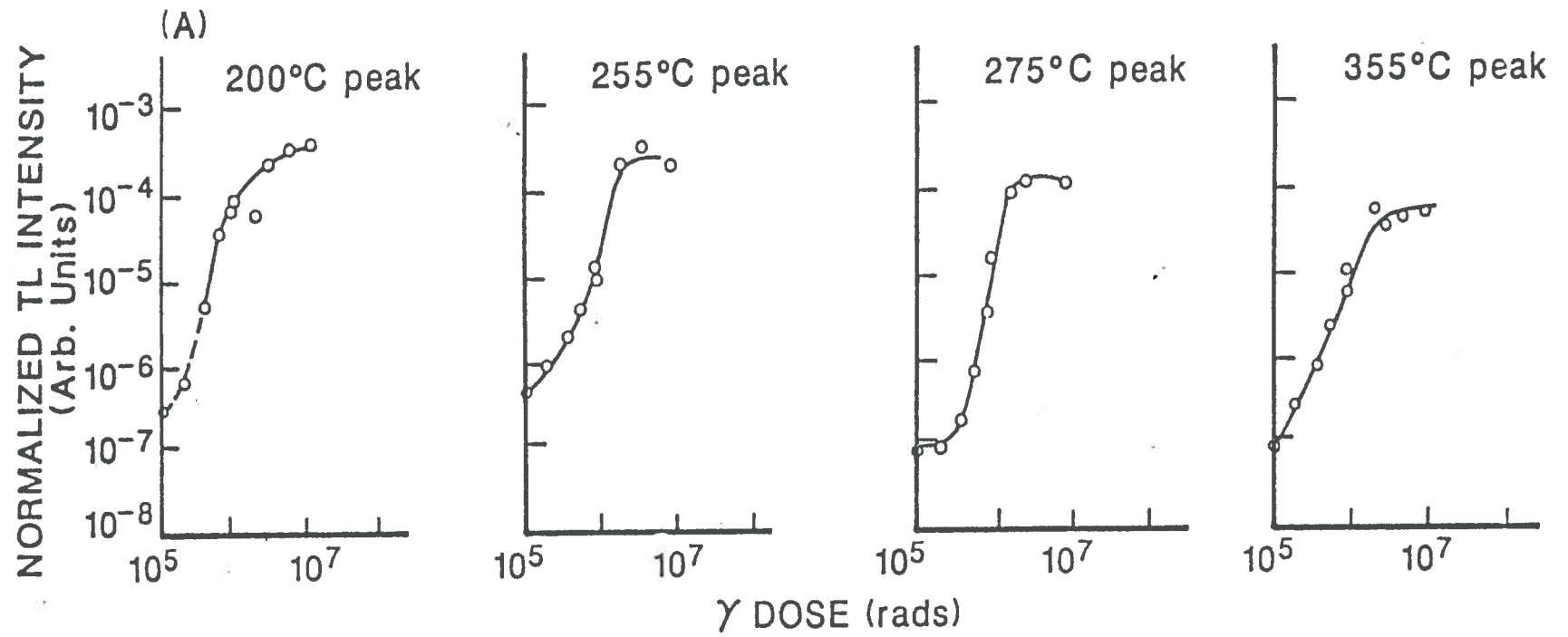


Figure 2.27 Change in TL intensity and sensitivity of four glow peaks in Brazilian quartz as a function of radiation dose (after Durrani et al 1977a).

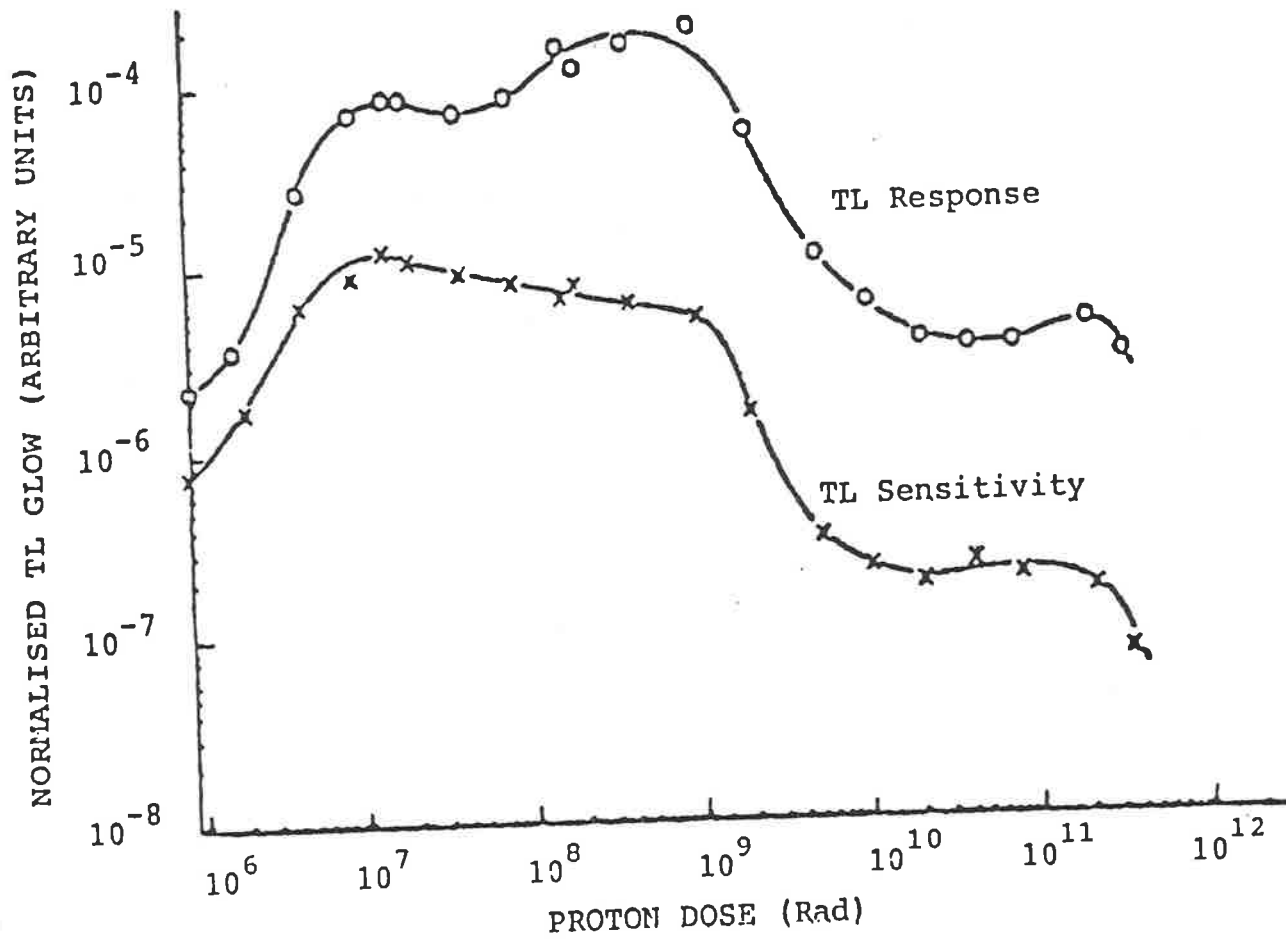


Figure 2.28 Change in TL response (area under glow curve from 240°C to 480°C) and TL sensitivity in quartz as a function of proton irradiation dose (after Durrani et al 1977a).

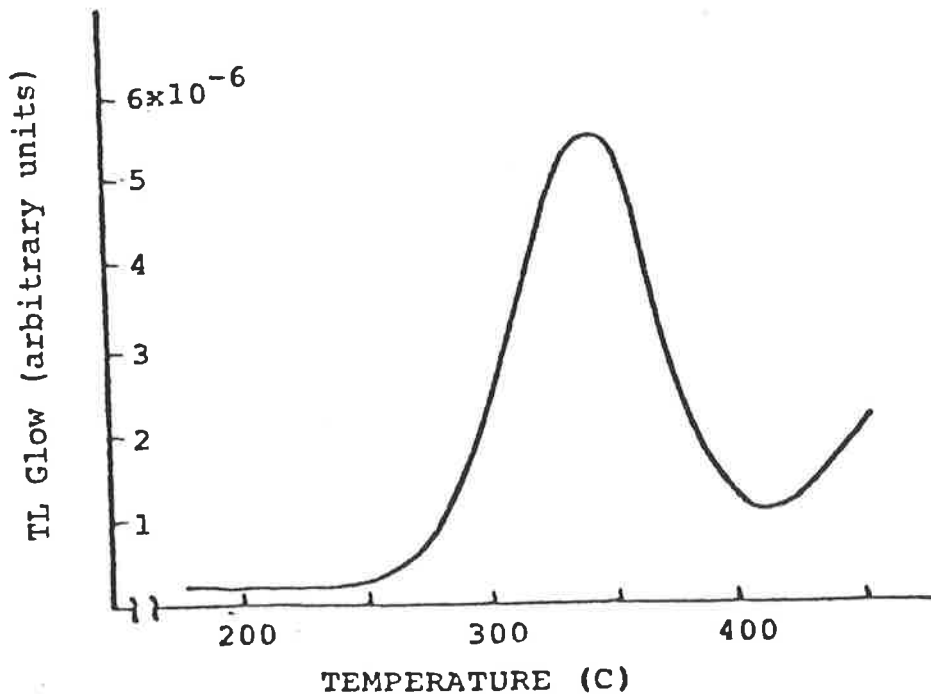
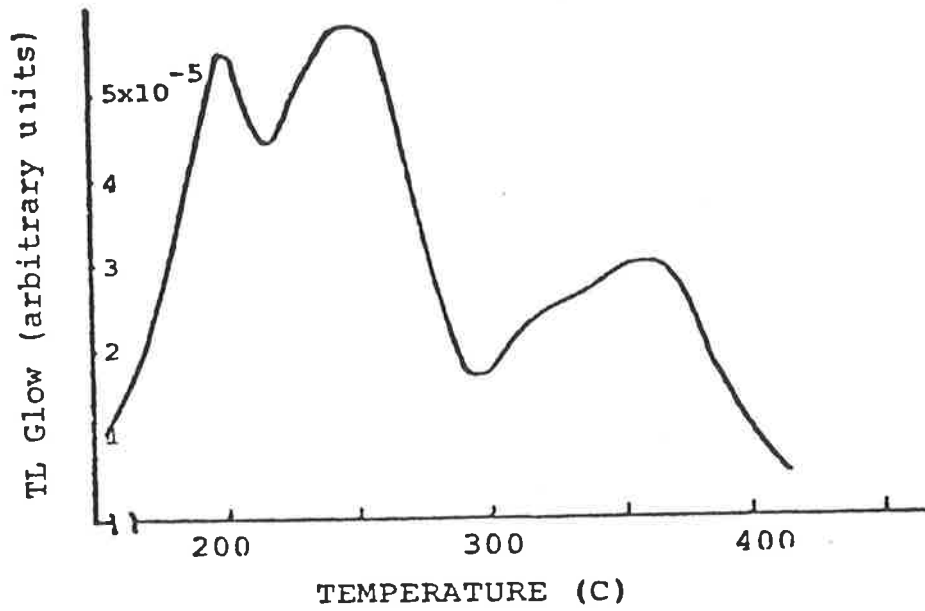


Figure 2.29 (a) TL glow curve for quartz slice irradiated with a dose of 10^7 rad 10 MeV protons, and
 (b) 2×10^{10} rad 10 MeV protons (after Durrani et al 1977a).

approximately 350°C. The low temperature and middle temperature glow peaks are not apparent.

Superficially, such results would appear to be contradictory to the interactive kinetic modelling of Levy (1985a,b) who found that the high temperature glow peak should predominate and overwhelm lower temperature glow peaks at low initial charge doses rather than high initial charge doses. However, the two studies are compatible, as will be discussed in chapter 4.

Durrani et al (op.cit) also showed that proton irradiation is much less efficient in producing TL than gamma radiation. This is illustrated in figure 2.30 where for a given radiation dose the TL sensitivity caused by proton irradiation may be up to two orders of magnitude less than that caused by gamma irradiation. This information is used by Durrani et al (op.cit) to explain their model for sensitization of quartz and will be discussed in the following section (2.5.2.1).

Perhaps the single most important observation regarding the use of TL in uranium exploration is that of Levy (1979), that quartz "remembers" exposure to previous large irradiations. The earlier quoted works of Durrani et al and Ichikawa showed that increasing radiation doses resulted in sensitization phenomena and also in a change in TL glow curve shape. However, the main weakness of their results were that such changes were observed as a result of sensitization rather than test doses. (It is true that Durrani et al also showed an increase in TL sensitivity but they did not show that the increase in TL sensitivity was intimately related to the increase TL response with sensitization dose). In the geological environment, where under ordinary burial and diagenetic conditions, ambient temperatures may be 100°C or more much of a large accumulated natural dose (as an equivalent of a

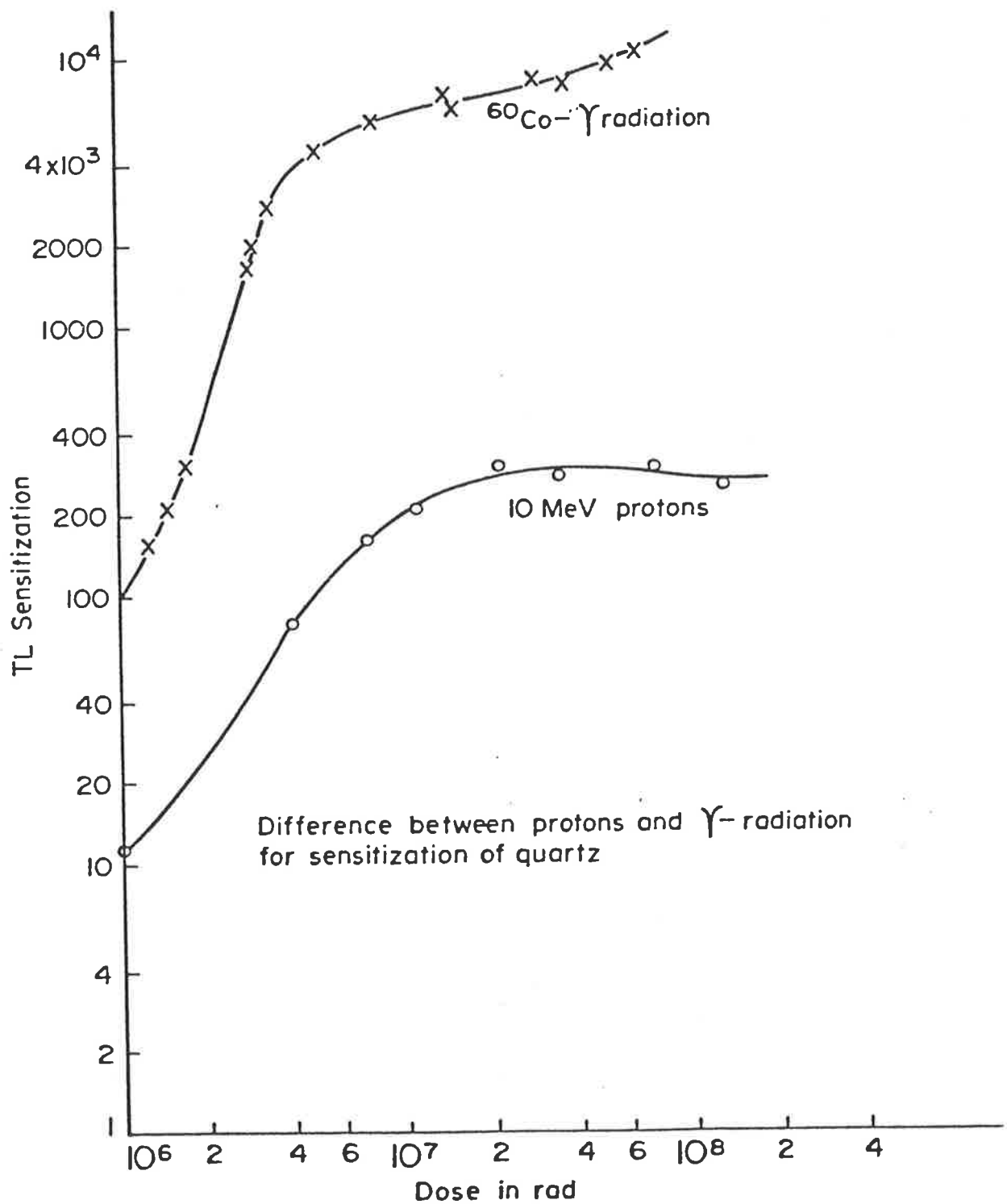


Figure 2.30 A comparison of the TL sensitivity in quartz induced by gamma and proton irradiation (after Durrani et al 1977a).

sensitization dose) may have been lost. What would therefore be useful is to have a method by which these large previous and partially bleached sensitization doses could be re-read or re-known. The significance of Levy's (op.cit) work is that it shows that quartz does have this capability to re-read previously accumulated radiation doses after exposure to a fixed laboratory test dose. His results are shown in figure 2.31. In order to determine how the radiation induced TL (artificial TL) of quartz depends on previous exposure to radiation, samples were subjected to three irradiations:

- (a) a fixed test dose of 2×10^5 rad,
- (b) a sensitizing dose between 10^5 and 10^9 rad,
- (c) a further test dose of 2×10^5 rad.

Following each of the three irradiations the TL was measured. Figure 2.31 shows that when the sensitizing dose exceeded 5×10^5 rad, the response to the second test dose was noticeably larger than that obtained for the first test dose, i.e. quartz "remembered" the previous exposure to a large sensitizing dose. The significance of this in uranium exploration is that TL can be used as a measure of the past irradiation history of a quartz sample, which given the high mobility of uranium under near surface oxidizing conditions, could be useful in tracing pathways of uranium bearing solutions. Applications of this type are contained in chapters 3 and 6.

Further points of interest from the study by Levy (op.cit) are (a) that sensitization begins at approximately 5×10^5 rad. (b) a plateau of TL response is reached at approximately 5×10^6 rad;

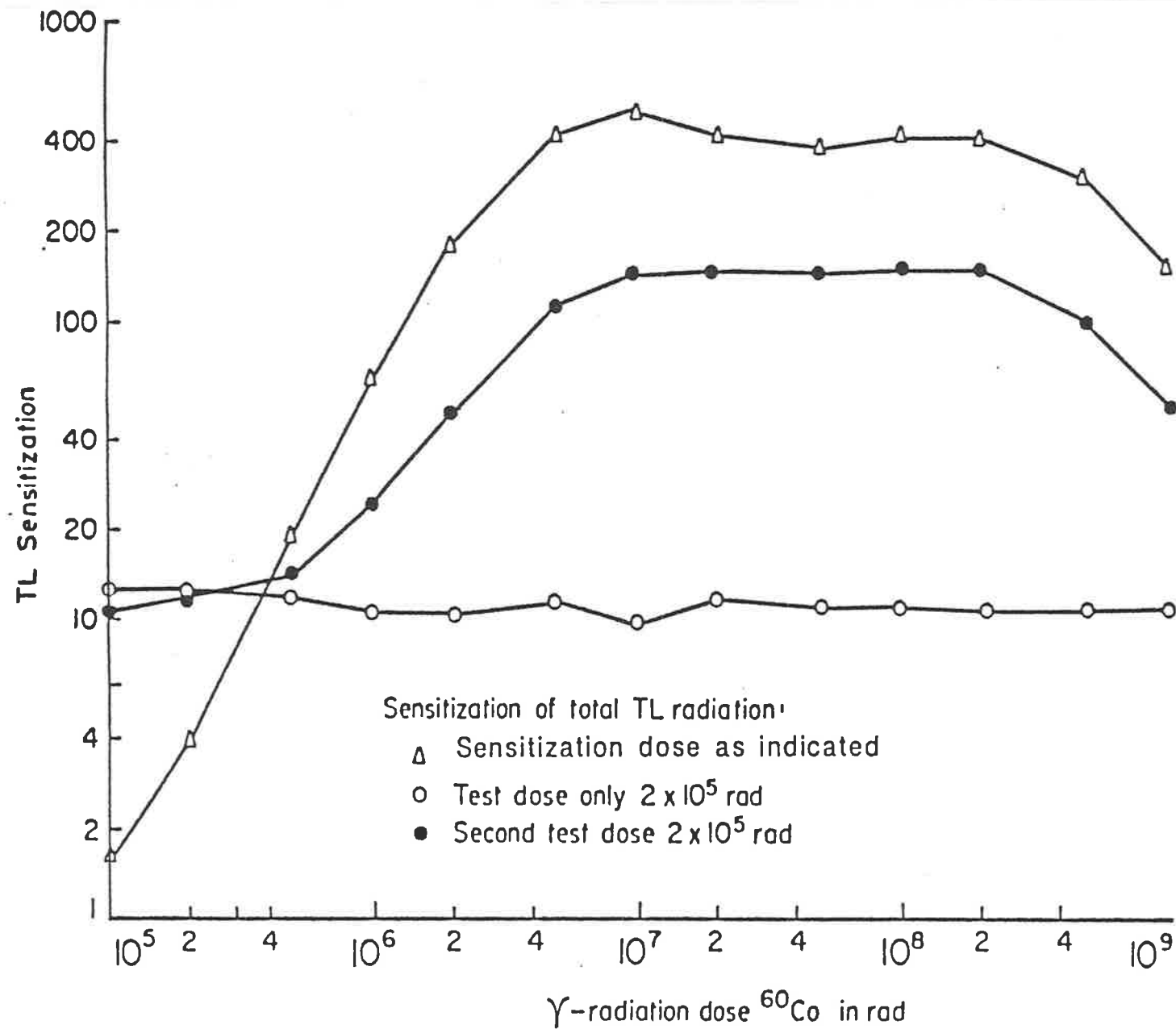


Figure 2.31 TL response in quartz following:
 (a) A test dose of 2×10^5 rad;
 (b) A variable sensitization dose and
 (c) A second test dose of 2×10^5 rad after thermal activation of the sensitization dose (after Levy, 1979)

(c) A decrease in TL response and TL sensitization occurs after approximately 10^8 rad. Durrani et al (1977) put the decrease in TL response and sensitivity at 10^9 rad proton irradiation, which corresponds with their observation that proton irradiation is less efficient in producing TL sensitization than gamma irradiation.

Before discussing sensitization models for quartz in an attempt to explain the increased, (and subsequent decreased), TL response and sensitivity of quartz as a function of radiation, mention should also be made of an earlier work on quartz from uranium deposits by Shekhmamteev (1973).

Shekhmametev (op.cit) examined the TL response of quartz from unnamed uranium deposits of Hercynian age (300M.y). The quartz samples were divided into three groups determined by their radioactive element concentration.

-Group 1 consisted of samples with no anomalous radioactive element concentration.

-Group 2 contained samples with uranium contents ranging from 0.001 to 10% .

-Group 3 consisted of samples which had no present anomalous radioactive element concentration, but were presumed to have had high concentrations in the geological past, ie. the uranium had been leached from these samples.

Natural TL (NTL) measurements of samples from all these groups were low and no well-defined dependence of NTL curve shape or intensity on the radioactive element content was found.

Artificial TL was induced by exposing samples to an unspecified dose of x-rays. Samples from all groups exhibited glow peaks at 180°C and 300°C with some samples also containing a glow peak at approximately 230°C . What Shekhmametev (op.cit) found significant however, was firstly that there was a change in TL

intensity of two orders of magnitude between groups 1 and 2 with the first group having the greatest intensity. It seems plausible that this large decrease in TL intensity in the natural environment should correspond to the desensitization mentioned in the previously quoted laboratory works of Levy and Durrani.

Shekhmametev (op.cit) placed the threshold at which this decrease in TL intensity occurs at 0.001% (10ppm U) over 300m.y. This corresponds to a model total dose of 10^9 rad.

Secondly, and importantly, Shekhmametev (op.cit) found that after X-irradiation samples of group 3 had similar glow curve shapes and intensities as those in group 2, ie. TL intensity was very low albiet that geochemically the samples of group 3 had no anomalous radioactive element concentrations. This can also be taken as indicating that quartz "remembers" exposure to previous large irradiations - even in the natural geological environment where annealing conditions may have been present over millions of years.

2.5.2.1 Sensitization Models For Quartz

McKeever (1985) lists three general models that have been proposed to explain sensitization effects. These are (a) the competing trap model where irradiation and heat treatment fill deep traps such that re-irradiation with a test dose can fill lower temperature traps without the competitive interference of higher temperature traps; (b) the centre conversion model, where radiation induces a conversion of one type of trap to another such that the luminescence resulting from the newly created traps is enhanced, and (c) the trap-creation models where radiation or thermal

treatment creates more defects - usually accepted as being of similar type to those pre-existent in the original crystal.

Variations of models (a) and (b) have been used to attempt to explain sensitization phenomena in alkali halides, though they have not been used to develop any widely accepted explanation of sensitization in quartz. It could however be argued that the model proposed by Zimmerman (1971) to explain the sensitization of the quartz 110°C glow peak, fits into the category of a competing trap model, with R and L as competing luminescent centres.

A model similar to, or along the lines of model (c), the trap creation model, has been proposed by Durrani et al (1977) as a viable means of explaining both sensitization and subsequent desensitization phenomena in quartz. They base their explanation on changes in the concentration of Al/alkali hole trapping centres and electron traps. Their work assumes that the Al/alkali centre acts as the luminescent recombination centre and the main hole trapping centre in quartz. (Electron traps are constituted by substitutional Ge and Ti ions (McKeever 1984), non bridging oxygens, alkali ions which do not compensate an Al^{3+} ion and oxygen vacancies). Furthermore, Durrani et al (op.cit) consider that initially the number of potential hole traps is greater than the total number of electron traps. If true, this implies that "if additional electron traps were to be created (by radiation) that there would initially be sufficient hole traps to compensate for them".

Given such a scenario it can be seen how sensitization can be explained. Gamma radiation creates electron-hole ionization pairs such that a hole may be trapped at an Al^{3+} site thus obviating the need for a charge balancing alkali ion. Such alkali ions can diffuse away from the Al centre, possibly along a c-axis channelway

where it may, or may not function as an electron trap. During thermal activation a trapped electron may be freed to recombine with the trapped hole with radiative emission and allowing the alkali ion to migrate back to the Al centre, thus restoring the Al/alkali site as a hole trap.

His model states that not only does ionizing radiation create electron hole ionization pairs, but that it also creates additional defects. These additional defects occur when strained Si-O bonds associated with the alkali ion at the Al/alkali centre are broken by ionizing radiation. Strained bonds will require less energy to be ruptured than unstrained bonds (Arnold and Compton 1959, McKeever 1985). The additional defects consist of additional oxygen vacancies and oxygen interstitials. The nett effect is the creation of additional electron traps. Implicit in the process is the destruction of the Al/alkali centre as a recombination centre.

Because it is necessary to retain charge neutrality, then a change in the concentration of one type of trapped charge will result in a change in concentration of the other type also. Therefore if the number of recombination centres (hole traps) is initially much larger than the number of electron traps, then even though radiation reduces the number of recombination centres, the population of trapped electrons may continue to increase with increasing radiation because the concentration of electron traps is increasing until such time as the concentration of available hole traps equals the population of trapped electrons. The result of more charges being trapped means that following a thermal cycle more charges are released to recombine at Al/hole recombination centres with resultant emission of light. This could explain the increased TL sensitivity as a result of increased radiation exposure.

In their model it is assumed that additional radiation would result in a decrease in the number of available hole traps, (and hence trapped holes) and therefore in order to conserve charge neutrality the number of trapped electrons would also decrease (even though the number of available electron traps continued to increase). Following a thermal cycle and TL measurement, less charges would be available for recombination, and thus less light emitted, i.e. TL response and sensitivity would decrease.

Other adherents of the trap creation model to explain sensitization of quartz include Ichikawa (1968). Although not advancing a complete explanation of sensitization and subsequent desensitization, Ichikawa (op.cit) also considered that gamma radiation created additional defects at pre-existent impurity and lattice defect sites. He advanced the theory that gamma radiation resulted firstly in multiple ionization and displacement of the oxygen ion into an interstitial position and secondly in the "scission" and rearrangement of chemical bonds.

Although trap creation models seem internally consistent in explaining the sensitization phenomena, direct confirmatory evidence as to the ability of non-displacive ionizing radiation to create additional defects has been lacking. Support may have come in a recent study by Chatagnon (1986) on the concentration of E' centres in heavily irradiated natural quartz. Chatagnon (op.cit) used Paramagnetic Electronic Resonance (EPR) techniques to monitor the change in concentration of E' centres in natural quartz following alpha, neutron and gamma irradiations. His data are contained in table 2.3 with results for three gamma irradiations at the top. These show that an increase in radiation dose from 3.2×10^8 rad to 1.2×10^{10} rad results in an increase in E₁' centre concentration i.e. an increase in potential electron traps.

rayonnement	rad /g	AR	170°C	300°C	Echantillon	
gamma	$3,2 \cdot 10^8$	1,6	1,5		Brésil	
	$\approx 10^9$	8,4	7,6	36	Mt Blanc	
	$1,2 \cdot 10^{10}$	65			Brésil	
$e^-: 5 \cdot 10^{18}/cm^2$ 3MeV	$3,1 \cdot 10^{11}$	1312		3017	Brésil	
neutrons/cm ²	10^{16}		1,5	1	3,5	Mt Blanc
	10^{16}		2	1,4	3	Gardette
	10^{18}		23150	22000	22580	Mt Blanc
	10^{18}		26050	22580	28900	Gardette
	$1,2 \cdot 10^{18}$	$1,3 \cdot 10^{10}$	39400			Brésil
alpha $4 \cdot 10^{14}/cm^2$	100 KeV		1625		1600	Mt Blanc
			1500		1500	Gardette
	400 KeV	$8 \cdot 10^9$	2437		2200	Mt Blanc
		$8 \cdot 10^9$	2500		2500	Gardette

Table 2.3 Increase in E_1' centre signal in response to gamma doses from $3,2 \times 10^8$ rad to $1,2 \times 10^{10}$ rad. Increase in E_1' centre signal with alpha and neutron irradiation is also observed (after Chatagnon, 1986).

Mattern et al (1975) suggest an alternative explanation for sensitization in quartz which may broadly be categorized as a competing-trap model. Their work examined the change in optical absorption (specifically "A" band growth) with increasing radiation doses. Their data for natural Brazilian quartz crystals measured at 85K and 300K are shown in figure 2.32 and show an initial rapidly increasing portion of the growth curve (up to approximately 1.5×10^5 rad) followed by a linearly increasing region.

Mattern et al (op.cit) suggest that the radiation induced color centre may be a hole trapped at a precursor site consisting of a substitutionary Al^{3+} ion with nearby compensating alkali metal (M^+) or hydrogen (H^+) ion. In addition to compensated Al^{3+} sites they also refer to suggest the existence of uncompensated Al^{3+} ions. Such uncompensated Al^{3+} ions would have a large capture cross section for radiation induced holes.

During irradiation uncompensated Al^{3+} ions would strongly attract radiation induced holes and be quickly converted to color centres. This process would lead to the quickly saturating exponential component observed in figure 2.32. Simultaneously holes would interact with compensated Al^{3+} defect sites, though at a less rapid rate, with subsequent diffusion of the compensatory monovalent ions. Luminescence occurs when ionization electrons recombine with holes trapped at Al^{3+} ions.

This process restores an uncompensated Al^{3+} ion which may again function as a hole trap. The processes actually occurring are likely to be quite complex and dependant upon several factors: ie. on the temperature of irradiation (which will influence the rate of M^+ diffusion); the cross sections for the Al^{3+} /hole + e recombination centre formation and Al^{3+} /hole colour centre

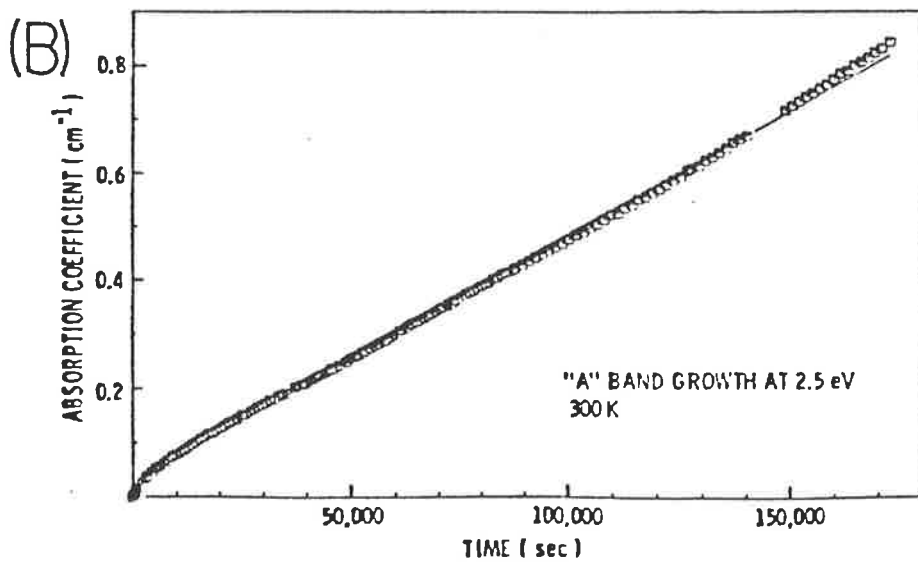
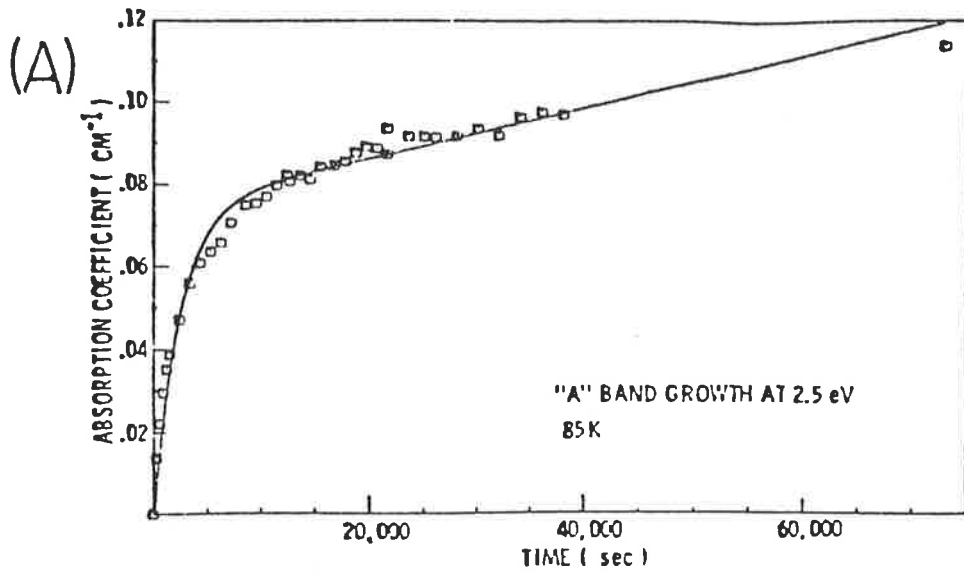


Figure 2.32 Change in A band optical absorption with radiation (after Mattern et al 1975). (A) shows two stage band growth and (B) essentially linear band growth.

formation; the concentration and cross-sections of all electron and hole traps and the radiation dose.

Despite the complexity and non-quantitatively defined nature of processes occurring, the model still seems potentially able to explain sensitization in quartz. One criticism may concern the lack of an explanation of de-sensitization at high radiation doses.

Finally, although not a physical model, the interactive kinetic modelling of Levy discussed earlier (Levy 1984, 1985a,b) has been able to explain the closely related phenomena of supralinearity in quartz (see figure 2.14). The increased sensitization as a result of exposure to increasing radiation doses, may therefore possibly be explained simply by retrapping of electrons (at least for lower temperature glow peaks). Physically, this could be expected to occur: 1) when there is a large number of electron traps, 2) the relative cross section of a recombination centre is low i.e. retrapping is non-negligible. It is interesting to speculate on how the creation of additional electron traps by ionizing radiation could contribute to a physical or conceptual understanding of interactive kinetic modelling. Such speculations are contained in chapter 4 where observed changes on TL response in the vicinity of uranium ore bodies have been tentatively interpreted in terms of interactive kinetic models and additional trap creation.

2.5.2.2. Changes in the Quartz Thermoluminescence Glow Curve With Radiation

Regardless of which model is best able to explain sensitization and de-sensitization phenomena in quartz, from purely empirical considerations there have been several factors mentioned

which suggest that TL should be of use in uranium exploration. There are: 1) that quartz "remembers" exposure to previous large doses of ionizing radiation (Levy, 1979); 2) that the shape of quartz TL glow curves changes as a function of radiation (Ichikawa 1968, Durrani et al 1977); 3) that sensitization occurs in different radiation ranges for different glow peaks in quartz (Ichikawa, op.cit. Durrani et al op.cit, David et al 1978); 4) that there is a decrease in TL response over two orders of magnitude for quartz associated with anomalously radioactive samples in uranium ore deposits (Shekhmametev, 1973) and 5) the fact that the TL properties of natural (and synthetic) quartz from different localities- as well as different samples from the same locality - show a very large range of TL glow peaks and emission bands.

What would therefore be useful for the exploration geologist would be to have a knowledge of how the TL glow curve of quartz changes in response to radiation. If a systematic variation in TL glow curves occurs then it should be theoretically possible to detect areas of past uranium concentration and pathways of uraniumiferous protore movement by observing the radiation "sensitization and damage" effects to host rock quartz.

As stated above, work by Durrani et al (1977b), David et al (1978) and Levy (1979) has indicated a decrease in the lower temperature glow peak intensities at doses of approximately 10^7 - 10^8 rad of gamma radiation. Experiments have not proceeded far beyond these gamma radiation doses, thus it is not yet possible to trace the radiation effects on quartz, or to assign precise radiation dose levels at which middle and higher temperature glow peaks will begin to decrease. Much of the remainder of this section must therefore remain qualitative rather than quantitative.

Notwithstanding the paucity of data on quartz beyond gamma radiation doses of 10^8 rad, extensive similar work at lower doses has been accomplished on alkali halides. Mattern et al (1970) and Fairchild et al (1975) have demonstrated that in the range from 800 rad - 3×10^7 rad there is an increase in intensity of each glow peak in the LiF glow curve, beginning with the low temperature glow peaks, followed by a decrease after each glow peak has reached a maximum intensity. This decrease in TL intensity has been referred to as desensitization (McKeever, 1984). The change in the LiF glow curve shape within this radiation dose range is shown in figure 2.33. This indicates a generally systematic change in glow peaks with increasing radiation, ie. a progressive increase then decrease of glow peaks beginning with low temperature glow peaks. Though generally systematic, the change in individual glow peaks intensities with increasing radiation is not strictly linear as some peaks will respond strongly to only a small incremental increase in radiation (eg. peaks 8 and 9 in figure 2.33 (e) and (f)) whereas others will not. This is not unexpected as other factors such as trap type and density will also influence the response of each peak. At the upper end of the radiation range, only the middle and high temperature glow peaks are left (270°C - 370°C) with the high temperature peaks being dominant.

Based on: (a) the above experimental work on alkali halides; (b) the observation by Ichikawa (1968), Durrani et al (1977), David et al (1978) and Levy (1979) that the low temperature glow peaks of quartz reach a maximum at 10^7 - 10^8 rad and then decrease with increasing radiation; (c) the low natural and radiation induced TL of quartz associated with uranium deposits by Shekhmametev (1973); (d) the dominance of high temperature glow peaks in old uranium bearing areas (Shekhmametev, 1973) and (e)

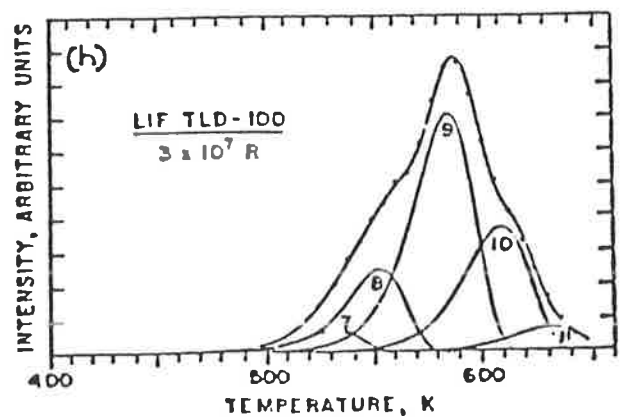
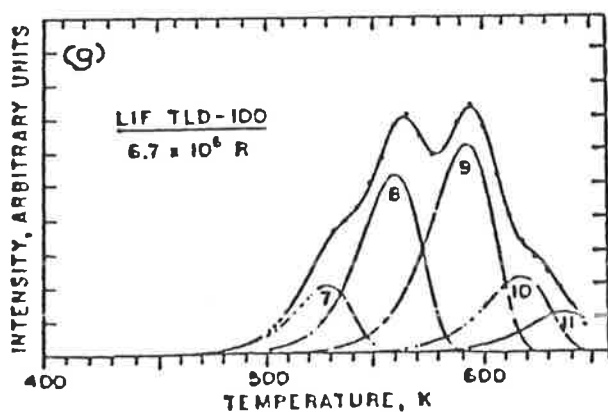
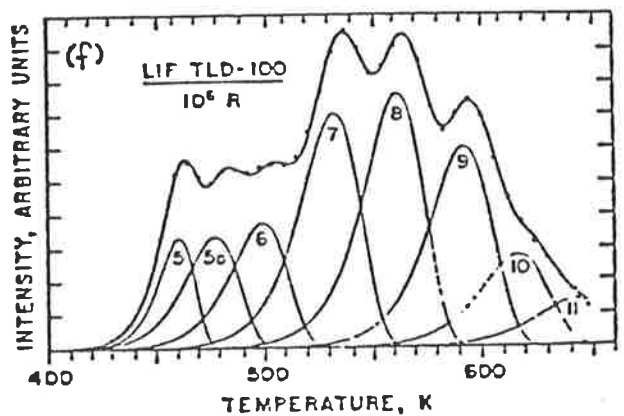
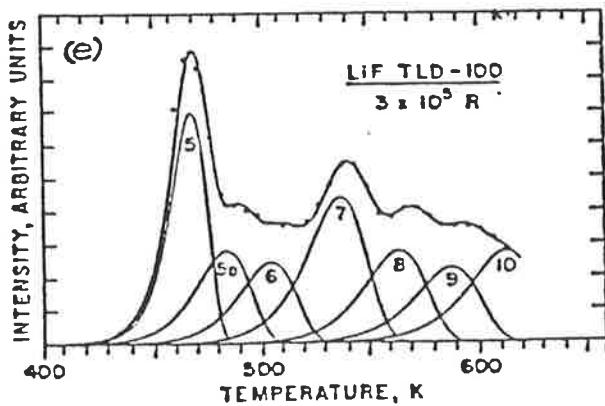
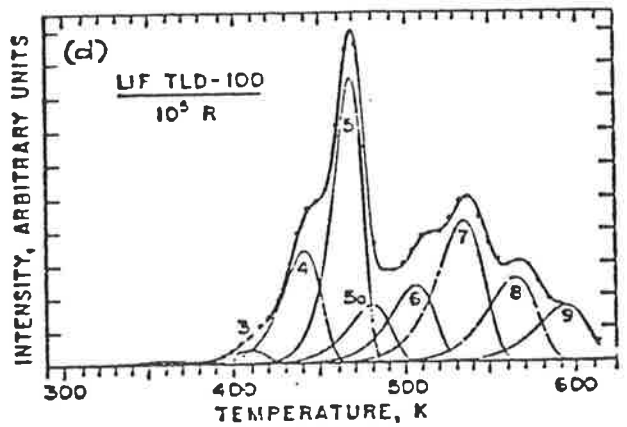
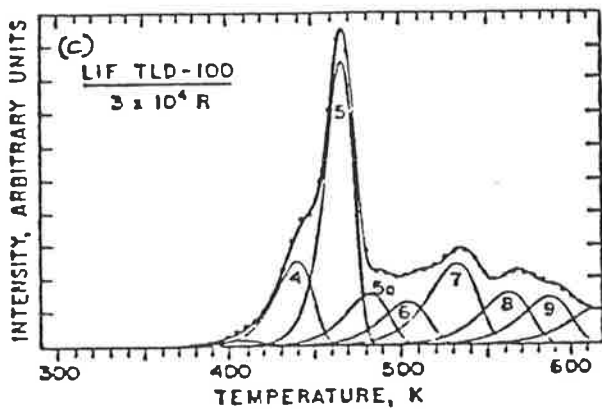
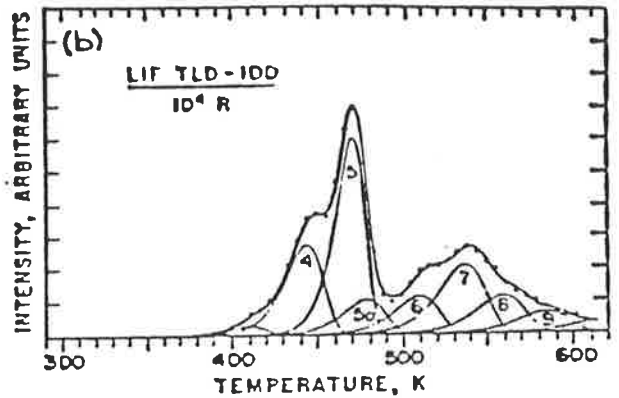
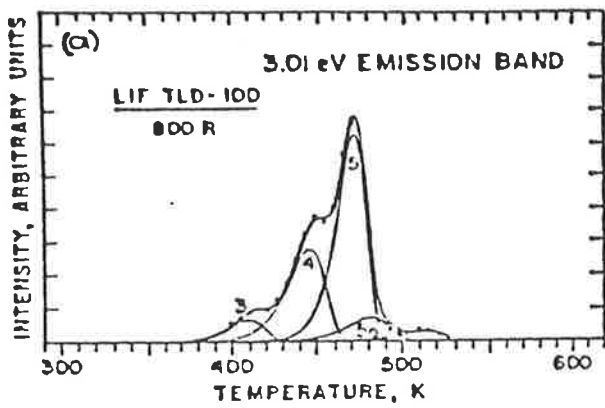


Figure 2.33 Change in LiF glow curve shape with gamma radiation from 800 rad to 3×10^7 rad (after Fairchild et al, 1975).

observations of TL glow curves of quartz from a number of different geological radiation environments, it is possible to construct a set of generalized glow curves very roughly representing the change in the quartz TL glow curve with increasing radiation. These generalized glow curves are shown in figure 2.34. It should be emphasized that: (a) these are schematic illustrations of glow curves - glow curves from actual samples are found in chapters 3 and 6 (b) these are, at this stage, expected variations in glow curves of quartz with increasing radiation. As will be seen, particularly in chapter 3 and 6, glow curves obtained approaching the Beverley ore bodies and to a lesser extent the Westmoreland ore deposits do generally conform to the expected variations.

Figure 2.34(a) shows a glow curve for quartz which has not been exposed to more than small amounts of radiation. The 110°C glow peak is well known in archaeometric geological literature and could be expected to dominate at low doses - the fact that the 110°C glow peak was not observed in this study is examined in Chpt 2.6.2. Quartz has several glow peaks. The exact temperature at which they occur depends on the heating rate. For this reason, and for simplicity (as this is a representation of expected glow curve variations rather than actual glow curve variations), only three glow peaks will be shown in subsequent diagrams, rather than all known glow peaks of quartz. The three glow peaks will be referred to as the low temperature, middle temperature and high temperature glow peaks (LT,MT,HT).

As the radiation dose increases one would expect the process of sensitization to begin. From Levy (1979) sensitization is expected to begin at approximately 5×10^5 rad gamma radiation. For doses in excess of 5×10^5 rad the LT glow peak increases in intensity, such that it obscures all other glow peaks. The

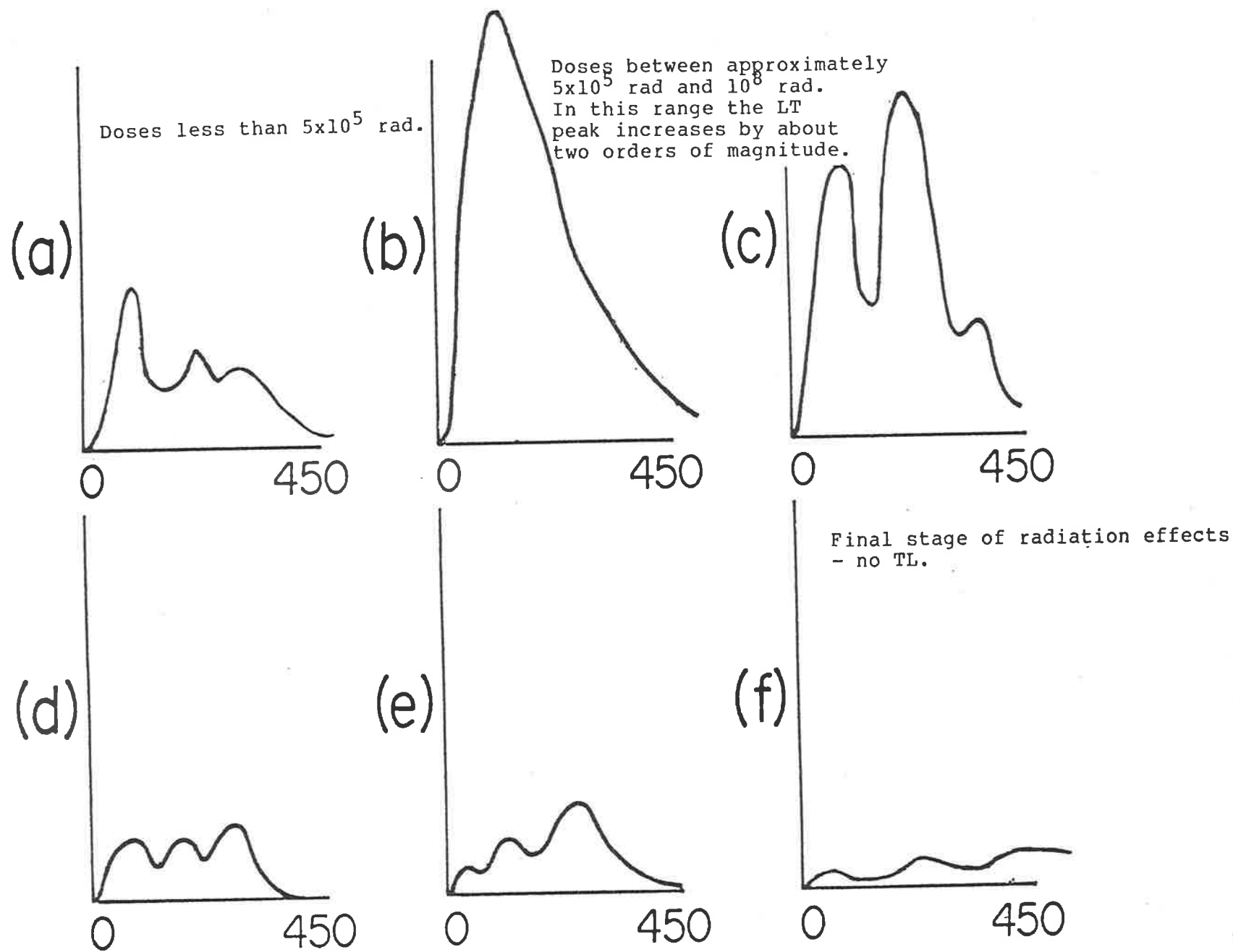


Figure 2.34 Expected change in generalized quartz glow curve shape

increase in LT peak intensity may be two or three orders of magnitude relative to the initial intensity. This is indicated in figure 2.34(b). The sensitization of the LT glow peak should continue up to doses in the vicinity of 10^7 - 10^8 rad gamma radiation. Beyond these dose levels, by reference to the works of Ichikawa (1968), Durrani et al (1977) and Levy (1979), one expects that de-sensitization of the LT glow peak could occur. The decrease in LT peak intensity is illustrated in figure 2.34(c). Figure 2.34(d) indicates the expected glow curve shape when the MT glow peak is also de-sensitized. The radiation dose at which this occurs is unknown. Further radiation will result in the HT peak being the only glow peak to continue increasing in intensity, whilst the LT and MT peaks continue to decrease in intensity (figure 2.34(e)). Durrani et al (op.cit) obtained a glow curve with only one HT glow peak remaining after a dose of 10^{10} 10 MeV protons (illustrated in figure 2.29). Reference to figure 2.30 implies that the equivalent gamma dose should be higher than 10^{10} rad; perhaps as high as 10^{11} or 10^{12} rad gamma radiation.

Durrani et al (1975) examined samples from the natural reactor core at the Oklo uranium deposit which exhibited no artificial TL at all. This is illustrated in figure 2.34(f) and may represent the end point of radiation damage in quartz as observable by TL.

It need be emphasized once more that the expected glow curve variations illustrated in figure 2.34 represent an "educated guess" based on the five observations mentioned previously. The fact that such variations do occur around some uranium deposits is indicative that the educated guess may have some basis. This basis will be discussed in chapter 4 after presentation of results at Beverley.

2.6 Experimental Procedure

2.6.1 Samples Studied

The samples analyzed (approximately 1,000) were in the form of drillhole core and cuttings or surface rock samples. The two major areas studied were the Beverley Deposit (chapter 3) in the Frome Embayment of South Australia (100 samples) and the Westmoreland Deposit (chapters 5 and 6) on the Murphy Tectonic Ridge in Queensland (800 samples). Further studies were also carried out in the Bremer River Prospect in the Murray Basin, South Australia (chapter 3, 100 samples). Generally samples from Westmoreland were drill core though minor cuttings were used. Samples from Beverley were generally percussion or rotary hole cuttings though some core was also collected.

Samples from both major areas were lithic sandstones, generally well sorted with well rounded quartz grains and very little feldspar. Individual binocular microscope descriptions for samples are contained in the appendices.

In the case of Beverley, all samples from the suspected ore transport horizon were collected from the same stratigraphic horizon between depths of 120-140 metres below surface. Samples were also collected from 10 metres above and below the ore transport horizon. The fact that samples are from the same stratigraphic horizon should guarantee the same provenance and hence a similar initial internal chemistry. Differing thermal or pressure histories between samples can also be ruled out given the similar collection depth.

The majority of samples from Westmoreland were also from the same stratigraphic horizon (Westmoreland Conglomerate Unit 4). Depths ranged from near surface to 140 metres. Occasional samples from underlying units are marked in the appropriate diagrams.

Given that in both of the above cases, samples have few inherent source, temperature or pressure differences, and that both areas have mobile uranium, it then seems reasonable to attempt to explain observed differences in TL characteristics between samples on the basis of differing radiation effects.

(Though not strictly forming a part of this thesis it is interesting to note in the appended publication by Ypma and Hochman 1987 that in a study on the Eyre Peninsular, South Australia, even when samples were taken transcending stratigraphic boundaries, that the effect of radiation produced a common trend, ie. high temperature TL peak increasing as a proportional of total TL).

All core samples from Westmoreland were collected from trays arrayed in core racks in direct sunlight. The history of cuttings from Beverley is not known prior to bagging though it is likely that they too would have been exposed to sunlight during drilling and bagging. For this reason, and given that this thesis is concerned with investigating the use of artificial (rather than natural) TL in uranium exploration no wholesale natural TL measurements were undertaken. This is further discussed and justified in chapter 2.6.2.

2.6.2 Sample Preparation

All samples, whether core, cuttings or whole rock were gently crushed in the laboratory which was fitted with unfiltered fluorescent lights. The crushings were then sieved manually

through 30 and 120# sieves (125-500 microns). The -30+120# fraction was washed and decanted several times to remove any dust sized particles remaining. Approximately one gram of sample was then agitated in an ultrasonic bath (the solvent was water) to further cleanse grains.

The washed sample was placed in a filter cone and further washed with acetone and then dried at room temperature in a fume cupboard.

Once dried the sample was passed through a Frantz isodynamic electromagnetic separator. Each sample consisted initially of greater than 95% quartz so the amount of impurity material to be removed was small. The Frantz was set at a reverse slope of -2° such that the natural tendency of all minerals would be to roll down the gravity slope. However when a strong magnetic field is applied (current of greater than 1.4 amps), quartz, being weakly diamagnetic is forced out of the magnetic field, upslope into the non-magnetic stream. The natural tendency of other minerals such as feldspar and zircon is to roll into the gravity stream (which is also the magnetic stream). This procedure is not 100% effective as a lot of quartz is also lost into the gravity/magnetic stream though it does ensure that the material coming out of the non-magnetic stream is greater than 99% quartz.

Each sample gained from the non magnetic stream of the Frantz was then checked for purity under a binocular microscope. Any remaining obvious impurities were removed by handpicking. Tabulated binocular microscope descriptions of each sample are contained in Appendix 1.

Samples were then placed in individual gelatin capsules which were irradiated to a total dose of 5×10^5 rad (5KGy) Co^{60} gamma radiation (rationale in chapter 2.6.3), removed from the source in

the dark and wrapped in aluminium foil. They were then left 24-72 hours before measurement to allow any phosphorescence to decay. During this period low temperature TL peaks can also be expected to decay including the 110°C peak which has a short half life. The 110°C peak was not subsequently observed in any glow curves. Measurement procedures are detailed in chapter 2.6.4.

There are a number of points in the above sample preparation technique which are different to those employed in pottery and sediment TL dating and which need to be further addressed. The technique used here is, in general, much simpler and less time consuming and could not be utilized in sediment dating TL preparation to give accurate results.

Firstly, the aim of this project is to find a comparative difference in TL response between many samples analyzed than to find absolute radiation doses accumulated in a few samples. In this regard the same sample preparation procedures were employed for all samples. If any errors are introduced by this procedure then they should be systematic.

Secondly, techniques were designed to meet the needs of the uranium exploration industry rather absolute dating. If artificial TL is to be useful in the uranium exploration industry then it must be quick and cheap, amenable to bulk analysis, rather than time consuming and expensive as is the case with the more extensive procedures adopted in sediment TL dating.

Thirdly the starting material must also be considered. The sediments used in this study were of Tertiary (15 m.y) and Mid-Proterozoic (1,600 m.y) age. During geologic history (and surface exposure) much of the contaminating feldspar has been altered and weathered such that the sandstones are relatively pure or clean. This contrasts with many of the sediments studied by TL

archaeometrists which may be only several tens of thousands of years old and may still have a major feldspar component.

Notwithstanding these three points, even with the simplified experimental procedure adopted in this study there must still be a reproducibility and reasonable accuracy of results. The following issues therefore need to be further considered.

2.6.2.1 Thermal Bleaching or Pre-annealing

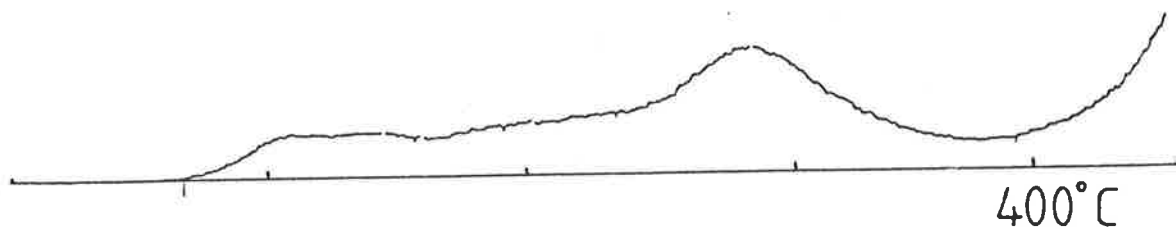
No thermal bleaching of samples was undertaken prior to Co^{60} irradiation to drain any remaining natural TL. Because samples had been stored in the sunlight after drilling and prepared in the laboratory under unfiltered lights it was assumed that a significant proportion of the natural TL (NTL) would have been bleached. Furthermore it was also assumed that any remaining NTL would be insignificant compared to the artificial TL (ATL) induced by 5×10^5 rad Co^{60} gamma irradiation. This is justified by reference to figure 2.35 where (a) represents a sample where NTL was drained by pre-heating to 460°C then cooled in air and irradiated with a 5×10^5 rad Co^{60} gamma test dose i.e. ATL only. Figure 2.35(b) is a sample irradiated with the same test dose with no prior pre-heating i.e. NTL+ATL. The strong similarity between the two curves validates the initial assumption.

2.6.2.2 The Lack of Hydrofluoric (HF) Acid Etching

It is usual when attempting TL dating on large grains by the quartz inclusion method to etch the sample with HF. This is done for three reasons. (a) to remove any contaminating minerals such as feldspars, (b) to remove the outer skin of the quartz which has

(A)

ATL + NTL



(B)

ATL only

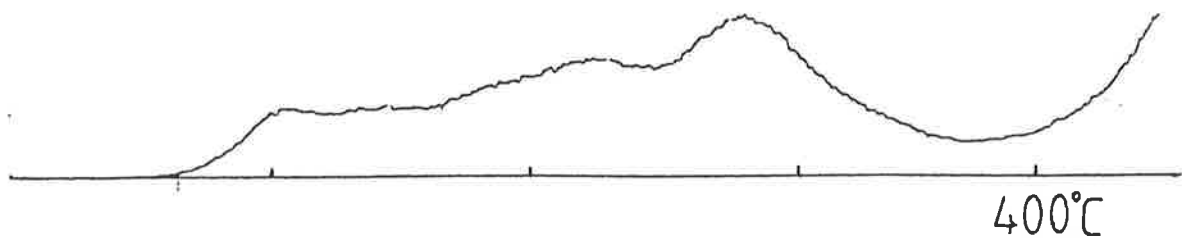


Figure 2.35 Glow curves for quartz where

- (a) NTL was drained and ATL induced with a standard test dose and
- (b) NTL was not drained prior to the standard test dose.

been affected by a variable alpha particle flux thereby simplifying subsequent dose rate calculations and (c) to "clean" the grains.

HF etching was not considered necessary in this study for the following reasons:

- (a) There was little feldspar in samples initially, even less after Frantz treatment and any remaining contaminating minerals (of which there were very few) were detected during binocular microscope examination.
- (b) The large grain size used (125-500 microns) greatly reduced the ratio of α particle induced TL signal to the electron and gamma ray induced signal. There are two interplaying factors here; (i) that the larger the grains used, the smaller the volume of the outer alpha affected skin becomes relative to the beta and gamma affected interior volume and (ii) that alpha particles are inherently less efficient as a radiation dose in producing TL than either beta or gamma radiation (possibly because the large number of ionization events per unit path length with alpha radiation also results in a greater percentage of instantaneous recombinations).

When considering both factors the alpha particle contribution to large grains becomes very small.

Further to these reasons, experimental work in this study also indicated that HF does have an effect on the TL response of some types of quartz grains resulting in a great diminution of the TL intensity of one peak in quartz (the 130°C peak).

This is shown in figures 2.36 and 2.37 where the former figure shows the effect of HF for varying periods on the TL glow curve of quartz from a high radiation environment (taken from within the Westmoreland uranium ore body). There is only a 3%

Sample UMD 77/22
37.7 metres
HF Etching followed by 5×10^5 rad $\text{Co}^{60} \gamma$

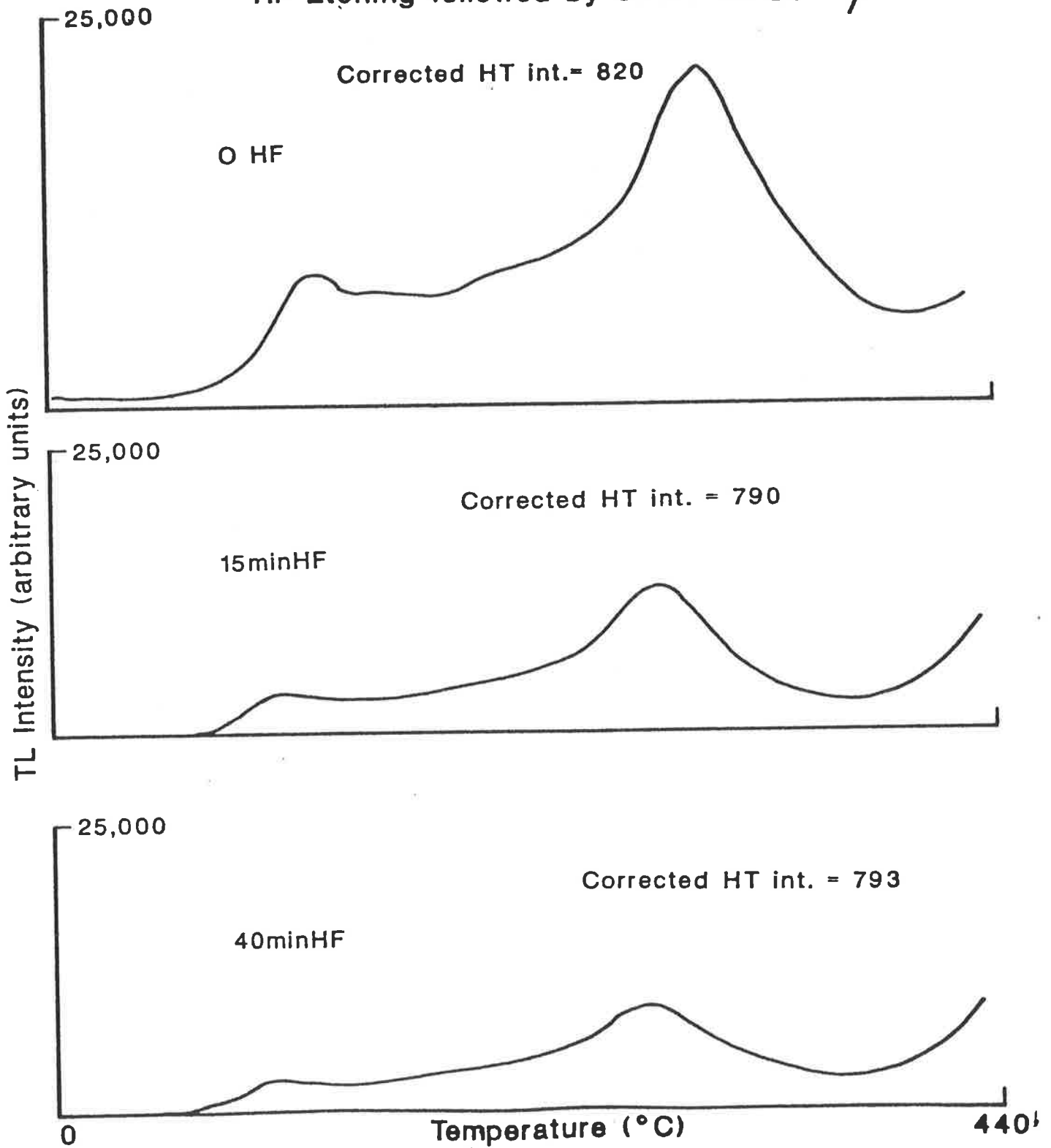


Figure 2.36 Effect of HF on quartz from the Westmoreland area which has been subject to high radiation exposure. Little change in TL is observed with etching time. The test dose used was 5×10^5 rad.

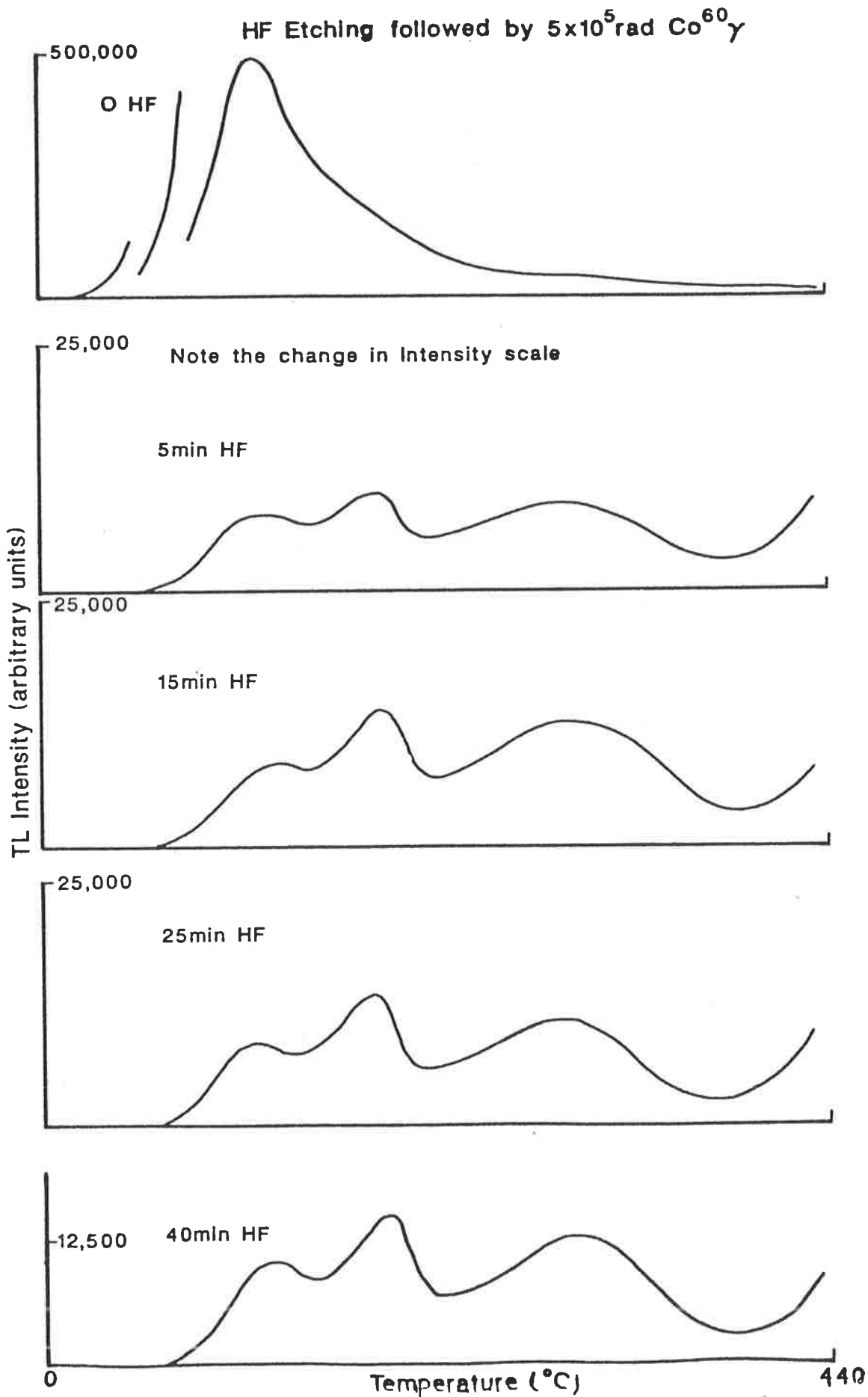


Figure 2.37 Effect of HF on quartz from the background Beverley host rock (low radiation exposure) showing a large decrease in TL intensity of the low temperature glow peak. The test dose used was 5×10^5 rad.

change in intensity of the 350°C glow peak from 0 to 40 minutes HF. In contrast figure 2.37 shows the TL of quartz from a low radiation environment (the up-dip host rock of the Beverley ore deposit). A drastic change in intensity of the 130°C glow peak occurs over an order of magnitude for just 5 minutes of HF etching. It is tempting to immediately think that the initial glow curve is not due to quartz but to a bright contaminating mineral such as feldspar or carbonate which is quickly attacked by HF. This however cannot be the case as the same result occurred when quartz was handpicked from the sediment (which was 95% quartz to begin with).

Aitken (1985) suggests that although early workers (Fleming) thought that HF upset pre-dose dating that this was not now generally accepted and that furthermore if HF did affect any TL glow peaks they were only low temperature glow peaks attributable to surface defects. To test this possibility the sample in question (186-30) was subjected to mechanical abrasion in an abraidor similar to that devised by Krogh (1982) for abraiding the rims of zoned zircons used in U-Pb geochronological studies.

Figure 2.38 shows the effect of abraiding approximately 50mg of sample for periods up to 5 minutes and figure 2.39 for periods up to 137 minutes at 30p.s.i. (These results should be compared with the average period for abraiding zircons which is approximately 5 minutes at 5p.s.i). Although some variations in intensity of the 130°C glow peak occur, there is no systematic decrease in intensity with abrasion and certainly no dramatic change in intensity as observed with HF etching. This would seem to rule out the possibility of surface defects being responsible for the 130°C glow peak. These results could also further argue against the possibility of feldspar remaining in the sample and

SAMPLE 186 - 30, MECHANICAL ABRASION
followed by 5×10^5 rad $\text{Co}^{60} \gamma$

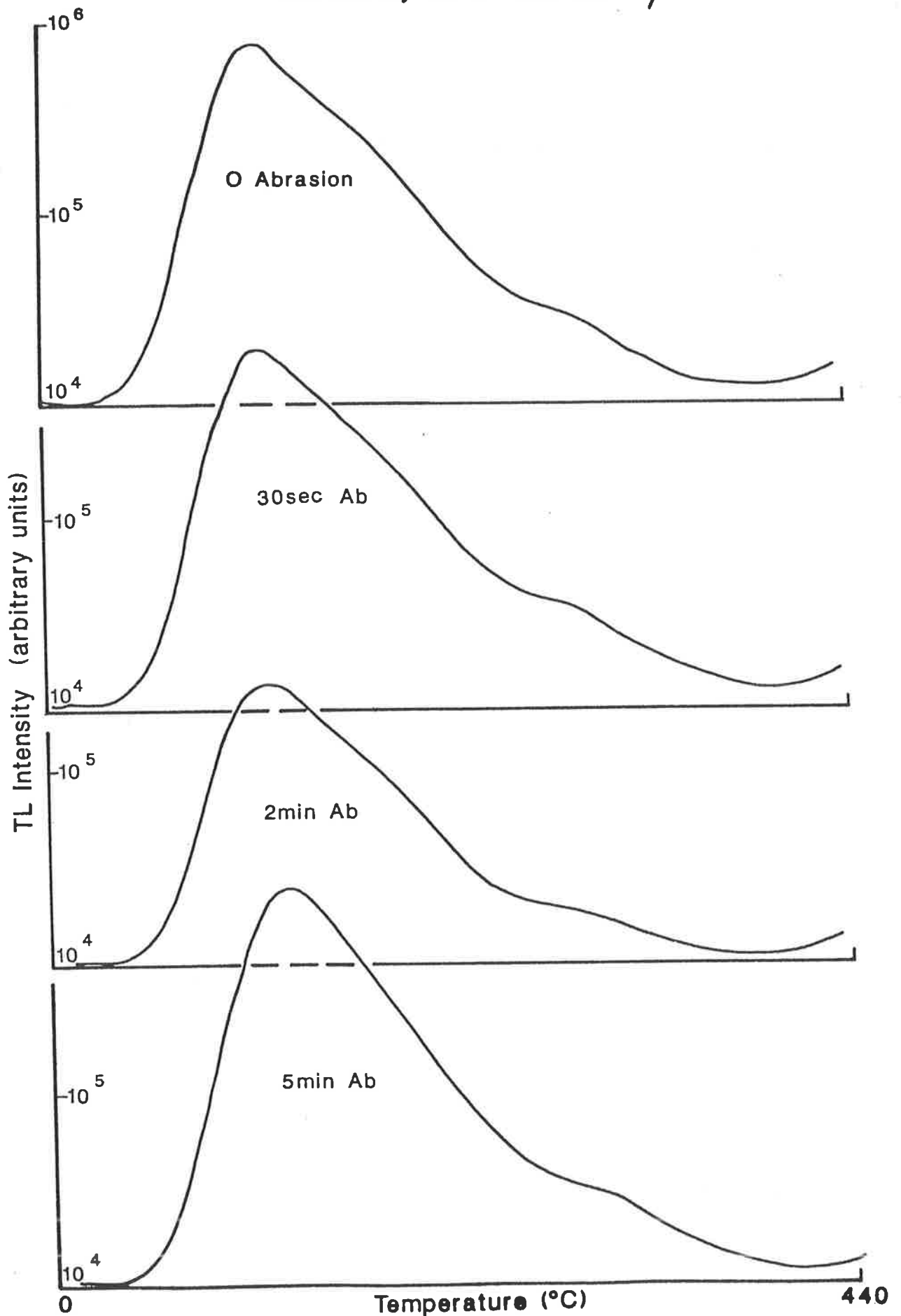


Figure 2.38 Effect of air abrasion on the TL of quartz from the background Beverley host rock showing little change in TL intensity. The time of abrasion was between 0 and 5 minutes. Test dose was 5×10^5 rad.

SAMPLE 186 - 30 MECHANICAL ABRASION
followed by 5×10^5 rad $\text{Co}^{60} \gamma$.

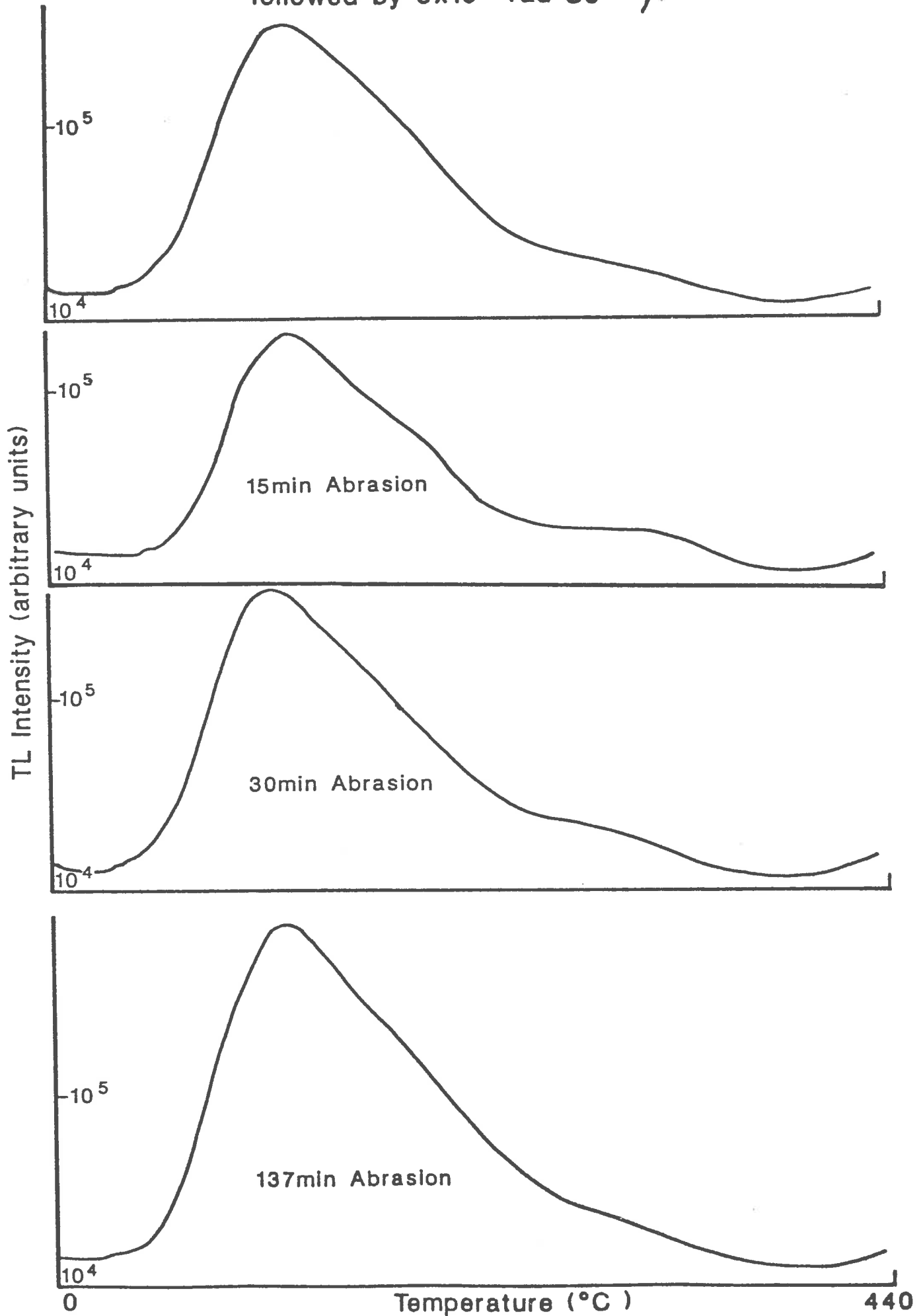


Figure 2.39 Effect of air abrasion on the TL of quartz from the background Beverley host rock showing a small change in TL intensity with abrasion. The time of abrasion was between 0 and 137 minutes. Test dose was 5×10^5 rad.

being responsible for the 130°C glow peak. The feed material abraided was a -30+60# fraction (500-250 microns) and the escape mesh bolting cloth used was 60# (250 microns). After 137 minutes abrasion it could be expected that any feldspar initially in the starting material would have been removed; being fractured and broken because of its relative softness (compared to quartz) and prominent cleavage. After fracturing the fragments would sift through the 60# bolting cloth leaving only the more resistant quartz.

The exact reason why HF should drastically affect the ATL of one type of quartz relative to another is not known. In this study, which involved the application of changing ratios of glow peaks with radiation, the avoidance of HF in sample preparation obviated the problems associated with it.

2.6.2.3 The ATL Test Dose

The test dose chosen was 5×10^5 rad (5KGy) Co^{60} gamma. This was based on: (a) the work by Levy (1979) which showed that the quartz "memory" for previous radiation did not begin until a dose of approximately 4 or 5×10^5 rad; (b) Previous unpublished work, by P. Ypma (pers. comm. 1987) at the Brookhaven National Laboratory showed that doses of 5×10^4 rad produced smaller intensity differences between samples known to have different radiation histories, than was produced by a 5×10^5 rad test dose.

2.6.3 Apparatus Used

2.6.3.1 Radiation Sources

Samples were irradiated in two sources, depending on their availability.

The first Co^{60} gamma source used (in the period 1979 - mid 1983) was housed in the Department of Physical and Inorganic Chemistry at the University of Adelaide. The source was kept under water and was raised by remote control to a fixed point above a hole in the floor. (Naturally the room had heavily shielded walls). Samples, in gelatin capsules inside plastic vials, were placed in predetermined positions around the hole through which the source was raised. Dose rates were determined previously by chemical dosimetry. In February 1979 the dose rate was 2.5×10^4 rad/hr. Following irradiation to a total dose of 5×10^5 rad the plastic vials, (which were wrapped in aluminium foil before irradiation), were stored 24 to 72 hours before measurements were made.

The second Co^{60} gamma source used, mainly for the Beverley samples, was housed in the Department of Geology and Geophysics, University of Adelaide. This was in use from mid 1983. The dose rate (from chemical dosimetry) was 4.5×10^5 rad/hour.

2.6.3.2 Thermoluminescence Apparatus

The TL equipment was obtained from Littlemore Scientific Engineering Company (Thermoluminescence Apparatus Type 711). The equipment consisted of a glow oven with a heating strip electronically controlled to increase temperature linearly at a

specified rate, a photon ratemeter, and a light detection system with accompanying EHT supply. An EMI 9635QA photomultiplier and a ND2 filter were used in all measurements. The photomultiplier response appeared on the Y axis of an HP3390A chart recorder. The thermocouple output (cold junction at room temperature) was simultaneously recorded on the X axis of the recorder.

2.6.4 Measurement Procedure

After irradiation and being "stored" for 24-72 hours, grains for TL measurement were "shaken" onto stainless steel discs, levelled to a monolayer by removing excess grains and then tapping the lip of the disc. Care was taken to use a single layer of grains as light from underlying grains is blocked by overlying grains. Also, samples not in contact with the heating strip thermally lag behind those that are in contact. All sample mounting and measuring was carried out under yellow filtered light to inhibit bleaching of the ATL.

For the TL measurement previously prepared discs were placed on the heating strip and centred on a premarked spot to aid reproduceable positioning. A black body shield, mounted on ceramic strips, was placed around the sample to mask thermal radiation from the heating strip at elevated temperatures, whilst allowing passage of the signal from the sample.

To reduce spurious TL the glow oven chamber was evacuated to 0.06 Torr and then flooded with high purity nitrogen. The heating cycle and TL measurement were recorded with the sample in an atmosphere of flowing high purity nitrogen. The second heating of all samples did not produce a measurable signal other than that attributable to thermal glow of the heating strip.

All TL measurements were made under the following conditions:

- (a) heating rate = 1.23°C/sec,
 - (b) initial temperature = 20°C,
 - (c) final temperature = 460°C,
 - (d) phototube voltage = 1364 volts,
 - (e) photon ratemeter setting = 50KHz for Westmoreland samples,
(this was increased for some samples to keep glow curves on scale).
- = Log scale for Beverley samples.
- (f) ND2 filter between the photomultiplier and the sample,
 - (g) attenuation factor on chart recorder = 256.

Following each TL measurement the disc and sample were weighed accurately on a Mettler H-5 balance. Grains were removed with a tissue and the disc reweighed to calculate the weight of sample. The measured glow peak intensities were then divided by the weight to express the data on a TL/mg basis.

Typical measured glow curves are shown in chapters 3 and 6.

Reproducibility of samples from the same core is $\pm 10\%$ for glow peak intensity and $\pm 5\%$ for glow peak temperatures.

No changes in glow curves were noticed during the 24-72 hour storage period in contrast to Schwartzmann et al. (1983) who found the glow curves of quartz handpicked from granite changed significantly in the 24-72 hour period.

2.6.5 Data Analysis

No kinetic analyses were undertaken. All glow peak parameters used (intensity, glow peak temperature etc) were measured from the glow curve manually and all computations were done manually.

Glow peak temperatures were measured wherever a peak maximum was evident. All curves contained 3, 4, 5 or 6 glow peaks. The height of the curve at each glow peak maximum was regarded as the peak intensity. Measurements of peak height were made with a ruler, i.e. the difference between the peak and the base line. These were divided into low, middle or high temperature peak zones (LT,MT,HT) in accord with the following: below 200°C, LT; between 201°C-300°C, MT and HT above 300°C.

The numerical intensity used in all tabulated results of each glow peak was computed from the following formulae:

$$\text{Intensity} = \frac{x}{150} \times \frac{\text{Scale}}{\text{Weight}}$$

where x = height of the peak in m.m above the base line
 150 = full scale of the chart recorder in m.m.
 scale = setting on photon ratemeter (usually 50,000 Hz)
 weight = weight of sample in mg.

(Dividing by 150 is unnecessary, but this was not realized until after numerous measurements were made).

The percentage of the LT, MT or HT component was calculated, i.e. the intensities of the LT, MT and HT peaks were totalled and then the proportion of LT, MT and HT expressed as a percentage of the total. (If several glow peaks existed within any of the LT, MT or HT zones, then their intensities were averaged when calculating percentages).

Glow peak ratios were calculated simply by dividing the intensities of the relevant peaks. Again, if more than one peak existed in an interval an average intensity was used.

CHAPTER 3

THE APPLICATION OF THERMOLUMINESCENCE TO EXPLORATION
FOR URANIUM IN TERTIARY SANDSTONES

CHAPTER 3: THE APPLICATION OF THERMOLUMINESCENCE TO EXPLORATION
FOR URANIUM IN TERTIARY SANDSTONES

- Summary of Chapter

This chapter applies artificial thermoluminescence (ATL) to quartz from the environs of the Beverley uranium deposits in the Lake Frome Embayment, South Australia. From the theoretically derived quartz ATL glow curves presented in chapter 2, it would be expected that as radiation effects on quartz increase, that low temperature (LT) and middle temperature (MT) glow peaks would progressively decrease whilst the high temperature (HT) glow peak would increase. Samples collected over an eight kilometre traverse from the suspected source of uranium, (Mt. Painter), towards the deposit itself, show a progressive change in glow curve shape consistent with that previously predicted. Glow curves conform to three major overlapping groups: The background group have dominant LT peaks indicative of only low radiation effects and occur nearest to the uraniferous source; The marginal group have glow curves where the LT glow peak has decreased and the MT peak is more prominent - these occur between the suspected source and the deposit; The third group, the ore-type group, show greatly diminished LT and MT glow peaks such that the HT peak is dominant. This group has suffered greater radiation effects than the previous two groups and occurs near to the uranium orebody.

The progressive increase in radiation effects along the transport pathway enables establishment of: (a) the fact that uranium has been mobilized along this route and (b) where an individual sample is likely to be in relation to the orebody. ATL is thus of direct use in exploration for this type of deposit.

The progressive increase in radiation effects along the transport horizon also suggests that, if uranium transport proceeds at an approximately constant rate, then the concentration of uranium must be increasing during transport, i.e. uranium is "snowballing".

Similar studies at the Tertiary Bremer River prospect in South Australia indicated an absence of increasing radiation trends and hence prospectivity for Tertiary roll-front deposits was low.

* * *

3.1 Previous Geological Uses Of Thermoluminescence

Over the last 25-30 years TL has been most commonly used in the field of archaeology as a dating tool for pieces of fired pottery and other native artefacts which have had their TL clocks reset by a heating process at the time of their usage, e.g. camp fires, heat strengthening of tools. The method of age determination has been to use TL to gain a measure of the amount of radiation to which the sample has been exposed, and then knowing both (1) the concentration of radioactive elements present, and (2) their radiation dosage rates, an age for the sample can be determined. A more detailed account of this technique is given in Aitken (1985) and Levy (1974).

In recent years the scope of TL application has widened dramatically such that it can now be used for such diverse things as dating recent ocean floor sediments (Wintle and Huntley, 1980), dating the ice on the polar caps (Zeller 1968), determining the orbital patterns of meteorites (McKeever and Sears 1980) and exploring for geothermal anomalies (Takashima, 1987).

Further geological applications of TL are contained in McDougall (1968) and McKeever (1985).

A number of applications have also been made in exploration geology, i.e. in an attempt to use TL to detect mineral deposits. Some of the earliest workers in this field were McDiarmid (1960, 1963) and McDougall (1964), who concentrated on carbonate hosted lead-zinc deposits observing the variation in natural TL away from mineralized areas. Results, summarized in McDiarmid (1968) were considered discouraging. It was suggested in this summary that future studies involve laboratory radiation techniques, i.e. artificially induced TL. Such a method was employed by Levy et al. (1977) who found that TL intensity irregularly increased from a distance of approximately 100 metres from the orebody to a maximum 6-30 metres from ore and to then decrease sharply to much below background levels in the ore. The maximum was two to ten times higher than the TL intensity within the ore itself. Similar patterns were obtained for curves showing ratios of glow peak intensities vs distance from ore. Curves of glow peak temperature and emission spectrum peak energy (equivalent to the wavelength of light) also showed variations with distance. No further work has been done on the application of TL in lead-zinc exploration and McKeever (1985 p.320) rightly states that the potential has remained undeveloped.

The number of workers using TL as a prospecting tool in uranium exploration has, until recently, been few, perhaps remembering the words of Daniels (1968), "Thermoluminescence was found to be much too sensitive a test for prospecting, because many rocks of very low uranium content give bright thermoluminescence". However it is this brightness and its relative change (i.e. the change in TL intensity) that is useful in uranium exploration. Again, McKeever (op.cit. p.320) concludes that promise has exceeded demonstration in exploration applications of TL.

TL may be used in two ways in uranium exploration. The first relates to the use of TL as a dosimeter. Such usage is only applicable where the total radiation dose does not exceed a radiation dose where

significant sensitization phenomena are observed. (In quartz this is approximately 5×10^5 rad).

The second application uses artificial TL (ATL) and relates to the permanent change in the TL glow curve intensity and shape as described in section 2.5.2. These changes reflect the total or cumulative dose to which the host quartz has been exposed even after the radioactive elements causing this dose have migrated, i.e., having a "memory" (Levy, 1979) for past radiation effects. Herein lies the advantage of TL in uranium exploration over many conventional geochemical techniques which, because they detect only present radiation effects, rely on proximity to mineralization. However, because TL measures cumulative radiation doses it may be able to track pathways of uranium protore movement over a distance of kilometres from the present ore position and also to assess the permanency of radiometric and uranium-related geochemical anomalies by means of determining cumulative radiation effects vs present uranium content. This principle is illustrated in the studies at Beverley (section 3.2) and Bremer River (section 3.3) as well as at Westmoreland in the following chapters.

3.1.1. Previous Uranium Case Histories Utilizing Thermoluminescence

3.1.1.1. A South Texas Roll-Front Type Uranium Deposit.

1) Spirakis et al. (1977) published a report on quartz TL studies of the Tertiary South Texas roll-front type uranium deposits. The geology of this deposit is described by Galloway (1978), Reynolds and Goldhaber (1978) and Goldhaber et al. (1978). Spirakis et al. (op.cit) used the increase of the low temperature (LT) glow peaks towards mineralization as a means of monitoring roll-front positions in the Miocene (20 M.y.) Catahoula Sandstone. The uranium deposit is low grade (up to 0.1% U_3O_8 but more commonly 0.05% U_3O_8) but for the TL study the

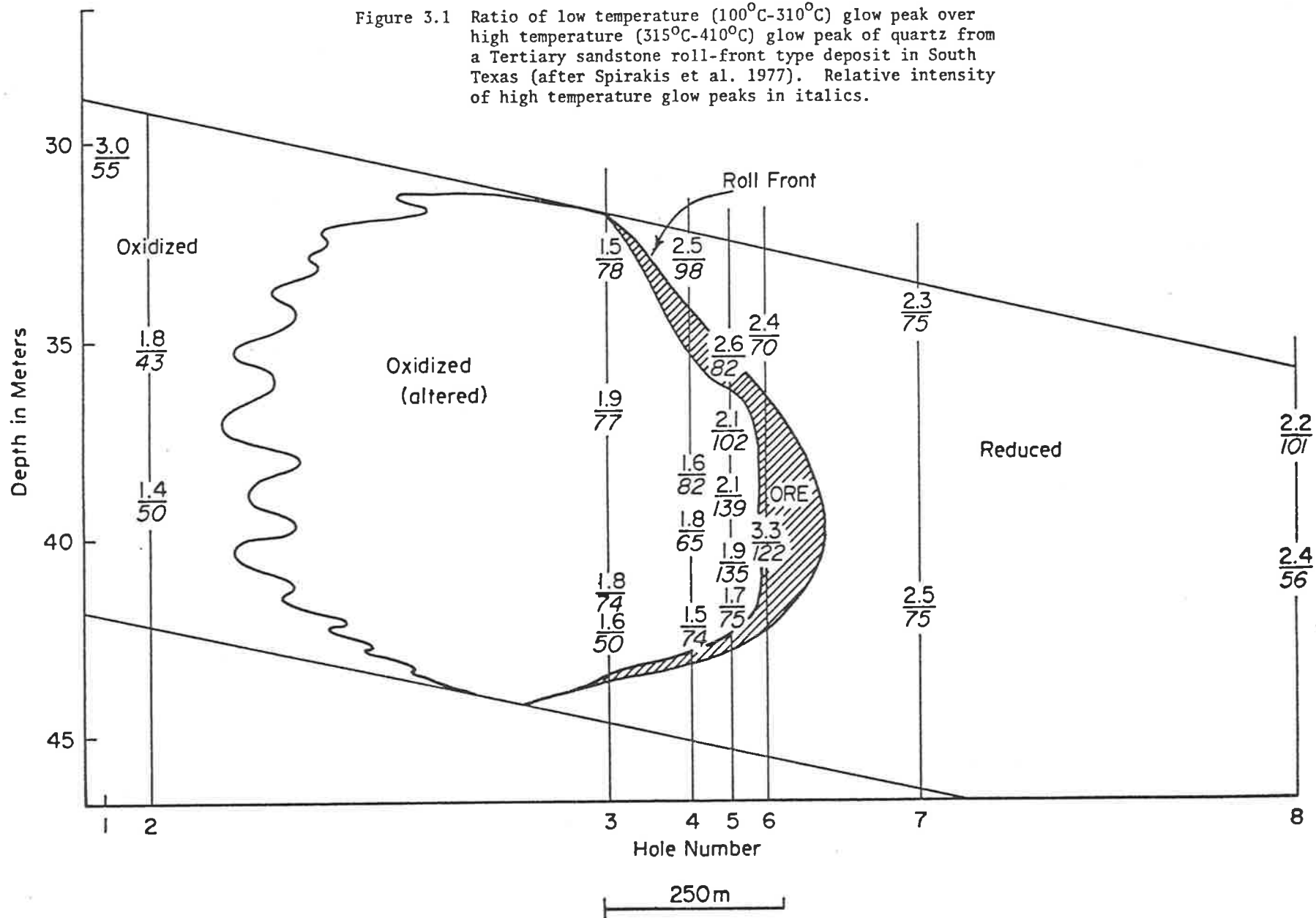
advantage was that ambient temperatures were probably never above 35°C. Their data is contained in figure 3.1. The conclusions that they reached are:

- (a) Total increased TL response in areas through which the roll-front must have passed, e.g. the high values of the high temperature (HT) glow peaks in hole numbers 4, 5 and 6.
- (b) The increase in the LT glow peak over the HT for areas that contain a higher proportion of immobile uranium, e.g. the front of the ore zone and the reduced environments.
- (c) Uraniferous solutions have moved down dip in an oxidized mobile environment. However these uraniferous waters were unable to produce a significant increase in radiation effects, probably due to their inherently low concentrations of 10-100 ppb uranium.
- (d) TL studies measure movement of ore rather than passageways of uraniferous solutions.

3.1.1.2. The "Blaton" Anomaly, Mons, Belgium.

Charlet et al. (1978) conducted a TL study on the Blaton anomaly near Mons (Belgium) where a series of Viséan-Namurian strata (limestones, black shales and cherts) are covered by Tertiary sands. Their studies were concentrated on the sands in an attempt to detect buried uranium mineralization using natural TL. The study succeeded in detecting several new low anomalies (eU:100 ppm at most) located in the Viséan black shales and one in a Cenomanian conglomerate with a palaeochannel shape. Typical TL anomalies using the 280°C glow peak (Charlet's H4 peak) were on the order of 1.5-2 x TL background.

Figure 3.1 Ratio of low temperature (100°C-310°C) glow peak over high temperature (315°C-410°C) glow peak of quartz from a Tertiary sandstone roll-front type deposit in South Texas (after Spirakis et al. 1977). Relative intensity of high temperature glow peaks in italics.



The authors concluded that TL could be used in exploration for uranium mineralization buried at too great a depth to be detected by scintillometer techniques.

3.1.1.3. Ambrosia Lake, U.S.A.

A geological application using quartz as a dosimeter has been undertaken by Hayslip and Renault (1976). They used the intensity of the high temperature peaks (300°C to 410°C) to monitor the U-content of Ambrosia Lake sandstone type uranium deposits, for "grades" of 10 to 100 ppm U. No effect was visible for 10 ppm but an increase to 15 to 20 ppm U triggered a proportional increase in the TL signal. They determined an empirical ratio of $ITL = 0.006 \times \text{ppm U} + 1.16$. It is of interest that their results indicated that U concentrations of less than 10 ppm U had no effect. Yet the age of the Jurassic Morrison Formation (host rock at Ambrosia Lake) and the alleged pene-diagenetic emplacement of the uranium mineralization, leads to the assumption of at least 100 m.y. residence time. One ppm U contributes a radiation dose of 0.312 rads/year to its environment. As such, uranium is the most efficient radiation source (1 ppm Th results in 0.079 rads/year and 1% K₂O in 0.112 rads/year (Levy, 1974)). Most of the radiation dose of uranium derives from alpha radiation. As we are concerned mainly with gamma radiation because of its depth of penetration, it is more appropriate to use a value of 0.1 rad/year for 1 ppm U. A residence time of 100 m.y. and a uranium concentration of 10 ppm would have produced a dose of 10⁸ rads over the lifetime of quartz in the Morrison Formation. This dose in laboratory conditions is sufficient not only to produce a maximal charge of traps but also to alter the number of available traps (see under 2.5.2). It is thus important to keep in mind, that a radiation dose created by 10 ppm U or less under geological conditions, may be below a threshold of charges

retained by the crystal. This threshold value may be the result of annealing of quartz, i.e. remaining at elevated ambient temperatures, which in the case of the Morrison Formation may have been between 80°C - 120°C, (based on a thermal gradient of 2°C/100 metres and a maximum Jurassic cover in the Colorado Plateau of 5000 metres).

3.1.1.4. Narlaby Palaeochannel, Eyre Peninsula, South Australia

Burns (1985) using the artificial TL (ATL) techniques described in Hochman and Ypma (1984a,b - appended), studied uranium movement in the Tertiary Narlaby palaeochannel on the Western Eyre Peninsula, South Australia. He sampled holes over a six kilometre traverse towards areas of known localized mineralization (100-340 ppm U) and discerned three points:

- (a) That there was a decrease in the ATL intensity of the quartz middle temperature glow peak (230°C) towards mineralization and a corresponding increase in the high temperature (350°C) peak percentage (as a function of the sum of low, middle and high temperature peak intensities). This was interpreted to represent a trend of increasing radiation effects.
- (b) that there was a sharp decrease in radiation effects (an increase in the 230°C peak intensity) once past the zone of maximum uranium concentrations, and
- (c) that these effects were detectable by ATL despite the low concentrations of uranium and their short residence times (less than Pliocene age).

Burns (op.cit) thus concluded that ATL studies of quartz could be used in uranium exploration for Tertiary sandstone hosted uranium mineralization.

3.1.1.5 Other Studies

Preliminary work by Spirakis (1979) has shown that the TL of quartz and feldspar grains from soils overlying vein type uranium mineralization in New Mexico, U.S.A. may be useful in locating veins that have been leached of uranium along their outcrops.

Renault (1981) considered a number of influencing parameters (including geological constraints and sample preparation techniques) on the TL of quartz when used in uranium exploration and found that radiation effects due to uranium deposit migration were sufficiently high to obscure TL due to other effects.

Dhana Raja et.al (1984) conducted a natural TL (NTL) study on whole rock samples along a drill-hole through the Singhbhum shear zone, Bular, India. They found that in a given rock type the NTL showed a marked increase over a known radioactive horizon and concluded that similar increases could be helpful in localizing radioactive ore bodies. Their NTL anomalies however, closely mimiced the existing radiometric haloes and thus did not demonstrate any significant advantage of TL over radiometric techniques.

Other previous uses of TL in assessing radiometric anomalies may be found in a review by Sankaran et al. (1983).

3.2 The Beverley Uranium Deposit, Frome Embayment, South Australia

3.2.1 Introduction to the Geology and Genesis of Tertiary "Roll Front" Uranium Deposits.

Sandstone-hosted uranium deposits (commonly of Tertiary age) have been well studied and constitute a major present source of U. These deposits are well known in the western U.S.A. and in Africa, and in recent years a growing number have been found in Australia. These

include Beverley (Haynes, 1976). Honeymoon (Brunt, 1978), those of the Billeroo Channel (Ellis, 1980) and those of the Narlaby Palaeochannel (Binks and Hooper, 1984). All of these occur in the state of South Australia, being in reasonably close proximity to different Middle Proterozoic granitoid and metamorphic basement complexes.

The genesis of sandstone-hosted U deposits has, in general, been well studied - particularly those of the western U.S.A. It is generally agreed that such deposits form by precipitation of U from oxidizing groundwaters upon encountering reduced environments which may contain pyrite, carbonaceous materials or other reductants. As such orebodies usually represent an addition of <1% to the host rock (Rackley, 1976), there are few mineralogical effects noticeable on the host rock e.g. addition of some epigenetic minerals. Rackley (1976) consequently suggests that the means of recognition of alteration within such a geochemical cell deserves more research.

Although it is generally agreed that U is transported in oxidizing ground waters down a hydrodynamic gradient within a semi-confined aquifer, there has been comparatively little work done, demonstrating the accretionary migration or "snowballing" of uranium protore movement. Previous works of this kind include the equilibrium/disequilibrium studies of Rosholt (1961), Robinson and Rosholt (1961) and more recently Ludwig et al. (1982).

The Beverley uranium deposit in the Frome Embayment, South Australia has been likened to sandstone roll front type deposits in the western U.S.A. It provides a suitable example to study both the uranium exploration applications of ATL and the "snowballing" movement of uranium by means of assessing cumulative radiation effects.

3.2.2 Geology of the Beverley Uranium Deposit

The Beverley U deposit occurs in the Tertiary Frome Embayment to the east of the Mount Painter Block, north of the Olary Ranges and west of the Barrier Ranges - all of Middle Proterozoic age. Callen (1975) describes the Frome Embayment as a lobe in the extensive Great Arterian Basin of northern Australia formed during Early Jurassic times. Its present configuration is the result of Late Tertiary and Quaternary tectonic events.

Spatially, the Beverley U deposit is closest to the Mt. Painter basement - a complex consisting of metamorphosed sediments (the Radium Creek Metamorphics), a suite of "older granites" dated as Carpentarian (1600 M.yr.), Late Proterozoic sediments and basic volcanics, and a suite of younger granites intruded during the Ordovician. Both suites of granites have higher than background radioactive element contents. Blight (1977) reports U contents up to 22 ppm for some of the granitoids of the "younger granite" suite.

Within the Frome Embayment, Precambrian basement is overlain by folded Cambrian redbeds and limestones, Jurassic fluviatile sediments, transgressive marine Cretaceous beds and later by regressive non-marine units. Callen (1976) has broadly divided the overlying Tertiary into two units: (1) the Palaeocene-Eocene Eyre Formation; and (2) Oligocene-Miocene sands, silts, carbonaceous and non-carbonaceous clays and some carbonates. U occurrences are known within Palaeocene medium- to coarse-grained sands, Eocene medium- to coarse-grained sands and silts to fine-grained sands, and in Miocene medium- to coarse-grained sands, carbonaceous in part with occasional pebbles.

Within the Beverley region, U mineralization occurs in sand lenses within fine unconsolidated argillaceous sediments of Miocene age overlying thin carbonaceous clays. These unconformably overlie

Cretaceous shales and sandstones which directly overlie the Precambrian basement. The Miocene sediments are overlain by possible Pleistocene argillaceous and occasional clastic sediments with some boulder beds.

The orebody consists of very finely divided uraninite absorbed on clay within a series of north-south-trending sands at an oxidation-reduction interface with the underlying carbonaceous clays (Haynes, 1976). U values occasionally extend into the underlying carbonaceous clays. Total reserves are estimated at 15,800 tonnes U_3O_8 at a recoverable grade of 0.24% U_3O_8 .

3.2.3 Results

The exploration model by the Oilmin N.L., Transoil N.L. and Petromin N.L. group was based on the premise that uplift of the uraniferous Mt. Painter Block established a hydraulic head driving uranium-bearing solutions into the sedimentary pediment of the Lake Frome embayment. Drilling started close to the Mt. Painter area and proceeded eastward along creek beds, under the assumption that Tertiary channels had similar locations.

Samples for a TL study were collected from a series of drill holes extending away from the Mt. Painter basement towards the Beverley orebody, and from other holes around the orebody. Location of Beverley is contained in figure 3.2 and of the drill holes sampled in figure 3.3. Note in figure 3.3 that holes with the same prefix, e.g. 39, 39A, 39A56W etc. indicate holes drilled close to hole 39.

Three samples were collected from each hole - one from the arenaceous formation hosting the mineralization and one each from the intervals 10 metres above and 10 metres below this unit. Experimental procedure was as described in chapter 2.6. Approximately 100 samples were measured in total.

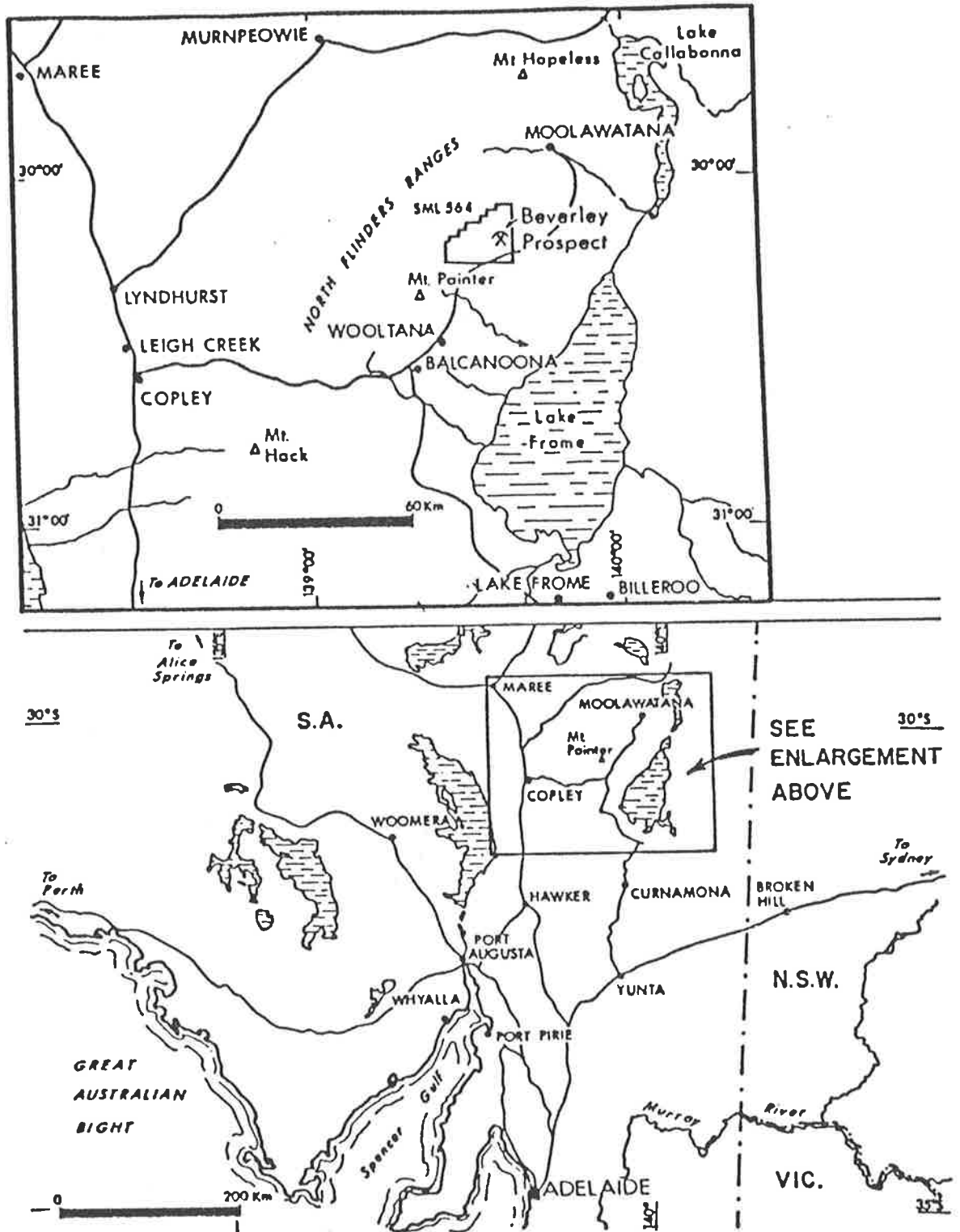


Figure 3.2 Location of the Beverley uranium deposit, South Australia (after Haynes, 1975).

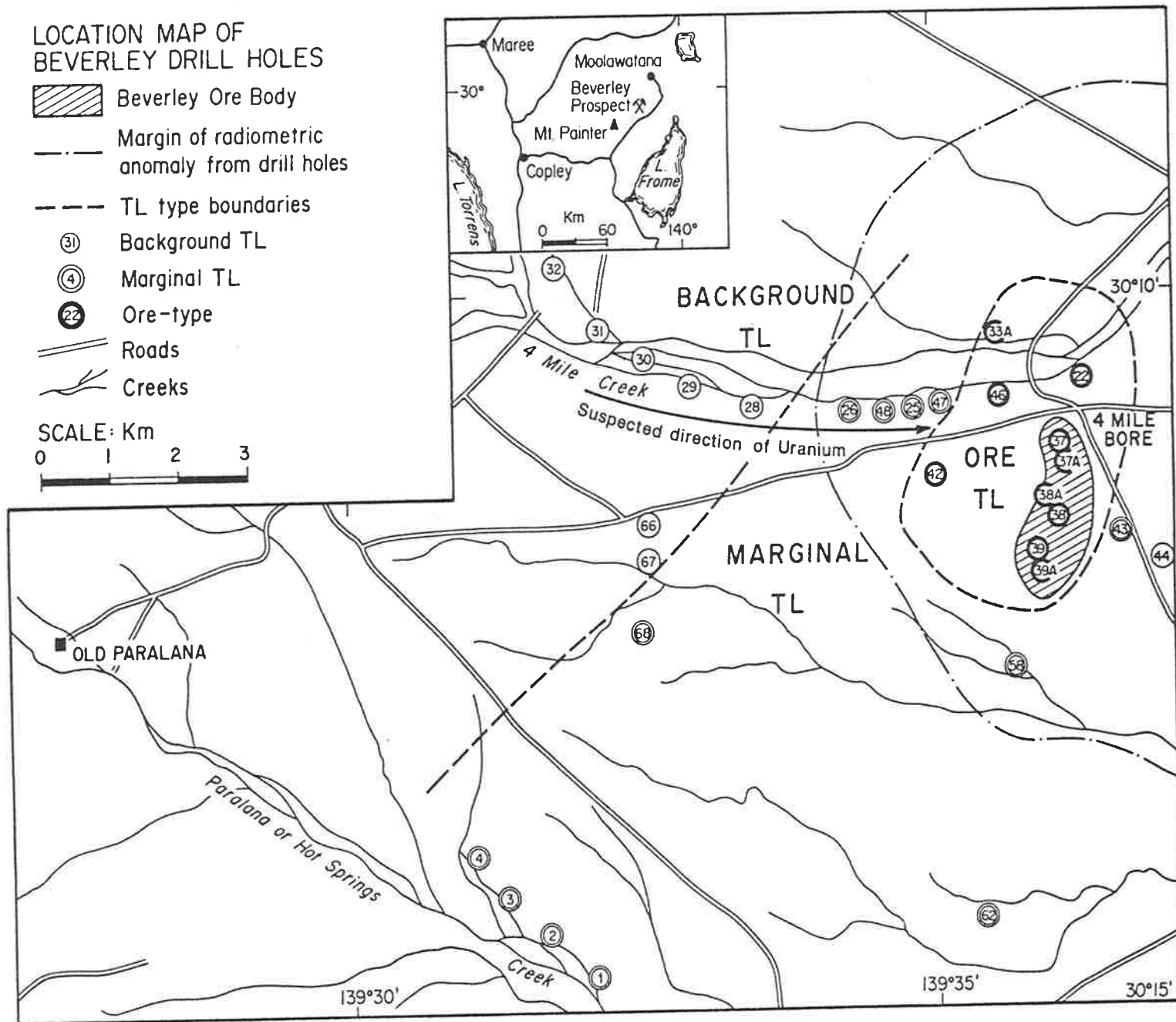


Figure 3.3 Beverley drill hole locations showing zones of background, marginal and ore-type quartz TL glow curves.

ATL results for the ore horizon are shown in figure 3.3 and 3.4. Results for samples 10 metres above the ore horizon are plotted in figure 3.5 and 10 metres below the ore horizon in figure 3.6.

Figures 3.3 and 3.4 indicate a progressive increase in radiation effects in the ore horizon upon approaching the ore body with data fitting into three main categories:

- (a) Background TL (up-stream of the orebody). Samples in this group show few radiation effects. A typical glow curve is illustrated in Fig. 3.7 which can be compared with the experimentally derived Fig. 2.34(b); i.e. a large LT glow peak which obscures the MT and HT glow peaks. Such a glow curve is the common one for unsensitized sands in the Lake Frome Embayment.
- (b) Marginal TL (further downstream though not in close proximity to the orebody and occupying a very large territory in Fig. 3.3). TL glow curves in this group are generally similar to those in Fig. 2.34(c) and (d). A typical glow curve in the marginal TL group is shown in Fig. 3.8 with a reduced LT and MT glow peak intensity. Proportionately the LT glow peak has decreased more than the MT glow peak.
- (c) Ore-type TL (within close proximity to the orebody). These glow curves are similar to those in Fig. 2.34(d) and (e) - more particularly Fig. 2.34(e). A typical glow curve from this category at Beverley is contained in Fig. 3.9. It shows even more reduction in the LT and MT glow peaks than in the marginal zone and also a corresponding increase in the HT glow peak.

Along Four Mile Creek eastwards towards the orebody there is a gradual increase in radiation effects and TL glow curves in the ore transport horizon from background to marginal to ore-type. Beyond the ore body (holes 43 and 44) TL glow curves return quickly to background.

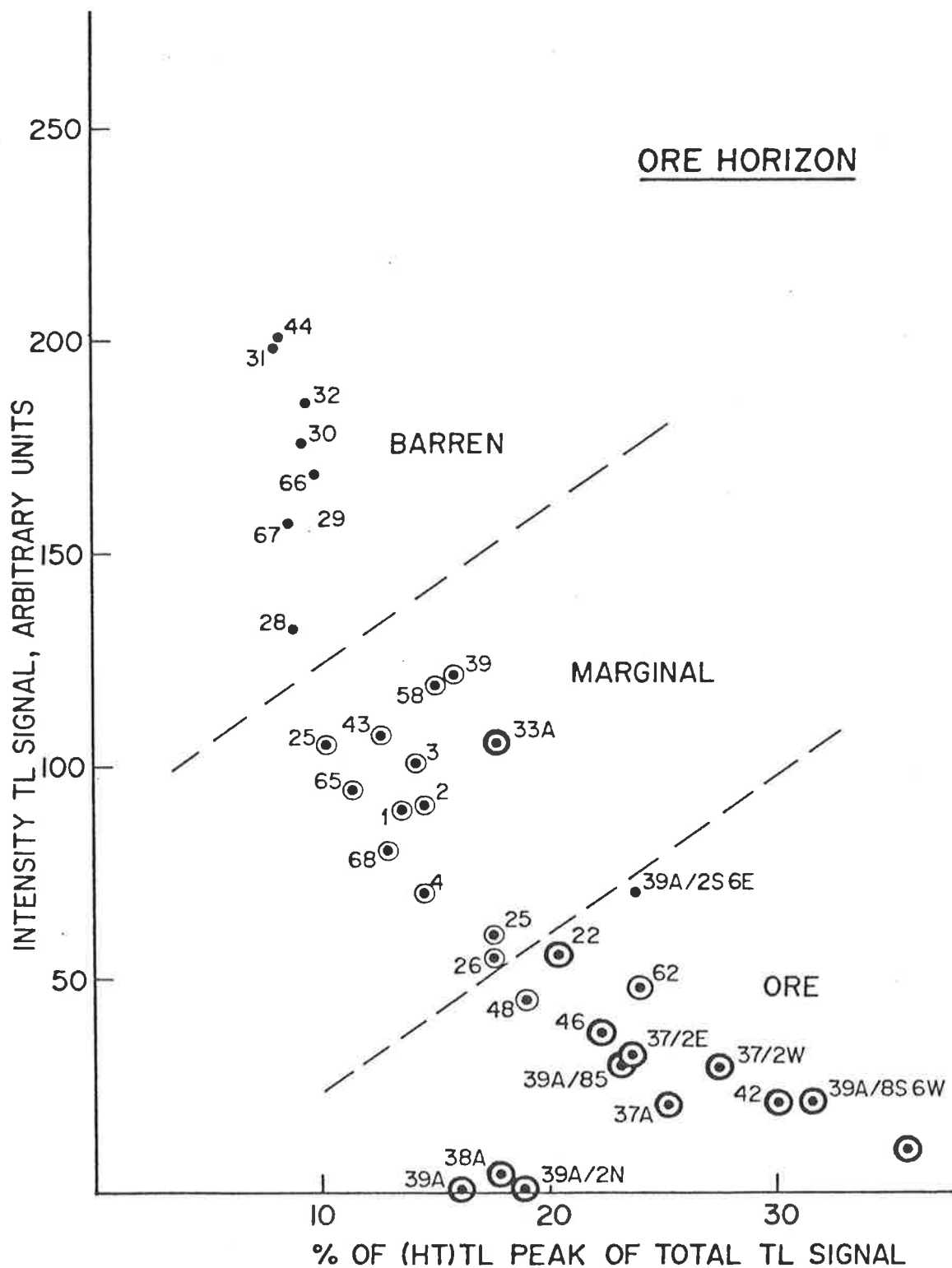


Figure 3.4 The change in quartz LT peak intensity and HT peak percentage in samples from the ore transport horizon in the Beverley region.

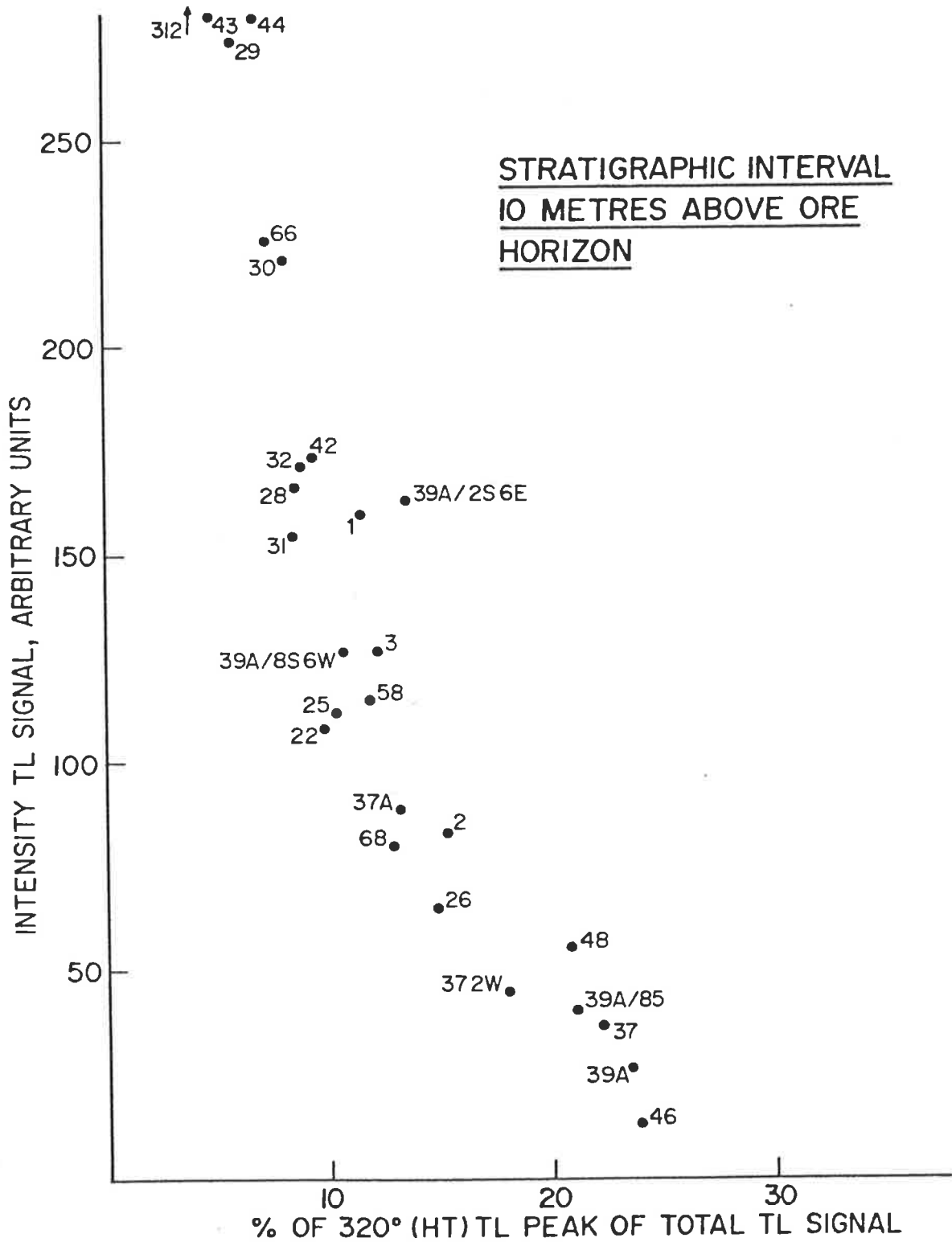


Figure 3.5 Change in quartz TL for samples from the Beverley region taken 10 metres stratigraphically above the ore transport horizon.

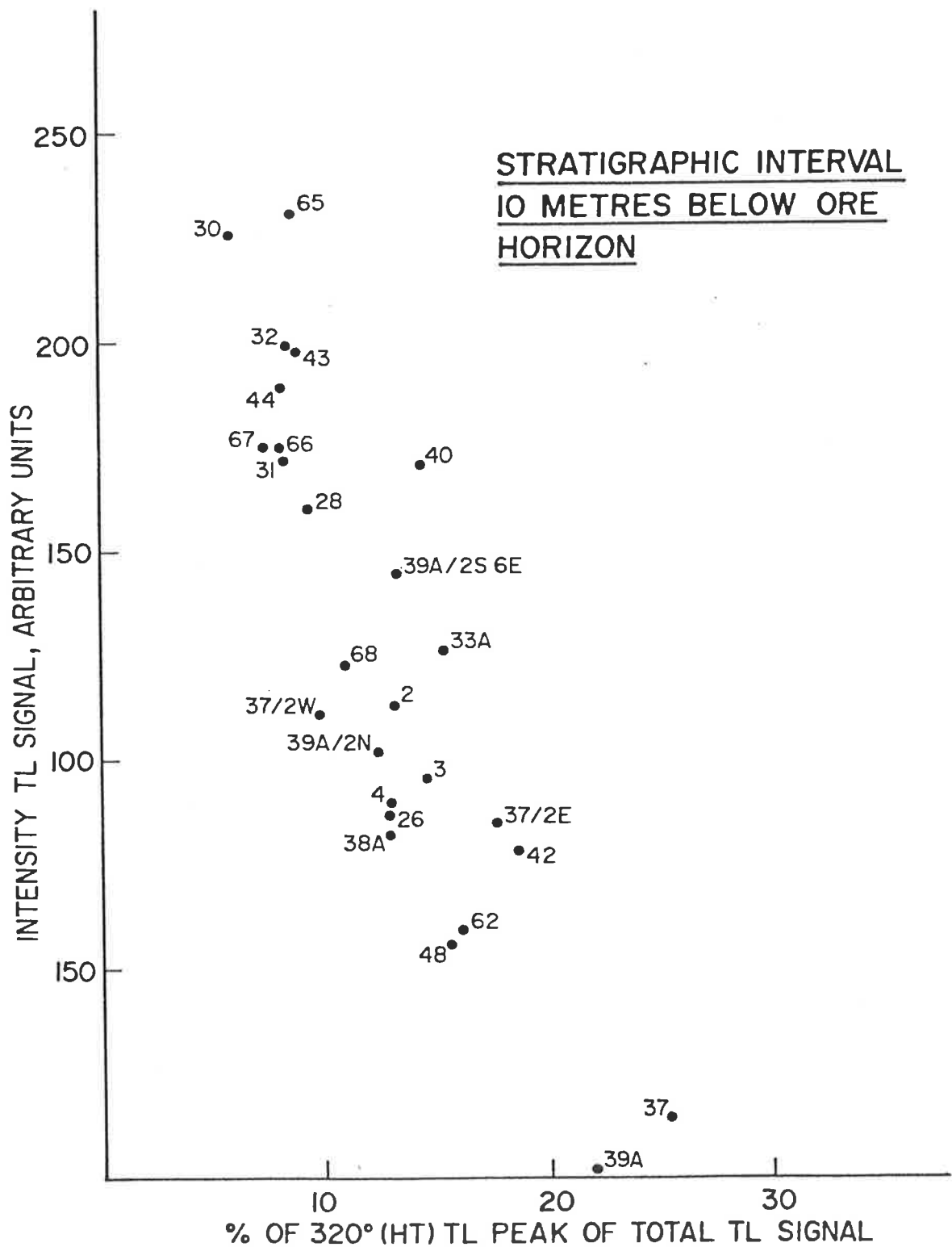


Figure 3.6 Change in quartz TL for samples from the Beverley region taken 10 metres stratigraphically below the ore transport horizon.

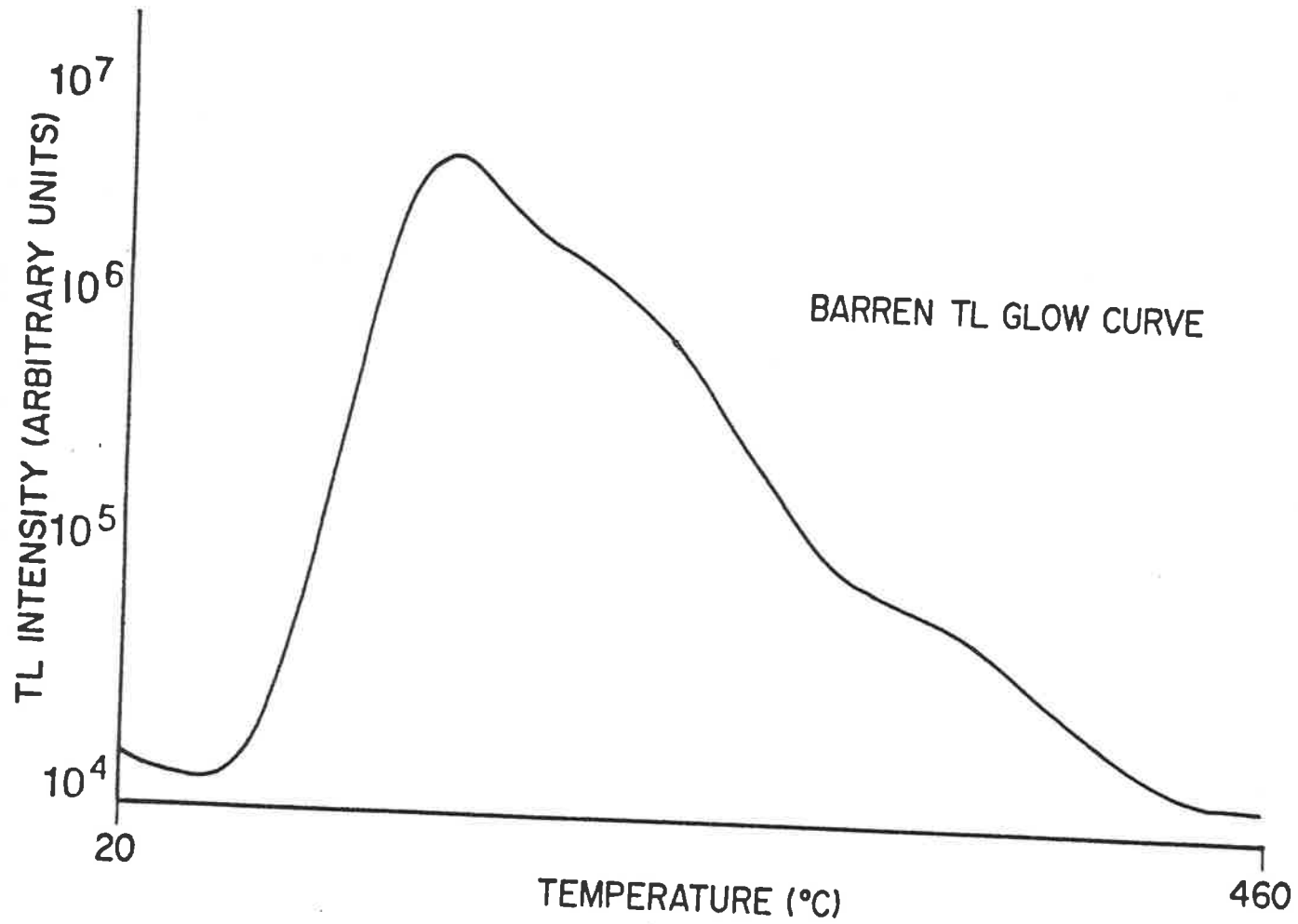


Figure 3.7 Typical TL glow curve for quartz from the background zone at Beverley.

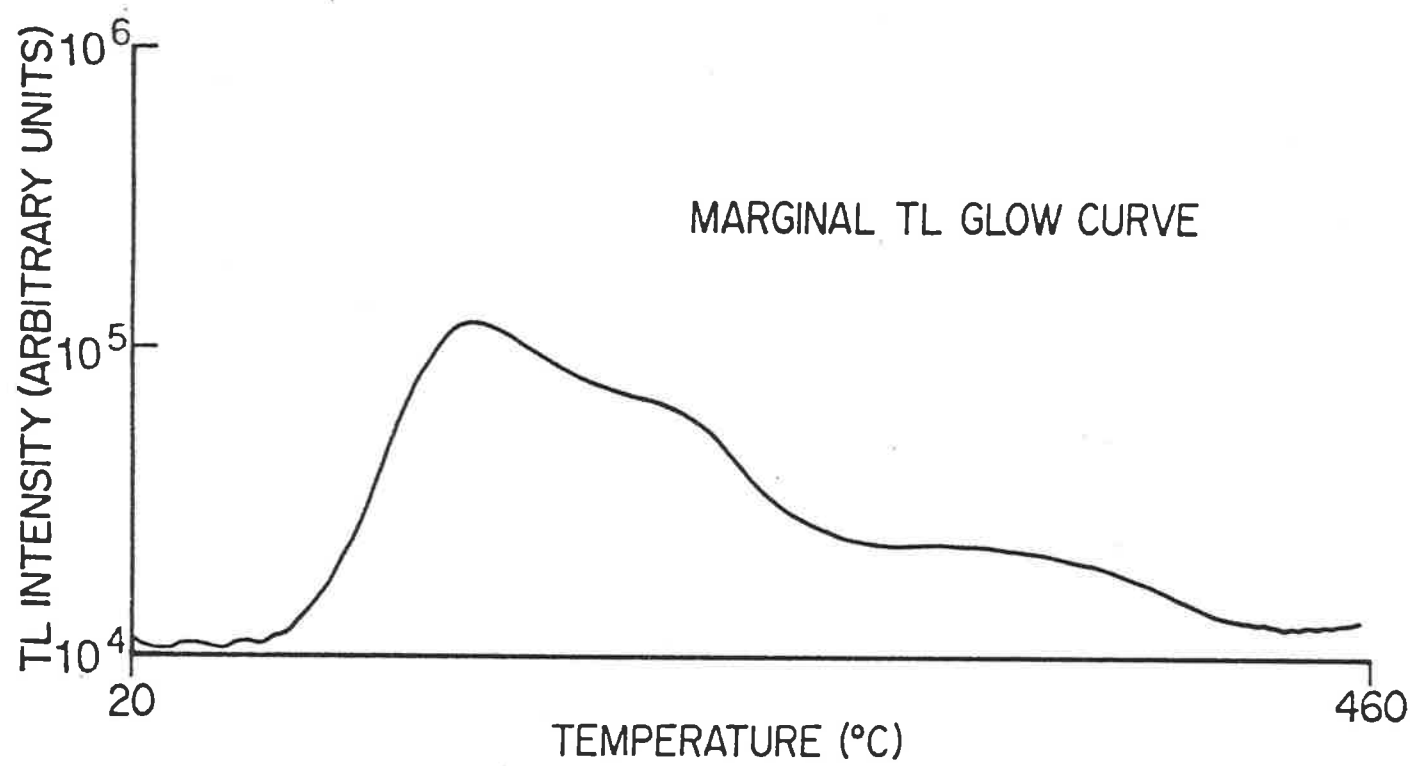


Figure 3.8 Typical TL glow curve for quartz from the marginal TL zone at Beverley.

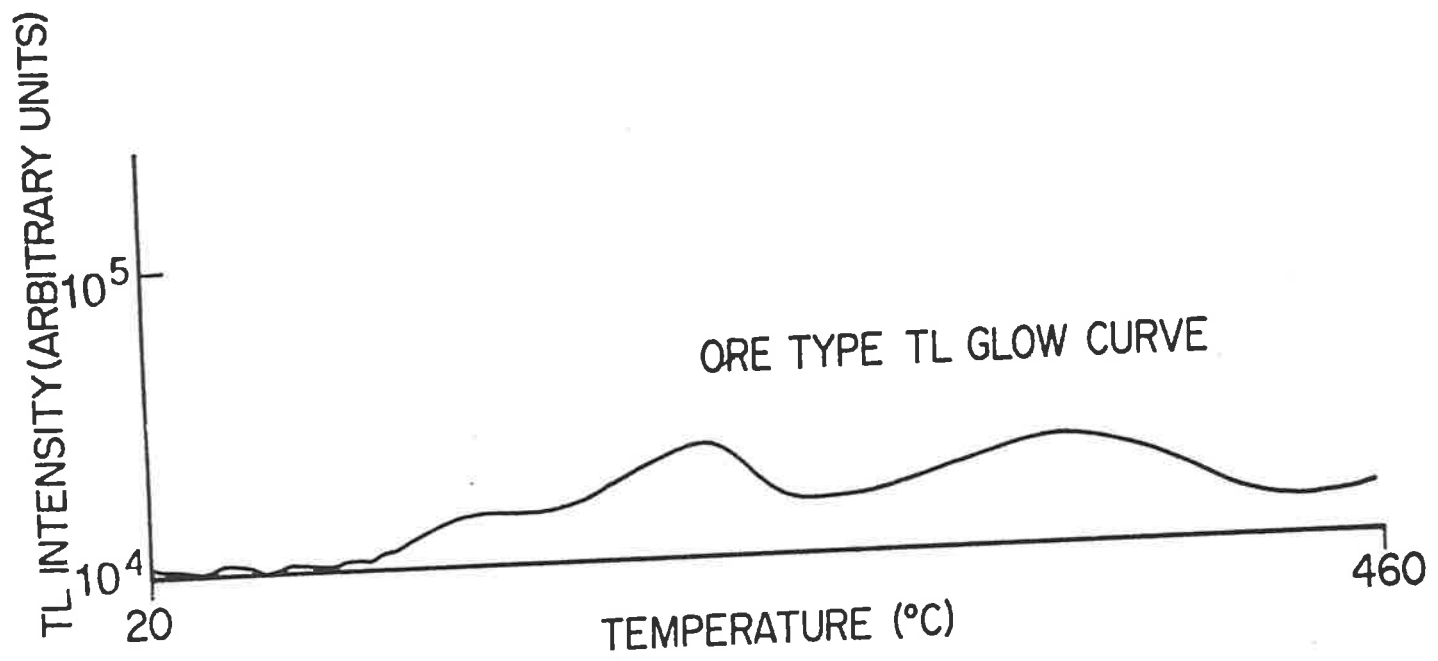


Figure 3.9 Typical TL glow curve for quartz from the ore-type TL zone at Beverley.

Samples taken from the stratigraphic interval, 10m above the ore horizon show a similar trend of increasing radiation effects towards Beverley, though the overall radiation effects are less than for the ore horizon. This is illustrated in that samples from any given drill hole, in this interval show less radiation effects than their corresponding samples from the ore horizon. This is particularly noticeable for some samples within the orebody, where the samples 10m above the ore horizon plot in the marginal, rather than ore-type TL categories, e.g. 39A/2S6E and 39A/8S6W.

Samples taken from 10m below the ore horizon show even less radiation effects again. A progressive increase in radiation effects is still discernible along this horizon with samples from particular drill holes again showing less sensitization than their corresponding samples from the ore horizon.

3.2.4 Uranium Exploration Implications of Thermoluminescence from the Beverley Results

Recognition of the degree of cumulative radiation damage has important implications in exploration for such deposits.

The Beverley orebody has no surface geochemical or radiometric anomaly. The radiometric anomaly indicated in Fig. 3.3 is subsurface. Comparison of the marginal TL zone incorporating holes 1-4, 62, 58 and 68, as well as non-mineralized holes along Four Mile Creek, has enlarged the secondary target zone far beyond that of the radiometric halo - it may possibly even be too large. However, even within the marginal TL zone, holes closer to the ore zone (though still 3km distant) such as 26, 48 and 25 show greater radiation effects than holes further away within this halo such as 58, 68 and 62.

Within the marginal TL zone is the ore-type TL halo (where all glow curves essentially conform to Fig. 2.34(d)-(e). A significant point is that some holes within this zone (42, 22, 46, 33A) contain no U mineralization yet still have TL glow curves as expected for mineralized samples. Thus recognition of such TL glow curves despite discouraging geochemical results would have indicated not only the presence of U mineralization but also proximity to such mineralization. From Fig. 3.3 it can also be noted that this zone of "mineralized" ore-type TL is four to five times larger than the orebody itself and thus has enlarged the primary target zone.

Probably the most useful observation from the point of view of uranium exploration is that along Four Mile Creek (the suspected loci for uranium transport) a trend of increasing radiation effects is seen over a distance of eight kilometres from Mt. Painter in the west, eastward towards the orebody. This trend is best portrayed in figure 3.4. Therefore, TL measurements from drill holes along Four Mile Creek during exploration, would have indicated an increasing trend of radiation effects to the east. Such recognition could give confidence for further drilling along Four Mile Creek.

This can be contrasted with results from Paralana Creek to the south, where holes 1, 2, 3 and 4 were drilled over a distance of 2.5 kilometres and where there is little or no change in radiation effects. This is in contrast to those holes drilled along Four Mile Creek where there is a progressive change in radiation effects, as illustrated in figure 3.4. Notwithstanding the benefits of hindsight, TL measurements at an early stage of drilling would have confirmed the existence of increasing radiation effects in Four Mile Creek as opposed to Paralana Creek and thus may have reduced the amount of exploratory drilling needed.

3.2.5 Genesis of the Beverley Deposit - Source of the Uranium

TL may also be used to give some evidence regarding the source of U for the Beverley deposit.

For Tertiary sandstone-type deposits in general, three principal ideas exist regarding U sources:

- (a) leaching of U from a granitic hinterland at some time after sediment deposition (Harshman, 1972);
- (b) leaching of U from within the original host sandstone or arkose (Shockey et al., 1968); and
- (c) derivation from devitrified or leached volcanic debris, tuffs and flows within or overlying the host rock (Davis, 1969). Many authors including the above acknowledge that combinations of the above possibilities may occur and that different mechanisms and sources are applicable for different deposits.

In the case of the Beverley deposit the possibility of leaching of an interbedded volcanic source can be ruled out because of the absence of such volcanic interbeds. Further, Callen (1976) reports clay mineralogy as montmorillonite rather than tuffaceous bentonite as is commonly found in the United States deposits. No volcanic quartz or glass shards have been found.

It is also unlikely that the U has been derived from within the sandstone as the sandstone layers are thin and could not have supplied the necessary volume of U. Further to this, the TL data for samples 10m above and below the host unit, and also from the host unit itself downdip of the orebody, all indicated the non-sensitized nature of the sandstone and hence its low inherent U content.

Modern groundwater draining the Mt. Painter granitic basement is rich in U and the dating of U within the basement indicates mobilization within the last 1 Myr. (Callen, 1976). Further to this, as mentioned

previously, granites of the Mt. Painter province are enriched in uranium.

When accompanied with the TL data indicating the progressive increase in radiation effects eastwards away from the Mt. Painter basement, it seems likely that, in the case of the Beverley deposit, uranium has been derived by leaching of the uraniferous Mt. Painter basement rocks.

3.2.6 Genesis of the Beverley Deposit - The Accretionary Movement of Uranium

The degree of radiation effects when considering (1) the threshold effect of U needed to initiate radiation effects; and (2) the young age of the deposit, suggests that the marginal TL type is due to actual U mineralization (i.e. protore) which has been displaced downdip by oxidizing U-bearing solutions. The U content expected in such solutions (100-1000 ppb) is too low to have produced the radiation damage observed.

Studies by Hayslip and Renault (1976) (chapter 3.1.3) found that under geological conditions (as opposed to laboratory conditions) a threshold of 10ppm U for a +100 Ma old deposit was needed to initiate TL in the HT glow peak. This suggests that the marginal TL type may be due to U concentrations greater than 10ppm. The fact that many, if not most, of the drill holes in this region currently contain less than 10ppm U indicates that the U has moved, and illustrates the usefulness of the TL technique in measuring past, as well as present radiation effects.

As the radiation damage is due to displacement of uranium protore, then the progressive increase in the radiation effects, observed over a distance of 8km eastwards towards the orebody, is consistent with the accretionary or "snowballing" concentration of U during transport. In fact these results actually suggest such a concentration mechanism for U. If the period of time for which the U has remained in each spot during

transport is approximately constant, then the increase in radiation effects can only be due to increasing concentrations of U. That is, as TL measures cumulative radiation effects - (time) x (concentration) - and if time has been approximately the same for each point in the migratory pathway, then concentration of U must be increasing in order to explain the increasing radiation effects observed, i.e. the uranium is accreting or "snowballing" during transport.

That such an increase in radiation effects is not merely a function of proximity to mineralization is obvious by the rapid return to background TL, or non-radiation damaged levels, beyond the orebody. For example, hole 43 ~ 500m east of the orebody (downdip) has only marginal TL, and hole 44 ~ 1000m east of the orebody has background TL. Holes a similar distance west of the orebody (updip), e.g. 42 and 46, show far more radiation effects.

The lesser radiation effects in horizons 10m above and below the ore horizon in some cases even within the ore body - indicate that transport and accretionary movement has been more or less confined to one stratigraphic horizon. This indicates that during a U exploration programme it may be just as necessary to identify the correct stratigraphy for U transport as it is to identify the correct geographical region.

3.3 Bremer River Prospect, South Australia

An opportunity to utilize TL in the exploration program for roll front type uranium deposits was provided by CRA Exploration in E.L. 547, Bremer River, South Australia (Andrews, 1980). Water sampling within the exploration lease had indicated variable values of uranium in groundwater with a possible oxidation front. However, contamination of water bores as a result of organic materials led to difficulty in assessing the

hydrogeochemical results, i.e. whether spot high uranium values were due to the scavenging effect of recent decaying organic material rather than truly reflecting anomalous uranium concentrations. For this purpose, it was felt that a knowledge of the past presence or absence of uranium would be useful and hence a TL study was undertaken to determine:

- (1) whether there was any evidence of anomalous uranium/protore within the exploration lease;
- (2) whether there was evidence of a roll front uranium situation which had resulted in radiation effects to the host rock and
- (3) whether any particular stratigraphic horizon appeared more prospective than others.

3.3.1 Geological Setting of the Bremer River Exploration Lease

The TL study was conducted in the Bremer River Basin, South Australia. Samples were collected from carbonaceous sands and clays of Oligocene-Eocene age informally named the "Continental Group". This target horizon is overlain by the Early to Middle Oligocene Ettrick Formation, the Miocene Mannum Formation and the late Pliocene Parilla sands. It is underlain by Cambrian quartzites and micaceous schists of the Kanmantoo Group which constitute basement.

Basement outcrops as part of the Adelaide Hills to the northwest of the basin and the Tertiary cover units increase in thickness to the south-east way from the outcropping basement thus confirming the basinal nature of the region. The approximate limit of the Kanmantoo Group is shown in the northwest of figure 3.10.

Possible sources for uranium were thought to include acidic tuffaceous members near the Nairne Pyrite Horizon and quartzites of the uppermost units of the Cambrian Kanmantoo Group. Background uranium values within the basement were generally low (less than 4ppm) with spot

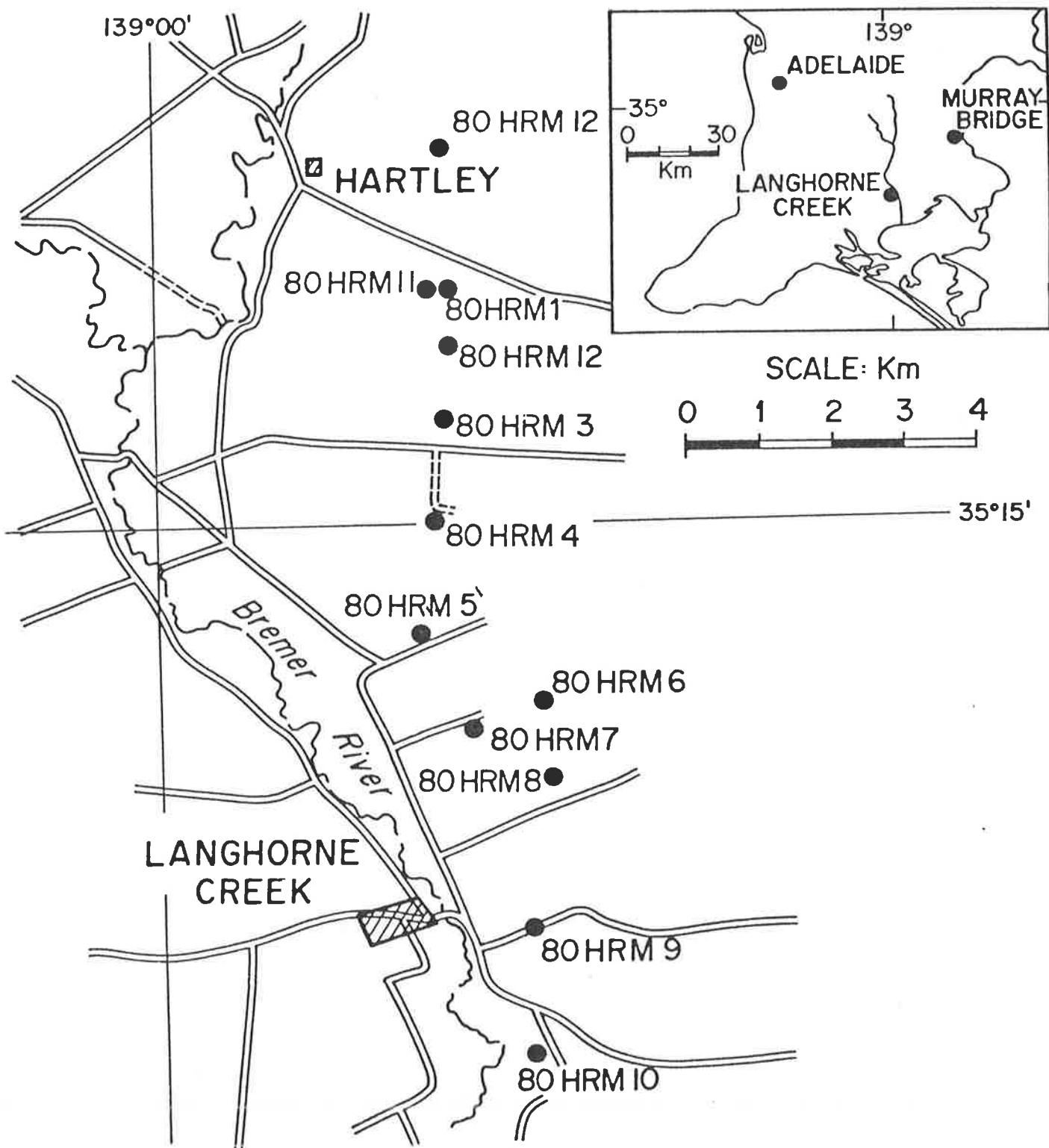


Figure 3.10 Location of the Bremer River prospect, South Australia.

values up to 30 ppm, thus necessitating scavenging of a large drainage area to accumulate appreciable quantities of uranium.

3.3.2 Results

Approximately 100 samples were analyzed from rotary drill holes designed to test the possibility of a mobile uranium front. Their locations are shown in figure 3.10. A summary of results is contained in figure 3.11 from raw data contained in Hochman (1981).

Since many samples were in the sensitization stage of TL (glow curves as in figure 2.34c) the principal methods employed involved studying variations in the intensity of the low temperature glow peak (LT) and in the high temperature to low temperature glow peak ratio (HT/LT) along the line of drill holes extending away from the basement. Since at this stage of radiation sensitization the LT glow peak will be decreasing and the HT glow peak will be increasing, increasing radiation effects should be reflected by a decrease in the LT glow peak intensity and an increase in the HT/LT glow peak ratio.

Figure 3.11 portrays results from two stratigraphic levels:

(1) from samples taken up to six metres below the limestone of the Mannum Formation and (2) from a fluvial channel sequence 20-34 metres below the limestone base. The latter area corresponds to the "Continental Group". Figure 3.11(a) shows little systematic variation in either of the TL parameters implying that no significant uranium concentrations have resided in this stratigraphic interval. Figure 3.11(b) indicates that the LT glow peak intensity is least and the HT/LT glow peak ratio at a maximum in holes 80HRM 12 and 11, implying greatest sensitization has occurred in this region.

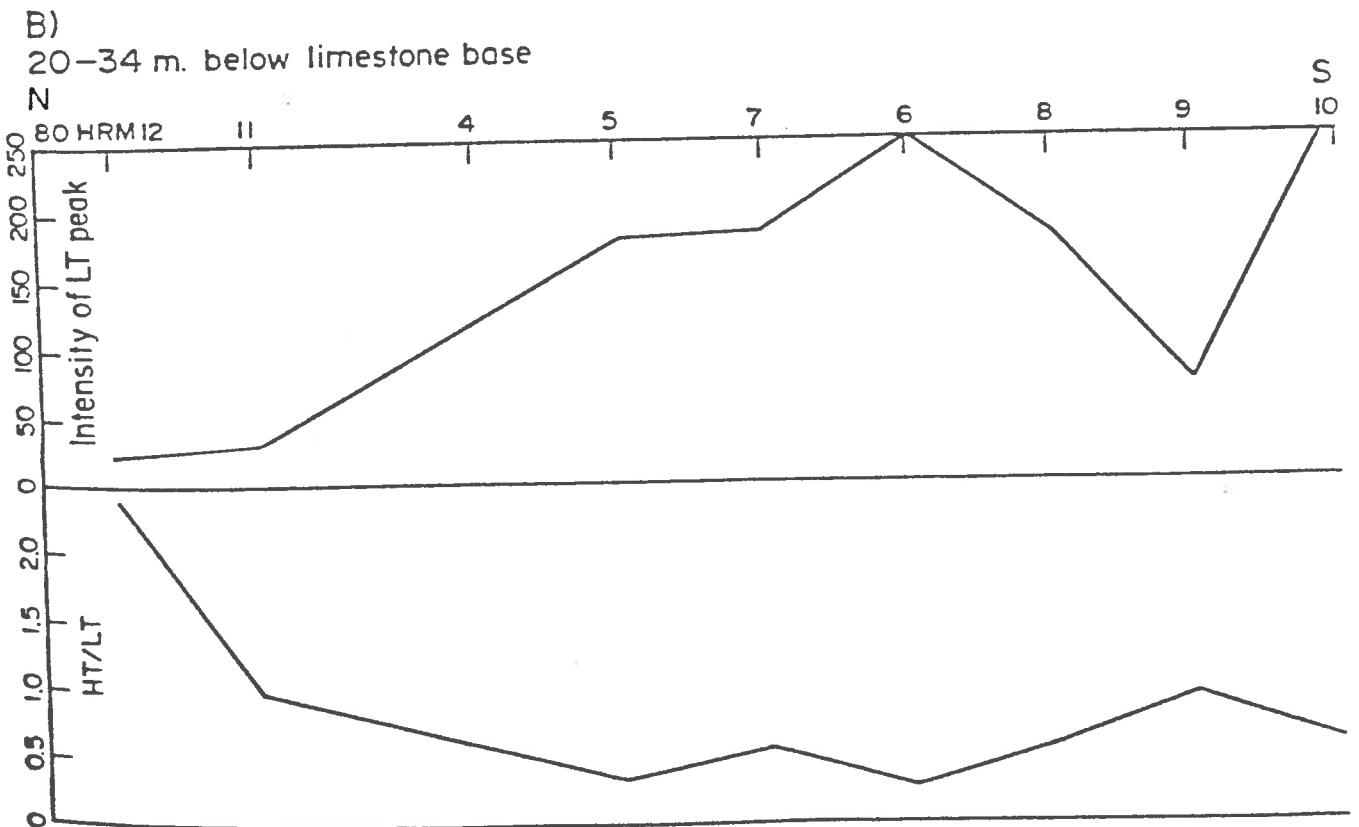
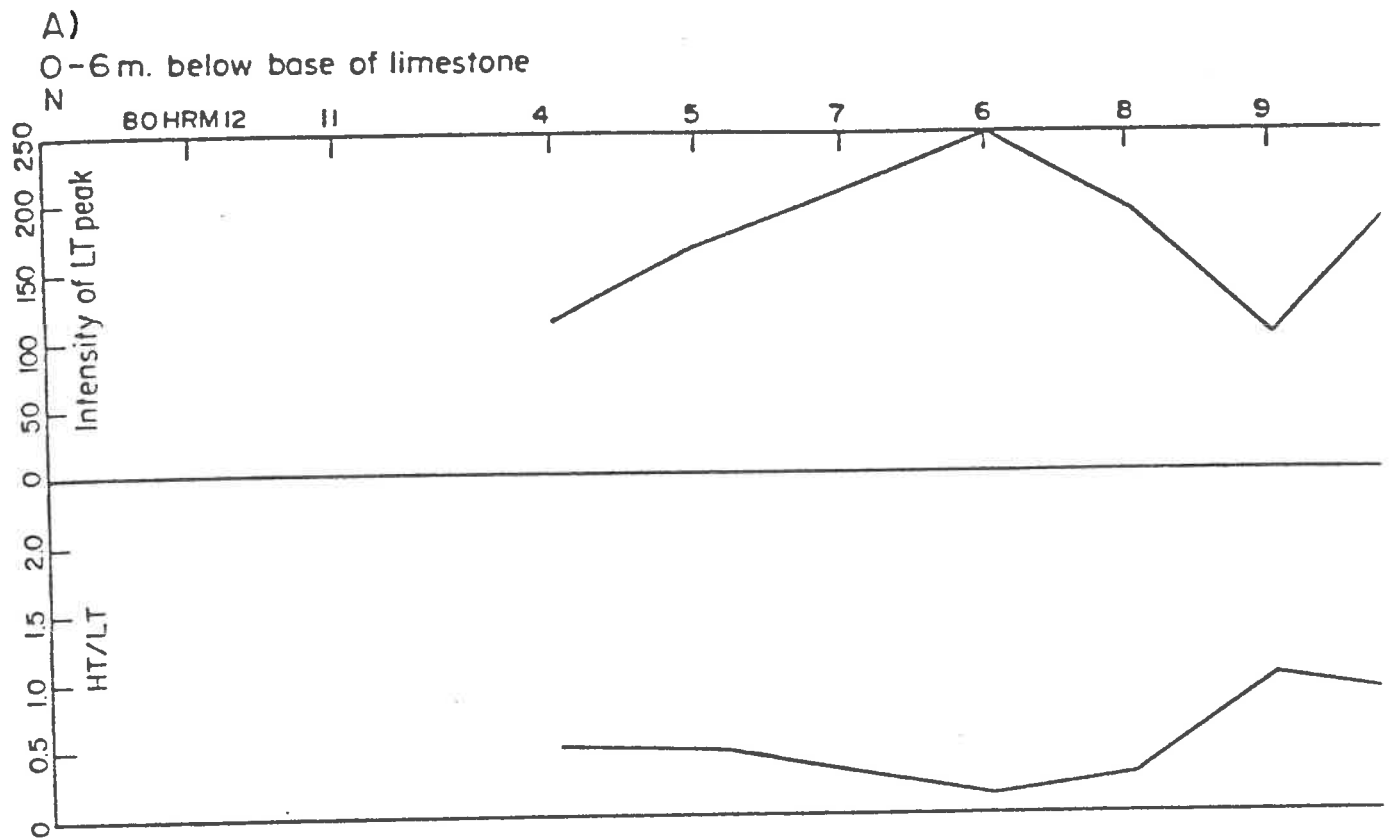


Figure 3.11 Bremer River data examining variations in quartz glow peak intensities and ratios for different stratigraphic levels within the "Continental Group".

Apart from these anomalies the rest of the fluviatile channel sands showed no more sensitization than any other stratigraphic interval sampled within the "Continental Group".

3.3.3 Discussion

The lack of radiation effects through holes 80HRM 4-10 and lack of any systematic change in radiation effects in these same holes, indicated that there had not been substantial uranium protore movement, in the form of a snowballing roll front, through these strata.

Holes 80HRM 12 and 11 which had shown radiation sensitization were drilled adjacent to the basement on the basin margin and hence intersected the thinnest limestone cover and thinnest fluviatile channel sands. These anomalies may possibly be explained by their proximity to basement i.e. local concentrations leached from the basement into the immediately adjacent sediments.

On the basis of the above two points, coupled with the hydrogeochemical and other results, the potential for economic uranium accumulations within the basin was considered remote and hence the recommendation could be made to the company concerned to relinquish this exploration lease without the need for further exploratory drilling.

3.4 Conclusions on the Use of Thermoluminescence in Exploration for Tertiary Sandstone Hosted Uranium Deposits

The examples utilizing artificial TL and the change in glow curve shape due to radiation in sections 3.2 and 3.3, suggest that TL is useful in uranium exploration for this type of deposit for the following reasons:

- (1) TL has detected an eastward trend of increasing radiation sensitization in the Frome Embayment which may be related to an eastward moving mobile orefront. This trend is visible along the Four Mile Creek over a distance of some eight kilometres despite the absence of any associated geochemical or radiometric anomalies
- (2) The zone of marginal TL around the Beverley orebody is larger than the subsurface radiometric halo.
- (3) The zone of "ore type" TL immediately surrounding the orebody is four to five times larger than the orebody itself even though some holes within this halo have little or no uranium. Thus recognition of an "ore type" TL glow curve expanded the target of uranium mineralization.
- (4) TL does detect areas of past uranium concentrations (as well as present concentrations) as evidenced by the areas immediately west of the Beverley orebody. Thus Levy's (1979) conclusion of quartz "remembering" exposure to past radiation has been confirmed under geological conditions.
- (5) TL is useful in helping to determine the prospectivity or unsuitability of an area for economic uranium accumulation as illustrated at Bremer River and may, therefore, be useful in terms of area selection for further exploration.

These conclusions agree with that of Andrews (1983) who considered that TL was of direct uranium exploration value and predicted more widespread use of the technique for uranium mineralization.

CHAPTER 4

A PROPOSED MODEL FOR THE GAMMA RAY INDUCED VARIATION
OF QUARTZ THERMOLUMINESCENCE GLOW CURVES

CHAPTER 4: A PROPOSED MODEL FOR THE GAMMA RAY INDUCED VARIATION
OF QUARTZ THERMOLUMINESCENCE GLOW CURVES

- Summary of Chapter

Chapter 4 speculates on variations in quartz ATL glow curves observed at the Beverley uranium deposit in terms of physical and kinetic models. In the case of physical changes in the quartz lattice it is assumed, from literature research, that defects acting as traps for the LT, MT and HT peaks are Al-M⁺ sites, M⁺ interstitials and oxygen vacancies respectively. The Al³⁺ site is assumed to be the only luminescent recombination centre. It is speculated that initially, Al³⁺ - M⁺ sites are the major trapping site. As radiation on the quartz continues the M⁺ ions are moved from the Al³⁺ - M⁺ sites by gamma radiation and form interstitial M⁺ sites. These act as trapping centres for electrons which, after recombination, result in the MT glow peak. Thus with increasing incident radiation the quartz LT peak should decrease and MT peak correspondingly increase. As radiation continues many extra defects, including oxygen vacancies are being formed. If oxygen vacancies act as electron traps for the HT glow peak, then, at high radiation doses, given an increasing abundance of oxygen vacancies, the HT peak would be the dominant glow peak.

*

*

*

4.1 Introduction

Chapter 2 described principles of TL - especially the effect of radiation on quartz TL glow curves - and suggested theoretical shapes of, and variations between, such glow curves with progressively increasing radiation doses. Chapter 3 showed the quartz artificial TL glow curves obtained with increasing palaeoradiation doses in the environment of an actual uranium deposit. These observed glow curves were found to be quite similar to those predicted in Chapter 2. This chapter (Chapter 4) is an attempt to explain why the predicted and observed quartz artificial TL glow curves vary in response to radiation dose. The attempted explanation is in terms of both physical and kinetic models though much of the following explanation must remain qualitative rather than quantitative, especially when an attempt is made to explain the variations in terms of kinetic models.

The principal points to be explained are:

- (a) The overall variation in TL glow curve shape as a function of distance from uranium mineralization and
- (b) The sensitization and subsequent desensitization of LT and MT glow peaks as the distance from uranium mineralization decreases.

Glow curves from Beverley samples, representing background, marginal and ore type TL glow curves are shown in figure 4.1. These curves approximate (b), (c) and (e) in the expected generalized glow curves of figure 2.34 and are representative of the variation in glow curve shapes exhibited by samples obtained at decreasing distances from the Beverley ore body. The explanations presented will be based on the three glow curves in figure 4.1.

Before stating assumptions and considering possible models, one additional piece of information must be given. As was mentioned in section 2.5.2.1, EPR work on artificially irradiated quartz (gamma,

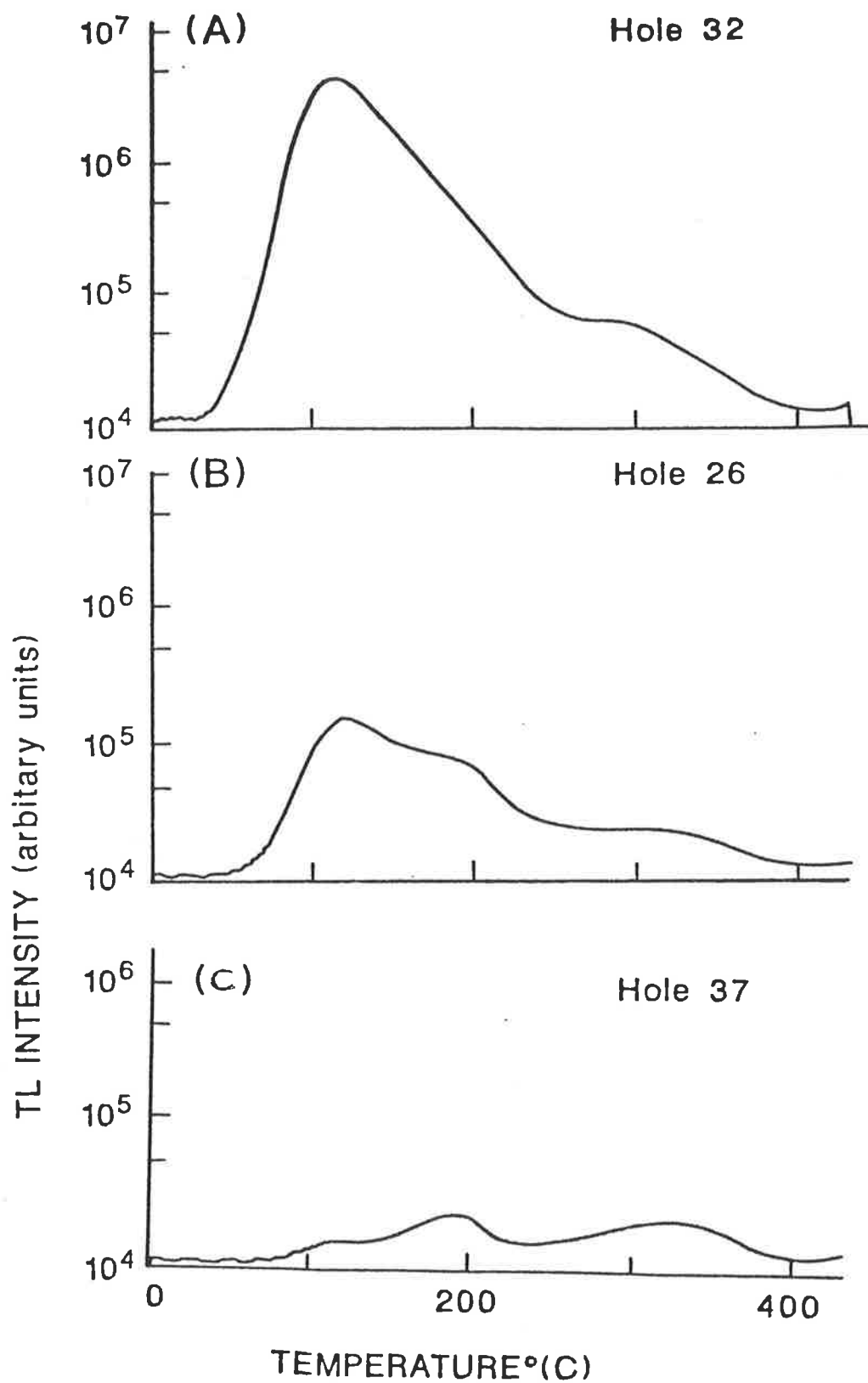


Figure 4.1 TL glow curves for quartz samples from the Beverley region representing

- (a) the background TL zone (low radiation),
- (b) the marginal TL zone (intermediate radiation) and
- (c) the "ore-type" TL zone (high radiation).

neutron and alpha radiation) by Chatagnon (1986) has shown an increase in E' centre concentration with increasing radiation. This trend was observed for gamma radiation as well as for alpha radiation. E' centres are usually correlated with oxygen vacancies. Therefore Chatagnon's (op.cit) results imply that oxygen vacancy concentration increases with increasing irradiation. It is interesting that a number of TL properties also change with radiation eg. glow peak intensities, ratios and glow curve shape.

Knowing that samples from the Beverley uranium deposit showed systematic TL variations (e.g. decrease in LT intensity and increase in HT percentage), it was decided to investigate a possible change in E' concentration in the same samples. Seven quartz samples from the Frome Embayment, at different distances from the Beverley ore body have been subjected to EPR analysis by Chatagnon. The location of the samples used is shown in figure 4.2, and intensity of the E' signal (in arbitrary units) is contained in table 4.1. These results show an increasing E'₁ signal (from 73 in the background sample, to 437 in the sample from the marginal palaeoradiation zone to a maximum of 1913 for a sample within the ore body. A more extensive discussion of these results is to be given elsewhere (Ypma et al, in prep).

Since E'₁ centres are correlated with oxygen vacancies, these EPR results indicate that the oxygen vacancy concentration in quartz increases through the areas of background palaeoradiation and marginal palaeoradiation, to a maximum within the orebody, i.e. the concentration of a particular type of defect, which could function as an electron trap increases, as TL properties also change: LT peak intensities decrease and HT peak percentages increase. An increase in E' centres in quartz with radiation has also been observed by Bossoli et al (1982) and Jani et al (1983). As well as the observed increase in E' centres it is possible that other defects will also be created as a result of radiation.

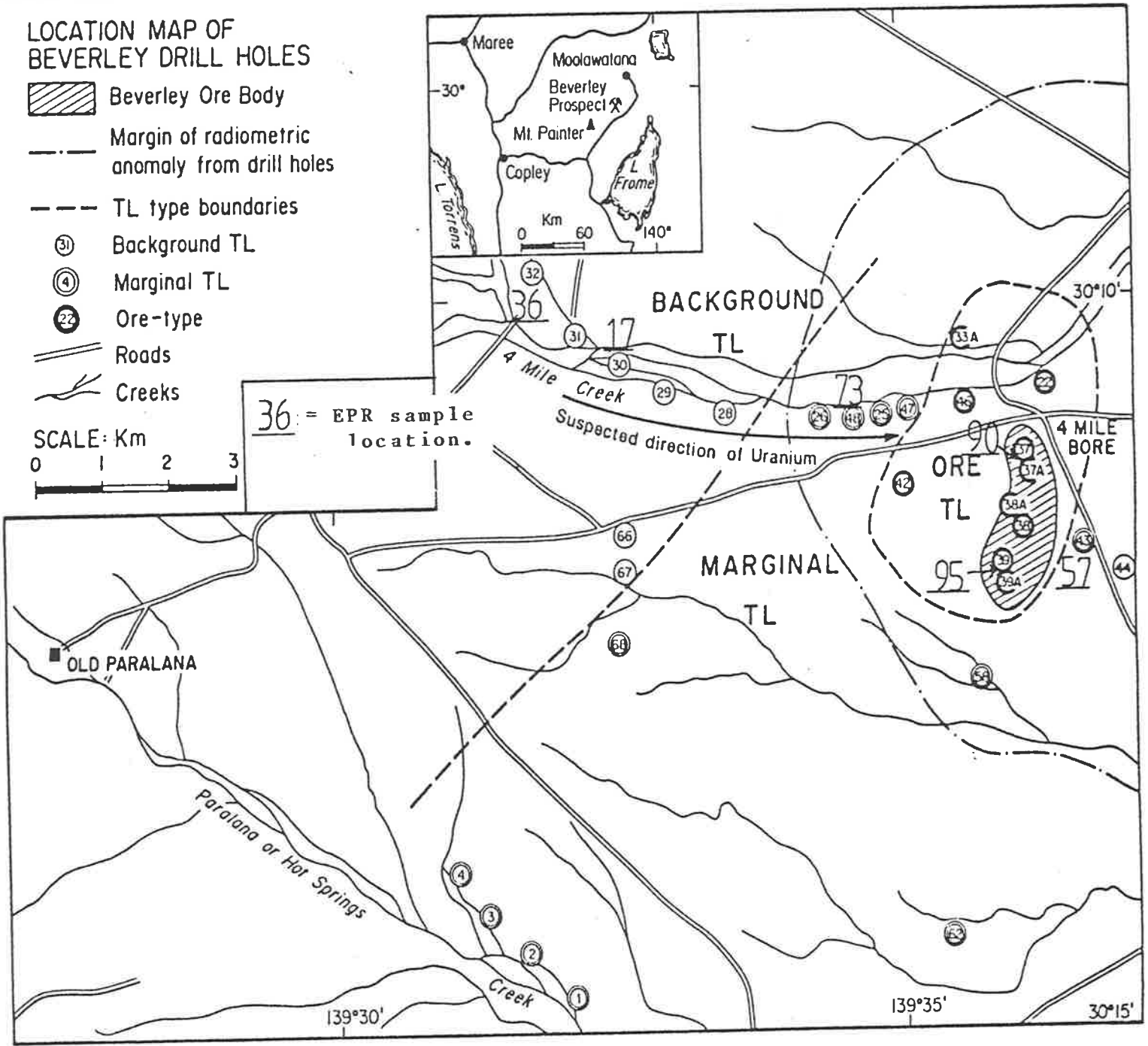


Figure 4.2 Location of EPR samples taken from the Beverley region.

Echantillon	$E'1$	$E'1$ recuit	$R (E'r/E'1)$
17	73	287	3,9
36	140,5	303	2,15
42	148,2	232	1,56
57	139,6	218	1,56
73	437	895	2,04
90	740	1602	2,16
95	1913,3	1940,7	1,01

Table 4.1 The change in E_1' centre signal in quartz samples from positions of variable palaeoradiation dose in the Beverley uranium region. Location of samples is given in figure 4.2.
 Echantillon = sample number.
 $E'1$ = natural $E'1$ centre signal.
 $E'1$ recuit = $E'1$ centre signal after a radiation dose. (Radiation dose is unspecified).
 R = ratio of $E'1$ recuit/ $E'1$.

Durrani et al (1977a) suggest that oxygen interstitials will be created by radiation. Kitt and Martin (1983) and Martini et al (1986) suggest that interstitial alkali-ions and Al-OH centres are created by radiation. It could be expected that these defects would also function as electron or hole traps and influence TL.

These EPR results, in conjunction with the previously described work of Ichikawa (1968) and Durrani et al (1977) suggest at least to this author, that a trap creation model to explain the sensitization and desensitization phenomena observed in quartz with increasing radiation dose, is to be preferred to a competing trap model.

Ichikawa (1968) and Durrani et al (1977) favoured trap creation models to explain sensitization phenomena in Brazilian quartz. However, their models were an attempt to explain the supralinear growth of an integrated TL intensity glow curve area between 240°C and 480°C versus radiation dose. Since this study is concerned with variations in glow curve shapes for a given test dose i.e. individual glow peak intensities and ratios, the model must contain features other than those given by Ichikawa (op.cit) and Durrani et al (op.cit). More specifically, it must explain the sensitization and desensitization of several individual glow peaks rather than the TL response determined from a single glow peak and integrated glow peak areas. A description of the proposed physical model for the observed TL glow curve variations is presented here. A qualitative explanation in terms of Levy's (1984,1985,a,b) interactive kinetic models will also be considered.

4.2 The Model

The model described here is based on the assumption that there is only one hole trap, with concentration N_r , and three electron traps with concentrations N_1 , N_2 , N_3 . (Similar models have been presented by Levy

1983b, 1984b). The concentration of trapped charge in each electron trap is n_{10} , n_{20} , n_{30} and in the hole trap is n_{r0} . n_r is always greater than $N_1+N_2+N_3$ and $n_{r0} = n_{10}+n_{20}+n_{30}$. Physically n_r could be assumed to be an Al^{3+} /alkali ion (M^+) centre which also acts as the only recombination centre. The ratio of radiative to non-radiative recombination is assumed to be constant. N_1 , N_2 and N_3 are assumed to correspond to electron traps contributing to luminescence of LT, MT and HT glow peaks respectively. An additional assumption is that initially, for a given test dose, n_{10} should be $> n_{20}+n_{30}$, possibly as a result of $N_1 \sigma_1$ being $> N_2 \sigma_2$ and $N_3 \sigma_3$.

Figure 4.3 after Levy (1983b) shows that in the three electron trap situation the shape of a glow curve depends on the initial trapped charge concentration distribution. When $n_{10} > n_{20}$ and n_{30} the LT peak is the dominant peak. In figure 4.3 the LT peak is at a maximum when a dominant fraction of the initial charge is in the low temperature trap.

A TL kinetic explanation for the behaviour shown in figure 4.1(a) has not yet been devised. One can speculate in a non-quantitative way that if n_{10} increased (implying an increase in n_{10}/N_1) that the LT peak intensity would increase to the extent that it may mask the MT and HT glow peaks and resemble the glow curve in figure 4.1(a) (obtained with samples from the Frome Embayment background zone). Put alternatively, the glow curve in figure 4.1(a) may be approximated under conditions where the trapped charge concentration in n_{01} is high, i.e. the ratio n_{01}/N_1 is high.

Next to be attempted is an explanation of why the LT glow peak decreases in intensity in comparison with the MT peak, as shown in figure 4.1(b). Now, in terms of interactive kinetics, glow curves approximating figure 4.1(b) can occur when the initial trapped charge ratio n_{20}/N_2 is comparable to or greater than n_{10}/N_1 and n_{30}/N_3 . One of the computed

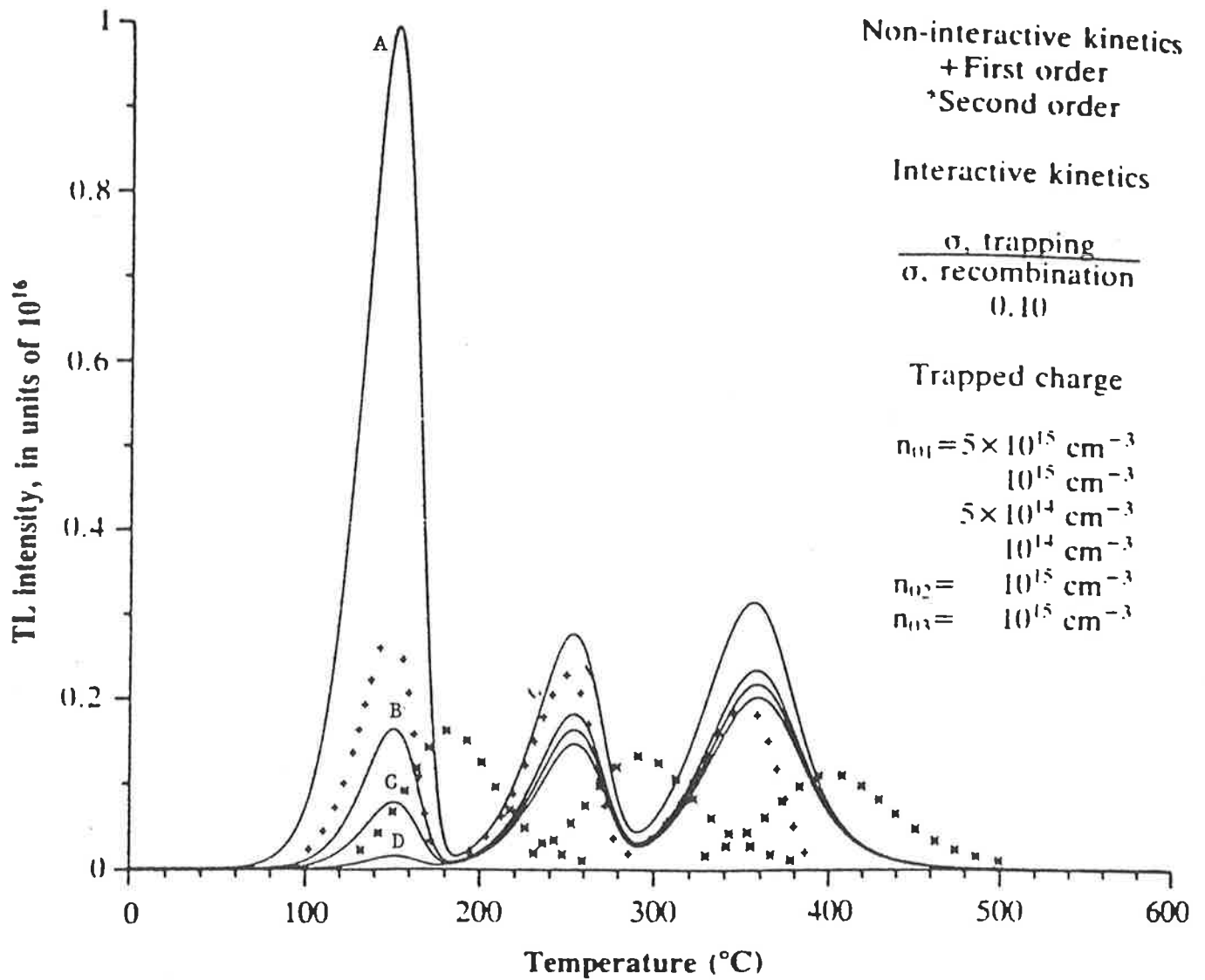


Figure 4.3 A computed glow curve where the initial trapped charge is distributed such that:
 (a) $n_{01} = n_{02} = n_{03}$;
 (b) $n_{01} = n_{02} = n_{03}$;
 (c) $n_{01} = n_{02} = n_{03}$;
 (d) $n_{01} = n_{02} = n_{03}$, after (Levy, 1983b).
 Case (a) is similar to the glow curve obtained in figure 4.1 for quartz from the Beverley background.

glow curves from Levy (1984b) when $n_{20} = 5 \times 10^{15}$ and $N_2 = 10^{16}$ approximates this situation, i.e. figure 4.1(b).

As the radiation dose increases, additional traps will be created in the quartz, i.e. the sum of $N_1 + N_2 + N_3$ will increase. It could therefore be reasonably expected that $N_1 + N_2 + N_3$ for the quartz represented by figure 4.1(b) will be greater than $N_1 + N_2 + N_3$ for the quartz represented by figure 4.1(a). In response to a fixed test dose the total trapped charge concentration ($n_{10} + n_{20} + n_{30}$) is also likely to increase because of increased trapping probabilities and therefore $n_{10} + n_{20} + n_{30}$ for the quartz represented by figure 4.1(b) will be greater than $n_{10} + n_{20} + n_{30}$ for the quartz represented by figure 4.1(a).

Since there will be a higher trapped charge concentration in the quartz represented by figure 4.1(b) than in that represented by figure 4.1(a), then the desensitization of the LT peak and sensitization of the MT peak in figure 4.1(b), could be explained in terms of an increase in N_2 or $\sigma_2 N_2$ (and/or possibly a decrease in N_1 or $\sigma_1 N_1$). Therefore, it is useful here, to consider what physical mechanisms may be involved in production of glow curves such as figure 4.1(a), (b) and (c).

The physical conditions under which a glow curve has a dominant LT glow peak can occur when there is a large concentration of electron traps which play a role in LT luminescence. Usually this requires that $\sigma_1 (N_1 - n_1)$ or $[\sigma_1 N_1]$ is appreciably greater than $\sigma_2 (N_2 - n_2)$ and/or $\sigma_3 (N_3 - n_3)$. Detailed studies on the nature of lattice defects and impurities responsible for individual glow peak emission in quartz do not explain all peaks. However Ichikawa (1968) suggested that the MT peaks of Brazilian quartz were due to centres that included interstitial alkali ions. Thus the Li^+ interstitial could be an electron trap producing the 230°C glow peak and Na^+ responsible for the 270°C glow peak. More recently Jani et al (1983), Kitt and Martin (1983) and Martini et al (1986) have also suggested that glow peaks in quartz between 200°C and



300°C are related to interstitial alkali ions. Ichikawa (op.cit) also suggested that the LT glow peak (180°C) was associated with a compensated Al^{3+} -(hole)- Li^+ -(e) centre. Ichikawa (op.cit) suggested that sensitization of the LT peak occurred when most of the Li interstitials, responsible for MT glow peak, had captured electrons and then moved, by interaction with gamma rays, to Al^{3+} hole sites, to act as LT electron traps. The major evidence for this hypothesis was that the MT peak (Ichikawa's B2 glow peak) saturated at a lower dose than the LT glow peak (Ichikawa's B1 glow peak). Three objections to this can be cited:

- (a) It does not explain the desensitization of the LT glow peak.
- (b) It cannot explain why the MT glow peak is sensitized after desensitization of the LT glow peak (as observed in samples from the marginal TL zone around the Beverley ore body, figure 4.1(b)).
- (c) Why $\text{M}^+ + \text{e}$ should move to Al^{3+} which have acquired h^+ beforehand and should therefore be electrically compensated.

Whilst accepting Ichikawa's (op.cit) defect sites responsible for LT and MT, TL emission, a reinterpretation of the data suggests the following model. Assume that initially most electron traps are of the type proposed by Ichikawa (op.cit) for the 180°C glow peak i.e. $\text{Al}^{3+} - \text{Li}^+$ sites and that interstitial Li^+ unrelated to Al^{3+} sites is much less abundant than the compensating Li of the $\text{Al}^{3+} - \text{Li}^+$ sites. As radiation is incident on the crystal electron-hole ionization pairs will be produced and some holes and electrons will be trapped on a range of trapping sites. The initial sensitization of the LT peak can be explained in terms of interactive kinetics as illustrated in figure 2.14 after Levy (1985a,b) i.e. by retrapping of electrons at the Al^{3+} - Li^+ sites or also by assuming more radiative recombinations than non-radiative recombinations occurring at this site (Levy, pers. comm. 1987). However, as radiation continues it is proposed that two additional effects occur:

(a) Oxygen vacancies are created, as discussed in section 2.5.2.1, which also creates oxygen interstitials. This effect has been mentioned by both Ichikawa (1968) and Durrani et al (1977),

(b) As holes are trapped on Al^{3+} centres, the compensatory alkali ions are free to move away from the Al^{3+} hole sites. Ichikawa (op.cit) suggest that Li^+ ions might be mobile during incident gamma-irradiation. Durrani et al (op.cit) suggested that process (a) occurs at already strained Si-O bonds in the vicinity of Al^{3+} - alkali ion centres. After the compensatory alkali ion has moved away from the Al^{3+} hole centre, interstitial oxygens may block its pathway so that it cannot diffuse back to the uncompensated Al^{3+} hole centre created even after an electron has recombined with the trapped hole. The net effect is an increase in the concentration of interstitial alkali centres which Ichikawa (op.cit), Kitt and Martin (1983) and Martini et al. (1986) have attributed to the electron traps responsible for the MT glow peaks. Durrani et al (op.cit) have also suggested that oxygen interstitials may prevent an alkali ion from moving back to the Al^{3+} site. However they did not discuss what would happen to the alkali ion and did not, apparently, consider the possibility that such an ion could then act as an electron trap. Ichikawa (op.cit) on the other hand, considered the possibility that interstitial alkali ions could act as electron traps for the MT peaks, but apparently did not consider the possibility that interstitial oxygens ions would curtail the movement of alkali ions, or that large radiation doses could create more interstitial alkali ions. Thus, it is suggested (here) that radiation will create interstitial alkali ions that can act as electron traps, for MT glow peaks, at the expense of Al^{3+} - Li^+ centres which were responsible for luminescence of the LT glow peak.

The overall effect is that as radiation proceeds there will be:

(a) a limitation of the number of hole traps, and

(b) the creation of additional traps which may function as electron traps. Both of these factors will aid retrapping.

One could expect therefore that (with the number of MT traps increasing and retrapping also increasing) the LT peak could decrease in intensity and the MT peak increase. A resultant glow curve would therefore resemble figure 4.1(b). As the concentration of alkali ions is finite, and the concentration of interstitial alkali ions is expected to be less than the total concentration of all alkalis, then as radiation increases there will come a stage when all M^+ ions have become electron traps. Because the concentration of initial interstitial alkalis, particularly Li^+ , is small, then it is not surprising that the B2 glow peak ($230^\circ C$) of Ichikawa (op.cit) reaches saturation at the comparatively small dose of 8×10^4 rad. Ichikawa (op.cit) also suggests that the $270^\circ C$ glow peak results from electrons trapped on Na^+ interstitials. This glow peak does not reach saturation for doses up to 9.2×10^6 rad and can contribute to the MT peak intensity over this entire range.

At higher doses, it is postulated that additional oxygen vacancies are created which act as electron traps. Ichikawa (op.cit) suggests that O vacancies are electron traps which contribute to luminescence of the HT glow peak. Therefore the creation of more HT electron traps should cause an increase in the luminescent intensity of the HT glow peak, as shown in figure 4.1(c). Therefore at high radiation doses only the HT glow peak remains. This was noticed by Durrani et al (1977) and was portrayed in figure 2.29.

Levy's (1984,1985a,b) interactive kinetic model predicts that a glow curve where only the HT glow peak remains should occur at low doses, not at high doses as found by Durrani et al (op.cit) and in "ore type" glow curves (high radiation dose) in this thesis. The interactive kinetic model is perfectly compatible with these observations however if one aspect is further explained.

Initially it was assumed that the ratio of radiative recombinations to non-radiative recombinations was constant. However, if this ratio is not constant, but changes in response to increasing radiation dose, i.e. proportionately more non-radiative recombinations occur at higher radiation doses than at lower doses, then overall TL intensity would decrease and the HT peak would be increased relative to the LT and MT peaks (Levy, pers. comm. 1987).

Physically, this situation could occur if some of the extra traps created by large doses of radiation, also functioned as non-radiative recombination centres. Then, as the radiation dose increased, the number of these centres would increase and the ratio of radiative to non-radiative recombination centres would decrease. This would lead to a decrease in TL intensity as observed in figure 4.1(c). The physical nature of such centres is not, as yet, known.

PART 2

USE OF THERMOLUMINESCENCE IN URANIUM EXPLORATION FOR PROTEROZOIC
URANIUM DEPOSITS. THE CASE OF THE WESTMORELAND URANIUM DEPOSIT,
NORTHWEST QUEENSLAND.

CHAPTER 5

GEOLOGY OF THE WESTMORELAND REGION

5.1 Introduction

Although ATL worked well in uranium exploration in the simple cases encountered in Tertiary sandstones, usage and interpretation can be expected to be complicated in Proterozoic sandstones where the age of mineralization is much older and uranium may have been redistributed during geological history. It is therefore important to have a good understanding of the geology of such areas and the implications of other geological and geochemical studies when interpreting TL results. For this reason in Chapter 5 a more comprehensive account of the geology of the Westmoreland region is given than was felt necessary for the Beverley and Bremer River studies. A more detailed knowledge of the geology will also be helpful when formulating a genetic model for the Westmoreland Uranium Deposits in Chapter 6 and when considering Proterozoic uranium deposits in general in Chapter 7.

5.1.1 Location and Access

The Westmoreland uranium deposits are located in northwest Queensland at latitude $17^{\circ}30'$, longitude $138^{\circ}10'$. They are 10 kilometres east of the Northern Territory border, approximately 400km northwest of Mt. Isa, and are within the pastoral lease of the Westmoreland Station (figure 5.1). Access is possible by vehicle along bitumen roads followed by unsealed roads from Mt. Isa via Doomadgee Mission, or by light aircraft from Mt. Isa to Mangaroo Airstrip - a company maintained airstrip approximately two kilometres from the exploration base, Camp Ridgeway. Access to the area is not possible during the summer wet season extending from November till March or April.

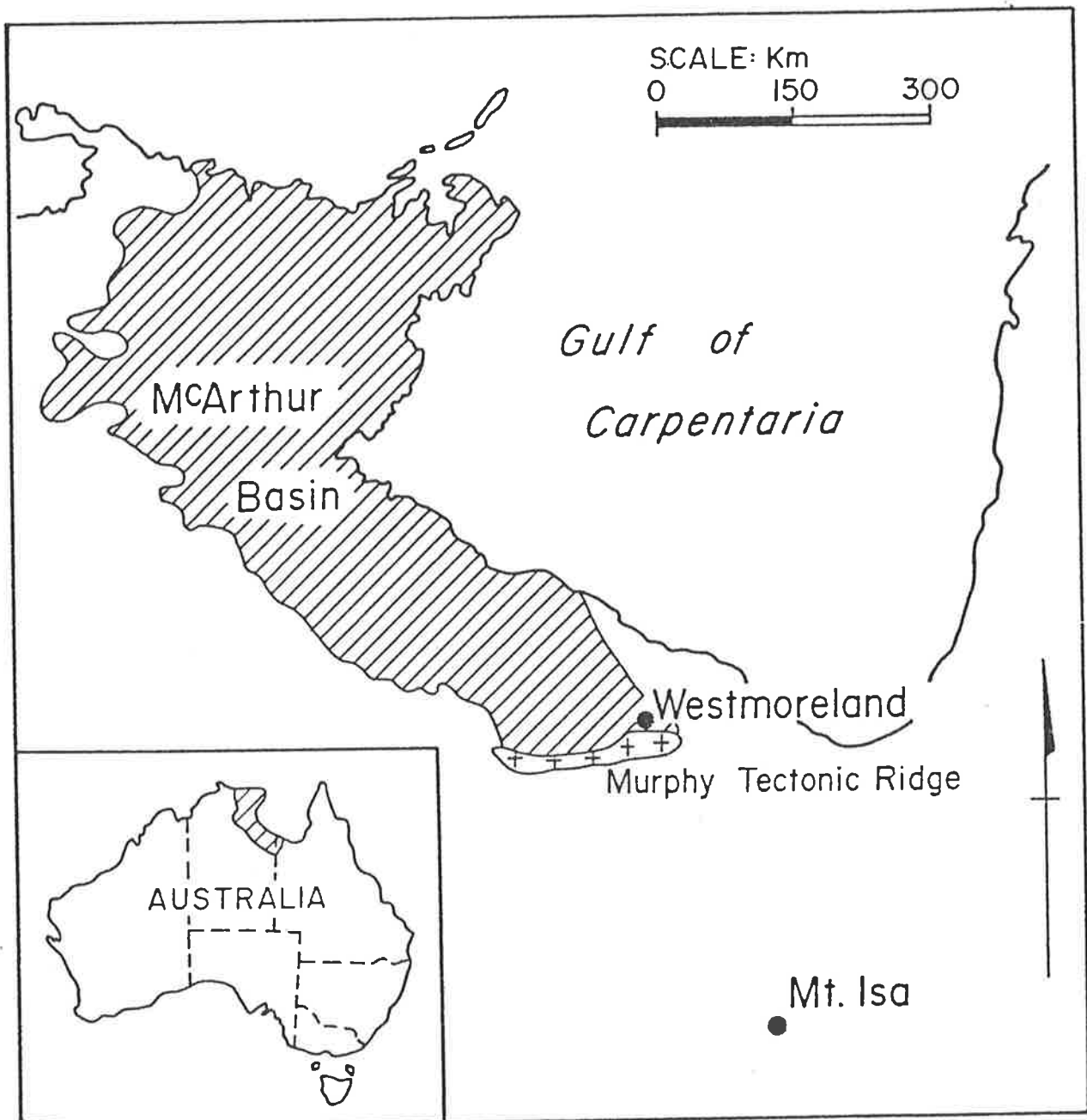


Figure 5.1 Location of Westmoreland.

5.1.2 Previous Investigations

Mineralization at Westmoreland was first reported in 1956 by Mount Isa Mines (MIM) prospectors leading the Bureau of Mineral Resources (BMR) to carry out an airborne radiometric survey which subsequently led to the discovery of the Livingstone Prospect. This was renamed the Redtree Prospect by an MIM-CRA (Conzinc Riotinto of Australia) joint venture during one of the sporadic investigations of the area which continued until 1967 when Queensland Mines Limited (QML) and Broken Hill Proprietary Limited (BHP) renewed active exploration.

In the period from 1969 to 1971 QML carried out an intensive exploration program (540 diamond and percussion drill holes) which revealed and delineated the then known orebodies, the Jack, Garee and Langi Lenses.

Urangesellschaft Australia Pty. Ltd. (UGA), the present operating company, entered into a joint venture with QML resumed exploration in 1975, resulting in the discovery of the Junnagunna, Sue and Outcamp Prospects. Locations of all prospects are given in figure 5.2.

5.2 Regional Geology of the Westmoreland Area

The host rock of the Westmoreland uranium deposits is the Westmoreland Conglomerate which is the basal unit of the Tawallah Group which itself constitutes the basal portion of the McArthur Basin, the major unit of the North Australian Platform Cover. The study area is at the southern most end of the McArthur Basin where the sedimentary sequence unlaps the Lower Proterozoic basement of the Murphy Tectonic Ridge.

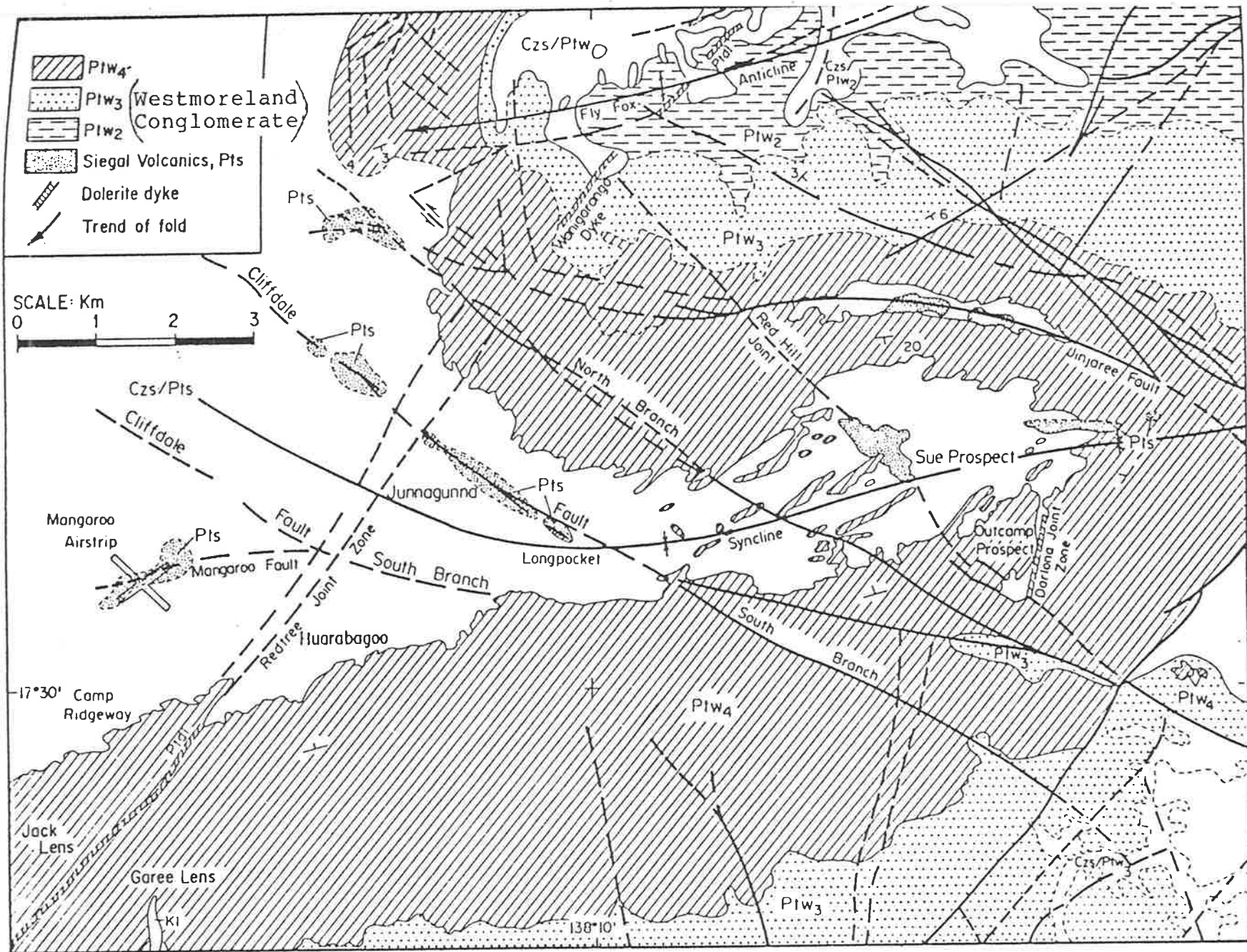


Figure 5.2 Local geology of the Westmoreland region.

The Murphy Tectonic Ridge is a Lower Proterozoic inlier comprised of the following three lithotypes - the Murphy Metamorphics, the Nicholson Granite Complex and the Cliffdale Volcanics.

The Murphy Metamorphics are the oldest of the units comprising the Murphy Tectonic Ridge. They are at least 1900 m.y. and possibly 2100 m.y. old (Plumb and Derrick 1975), and are intruded by the Nicholson Granite Complex. In places they are overlain by the Cliffdale Volcanics, and rarely by the Westmoreland Conglomerate.

Structural trends within the Ridge are reflected in the Murphy Metamorphics and are dominantly east-west. This unit has passed through an episode of regional metamorphism and deformation that has not affected the overlying units. Metamorphism took place in the greenschist facies.

The units are comprised of tight to isoclinally folded quartz-albite-biotite-chlorite \pm muscovite \pm epidote schists with a biotite defined foliation striking slightly north of west and dipping steeply north. (Gardner, 1978).

These rocks are similar in lithology and metamorphic grade to the Yaringa Metamorphics in the Mt. Isa Block and have been correlated with basement inliers in eastern Arnhem Land, i.e. the Grindall Metamorphics, Bradshaw Granite and Mirarramina Complex. Plumb and Derrick (op.cit) have suggested that they may also be continuous with the Pine Creek Geosyncline metamorphic sequences in sub-surface.

The Nicholson Granite in general covers the western part of the Murphy Tectonic Ridge. Gardner (op.cit) divided the complex into seven sub-divisions: Pgn₁, Pgn₂, Pgn₃₋₄, Pgn₅, Pgn₆, Pgn₇ and Pgn₈ with Pgn₁ representing the earliest intrusion and Pgn₈ the last, though the relative sequence of intrusions between these is not entirely certain.

Pgn₁ and Pgn₂ are coarse-grained porphyritic hornblende-microcline-albite and albite-microcline granites respectively, representing sub-

solvus two feldspar granites having been formed in the mesozone of Buddington (1959) at a depth of approximately 10 kilometres.

Pgn₅, Pgn₆ and Pgn₇ are distinguishable as a group from Pgn₁, Pgn₂ and Pgn₃₋₄ in being red, even grained (biotite-) alkali feldspar granites with associated aplite and microgranite dykes. These represent hypersolvus one feldspar granites having been formed at shallower depths than the first group (approximately 7 kilometres).

Pgn₃₋₄ are granodiorite and microgranodiorite stocks and ring dykes which were emplaced at various times during the history of the complex, intruding Pgn_{1,2,5} and 6.

Pgn₈ is distinguished from the other granites by its finer and more even grain size, the presence of muscovite in preference to biotite and its high proportion of plagioclase. It is termed a white, aplitic, muscovite-bearing, microcline-albite leucogranite. Pegmatites are also common in this stage of intrusion.

Compared with average granites (Taylor 1968), all the granites of the Nicholson Granite Complex are enriched in K₂O and total Fe. Minor elements show enrichment in U, Th, Ba, Rb and Ce, and are depleted in W and Sn.

Initial Sr⁸⁷/Sr⁸⁶ ratio values of 0.7069 ± 0.0040 have been obtained for the "older" granite part of the intrusions, and 0.7178 ± 0.0038 for the "younger" granite portion (Webb 1973, 1975). These further confirm the more primitive nature of the "older" granites, e.g. Pgn₁ and Pgn₂. Gardner (1978) reports radiometric ages of 1843 ± 8 Ma and 1860 ± 103 Ma for the "older" granites and several ages around 1770 Ma for the "younger" granites.

Similar groupings of granites have been found in the Pine Creek Geosyncline by Ferguson et al. (1980) and Riley (1980). These groupings are not so much based on age but on geochemistry and Sr⁸⁷/Sr⁸⁶ initial ratios. In the Pine Creek Geosyncline the older granites e.g. the

Nanamba and Nimbuwah Complexes are considered by Ferguson et al (1980) to be the possible original sources of uranium for the East Alligator uranium deposits.

The Cliffdale Volcanics are the third unit of the Murphy Tectonic Ridge and comprise its eastern part. The Cliffdale Volcanics are a sequence of rhyolitic to andesitic ignimbrites, flow banded rhyolitic lavas and acid tuffs erupted as numerous lava flows and pyroclastic extrusions forming a near continuous belt 7 to 18km wide and 48km long. They are essentially flat lying flows, although they dip more steeply adjacent to faults and granite contacts. The only metamorphism effects present are those attributed to contact metamorphism near to granite intrusions.

Webb (1973) dated the volcanics at 1770 ± 20 m.y. and as such, they define the base of the Carpentarian in Australia. Similar acid volcanics are found in other Proterozoic inliers and blocks throughout Australia which mark the local base of the Carpentarian in these areas. These include the Edith River Volcanics in the Pine Creek Geosyncline, acid volcanics in the Mt. Winnecke Formation and associated Winnecke Granophyre in the Granites-Tanami region, the Argylla Formation in the Tewinga Group at Mt. Isa, and the volcanics of the Hatches Creek Group in the Tennant Creek Block.

5.2.1 Uranium Mineralization of the Murphy Tectonic Ridge

Uranium mineralization is known in many parts of the Murphy Tectonic Ridge, which includes the Westmoreland area. Mineralization has been identified within the Nicholson Granite Complex, the Cliffdale Volcanics, the Westmoreland Conglomerate and the overlying Siegal Volcanics. The largest of the deposits, outside of Westmoreland, is the Pandanus Creek uranium mine also known as the Eva mine, situated on the

Northern Territory side of the border. Mineralization is primarily pitchblende with secondary sklodowskite and beta-uranophane. These are irregularly distributed in sheared acid to intermediate lavas and interbedded sandstones of the Cliffdale Volcanics immediately below the unconformably overlying Westmoreland Conglomerate. The ore is localized by faults and is associated with a high degree of chloritic alteration of the host rock (Crohn 1975, Curtis 1976). Morgan (1965) records production of 306 tonnes of uranium ore at 8.37% U_3O_8 from the Eva mine.

A further group of small mines, the largest of which is the Cobar II deposit, is situated approximately 20km north of Eva. These mines occur within the Siegal Volcanics. Individual ore shoots are confined to shear zones and are associated with extensive hematitic replacement of the country rocks. Crohn (op.cit) reports 6.3 tonnes of U_3O_8 at a grade of 10.5%. Geographic positions of these orebodies are given in figure 5.3. Other minor deposits in the Siegal Volcanics include El Hussein and King's Ransom mines. No details of geological setting or production figures are known.

At least 20 occurrences of mineralization within the Westmoreland Conglomerate are known in Queensland. The most significant of these are those at the Redtree, Junnagunna and Longpocket areas hereafter collectively referred to as the Westmoreland Deposits. These constitute the largest uranium deposits known as yet in Queensland and have been the subject of this study.

5.3 Local Geology of the Westmoreland Area

In the Westmoreland area the Middle Proterozoic McArthur Basin succession is not fully developed. The only units present are the Westmoreland Conglomerate and the Siegal Volcanics, the two lowermost units of the Tawallah Group which unconformably overlies the Murphy

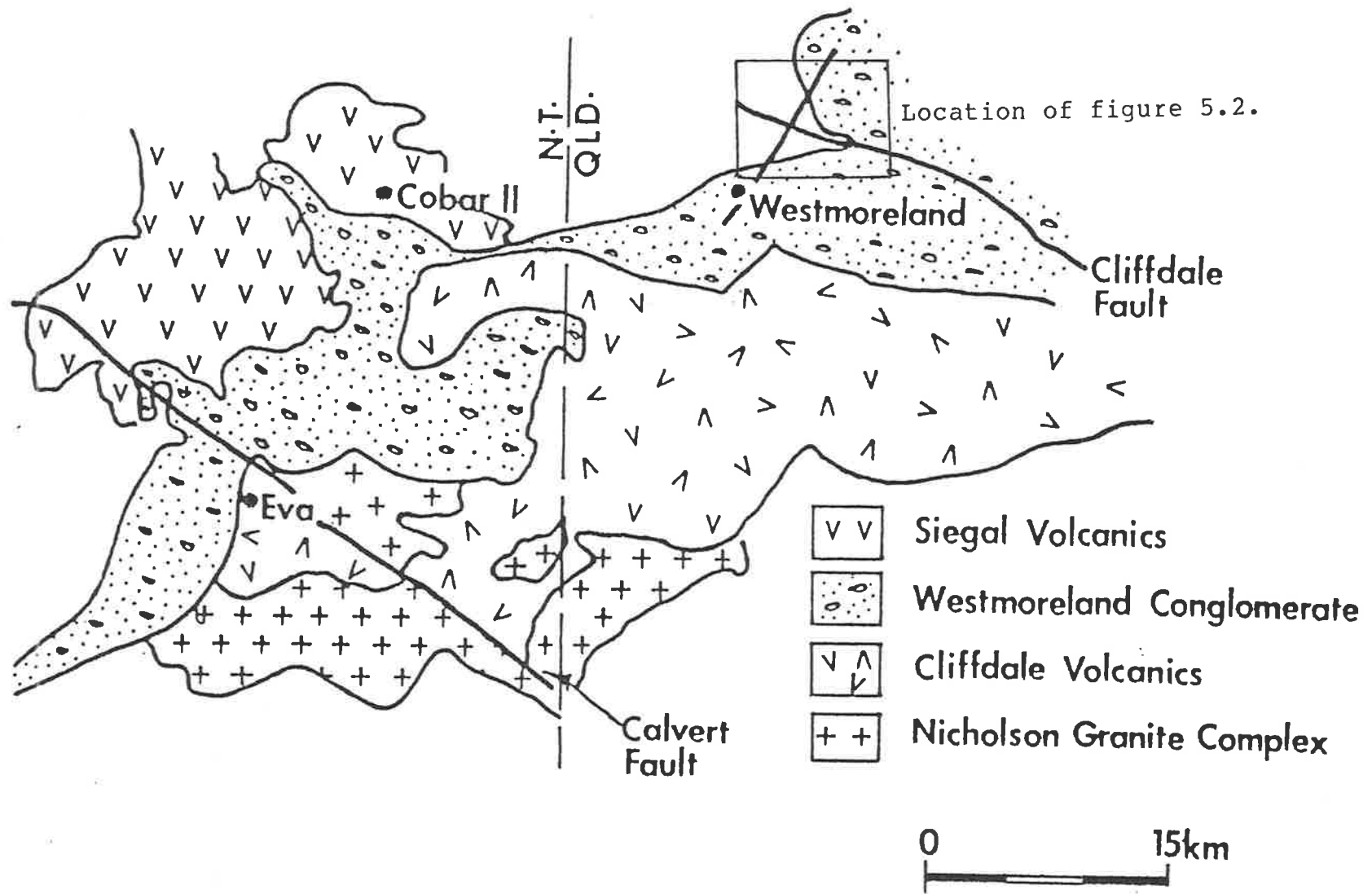


Figure 5.3 Location of uranium deposits on the Murphy Tectonic Ridge.

basement Ridge. The overlying Wollongorang Formation is present in discontinuous outcrops 20km to the north where this and other units of the Tawallah Group begin to thicken towards the north and west.

5.3.1 The Westmoreland Conglomerate

The Westmoreland Conglomerate unconformably overlies the basement Murphy Tectonic Ridge. It has been divided into four units with conformable contacts between each.

Unit 1 is the basal unit unconformably overlying the Cliffdale Volcanics. A basal boulder conglomerate may be locally present and is composed of a valley fill deposit with subrounded cobbles of tuff and acid volcanics in a matrix of coarse sandstone (Sweet and Slater 1975). Particle size decreases upwards grading into a coarse sandstone with pebble layers and then to a thick medium bedded sandstone and coarse-grained orthoquartzite which may be hematitic. The overall thickness of this unit is between 150m and 200m.

Unit 2 is composed of a uniform sequence of massive bedded, coarse-grained, poorly sorted sandstones. Hematite staining may occur. Pebbles of vein quartz and acid volcanics are common. Trough and occasional tabular crossbeds have been found. The approximate thickness of Unit 2 is 450m.

Unit 3 is a light brown, very coarse pebbly or cobbly conglomerate. Rounded pebbles of vein quartz, metamorphic quartz, red orthoquartzite, quartz arenite and acid volcanics occur in varying proportions in a matrix of poorly sorted coarse-grained hematitic sandstone. Trough cross bedding is common. The upper boundary of unit 3 is commonly placed above the last cobble bed (Sweet and Slater op.cit). Maximum thickness of this unit is approximately 350m.

Unit 4 is comprised of coarse to very coarse, poorly sorted sublitharenites with occasional discontinuous pebble beds and large cobbles scattered throughout the sequence. Medium to large-scale trough and tabular cross-bedding is common. At the top of Unit 4, low energy sedimentary structures such as ripple pavements and flat lying graded beds are also common. Less common, but also present, are slump structures of unconsolidated sediments. Maximum thickness of unit 4 is 100m.

Unit 4 also contains a volcanic/volcanoclastic component. Basic sills, e.g. the Outcamp Sill, occur in the upper half of the unit in the Longpocket and Flying Fox Anticline areas. These are geochemically and petrologically similar to the overlying Siegal Volcanics (see further in Appendix 4). Also present are interbedded waterlain tuffs and sandy tuffs which occur as thin bands, usually less than 10cm thick though up to 2m thick. These are present throughout the entire Unit 4 succession and may possibly be present in underlying units also, though the paucity of drill holes intersecting Units 1, 2 and 3 cannot confirm or deny this. The tuffs are not recognized in surface outcrop, no doubt due to the susceptibility of their component minerals.

Petrologically the Unit 4 sandstones are classified as coarse-grained sublitharenites comprised of 85% quartz, 5% lithic fragments and a variable amount of rounded feldspar (less than 5%), with minor zircon. The cementing agent is a secondary quartz development forming quartz overgrowths as well as clay and chlorite. Earthy hematite and rare sulphides complete the accessory minerals. In samples which contain pitchblende, specular hematite and small euhedral quartz grains are also present. The clay and chlorite content of the unit increases towards its top coincident with a fining of the sandstone, Manning (1979).

5.3.1.1 Environment of Deposition of the Westmoreland Conglomerate

Sediment for the Westmoreland Conglomerate was provided by the units of the Murphy Tectonic Ridge, particularly the Nicholson Granite Complex and the Cliffdale Volcanics (Manning 1979). Initially the Murphy Tectonic Ridge formed a strong positive topographic feature with localized boulder conglomerates developed as valley fill deposits as represented by Unit 1. Sediment supply from the erosion of the ridge and deposition of this led to the thick uniform fluvial sequence represented by Unit 2. Unit 3 represents rejuvenation and uplift of the Murphy Tectonic Ridge source rocks and lower units of the Westmoreland Conglomerate. It is a thick sequence of pebble and cobble conglomerates with clasts of quartzite and sandstone which indicate cannibalism of earlier deposits. This also occurs in Unit 4 which is characterized by extensive erosion and abundant sediment supply, resulting in the formation of extensive accumulations of continental sediments. The environment of deposition was likely to have been high energy braided stream, as indicated by the large-scale trough cross-bedding, discontinuous cobble beds, low proportion of fine materials and textural maturity of the sands. Conditions of sedimentation were semi-arid (indicated by the presence of rounded feldspar grains) and deposition was during sporadic aqueous events rather than continuous water transport (Sweet and Slater, 1975).

5.3.2 The Siegal Volcanics

The Siegal Volcanics interfinger with the underlying Unit 4, to produce a gradational boundary often marked by a thin tuffaceous/shaley horizon up to 30cm thick. They are conformably overlain by either the McDermott Formation or the Sly Creek Sandstone.

The Siegal Volcanics are composed of a series of amygdaloidal extrusive basaltic to andesitic lava flows with minor interbeds of siltstone and sandstone. They range from 1,000m to 1,600m thick in complete section, with individual flows up to 200m thick.

The lavas are usually totally altered though relict fabrics are well preserved enabling them to be broadly classified. Thin section examination (appended) indicates that these flows were originally composed of plagioclase laths and clinopyroxene phenocrysts in a matrix of fine plagioclase and glass \pm olivine depending on composition. Magnetite appears to have been a common accessory mineral. The lavas thus appear of tholeiitic composition. Compositional variations did originally exist as is verified by differences from sample to sample in the proportions of the above minerals.

Alteration has been attributed to metasomatism, diagenesis and later mineralizing solutions (Fander 1976) and has resulted in a complete alteration of all minerals. Plagioclase has been totally sericitized, clinopyroxene has been replaced by chlorite, the groundmass has been altered to a clay (illite) and magnetite has been converted to leucoxene. Vesicles are commonly filled with quartz or magnesite. Near surface samples are often altered to a white weathered kunkar/magnesite.

Despite alteration, rare fresh samples do exist. These are usually a darker green color with a less weathered appearance comprised mainly of labradorite and clinopyroxene.

The contacts between dykes and the underlying sandstone are sharp, implying that their intrusion was a post-lithification event.

In the Westmoreland region proper, the thickness of the Siegal Volcanics is much less than in the type section (usually less than 35m at Junnugunna) but increases in a westerly direction along plunge of the major folds.

5.3.3 Dolerite Dykes

Dolerite dykes such as the Redtree dyke extending from south of the Jack and Garee orebodies to the Cliffdale Fault, are intrusive into the Westmoreland Conglomerate and Siegal Volcanics, but not the overlying units.

This dyke and its proposed equivalents in the Darlona and Wanigarango Joint Zones is petrologically similar to the Siegal Volcanics consisting of plagioclase, clinopyroxene, chlorite \pm quartz with minor accessory magnetite. Alteration is similar to that in the extrusives and the dykes are usually expressed as rubble covered gullies in the middle of large sandstone ridges. Mechanisms responsible for alteration of the dykes are probably the same as operating in the Siegal Volcanics, i.e. deuteric, diagenetic and mineralizing solutions. Petrological descriptions are appended.

5.3.4 Geochemistry of the Siegal Volcanics, Dykes and Tuffs

A geochemical study of basic volcanics at Westmoreland (the extrusive Siegal Volcanics, intrusive Redtree dolerite dyke and minor interbedded tuffs and tuffaceous shales, has been undertaken in order to establish their suitability as uranium suppliers. Results for 35 whole rock samples and trace elements are in Appendix 4 and indicate that the extrusive rocks are best classified as basalts and the intrusive rocks as dolerites. As such they are unlikely to be major suppliers of uranium to the Westmoreland Uranium Deposits. For reasons of continuity of text a discussion of the geochemical results and their relationship to other Northern Australian basic suites is also confined to Appendix 4.

5.3.5 Structure and Metamorphism

The Tawallah Group is folded over the Murphy Tectonic Ridge in open, concentric folds. In the Westmoreland area the major fold structures are the Flying Fox Anticline and the Longpocket Syncline. Amplitudes of the folds are large, up to two kilometres, and the fold axes trend east-west and plunge gently westward.

Two dominant fault trends are prominent not only in this area but throughout the Murphy Tectonic Ridge (Gardner, 1978). The orientations of these faults are north-east (N.E.) and west-northwest (WNW).

The NE trending system is often intruded by dolerite dykes and includes the Redtree and Darlona Joint Zones. The Redtree Joint Zone is the major structural feature related to mineralization in the Redtree area and the Darlona Joint Zone is also spatially related to the Outcamp and Sue prospects in the Longpocket Syncline. Such zones are characterized by little vertical or lateral movement. Displacement on the Redtree Joint Zone is mainly vertical with the eastern side having been upthrust by ten metres (B.G. Penny, pers. comm.).

Dominant faults in the WNW trending system are the Cliffdale, Mangaroo and Namalangi Faults, and outside of the Westmoreland area include the Calvert Fault. These structures are marked by large quartz ridges commonly 20m high. Examination of this quartz shows angular shapes of relic Siegal Volcanic fragments which fit together (much like a jigsaw). This indicates that these are a fault breccia rather than a solution breccia which would have formed by upwelling siliceous solutions dissolving the volcanics rather than first fragmenting them, i.e. the Siegal Volcanics have first been brecciated by fault activity and then later cemented by siliceous solutions in this fault system.

5.3.6 Uranium Mineralization at Westmoreland

The Westmoreland Uranium Deposits are composed of the Redtree Namalangi (Jack, Garee and Langi lenses) - Huarabagoo, Junnagunna, Outcamp, Sue and Red Hill deposits and prospects as well as many other minor occurrences and prospects including Black Hill and Longpocket. Locations of all areas are shown in figure 5.4. A brief geological description of each area is given below.

Mineralization occurs as two types:

- 1) as vertical lenses and pods along the strike of the Redtree dyke through the Redtree, Huarabagoo and Junnagunna areas and
- 2) as sub-horizontal blankets fanning out laterally at shallow depth from the Redtree dyke and the postulated dyke in the Outcamp Sue area.

It is considered that a continuum exists between the thin vertical lenses and the horizontal mineralization (illustrated in figure 5.5, though this has not yet been verified by either drilling or trenching. The grade is variable from deposit to deposit but averages 0.15% U_3O_8 .

All major mineralization occurs within Unit 4 of the Westmoreland Conglomerate. Horizontal mineralization is almost always within ten metres of the overlying Siegal Volcanics or underlying the Outcamp Sill, and usually occurs adjacent to the contact and stretching one to two metres below it. Vertical mineralization occurs at a greater variety of depths throughout Unit 4, up to 20m below the surface, though always occurs in close proximity to the dykes themselves. Mineralization can also occur within the volcanics or dykes though only at the contact in the highly altered portions or in sandstone interbeds.

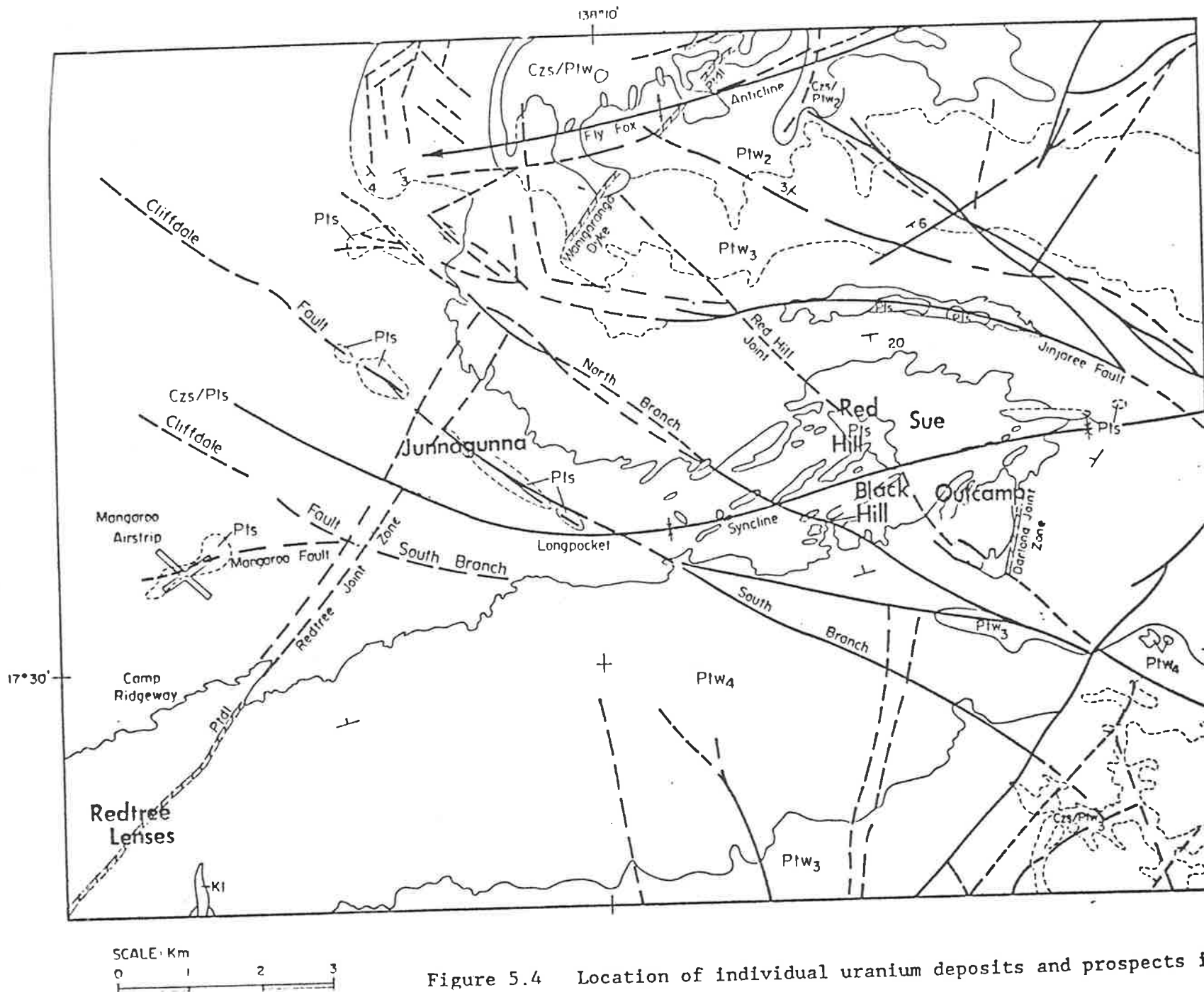


Figure 5.4 Location of individual uranium deposits and prospects in

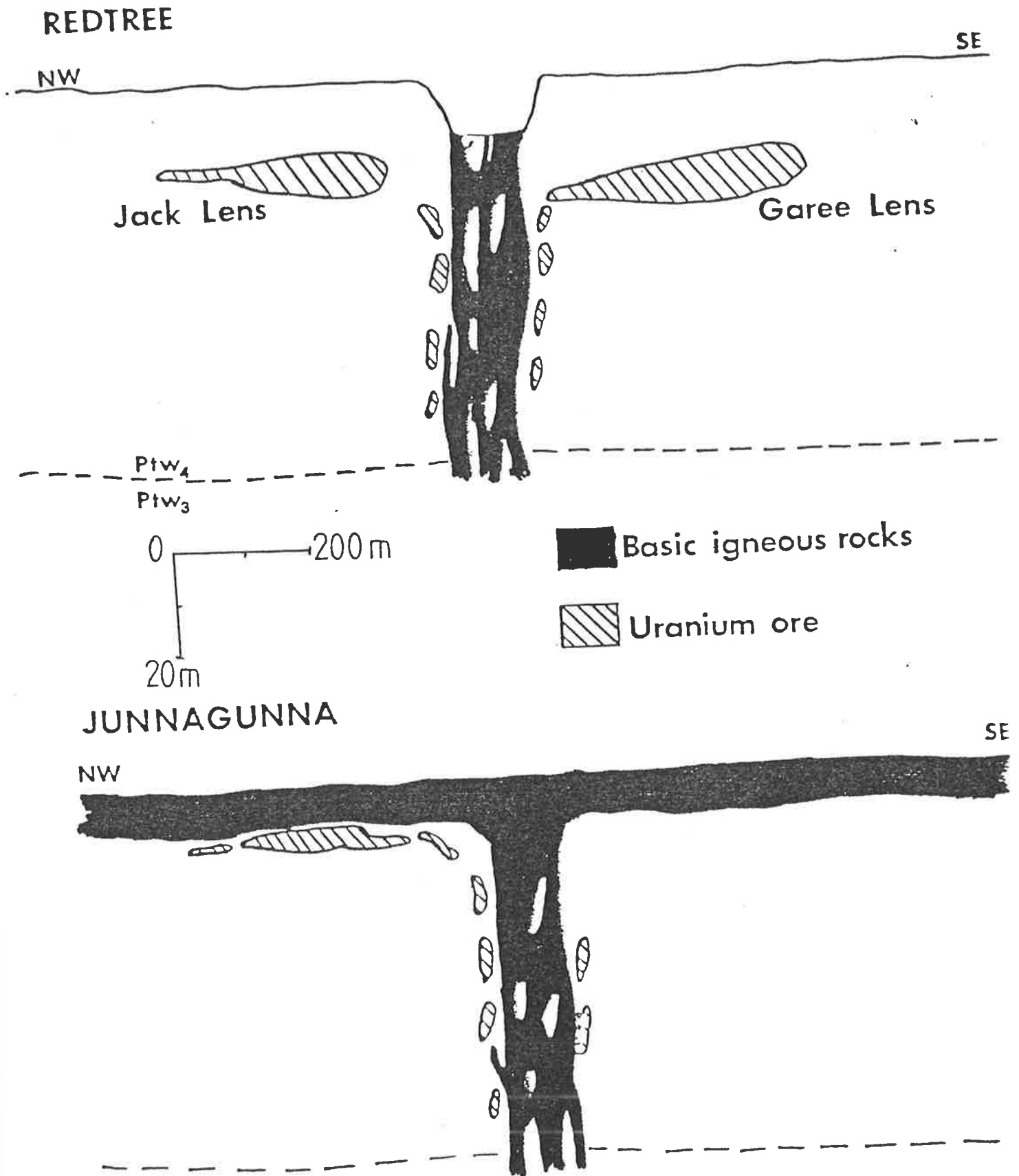


Figure 5.5 Vertical and horizontal mineralization styles at Westmoreland.

The strong affinity between ore and basic volcanics led some previous workers to suggest that the basalts and dolerites had supplied mineralizing fluids to the sandstone. This seems unlikely as field evidence indicates that mineralization within these units is absent or erratic, and coupled with the restriction of mineralization to volcanic contacts with the sandstones, suggests an introduction from the sandstone instead. Further, highly altered portions of the dyke away from the contact are unmineralized and the inherently low uranium content of such rocks renders them unlikely uranium sources (Clarke et al. 1966). This theory is therefore virtually ignored in the discussion of previous theories in section 6.1.

The primary mineralization in these deposits (in both horizontal and vertical lenses) is pitchblende, though brannerite has also been recognized in the dykes. Pitchblende occurs as massive anhedral and rarely euhedral grains, as colloform masses, and as sooty films which are interstitial and infilling cracks in grains. Brannerite formed by alteration of titanomagnetite in the dyke along with uranium introduction (Pohl 1970).

Secondary mineralization is a supergene surface expression of primary mineralization. The most common minerals are carnotite, torbenite and metatorbenite, occurring as interstitial cements or as crystal growths on grain and rock surfaces. Other reported secondary minerals include soddyite, sklodowskite, vandendriesscheite, uranosprite, zeunerite, phosphuranylite, renardite and parsonite (Hills and Thakur, 1975).

Pitchblende is intimately associated with hematite, euhedral quartz crystals and usually chlorite. Other minerals often associated with uranium mineralization include pyrite, chalcopryrite and galena and Hills and Thakur (op.cit) report gold inclusions up to ten microns in diameter in either the pitchblende or gangue minerals.

Hills and Richards (1972), using the U-Pb dating method, put the age of uranium mineralization between 820Ma-900Ma with a second younger mineralizing event at approximately 450Ma.

Recently, further gold mineralization has been reported in the Junnagunna area with a loose spatial relationship to uranium mineralization (Schindlmayr and Beerbaum, 1984). Gold grades reach 80 grams/tonne though more commonly are 0.2-7 grams/tonne.

Geochemically uranium correlates with total iron (ΣFe) and vanadium (V) (Manning 1979) and to a lesser extent with chromium (Cr) and radiogenic lead (Pb) (Curtis 1976). Surprisingly, mineralization occurs in areas with higher $\text{Fe}^{3+}/\text{Fe}^{2+}$ ratios than those of non-mineralized areas.

A detailed statistical study of mineralization at Jack and Garee Lenses was undertaken by Clavarino (1975), and resulted in the following five points:

- 1) Hematite is abundant at the surface and becomes less common with depth, whereas chlorite is rare at surface and increases in abundance with depth. It should be mentioned here that Manning (1979), who studied the Junnagunna prospect, which is capped by the Siegal Volcanics, found that chlorite content increases up the Unit 4 sequence, no doubt reflecting proximity to the capping basic volcanics.
- 2) Mineralization is preferentially biased to the hematite rocks.
- 3) Grain size is not a controlling factor on presence or grade of mineralization.
- 4) There is no preferential distribution of grade with depth, though deeper mineralization is preferentially closer to the dyke.
- 5) Most of the economic mineralization (more than 75%) is within 38m of the surface.

Giblin (1980b) studied the activities and concentration of many ionic species within the groundwater at many of the Westmoreland prospects and found that:

- 1) areas such as Jack and Garee lens which occurred beneath outcropping sandstone had higher Eh and lower pH values than areas such as Junnagunna and Sue which were covered by basalts, i.e. the former areas are more oxidized than the latter.
- 2) These more highly oxidized areas have a higher uranium content in groundwater leaching the ore, than do the more relatively reduced areas.

5.3.6.1 Geology of Individual Prospects at Westmoreland Where Thermoluminescence Studies Were Undertaken

A brief geological description of each of the prospects is now given in order to familiarize the reader with information which will prove helpful in further considerations of the data and in formulating a genetic model. Figure 4.16 may also prove helpful in locating these prospects. Further details of individual prospects may be found in Hills and Thakur (1975), Fuchs and Schindlmayr (1981) and Schindlmayr and Beerbaum (1984).

1) Jack/Garee/Langi Lens

These occur on the southern slopes of the Longpocket Syncline dipping gently to the north, and in Unit 4 of the Westmoreland Conglomerate. This area - the Redtree area - is transgressed by a NE trending joint zone - the Redtree Joint Zone - which has been intruded by a dolerite dyke. Horizontal mineralization is found some 40 metres below surface and is associated with an oxidizing environment and high uranium in

groundwater. No volcanic capping is present over the Westmoreland Conglomerate at this project.

The Jack Lens is approximately 600 metres long and 250 metres wide, whereas the Garee Lens measures approximately 300 metres by 200 metres.

2) Junnagunna

This prospect occurs in flat lying Unit 4 sandstone covered by a variable thickness of Siegal Volcanics up to 25m. The thickness of these basalts increases in a westerly direction in response to the westerly plunge of the Longpocket Syncline.

Junnagunna occurs in the south-west corner of the intersection of the Redtree Joint Zone with the Cliffdale Fault. Movement on the Cliffdale Fault is left lateral with a displacement of 200-250m and on the Redtree Joint Zone is eastern block upthrown by ten metres (Evans 1978). Mineralization occurs immediately beneath the contact of the Siegal Volcanics and Westmoreland Conglomerates as flat sub-horizontal sheets and nearer to the margin of the Redtree Dyke as small vertical pods.

The Junnagunna ore lens occupies an area approximately 700 metres x 500 metres.

3) Outcamp

The Outcamp prospect occurs close to the Darlona Joint Zone and as such is similar to the Jack and Garee Lenses along the Redtree Joint Zone. As yet, no unequivocal proof of the existence of a dyke in the Darlona Joint Zone has been discovered, though the structural similarities with the Redtree Joint Zone exist. A basaltic to andesitic sill occurs within

this area, is usually only a few metres thick and anywhere from 14m to 37m below surface. Its thickness varies but increases in an easterly direction towards the Darlona Joint Zone which may possibly have been a feeder vent for the sill.

Geochemically the sill is similar to the Siegal Volcanics indicating that it was intruded into the sandstone at the same time as extrusion of the Siegal Volcanics occurred.

4) Sue

The Sue prospect abuts the Outcamp prospect on its north-west margin. The sill is thin to absent and thins as the overlying Siegal Volcanics thicken to the west. Mineralization occurs either at the Siegal Volcanic - Unit 4 or at the lower margin, and occasionally also the upper margin of the sill.

5) Black Hill, Red Hill

These are elongated hills of outcropping quartz filled faults with basic volcanics. A dyke has been found at Black Hill and the possibility of an east-west trending dyke exists at Red Hill. Mineralization at both areas is minor.

Total tonnage at all five prospect areas is approximately 15,000 tonnes U_3O_8 at an average grade of 0.17% U_3O_8 .

CHAPTER 6

THE USE OF THERMOLUMINESCENCE IN URANIUM

EXPLORATION AT WESTMORELAND

CHAPTER 6: THE USE OF THERMOLUMINESCENCE IN URANIUM
EXPLORATION AT WESTMORELAND

- Summary of Chapter

All quartz at Westmoreland had ATL glow curves which at the Beverley uranium deposit occurred only in the ore type TL zone. This meant that all quartz at Westmoreland had suffered large radiation effects and therefore only small intensity variations were present approaching known ore-bodies.

For this reason, studies at Westmoreland concentrated on closely spaced geographic and stratigraphic sampling around uranium deposits to see if consistent intensity variations occurred which could be used to predict extensions to, or repetitions of, the known mineralization.

Intensity variations alone were an unreliable guide to proximity to mineralization, though generally HT intensity was at a maximum within mineralization. Ratios of glow peaks were a more reliable guide of proximity to mineralization with the HT/LT ratio increasing towards uranium concentrations.

Traverses examining the glow peak temperature of the HT peak revealed that in areas of uranium mineralization the HT peak temperature was at a minimum i.e. less than 340°C.

Studies of the stratigraphic distribution of radiation effects showed that a vertical homogenization occurs - in some areas high radiation effects occur throughout a drillhole in other areas low radiation effects occur throughout the drillhole, regardless of current uranium contents. In all cases sandstone samples in close proximity to (within three to five metres) the overlying Siegal Volcanics show higher radiation effects than samples further away from this stratigraphic boundary.

Using the observations above, extensive ATL measurements over the rest of the Westmoreland region were conducted to attempt to find other areas with potential for uranium occurrences. Several areas were found.

A single surface traverse over known buried mineralization showed an increase in HT/LT ratio over the known uranium occurrence.

* * *

6.1 Westmoreland - Introduction to Data

More than 700 samples from the Westmoreland area, both on a regional and a very localized scale, were analyzed for their artificial TL characteristics.

The purpose of regional sampling was to examine whether large TL intensity variations seen approaching the Tertiary Beverley deposit, would also be present around Proterozoic deposits which had a very different genetic history. The purpose of the local, or closely spaced, analyses were to see if any consistent trends in TL glow curve parameters occurred across known mineralization. Such trends, if consistently present, could be used to evaluate the proximity of randomly chosen samples in an uraniferous district to further mineralization.

The most striking factor of this study in general is that every one of the 700 samples measured had suffered major radiation effects, i.e. TL intensity was strikingly low and HT peak percentage large, with all glow curves corresponding to those of figure 2.34(d) and (e). This was true regardless of whether the sample was taken from within the ore zone, 10 metres away from it or even 10km away. It also held true, regardless of the direction away from ore, i.e. north, south, east or west. Because of this, the large regional variations in TL intensity present in Tertiary sandstone hosted deposits upon approaching mineralization, were not present at Westmoreland. This also meant that interpretations of TL for

exploration purposes would be more complex as the small variations still present would only correspond to variations of the type presented in figures 2.34(d) and (e).

For this reason work was concentrated on a number of closely spaced local studies across known ore occurrences, or in individual prospects. The purpose of such closely spaced studies was to examine whether consistent variations in TL parameters occurred approaching uranium mineralization and whether such findings could then be used to indicate extensions to, or repetitions of, known mineralization.

The principal area chosen to investigate variations in TL parameters upon approaching mineralization was the Junnagunna prospect. This deposit is well defined and occurs in the south-west quadrant formed by the intersection of the Redtree joint zone and the Cliffdale Fault (figure 5.1). The Junnagunna region was chosen as the large number of drill holes on a gridded pattern made closely spaced sample selection possible. The geology is also relatively uncomplicated with mineralization occurring as flat lying sheets immediately beneath the Siegal Volcanics/Westmoreland Conglomerate contact. Further geological detail is contained in Chapter 5 and also in Fuchs and Schindlmayer (1981).

Other ore occurrences studied were the Jack, Garee and Langi deposits which constitute the Redtree Lenses and the Sue and Outcamp deposits in the Longpocket Syncline. Other prospects studied where mineralization was not well defined were the Huarabagoo, Lilypond, Red Hill, Jinjaree Valley and Flying Fox Anticline areas.

A summary of TL results at Westmoreland are presented in the attached publications; Hochman and Ypma (1984a) dealing with genesis of the Westmoreland uranium deposits and (1984b) - dealing with uranium exploration applications of TL at Westmoreland and other deposits.

6.2 Junnagunna Area

6.2.1 Interpretive Methods Used

Traverses across the Junnagunna orebody examined variations in:

- 1) the intensity of the LT peak;
- 2) the intensity of the HT peak, and
- 3) the HT/LT peak ratio.

Considering small fluctuations in glow peaks at this stage of radiation effects, one would expect the LT peak intensity to decrease, and the HT peak intensity to increase towards an area of mineralization. The HT/LT peak ratio should therefore also increase towards mineralization.

For convenience, trends of increasing radiation effects are referred to as sensitization trends or effects, i.e. the standard test dose results in a stronger HT peak in samples which have been exposed to higher palaeoradiation doses.

The results of this study are presented in figure 6.2 (raw data is given in Appendices 1 and 2). Each data point shown on the traverses has been taken from within ten metres of the Siegal Volcanics Westmoreland Conglomerate contact, i.e. samples are from the same approximate stratigraphic position. A brief resumé of each traverse is given, followed by general conclusions. Locations of drill holes sampled are shown in figure 6.1.

6.2.2 Variations in Glow Peak Intensities

Figure 6.2(A): No discernable trends are observed upon approaching mineralization with the LT peak intensity at a minimum within mineralized holes and the HT peak intensity at a maximum away from mineralization.

Figure 6.2(B): No absolute intensities are available for this traverse.

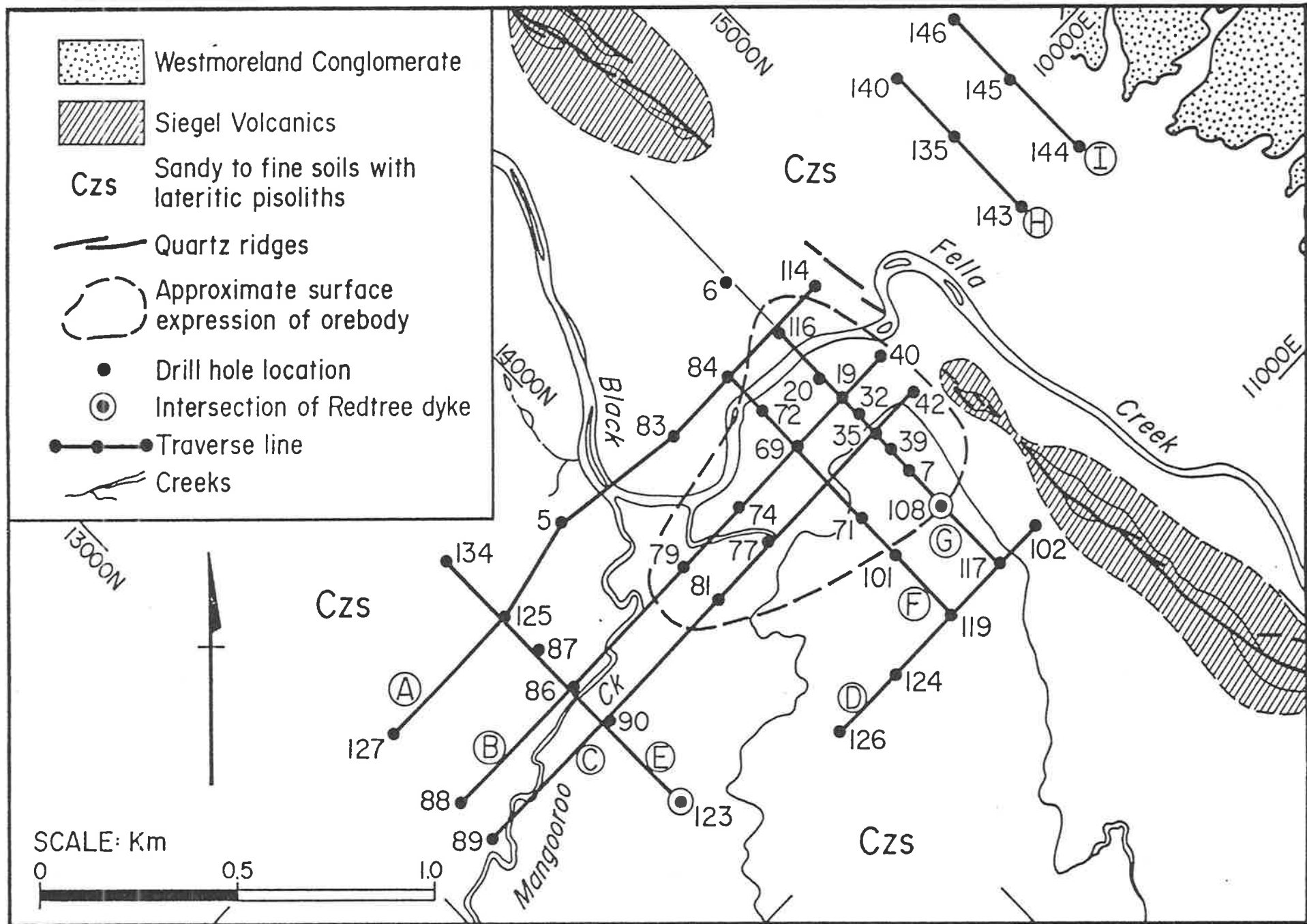


Figure 6.1 Location of Junnagunna drill holes used in TL traverses.

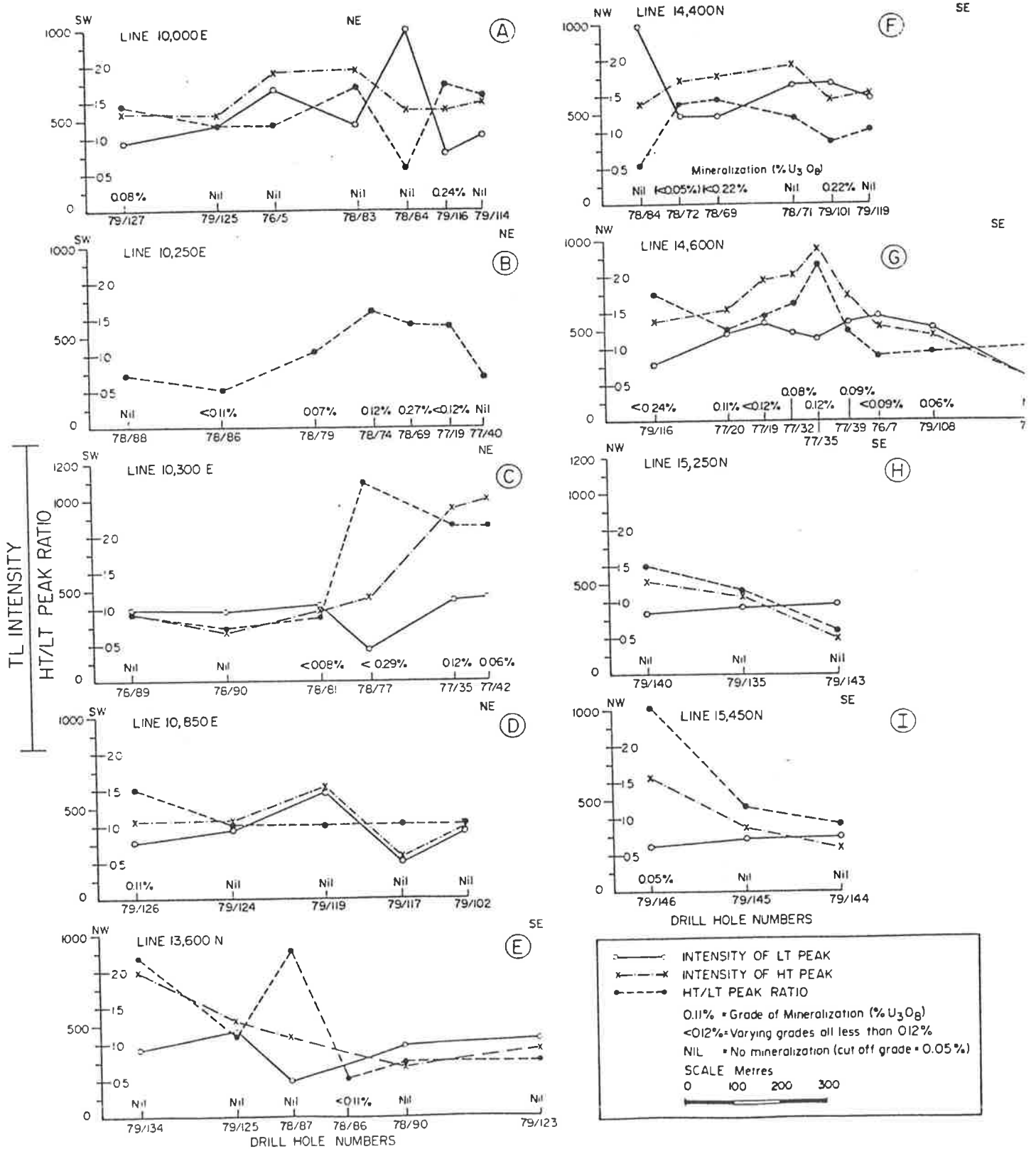


Figure 6.2 Variation in TL glow peak intensities and ratios across the Junnagunna orebody. Drillhole locations are in figure 6.1.

Figure 6.2(C): The LT and HT peak intensities remain consistent whilst approaching mineralization, then the HT peak increases while the LT peak initially decreases and then recovers.

Figure 6.2(D): No systematic variation in either HT or LT peak intensity is observed away from the one mineralized hole (79/126).

Figure 6.2(E): The LT peak intensity varies randomly, whereas the HT peak intensity constantly increases in a NW direction toward hole 79/134. Such a systematic increase is consistent with the theory of increasing proximity to mineralization, and although hole 79/134 is unmineralized, the nearby hole 79/133 contains 0.05% U_3O_8 .

Figure 6.2(F): The HT peak intensity shows no systematic variation through a series of mineralized and unmineralized holes. The LT peak intensity decreases markedly from hole 78/84 (outside the orebody) to hole 78/72 (within the orebody) then slowly increases to the SE.

Figure 6.2(G): The HT peak intensity is at a maximum within the centre of the orebody, decreasing to the NW and SE margins. The LT peak intensity shows no systematic variation.

Figure 6.2(H): The HT peak intensity increases and that of the LT decreases in a NW direction towards 79/140. Such a trend is consistent with the theory of increasing proximity to mineralization and it is worthwhile noting that nearby hole 79/146 contains 0.05% U_3O_8 .

Figure 6.2(I): Similar trends to traverse (H) can be observed though the increase in HT peak intensity is more pronounced.

6.2.2.1 Discussion

A number of points are immediately discernible from the above data, e.g. that no absolute correlation exists between peak intensity and the grade of mineralization. This is not surprising as TL is a measure of the cumulative radiation dose rather than instantaneous ore grade,

therefore it can be expected that some current high grade ore areas should show relatively low sensitization effects (indicative that the high grade ore is of recent origin) and that some currently low grade ore areas show high sensitization effects (indicative of higher ore grades in the past).

Despite this there is a positive correlation in some instances between peak intensity and the geographical ore position (regardless of grade). For example, in figure 6.2(F) the LT peak doubles in intensity away from ore. A smaller increase in LT peak intensity is also observed away from mineralization in 6.2(I), however, the opposite trend is observed in 6.2(G) with LT peak intensity decreasing away from ore. In other traverses the LT peak intensity is variable and no distinct trends are present.

The HT peak intensity is generally at a maximum within the mineralized zones and decreases away from the mineralization, e.g. figures 6.2(C) (G) and (I) and to a lesser extent figure 6.2(F).

No absolute LT or HT peak intensity is characteristic of mineralization, e.g. a HT peak intensity of 600-700 in 5.2(F) corresponds to a grade of 0.22% U_3O_8 , whereas a HT peak intensity of 700-800 in 6.2(A) occurs in a non-mineralized zone. This suggests that absolute peak intensity is of doubtful value as a regional indicator of proximity to mineralization in Proterozoic uranium deposits where there is likely to have been much mobilization and redistribution of mineralization.

Interpretations of these evaluation techniques in this instance are as follows:

- 1) Superimposed upon the regional doses further incident radiation should cause the LT glow peak to decrease and the HT glow peak to increase, as is the case when approaching mineralized zones at Beverley (see Chapter 3).

2) Local fluctuations and some non-linearity can be expected as TL measures positions of both past and present ore, and for this reason, no correlation is expected between present ore grade and TL intensity.

3) Further fluctuations can be caused by the variable concentration of initial hole and electron traps in samples of different origin and by a variable ionization effect caused by short range alpha-particles.

Despite such local fluctuations overall trends are present in some cases. Figure 6.2 indicates that these local fluctuations affect the LT traps more than the HT traps and therefore LT peak intensity alone is not a reliable guide of proximity to this particular type of mineralization. The HT peak intensity is less susceptible to local fluctuation and may be of localized use within known orebodies, e.g. in exploration for extensions of, or repetitions to those already known as illustrated in interpretation of the trend in figure 6.2(H).

6.2.3 Variations in Glow Peak Ratios

The HT/LT peak ratios are also shown in figure 6.2(A).

Figure 6.2(A): The HT/LT peak ratio varies irregularly through non-mineralized holes, increasing in mineralized holes.

Figure 6.2(B): The HT/LT peak ratio is at a maximum within the centre of the orebody and a minimum outside it.

Figure 6.2(C): Again there is a sharp increase in the HT/LT peak ratio within the orebody.

Figure 6.2(D): The HT/LT peak ratio is constant in non-mineralized holes and increases by 50% in the mineralized hole.

Figure 6.2(E): An irregular pattern through non-mineralized holes.

Figure 6.2(F): The HT/LT peak ratio is a maximum within the mineralized area.

Figure 6.2(G): The same trend as in traverse (F) with the HT/LT peak ratio increasing to a maximum within the centre of the orebody.

Figure 6.2(H) and (I): Both diagrams show the same trend as their peak intensity diagrams, i.e. increasing sensitization to the north-west.

6.2.3.1 Discussion

The HT/LT peak ratio generally mimics the mineralization. As with intensity, there is no absolute correlation between peak ratio values and ore grade, but again, this is to be expected as TL measures cumulative rather than instantaneous radiation effects.

As the LT glow peak decreases and the HT glow peak increases, the HT/LT glow peak ratio should also increase. This ratio has generally been observed to be a reliable indicator of increasing radiation sensitization, moreso than peak intensities, because individual intensity fluctuations mentioned above will be cancelled out.

The HT/LT peak ratio in figure 6.2 increases upon approaching the orebody (figures 6.2(B), (C), (F) and (G)) or mineralization (figure 6.2(I)). In these traverses a HT/LT peak ratio of greater than 1.4 indicates proximity to the orebody. Many presently non-mineralized samples have a HT/LT peak ratio of greater than 1.0, indicating that they have suffered radiation damage almost to the same extent as presently mineralized samples. This may suggest that these too may have been mineralized at some stage in the past, that is, they are areas formerly occupied by mineralization.

6.2.4 Further Prospective Areas for Uranium Exploration

Analysis of these three parameters, particularly the HT/LT peak ratio and to a lesser extent the HT peak intensity, could prove useful within a known uraniferous area to identify, in areas distant from the orebody, increasing sensitization trends which are similar to those observed upon approaching the orebody. Such trends can be used to suggest sites for extensions to the orebody or even new orebodies (Figures 6.2(E), 6.2(H) and (I)).

Figures 6.2(H) and (I) show two parallel northwest-southeast trending traverses away from the proposed extension of Redtree dyke (assumed to be close to holes 143 and 144 and having a north-easterly trend). Both traverses indicate increasing sensitization to the northwest with HT/LT peak ratios greater than 1.4 in holes 146 and 140, and intersection of minor mineralization in hole 146. This trend is similar to that observed upon approaching the main Junnagunna orebody and is consistent with the idea of increasing proximity to further mineralization.

Similarly, increasing sensitization to the northwest is shown in figure 6.2(E) towards a locality near which minor mineralization had previously been detected. Results of follow-up work on these sensitization trends are not yet known.

6.2.5 Glow Peak Temperature Traverses

Levy et al (1977) noticed a shift in glow peak temperature with distance from carbonate hosted Pb-Zn deposits. A shift in the temperature of individual glow peaks which is present in or near ore samples could also be used as a potential indicator of proximity to mineralization. Figure 6.3 shows the variation of the HT glow peak

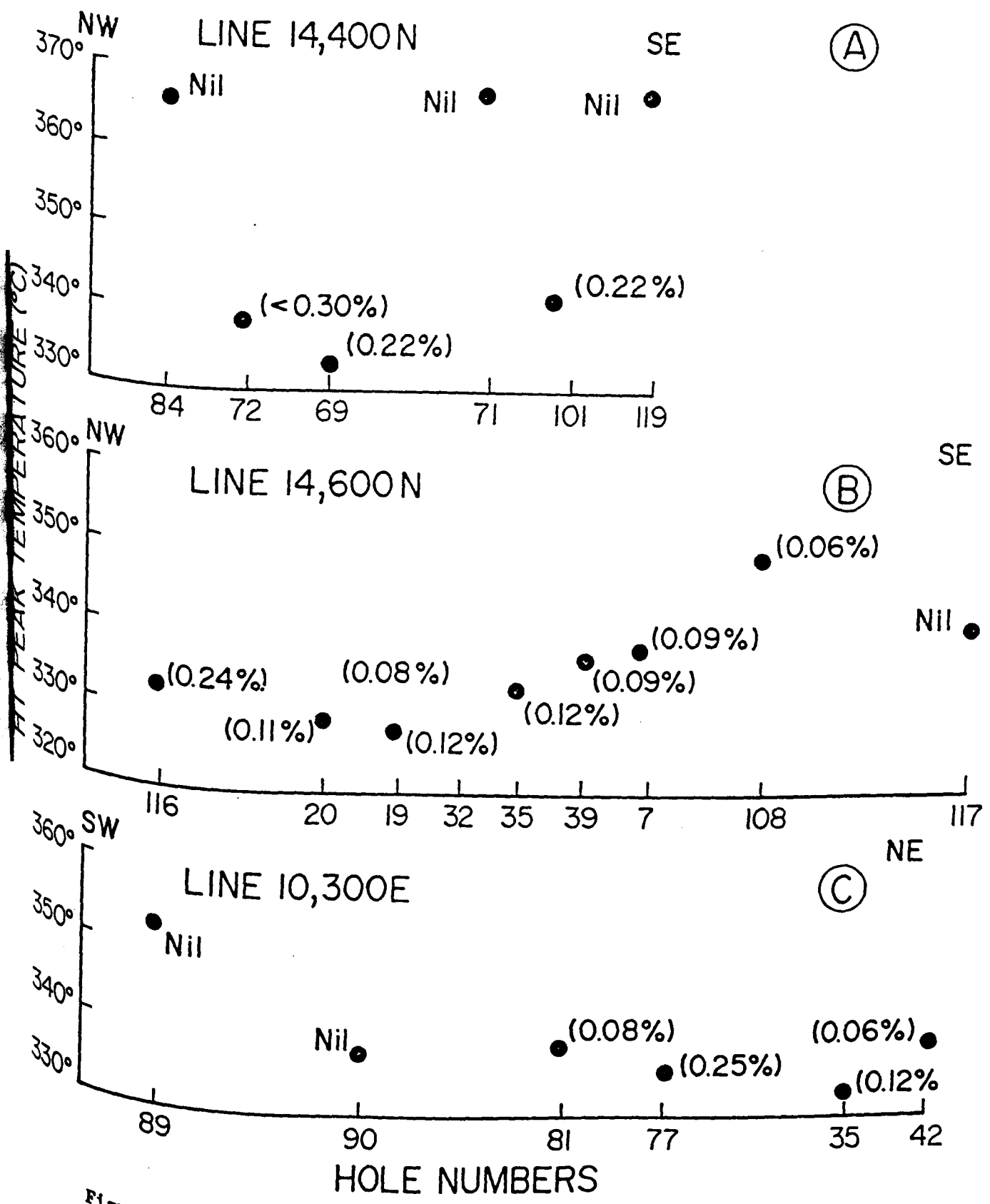


Figure 6.3 Variation in the HT glow peak (350°C) temperature across the Junnagunna orebody.

temperature across three of the previously selected traverses. Figure 6.3(A), indicates that all non-mineralized samples have a HT glow peak temperature greater than 365°C, whereas for two of the three mineralized samples less than 340°C. Figure 6.3(B) indicates a wide spread of HT glow peak temperatures (328°C-352°C) in ore through generally less than 340°C. The temperature is lowest in the central part of the orebody. Figure 6.3(C) again shows all mineralized samples as having a HT glow peak temperature of less than 340°C, as does one non-mineralized sample.

6.2.5.1 Discussion

In general (13 out of 15 samples), the HT glow peak of mineralized samples shows a shift towards a lower temperature of less than 340°C. As this is related to cumulative radiation effects it will not vary according to the time of ore formation, that is, some recently formed ore samples may not show a low temperature shift. Conversely some presently non-mineralized samples may show a low temperature shift indicating that at some past stage uranium was present. The non-mineralized samples from hole 90 in figure 6.3(C) and hole 117 in figure 6.3(B) may represent such cases. As such, this low temperature shift may represent a useful tool (for quartz of the same provenance) to detect areas of past mineralization if accompanied by other signs such as high HT percentage etc.

6.2.6 A Vertical Profile Study Through Westmoreland Conglomerate, Unit 4

Two holes from within the Junnagunna prospect, UMD 78/60 and UMD 78/77 were sampled at intervals of one metre from the area immediately below the overlying Siegal Volcanics, to the end of the hole and their TL characteristics were determined.

UMD 78/60 is situated at 10260E, 14749N (on the grid in figure 6.1) and is an angled hole through the Cliffdale Fault with an azimuth of 045/45. UMD 78/77 is a vertical hole from within the orebody. It is located at 10349E, 14178N. The aim of this portion of the study was to observe the variation in radiation effects down the drill hole as a result of mineralization, and geology. By this, one could gain an idea of the vertical extent of a TL "mineralized" glow curve pattern. A further aim was to test for any areas of greater radiation effects (away from mineralization) to examine the suggestion that there were, or had been, bands of uraniferous heavy minerals which had contributed uranium to these deposits. If so, such bands should be identifiable as regions of greater than background radiation effects. The data and a simple stratigraphic column for each hole is presented in figures 6.4(a) and (b).

6.2.6.1 Hole UMD 78/60

The intensity of the HT glow peak fluctuates down the hole. Generally it is at a maximum at the top of the hole, corresponding to mineralization in the areas between 58m to 80m and again below 125m. The area between 58m and 80m corresponds to the intersection of the Cliffdale Fault which appears to be bifurcated around blocks of the sandstone, containing inclusions of sandstone, e.g. 75m-82m. This area is characterized by having a large portion of fault breccia quartz. (The fault breccia quartz has been affected by the widespread movement of uranium and its TL glow patterns are very similar to those of the Westmoreland Conglomerate - see data in Appendix 1 and 2 where C2 and C3 represent Cliffdale Fault quartz).

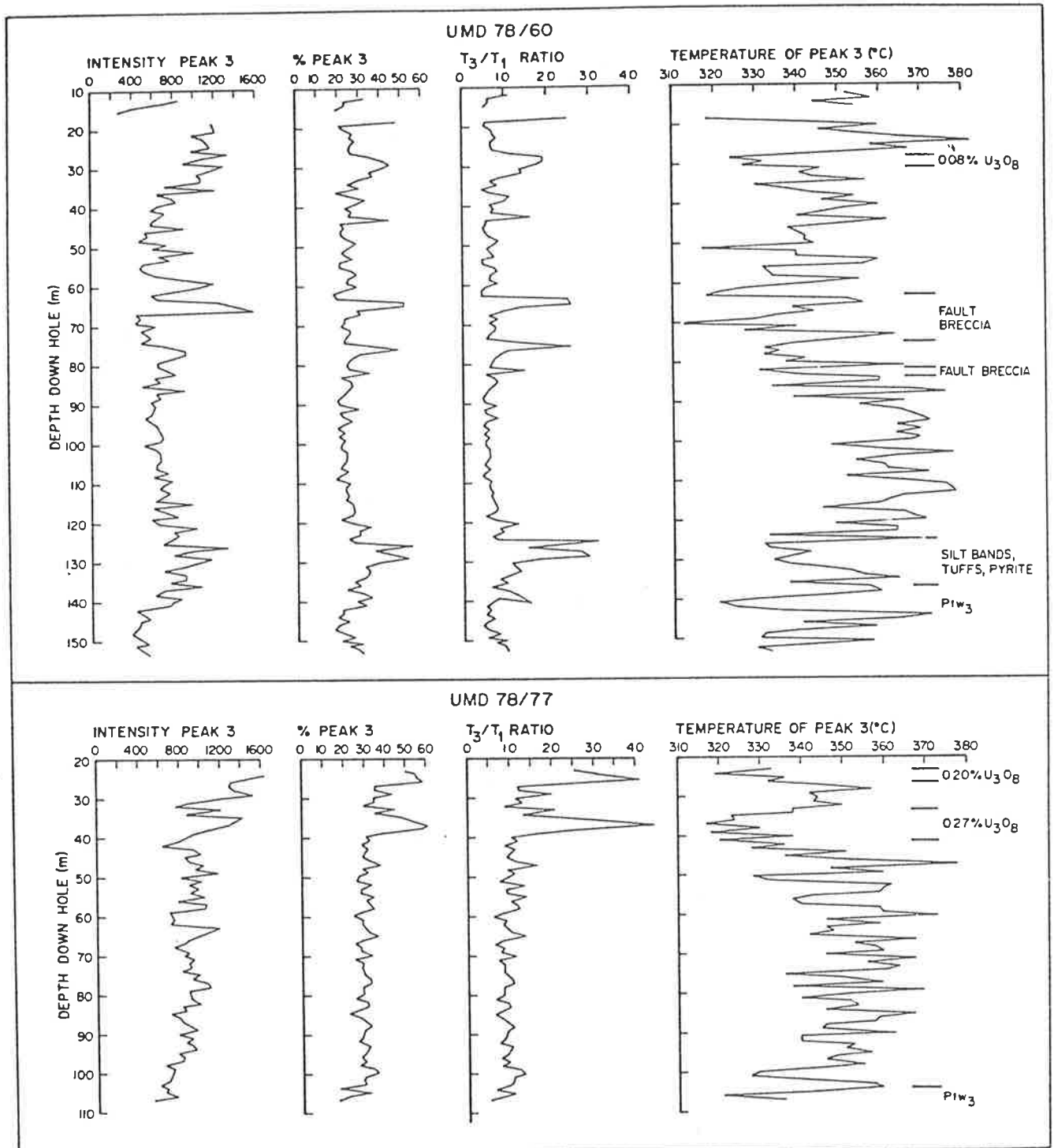


Figure 6.4 Vertical profiles through Unit 4 of the Westmoreland Conglomerate showing variations in glow peak intensity (peak 3 is the HT peak) peak percentages, ratios and temperatures for
 (a) hole UMD 78/60 and
 (b) hole UMD 78/77.
 The sample interval is one metre.

The area between 125m and 137m contains fine grained sandstones with siltstone and tuffaceous bands. Pyrite is also present. Such an area would provide reducing conditions for precipitation of uranium and may also have been host to sub-economic uranium accumulations in the past. The HT peak percentage and HT/LT peak ratios echo that of the HT peak intensity, i.e. being at a maximum within the same areas as above. Generally fluctuations in these parameters are less than those of the intensities.

The HT peak temperature is extremely variable, alternating between low temperature shifts and high temperature shifts within the space of a few metres. Overall though, the following observations can be made:

- 1) that the temperature is at a minimum within the areas where the above parameters are at a maximum;
- 2) the temperature is high in areas that are not mineralized or have no other anomalous features, i.e. "ordinary" sandstone between 90m-120m;
- 3) the "ordinary" sandstone in the upper portion of the hole, 35m-58m, has a lower mean temperature than the "ordinary" sandstone in the lower part of the hole, 90m-120m, indicating a slightly greater sensitization in the upper part of the hole.

6.2.6.2 Hole UMD 78/77

As was the case in UMD 78/60, the intensity of the HT peak fluctuates down the hole though is at a maximum within the mineralized areas. The same is true of the total percentage of the HT peak and of the HT/LT peak ratio, and again these are more stable than the intensity itself.

The temperature of the HT glow peak is extremely variable, varying from a low temperature to high temperature shift within a few metres as

was the case in UMD 78/60. Once again, the areas of mineralization correspond to areas with a low temperature shift.

UMD 78/77 is different to UMD 78/60 in that the "background" values of the HT peak percentage and the HT/LT peak ratio are higher, i.e. around 30% and 1.0 respectively as compared to 20-30% and 0.6-0.7. This points to a higher background sensitization in UMD 78/77 which is not unexpected as this hole is within the present orebody, whereas UMD 78/60 is not. An interesting feature is the consistency of patterns and parameters within the hole which points to a uniform sensitization which has affected the entire hole. The uppermost portion beneath the Siegal Volcanics shows highest sensitization, then the rest of the hole shows a uniform sensitization. This uniform sensitization has been found to be a feature of other holes within the Junnagunna area and is discussed in a following section.

Many variations in TL parameters can be related to variations in host rock stratigraphy, e.g. higher sensitization with fault breccias in UMD 78/60 or silts with chlorite in UMD 78/77. No evidence is found away from presently mineralized zones of bands of higher than background radiation effects which may be indicative of uraniferous heavy mineral bands.

6.2.7 Vertical Homogenization of Thermoluminescence with Drill holes

The consistency with which the TL pattern was repeated for UMD 78/77 has also been found to occur in other holes away from the dyke. Figure 6.6 contains illustrations of the glow curve patterns for some of these holes. Figure 6.5 is a more detailed drill hole location map of Junnagunna, including holes not on traverses of figure 6.1. Although samples are spread over the length of the hole, the similarity of glow curve patterns is interesting, with many holes showing little variation

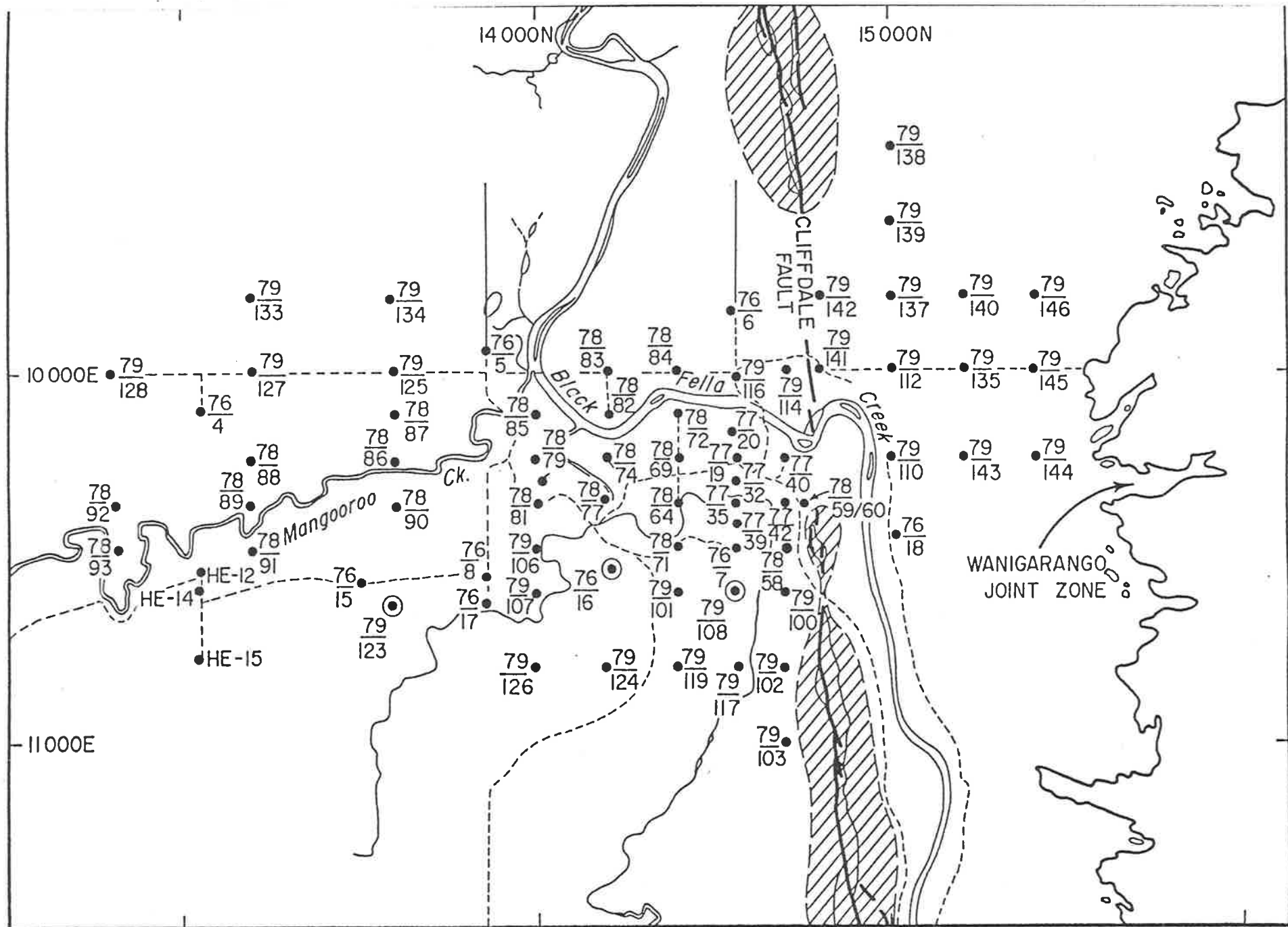


Figure 6.5 Detailed drill hole location map of the Junnagunna region.

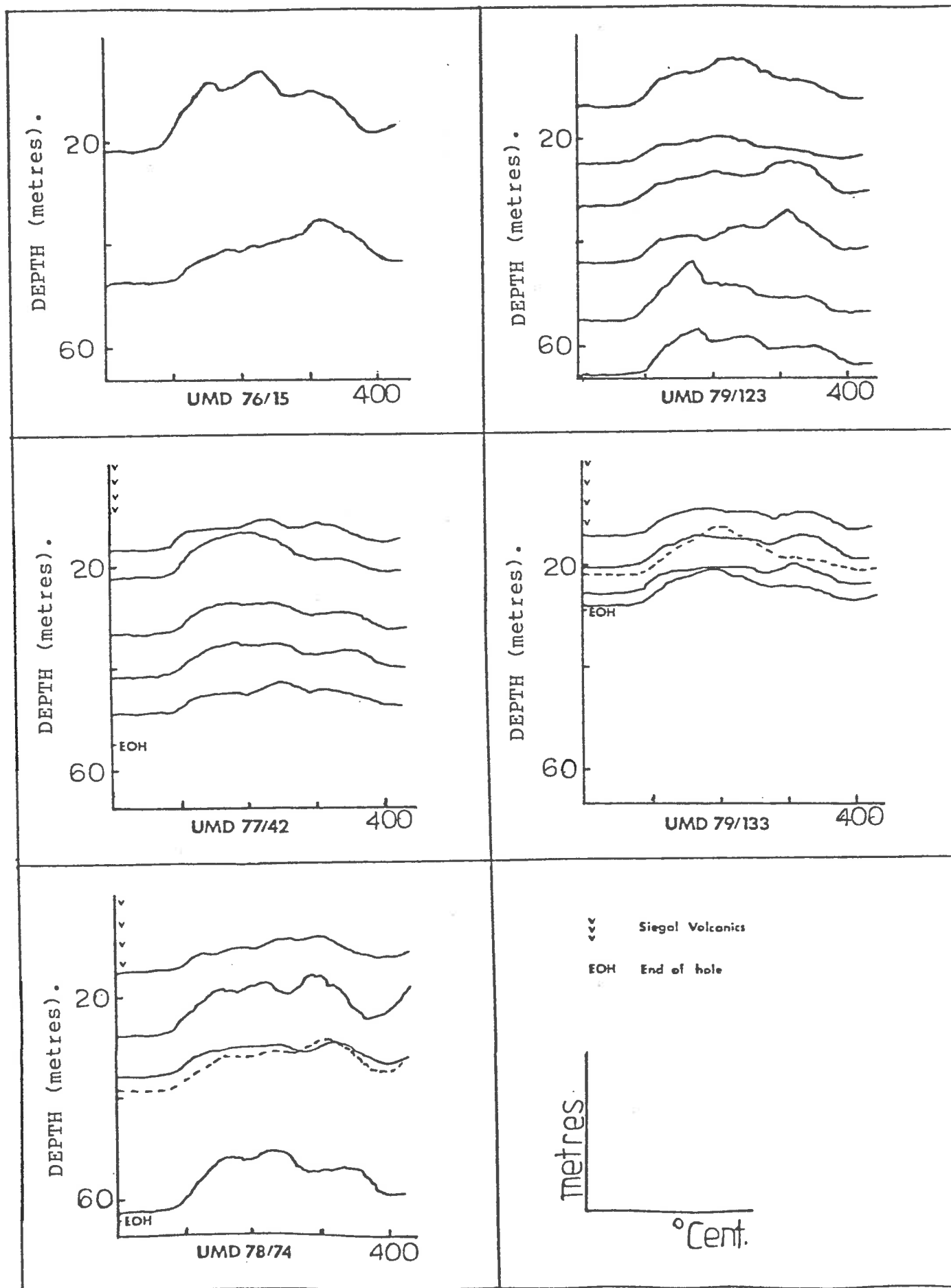
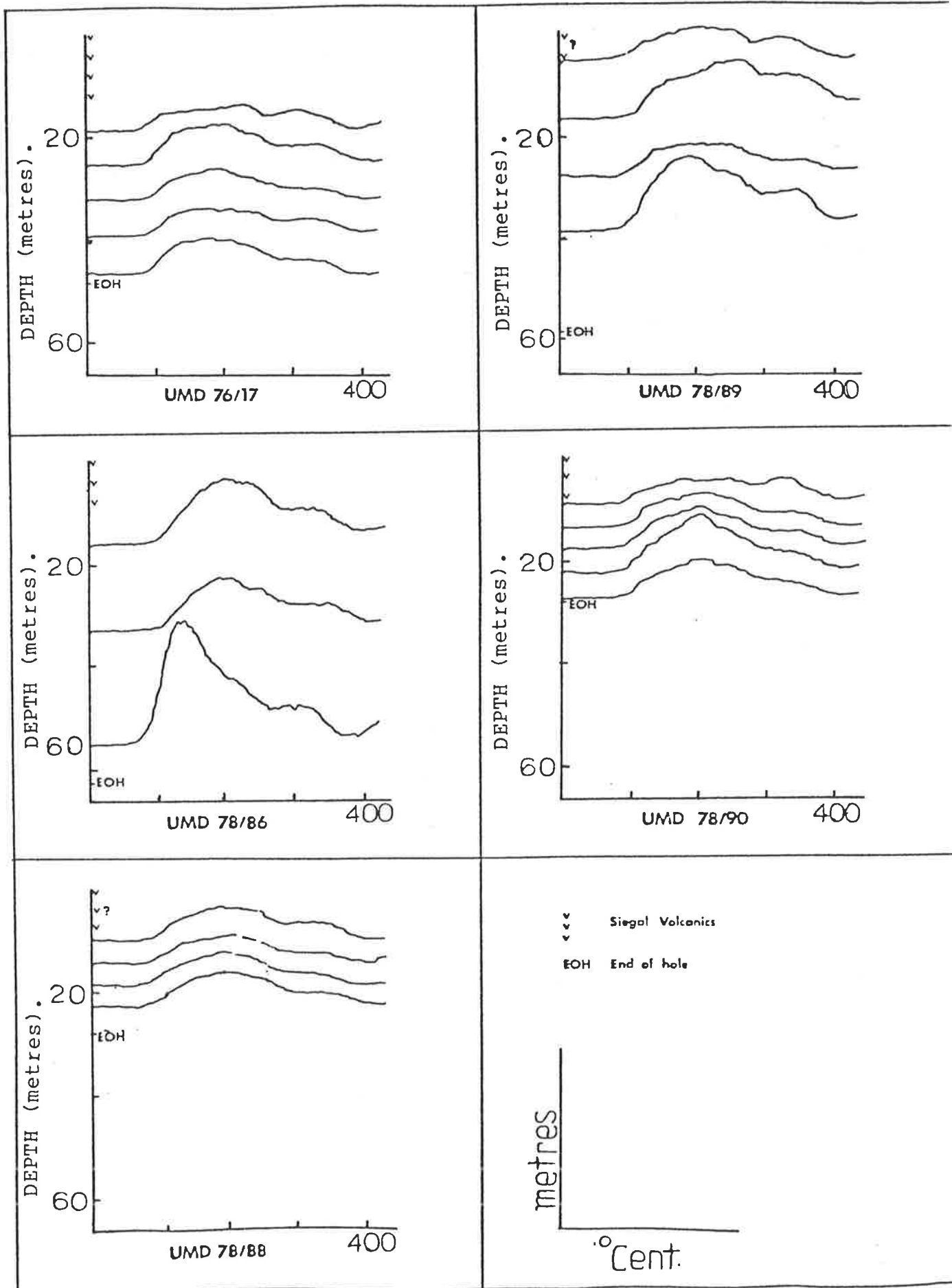


Figure 6.6 Examples of the vertical homogeneity of ATL quartz glow curves in drillholes at Junnagunna: (a) Holes showing an approximate uniform sensitization;



(b) Holes showing an approximate lack of uniform sensitization.

of pattern at all. Sometimes these holes point to high sensitization irrespective of actual grades, e.g. UMD 77/42, UMD 79/133, UMD 79/123, UMD 76/15, UMD 78/74 (figure 6.6(a)); in other cases sensitizations are consistently low regardless of some spurious uranium values, e.g. UMD 78/86, UMD 78/89, UMD 78/88, UMD 78/90, UMD 76/17 (figure 6.6(b)).

Interestingly this apparent vertical homogenization only occurs in areas with a volcanic capping, e.g. Junnagunna, Longpocket, but was not found in areas devoid of such a volcanic capping, e.g. the Redtree lenses. (see further in section 6.3.1).

Given the uniform provenance of the Unit 4 sandstone, the vertical homogenization may indicate vertical movement of uranium through the strata, such that actual uranium concentrations are displaced up and down the stratigraphic column thus sensitizing the host rock over the entire hole rather than isolated spots. Such a factor is seen to be important in the genesis of the deposits and is discussed further in Chapter 7.

6.2.8 Distribution of Sensitization: Contour Maps

Since TL measures the cumulative radiation dose rather than instantaneous ore grade, it can be used to distinguish between areas of different radiation sensitization and to point out trends of increasing sensitization. A comparison of these trends at varying stratigraphic levels may lead to an understanding of protore movement within the Junnagunna prospect.

Contour maps of HT/LT peak ratios are shown in figure 6.7. Values of HT/LT peak ratios were contoured from "slices" of the sandstone beneath the Siegal Volcanics, i.e. the peak ratio value was taken for each hole within a particular 10-20 metre sandstone interval and these values were grouped according to their similarity to obtain an overall sensitization pattern for the Junnagunna region. If any interval

contained more than one sample point the highest value of the HT/LT peak ratio was selected, i.e. the most highly radiation affected sample (recalling that the HT/LT peak ratio increases with increasing radiation).

This method of presentation of the data thus makes it possible to observe large areas of radiation effects within a particular stratigraphic interval. A description of data presented in each diagram, along with interpretation, follows:

Figure 6.7(a). This is the contour map of the HT/LT peak ratio in the 10 metre slice beneath the Siegal Volcanics. Within the Junnagunna region the area of highest radiation effects occur in a north-westerly trending belt between grid lines 14,000N and 14,300N. This area then turns northerly and continues to the Cliffdale Fault. A comparison of this diagram with that of the distribution of mineralization (figure 6.8) indicates that this area of highest radiation effects coincides with the most highly mineralized area. Other areas of higher radiation effects occur as isolated patches either within the mineralized area, e.g. UMD 77/42, UMD 77/35, UMD 77/32 or outside of it, e.g. UMD 78/91, UMD 78/87, and UMD 79/134.

In the Junnagunna North area where mineralization is too sparse to be contoured, the area of highest radiation effects occurs at the most north-westerly edge of the prospect. Recalling the trends observed in figures 6.2(H) and (I), indicative of increasing proximity to mineralization, it thus confirms the potential of this area for further exploration. A similar argument can also be used for the radiation effects in UMD 79/134 which had also been previously found to be sensitized though not mineralized.

Two areas of lower radiation effects are prominent: 1) the area to the south-east of the dyke (apart from UMD 79/107 which is strongly mineralized both at surface and depth) and 2) the region between 10,100E

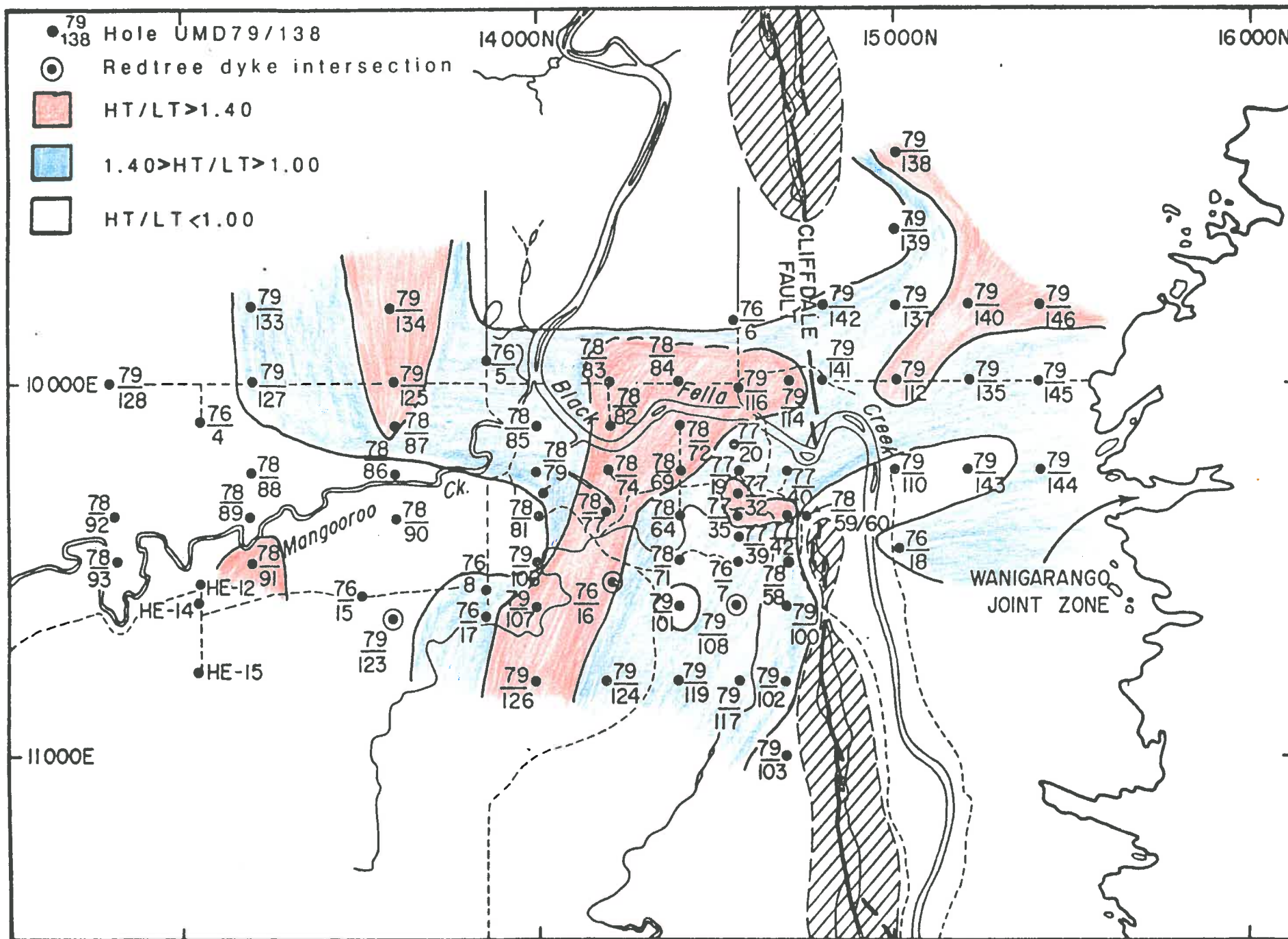


Figure 6.7(a) Contour maps showing distribution of sensitization at Junnagunna: for the 10 metres below the Siegal Volcanic/Westmoreland Conglomerate contact.

and 10,400E parallel to the dyke, despite isolated patches of mineralization, e.g. UMD 78/86. The former may be explained by the lack of mineralization on the east side of the dyke, which itself reflects the uplift and erosion of the upper 10 metres of Westmoreland Conglomerate, thus removing the (upper more silty and chloritic) part of the sandstone suitable for uranium precipitation. The latter reflects the lack of near-surface mineralization related to the dyke.

Figure 6.8(b). This diagram represents the HT/LT peak ratio contour map of the slice 10m-30m below the Siegal Volcanic contact. It is immediately obvious that overall radiation effects are lower than for the overlying 10m of sandstone, again reflecting the greater suitability of the uppermost part of the sandstone as a host for uranium. Three main areas of interest are discernable:

- 1) Areas of higher radiation effects occurring within the orebody and due to the presence of mineralization extending over greater vertical depth either in the central portion of the orebody, or closer to the dyke margins.
- 2) Areas of higher radiation effects occurring parallel, and close to, the Cliffdale Fault. A sharp drop in peak ratio values occurs in the surrounding areas, i.e. there is a distinct difference between highly and lowly radiation affected areas. Areas of higher radiation effects reflect in part the slightly deeper mineralization in these areas, but may also be the result of a banking up of uraniferous solutions or protore, at the impermeable quartz-filled Cliffdale Fault. Such solutions may have been derived by leaching of the present orebody and then moving down dip in the sandstone towards the fault.

- 3) An anomaly at Junnagunna North reflects both proximity to the assumed extension of the Redtree dyke near holes UMD 79/140 and UMD 79/143, and also the occurrence of tuffaceous layers in UMD 79/139.

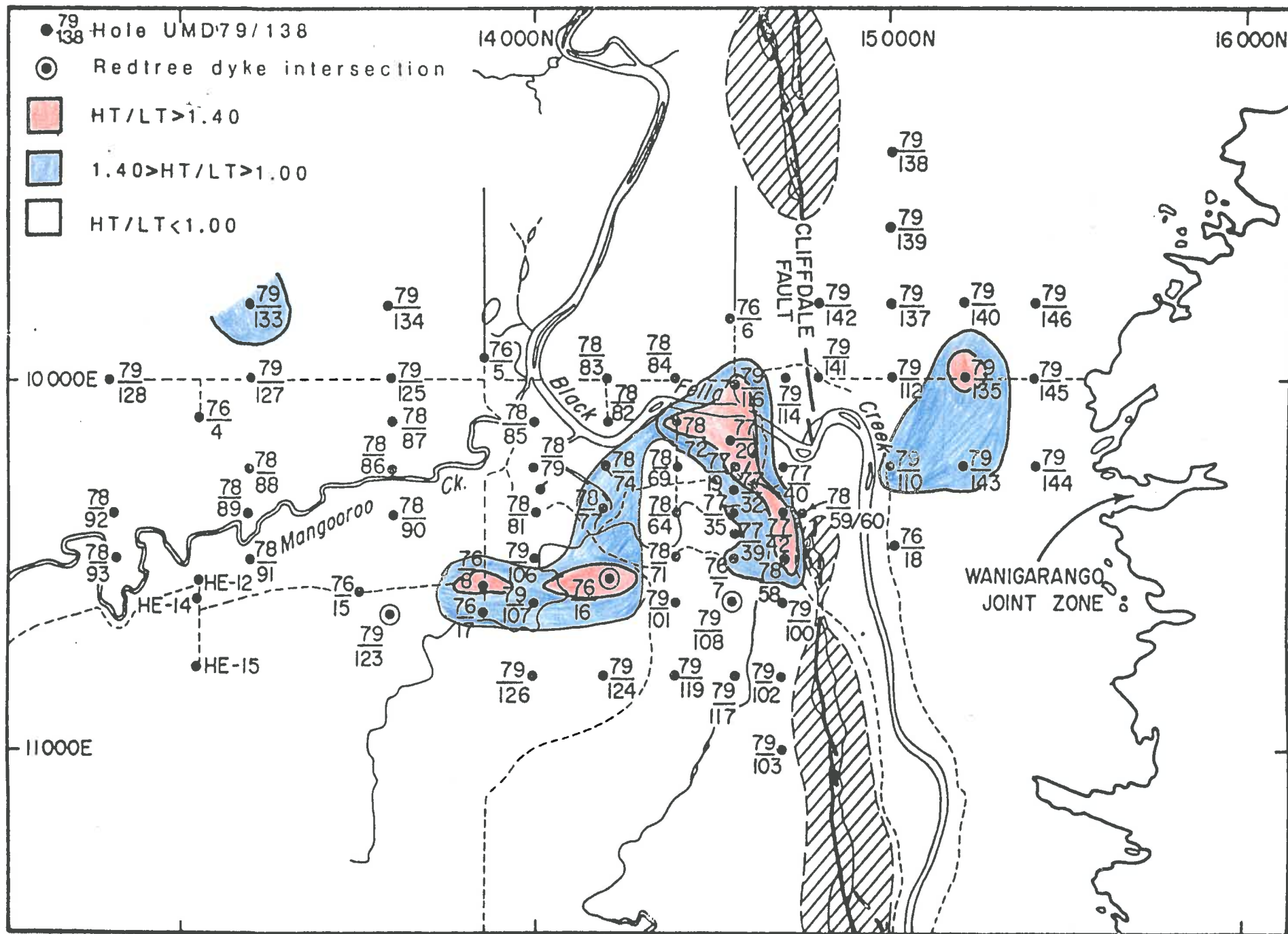
Figure 6.8(c) represents the HT/LT peak ratio contour map for the sandstone slice 30m-50m below the Siegal Volcanics.

A trend of higher radiation effects can be observed through the holes UMD 79/123, UMD 76/8, UMD 76/16 and UMD 79/108, all of which intersect, or are very near to the Redtree dyke. A similar trend is observed at UMD 79/110 in Junnagunna North which is close to the assumed dyke extension.

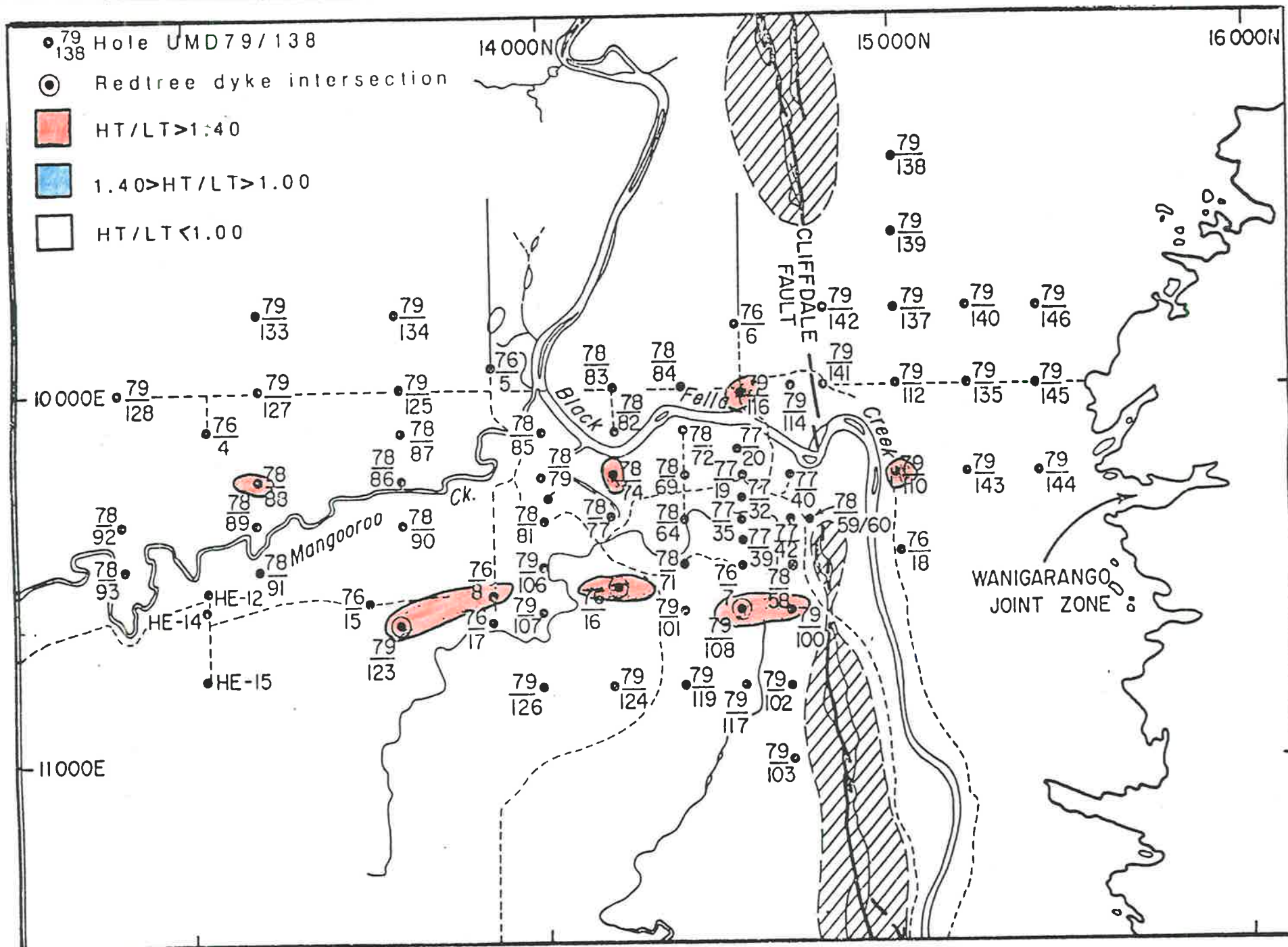
The anomalously high radiation effects in UMD 78/59 (HT/LT=2.59) is due to the presence of mineralization at this depth, near to the Cliffdale Fault. Other areas of higher radiation effects, e.g. UMD 79/116, UMD 79/103 and UMD 78/88 are due to the presence of tuffs or tuffaceous sediments.

6.2.8.1 Discussion

Generally, higher sensitization in the upper portions of the sandstone coincide with mineralization, though a strong anomaly in the non-mineralized Junnagunna North prospect further illustrates its potential. Higher sensitization at depth was also found to coincide with 1) the margins of the dyke related to pods of vertical mineralization and 2) the Cliffdale Fault, which, coupled with an increased proportion of deep mineralization in this area leads to the hypothesis of down-dip movement of protore/ore towards the impermeable Cliffdale Fault. No wholesale lateral or vertical sensitization trends, indicative of transport directions, are discernable. This argues against hydrothermal introduction of uranium from the dyke, or solutions emanating from



(b) Contour maps showing distribution of sensitization at Junnagunna: 10-30 metres below the contact



(c) Contour maps showing distribution of sensitization at Junnagunna: 30-50 metres below the contact.

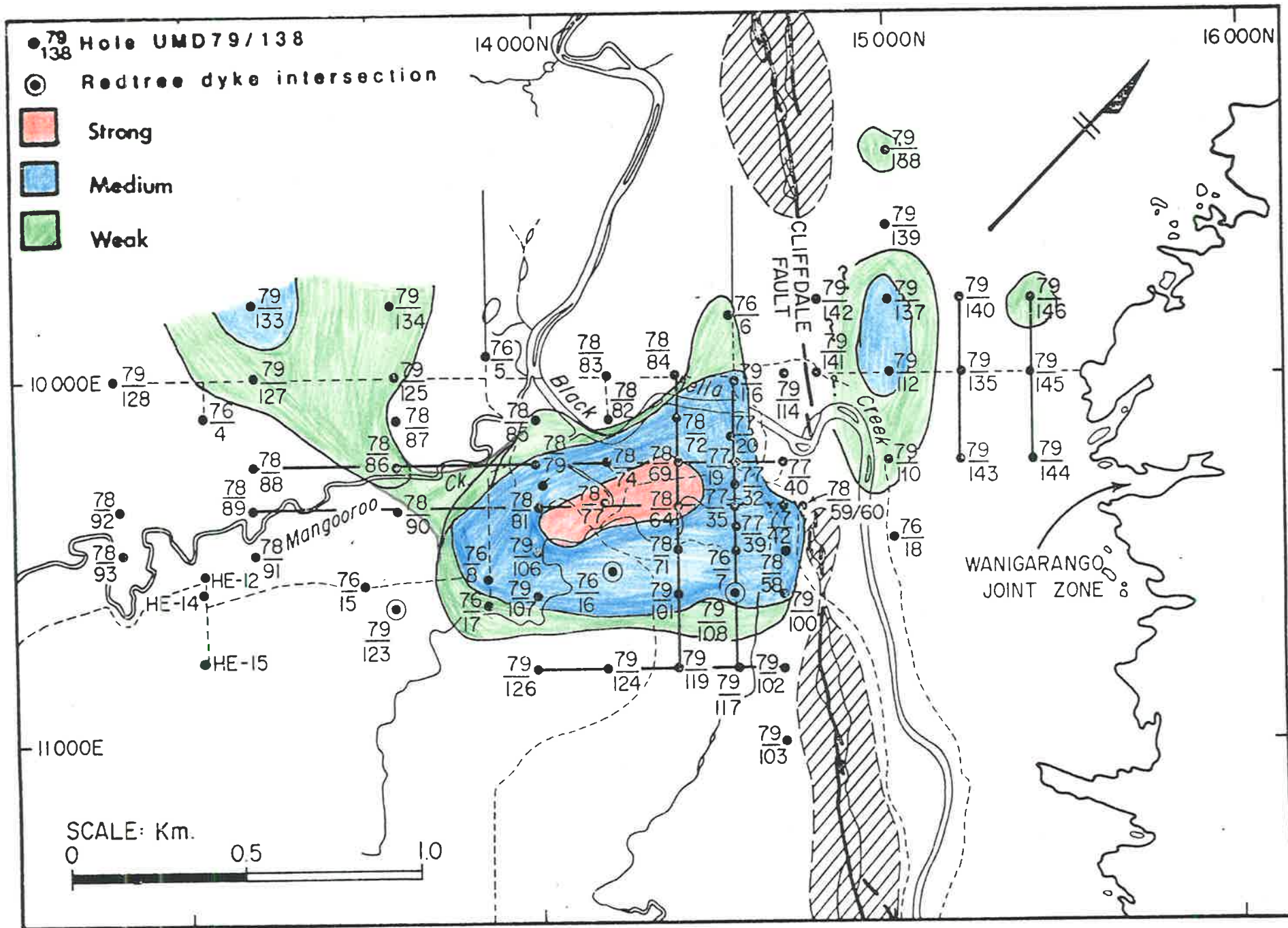


Figure 6.8 Distribution of mineralization at Junnagunna.

faults, as vertical and/or lateral radiation zones would be expected around such features if such were the case.

6.3 Variation Diagrams: 190°C Peak (LT)/260°C Peak (MT) vs 350°C Peak (HT) Percentage

Although the methods discussed previously demonstrate the applicability of TL as an exploration tool for sandstone hosted uranium deposits, only one variable of data, or data for one specific depth, can be presented at any one time. A method of incorporating several data parameters (peak percentages, ratios and the apparent low temperature shift (LTS) in the HT glow peak temperature) at all depths, has been derived and is shown in figure 6.9. This plot involved a calculation of the percentage of each of the three major glow peaks as described in Chapter 2.6. The ratio of the LT (190°C) peak over the MT (260°C) peak has been plotted on the ordinate, and the total percentage of the HT (350°C) peak on the abscissa. For these ATL studies, samples in a normal or low level gamma radiation environment, i.e. not subject to large amounts of radioactivity from the presence of uranium or other radioactive materials, would have a LT peak which would dominate over the others. Hence, the LT/MT peak ratio would be high and the percentage of the HT peak correspondingly low. Such samples would therefore plot in the field indicated in the upper left-hand corner of figure 6.9.

One could expect the LT/MT peak ratio to decrease for increasing sensitization, and the HT peak percentage to increase proportionately over LT and MT peak percentage. Such samples would be expected to progress through the middle increasing sensitization-protore-ore fields of figure 6.9. This trend is indeed very accurately followed as will be seen in examples below, where all data points in the lower right-hand corner of the diagram are from ore grade material.

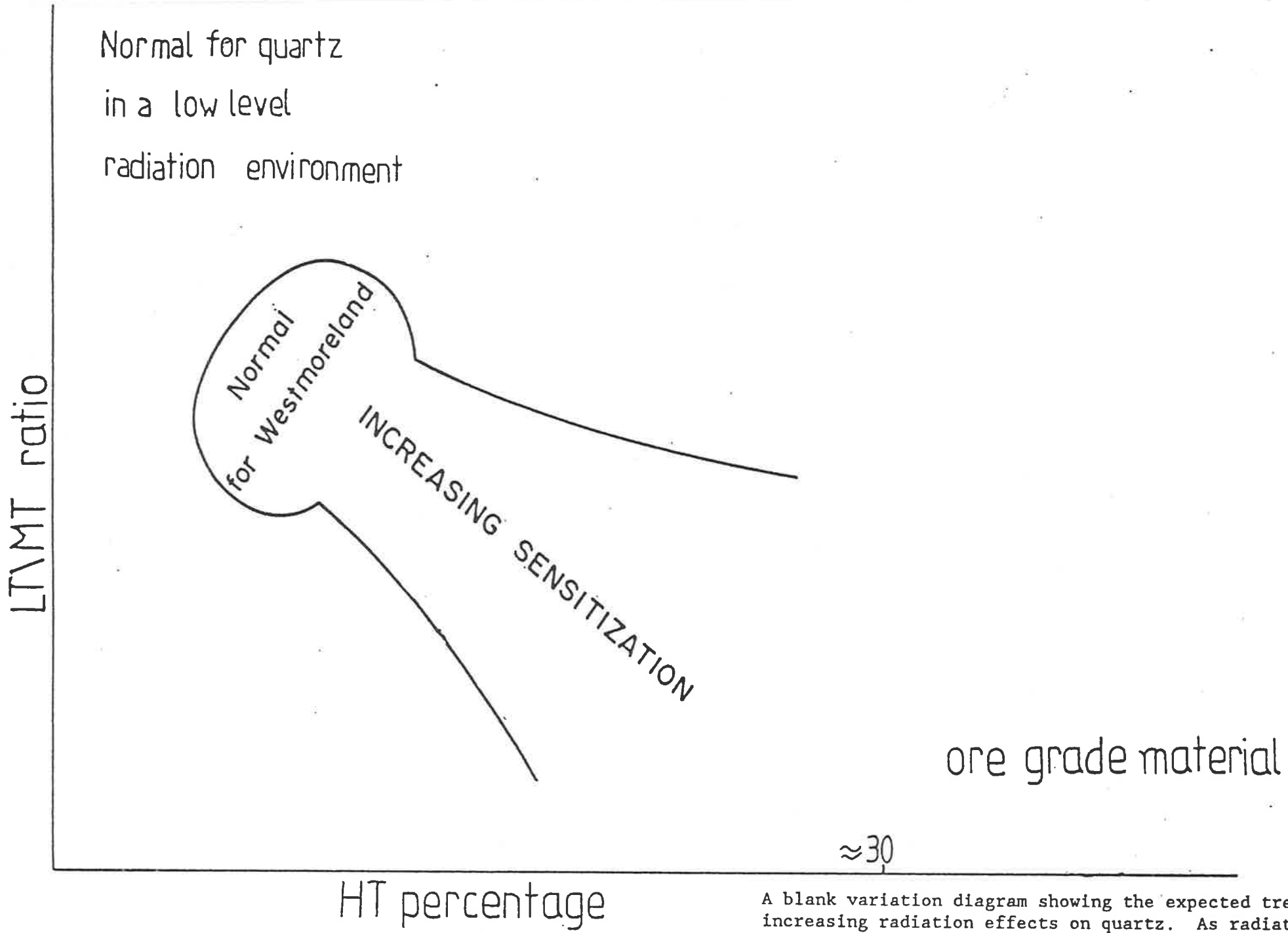


Figure 6.9

A blank variation diagram showing the expected trends of increasing radiation effects on quartz. As radiation effects increase the LT/MT ratio should decrease and the HT percentage should increase.

Wherever a LTS in the HT peak occurs it is marked thus:<. If a LTS occurs in an area not presently mineralized then it could possibly represent an area of past mineralization,)i.e. an area from which uranium has recently been leached) especially if accompanied by a strong HT peak.

Data for different ore occurrences and prospects are now presented on these variation diagrams in order to examine:

- 1) the overall patterns of ore movement, and
- 2) the suitability of other potentially interesting areas for the presence of uranium ore. It is in these latter areas that the advantage of these diagrams is apparent, i.e. the paucity of data prevents the use of intensity, ratio or temperature traverses to determine prospective areas, but these diagrams help to classify individual samples as indicative of normal, protore or ore.

6.3.1 Jack-Garee-Langi Uranium Deposits (Redtree Lenses)

Each point on the diagram represents a sample taken from a particular hole at a particular depth. Drill hole locations in the Redtree area are contained in figure 6.10. Raw data for each of these points is contained in Appendix 1. The data for the Jack-Garee-Langi Lenses is plotted in figure 6.11. The following points are discernible:

- 1) The radiation effects and sensitization at Jack and Garee Lenses are far stronger than in any other area (as will be borne out by discussion on further areas). More samples plot in "strong" ore positions and there are proportionately less "normal" samples, e.g. UMD 77/22, 24.7m, 37.7m; 63.3m and N130 42m plot in the extreme right-hand corner, or beyond. Many

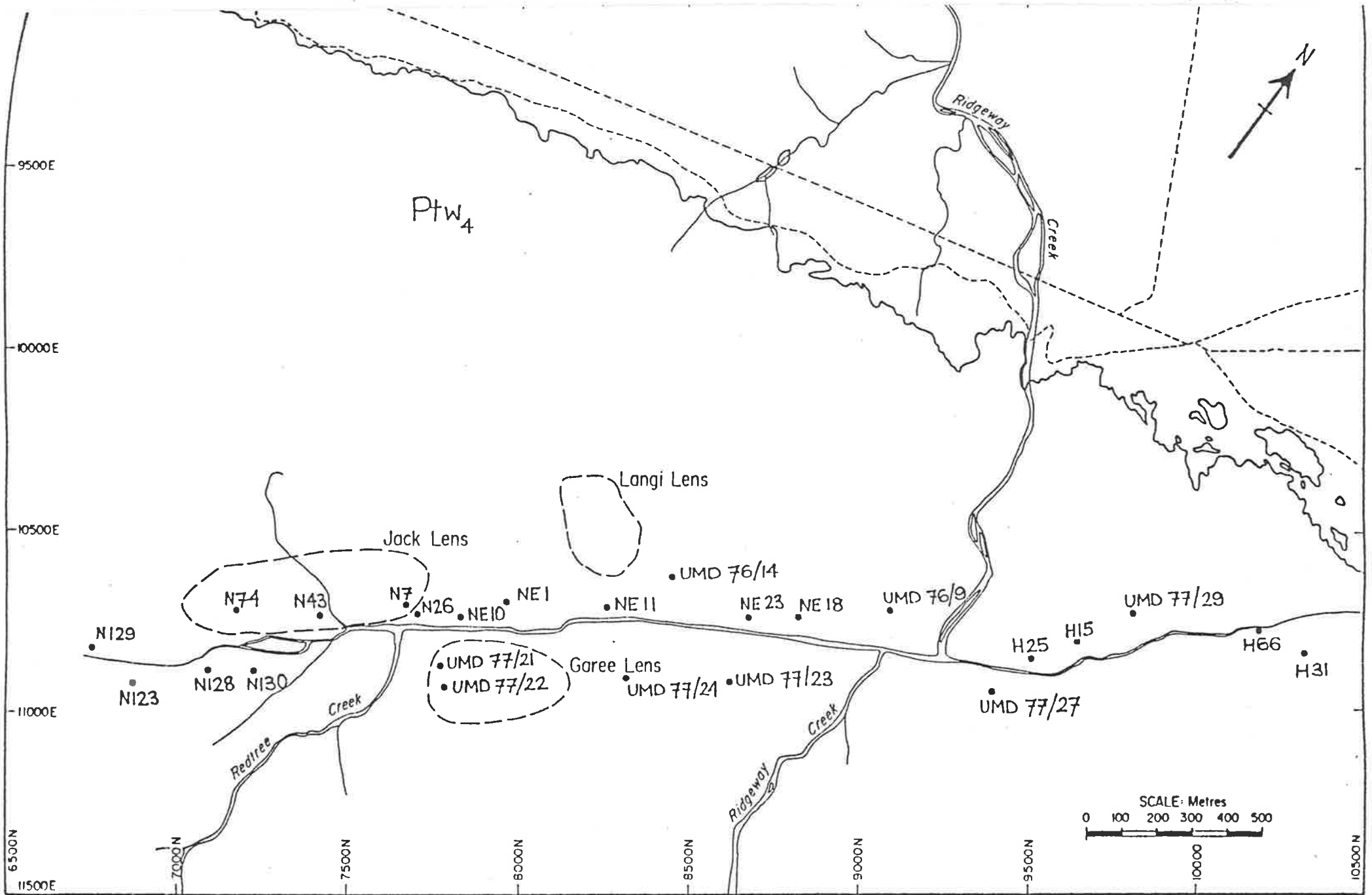


Figure 6.10 Location of drill holes sampled at the Redtree Lenses and Huarabagoo prospect.

samples plot in the protore type TL field with comparatively few in the normal or low level field.

- 2) The most highly radiation affected material occurs to the south-west of Jack Lens. Much of the sample material taken from this area, showing high radiation effects is not ore, e.g. N128 71m and N123 54m. Considering current grades and location of mineralization, it therefore appears that this area could have contained the highest grade mineralization over the most extended period of time. As such, this area, i.e. in the vicinity of N129, N123, N128, and also the area further to the south-west along the dyke, is worthy of further exploration for high grade ore.
- 3) Samples taken from within the Jack and Garee Lenses also show large radiation effects reflecting the ore grade and/or residence time, e.g. N74 2m, 76m; UMD 77/22 24.7m 37.7m. It should be noted, however, that some (not all) high grade ore samples from the Garee Lens do not plot in strong ore positions but only on the ore/protore type TL boundary, e.g. UMD 77/21 15.6m; UMD 77/22 10m.

This implies a more recent derivation for these ore samples - perhaps a leaching and reprecipitation of older ore. Such an idea is supported by the work of Giblin (1980b) who showed that the ore in the Jack and Garee Lenses was more oxidized than any other in the Westmoreland region, and that groundwater washing these orebodies also had the highest uranium content of those sampled. This indicates a greater leaching and reprecipitation rate in the Redtree ore zones. Further confirmation of this is seen in the greater abundance of secondary surface mineralization coating the underside of half buried rocks above the Jack, Garee and Langi Lenses.

- 4) Radiation effects decrease along the dyke to the north-east, i.e. towards Huarabagoo and Junnagunna. This coincides with:
- a) a decrease in ore grade;
 - b) an absence of large mineralized blankets or lenses, and
 - c) an appearance and gradual increase in thickness of the basaltic Siegal Volcanics.
- 5) When compared to the Junnagunna prospect (following section) the total sensitization is stronger in areas capped by extrusive volcanics, e.g. Junnagunna, than in areas devoid of these, e.g. Jack and Garee Lenses, whereas the sensitization at some individual spots is much higher in the Jack and Garee Lenses than at Junnagunna.

The significance of this observation is that sensitization at Jack and Garee Lenses is confined to a few high grade spots which could indicate that the ore has been vertically less mobile than at Junnagunna. As an example of this localized sensitization, at Jack Lens, an apparent recovery of low temperature peaks has occurred in holes N128 and N129 without affecting the sensitization of the high temperature peaks or the LTS. Total TL intensity of these samples is therefore very strong. The lack of vertical mobility of ore here is also indicated by the lack of vertical homogenization throughout the hole in contrast to Junnagunna, Lilypond, Sue and Red Hill - all areas that are capped by volcanics.

- 6) Some samples plotting within the ore field of 6.11 are not actually mineralized, e.g. UMD 77/24 45m. This implies that samples such as this either have not been mineralized until very recently, or that mineralization is very close by. Hole UMD 77/24 is 200 metres down-dip from the Garee Lens, and given the high leaching rate of these ore zones it is possible that small orebodies could be formed down-dip from the major

orebodies. In fact, the Langi Lens - a small orebody containing approximately 300-400 tonnes U_3O_8 - is thought to have formed by such a mechanism, i.e. down-dip leaching and reprecipitation of ore from the Jack Lens.

As UMD 77/24 30m-45m shows the TL attributes of ore and protore, and UMD 77/23 31m the presence of protore, then it is therefore possible that Langi Lens type mineralization could be found in this area.

A further encouraging sign regarding the potential of the UMD 77/24 - UMD 77/23 area is its geographical position, i.e. adjacent to the Langi Lens on the opposite side of the Redtree dyke.

- 7) The distribution of protore type TL within the Jack and Garee Lenses is usually confined to samples of the underlying unit (Ptw₃), e.g. N123 111m, N129 106m and N128 110m. This may indicate the presence of ore in these conglomerates at some past stage, though more likely reflects the lithology of the unit itself which is characterized by having a high volcanic component. This has important genetic implications which will be further discussed in the following chapter.

Protore type TL within the Unit 4 sandstone only appears further towards the Huarabagoo area. This too may indicate a down-dip movement of leached ore solutions or may be related to the absence of horizontal mineralization and increasing presence of vertical pods.

- 8) Two sandstone samples taken from sandstone intervals within the Redtree dyke show slightly less radiation effects than all other samples. These samples N123 84m and NE1 70m have LT peak intensities twice as high as other Westmoreland sandstones. In comparison with host rock of the Beverley area (Chapter 3) they have still however, suffered radiation effects and are still two orders of magnitude less bright than the background

host rock of Beverley. These samples may represent background material for Westmoreland.

Possible explanations for the increased LT peak intensities are:

- a) The dyke may have acted as a permeability barrier to mineralizing solutions resulting in less radiation exposure to these samples.
- b) The heat of the dyke has caused annealing of the crystal lattice to such an extent that restoration of some low energy electron and hole traps occurred.
- c) The LT peaks have been resensitized as part of recovery after large radiation effects. This possibility is not considered likely, due to the absence of an accompanying low temperature shift in the HT peak.

A combination of a) and b) seems the most likely explanation. Studies by Durrani et al. (1977a) show that higher temperatures accompanying irradiation result in an increased TL signal. Annealing experiments by Kaul et al. (1972) also indicate increased TL intensity accompanying heat. This is in agreement with possibility b) above, though absolute influences of the heat of the dyke cannot be known or accurately equated with laboratory annealing experiments, as a cooling basic magma will have a heat effect far in excess of the time presented in laboratory experiments.

Protection of this quartz from outside influences after cooling of the dyke led to the quartz being preserved in its then present state, whereas similar heat affected quartz on the margins of the dyke would have suffered further radiation effects in the course of uranium protore and ore movement.

The significance of this observation is that it indicates that the quartz comprising the Unit 4 sandstone had already suffered major radiation effects, prior to being affected by radiation from the ore.

6.3.2 Junnagunna Area

Data for the Junnagunna region is shown in figure 6.12. Despite crowding due to the number of data points, the following points are discernable.

- 1) Compared to the Jack and Garee Lenses, samples at Junnagunna have less radiation effects. This is borne out by a number of points, that is:
 - a) the lack of "strong" ore type TL such that the HT peak percentage is never greater than 60%. This is further illustrated in figure 6.13 which is a plot exclusively of mineralized samples at Junnagunna;
 - b) the greater proportion of samples in the "normal" type TL position as opposed to protore type TL positions in the Redtree area;
 - c) the fact that fewer samples have a distinct low temperature shift in the HT peak.
 - d) the position of many presently mineralized samples away from the main orebody which plot in the protore type TL field rather than the ore type TL field, e.g. UMD 79/133 25m, UMD 79/125 25m, UMD 79/126 27m and UMD 78/69 26m.

These observations indicate that ore residence time is likely to have been shorter here than at Jack and Garee Lenses.

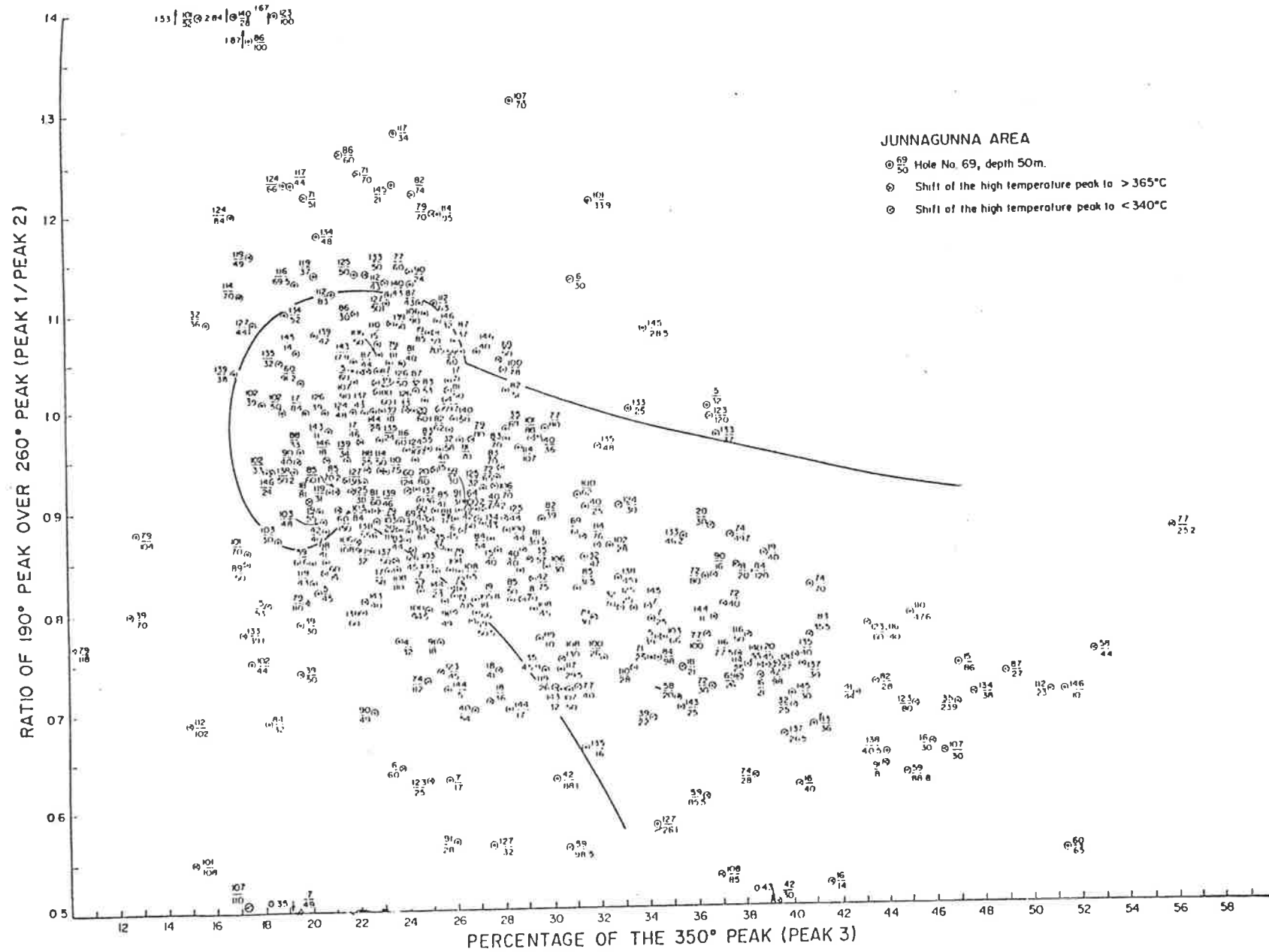


Figure 6.12 Variation diagram for the Junnagunna area.

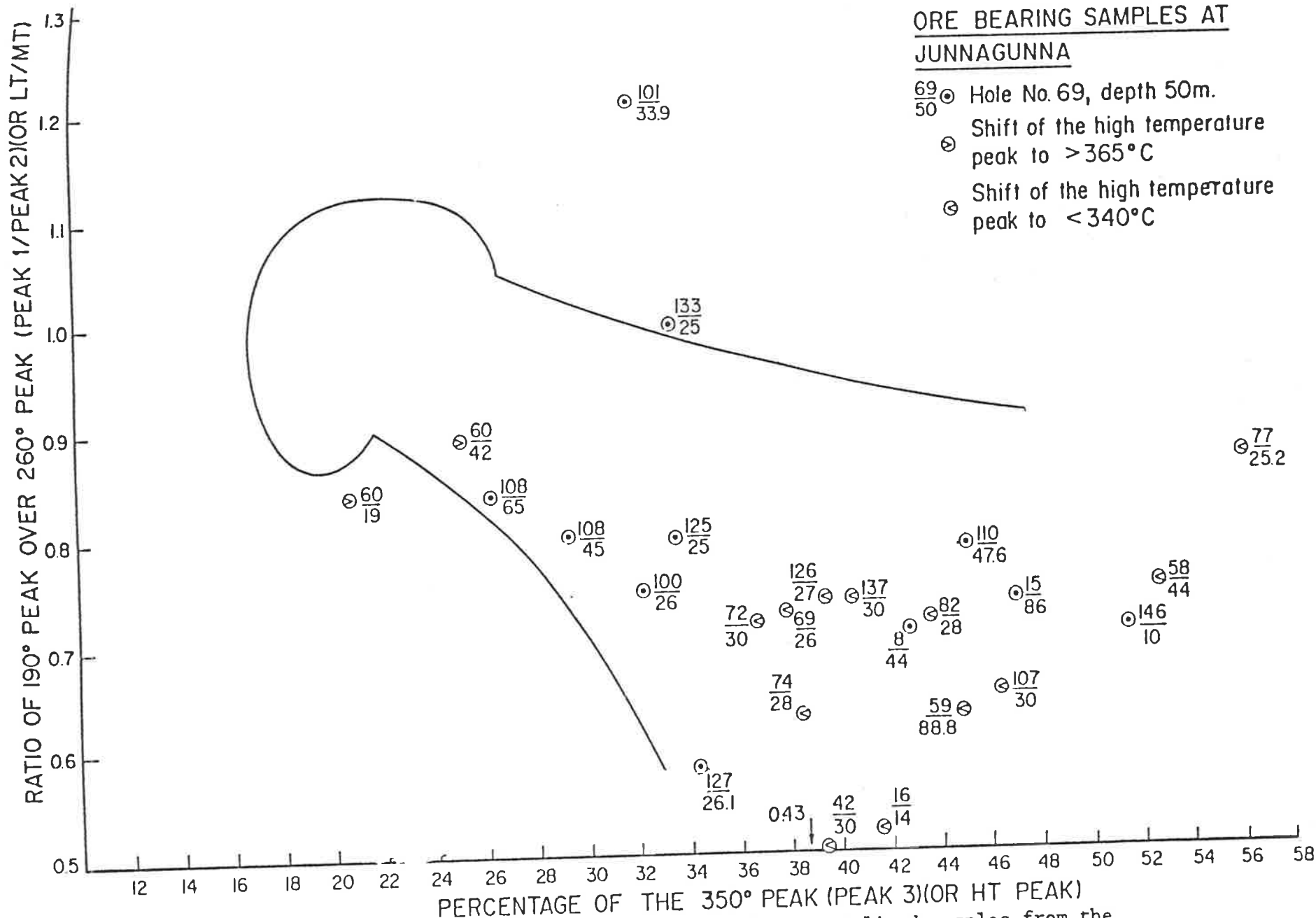


Figure 6.13 Variation diagram for mineralized samples from the Junnagunna area.

- 2) In almost every hole the area immediately below the Siegal Volcanics-sandstone contact shows sensitization features regardless of whether there is mineralization present or not. Figure 6.14 shows only the top samples from each hole. A comparison with figure 6.12 indicates the generally more radiation sensitized nature of the top samples. Samples plot in the protore type TL field or in the ore type TL field (however, no non-mineralized samples plot as ore). This suggests previous movement of protore and/or ore along this contact.
- 3) Holes close to the dyke show sensitization not only at the contact with the Siegal Volcanics but throughout their depth, reflecting the presence of vertical pods of mineralization at depth, close to the dyke. This, in turn, reflects the more suitable environment for uranium precipitation close to the basic rocks.
- 4) With increasing distance away from the dyke, the sensitization at depth decreases. Generally, with increasing distance from the dyke, the total radiation effects in the hole decrease, except for holes within the orebody.

The situation therefore is one where the uppermost portion of the hole will show strong radiation effects due to ore/protore movement and the rest of the hole show a vertical homogenization, either uniformly higher or lower radiation effects.

- 5) The area to the south-west of 13,200N has a lack of ore at the volcanic sandstone contact. There is a gradual increase in the amount of ore and protore from this position (13,200N) in a north-easterly direction towards the Cliffdale Fault.

The distribution of ore and protore type TL also changes beginning as only present at the contact, then also becoming more abundant with

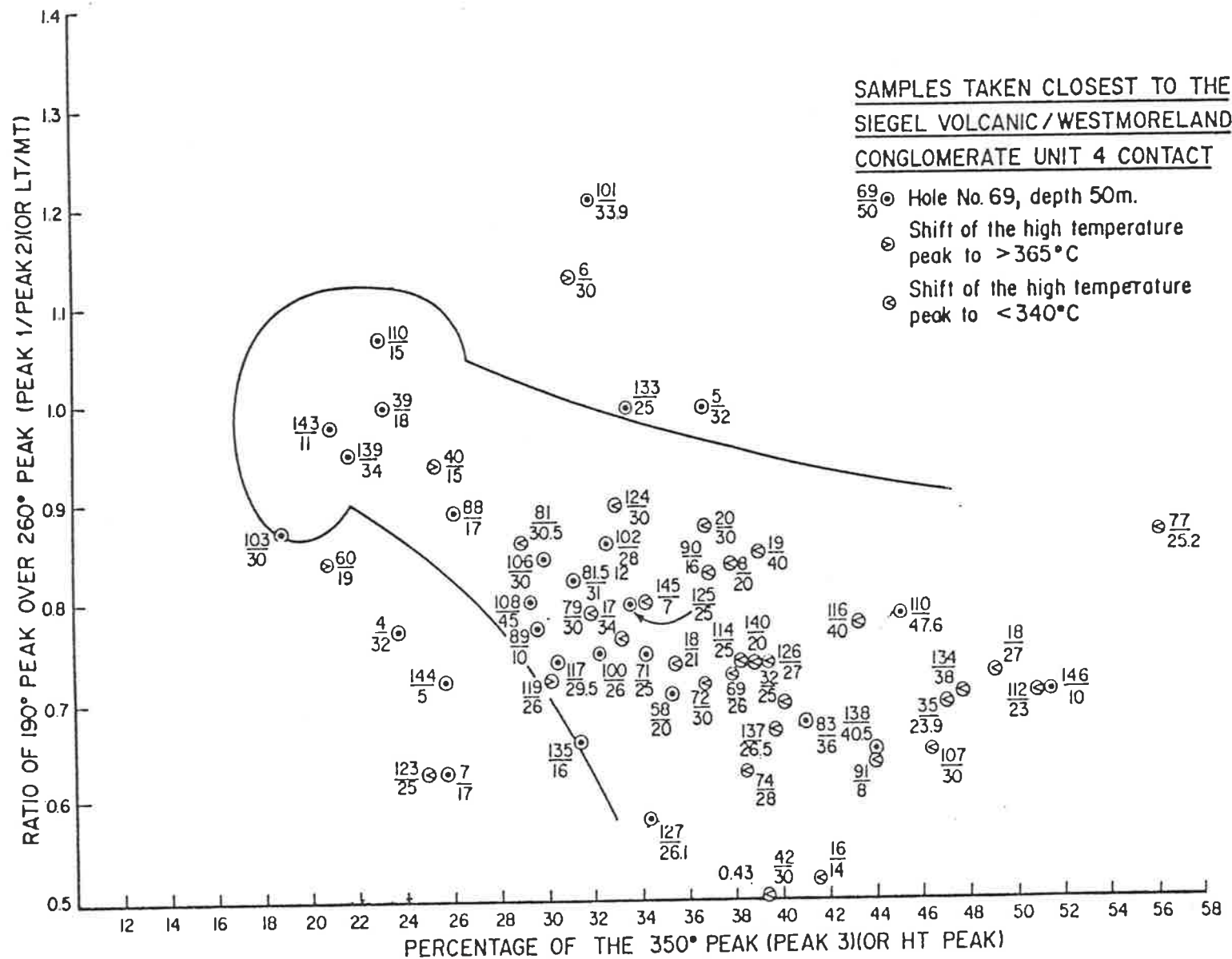


Figure 6.14 Variation diagram for samples from the Siegal Volcanics/Westmoreland Conglomerate Contact.

depth, i.e. present at the contact and further down the hole. Once again, this indicates the possibility of the previously discussed banking-up of ore and ore-bearing solutions at the Cliffdale Fault following down-dip movement in a north-easterly direction.

- 6) The area on the south-eastern side of the Redtree dyke always shows less radiation effects than the opposite side. This was also indicated by the contour maps in section 6.2.8. This observation does not apply to holes in close proximity to the Redtree dyke which are sensitized at all depths and also contain vertical pods of mineralization, but rather applies to holes at a greater distance from the dyke. Reasons for the lack of mineralization and sensitization were previously discussed, i.e. uplift and erosion of the upper 10 metres of silty chloritic sandstone suitable for uranium precipitation on the south-east side of the dyke.
- 7) As at the Jack and Garee Lenses, some samples from the underlying Unit 3 conglomerate, or close to the Unit 4 - Unit 3 contact plot as protore type TL reflecting:
 - a) the sensitized nature of the Unit 3 conglomerates with their abundance of acid volcanic clasts, and
 - b) the possibility of accumulation of uranium during solution transport and movement near this contact.
- 8) The prospectivity of the area in the vicinity of UMD 79/133 and UMD 79/134 is reflected by the positions in which samples from these holes are found, i.e. in the protore type TL fields.

6.3.3 Junnagunna North

The information for Junnagunna North is also plotted in figure 6.12 in relation to all Junnagunna data and is plotted separately on figure 6.15.

The situation is basically the same as at Junnagunna proper, i.e. ore grade mineralization plots in a less sensitized area than at Jack and Garee Lenses and so is presumably more recent, e.g. UMD 79/137 30m has a grade of 0.39% U_3O_8 yet only plots in the protore type TL field. Other interesting points distinct from Junnagunna include:

- 1) The Wanigarango Joint Zone (passing through approximately 10,350E) is the extension of the Redtree Joint Zone/Redtree dyke. As yet, no dolerite has been found within the Wanigarango Joint Zone but is presumed present, e.g. holes UMD 79/110, UMD 79/143 and UMD 79/144 show little sensitization at surface, but increasing sensitization with depth in a similar fashion to holes UMD 76/16, UMD 79/107 and UMD 79/101 close to the Redtree dyke in the main Junnagunna prospect; this illustrates usage of TL as a lithological indicator.
- 2) Once again, as observed in sections 6.2.2, 6.2.3 and 6.2.8, the trend of increasing sensitization to the north-west away from the presumed dyke can be seen, i.e. from holes UMD 79/143 to UMD 79/135 to UMD 79/140 and UMD 79/144 to UMD 79/145 to UMD 79/146. UMD 79/146 which has a marginally economic grade of 0.05% U_3O_8 plots in a "strong" ore position. This again implies that further uranium may be present at a slightly greater distance from the presumed dyke than UMD 79/146.

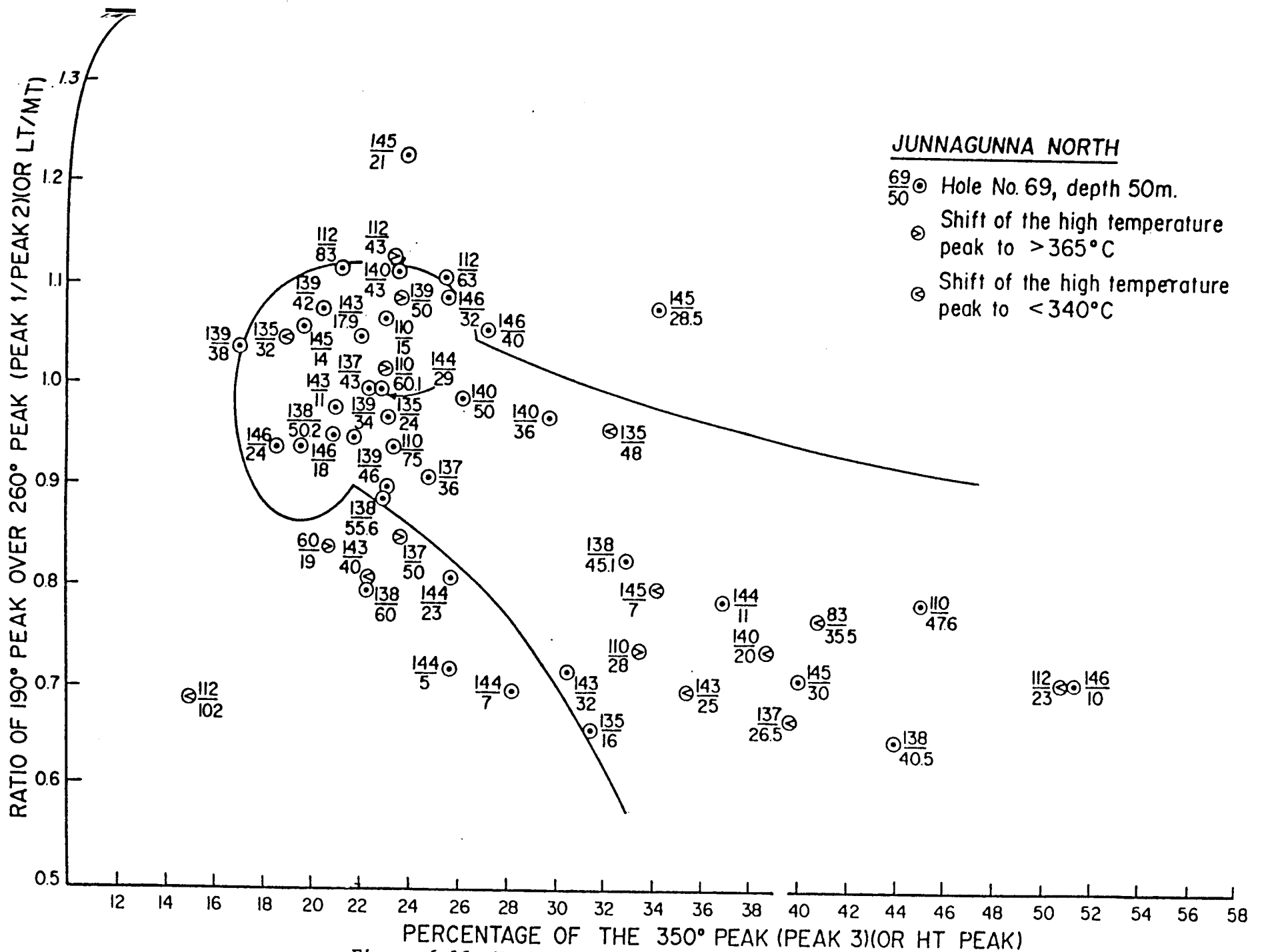


Figure 6.15 Variation diagram for samples from the Junnagunna North

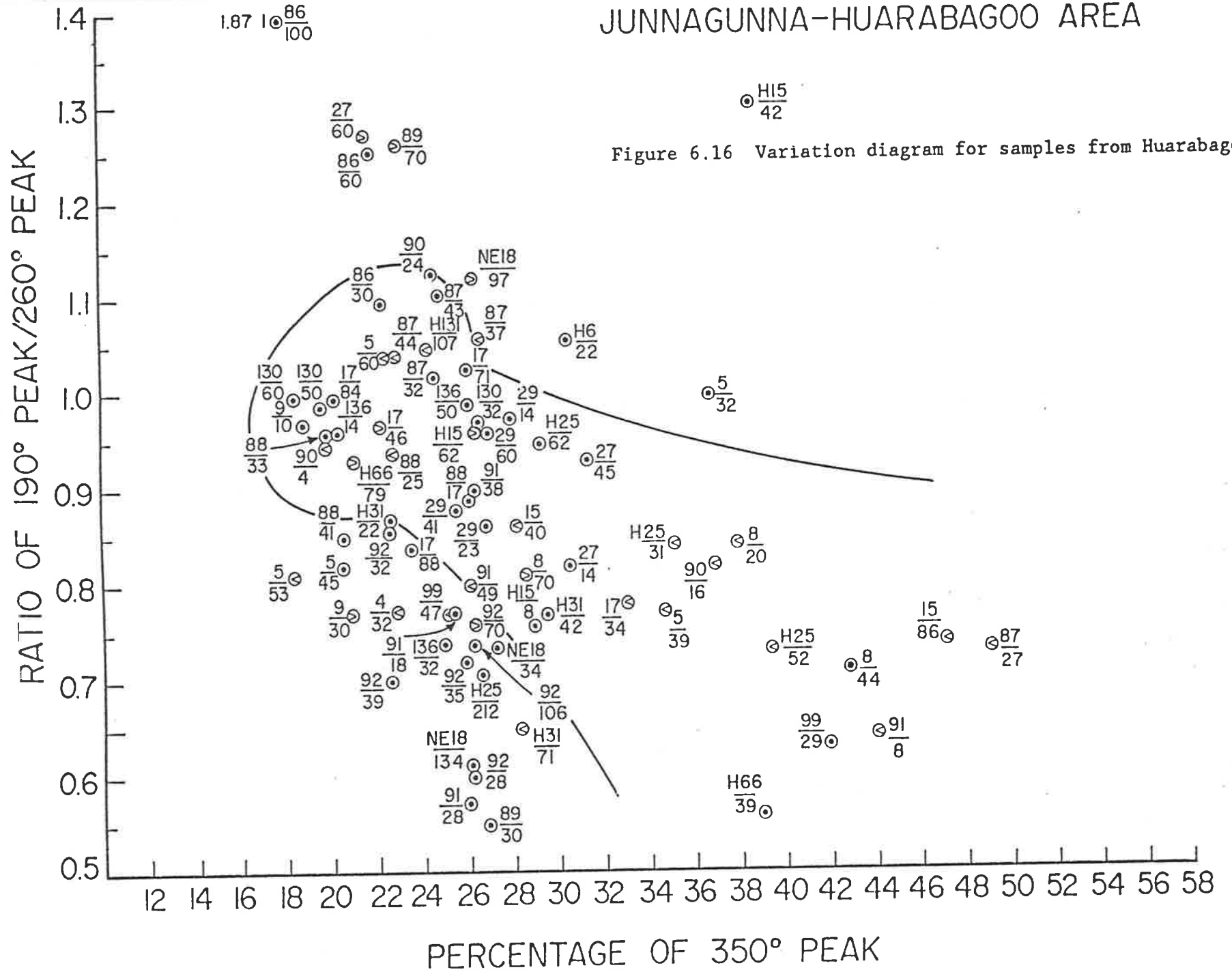
6.3.4 Huarabagoo

Huarabagoo is usually taken to mean the area along the margins of the Redtree dyke in the region situated between the Redtree ore lenses and Junnagunna. Drill hole locations of samples used in the study are found in figure 6.10, and the data for this project is contained in figure 6.16, from which the following points arise:

- 1) Ore type TL positions are variable, occurring as vertical pods down to 85 metres below the surface. Protore type TL is also randomly scattered along the length of the dyke, generally at depths of less than 40 metres and noticeably only in those areas which still have a volcanic capping. Areas which do not have a capping of Siegal Volcanics do not contain protore. The implication is that this ore has been fixed in its present position, i.e. was less vertically mobile than in areas with a volcanic capping.
- 2) The Huarabagoo area contains numerous samples with a strong LTS in contrast to the Redtree and Junnagunna areas, e.g. UMD 76/4 32m, H31 71m; which could mean that uranium mineralization has been higher grade in the past than at present.

A further point of interest concerns the position of the possible "past uranium" occurrences, (areas with a strong HT peak percentage, a LTS, but no mineralization), which occur at depths from 22m in H25 to 134m in NE18. This, coupled with the random distribution of present ore reflects the suitability of the entire dyke for provision of the reducing environment necessary for precipitation of uranium - regardless of depth though within Unit 4 of the Westmoreland Conglomerate (Ptw₄).

JUNNAGUNNA-HUARABAGOO AREA



6.4 Further Usage of Variation Diagrams in Non-Mineralized Areas and Areas Distant from the Redtree Joint Zone

Apart from determining relationships between present mineralization and protore within prospects, the LT/MT peak ratio vs HT peak percentage variation diagrams can also be used to consider the prospectivity of areas where no mineralization is currently present. This can compensate for a lack of data suitable for usage on traverses. It is in this context that the method is used in the following areas, i.e. to determine their prospectivity for uranium occurrences.

6.4.1 Jinjaree Valley

The Jinjaree Valley is situated on the northern dip slope of the Longpocket Syncline in a small open fold within the sandstone which creates a valley, surrounded by sandstone with an occasional covering of Siegal Volcanics. The Siegal Volcanics are present as a thin sill within a few metres of the surface in the eastern part of the valley, rather than as an extrusive. The location is shown in figure 6.17.

A total of five diamond holes were drilled in the eastern two thirds of the valley based on the detection of two large alpha meter anomalies. No mineralization at all was detected in the holes.

Samples have been taken from these holes to compare their TL response with those of known ore containing areas, discussed above, and to detect proximity to ore, if any. Results are presented in figure 6.18. Drill hole locations are contained in figure 6.19.

- 1) As with other areas, all samples have suffered major radiation effects and the area below the sandstone-basalt contact usually shows sensitization. In general, however, the strata below this contact shows less sensitization than the equivalent

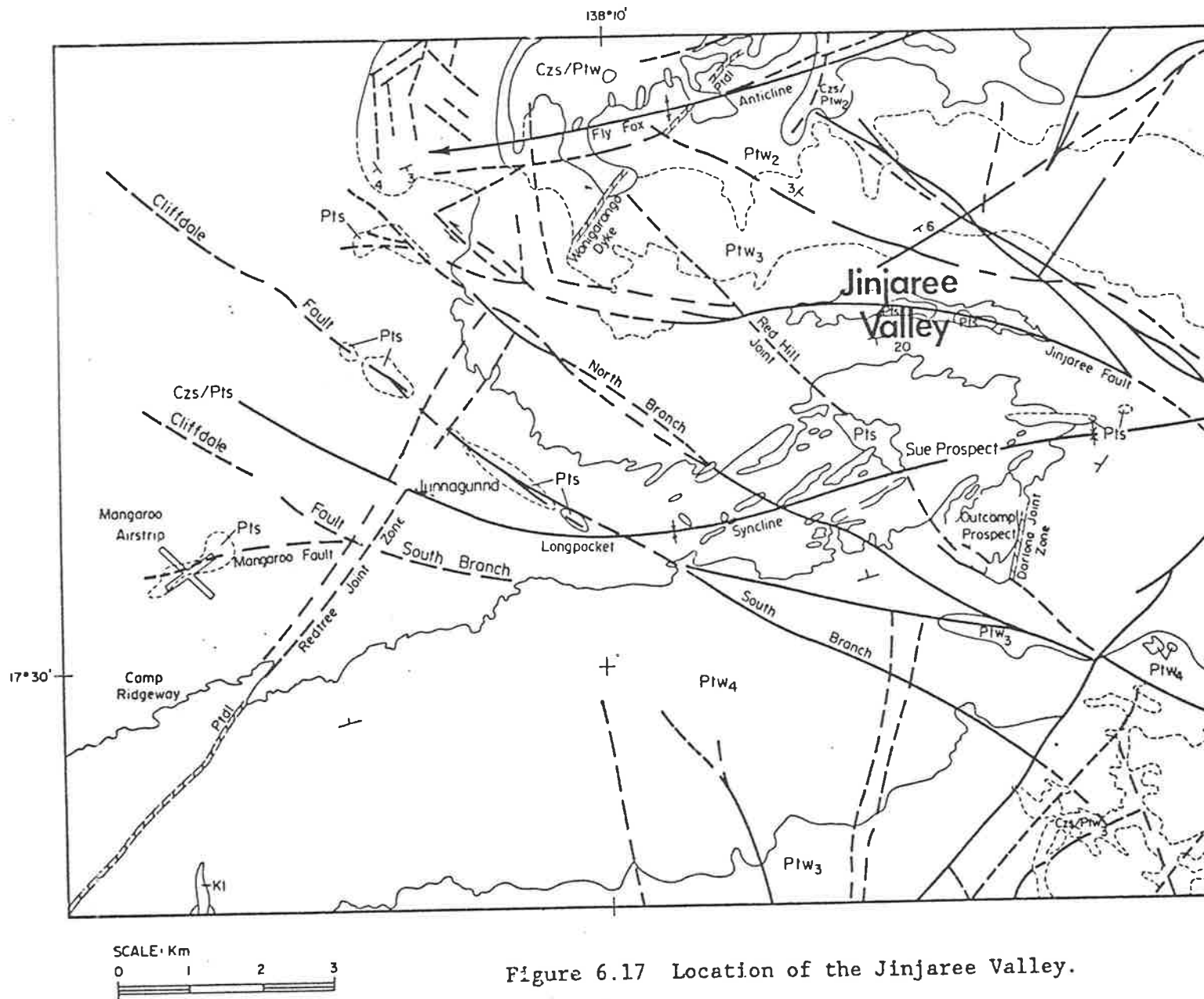


Figure 6.17 Location of the Jinjaree Valley.

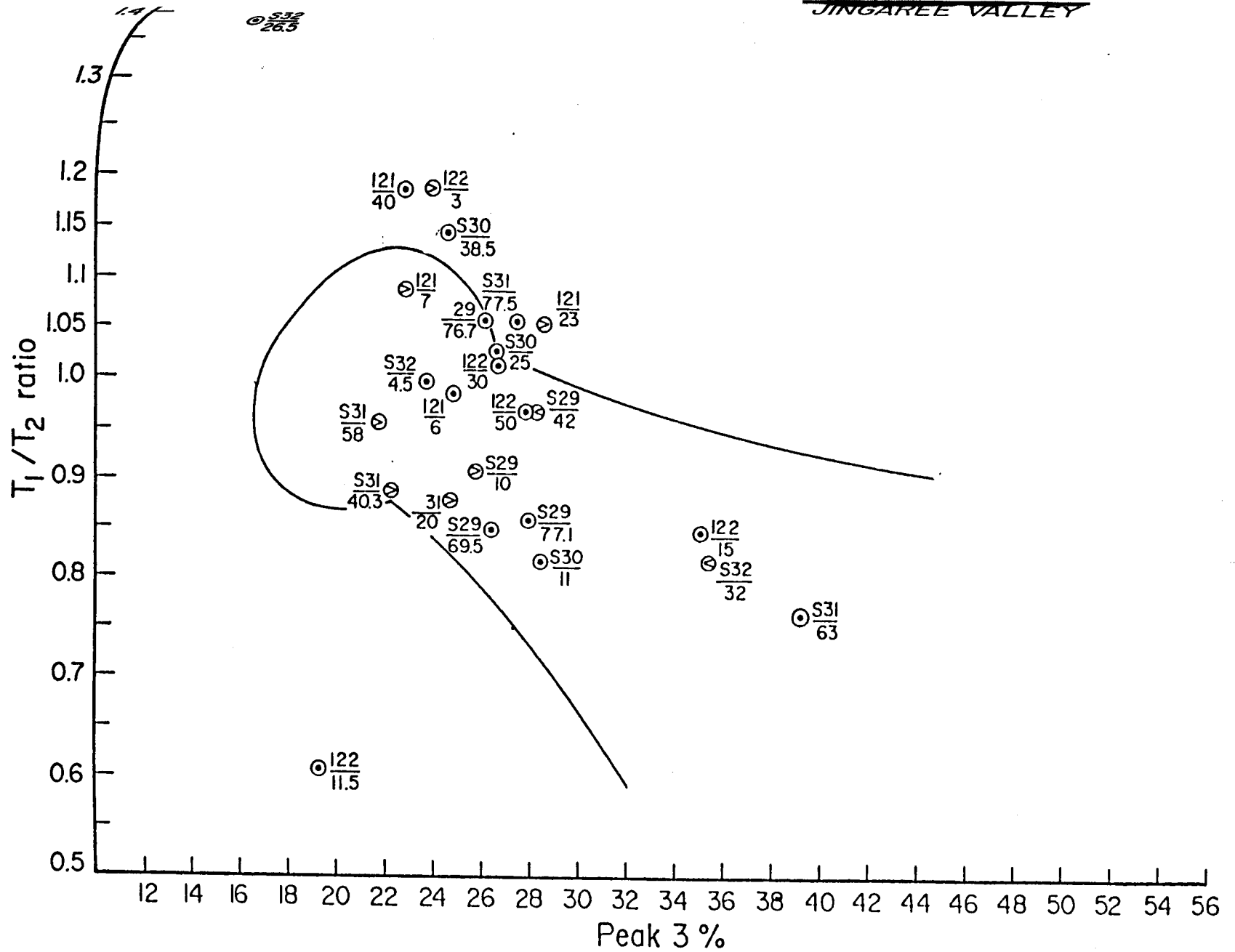


Figure 6.18 Variation diagram for samples from Jinjaree Valley.

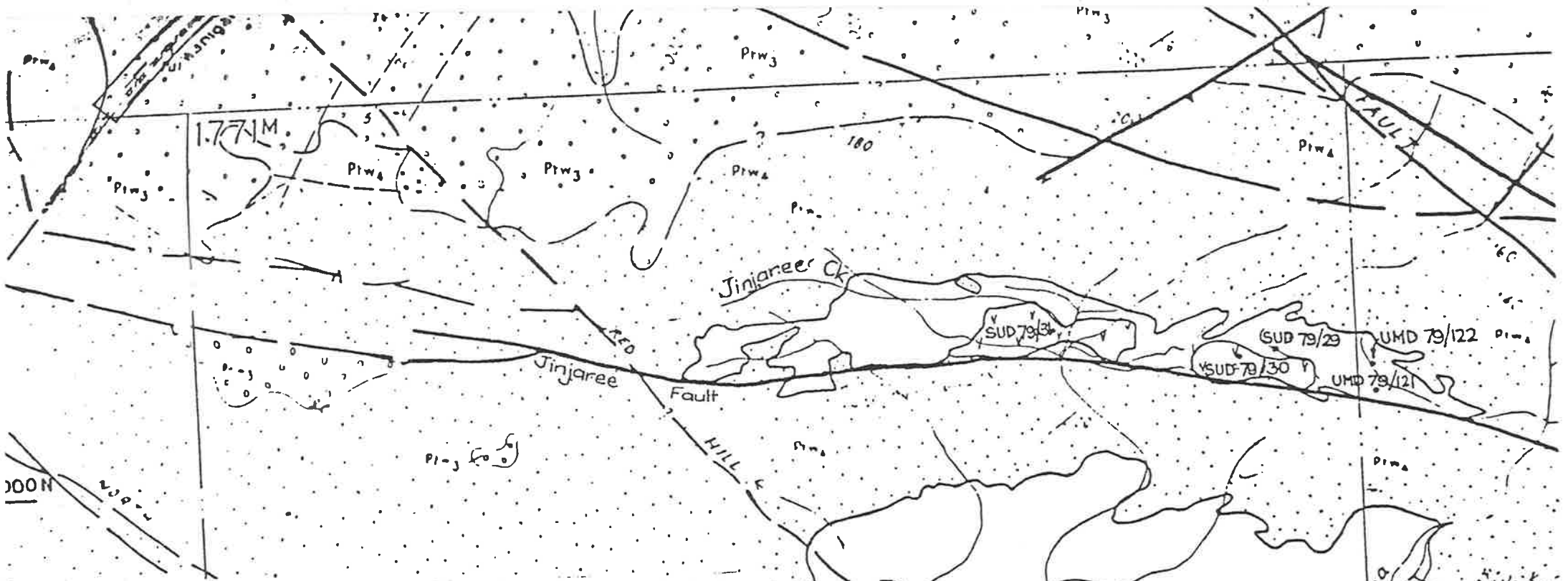


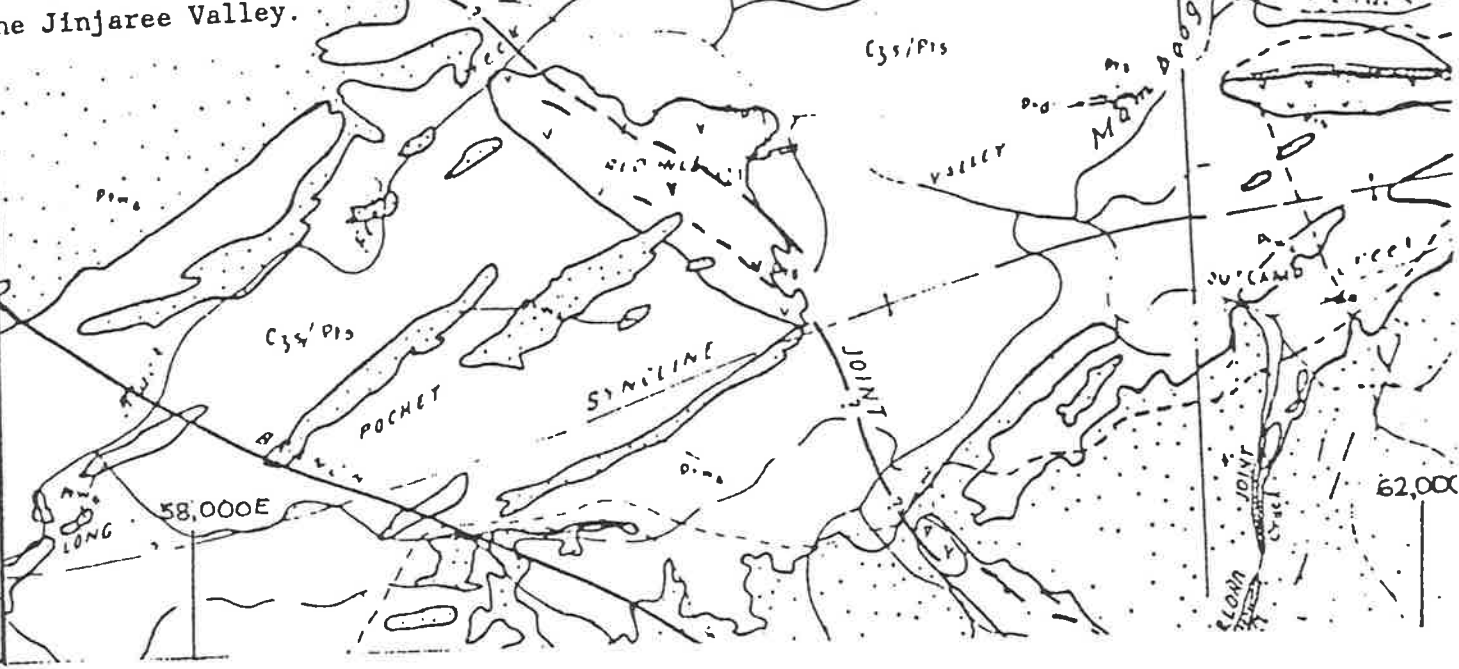


Figure 6.19 Location of holes sampled in the Jinjaree Valley.

LEGEND

- SUD 79/32 Drill hole location
-  Creek
- PtW₄ Westmoreland Conglomerate
-  Siegal Volcanics
- Cz_s Alluvium (Recent)

Scale 0 500m



horizon in other areas, say Junnagunna or Huarabagoo. An explanation of this would require that there has been movement of less protore, or even less protore in this area.

- 2) Holes UMD 79/121, UMD 79/122 and SUD 79/29 were drilled to intersect major alpha-meter anomalies with alpha counts of greater than 1,000 per hour. Figure 6.18 indicates that even these holes are not strongly sensitized. Coupled with the absence of mineralization, these areas therefore appear unprospective despite the large alpha-counts.

The holes which are more strongly sensitized in the Jingaree Valley are those which are closest to the sandstone edge, e.g. UMD 79/122 and SUD 79/32. The samples taken from just below the volcanics in these holes (15m and 32m respectively) plot in protore type TL positions. This may imply one of two possibilities:

- a) an increased drainage flow from the sandstone edge providing more uranium, or
- b) the possibility of mineralization further up the sandstone slope.

This latter situation would parallel that of the anomaly 22 area (to be discussed later) where UMD 79/109 was drilled at the sandstone edge of the southern dip slope of the Longpocket Syncline to intersect a major alpha-meter anomaly. No mineralization was detected and the conclusion drawn was that the anomaly itself was caused by leaching of uranium from the Jack Lens further up the sandstone slope.

- 3) Despite the presence of the alpha meter anomalies in the easternmost portion of the Jinjaree Valley, the TL sensitization increases towards the west. A lack of holes makes this trend speculative rather than conclusive, but if real it would suggest that further exploration could be continued in the western portion of the valley.

- 4) A further point of interest is the lower degree of sensitization in samples SUD 79/32 26.5m and UMD 79/122 3m taken from sandstone within the volcanics and above the volcanics respectively. Although lower in sensitization they have still suffered major radiation effects. As such, they are similar to the previously discussed samples NE1 70m and N123 80m from the Jack and Garee Lenses area, taken from within the Redtree dyke. These Jinjaree samples also indicate:
- a) the inherently high radiation effects in the Unit 4 sandstone prior to further exposure to uranium ore, and
 - b) the further sensitization effects caused by ore movement beneath the volcanics.

6.4.2 Longpocket

The Longpocket area comprises the Outcamp and Sue Prospects - two small mineralized bodies each totalling a few hundred tonnes contained U_3O_8 . They are situated in the hinge zone of the Longpocket Syncline. The Darlona Joint Zone, with a postulated, though as yet undetected, dyke, runs adjacent to the eastern margin of Outcamp approximately along the grid line 61,000E. Locations of prospects and drill holes are contained in figure 6.20 and data is presented in figure 6.21. Major observations are as follows:

- 1) The area is a mixture of strongly sensitized and ordinary sandstone. Areas of ore plot either in the "strong" ore type TL field, e.g. UMD 77/44 40m (despite a low grade of 0.05% U_3O_8) or in the protore type TL field, e.g. UMD 78/70 48m (also 0.05% U_3O_8) illustrating that this area has been subject to much redistribution of ore as have the Junnagunna and Huarabagoo areas.

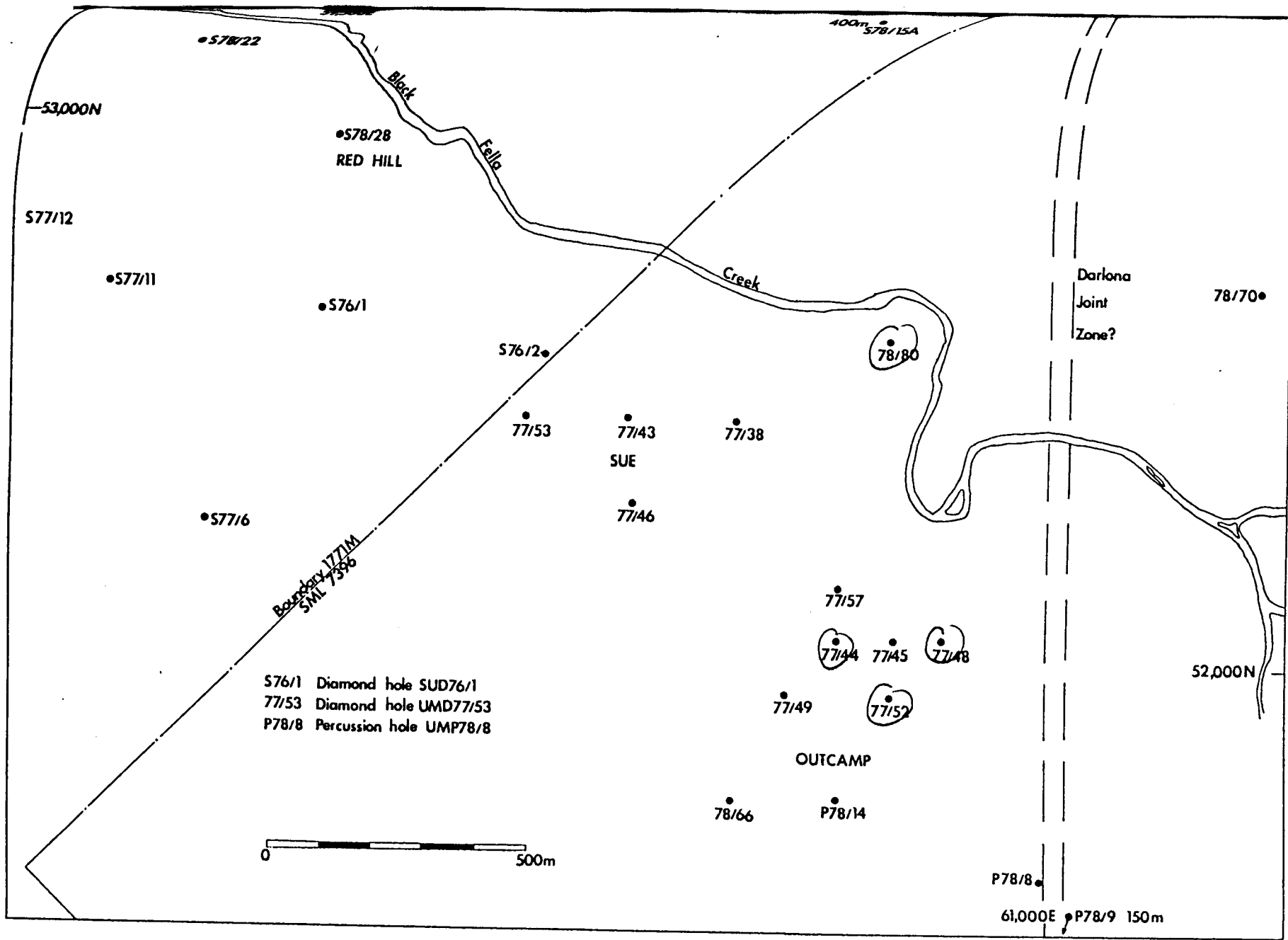


Figure 6.20 Location of holes sampled at Longpocket and Red Hill.

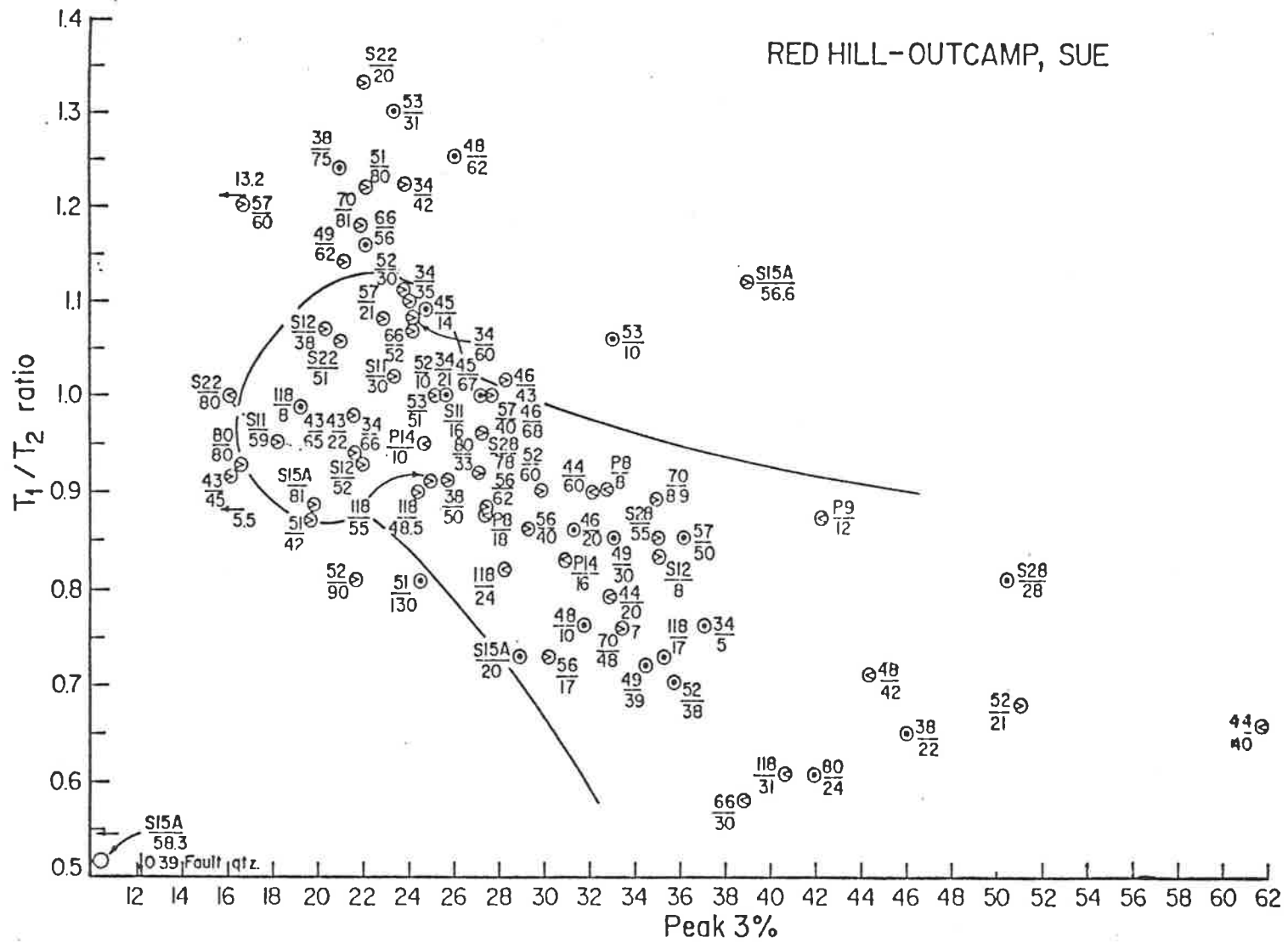


Figure 6.21 Variation diagram for samples from Longpocket.

- 2) From the point of further exploration potential, a trend of increasing sensitization southwards along the joint zone through UMP 78/8 and UMP 78/9 is present, leading into the Golara area. Hole UMD 79/118 (not shown on location map) in the Golara area has intersected ore with a grade of 0.28% U_3O_8 thus firming the potential of this area for mineralization analogous to the Redtree type.
- 3) The Red Hill prospect, to the north of Sue (data separate in figure 6.22) is situated along an east-west trending quartz-filled fault with fragments of surrounding basic volcanics. The only mineralization intersected SUD 78/28 28m plots in the ore type TL field in figure 6.22 but has no LTS. No distinct pattern can be drawn between TL response and geological position for this area, which may indicate recent remobilization and redistribution of uranium rather than permanent high grade mineralization.

6.4.3 Flying Fox Anticline

The location of the Flying Fox Anticline is shown in figure 6.23. Six drill holes were sampled from around the anticline in three prospects: Lagoon Creek, South West Corner and Battle Creek. These are also marked on figure 6.23 and data is presented in figure 6.24.

- a) South West Corner occurs in an embayment in Unit 4 sandstone such that it is enclosed to the north, east and west. Siegal Volcanics cover increase to the south-west. None of the samples from either WD6 or WD8 show major sensitization apart from WD8 64m which is a tuffaceous horizon.

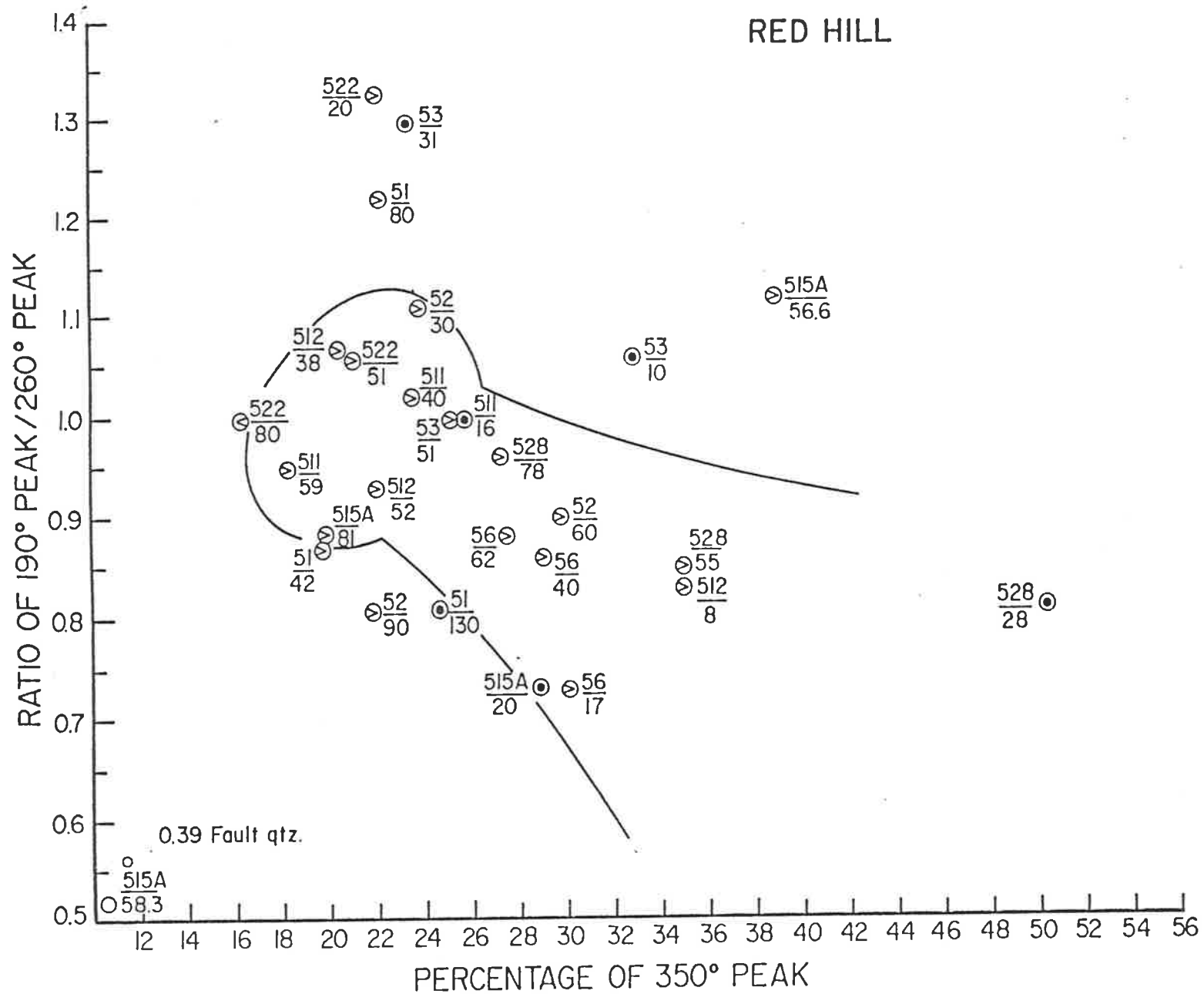


Figure 6.22 Variation diagram for samples from Red Hill.

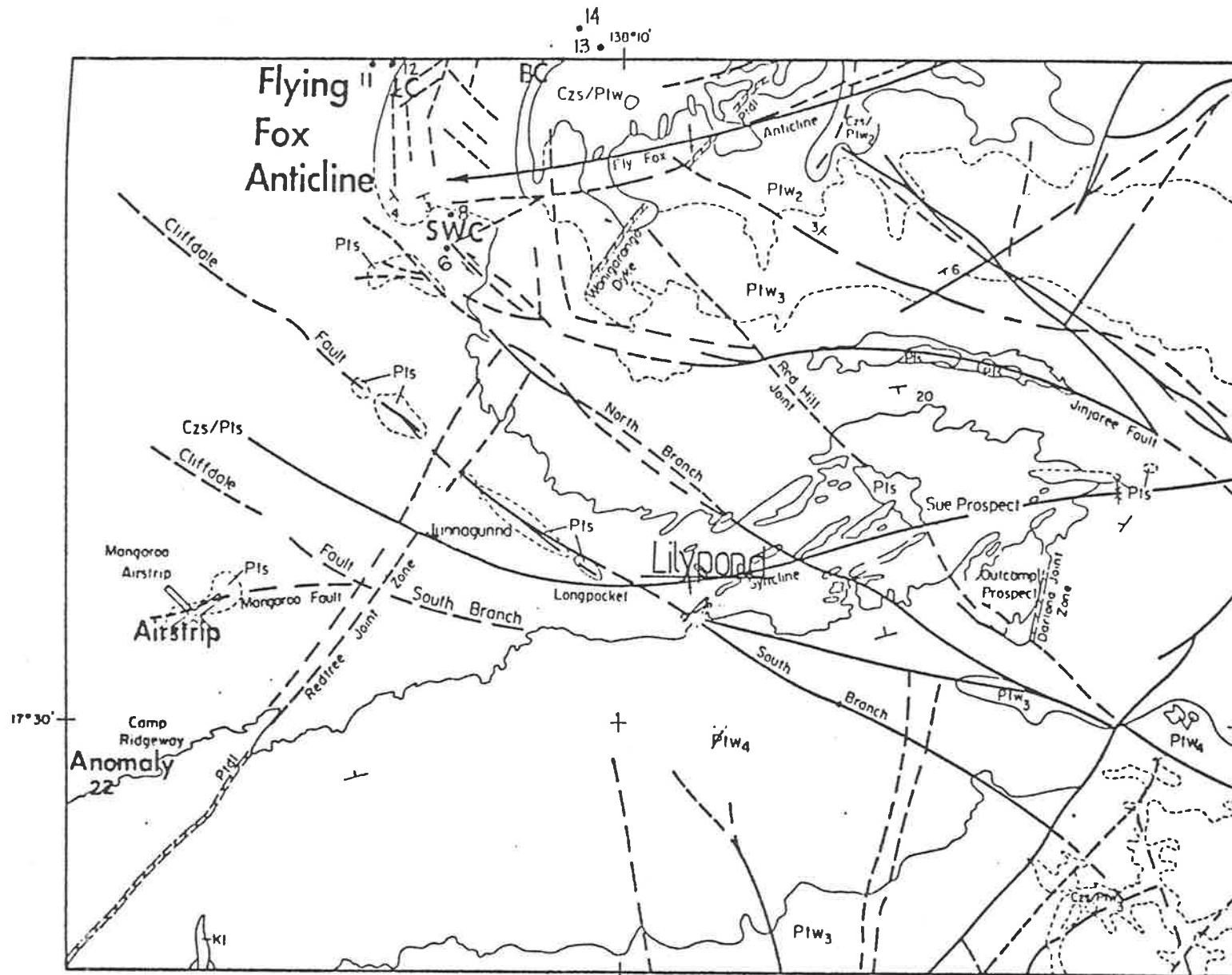


Figure 6.23 Location of the Flying Fox Anticline with holes sampled. SWC - South West Corner, BC - Battle Creek and LC - Lagoon Creek.

FLYING FOX ANTICLINE

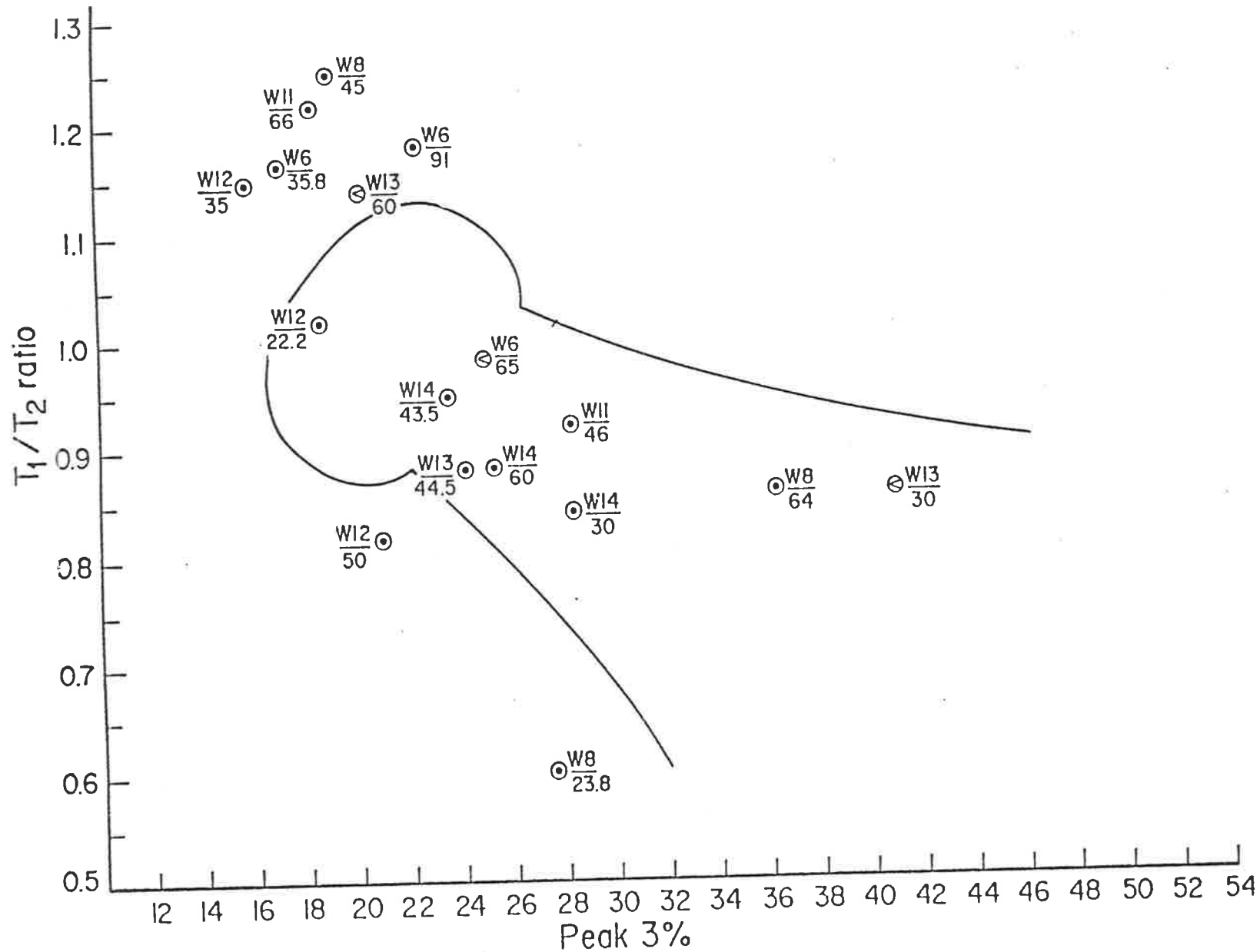


Figure 6.24. Variation diagram for the Flying Fox Anticline samples.

- b) Lagoon Creek is situated on the western margin of large Unit 4 outcrops and is covered by weathered Siegal Volcanics containing a five metre wide layer of alluvial gravels and silicified sandstone. None of these samples from WD11 or WD12 show strong sensitization, and only minor sensitization is present below the contact.
- c) Battle Creek is situated adjacent to the margin of the northern dip slope outcrops of the Flying Fox Anticline. This prospect is the most promising of the three. Samples taken from just below the Siegal Volcanic contact show evidence of sensitization by their plotting in the protore type TL field - in particular WD 13 30m which also has a LTS, and to a lesser extent W14 30m also.

WD 13 is situated closer to the sandstone outcrop than WD 14 hence the increased sensitization may be a result of leaching from mildly uraniferous areas such as Conglomerate Hill in which the Embayment prospect occurs. This prospect was explored and tested by BHP during the early-mid 1970's without any major ore discoveries.

6.4.4 Lilypond

Lilypond is the area in the Longpocket Syncline between Junnagunna and the Outcamp/Sue prospects. As yet, no mineralization has been discovered in this area so five random holes were sampled to determine their TL sensitization characteristics. Although all have suffered radiation effects, figure 6.25 shows that none of them show any further sensitization attributable to mineralization. This further downgrades

LILYPOND

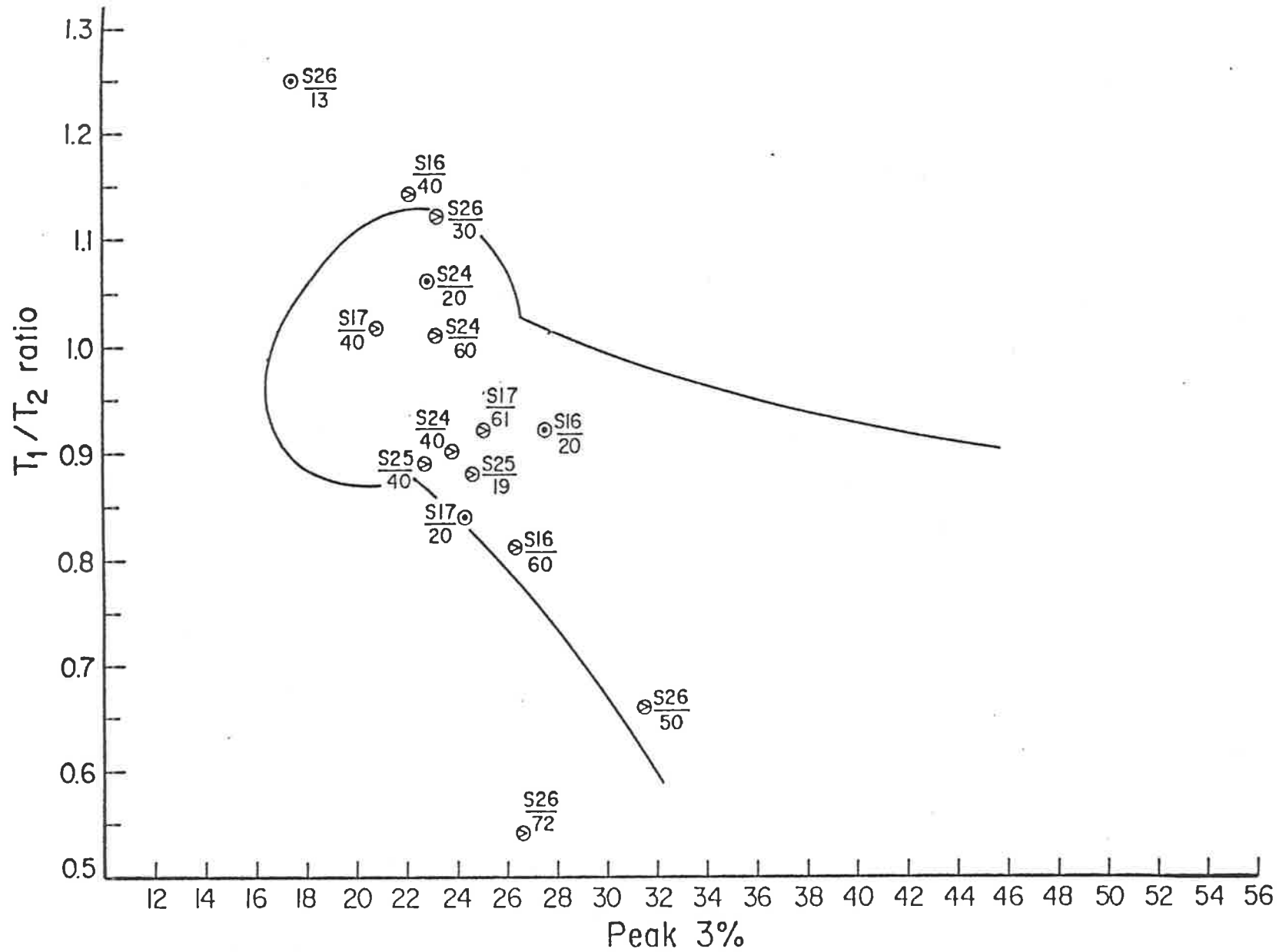


Figure 6.25 Variation diagram for samples from the Lilydale area.

the potential of this area for discoveries of economic uranium accumulations.

6.4.5 Others

Samples from two other prospects (Anomaly 22 and Airstrip) where the lack of drill holes prevents an exhaustive examination of data, are plotted on figure 6.26. Observations are that:

- 1) UMD 79/109 does not show any strong sensitization despite the alpha-meter anomaly causative of the drilling of the hole.
- 2) The only hole to show any sensitization above normal levels at the Airstrip prospect is SUD 79/34 132m - a shaley tuff forming the base of the volcanics.
- 3) SUD 79/34 141.2m - a sample of late-stage quartz veins with pyrite shows little sensitization above normal background Westmoreland Conglomerate.

6.5 Surface Traverse Results

Charlet (1978) used TL to indicate the presence of anomalous uranium buried beneath Tertiary sands at too great a depth to be detected by conventional scintillometer techniques. If confirmed by further work, TL would thus have great potential as a quick time and money saving tool in detecting buried mineralization and siting drill holes. A very limited test program was undertaken in this study. Nineteen samples have been taken from the surface of Unit 4 sandstone outcrops in a traverse across the Redtree dyke. Samples were taken approximately 100m apart along the line 9645N starting 11,550E, 9,645N (sample T1) such that sample T11 was taken from the south-east margin of the dyke and sample T12 from just past the north-west margin overlying hole H15.

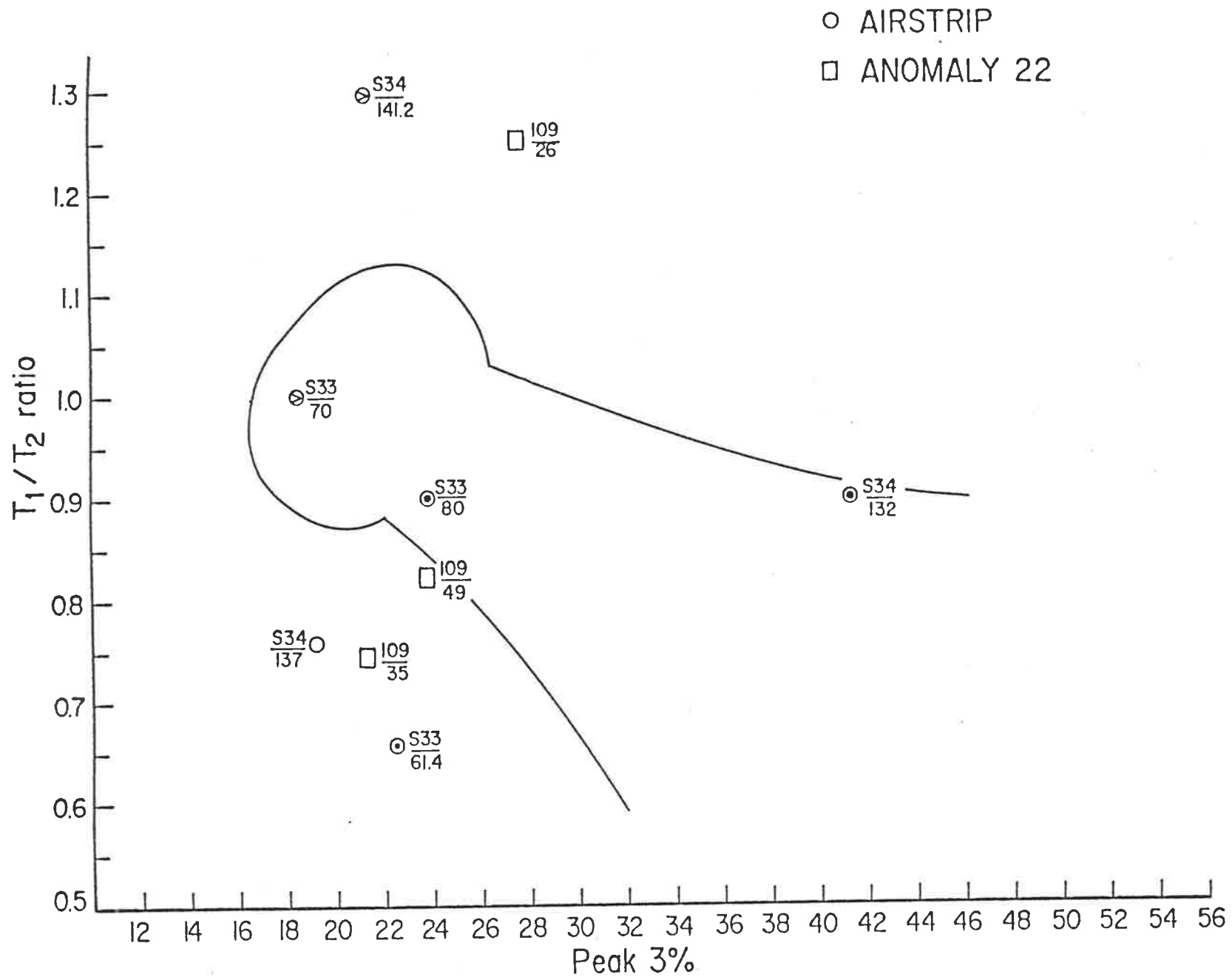


Figure 6.26 Variation diagram for samples from minor localities.

The aim of this study was to see if any change in TL characteristics were obvious when approaching the dyke (and buried mineralization) on the surface outcrops. TL intensity and ratio data is plotted in figure 6.27.

On the intensity traverse, the intensity of the LT peak is erratic, firstly increasing dramatically at a distance of 200 metres from the dyke and then decreasing by 50% at the dyke margin. No other systematic variation can be discerned.

The intensity of the HT peak increases by approximately 75% at sample location T7 (400 metres from the dyke) then remains high showing no further fluctuation across the dyke. Minor fluctuations occur at T15 and T18.

The HT/LT peak ratio shows a distinct increase across the dyke (T11 and T12). Further elevated ratio values at T7 and T14 are discussed below.

In figure 6.28 traverse samples are plotted on a variation diagram. Some individual samples do exhibit sensitization features, e.g. sample T11 and T12 from the dyke margin plot half way along the sensitization curve. Both have a LTS.

Sample T12 is situated above drillhole H15 which is mineralized from 23.8m-24.9m at a grade of 0.09% U_3O_8 . The sensitization in T12 may have resulted from this mineralization, i.e. by upward leaching and redistribution. If such is the case, then T14 which plots in a similar position to T12 in figure 6.28, and also has LTS, could also be indicative of a similar occurrence. Further groundwork indicating any significant radiometric anomaly or locating surficial secondary mineralization would help to confirm or negate the potential of this site. T7 also plots in a similar position but does not have a LTS. This site too, could therefore warrant further exploration.

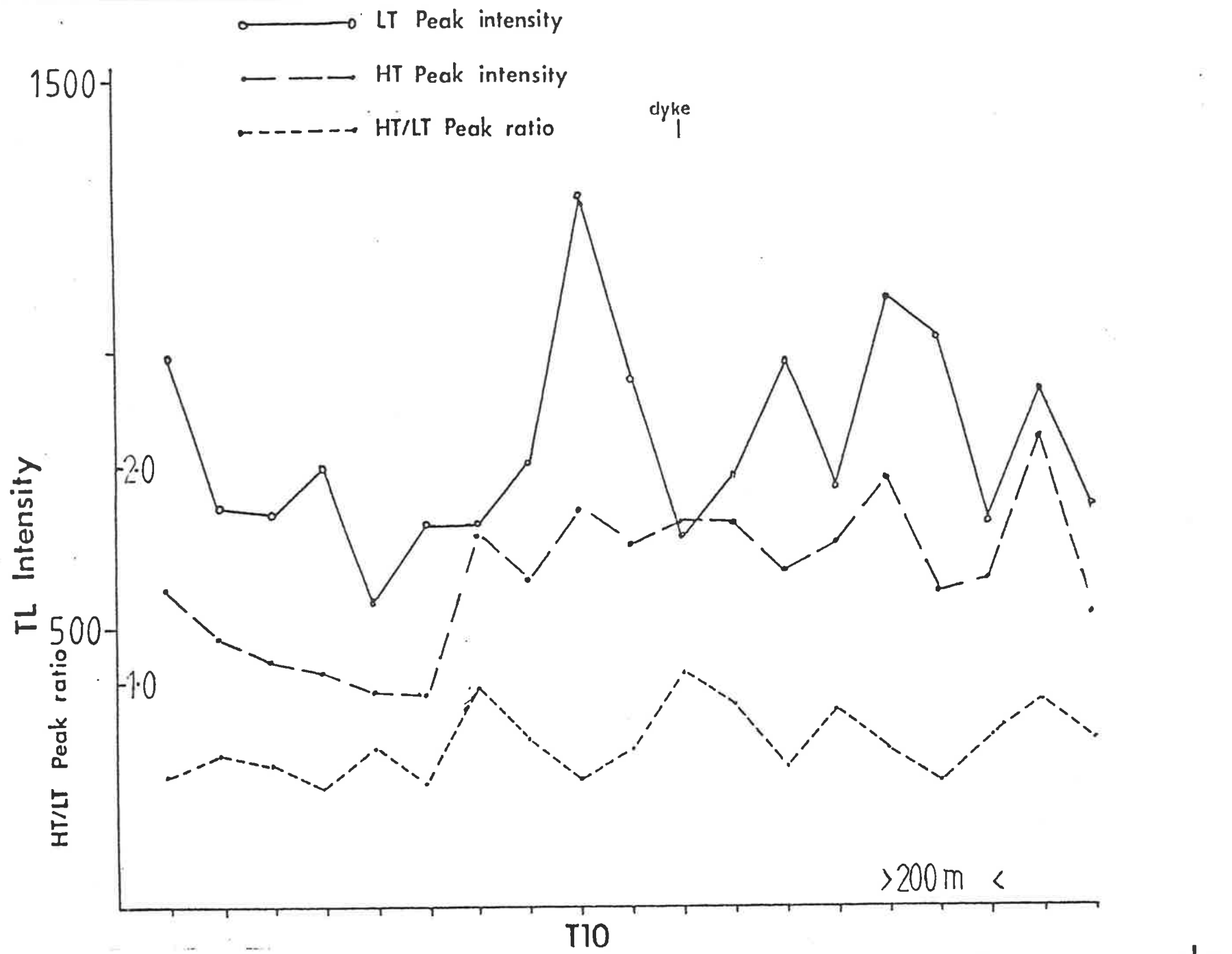


Figure 6.27 Variation in TL intensity and ratios for quartz samples taken along a surface traverse over the Redtree dyke.

Traverse samples

TRAVERSE 9645N

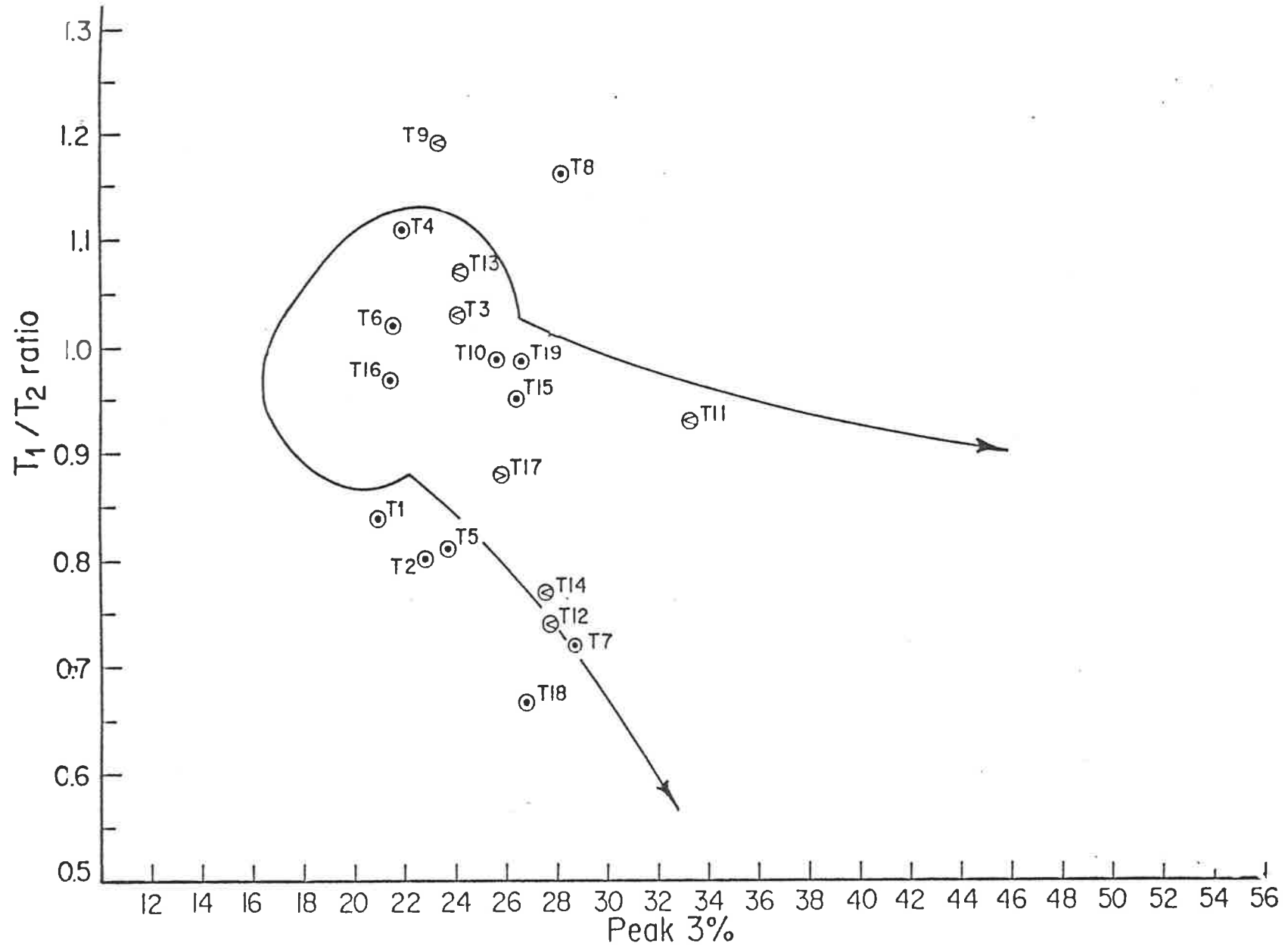


Figure 6.28 Variation diagram for samples on a surface traverse over the Redtree dyke.

An assessment of the potential of this method thus indicates the following:

- 1) In Proterozoic sandstones where there has been considerable time for much redistribution of uranium, intensities of either HT and/or LT peaks are variable for surface samples and may not be the most useful technique in detecting buried mineralization.
- 2) HT/LT peak ratio and LT/MT vs HT variation diagrams may be of more use in detecting possible anomalous areas which may then be reassessed by later groundwork.

Further work must be done however, to more fully assess the use of ATL as a surface prospecting technique.

6.6 Conclusions on the Use of Thermoluminescence in Exploration for Uranium in the Proterozoic Sandstone Hosted Deposits at Westmoreland

- 1) Large variations in TL intensity (ie. orders of magnitude variations as observed at the Tertiary Beverley deposit), do not occur on a regional scale approaching the Proterozoic Westmoreland Deposits. As a consequence TL may not be as useful an exploration tool for these type of uranium deposits as it undoubtedly is for the simpler Tertiary roll-front type deposits. Nevertheless TL may still, in some instances, be of use on a localized scale in detecting further mineralization in a known uraniferous district. Such usages however, will require a large number of samples to be analyzed.
- 2) Of the methods used at Westmoreland, traverses examining variations in the LT glow peak and HT glow peak intensities across the Junnagunna orebody do not show unambiguous variations associated with ore, though generally the HT peak

intensity is at a maximum within the ore zones. The LT peak intensity fluctuates markedly upon approaching the ore zones and within mineralization itself and thus is not a useful parameter in Proterozoic sandstones by itself.

- 3) HT/LT glow peak ratios are better indicators of proximity to mineralization, as many fluctuations associated with intensity alone are cancelled out. The HT/LT glow peak ratio increases towards uranium mineralization and a value of 1.4 or more is usually associated with mineralization.
- 4) The HT peak temperature generally shows a shift to temperatures less than 340°C in areas of present uranium mineralization. The same LTS is also found in quartz that is spatially related to uranium mineralization but is not mineralized at present. Occurrence of a LTS in a non-mineralized sample with a strong HT peak percentage may therefore represent an area previously mineralized.
- 5) Variation diagrams incorporating peak ratios, percentages and the LTS are a means of portraying a maximum amount of beneficial data and are useful in determining relative radiation effects on a small number of samples which may preclude the use of traverses etc.
- 6) Variations in TL characteristics have allowed the determination of a number of prospective areas for further exploration. The most promising of these, not necessarily in order of suitability are:
 - a) The area to the north-west away from the Redtree dyke extension in Junnagunna North, i.e. further north-west than the line of holes UMD 79/146, UMD 79/140 and UMD 79/137.

- b) The area downdip of the Garee Lens in the vicinity of UMD 77/23 and perhaps UMD 77/24 for the possibility of further Langi Lens type mineralization.
 - c) The area to the south of the present Jack and Garee Lenses based on the larger amounts of radiation damage in these areas than even in some of the ore lenses. As a point of interest, the area to the south of the Garee Lens was also mentioned by Curtis (1976) as being worthy of further exploration, as the Garee Lens dispersion halo extended predominantly into this area rather than symmetrically overlapping the orebody.
 - d) The possibility of mineralization at depth below sample T14 taken on the surface traverse.
 - e) The possibility of mineralization in the Jinjaree Valley on the southern sandstone slopes based on the presence of a TL anomaly and alpha-meter anomaly in holes at the edge of the sandstone in the valley and similarity to the Anomaly 22 site.
 - f) The area at Junnagunna close to, or slightly north-west of, holes UMD 79/133 and UMD 79/134 which showed sensitization and minor mineralization.
- 7) A surface anomaly associated with buried mineralization in hole H15 indicates that TL surface traverses may be a means of detecting buried mineralization, though further work is needed to more exhaustively test this usage.
- 8) TL may also be of indirect use in uranium exploration by contributing to a knowledge of the genesis of such deposits - in this case the radiation effects suffered by all samples, the sensitization beneath the Siegal Volcanics/Westmoreland

Conglomerate contact, the vertical homogenization within areas capped by volcanics and absence in areas without a volcanic capping. These and other considerations will be more fully discussed in the following chapters.

CHAPTER 7

GENESIS OF THE WESTMORELAND URANIUM DEPOSITS

CHAPTER 7: GENESIS OF THE WESTMORELAND URANIUM DEPOSITS

- Summary of Chapter

In Chapter 6 several previously unknown observations regarding the genesis of the Westmoreland Uranium Deposits were revealed by TL measurements. These included the widespread radiation effects throughout the entire Westmoreland Conglomerate, the radiation sensitization along the Westmoreland Conglomerate/Siegal Volcanics contact and the vertical homogenization of radiation effects within drill holes. These are coupled with existing geological, mineralogical and geochemical data to suggest a genetic model for the Westmoreland deposits.

The ubiquitous radiation effects are interpreted to indicate an initial high background uranium content for the Westmoreland Conglomerate, which was derived from the acid igneous source rocks for the clastic sequence. It is suggested that this precontained uranium was remobilized during an unspecified thermal event, possibly associated with intrusion of dolerite dykes. The remobilized uranium was moved in convective cell systems - upward near to the heated dykes, horizontally along the sediment/volcanic stratigraphic boundary and then downwards at some distance from the dykes.

Precipitation of uranium occurred at the margins of dolerite dykes or beneath the basaltic volcanics, where suitable reducing conditions existed.

Subsequent massive extrusive volcanism then protected the uranium deposits from the effects of weathering.

*

*

*

Parts 1 and 2 of this study have examined the direct use of TL in uranium exploration: Part 1 in the simple, Tertiary, sandstone hosted deposits; Part 2 in the more complicated Proterozoic, sandstone hosted deposits exemplified at Westmoreland. The following two chapters (7 and 8), which constitute Part 3 of this thesis, use the TL results obtained at the Westmoreland deposits to assist in developing genetic models for such deposits.

Genetic models, not only for the Westmoreland Uranium Deposits, but for all Proterozoic sandstone hosted uranium deposits are many and varied. Because of the ability of quartz to "remember" previous exposure to radiation, it is to be hoped that TL studies may add extra information to these genetic studies, perhaps in determining source or permanency of uranium.

In chapter 7 only the Westmoreland Uranium Deposits are discussed. TL results are added to existing geochemical and geological results and previous theories are examined in the light of this integrated information. A genetic model, compatible with the existing information is then suggested.

In chapter 8 information from other Proterozoic sandstone hosted uranium deposits is synthesized, similarities and differences between these deposits are highlighted, then with new results gained by TL studies at Westmoreland a possible speculative classification of this class of deposits is suggested.

7.1 Previous Genetic Theories for the Westmoreland Uranium Deposits

After discovery of the Redtree Lenses in the 1950's, one of the first genetic models proposed was that of Newton and McGrath (1958) who considered that hydrothermal fluids derived from the intrusion of the Nicholson and Norris Granites (now the Nicholson Granite Complex)

supplied uranium mineralization along the pre-existing fault and joint systems. Morgan (1965) also suggested that hydrothermal mineralizing solutions derived from the Nicholson Granite had led to the presence of mineralization at the Eva mine, 50km north of Westmoreland.

Hills and Thakur (1975) consider that since the Nicholson Granite Complex predates the Westmoreland Conglomerate, it could not have supplied uranium-rich fluids at Westmoreland. However, this may possibly have occurred at the Eva mine, where mineralization is located in a sandy lens in the Cliffdale Volcanics which was intruded by a later granite phase. The occurrence of epidotization and talc schist formation at Eva also suggest some type of hydrothermal metasomatic activity related to mineralization. Against this theory is the age of mineralization at Eva which has been put at 430 m.y. by Hills and Richards (1972), and is too young to have been derived from granites intruded during Early-Mid Proterozoic times. This age however was gained using the U-Pb technique on pitchblende and it may relate to a remobilization of uranium at a later time.

Another younger granite to which the same reasoning could be applied for the Westmoreland deposits is the Packsaddle Microgranite, intruded during the mid-Carpentarian and marking the top of the Tawallah Group. This is also considered an unlikely source due to its limited size and distance from Westmoreland.

Davidson (1964) considered the fact that the Westmoreland Conglomerate was sandwiched between two supposedly acid-intermediate volcanic units - the Cliffdale Volcanics and the Siegal Volcanics, and thought that uranium could be derived from leaching of both presumed uranium-rich units. Since then, however, the Siegal Volcanics have been found to be basaltic to andesitic rather than andesitic to dacitic and their inherent uranium concentrations are hence lower than would have been expected (as discussed in section 5.3 and Appendix 4).

Queensland Mines geologists of the late 1960's postulated a relationship between the Westmoreland deposits and the then newly discovered Narbalek deposit in the Pine Creek Geosyncline in the Northern Territory. Both deposits were spatially related to intrusive dolerites which led to the theory that the dykes themselves may have been the uranium source for hydrothermal mineralizing fluids. Since then, many differences between the two deposits have been found particularly in host rock lithology (unmetamorphosed conglomeratic sandstones at Westmoreland and graphitic quartz feldspar schists and pelites at Narbarlek), in stratigraphic position (above the Carpentarian unconformity at Westmoreland and below it at Narbarlek) and in ore grade (0.15% U_3O_8 at Westmoreland, average 1.9% U_3O_8 and spots up to 10% U_3O_8 at Narbarlek), thus negating such a genetic link. Further to this, basic igneous rocks have an inherently low uranium content rendering them unsuitable source rocks for uranium deposits as previously discussed in Chapter 5.3.

Hills and Richards (1972, 1976) advanced no genetic model as such for the Westmoreland deposits, but upon examination of the U-Pb isotopic compositions at Westmoreland and the U-Pb, K-Ar and Rb-Sr systematics in the East Alligator Uranium Field reached the conclusion that accumulation of uranium took place under low grade conditions as no evidence of metamorphism of the same age of mineralization (900 m.y. 500 m.y.) could be found in the K-Ar or Rb-Sr isotopic records.

This led to the thought that the formation of primary pitchblende reflects the oxidation-reduction state of the environment and its effect on the kinetics of uranium precipitation, rather than the temperature and pressure of formation, i.e. precipitation of uranium was in response to redox changes rather than to temperature and pressure changes.

Hills and Thakur (1975) considered that the dolerite dykes and faults along which they were emplaced, acted as channelways for later mineralizing solutions from an unknown source. They envisaged these

solutions as causing the widespread alteration of the dyke and the chloritic alteration of the sandstone and considered that the vertical ore lenses within the dyke and the sandstone were of hypogene origin, with the peneconcordant mineralization in the sandstone being of supergene origin.

A number of points render this model questionable including the lack of a suitable source for the mineralizing solutions as well as the lack of supposedly supergene lenses at Huarabagoo.

Further to this, Fander (1976) considered that the mineralizing fluids were not responsible for the large scale alteration of the dyke (although they may have made a minor contribution) as mineralization in the dyke was erratic and more likely to have formed by migration of uranium into altered dyke rocks during a low temperature metasomatic alteration. Alteration in the dyke and overlying volcanics as well as in the basement Cliffdale Volcanics is accompanied by large scale introduction of potassium and depletion in sodium and calcium, rather than by introduction of uranium, and hence should be attributed to a regional deuteric alteration of the Westmoreland province.

Lastly, no data exists to suggest that the vertical and horizontal ore lenses represent hypogene and supergene mineralization respectively, in fact it is more consistent to believe that both are contemporaneous, related to the one major mineralizing event as will be advanced in section 6.3.

Renewed exploration interest in Westmoreland in 1975 by Minad and Urangesellschaft Australia lead to a new genetic concept quite distinct to those advanced above. Clavarino (1975) and Curtis (1976) summarized thinking with a nine point model as follows:

- 1) Uranium is present in an Archaean basement.
- 2) Detritally contained uranium is concentrated in Lower Proterozoic metasediments.

- 3) Formation of the Murphy Tectonic Ridge and its lateral basins, followed by metamorphism of Lower Proterozoic rocks and intrusion of the Nicholson Granite Complex causes local hydrothermal remobilization of uranium.
- 4) Further development of the Murphy Tectonic Ridge, erosion of the granites and initiation of acid volcanism. Continued hydrothermal uranium remobilization in metasediments, granites and the Cliffdale Volcanics.
- 5) Deposition of the Tawallah Group with uranium locked detritally into sediments derived from the ridge except where volcanic events and fissures permit further hydrothermal remobilization.
- 6) Devitrification of acid volcanics takes place during the final stages of development of the Tawallah Group, releasing uranium from within the Cliffdale Volcanics and the Cliffdale Volcanic clastic component within the Westmoreland Conglomerate.
- 7) Development of a groundwater transport regime within the Westmoreland Conglomerate in restricted aquifers from which uranium in solution is precipitated where suitable reducing conditions exist at contacts with other lithologies, or internally.
- 8) Burial by later stratigraphic sequences may or may not have affected this process.
- 9) Weathering to present day exposure releasing uranium into the drainage system and supergene concentration at sites of pre-existing uranium occurrences.

This model is therefore quite different to previous ones which postulated hydrothermal fluids as supplying uranium in that, in this case, the uranium is derived by low temperature phenomena, i.e. devitrification of acid volcanics and derivation of uranium from within the sandstone in the final analysis.

Certain assumptions, however, such as the pre-existence of an Archaean basement to supply uranium, and the continuing hydrothermal remobilization of uranium in stages 3, 4 and 5, may be argued against, particularly the former, in view of the absence of Archaean aged rocks within the province. The closest Archaean rocks occur in the Pine Creek Geosyncline some several hundred kms to north-west. The lack of obvious hydrothermal veining also precludes the need for continuing hydrothermal remobilization.

Other debatable points include the role of the Murphy Metamorphics in supplying uranium by erosion from the Murphy Tectonic Ridge in view of their low uranium contents when compared with the Nicholson Granite Complex and the Cliffdale Volcanics and the role of a simple hydrodynamic groundwater transport regime in concentrating uranium, particularly in the vertical lenses.

Despite these objections, the present author favours some points of this model, i.e.

- 1) low temperature derivation of uranium from the sandstone, as opposed to the earlier models of high temperature hydrothermal introduction of uranium from unknown source, and
- 2) precipitation in response to oxidation reduction changes from oxidizing uranium bearing solutions encountering reducing environments at sandstone volcanic interfaces.

Other authors, without having advanced an genetic model, have seen fit to classify the Westmoreland deposits as sandstone type deposits, e.g. Dalkamph (1978) and Tilsley (1981). In those studies, no attempt has been made to sub-classify Westmoreland into a more particular genetic deposit type, though in view of the host rock age and lithology, and the age and associations of mineralization, it is assumed that the uranium mineralization of the Athabasca unconformity type is being suggested.

7.2 Characteristics of the Westmoreland Deposits

In order to be wholly satisfactory, any genetic model advanced would have to account for the following properties of the Westmoreland area, its uranium deposits and mineralization associations:

7.2.1 Thermoluminescence Characteristics

The model advanced must be able to explain the following TL characteristics as determined in Chapters 6.2, 6.3, 6.4 and 6.6:

- 1) The fact that all quartz in the Unit 4 sandstone has suffered major radiation effects comparable with a near-ore position at the younger Beverley deposit.
- 2) Why the sandstone immediately below the Siegal Volcanic Westmoreland Conglomerate contact is sensitized, often strongly, irrespective of actual mineralization.
- 3) The reason why sandstone within the basic dykes themselves, although showing some radiation effects, is not as strongly sensitized as the Unit 4 sandstone.
- 4) Why sensitization often decreases with distance away from the volcanic contact, but in holes close to the dyke remains strong regardless of depth.
- 5) Even though sensitization tends to decrease away from the Siegal Volcanics contact, a vertical homogenization of sorts in TL patterns is present in holes from Junnagunna, Longpocket and Lilypond.
- 6) Why such a vertical homogenization is not present at Huarabagoo or at the Jack and Garee Lenses, and why extremely strong localized sensitization is observed in the latter area.

- 7) The TL characteristics and sensitized nature of clasts of the early acid volcanics as found in the Unit 3 conglomerate.
- 8) The TL characteristics and role of the tuffs interbedded within Unit 4.
- 9) Why all types of quartz within the Westmoreland area including vein quartz and small euhedral quartz crystals, whether in faults or associated with mineralization, all show major radiation effects.

7.2.2 Geochemical and Mineralogical Characteristics

A statistical study of uranium mineralization beneath the Siegal Volcanics and its mineralogical associations has been undertaken at the Junnagunna orebody holes to see if any mineralogical difference exists between mineralized and unmineralized areas. Data is given in Table 7.1 and points of interest are as follows:

- A distinct relationship exists between mineralization and hematite/chlorite content, i.e. all mineralized holes contain hematite associated with uranium minerals, and practically all contain chlorite also. The converse, however, does not apply, i.e. hematite and/or chlorite may also exist in non-mineralized areas.
- The hematite associated with mineralization is a fine red-black variety - a micaceous specular hematite. Hematite further down the hole away from mineralization is an earthy red colour. Chlorite is dark green to black.
- Most non-mineralized holes also have hematite and chlorite at the sandstone contact with Siegal Volcanics. The only major exception is in the region of UMD 79/143 - UMD 79/146, where moderate hematite is present with chlorite being sparse or absent.

Hole number	Hem.	Chl.	Sulph.	Fe-Oxid.	Others	Mineral'n (>0.05%)	Silici- fication
UMD76/5	✓	✓			shale		
76/6	✓	✓					
76/7	✓	✓			siltst.	✓	
76/7 (vertical)	✓	✓				✓	
76/8	minor	minor		limonite		✓	
76/8 (vertical)	✓	✓		limonite		✓	
76/15	minor	minor		lim-goeth			
76/15 (vertical)	weak	✓			green clay		
76/16	✓	✓		limonite	clay	✓	
76/17	✓	✓	pyrite	limonite		✓	
76/18	✓	✓		limonite			
77/19	✓	✓		limonite	shale/ tuff.	✓	porous
77/20	✓	✓	py-chalc			✓	✓
77/32	✓	✓	chalc, gna	limonite	shale/ tuff.	✓	moderate
77/35	✓	✓	py,chalc	limonite		✓	poor porosity
77/39	✓	✓	rare py.			x	
77/40	✓	✓				x	
77/42	✓	✓	py,gna.	limonite above min.		✓	
78/58	✓	✓		limonite	clay/ chert	x	
78/59	✓	✓		lim/goeth above min.		✓	✓
78/59 (vertical)	✓				sericite	✓	
78/60	✓	✓	py in faults	limonite + pyrite.		✓	✓
78/64	✓	✓	py			✓	
78/69	✓	✓	py-chalc			✓	✓
78/71	✓	✓	py	lim.in volcs.		x	
78/72	✓	✓	py	limonite		✓	mod. well
78/74	✓	✓	chalc- py			✓	✓
78/77	✓	✓	py,chal aspy.	lim+qtz		✓	mod. well
78/79	✓	✓	py, aspy			✓	moderate
78/81	✓	✓	py			✓	moderate

Table 7.1 Mineral associations with uranium at the Junnagunna prospect, Westmoreland.

Hole number	Hem.	Chl.	Sulph.	Fe-Oxid.	Others	Mineral'n (>0.05%)	Silici- fication
UMD78/82	✓	✓				✓	✓
78/83	✓	✓					
78/84	✓	✓	py. in volcs.	limonite	sericite		
78/85	✓	✓	py, chalc			✓	✓
78/86	✓	✓	py, chalc			✓	mod.
78/87	patchy	✓	py	limonite			
78/88	✓	✓					
78/89	✓	✓		limonite			
78/90	mod.	minor		limonite			
78/91	patchy	✓		limonite	sericite		
79/100	✓	✓	py		alter'n	✓	
79/101	✓	✓		limonite		✓	mod.
79/102	✓	✓	py				
79/103	✓	✓					
79/106	✓	✓		limonite above min'n.		✓	✓
79/107	✓	✓	py			✓	
79/108	✓	✓		lim. in volcs.		✓	partial
79/108 (vertical)	✓	✓	py. in dyke			✓	partial
79/110	✓	✓		lim. in volcs.			
79/112	✓	✓	py	limonite		✓	✓
79/114	✓	✓		limonite	clayey		
79/116	✓	minor	marcasite	limonite	chert	✓	partial
79/117	✓	not in ss		tuffa- ceous			
79/119	✓	✓					
79/123	weak			limonite			
79/124		✓					
79/125	✓	✓				✓	✓
79/126	✓	✓		limonite			
79/127	✓	✓				✓	✓
79/133	✓	✓	py			✓	partial
79/134	✓	✓		weak lim.		✓	
79/135	✓	minor					
79/137	✓	✓				✓	partial
79/138	✓	✓			clay		
79/139	✓	✓					
79/140	✓	✓	py	limonite		✓	✓

Table 7.1 Mineral associations with uranium at the Junnagunna prospect Westmoreland.

Hole number	Hem.	Chl.	Sulph.	Fe-Oxid.	Others	Mineral'n (>0.05%)	Silici- fication
UMD79/141	✓	✓	py			✓	✓
79/142	✓	✓	py				
79/143				limonite			
79/144				limonite			
79/145	at depth	at depth					
79/146	at depth	at depth		limonite		✓	✓

Table 7.1 Mineral associations with uranium at the Junnagunna prospect, Westmoreland.

- No direct relationship exists between mineralization and silicification. Mineralization generally occurs in well silicified areas, though well silicified areas need not necessarily be mineralized.
- Small euhedral quartz crystals are associated with mineralization. They also occur away from mineralization in small joints and faults. These probably represent different modes of formation. (As reported previously the TL characteristics of the crystal quartz are very similar to those of most sandstone).
- Limonite is not associated with mineralization. 50% of limonite occurrences are in completely non-mineralized holes, and when occurring in mineralized holes is not spatially related to pitchblende but usually occurs below, and rarely above ore. Some limonite represents oxidation from pyrite. The lack of limonite and the presence of hematite in mineralized zones may represent a further conversion of limonite to hematite accompanying the mineralization process.
- Twenty nine occurrences of sulphides are recorded in the Junnagunna drill logs - 23 occurring in mineralized holes and six in non-mineralized holes. Of the 39 mineralized holes at Junnagunna, 23 contain sulphides.

Sulphides occur in three forms:

- a) Detrital grains which are original constituents of the sandstone. The sulphide is pyrite and is extremely rare, being scattered at random throughout Unit 4. This detrital sulphide is certainly not abundant enough to cause precipitation of uranium.
- b) Grains associated with mineralization. These are also usually pyrite, though chalcopyrite and galena also occur. Being

associated with mineralization means that they occur close to the Siegal Volcanics or the Redtree dyke. As such, they may have formed by release of sulphur complexes into the upper few metres of sandstone contemporaneous with the migration of Fe^{2+} and Mg^{2+} during extrusion of the basalts or intrusion of the dolerites (Fander 1976), or during deuteric alteration of the volcanic flows and dykes.

- c) Veins and veinlets of pyrite, chalcopyrite and galena, with minor sphalerite associated with euhedral quartz crystal development along microfaults and joints. Pyrite is often oxidized to marcasite and limonite. These represent a later stage feature than mineralization (Hills 1973, Manning 1979) and are not associated with ore development.

(Microscope descriptions of the different sulphide forms are given in Appendix 3).

The geochemical and mineralogical associations of the mineralization that must therefore be explained by the proposed genetic model are:

- 1) The intimate presence of hematite, chlorite and euhedral quartz with mineralization and the frequent occurrence of clays and sulphides as well.
- 2) The lack of association between limonite and pitchblende.
- 3) The geochemical relationship between U, V and ΣFe and the unexpected association of those elements with high $\text{Fe}^{3+}/\text{Fe}^{2+}$ ratios (Curtis 1976, Manning 1979).
- 4) Why the mineralization at the Jack, Garee and also Outcamp Lenses, where capping volcanics are missing, is more oxidizing than in areas such as Junnagunna and Sue, i.e. with with capping volcanics.

- 5) Why mineralization has remained fixed in an oxidizing redbed environment.

7.2.3 Location and Structural Characteristics

The geomorphological and structural points needed to be accounted for are:

- 1) The presence of mineralization immediately below the volcanic contact yet the sparsity within the basalts themselves, and the almost complete absence of mineralization away from the upper few metres of Unit 4 at Junnagunna and Sue.
- 2) The spatial association of the horizontal lenses with the dyke.
- 3) The proximity of vertical pods of mineralization to the dyke.
- 4) The association of the Jack and Garee Lenses with the Redtree dyke with mineralization occurring at a depth of approximately 40m from the top of Unit 4 as opposed to areas such as Junnagunna, where mineralization is within the upper few metres.
- 5) The proximity of the Junnagunna orebody to the Cliffdale Fault.
- 6) The confinement of mineralization to the Unit 4 sandstone and absence in the underlying three units.

7.3 Genetic Model

In determining a genetic model, the following four points need to be known:

- 1) The original source of the uranium.
- 2) The method of fixing the uranium within the sandstone until concentration and precipitation.

- 3) A transport and precipitation mechanism to concentrate the ore,
and
- 4) a means of preserving it to its present state.

A knowledge of these four properties would also explain many of the points raised in section 7.2.

7.3.1 Source of Uranium

As was previously suggested, the original sources of uranium for the Westmoreland deposits have included hydrothermal mineralizing solutions from granites (Newton and McGrath, 1958), dykes (unnamed Queensland Mine geologists), or an unknown source (Hills and Thakur, 1975), devitrification of the Cliffdale Volcanics and its clasts (Curtis, 1976) and an Archean basement (Clavarino 1975). Other possibilities that have been proposed in recent years include placer deposits of detrital heavy minerals, deposited along positive topographic features represented by the Cliffdale Fault (Evans 1979), uraniferous heavy mineral bands within the Westmoreland Conglomerate (Ahmad et al. 1984) the tuffs and tuffaceous sandstones recently identified as being interbedded within the Unit 4 sandstone, and the possibility of remobilization of deeper higher grade mineralization (Schindlmayr and Beerbaum, 1984).

The first of the more recent suggestions seems unlikely, in view of the limited association of mineralization with faults in the Westmoreland area, other than the Cliffdale Fault, and even then, only in the Junnagunna area.

Page (1981) studied acid tuffs in the Barney Creek Formation in the McArthur Group (overlying the Tawallah Group) and found that they had uranium contents of up to 230 ppm. As such, these could have been excellent uranium source rocks, however, the Westmoreland tuffs are

different to these both in uranium content and in mode of formation, (discussed further with geochemical results in Appendix 4).

Croxford (1964, 1968) and Croxford and Jephcott (1973) considered that the McArthur River tuffs and corresponding ones at Mt. Isa were derived from a rhyolitic parent magma and would therefore be expected to be enriched in uranium. On the other hand, the Westmoreland tuffs and overlying volcanics are more basic in nature (section 5.3 and discussion in Appendix 4), and would thus have a lower uranium content than those at McArthur River and Mt. Isa.

TL work on the Westmoreland tuffs shows that they have a dominant MT peak and a large intensity (figure 7.1), and therefore could be considered to show some sensitization. However, these are probably still in the transition stage to major radiation effects (observation 7.2.1(8)). Hence, they are less radiation-effected than would be expected if they were major suppliers of uranium.

Volumetric considerations also rule out the tuffs as a viable possibility to supply sufficient uranium, as they are quite thin (usually less than 10cm thick, though up to 30cm) and do not form a major constituent of the sandstone.

Clavarino (1975) and Curtis (1976) invoked devitrification of the Cliffdale Volcanics to supply uranium. Many samples from the Unit 3 conglomerate show a distinctive TL pattern (figure 7.2), with the MT glow peak having maximal intensity (observation 7.2.1(7)). These rocks are all petrologically characterized by acid volcanic fragments. The quartz is thus also possibly volcanogenically derived. Giles (1980) found that many Middle to Lower Proterozoic acid volcanics throughout Australia are significantly enriched in large-ion-lithophile elements including uranium relative to their Archaean and Palaeozoic counterparts. Uranium contents were up to 50 ppm. Similarly, Teale (Ph.D. at Univ. of Adelaide in prep.) has found that many similar aged acid volcanics in South Australia

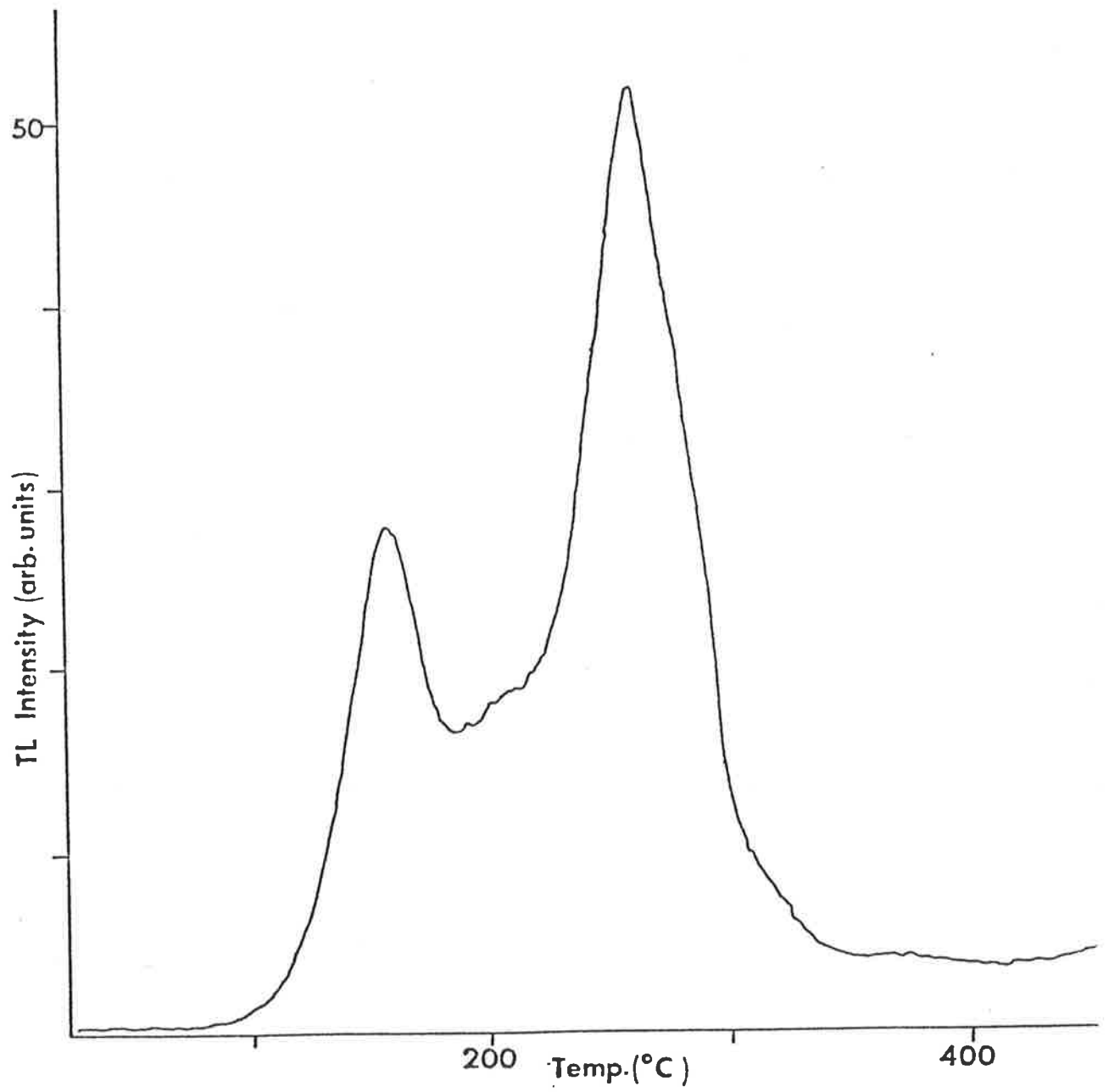


Figure 7.1 TL glow curve of quartz from tuffs within Unit 4 of the Westmoreland Conglomerate.

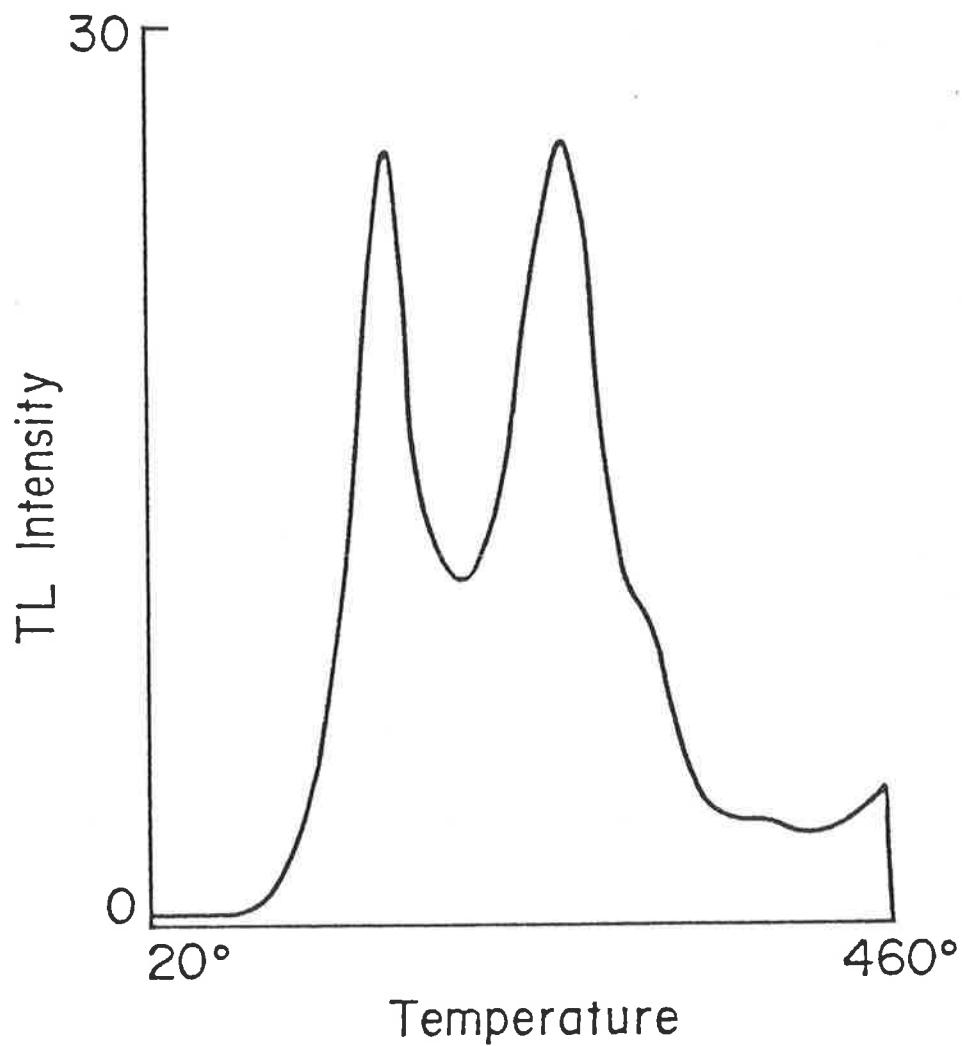


Figure 7.2 TL glow curve of quartz from the Westmoreland Conglomerate, Unit 3.

and the Northern Territory contain uranium concentrations up to 70 ppm.

Uranium analyses by Ayres and Eadington (1975) on the Edith River Volcanics in the Pine Creek Geosyncline (which are equivalent to the Cliffdale Volcanics) range from 12 ppm to 56 ppm with a mean of 13.4 ppm. They consider the work of Rosholt and Noble (1969) and Rosholt et al. (1971), who showed that recrystallized volcanic rocks have probably lost 60% of their original uranium, to conclude that the original uranium content of the Edith River Volcanics was high (33.5 ppm assuming a 60% loss). Further to this, they consider a high Th/U ratio in the Edith River Volcanics of 2.8 (vs 2.1 for the average rhyolite (Imbo, 1968) to indicate that uranium has been lost from the volcanics. The Th/U ratio of the Cliffdale Volcanics is 3.5 (average of 12 samples from Mitchell (1976)) pointing to the possibility of a larger uranium loss than that for the Edith River Volcanics.

Further evidence of large uranium loss from such acid rocks is supplied by Labhart and Rybach (1974), who show that 90% of uranium may be leached from such rocks without any apparent weathering effects and by Hart et al. (1981), who used U-Pb isotope studies to indicate an 80% uranium loss from basement rocks in the Vredefort Dome, South Africa.

Applying this reasoning and considering the work of Giles (op. cit) and Teale (op. cit), as well as the TL characteristics of Cliffdale Volcanic fragments and clasts, the Cliffdale Volcanics thus appear an attractive original source for uranium, as does the coeval Nicholson Granite Complex which is similarly enriched.

All of the 700 or so samples measured of Unit 4 of the Westmoreland Conglomerate have lower LT/MT peak ratios than for most common sandstones. The displacement of this ratio towards 1.0 could indicate that the quartz is derived from material with a generally high background value of uranium in Unit 4 sandstone, which led to a sensitization affecting all quartz.

This is further confirmed when one considers that all samples are over the threshold at which major radiation effects (ie. the drastic decrease in ATL intensity) occurs. Shekhmametev (1973) placed this threshold at 10 ppm U over a 300 m.y. period.

Further to this, as discussed in section 3.1, Hayslip and Renault (1976) found that concentrations of uranium in the Jurassic Morrison Formation below 10 ppm, had no effect on the intensity of the HT glow peak, even though under laboratory conditions, a radiation dose created by such concentrations should have caused major radiation effects. The conclusion reached is that a radiation dose created by 10 ppm U or less under the burial conditions experienced by the Morrison Formation (which are similar to those of the Westmoreland Conglomerate), is not large enough to produce major radiation effects in the host sandstone.

It is important here to re-emphasize the fact that radiation doses caused by uranium concentrations of 10 ppm or less, apparently have little effect on the TL signal. Therefore, according to this reasoning any sensitization or radiation effects in the Westmoreland Conglomerate should be caused by uranium concentrations of at least 10 ppm and possibly more.

This value, although high for sandstones, seems plausible in view of the work of Manning (1979), who found that the Westmoreland Conglomerate had been derived dominantly from the Cliffdale Volcanics and the Nicholson Granite Complex rather than the metasedimentary Murphy Metamorphics. It also appears possible in view of:

- 1) the high uranium contents of these acid igneous rocks, as previously established;
- 2) the massive erosion of these rocks - an estimated 10,000 metres has been eroded from the upper portions of the Nicholson Granite Complex and therefore the coeval Cliffdale Volcanics as well (Gardner, 1978) and,

- 3) the availability of the uranium for leaching, i.e. McAndrew et al. (1980) found that uranium in the granites of the Pine Creek geosyncline tended to form uraninite rather than be locked into accessory minerals. Teale (pers. comm.) has also shown by electron microprobe analyses that uranium in Proterozoic acid volcanics tends to be found in the glassy and leachable components of the extrusive rather than being incorporated into accessory minerals such as zircon, leucoxene, monazite etc.

It should also be noted here that the regional sandstone background uranium content within the Westmoreland Conglomerate is still 4-6 ppm (Schindlmayr and Beerbaum, 1984).

Other workers have also established a link between the uranium content of a sediment and the provenance rocks of the sediment. For example, Ishihara et al. (1981) determined the thorium and uranium contents of sandstones and shales derived from a number of different sources in western Shikoku, Japan. They discovered that the sandstones of the Izumi Group, which were derived from a granitic and rhyolitic provenance area, had higher uranium and thorium contents than the sandstones and shales derived from other source rocks of sediments and mafic volcanics, the Shimanto Supergroup and Chichibu Group. Similarly, Beeson (1981) who studied the associations of uranium in the Permian-Triassic Beaufort Basin of South Africa, concluded that the bulk of the established uranium mineralization was related to the presence of source lithologies capable of providing uranium.

The favoured source for the uranium for the Westmoreland Uranium Deposits is therefore from within the Westmoreland Conglomerate itself, which was derived by erosion from Proterozoic acid igneous rocks which themselves had an inherently high uranium content. Thus the derived sandstone was also significantly enriched in uranium, leading to the major radiation effects observed in the entire sequence. This is similar

to the ideas of Clavarino (1975) and Curtis (1976) who recognized the potential of the Cliffdale Volcanics clasts in the Westmoreland Conglomerate to provide uranium upon devitrification, though this suggested uranium source differs from their need to invoke the existence of a uranium-rich Archaean basement, to originally provide uranium.

7.3.2 The Mechanism to Hold Uranium Within the Westmoreland Conglomerate

After deposition of the Westmoreland Conglomerate, the contained uranium would have been quickly leached out of the sandstone (given its redbed nature) by oxidizing groundwaters unless a suitable reducing agent or barrier mechanism was available. Such an agent may have been the interstitial sulphides or perhaps the clay and chlorite contained within the upper metres of the sandstone, thus accounting for observation 7.2.2(1). However the interstitial sulphides are so rare that they are not considered a viable reductant, though the clay and chlorite may well have slowed down the leaching of uranium.

The preferred retention mechanism involves the high concentrations of vanadium found, particularly in mineralized areas, but also in non-mineralized areas. The background vanadium content of Unit 4 of the Westmoreland Conglomerate is usually greater than 50 ppm and up to 420 ppm (Curtis 1976, Manning 1979), as opposed to 20 ppm for the average sandstone (Rankama and Sahama, 1950). Vanadium was supplied to the sandstone during pyroclastic and basic tuffaceous extrusion - the tuffs have high vanadium concentrations in excess of 500 ppm. Vanadium would also have been supplied by surface alteration of magnetite.

Uranium in the oxidized state would complex with the excess vanadium in the groundwater regime and form a uranyl vanadate which would thus immobilize the uranium in the sandstone and prevent further leaching. Such a mechanism may also help to explain the intimate

association of uranium and vanadium, not only at Westmoreland (observation 7.2.2(3)) but also in many other similar aged deposits as noticed by other workers, e.g. Ayres and Eadington (1975) in the South Alligator Valley; Brookins (1980) at Oklo; and Giblin (pers. comm.) at Ranger.

Ayres and Eadington (op.cit) found that uranium was strongly associated with vanadium in the South Alligator Valley, but not with total carbon, thereby implying that uranium was not introduced with reduced carbon in carbonaceous shales, but that these had provided a reducing environment at a later time for uranium which was associated with vanadium being transported together as a uranyl complex.

Thus, the blocking of uranium by vanadium would allow further accumulation of hematite by surface alteration of magnetite, enabling further development of the red bed nature of the sandstone. Subsequent massive extrusive volcanism would then halt the effects of further surface alteration and lock the uranyl vanadate into the sandstone.

7.3.3 Transport and Precipitation

The situation thus far, therefore, is one of the Westmoreland Conglomerate with overlying Siegal Volcanics, with uranium fixed in the Westmoreland Conglomerate as a uranyl vanadate but still in a dispersed form, i.e. is not concentrated to form an orebody. The mechanism proposed by Clavarino (1975) and Curtis (1976) to transport and concentrate the uranium involved groundwater movement. Although this undoubtedly played a part, it is not sufficient to explain certain properties of the deposit such as the present ore positions of vertical lenses, or the vertical homogenization of TL patterns within individual holes.

One way of explaining such facts is to invoke the vertical dykes having triggered a convective groundwater flow, upwards along the dykes due to localized heat flow and downwards because of higher salinity (density) differences during cooling. As the convective flow involved oxygenated waters from the more oxidizing sandstones, uranium could have been mobilized in this way, flowing towards the intrusives and their surface extrusives, and be precipitated as pitchblende in the more reducing conditions. Transport through the sandstone would be as a uranyl vanadate. Langmuir (1978) has suggested that these soluble complexes exist in oxidizing conditions with an excess of vanadium, but due to the lack of available data he has been unable to either identify the soluble complexes, or classify the precise thermodynamic conditions under which they exist. Schindlmayr and Beerbaum (1984) also support the idea of a convective cell concentrating uranium, though they favour a heat flow event along rejuvenated dyke filled structures at 820 m.y. - the oldest pitchblende ages. As yet, no tectonic event or igneous activity of this age is known within the Westmoreland region.

Once the first uranium concentrations were formed in this way, the system may even have had enough heat generating potential to continue a vertical convective current due to radiogenic heat production which would displace actual uranium concentrations up and down the stratigraphic column. The direction of flow would be determined by heat (up) and/or the density of solution (down) with lateral movement along the Siegal Volcanic contact. This mechanism would account for observations 7.2.1(2) (4) and (5). The principle of this mechanism has been worked out by Fehn et al. (1978) who show that radiogenic heat derived from a mildly uranium and thorium enriched granite can drive such convective cells. A model involving convective cells driven by radiogenic heat has also been previously proposed by Tilsley (1980, 1981) and Hoeve et al. (1980,1987) for the Athabasca uranium deposits.

A cartoon sketch of the Westmoreland system is given in figure 7.3.

The impermeable nature of the dolerite dykes and overlying basalts would prevent major penetration of the convecting uranium-bearing solutions which explains the sparsity of mineralization within the volcanics, as well as the lesser sensitization shown by the sandstone inclusions in dykes and/or volcanics (observation 7.2.1(3)). Such a model would also account for the close spatial relationship of horizontal lenses with the dyke (observation 7.2.3(2)) and the proximity of vertical pods to the dyke (observation 7.2.3(3)). Precipitation of uranium as pitchblende would occur at the more reduced conditions close to the dolerite dykes and their surface extrusives (observations 7.2.3(1) and (6)). Such conditions would promote alteration of the volcanics and dykes and the migration of Fe^{2+} and Mg^{2+} and sulphur complexes into the surrounding sandstone. This would lead to the formation of sulphides (pyrite) and conversion of clays to chlorite (Ferguson and Rowntree, 1980) within the few metres of sandstone close to the volcanics. Upon encountering these reducing conditions, uranium would form pitchblende along with liberation of vanadium into the sandstone. Vanadium would probably be absorbed by clays and micas and indeed the vanadium mica roescolite has been identified in these areas by XRD analysis (Manning, 1979).

The uppermost portions of Unit 4 also contain abundant clays and given the sorptive properties of clays and uranium (Muto 1965; Giblin 1980a) these too could immobilize uranium.

A third mechanism for reduction and precipitation of uranium as pitchblende involves the scavenging iron oxy-hydroxides such as goethite. Fine-grained natural goethite has an enrichment factor of 4×10^3 and amorphous ferric oxy-hydroxides have an enrichment factor of $1.1 \times 10^6 - 2.7 \times 10^6$ (van der Weijden et al. 1976; Langmuir, 1978) and thus are capable of absorbing much uranium and retaining it within the convective

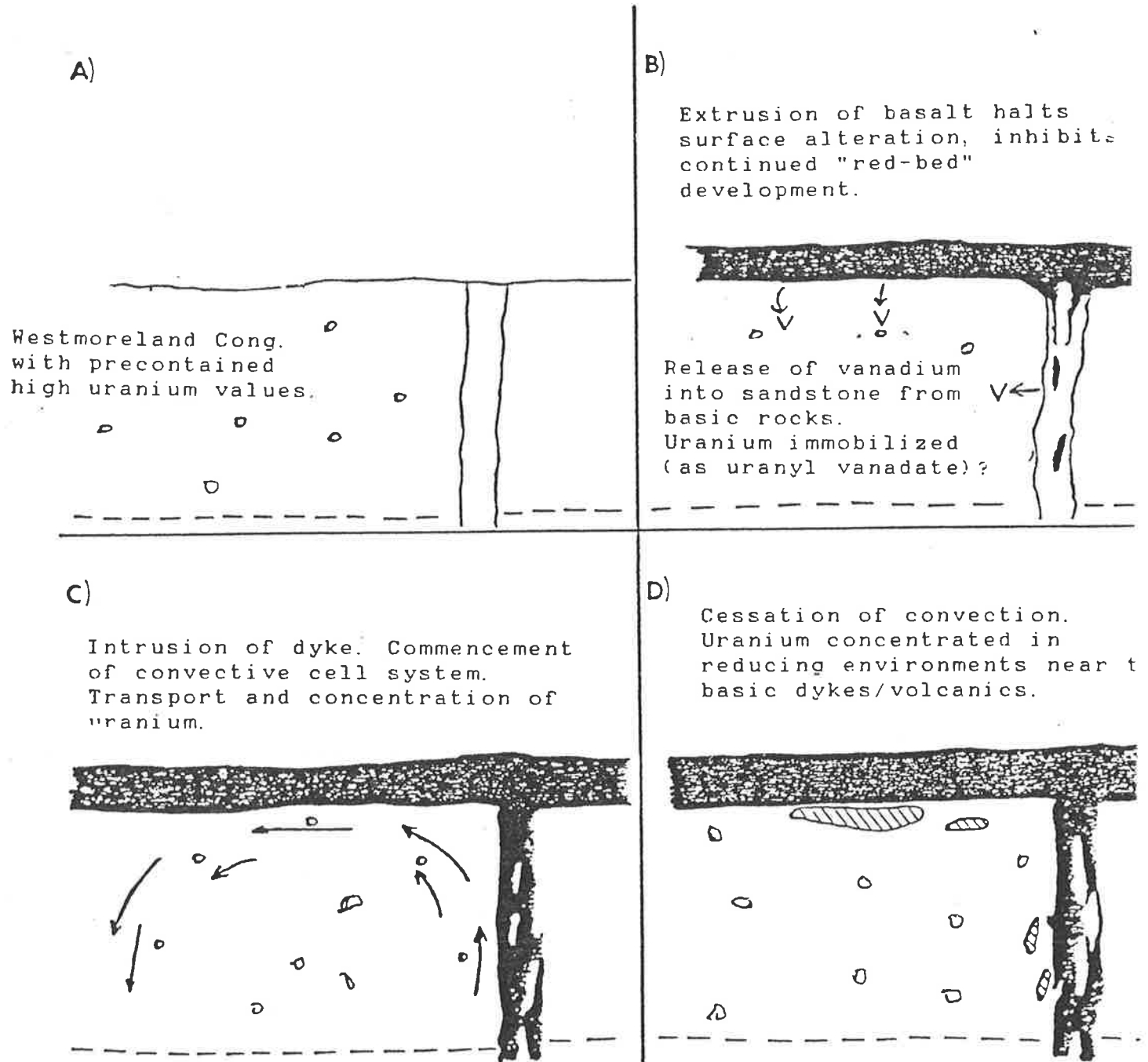


Figure 7.3 Cartoon sketch of the genetic model for the Westmoreland uranium deposits.

cell. Recent Russian work (Shmariovich, 1980) has indicated that some of the iron oxy-hydroxides may be reducing enough to allow precipitation of pitchblende. Such a mechanism has previously been proposed by Ferguson and Rowntree (1980), for the concentration of pitchblende at Narbarlek.

Such a mechanism would explain the intimate association of mineralization with hematite at Westmoreland as goethite, during charge couple transfer with the uranyl ion, would oxidize to hematite, i.e. $\text{goethite} \rightarrow \text{hematite} + \text{water}$ (Langmuir, 1971) (observations 7.2.2(1) and (2)). If the liberation of water in this reaction took place in mildly acidic conditions, it could have perhaps caused minor dissolution of silica and reprecipitation as the small euhedral quartz crystals which are associated with mineralization.

Finally, one has to consider the vanadium-rich nature of the mineralized samples (up to 850 ppm in sample N12 from the Jack Lens). As previously discussed, this also could help in retention of uranium. In fact, the secondary uranium mineralization found in sandstones above areas with no present volcanic capping is largely carnotite - a uranium vanadate.

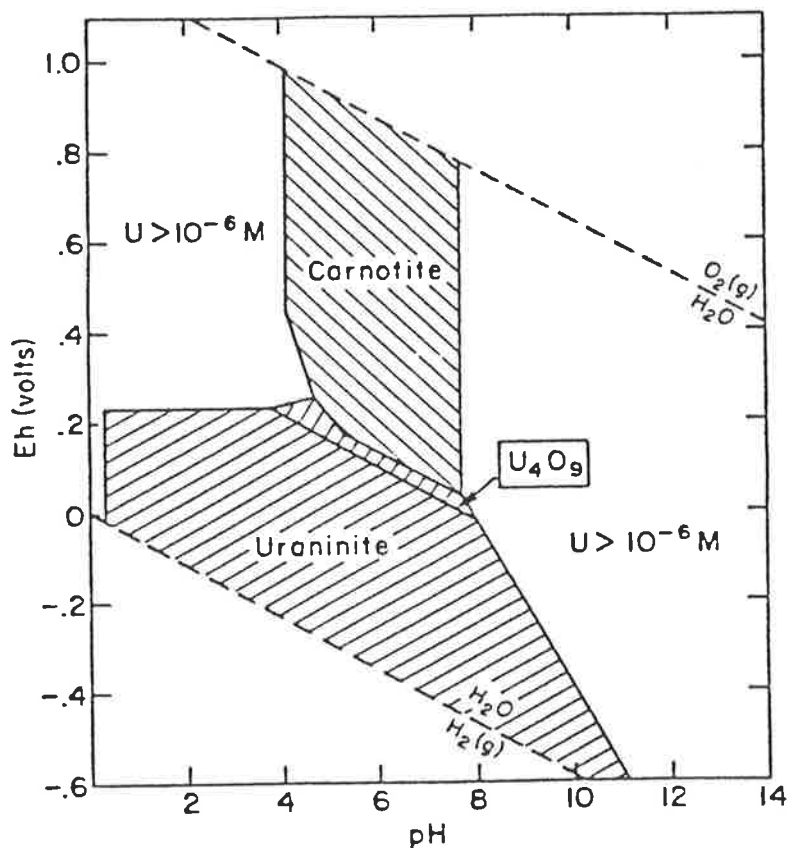
Therefore, despite the oxidizing red-bed nature of the sandstone, suitable reductants and reducing environments are present to cause precipitation of uranium as pitchblende in the upper few metres of the sandstone or in the sandstone close to the dyke. This explains observation 7.2.2(5).

7.3.4 Preservation

Preservation of Junnagunna type deposits would be achieved by protection from the effects of surface alteration and oxidation by a thick covering of Siegal Volcanics. These deposits would therefore be fixed in the positions in which they had been reduced.

This situation cannot be applied to the Redtree area where the sandstone has no volcanic capping. If the Jack and Garee Lenses had been at the contact after erosion of the Siegal Volcanics and hence exposed to the surface, then they may have been lost. These orebodies, however, occur at a depth of 30m-40m below surface. It is hypothesized that erosion of the overlying volcanic cover caused termination of the convective cell system. Once the capping was removed, convection would finish and the ore formed would remain at whatever depth it had been in the system prior to cessation of convection. This would account for observation 7.2.3(4). Once again, the presence of excess vanadium in the sandstone would prevent excessive leaching, though this ore would still not be as stable as that protected by a volcanic capping. This may explain the higher oxidation state in the Redtree area than in the Junnagunna or Sue areas ($E_h = +0.375$ V, $pH = 6$ in the Redtree area; vs $E_h +0.100$ V $pH = 7.5$ of Junnagunna) and also the higher uranium values in groundwater in the former as opposed to the latter (up to 1000 ppb U vs 20-30 ppb U); Giblin (1980b), and thus may explain observation 7.2.2(5). The work of Giblin (op.cit) also indicated that the oxidation potential tended to decrease with depth in the Jack and Garee Lenses, i.e. more reducing conditions were encountered at depth. For example, in N129 18m $E_h = +0.180$ V, $pH = 5.1$ which is suitably reducing for preservation of pitchblende, whereas at the surface, where redox conditions are more oxidizing, the major mineral is carnotite. This conforms with thermodynamic expectations as represented in figure 7.4 after Langmuir (1978).

The cessation of convection would also explain the lack of a vertical homogenization within holes in the Redtree area, and since the ore was relatively immobile, would also account for the strong localized sensitization found at the Jack and Garee Lens (observation 7.2.1(6)), but weaker spot sensitization in areas where convection has been



Eh-pH diagram in the system K-U-V-O₂-H₂O-CO₂ at 25°C. Given: K = 10⁻³ M (39 ppm), ΣU = 10⁻⁶ M (0.24 ppm) at mineral-solution boundaries, ΣV = 10⁻⁶ M (0.1 ppm as VO₄), and P_{CO₂} = 10⁻² atm.

Figure 7.4 Eh-pH stability fields of pitchblende and carnotite (after Langmuir, 1978).

continuous, e.g. Junnagunna. As convection continued in areas such as Junnagunna, this would lead to further vertical homogenization of TL patterns within individual areas. Continued convection would also dissipate mineralization and thus could account for the lower overall grade of mineralization at Junnagunna as opposed to the Redtree Lenses. Dissipation of mineralization would lessen the radiogenic heat production driving the cell, and thus could eventually lead to termination of the cell.

These deposits could therefore be preserved from either further Proterozoic or Cretaceous weathering to the present time, due to either a volcanic capping or their depth below surface. Down-dip movement from the deposits would occur after cessation of convection and may have led to formation of the Langi Lens and also to a banking up of ore-bearing solutions at the Cliffdale Fault resulting in the deeper sensitization and occasional mineralization found there.

7.4 Summary of the Genetic Model

A point by point model of the history of the Westmoreland region leading up to the formation of the uranium deposits and preservation until the present is as follows:

- 1) The formation of the Murphy Tectonic Ridge (as described in Chapter 5.2) comprises geosynclinal metasediments of Lower Proterozoic age, followed by multiple intrusions and widespread extrusion of uraniferous acid volcanics.
- 2) Uplift of the ridge and subsidence of the formative McArthur Basin with erosion of up to 10,000 metres of the Nicholson Granite Complex and an unknown amount of the Cliffdale Volcanics, resulting in deposition of the Westmoreland

Conglomerate, with an inherently high uranium content of at least 10 ppm and probably higher, (4-6 ppm is still left).

- 3) Contemporaneous with deposition of the Westmoreland Conglomerate is pyroclastic activity, resulting in the interbedded tuffs and tuffaceous shales within the sandstone. Vanadium released from the tuffs and from surface alteration of magnetite retains uranium in the sandstone, despite the oxidized nature of the sandstone and the groundwater regime within it. Clays, syngenetic chlorite and rare dispersed sulphides may have also contributed to the fixation of uranium.
- 4) Massive extrusive basic volcanism stops surface leaching and alteration effects. Migration of Fe^{2+} and Mg^{2+} with the introduction of sulphur complexes, creates a reducing environment close to the volcanics, which, coupled with clays, iron oxy-hydroxides and a high vanadium content, is suitable to precipitate uranium as pitchblende following the next step.
- 5) Intrusion of dolerite dykes or other sources of localized heat flow along rejuvenated joint zones (Schindlmayr and Beerbaum, 1984), sets up convective cell systems with oxygenated waters moving upward near the dyke because of localized heat flow and downward further away from the dyke because of salinity and density differences. In this way, uranium is transported along the contact of the Siegal Volcanics/Westmoreland Conglomerate and is reduced to pitchblende. At the same time, goethite is altered to hematite during sorption of uranium. Similar occurrences near to the dykes, at any depth, result in the vertical pods of mineralization.

- 6) Uplift and erosion of the overlying cover in the Redtree area halts convection, leaving the Jack and Garee Lenses at their present depths.
- 7) These are modified by later weathering and down-dip movement of uraniferous solutions to form the present day situation.

CHAPTER 8

PROTEROZOIC SANDSTONE HOSTED URANIUM DEPOSITS

- A BIMODAL CLASSIFICATION?

CHAPTER 8: PROTEROZOIC SANDSTONE HOSTED URANIUM DEPOSITS

- A BIMODAL CLASSIFICATION?

- Summary of Chapter

In chapter 7 it was suggested that the Westmoreland Conglomerate itself provided the uranium which was subsequently concentrated to form the current deposits.

Chapter 8 compares the Westmoreland deposits with other similarly aged uranium deposits and refers to TL studies on two other Australian Middle Proterozoic sandstones. These two referenced TL studies revealed that ubiquitous host rock radiation effects do not occur in all Middle Proterozoic sandstones. In turn, not all of these units have initial, high, pre-contained uranium contents. The initial uranium content of such a sandstone may reflect its provenance, with those being derived from uranium rich Middle Proterozoic acid igneous rocks having high uranium contents and those derived from uranium poor metasedimentary sequences having low inherent uranium contents.

The former are considered more likely for derivation of economic uranium deposits from within the sandstone itself.

* * *

Uranium mineralization in other Proterozoic aged sandstones and conglomerates is known throughout the world, notably the Athabasca Formation in Canada and the Franceville Series in Gabon. As yet, no extensive mineralization has been discovered in the Kombolgie Sandstone in the Alligator River Uranium Field of the Pine Creek Geosyncline (Northern Territory), though by comparison with the Athabasca Formation in Canada it does appear likely that discoveries may be made in the future.

Because ATL studies at Westmoreland have resulted in new discoveries and interpretations which may have wider applications (eg. the radiation affected nature of the entire Westmoreland Conglomerate), these results will be used to assist in a speculative classification of Middle Proterozoic sandstones and their uranium deposits.

Extensive ATL studies have also been conducted on two other Middle Proterozoic sandstones in South Australia which are referred to in this chapter. No extensive discussion of the studies is given other than to draw out the points relative to this chapter i.e. the radiation effects on the sandstones and its use in classification of Middle Proterozoic sandstones. One of the studies (on the Corunna Conglomerate) has in part, been published and is appended to the back of this thesis. Studies on the other sandstone (the Pandurra Formation) were part of contract work for a private company though now are on open file in the South Australian Department of Mines and Energy Envelope system. Details are given in the bibliography.

Considering that the Westmoreland Conglomerate is contemporaneous with the Kombolgie Sandstone which is, itself, considered an equivalent of the Athabasca Formation, it could be thought that these sandstones and their uranium deposits, or potential uranium deposits, would be similar. In order to discover any such similarities, (or to highlight differences) which may be useful in determining a general model for Proterozoic

sandstone uranium deposits, a comparison of the deposits made. A brief description of each area is given to acquaint the reader with necessary information concerning tectonic setting, host rock lithology, mineralization (if present) and current theories of genesis. The most important of these aspects are summarized in Table 8.1.

8.1 Comparison of the Westmoreland Uranium Deposits With Other Similarly Aged Uranium Deposits

8.1.1 The Athabasca Formation and its Uranium Deposits, Saskatchewan, Canada

The Athabasca uranium deposits are located in the Athabasca Basin of the Saskatchewan Shield. The shield area is part of the Churchill Structural Province and is comprised of Archaean granulites and continental crust overlain by Apebian (Lower Proterozoic) platform cover (Lewry and Sibbald, 1979). These have been deformed and metamorphosed by the Hudsonian orogeny (c.a. 1750 m.y.) during which time anatexis mobilization resulted in late tectonic granitoid intrusion (Hoeve et al. 1980).

The lithology and thickness of Lower Proterozoic metasediments varies within the province, however, where best exposed in the Wollaston Domain, they are composed of four main stratigraphic units. These are:

a basal clastic unit;

a graphitic pelitic unit with occasional quartzite psammite, calc-silicates and marble;

a thick often calcareous meta-arkose with interlayered calc-silicates and meta-pelites;

and

an amphibolite-quartzitic unit.

	Westmoreland	Oklo	Athabasca	Keewatin	East Alligator
<u>Basement</u>					
Lithology	Granite, acid volcs. metamorphics.	Granite, syenite metamorphics.	Granulites, metamorphics, granite.	Metamorphics, paragneisses.	Granite, metamorphics
Age	1800 M.a.	>2,200 M.a.	>2,200 M.a.	>2,200 M.a.	>2,200 M.a.
<u>Host rock</u>					
Lithology	Conglomerate, sandstone (Westmoreland Conglomerate).	Conglomerate, sandstone (Franceville Series).	Conglomerate, sandstone (Athabasca Formation).	Conglomerate, sandstone arkose (Karzan Arkose).	Conglomerate, sandstone (Kombolgie Sandstone).
Age	1,650-1,700 M.a.	1,700-2,000 M.a.	?1,700 M.a.	>1,766 M.a.	1,650 M.a.
Stratigraphic position.	U/C overlying acid volcanics, granites.	U/C overlying granite.	U/C overlying metasediments.	U/C overlying metasediments.	U/C overlying metasediments.
Source rocks	Granite, acid volcanics	Granite, syenite	Metasediments	Metasediments	Metasediments
<u>Mineralization</u>					
Ore minerals	Pitchblende	Pitchblende, uraninite	Pitchblende, uraninite	Pitchblende	
Average grade (Max. grade)	0.15% (2.0%)	0.4% (>50%)	0.3% (40%)	low	(The only uranium is contained in basement)
Age	900 M.a; 500 M.a.	2,000 M.a; 1,950 M.a.	89-370 M.a.	-	
Mineral/element associations.	Clay, chlorite, quartz hematite, V.	Clay, chlorite, hematite V.B.	Sulphides hematite.	Sulphides, clay Cu, Ag.	
Stratigraphic	Top unit of Westmoreland - conglomerate-Ptw ₄ .	Top unit of Franceville Series - FA _{n+4}	Base of Athabasca Formation.	Base of Karzan Arkose also near dykes.	
Source of uranium.	Within sandstone.	?Within sandstone. ?tuffs.	Older uranium deposits? within sandstone?	Overlying volcanics.	

Table 8.1 A comparison of worldwide Proterozoic sandstones and their uranium deposits (where present).

These are unconformably overlain by continental red beds - the Martin Formation which is folded but not metamorphosed, and the slightly younger Athabasca Formation which is undeformed and unmetamorphosed. The Athabasca Formation is a 1400m thick sequence of flat-lying, fluvial, poorly to well sorted, often clay-rich quartz sandstone with minor conglomerate, siltstone and mudstone. Conglomerate is concentrated towards the bottom of the sequence (Ramaekers, 1979). Much of the red-bed nature of the sandstone was acquired during diagenesis, i.e. most of the hematite formed during diagenesis rather than being an original component of the sandstone (Ramaekers, 1976).

Mineralization is pitchblende and uraninite is of three main types:

- 1) Late Hudsonian - metamorphic hydrothermal pitchblende deposits of simple mineralogy as at Beaverlodge. Primary mineralization is 1780 m.y. \pm 20 m.y.
- 2) Grenvillian - This is a more important episode and encompasses the unconformity type deposits in the Athabasca Basin. Primary mineralization is dated at 1000 m.y. - 1300 m.y. (Hoeve et al. 1980).
- 3) A later Palaeozoic type leading to mineralization within the Athabasca Formation. This type is the one to be compared with the Westmoreland deposits.

Current ideas for the genesis of this third type of deposit are:

- a) Displacement of older deposits into the cover rocks by post-ore faults (Kalliokski et al. 1978).
- b) Upward remobilization of older uranium by Kirchner et al. (1980), who point out that the age of this mineralization type varies from 107 m.y. - 250 m.y. at Key Lake, and by Tilsley (1980) who considers them epigenetic concentrations related to weathering.

- c) Derivation from within the sandstone itself during post cover rock diagenesis (Hoeve et al. 1980, 1987).

8.1.2 The Oklo Deposit, Gabon, West Africa

The uranium deposit of Oklo, Boysindi and Oklobondo occur within the Franceville n + 1 series which is a sandstone unit within the Franceville Basin. This is an intra-cratonic basin which overlies the Archaean Lower Proterozoic Congolese craton (Molina et al. 1975).

Basement is composed of Lower Proterozoic-Archaean granites and syenites with some acid volcanics. Ages range from 2,200 m.y. to 2,500 m.y. (Weber and Bonhomme, 1975). The Franceville Series unconformably overlies the basement acid igneous rocks. It is comprised of conglomerate, sandstones and interbedded tuffs up to 1,000 metres thick in the centre of the basin, but only 140 metres thick on the flanks as at Oklo (Pfiffelmann, 1975). The basal sandstone which hosts the uranium deposits (the FA1 series) is derived from the underlying basement which is reflected in the abundant feldspar and immature nature of the quartz grains. It is overlain by a 400 metre thick sequence of pelites with interbedded sandstones named the FB series (Chauvet, 1975).

The age of the sediments in the Franceville Basin is thought to be either 2,000 m.y. (Brookins, 1980) or 1850 m.y. (Weber and Bonhemme, 1975), though the latter is now interpreted as a post-orogenic diagenetic silicification age.

Mineralization occurs at the unconformity between the FA and FB series, and is of two types:

- 1) Low grade mineralization (0.4% U_3O_8) dated at 2,000 m.y. by Devillers et al. (1975), i.e. the same as the age of the formation of the FA series sandstone. This mineralization is associated with quartz, hematite, vanadium and boron.

- 2) High grade mineralization (up to 70% U_3O_8) tectonically concentrated in cracks and fissures by remobilization of older low grade ore. This is associated with hydrocarbons and hematite with an absence of quartz, vanadium and boron. This high grade ore underwent natural fission for a period of 0.5 - 2.0 m.y. approximately 1,950 m.y. ago (Weber and Bonhomme, 1975) and as such has attracted world-wide attention.

The original uranium is considered to have been derived dominantly from the basement with the interbedded tuffs also contributing some uranium. However, the similarity in age between the FA series sandstone and the low grade mineralization contained within it, certainly argues for a syngenetic concentration and early remobilization such that uranium may have been contained within the sandstone during deposition (following Brookins, 1980).

Further details regarding geological setting, mineralization and the natural fission reaction are covered very fully in the 1975 IAEA publication "Le phenomene d'Oklo".

8.1.3 Deposits of the Dubawnt Group, Keewatin, North West Territories, Canada

The Dubawnt Group overlies Archaean-Aphebian basement metasediments in the Baker Lake and Thelon Basins which are also contained in the Churchill Structural Province in the Keewatin District, North West Territories. It rests unconformably on the basement which is composed of belts of metavolcanic and metasedimentary rocks with a felsic ortho and paragneiss complex (Miller, 1980).

The basal unit of the Dubawnt Group is the South Channel Formation - a pebble supported conglomerate with minor sandstone interbeds. This is conformably overlain by the Karzan Formation - a 1000 metre thick

sequence of cross-bedded plagioclase-rich arkosic sandstone with interbedded mudstone and siltstone. The provenance area for both formations consists of biotite and hornblende-bearing felsic gneisses and metavolcanics with associated paragneisses. The iron-rich nature of these sediments is thought to have resulted from the breakdown of mafic detrital minerals derived from the basement (Miller, op.cit). These clastic units are overlain by thick sequences of pyroclastics and intermediate to acid lavas which are, in turn, overlain by the Thelon Formation - a pebbly sandstone/conglomerate considered equivalent to the Athabasca Formation in the Saskatchewan district.

Uranium mineralization occurs in six main types which are described in Curtis and Miller (1980). The Karzan Formation has the most potential of these types and is included as such in this study.

The uranium mineralization is associated with Cu and Ag, and occurs in a close spatial relationship with younger lamprophyre dykes intruding the South Channel Formation and the Karzan Formation.

Miller (1980) considers that the source of the uranium for this mineralization type was the overlying Christopher Island alkalic volcanic rocks rather than the Archaean-Aphebian basement, the lamprophyre dykes, or from within the sandstones themselves.

Concentration of uranium resulted when oxidized uraniferous waters encountered reducing environments created by disseminated epigenetic sulphide assemblages near to the lamprophyre dykes.

8.1.4 The Kombolgie Sandstone in the East Alligator Uranium Field, Northern Territory, Australia

The East Alligator Uranium Field (EAUF) is situated in the Pine Creek Geosyncline in the Northern Territory, Australia. It is broadly similar, geologically, to the Athabasca Basin. Basement rocks comprise

Archaean to Lower Proterozoic "S" type granites (following the terminology of Chappell and White, (1974)) and granulites (Ferguson et al. 1980a). These are the Archaean Rum Jungle Complex in the west of the geosyncline and the Lower Proterozoic-Archaean Nanambu Complex in the east (Page et al. 1980). These are overlain by 14 kilometres of metasediments with minor interbedded tuffs (Gerowie Tuff) which are recognizable in the west of the geosyncline but not in the east (Needham et al. 1980).

Within the Pine Creek Geosyncline, two distinct regional metamorphic zones are present. The boundary between these coincides, in part, with the north-northwest trending South Alligator Valley. To the west of this, the regional metamorphic grade is low, i.e. greenschist facies, and to the east is medium to high, i.e. upper amphibole to granulite facies (Ferguson 1980).

These Early Proterozoic sediments were deposited in an intracratonic basin under alternating continental and shallow marine environments (Stuart-Smith et al. 1980).

Late tectonic uranium-rich "I" type granites (of the Chappell and White (1974) terminology), equivalent to the Nicholson Granite Complex, intrude the entire geosyncline. These have not suffered regional metamorphism or deformation. Felsic volcanism (the Edith River Volcanics) accompanied granite intrusion, followed by intrusion of continental tholeiitic dolerites, such as the Oenpelli Dolerite dated at 1,688 m.y. (Stuart-Smith and Ferguson, 1978, Page et al. 1980).

The Edith River Volcanics are considered equivalent to the Cliffdale Volcanics in the Murphy Tectonic Ridge (Plumb and Derrick, 1975) and are unconformably overlain by the Kombolgie Formation, a sequence of conglomerate and sandstone with minor interbedded, dominantly intermediate, volcanics. The formation has a variable thickness of 600

metres - 1500 metres (Crick et al. 1980) and is considered equivalent to the Westmoreland Conglomerate.

Within the EAUF, the Kombolgie Formation overlies the Cahill Formation of the Lower Proterozoic metasediments with marked unconformity. The Edith River Volcanics are sparse to absent.

Within the South Alligator Valley, the Edith River Volcanics unconformably overlie the Lower Proterozoic Koolpin Formation and are, in turn, overlain by the Kombolgie Formation.

Major uranium mineralization is located within the Cahill Formation. It is beyond the scope of this thesis to fully examine genetic models for this type of uranium deposit and hence the reader is referred to Taylor and Rowntree (1980) for a summary of the three main proposals, i.e. hydrothermal introduction of uranium along faults (Binns et al. 1980), deposition in a brecciated karstified environment from uraniumiferous groundwaters (Ferguson et al. 1980b), and the mixing of two solutions close to the unconformity - one a low salinity uranium-rich solution, the other a highly concentrated CaCl_2 brine (Ypma and Fuzikawa, 1980).

No mineralization has yet been found within the Kombolgie Formation, apart from minor deposits in the South Alligator Valley such as the Skull deposit (Ayres and Eadington, 1975). The uranium source for this deposit and others in the South Alligator Valley is considered to have been the Edith River Volcanics, from which uranium was leached either by low temperature groundwater (Ayres and Eadington (op.cit) based on preliminary sulphur isotope data) or by hydrothermally heated groundwater (Crick et al. 1980, based on gangue mineralogy).

Despite the lack of significant mineralization in the Kombolgie Formation at the present time, potential exists for future discoveries, hence it is included in the ensuing discussion.

Limited TL measurements have been undertaken on the Kombolgie Formation. Twenty one samples from the chlorite injection zone at the base of the formation, immediately overlying the Jabiluka orebodies, all showed major radiation effects with glow curves as in figure 2.34(d), i.e. akin to background Westmoreland Conglomerate. Because of the limited regional and stratigraphic distribution of the samples, it is not known whether the radiation effects are:

- 1) an inherent feature of the Kombolgie Formation (as is the case of the Westmoreland Conglomerate);
- 2) a result of upward migration of uranium and daughter products
or
- 3) caused by uranium movement along the base of the Kombolgie Formation.

Further detailed sampling at varying stratigraphic levels from holes within the orebodies, at the margins of the orebodies and distant from mineralization would be needed to distinguish between the above three possibilities.

8.2 Discussion

The aim of this discussion is to examine the characteristics of the five sandstones and uranium deposits (or potential host rocks) with an examination of existing models, and to contribute to the formation of a genetic model for Proterozoic sandstone-hosted uranium deposits. A re-examination of Table 8.1 certainly indicates that many similarities do exist, e.g. host rock lithology, stratigraphic position and primary mineralization type, though some obvious differences also exist, e.g. the rock type immediately underlying the host rock, the provenance of the host rock and the grade of mineralization.

8.2.1 A Comparison of the Westmoreland and Oklo Deposits

The Oklo deposit is found to be most closely similar to those deposits at Westmoreland. A more detailed comparison of both is given in Table 8.2. This shows clearly the similarities between the two, even in those characteristic where the Westmoreland Conglomerate (and its deposits) differ from the Athabasca Sandstone (and its deposits) and the Kombolgie Formation. For example, both the Westmoreland Conglomerate and the Franceville FA Series have a similar tectonic setting, a similar basement of acid igneous rocks as well as less common metasediments. The lithology and thickness of the host rocks are similar, as are mineralization associations and positions. The ages of both host rocks are poorly defined though do also overlap.

The source of the uranium at Oklo is thought to be the basement acid igneous rocks with contribution from the interbedded tuffs. As was mentioned in the previous section, when considering the concentration mechanism of uranium and the source rocks of the FA Series sandstone, it does seem possible however, that uranium was contained within the sandstone during erosion from the basement and redeposition. Confirmation is provided by Weber and Bonhomme (1975) who consider the age of low grade mineralization and sedimentation to be almost identical. Brookins (1980) also considers that syngenetic and early epigenetic processes contributed to the low grade ore at Oklo. This is, therefore, another strong similarity between the two deposits, i.e. that original uranium contents within the Westmoreland Conglomerate and the FA Series sandstones were anomalously high and that the economic ore in both cases may have formed by remobilization of these inherently high concentrations. This is plausible considering that both sandstones were derived from Proterozoic acid rocks which are known to have inherently high uranium concentrations as was discussed in section 7.3.

WESTMORELAND

OKLO

	WESTMORELAND	OKLO
<u>TECTONIC SETTING</u>	<ul style="list-style-type: none"> • McArthur Basin • platform cover domain • immediately overlying basement. 	<ul style="list-style-type: none"> • Franceville Basin • intracratonic basin • immediately overlying basement.
<u>BASEMENT</u>		
Lithology	Granite, acid volcanics, schist.	Granite, syenite, schist, gneiss.
Age	1800 m.y.	>2200 m.y.
<u>HOST ROCK</u>		
Age	1650-1750 m.y.	1740-2000 m.y.
Lithology	Conglomerate, sandstone. Interbedded tuffs in upper beds.	Conglomerate, sandstone, interbedded tuffs.
Thickness	1000m (Ptw ₄ -100m)	140m? (Oklo), 1000m outside area.
Source rock	Granite, acid volcanics.	Granite.
Overlying Unit	Basalt (up to 1200m)	Pelite (400m)
<u>MINERALISATION</u>		
Ore Minerals	Pitchblende-disseminated, interstitial.	Uraninite (veins), pitchblende.
Average grade (max. grade)	0.15% (2%)	0.4% (>50%)
Age	900 m.y., 500 m.y.	2000 m.y., 1950 m.y.
Mineral/element associations.	Clay, chlorite, <u>haematite</u> , V.	Clay, chlorite, <u>haematite</u> , V, B.
Stratigraphic position.	Upper 5m of Ptw ₄ .	Upper 4-10m.
Source of U	Within Westmoreland Conglomerate.	Tuffs or basement.
Precipitation mechanism.	1st - fixation by V or Fe. 2nd - hydrothermal remobilisation in convective cell.	1st - fixation by hydrocarbons. 2nd - hydrothermal remobilisation & preferential precipitation in small scale faults and fractures.

DIFFERENCES: - Presence of hydrocarbons at Oklo.
- High grade ore at Oklo.

Table 8.2 A more detailed comparison of the geology of the Westmoreland and Oklo uranium deposits.

The major difference between the Westmoreland Uranium Deposits and those at Oklo is the presence of hydrocarbons and high grade ore at the latter. Muir et al. (1980) have reported the presence of hydrocarbons in the McArthur Group, overlying the Tawallah Group which they consider may have been derived from within the Tawallah Group. The presence of hydrocarbons within the Westmoreland Conglomerate is therefore a possibility which may be confirmed by later workers.

If suitable localizing structures are found within the Westmoreland Conglomerate, then higher grade ore than is known at present could also be discovered.

As a matter of interest, some thermoluminescence studies have been undertaken at Oklo by Durrani et al. (1975). In a very localized study, they took 15 quartz samples at 10 cm. intervals starting from the reactor core (high grade ore). Their results showed no TL at all for five samples taken within the high grade ore (50% U_3O_8), though samples taken outside this zone had TL patterns as shown in figure 8.1(a). Westmoreland samples from the Jack and Garee Lenses show TL patterns similar to this (figure 8.1(b)), indicative of similar, if not more radiation damage than the Oklo "low grade" ore samples. This may further confirm the prospectivity of the Redtree area for higher grade mineralization.

8.2.2 A Comparison of the Westmoreland and Oklo Deposits with those of the Athabasca, Keewatin and East Alligator Regions

The uranium deposits at Westmoreland and Oklo show some differences when compared with those of the Athabasca and Keewatin regions, i.e. in the position of mineralization, the age of mineralization and the mineralogical associations. To expand, the Westmoreland and Oklo deposits occur within the upper 10 metres of their respective host rocks

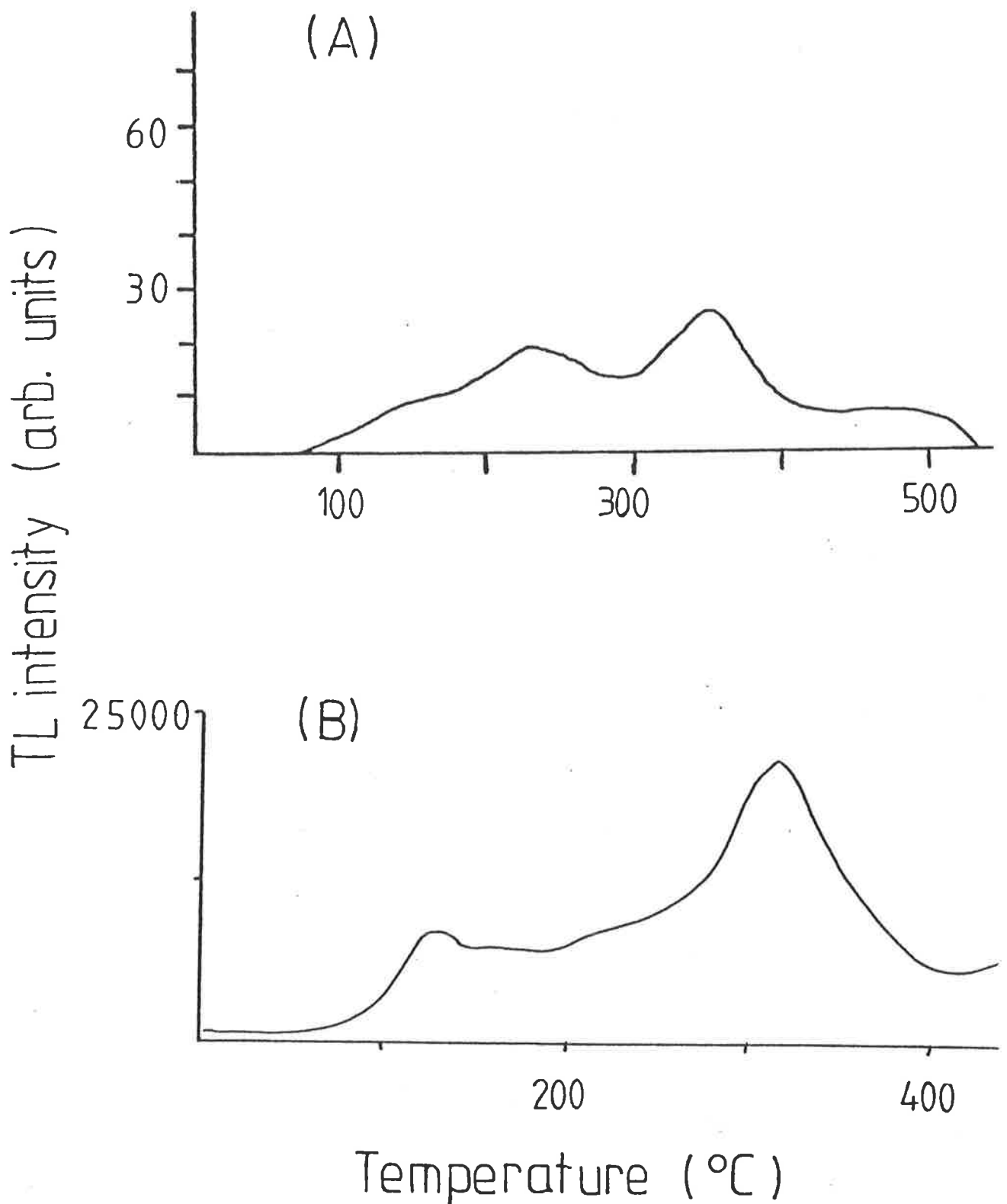


Figure 8.1 (a) TL glow curve of a sample outside the reactor core at the Oklo uranium deposit, Gabon (after Durrani et al 1975).
 (b) TL glow curve of quartz from within the Jack Lens deposit at Westmoreland.

and are overlain by more impermeable capping rocks (basalts and pelites respectively), whereas the deposits in the Athabasca Formation occur at its base, close to the contact with the underlying Lower Proterozoic metasediments (figure 8.2). This is also reflected in the age of the deposits where the Westmoreland and Oklo deposits are Precambrian, whereas the Athabasca ones are much younger, e.g. 107 m.y. - 250 m.y. for the Key Lake deposit (Kirchner et al. 1980) and are considered to be displacements or remobilizations of the older deposits in the underlying pelitic metasediments, e.g. Kalliokski et al. (1978), Kirchner et al. (1980) and Tilsley (1980). It should be pointed out however, that Hoeve et al. (1980) do not consider the uranium deposits within the Athabasca Formation to have been derived from older deposits but from within the Athabasca Formation itself. They quote U-Pb isotopic studies by Gancarz (1979) which show that the ore constituents were not derived from precursor ores, but were leached from ordinary rocks not enriched in lead and uranium. Hoeve et al (1987) also suggest a variation on the convective cell model to derive economic uranium deposits within the Athabasca Group in which derivation of uranium from within the sandstone is an important part of the model.

The mineralization at Westmoreland and Oklo is associated with clay, chlorite, hematite and vanadium which is also different to the Athabasca and Keewatia situation where it is dominantly associated with sulphides and hematite.

Differences also exist in the host rock setting and provenance between the Westmoreland Conglomerate/FA Series sandstones and the Athabasca Formation/Karzan Arkose/Kombolgie Formation sandstones. The former unconformably overlie Lower Proterozoic granitic or syenitic basement and/or acid volcanics, whereas the latter unconformably overlie Lower Proterozoic metasediments (apart from the South Alligator Valley

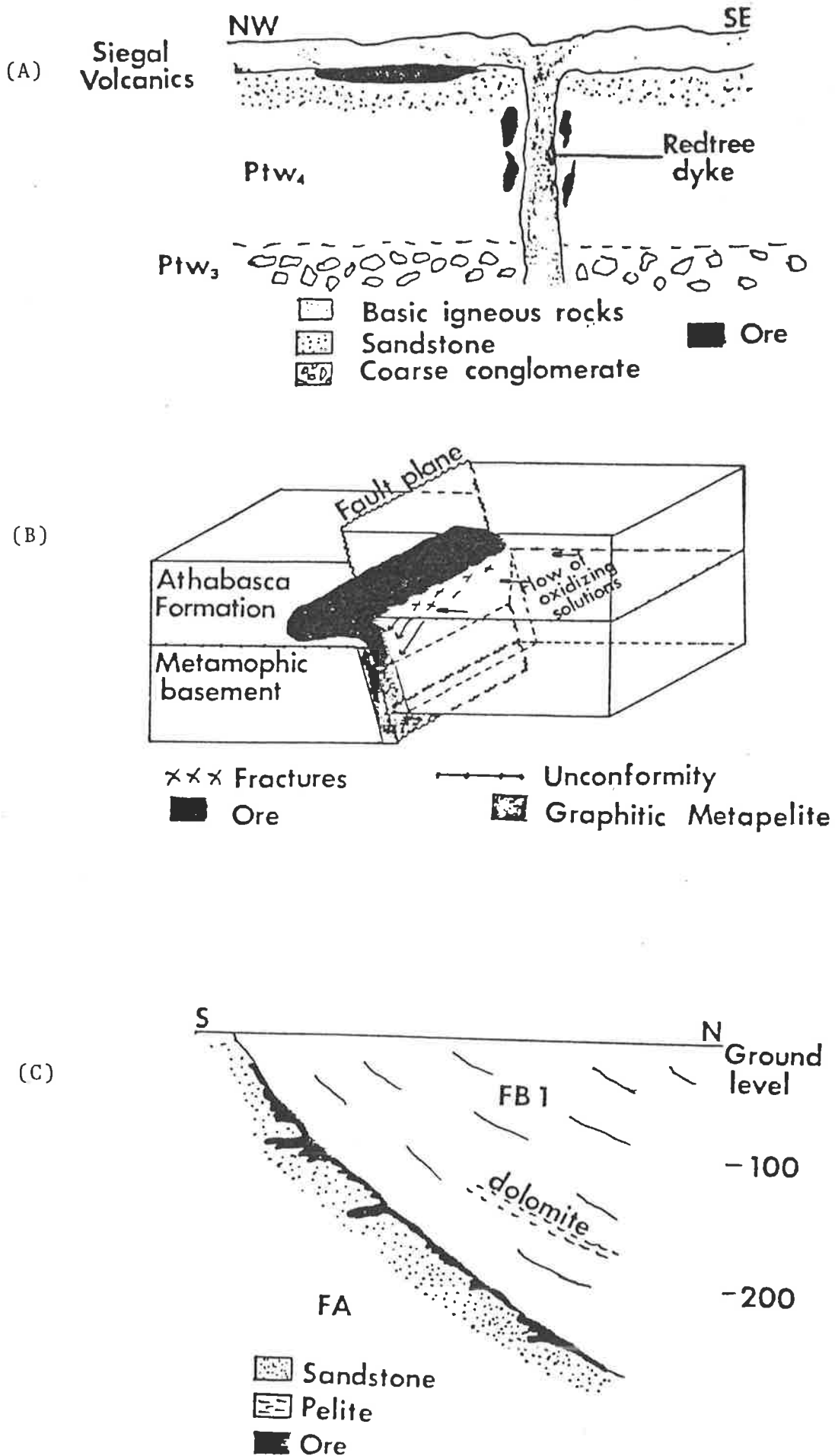


Figure 8.2 Stratigraphic position of uranium mineralization in the Westmoreland deposits, the Athabasca deposits (after Hovee et al 1980) and the Oklo deposit (after Pfiffelmann, 1975).

where the Kombolgie Formation overlies a thin (66 metres) portion of the Edith River Volcanics).

The Westmoreland Conglomerate and FA Series sandstone were derived from their underlying acid igneous basement, whereas the Karzan Formation and other similar units in Canada were derived from Lower Proterozoic metasediments, e.g. the Karzan and South Channel arkoses in the Keewatin District, North West Territories (equivalent to the Martin Formation in the Beaverlodge District) were derived from a provenance area of felsic gneisses, mafic metavolcanics and paragneisses (Miller, 1980).

No provenance studies have been accomplished as yet on the Kombolgie Formation. Likewise the provenance of the Athabasca Formation is unknown.

It is this difference, i.e. the provenance of the host rock sandstones to these uranium deposits, and implications for inherent uranium content, that is considered the most important. As has been proposed for the Westmoreland and Oklo deposits, the sandstones derived from Lower-Middle Proterozoic uranium-rich acid igneous rocks have a sufficiently high uranium concentration for economic uranium deposits to be derived from within the sandstones themselves. This would not be possible for sandstones derived from uranium-poor rocks such as Lower Proterozoic metasedimentary sequences or uranium-impoverished granitoids, as the derived sandstones themselves would not have an inherently high uranium concentration.

A method of testing this proposal would be in undertaking a TL study of a Proterozoic sandstone known to have been derived from uranium-poor source rocks. This model proposes that such a sandstone should have a low inherent uranium content and thus, in this case, not all samples from such a sandstone would have suffered major radiation damage.

8.3 The Corunna Conglomerate, South Australia

Such a study as mentioned above has been accomplished on the Middle Proterozoic Corunna Conglomerate in South Australia (Ypma and Hochman, 1987, copy appended). This unit is in the same stratigraphic position as the Kombolgie Formation and Westmoreland Conglomerate, overlying the Lower-Middle Proterozoic unconformity. Giles et al. (1980), J. Parker (pers. comm.) and N. Lemon (pers. comm. 1984) indicate that the majority of the Corunna Conglomerate is derived from the underlying uranium-poor Hutchinson Group and Middleback Sub-group metasediments with only local input from radiogenic granites such as the Burkitt Granite. This sandstone should have an overall low inherent uranium content. (Present uranium content is 1-2 ppm). The TL study indicated that not all of the Corunna Conglomerate had suffered major radiation effects, i.e. as the model predicted. The background glow curves had very large LT peak intensity like background glow curves of the Beverley host rock. "Ore-type" ATL glow curves were limited spatially and stratigraphically, being confined to either the Middle Proterozoic unconformity surface or being associated with shear zones with present minor concentrations of uranium.

Similar results were obtained by the author (Hochman, 1984) on the Middle Proterozoic Pandurra Formation in South Australia. This study showed that not all of the Pandurra Formation had suffered radiation effects - in fact, of 4 units within the Pandurra Formation radiation effects were confined to one stratigraphic layer which had been derived from a uranium enriched Middle Proterozoic granite (the Hiltaba Granite). The other three units (provenance unknown) had glow curves like those of the Beverley background, i.e. little radiation effects.

8.4 A Possible Bimodal Classification of Proterozoic Sandstones and Implications for Uranium Exploration

The significance of these observations is that not all Proterozoic sandstones show widespread major radiation effects. Those derived from basement uranium-rich acid igneous rocks do show widespread radiation effects, whereas those derived from uranium-poor source rocks (such as the Corunna Conglomerate) may not have ubiquitous radiation effects. A bimodal distinction between Middle Proterozoic sandstones and their uranium deposits may thus be possible and is summarized as follows:

Type 1: These are sandstones which are derived from uranium-rich Lower-Middle Proterozoic acid volcanics and granites. They have:

- 1) an inherently high uranium concentration which in the case of the Westmoreland Conglomerate may possibly be greater than 10 ppm, such that,
- 2) the entire sandstone will show major radiation effects.

Uranium deposits contained in the sandstone may be derived from within the sandstone itself. A proven example is Westmoreland. The Oklo deposits may also belong in this category.

Type 2: These are sandstones which are derived dominantly from uranium-poor Lower Proterozoic basement rocks including metasediments, basic to intermediate metavolcanics with only minor acid igneous influence. These derived sandstones should have:

- 1) an inherently low uranium concentration and therefore,
- 2) not all samples of these sandstones will have suffered major radiation effects.

Where radiation effects do occur they will be spatially and/or stratigraphically confined.

This type of sandstone may also contain uranium deposits though the uranium would probably not be derived from within the sandstone, but would have been introduced from outside of it and hence be of younger age, i.e. epigenetic or exogenic deposits. The Corunna Conglomerate in South Australia represents such a sandstone as does part of the Pandurra Formation. The Athabasca Formation deposits have young mineralization ages relative to the age of their host rock (as discussed previously), though since the original source of uranium for these deposits is disputed, it would be unwise to characterize them into either of Type 1 or Type 2 sandstones on the current (lack of) information. A similar case can be argued for the Karzan Arkose, Keewatin District, where even less information is currently available.

It needs to be stressed that although it has been shown that there are two types of Proterozoic sandstone based on their ATL characteristics, that the allocation of the Oklo uranium deposit into Type 1 is based on literature research than hard evidence. The only means of further testing of this proposal and subdivision, would be to undertake further TL studies on all of the Franceville Series, Athabasca Formation and Karzan Arkose.

It is not known at present where the Kombolgie Formation would fit in this classification, in view of the lack of knowledge regarding its provenance and the lack of known mineralization which could be compared with basement mineralization. Further TL studies would also be needed to clarify the position of the Kombolgie Formation.

The author also feels that it is important to re-emphasize here what is not being proposed, i.e. it is not proposed that a Proterozoic sandstone must be derived from uranium-rich acid igneous source rocks in order to contain a uranium deposit. What is being proposed is that if a Proterozoic sandstone is derived from such rocks, then an economic

uranium deposit may be formed from within the sandstone itself, as well as the possibility of being introduced at some later stage.

As a guide in exploration for such "syngenetically derived" uranium deposits, the following four factors would be necessary for economic uranium concentration. These criteria could be determined by examination of geological maps and notes, literature research etc., and confirmed by an ATL study of a suite of selected spatial and stratigraphic samples selected from the proposed host rock, to examine radiation effects before the commitment to an extensive field exploration program.

- 1) The presence of uranium-rich Lower-Middle Proterozoic acid volcanics and granitoids.
- 2) A (Middle) Proterozoic sandstone derived from such rocks and resting unconformably on them.
- 3) An overlying relatively impermeable cap rock to prevent uranium escape, or alternatively the presence of a fixing agent such as vanadium, hydrocarbons, iron oxyhydroxides etc. to immobilize the uranium in the sandstone.
- 4) A mechanism capable of concentrating uranium, e.g. intrusion of dykes as at Westmoreland to trigger a convective cell, the development of a groundwater transport regime in conjunction with a reducing environment, suitable structural characteristics, evidence of tectonic or heat flow activity capable of remobilizing syngenetic uranium.

Other factors which may also prove useful are to consider such areas as the above, close to the edges of the relevant basin where the basal sandstone is best exposed, and to look for the presence of a suitable reducing environment in which to precipitate uranium after transport.

CHAPTER 9

CONCLUSIONS ON THE USE OF ARTIFICIAL THERMOLUMINESCENCE IN
URANIUM EXPLORATION AND ORE GENESIS STUDIES
AND RECOMMENDATIONS FOR FURTHER RESEARCH

9.1 Introduction

Perhaps the most important observation recorded in this study is that the artificial thermoluminescence (ATL) glow curves of quartz, change in response to radiation, in a manner which could have been predicted by previous studies on LiF TLD-100 by Fairchild et al (1975). Fairchild et al (op.cit) showed for LiF TLD-100, that in the dose range 800 rad to 3×10^7 rad, there was an initial increase in the low temperature (LT) peak intensity, followed by a decrease in LT peak intensity. This was followed by a progressive increase and subsequent decrease in middle temperature (MT) peak intensities, till at the conclusion of the experiment (3×10^7 rad), only the high temperature (HT) glow peaks remained.

The importance of the present study, particularly at the Beverley uranium deposit, is that it has been shown that the same progressive change in glow peak shape occurs, in quartz, in a natural geological radiative environment. Initially, the LT peak intensity of quartz from the Beverley environment is large and dominates all other glow peaks. With increasing radiation the LT intensity decreases and the MT intensity increases. At still larger radiation doses, for quartz within the Beverley ore body, the MT peak intensity decreases, such that the HT peak is the dominant glow peak. (This change in glow curve shape is portrayed in figures 3.7-3.9). Admittedly this trend is not as well defined in quartz from a natural radiation environment, as in LiF TLD-100 in a controlled laboratory radiation environment, though the trend nevertheless does exist. The progressive change in glow curve shape with radiation is the basis on which this thesis is therefore based.

9.2 Conclusions Regarding the Use of Artificial Thermoluminescence in Uranium Exploration

The principal aim of this thesis was to test whether, or not, ATL could be advantageously used in exploration for uranium mineralization. Following case studies at the Beverley and Westmoreland uranium deposits and the Bremer River prospect, the answer must be a qualified, or guarded, yes. The qualification is necessary in that ATL seems better suited to exploration for certain types of uranium deposit.

In exploration for Tertiary sandstone hosted uranium deposits, such as the Beverley uranium deposit, ATL is not only useful, but has some very distinct advantages over other exploration methods. The advantages of ATL arise because of the extreme mobility of this type of uranium mineralization - in the Beverley case uranium is transported over a distance of eight kilometres. Conventional geochemical and geophysical exploration techniques rely on detecting the presence of uranium mineralization and/or daughter products and hence are not suited to identify areas which may previously have hosted mobile uranium. ATL, in contrast, detects cumulative radiation effects in a mineral lattice and can therefore identify areas through which uranium mineralization has passed. Trends of increasing radiation effects gained from several samples may then define a pathway of uranium transport, which may lead to the site of current deposition. At the Beverley uranium deposit this trend of increasing radiation effects was observed in drill-holes spread over the whole eight kilometres of uranium transport. The trend of increasing radiation effects was marked by a decrease in LT peak intensity of two orders of magnitude and a corresponding increase in the proportional percentage of the HT peak.

In addition to defining the transport pathway, ATL studies at Beverley also showed a zone of anomalous ATL, ("ore-type TL"), around the ore-body, which enlarged the primary exploration target by a factor of four to five.

ATL studies at the Tertiary Bremer River prospect in South Australia, in a series of drill-holes extending away from basement rocks, showed a lack of increasing radiation effects. This downgraded the potential of the prospect for mobile uranium "roll-front" type uranium deposits and a recommendation was able to be made to the exploration company to discontinue drilling.

Application of ATL at the Proterozoic sandstone hosted Westmoreland uranium deposits, in northwest Queensland, proved to be far more complicated than at their Tertiary counterparts. The complications were introduced by the elevated and ubiquitous uranium contents of the host sandstone and the much longer residence time of the uranium. These factors lead to a "normal" or "background" type of ATL glow curve pattern, which at the Beverley deposits had been found only in, or near, the orebody itself. Variations in ATL approaching mineralization were therefore more restricted than those encountered at the Beverley deposit.

Variations in ATL peak intensity approaching mineralization at the Junnagunna prospect, Westmoreland, were not conclusive, though generally the HT peak intensity was at a maximum within the ore-body. The HT/LT peak ratio was a much better indicator of increasing proximity to mineralization and generally a HT/LT ratio value of greater than 1.4 was associated with mineralization.

Limited traverses across the Junnagunna ore-body also examined the change in temperature of the HT glow peak. This was consistently found to be a minimum (below 340°C) within the ore-body and higher (greater than 355°C) outside the mineralized zone. The discovery of this low temperature shift (LTS) in the HT glow peak, when coupled with a strong

HT peak in samples presently unmineralized, was tentatively interpreted to indicate that such samples had hosted uranium mineralization in the past.

An extensive study at Westmoreland, comprising almost 800 samples, did identify several areas suitable for exploration for further uranium mineralization. However, whether ATL was advantageous in exploration in this instance, is debatable. The complexity of interpretation in terms of geological processes and uranium mobility, coupled with the large number of samples needed to make such interpretations, suggests that in small scale local mine environments, ATL, though providing some useful information, may not have significant advantages over other more common geochemical or geophysical techniques.

9.3 Conclusions Regarding the Use of Thermoluminescence in Ore Genesis Studies

9.3.1 The Beverley Uranium Deposit, South Australia

- (1) At the Beverley uranium deposit the discovery of an eastward trend of increasing radiation effects, and the rapid decrease in radiation effects past (down-dip) the orebody, represent conclusive proof of the accretionary migration, or "snow-balling" movement of uranium in Tertiary roll-front type uranium deposits.
- (2) The lack of sensitization within the Beverley host rock indicates that the source of the uranium, at Beverley, was not from within the host rock. Rather, the eastward trend of increasing radiation effects away from the granitic Mt. Painter basement suggests derivation of uranium from groundwaters draining the uranium-enriched Mt. Painter granitoids.

9.3.2 The Westmoreland Uranium Deposit, Queensland

- (1) ATL measurements at Westmoreland indicate that there is a ubiquitous radiation sensitization along the Westmoreland Conglomerate/Siegal Volcanics contact.
- (2) Within areas capped by basic volcanics there exists a vertical homogenization (of sorts) of ATL glow curve patterns within individual drill-holes. This vertical homogenization may indicate either strong radiation effects throughout the drill-hole, or in other cases, weaker radiation effects throughout the drill-hole.
- (3) Quartz from Unit 3 of the Westmoreland Conglomerate has a distinctive ATL glow curve indicative of radiation sensitization. This quartz is derived from the underlying uranium-enriched Cliffdale Volcanics.
- (4) The fact that all samples of the Westmoreland Conglomerate have ATL glow curves which at Beverley were found only in, or near, the ore-body, is best explained by a high inherent uranium content within the Westmoreland Conglomerate and a longer residence time. The present uranium content of the Westmoreland Conglomerate is still 4 to 6 ppm, the ATL data suggest an initial content of perhaps 10 ppm. This seems plausible in view of the derivation of the Westmoreland Conglomerate from the underlying Middle Proterozoic Cliffdale Volcanics, which themselves have an elevated uranium content.
- (5) A proposed model for the genesis of the Westmoreland uranium deposits, incorporating the ATL data and interpretations above, is as follows:

- (a) A high inherent uranium content within the Westmoreland Conglomerate is remobilized by heated groundwaters, possibly triggered by dolerite dyke intrusion, or by some, as yet unspecified, heat flow event along pre-existing lineaments;
 - (b) Uranium is transported in a convective cell system, upward near the margins of the dyke (due to heating of groundwaters), along the Westmoreland Conglomerate/Siegal Volcanics contact and downwards (due to cooling of the transporting solutions) away from the dyke. Such a convective cell system, transporting and concentrating uranium could explain the apparent vertical homogenization of radiation effects observed;
 - (c) Uranium is precipitated where suitable reducing conditions exist near to sandstone/basic volcanics contacts, and
 - (d) Preservation of the uranium deposits, once formed, is achieved by extrusion of massive basic volcanic flows preventing oxidation and dissipation of the deposits.
- (6) Although the entire Westmoreland Conglomerate has suffered major radiation effects, not all Proterozoic sandstones have suffered major radiation effects. ATL studies on the Corunna Conglomerate and Pandurra Formation in South Australia show that they have background glow curves identical to the background glow curves of Beverley host rock, i.e. glow curves with very dominant LT peaks - indicative of only minor radiation effects. This suggests that these sandstones, the Corunna Conglomerate in particular, have had only low inherent uranium contents as opposed to the high inherent uranium content proposed for the Westmoreland Conglomerate. The inherited uranium content is a function of the uranium content

of the source rock and a possible bimodal classification of Proterozoic sandstones (based on ATL results and literature research) may be thus possible into:

- (a) Those sandstones derived from uranium rich source rocks (Middle Proterozoic granites and acid volcanics), such that the derived sandstone has a high inherent uranium content and hence ubiquitous radiation effects. Examples of this type may include the Westmoreland Conglomerate and the Franceville Series (host to the Oklo uranium deposit);
- (b) Those sandstones derived from uranium poor source rocks (Lower Proterozoic metasediments), such that the derived sandstone has a low inherited uranium content and has not suffered ubiquitous radiation effects. Examples of this type include the Corunna Conglomerate, parts of the Pandurra Formation and possibly the Karzan Arkose in the Northwest Territories, Canada.

9.4 Recommendations for Further Research

Research opportunities into a newly developing field often seem limitless. It is not the purpose of this sub-chapter to enumerate all such opportunities, but rather to very briefly list some directions for advantageous research in further developing the uranium exploration applications of ATL.

The most pressing need in establishing widespread usage of ATL in uranium exploration is to calibrate known glow curve shapes against known radiation doses. For example, if each of the glow curves presented in Figure 2.34 could be universally calibrated against a known radiation dose, then, knowing the geological age of a sample, it would be possible to make a reasonable estimate of the uranium concentration required to

produce such a glow curve. (Such a calibration would also be beneficial in dating applications of TL and could allow extension of the age range datable by the TL method back to hundreds of millions of years).

Unfortunately such calibration is not foreseen in the short term future. Each quartz sample is different and responds differently to radiation depending on internal defect structures. When coupled with the problems in extrapolating results obtained at dose rates in the laboratory with dose rates in geological environments, such a universal calibration would conceivably have to await a far better understanding of what defects are responsible for quartz TL, how such defects respond to radiation, and how these defects are annealed under geological conditions.

A second useful piece of further research would be to more accurately determine the precise threshold, under variable geological conditions (e.g. host rock age and ambient temperature), at which sensitization is initiated in quartz. Such information would allow more confident back-calculation of uranium contents in rocks based on total dose estimates gained by ATL.

Further case studies examining the use of ATL in exploration for different types of uranium deposits would also be useful and may have the serendipitous side-effect of enabling some sort of rough empirical estimates to be made of the calibration doses and uranium thresholds mentioned above. In this context it should be mentioned here that in 1985 the Sirotope group, developing the use of lead isotopes in mineral exploration, had accumulated 400 case studies over 12 years to enhance and interpret their technique.

There remains much more basic research and many more case studies to be performed before ATL can be used in a quantitative way in uranium exploration, though there is no obstacle for its present application in qualitative or semi-quantitative ways.

BIBLIOGRAPHY.

BIBLIOGRAPHY.

- AHMAD, M., HALLENSTEIN, C.P. and WYGRALK, A. 1984: Palaeoplacer potential in the Mid-Proterozoic of the Northern Territory - a study of the Westmoreland Conglomerate. Aust. Inst. Min. Metall. Annual Conference Volume. Darwin, 1984. p.357-367.
- AITKEN, M.J. 1965: Thermoluminescence. Sci. J.,1,(4), p.32-38.
- AITKEN, M.J. 1979: Dose rate evaluation. PACT 3, Part 2. p.319.
- ANDREWS, D.L. 1980: Third quarterly report, Milang, E.L. 547, for the period ending 15 August 1980. S.A.D.M.E. open file report envelope number 3729, Adelaide, S.A. (unpubl.).
- ANDREWS, D.L. 1983: Thermoluminescence and its application to mineral exploration. M.Sc. Thesis, Imperial College, London. 128 pages. (unpubl.).
- ARNOLD, G.W. and COMPTON, W.D. 1959: Radiation effects in silica at low temperatures. Phys. Rev. 116, 802-11.
- ARTH, J.G. 1976: Behaviour of trace elements during magmatic processes - A summary of theoretical models and their applications. Jour. Research. U.S. Geol. Survey. Vol. 4, No. 1, p.41-47.(*)
- AYRES, D.E. and EADINGTON, P.J. 1975: Uranium mineralization in the South Alligator River Valley. Miner. Deposita, 10(1), p.27-42.
- BAILEY, R.V. and CHILDERS, M.O. 1977: Applied mineral exploration with special reference to uranium. Westview Press, Boulder, Colorado. 542 pages.
- BEESON, R. 1980: The relationship of siltstone geochemistry to sedimentary environments and uranium mineralization in the Beaufort Group, Cape Province, South Africa. Chem. Geol. 30, p.81-107.
- BERNHARDT, H. 1982: A contribution to high temperature thermoluminescence investigations in quartz crystals. Phys. Stat. Sol.(a) 74, p.159-165.
- BINNS, R.A., M^CANDREW, J. and SUN, S-S. 1980: Origin of uranium mineralization at Jabiluka. In Proc. of the I.U.S. on the Pine Creek Geosyncline. IAEA.(Vienna) p.543-562.
- BLAKE, D.H. 1978: The Proterozoic and Palaeozoic rocks of The Granites - Tanami region, Western Australia and Northern Territory, and interregional correlations. B.M.R. J. Aust. Geol. Geophys. 3, p.35-42.

- BROOKINS, D.G. 1980: Syngenetic model for some Early Proterozoic uranium deposits: evidence from Oklo. In Proc. of the I.U.S. on the Pine Creek Geosyncline. IAEA.(Vienna) p.709-720.
- CALLEN, R.A. 1975: Lake Frome area - regional geology, Tertiary stratigraphy and uranium localization. In Economic Geology of Australia and Papua New Guinea, 1. Metals. Aust. Inst. Min. Metall., Monogr. 5. Ed. G.L.Knight p.803-808.
- CARTER, E.K. 1959: Westmoreland 4 mile Geological Series. B.M.R. Aust. Explan. Notes, 14.
- CHARLET, J.M. 1971: Thermoluminescence of detrital rocks used in palaeogeographical problems. Mod. Geol. 2(4), p.265-274.
- CHARLET, J.M., DUPUIS, Ch. and QUINIF, Y. 1978: Mise en évidence par la thermoluminescence (TL) des sables landeniens d'anomalies radiométriques nouvelles dans la coupe du canal de Blaton. Ann. Soc. Geol. Belgique. 101. p.337-340.
- CHATAGNON, B. 1986: Use of EPR in Uranium exploration. Univ. of Paris, Ph.D thesis ~~3rd cycle~~ (in French, unpubl). *Doctorat d'Etat* no
- CHAUVET, R.J. 1975: Description de gisement d'Oklo. In The Oklo Phenomenon. IAEA. (Vienna).
- CHEN, C.C. 1976: Application of thermoluminescence to mineral exploration based on studies of replacement ore deposits in carbonate host rock at Charcas, Mexico; Toggenburg S.W. Africa and Bisbee, Arizona. Ph.D thesis, Columbia University, New York. 224 pages (unpubl.).
- CHEN, R. and KIRSH, Y. 1981: Analysis of thermally stimulated processes. Pergaman Press, Oxford.
- CLARKE, S.P. Jr., PETERMAN, Z.E. and HEIER, K.S. 1966: Abundances of uranium, thorium and potassium. In Handbook of Physical Constants. Geol. Soc. Am., Memoir 97. Ed. S.P. Clarke Jr. p.521-541.
- CLAVARINO, J.G. 1975: Unpublished company report for Mines Administration Pty. Ltd. regarding the Westmoreland uranium deposits.
- COHEN, A.J. 1960: Substitutional and interstitial Al impurity in quartz; Structure and color centre relationships. J. Phy. Chem. Solids 13, 321-5.
- COHEN, A.J. and MAKAR L.N. 1982: Models for color centres in smoky quartz. Phys. Stat. Sol. (a) 73, p. 593-6.
- COMPSTON, W., M^CDOUGALL, I. and HEIER, K.S. 1968: Geochemical comparison of the Mesozoic basaltic rocks of Antartica, South Africa, South America and Tasmania. Geochim. Cosmochim. Acta, 32, p.129-149.(*)

- CONDIE, K.C. 1978: Geochemistry of Proterozoic granitic plutons from New Mexico, U.S.A. *Chem. Geol.*, 21, p.131-151.(*)
- CONDIE, K.C. and HUNTER, D.R. 1976: Trace element geochemistry of Archaean granitic rocks from the Barberton Region, South Africa. *Earth Planet Sci. Lett.* 29, p.389-400.(*)
- CONDIE, K.C. and POTTS, M.J. 1969: Calc-alkaline volcanism and the thickness of the early Precambrian crust in North America. *Can. J. Earth Sci.* 6, p.1179-1184.(*)
- CRICK, I.H., MUIR, M.D., NEEDHAM, R.S. and ROARTY, M.J. 1980: The geology and mineralization of the South Alligator Valley uranium field. *In Proc. of the I.U.S. on the Pine Creek Geosyncline.* IAEA. (Vienna) p.273-286.
- CROHN, P.W. 1975: Mineralization in the M^CArthur and Nicholson Basins. *Econ. Geol. Austr. Aust. Inst. Min. Metall. Monograph 5, Chapter 9, p.327-329.*
- CROXFORD, N.J.W. 1964: Origin and significance of volcanic potassium-rich rocks from Mt. Isa. *Trans. I.M.M.* 74, p.33-43.
- CROXFORD, N.J.W. 1968: A mineralogical examination of the M^CArthur lead-zinc-silver deposit (with discussion). *Proc. A.I.M.M.* 226,2, p.97-109.
- CROXFORD, N.J.W. and JEPHCOTT, N. 1972: The M^CArthur lead-zinc-silver deposit, Northern Territory. *Proc. A.I.M.M.* 243, p.1-27.
- CURTIS, J.L. 1976: Annual Report 1975. Westmoreland. Authority to Prospect 996M (1,2,3) and adjoining leases. Company Report for UGA (unpubl.).
- CURTIS, L. and MILLER, A.R. 1980: Uranium geology in the Amer-Dubawnt-Yathked-Baker Lake region, Keewatin District, N.W.T. Canada; *In Proc. of the I.U.S. on the Pine Creek Geosyncline.* IAEA. (Vienna) p.595-617.
- DAHLKAMP, F.J. 1978: Classification of Uranium Deposits. *Mineral. Deposita*, 13, p.83-104.
- Dana's Manual of Mineralogy 18th Ed.. C.S. Hurlbut Jr Ed. John Wiley & Son Inc. 579p.
- DANIELS, F. 1968: Early studies of thermoluminescence in geology. *In Thermoluminescence of Geological Materials.* Academic Press London, p.3-14.
- DAVID, M., SUNTA, C.M. and GANGULY, A.K. 1977; Thermoluminescence of Quartz: Part I - Glow Curve and Spectral characteristics. *Indian J. Pure Appl. Phys.* 15, p.201-204.

- DAVID, M., SUNTA, C.M. and GANGULY, A.K. 1977: Thermoluminescence of Quartz: Part II - Sensitisation by Thermal Treatment. Indian J. Pure Appl. Phys. 15, p.277-280.
- DAVID, M., SUNTA, C.M., BAPAT, V.N. and GANGULY, A.K. 1978: Thermoluminescence of Quartz: Part III - Sensitisation by Pre-Gamma Exposure. Indian J. Pure Appl. Phys. 16, p.423-427.
- DAVID, M., SUNTA, C.M. and GANGULY, A.K. 1979: Thermoluminescence of Quartz: Part IV - Effect of Stress on Sensitivity. Indian J. Pure Appl. Phys. 17, p.655-657.
- DAVID, M., SUNTA, C.M. and GANGULY, A.K. 1979: Thermoluminescence of Quartz: Part V - Effect of Polarization on Sensitivity. Indian J. Pure Appl. Phys. 17, p.658-660.
- DAVID, M. and SUNTA, C.M. 1981: Thermoluminescence of Quartz: Part VI - Effect of Ultraviolet Rays. Indian J. Pure Appl. Phys. 19, p.1041-1047.
- DAVID, M. 1981: Thermoluminescence of Quartz. Part VII - Radiation Sensitivity of First Peak. Indian J. Pure Appl. Phys. 19, p.1048-1053.
- DAVID, M. and SUNTA, C.M. 1981: Thermoluminescence of Quartz. Part VIII - Estimation of Firing Temperature in Ancient Pottery Samples. Indian J. Pure Appl. Phys. 19, p.1054-1056.
- DAVID, M., KATHURIA, S.P. and SUNTA, C.M. 1982: Thermoluminescence of Quartz. Part IX - Kinetics of Glow Peaks. Indian J. Pure Appl. Phys. 20, p.519-523.
- DAVIDSON, C.F. 1964: The mode and origin of blanket ore bodies. Trans.I.M.M. 74, p.319-338.
- DAVIS, J.F. 1969: Uranium deposits of the Powder River Basin. Univ. Wyo. Contrib. Geol., 8(2, part 1): p.131-141.
- DEVILLERS, C., RUFFENACH, J.-C., MENES, J., LUCAS, M., HAGEMANN, R. and NIEF, G. 1975: Age de mineralisation de l'uranium et date de la reaction nucleaire. In The Oklo Phenomenon. Proceedings of a Symposium, Libreville, IAEA. (Vienna), p.299-304.
- DOE, B.R., STUCKLESS, J.S. and DeLEVAUX, M.H. 1983: The possible bearing of the granite of the UPH deep drill holes, Northern Illinois, on the origin of Mississippi Valley Type ore deposits. J. Geophys. Res. 88, B9, Sept. 10, p.7335-7345.
- DURRANI, S.A., KHAZAL, K.A.R., MALIK, S.R., FREMLIN, J.H. and HENDRY, G.L. 1975: Thermoluminescence and fission track studies of the Oklo fossil reactor materials. In The Oklo Phenomenon. Proceedings of a Symposium, Libreville IAEA. (Vienna), p.207-220.

- DURRANI, S.A., GROOM, P.J., KHAZAL, K.A.R. and M^CKEEVER, S.W.S. 1977b: The dependance of thermoluminescence sensitivity upon the temperature of radiation in quartz. Journ. Physics D. Appl. Physics, 10, p.1351-1361.
- DURRANI, S.A., KHAZAL, K.A.R., M^CKEEVER, S.W.S. and RILEY, R.J. 1977a: Studies of changes in the thermoluminescence sensitivity in quartz induced by proton and gamma radiation. Radiation Effects. 33, p.237-244.
- EVANS, R.C. 1966: An Introduction To Crystal Chemistry. Cambridge Univ. Press.
- EVANS, R.C. 1979: Annual report 1978. Authority to Prospect 996M and associated leases. (Held by Queensland Mines Limited). Company Report No. UGA 78/12A (unpubl.).
- Exploration for uranium ore deposits. Proceedings of a symposium Vienna, 29 March-2 April, 1976. IAEA. Vienna, 1976. 806p.
- FAIRCHILD, R.G., MATTERN, P.L., LENGWEILER, K. and LEVY, P.W. 1978: Thermoluminescence of LiF TLD-100 dosimeter crystals; glow curve kinetics. J. Appl. Phys. 49, 4523-4533.
- FANDER, W. 1976: In Annual report 1976, Westmoreland. Authority to Prospect 996M and adjoining leases. Vol.III. Company Report for Queensland Mines (unpubl.).
- FEHN, U., CATHLES, L.M. and HOLLAND, H.D. 1978: Hydrothermal convection and uranium deposits in abnormally radioactive plutons. Econ. Geol. 73, p.1556-1566.
- FERGUSON, J. 1980: Metamorphism in the Pine Creek Geosyncline and its bearing on stratigraphic correlations. In Proc. of the I.U.S. on the Pine Creek Geosyncline. IAEA. (Vienna), p.91-100.
- FERGUSON, J., CHAPPELL, B.W. and GOLBEY, A.B. 1980: Granitoids in the Pine Creek Geosyncline. In Proc. of the I.U.S. on the Pine Creek Geosyncline. IAEA. (Vienna), p.73-90.
- FERGUSON, J., EWERS, G.R. and DONNELLY, T.H. 1980: Model for the development of economic uranium mineralization in the Alligator Rivers uranium field. In Proc. of the I.U.S. on the Pine Creek Geosyncline. IAEA. (Vienna), p.563-574
- FERGUSON, J. and NEEDHAM, R.S. 1978: The Zamu Dolerite: A Lower Proterozoic preorogenic continental tholeiitic suite from the Northern Territory, Australia. J. Geol. Soc. Aust. 25, p.309-322.
- FERGUSON, J. and ROWNTREE, J.C. 1980: Vein-type uranium deposits in Proterozoic rocks. Revue de L'institut Francais du Petrole. 35, 3, p.485-496.

- FLOYD, P.A. and WINCHESTER, J.A. 1975: Magma type and tectonic setting discrimination using immobile elements. *Earth Planet. Sci. Lett.*, 27, p.211-218.(*)
- FORNACA-RINALDI, G. 1968: Some effects of heating on the radiation sensitivity of natural crystals. In Thermoluminescence of Geological Materials. Ed. D.J. M^cDougall. Academic Press, p.103-110.
- FREY, F.A., GREEN, D.H. and ROY, S.D. 1978: Integrated models of basalt petrogenesis: A study of quartz tholeiites to olivine melilitites from southeastern Australia utilizing geochemical and experimental petrological data. *J. Petrology*, 19, p.463-513.(*)
- FUCHS, H.S. and SCHINDLMAYER, W.E. 1981: The Westmoreland Uranium Deposit, Queensland, Australia. In "Uranium Case Histories". IAEA. (Vienna) p.59-73.
- FULLER, G.E. and LEVY, P.W. 1978: Thermoluminescence of natural quartz. *Bull. Amer. Phys. Soc.*, 23, p.324.
- GALLOWAY, W.E. 1978: Uranium mineralization in a coastal plain aquifer system: Catahoula Formation, Texas. *Econ. Geol.* 73, p.1655-1676.
- GANCARZ, A.J. 1979: Chronology of the Cluff Lake uranium deposit, Saskatchewan, Canada. In Extended Abstracts of the I.U.S. on the Pine Creek Geosyncline. p.91-94.
- GARDENER, C.M. 1978: Precambrian geology of the Westmoreland region, northern Australia, Part 3: Nicholson Granite Complex and Murphy Metamorphics. *Rec. B.M.R. Geol. Geophys. Aust.*, 1978/32, (unpubl.).
- GARLICK, G.F.J. and GIBSON A.F. 1948: The electron trap method of luminescence in sulphide and silicate phosphers. *Proc. R. Soc. Lond.* A60, 574-590.
- GIBLIN, A.M. 1980a: The role of clay adsorption in genesis of uranium ores. In Proc. of the I.U.S. on the Pine Creek Geosyncline. IAEA. (Vienna) p.521-530.
- GIBLIN, A.M. 1980b: Unpublished report to Urangesellschaft Aust. on oxidation-reduction potentials at Westmoreland.
- GILES, C.W. 1980: A comparative study of Archaean and Proterozoic felsic volcanic associations in southern Australia. Ph.D. Thesis, University of Adelaide. (Unpub.)
- GILES, C.W. and TEALE, G.S. 1979: A comparison of the geochemistry of the Roopena Volcanics and the Beda Volcanics. *Q. Geol. Notes, Geol. Surv. S. Aust.* 71, p.7-13.(*)
- GILL, J.B. 1978: Role of trace element coefficients in models of andesite genesis. *Geochim. Cosmochim. Acta.* 42, p.709-724.(*)

- GLIKSON, A.Y., DERRICK, G.M., WILSON, I.H. and HILL, R.M. 1976: Tectonic evolution and crustal setting of the Middle Proterozoic Leichhardt River fault trough, Mt. Isa region northwestern Queensland. B.M.R. J. Aust. Geol. Geophys. 1, p.115-129.(*)
- GOLDHABER, M.B., REYNOLDS, R.L. and RYE, R.O. 1978: Origin of a South Texas roll-type uranium deposit: 2, Petrology and sulphur isotope studies. Econ. Geol. 73, p.1690-1705.
- GRISCOM, D.L. 1978: Defects and impurities in -quartz and fused silica. In Physics of SiO₂ and its Interfaces. Ed. S.T. Pantelides, Pergamon, New York, p.323-52.
- GRISCOM, D.L. 1985: Naature of defedcts and defect generation in optical glasses. In Radiation effects in optical materials. Proc. of Society of Photographic Instrument Engineers SPIE 541. Ed. P.W. Levy.
- GRUNER, J.W. 1956: Concretion of uranium in sediments by multiple migration-accretion. Econ. Geol. 51, p.495-520.
- GUNN, B.M. 1966: Modal and elemental variation in Antarctic tholeiites. Geochim. Cosmochim. Acta. 30, p.881-920.(*)
- HART, R.J., NICOLAYSEN, L.O. and GALE, N.H. 1981: Radio-element concentration in the deep profile through Precambrian basement of the Vredefort Structure. J. Geophys. Res. 86, p.10639-10652.
- HARSHMAN, E.N. 1972: Geology and uranium deposits, Shirley Basin area, Wyoming. U.S. Geol. Surv. Prof. Pap., 745: 82p.
- HAYNES, R.W. 1976: Beverley sedimentary uranium orebody, Frome Embayment, S.A. In Economic Geology of Australia and Papua New Guinea. 1. Metals. A.I.M.M., Monogr. 5, Ed. C. L. Knight. p.343-347.
- HAYSLIP, D.L. and RENAULT, J.R. 1976: Potential of quartz thermoluminescence in uranium exploration. Abstract, 29th Ann. Mtg. Rocky Mnt. Sec. Geol. Soc. Amer. Albuquerque, N.M. p.590.
- HILLS, J.H. 1973: Lead isotopes and the regional geochemistry of northern Australian uranium deposits. Ph.D. thesis. Macquarie University. (unpubl.).
- HILLS, J.H. and RICHARDS, J.R. 1972: The age of uranium mineralization in northern Australia. Search 3, 10, p.382-385.
- HILLS, J.H. and RICHARDS, J.R. 1976: Pitchblende and galena ages in the Alligator Rivers Region, Northern Territory, Australia. Miner. Deposita. 11, p.133-154.

- HILLS, J.H. and THAKUR, K. 1975: The Westmoreland uranium deposits. *In* Economic Geology of Australia and Papua New Guinea. 1. Metals. A.I.M.M., Monogr. 5, Ed. C.L. Knight. p.609-612.
- HOCHMAN, M.B.M. 1981: Thermoluminescence of quartz in the Bremer River area, South Australia. C.R.A.E. Company Report No. 10463. (unpubl.).
- HOCHMAN, M.B.M. 1984: Report on thermoluminescence characteristics of some Pandurra Formation and igneous rock samples from the Panduura, Charlinga, Gunson and Lake Torrens exploration leases. CSR Minerals Limited, Company Report No. EMR37/84. (unpubl.).
- HOCHMAN, M.B.M. and YPMA, P.J.M. 1984a: Thermoluminescence as a tool in uranium exploration. *J. Geochem. Explor.* 22, p.315-331.
- HOCHMAN, M.B.M. and YPMA, P.J.M. 1984b: Thermoluminescence applied to uranium exploration and genesis of the Westmoreland uranium deposits—Implications for the Northern Territory. A.I.M.M. Ann. Conf. Vol. Darwin, N.T. 1984, P.215-224.
- HOCHMAN, M.B.M. and YPMA, P.J.M. 1987: The accretionary migration of uranium in Tertiary sandstones—Thermoluminescence evidence from the Beverley deposit South Australia. *Uranium 3*, p.245-259.
- HOCHMAN, M.B.M. and YPMA, P.J.M. 1988: Changes in the artificial thermoluminescence glow curves of quartz associated with uranium deposits. *Nucl. Tracks Radiat. Meas.* 14, p.105f.
- HOEVE, J., SIBBALD, T.I.I., RAEMAKERS, P. and LEWRY, J.F. 1980: Athabasca Basin unconformity type uranium deposits: A special class of sandstone-type deposits? *In* Proc. of the I.U.S. on the Pine Creek Geosyncline. I.A.E.A. (Vienna), p.575-594.
- HORNYAK W.E., LEVY P.W. and KIERSTEAD J.A. 1985: Nuc. Tracks & Rad. Meas. CaF_2 : Mn thermol: A single glow peak not described by 2nd order kinetics.
- ICHIKAWA, Y. 1968: Thermoluminescence of natural quartz irradiated by gamma rays. *Jap. Jour. Appl. Physics.*, 7, 3, p.220-226.
- IMBO, G., GASPARINI, P., LUONGO, G. and RAPOLLA, A. 1975: Contributions to the volcanological researches by determination of the radioactivity of eruptive rocks. *Bull. Volcanol.* 32, p.317-342.
- IRVINE, T.N. and BARAGAR, W.R.A. 1971: A guide to the chemical classification of the common volcanic rocks. *Can. J. Earth Sci.* 8, p.523-548.

- ISHIHARA, S., SAKAMAKI, Y., MOCHIZUKI, T., TERASHIMA S. and ENDO, Y. 1981: Distribution of K, Na, Th AND U in sandstones and shales from western Shikoku, Japan. Bull. Geol. Soc. Japan. 32, 6, p.329-342.
- JAKES, P. and WHITE. A.J.R. 1971: Composition of island arcs and continental growth. Earth Planet. Sci. Lett. 12, p.224-230.(*)
- JANI, M.G., BOSSOLI, R.B. and HALLIBURTON L.E. 1983: Further characteristics of the E_1 centre in crystalline quartz. Phys. Rev. B. 27, 2285-94.
- JANI, M.G., HALLIBURTON, L.E. and KOHNKE, E.E. 1984: Point defects in crystalline SiO_2 : Thermally Stimulated Luminescence above room temperature. J. Appl. Phys. 54, 6321-28.
- KALLIOKOSKI, J., LANGFORD, F.F. and OJAKANGAS, R.W. 1978: Criteria for uranium occurrences in Saskatchewan and Australia as guides to favourability for similar deposits in the United States. Technological University, Department of Geology and Geological Engineering. 480p.
- KAUL, I.K., GANGULI, D.K. and HESS, B.F.H. 1972: Influencing parameters in thermoluminescence of quartz. Mod. Geol. 3, p.201-207.
- KIRCHNER, G., LEHNERT-THIEL, K., RICH, J. and STRNAD, J.G. 1980: The Key Lake U-Ni deposits: A model for Lower Proterozoic uranium deposition. In Proc. of the I.U.S. on the Pine Creek Geosyncline. I.A.E.A. (Vienna) p.617-630.
- KITT, K.B. and MARTIN J.J. 1983: Radiation-induced mobility of lithium and sodium in -qtz. J. Appl. Phy. 54 (9), 5030-31.
- KNUTSON, J., FERGUSON, J., ROBERTS, W.M.B., DONNELLY, T.H. and LAMBERT, I.B. 1979: Petrogenesis of copper bearing breccia pipes Redbank, Northern Territory, Australia. Econ. Geol. 74, p.814-826.
- LABHART, T.P. and RHBACH, L. 1974: Granite und Uranvererzungen in den Schweizer Alpen. Geol. Rundschau. 63, p.135-147.
- LANGMUIR, D. 1971: The effect of particle size on the reaction goethite--hematite + water. Am. J. Sci. 271, p.147-156.
- LANGMUIR, D. 1978: Uranium solution-mineral equilibria at low temperatures with applications to sedimentary ore deposits. Geochim. Cosmochim. Acta. 42(6), p.547-569.
- Le phenomene d'Oklo 1975: Proceedings of a symposium, Libreville. I.A.E.A. (Vienna) 649p.

- LEVY, P.W. 1968: A brief summary of radiation effects applicable to geology problems. In Thermoluminescence of Geological Materials. Ed. D.J. McDougall, Academic Press, p.25-38.
- LEVY, P.W. 1973: Colour centres. Brookhaven National Laboratories Report No. BNL 24242 24p.
- LEVY, P.W. 1974: Physical principles of thermoluminescence and recent developments in its measurement. Presented at an international seminar on application of science to dating of works of art, Museum of Fine Arts, Boston, Mass. (unpubl.).
- LEVY, P.W. 1979: Thermoluminescence studies having application to geology and archaeometry. PACT J. 3, p.466-480.
- LEVY, P.W. 1981: Thermoluminescence. In Encyclopedia of Physics R.G. Lerner and G.L. Trigg, Editors, (Addison-Wesley, Reading, Mass., 1981), p.1036-1040.
- LEVY, P.W. 1982: Thermoluminescence and optical bleaching in minerals exhibiting second order kinetics and other charge retrapping characteristics. PACT 6, p.224-242.
- LEVY, P.W. 1983a: Thermoluminescence in systems not subject to the usual approximations for first and second order kinetics. Rad. Effects, 72, p.259-264.
- LEVY, P.W. 1983b: Characteristics of thermoluminescence glow curves for minerals exhibiting more than one glow peak. PACT 9, p.109-122.
- LEVY, P.W. 1984a: Thermoluminescence kinetics in systems more general than the usual 1st and 2nd order kinetics. J. Lumin. 31&32, p.133-135.
- LEVY, P.W. 1984b: Thermoluminescence systems with two or more glow peaks described by anomalous kinetic parameters. Nuc. Inst. and Methods in Phys. Res. B1, p.549-556.
- LEVY, P.W. 1985a: Recent developments in thermoluminescence kinetics. Proc. 1984 Nat. Sym. on Thermally Stimulated Luminescence and Related Phenomena, Ahmedabad, India. Nuc. Tracks and Rad. Meas.
- LEVY, P.W. 1985b: Thermoluminescence kinetics in materials exposed to the low doses applicable to dating and dosimetry. Nuc. Tracks and Rad. Meas.
- LEWRY, J.F. and SIBBALD, T.I.I. 1979: A review of pre-Athabasca basement geology in northern Saskatchewan. In Spec. Pubs. Geol. Soc. Sask. 4, p.19-58.
- MACDIARMID, R.A. 1960: An application of thermoluminescence for prospecting for hydrothermal ores. Econ. Geol. 55, p.1340-1341. (Abstract).

- MACDIARMID, R.A. 1963: The application of thermoluminescence to geothermometry. *Econ. Geol.* 58, p.1218-1228.
- MACDIARMID, R.A. 1968: Natural thermoluminescence as a prospecting tool for hydrothermal ores in carbonate host rocks. *In* Thermoluminescence of geological materials. Edit. D.J. McDougall, Academic Press, p.547-558.
- MACKEY, J.H. 1963: EPR study of impurity related colour centres in germanium doped quartz. *J. Chem. Phys.* 39, p.74-83.
- M^CANDREW, J. and FINLAY, C.J. 1980: The nature and significance of the occurrence of uranium in the Nanambu Complex of the Pine Creek Geosyncline. *In* Proc. of the I.U.S. on the Pine Creek Geosyncline. I.A.E.A. (Vienna) p.357-362.
- M^CDOUGALL, D.J. 1964: Thermal glow tests as a guide to ore deposits. *Econ. Geol.* 59, p.326-327. (Discussion.)
- M^CDOUGALL, D.J. 1968: (Editor). Thermoluminescence of geological materials. Academic Press, London. 578 pages.
- M^CDOUGALL, I. 1962: Differentiation of Tasmanian doerites: Red Hill dolerite-granophyre association. *Bull. Geol. Soc. Am.* 73, p.279-316.(*).
- M^CDOUGALL, I., DUNN, P.R., COMPSTON, W., WEBB, A.W., RICHARDS, J. and BOFINGER, V.M. 1965: Isotopic age determinations on Precambrian rocks of the Carpentaria region, Northern Territory, Australia. *J. Geol. Soc. Aust.* 12,1, p.67-90.
- M^CKEEVER, S.W.S. 1984: Thermoluminescence in quartz and silica. *Rad. Protect. Dos.* 8, 1/2, p.81-98.
- M^CKEEVER, S.W.S. 1985: Thermoluminescence of solids. Cambridge University Press. Cambridge Solid State Science Series. 376 pages.
- M^CKEEVER, S.W.S., CHEN, C.Y. and HALLIBURTON, L.E. 1985: Point defects and the pre-dose effect in natural quartz. *Nuc. Tracks.* 10, No. 4-6, p.489-495.
- M^CKEEVER, S.W.S. and SEARS, D.W. 1980: The natural thermoluminescence of meteorites: A pointer to meteorite orbits? *Mod. Geol.* 7,(3), p.137-146.
- M^CKEEVER, S.W.S., STRAIN, J.A., TOWNSEND, P.D. and UDVAL, P. 1983: Effects of thermal cycling on the thermoluminescence and radioluminescence of quartz. *PACT* 9, p.123-132.
- M^CKEEVER, S.W.S. and YANG, X.H. 1987: Characterization of the pre-dose effect using ESR and TL. *Nuc. Track Rad. Meas.* 14 1/2, p.75-79.
- M^CMORRIS, D.W. 1969: Trapped Electron Dating: ESR studies. *Nature* 222, 870-1 (1969).

- M^CMORRIS, D.W. 1971: Impurity Colour Centres in Quartz and Trapped Electron Dating: Electron Spin Resonance, Thermoluminescence Studies. *J. Geophys. Res.* 76, 7875-87.
- MALIK, D.M., KOHNKE, E.E. and SIBLEY, W.A. 1981: Low temperature stimulated luminescence in high quality quartz. *J. Appl. Phys.* 52, 3600-5.
- MANNING, R.A. 1979: Host rock petrology and geochemistry of the Westmoreland uranium deposits, northwest Queensland. B.Sc. (Hons.) thesis. Univ. of Adelaide, S.A. (unpubl.).
- MARFUNIN, A.S. 1979: Spectroscopy, Luminescence and Radiation Centres in Minerals. (Springer-Verlag, Berlin).
- MARTINI, M. SPINOLO, G, and VEDDA, A. 1986: Radiation-induced conductivity of as-grown and electrodiffused quartz. *J. Appl. Phys.* 60 (5), 1705-8.
- MATTERN, P.L., LENGWEILER, K., LEVY, P.W. and ESSER, P.D. 1970: Thermoluminescence of KCl:Tl between 30°C and 410°C determined by simultaneous intensity and spectral distribution measurements. *Phys. Rev. Letters.* 24, p.1287-1291.
- MEDLIN, W.L. 1963: Thermoluminescence in quartz. *J. Chem. Phys.* 38,(5), p.1132-1143.
- MELSON, W.G. and THOMPSON, G. 1971: Petrology of a transform fault zone and adjacent ridge segments. *Philos. Trans. R. Soc. London.* A268: p.423-441.
- MILLER, A.R. 1980: Uranium geology of the eastern Baker Lake Basin, District of Keewatin, Northwest Territories. *Geol. Surv. Canada Bull.* 330.
- MITCHELL, J. 1976: Precambrian geology of the Westmoreland region, Northern Australia. Part 2: Cliffdale Volcanics. *B.M.R. Geol. Geophys. Aust., Record* 1976/34.
- MOLINA, P. and BESOMBES, J.C. 1975: Place du Francevillien dans le contexte géologique de L'Afrique. In The Oklo Phenomenon. Proceedings of a symposium, Libreville, I.A.E.A. (Vienna) p.3-14.
- MORGAN, B.D. 1965: Uranium ore deposits of Pandanus Creek. In Geology of Australian ore deposits. (Edit. J. M^CAndrew), p.210-211. (Eighth Commonwealth Mining and Metallurgical Congress: Melbourne). A.I.M.M.
- MORTIMER, G.E. 1984: Early to Middle Proterozoic granitoids, basaltic dykes and associated layered rocks of S.E. Eyre Peninsula, South Australia.

- MUIR, M.D. 1980: Palaeontological evidence for the Early Cambrian age of the Bukalara Sandstone, M^CArthur Basin, Northern Territory. B.M.R. Jour. Aust. Geol. Geophys. 5, (2), p.159-160.
- MUIR, M.D. 1981: The microfossils from the Proterozoic Urquhart Shale Mt. Isa, Queensland, and their significance in relation to the depositional environment, diagenesis and mineralization. Miner. Deposita 16, (1), p.51-58.
- MUIR, M.D., ARMSTRONG, K.J. and JACKSON, M.J. 1980: Precambrian hydrocarbons in the M^CArthur Basin, Northern Territory. B.M.R. Jour. Aust. Geol. Geophys. 5, (4), p.301-305.
- MUTO, T., HIRONO, S. and KURATA, H. 1965: Some aspects of fixation of uranium from natural waters. Mining Geol. (Tokyo), 15, (74), p.287-297.
- NAUDET, R. 1978: Problemes poses par le deroulement de phenomene d'Oklo: tentative d'interpretation globale. In Natural Fission Reactors. Proceedings of a Technical Committee Meeting, Paris. I.A.E.A. p.715-734.
- NEEDHAM, R.S., CRICK, I.H. and STUART-SMITH, P.G. 1980: Regional geology of the Pine Creek Geosyncline. In Proc. of the I.U.S. on the Pine Creek Geosyncline. I.A.E.A. (Vienna) p.1-22.
- NEWTON, H.J. and M^CGRATH, M.G. 1958: The occurrence of uranium in the Milestone Authority to Prospect, Wollongorang District Northern Territory. In Stillwell Anniversary Volume, A.I.M.M., Melbourne, p.177-185.
- O'BRIEN, M.C.M. 1955: The structures of color centres in smokey quartz. Proc. Roy. Soc. London, A231, p.404-414.
- PAGE, R.W. 1981: Depositional ages of the stratiform base metal deposits at Mt. Isa and M^CArthur River, Australia, based on U-Pb zircon dating of concordant tuff horizons. Econ. Geol. 76, 3, p.648-658.
- PAGE, R.W., COMPSTON, W. and NEEDHAM, R.S. 1980: Geochronology and evolution of the late-Archaeon basement and Proterozoic rocks in the Alligator River Uranium Field, Northern Territory, Australia. In Proc. of the I.U.S. on the Pine Creek Geosyncline. I.A.E.A. (Vienna) p.39-68.
- PARKER, A.J. 1981: (Compiler). Symposium on the Gawler Craton, Extended Abstracts. Geol. Soc. Aust. S.A. Branch.
- PEARCE, J.A. and CANN, J.R. 1973: Tectonic setting of basic volcanic rocks determined using trace element analyses. Earth Planet. Sci. Lett. 19, p.290-300.(*).

- PEARCE, J.A., GORMAN, D.E. and BIRKETT, T.C. 1975: The TiO_2 - K_2O - P_2O_5 diagram: a method of discriminating between oceanic and non-oceanic basalts. *Earth Planet. Sci. Lett.* 24, p.419-426.(*)
- PFIFFELMANN, J-P. 1975: L'uranium dans le bassin de Franceville. In The Oklo Phenomenon. Proceedings of a Symposium, Libreville. IAEA (Vienna). p.37-53.
- PLUMB, K.A. 1979: The tectonic evolution of Australia. *Earth Sci. Rev.* 14, p.205-249.
- PLUMB, K.A. and DERRICK, G.M. 1975: Geology of the Proterozoic rocks of the Kimberley to Mt. Isa region. *Econ. Geol. Austr.*, Aust.I.M.M. Monograph 5, p.217-252.
- POHL, D.C. 1970: The geology of the uranium prospects of the Westmoreland area, northwest Queensland. B.A.(Hons) thesis. Macquarie University. (unpubl.).
- RACKLEY, R.I. 1976: Origin of Western States Type Uranium Mineralisation. In Handbook of Strata-bound and Strataform Ore Deposits. Elsevier, Amsterdam. Ed. K.H. Wolf. p.89-156.
- RAMAEKERS, P. 1976: Athabasca Formation, Northeast Edge (64L, 741 74P): Part 1. Reconnaissance Geology. Eds. J.E.Christopher and R. Macdonald. Summary of Investigations 1976. *Sask. Geol. Misc. Rep.* p.73-77.
- RANDALL, J.T. and WILKINS, M.H.F. 1945: Phosphorescence and electron traps. 1. The study of trap distributions. *Proc. Roy. Soc.* A184, p.366-389.
- RANKAMA, K. and SAHAMA. 1950: *Geochemistry*. Univ. of Chicago Press. 910p.
- RENAULT, J.R. 1981: Variations in the thermoluminescence properties of quartz associated with migrating uranium deposits. *Bull. de Mineral.* 104, 6, p.715-722.
- REYNOLDS, R.L. and GOLDBERGER, M.B. 1978: Origin of a South Texas roll front type uranium deposit: 1. Alteration of iron titanium oxide minerals. *Econ. Geol.* 73, p.1671-1689.
- RILEY, G.H. 1980: Granite ages in the Pine Creek Geosyncline. In Proc. of the I.U.S. on the Pine Creek Geosyncline. IAEA. p.69-72.
- ROBERTS, H.G., RHODES, J.M. and YATES, K.R. 1963: Calvert Hills, Queensland 1:250,000 geological series. BMR Aust. Explan. Notes. SE/53-8.
- ROSHOLT, J.N. and NOBLE, D.C. 1969: Loss of uranium from crystallised silicic volcanic rocks. *Earth Plan. Sci. Lett.* 6, p.268-270.

- ROSHOLT, J.N., PRIJANA, and NOBLE, D.C. 1971: Mobility of uranium and thorium in glassy and crystallised volcanic rocks. *Econ. Geol.* 66, p.1061-1069.
- ROSSITER, A.G. and FERGUSON, J. 1980: A Proterozoic model for northern Australia and its economic implications. In Proc. of the I.U.S. on the Pine Creek Geosyncline. IAEA. p.209-232.
- SANKARAN, A.V., NAMBI, K.S.V. and SUNTA, C.M. 1983: Progress of geological research on geological materials. Proc. Ind. Nat. Sci. Academy. 49A, No. 1, p.18-113.
- SCHINDLMAYR, W.E. and BEERBAUM, B. 1984: Structure related mineralisation in the Westmoreland district, Queensland, Australia. Proc. World Geological Congress, Uranium Session. Moscow, 1984.
- SCHLESINGER, M. 1964: Thermoluminescence in Aluminium bearing quartz. *Phys. Lett.* 10, p.49-50.
- SCHLESINGER, M. 1965: Optical studies of electron and hole trapping levels in quartz. *J. Phys. Chem. Solids* 26, 1761-6.
- SCOTT, R. 1966: Origin of chemical variations within ignimbrite cooling units. *Am. J. Sci.* 264, p.273-288(*).
- SEN, K.K. 1960: Some aspects of the distribution of Ba, Sr, Fe and Ti in plagioclase. *J. Geol.* 68, p.638-665(*).
- SHEKHMAMETEV, R.I. 1973: Effect of radiation from radioactive material on natural quartz thermoluminescence. *Opt. Spectrosk.*, 34, p.505-509.
- SHMARIOVICH, E.M. 1980: Behavior of iron during uranium ore formation by bed filtration. *Lithology and Mineral Resources.* 15, 3, p.271.
- SHOCKEY, P.N., RACKLEY, R.I. and DAHILL, M.P. 1968: Source beds and solution fronts. *Remarks Wyo. Met. Sect. AIME*, Feb. 27, 1968: 7 pages.
- SMITH, J.W. and CROXFORD, N.J.W. 1973: Sulphur isotope ratios in the McArthur lead-zinc-silver deposit. *Nature.* 245, p.10-12.
- SPIRAKIS, C.S. 1979: Some applications of thermoluminescence to uranium prospecting. U.S.G.S. Prof. Paper. 1150.
- SPIRAKIS, C.S., GOLDHABER, M.R. and REYNOLDS, R.L. 1977: Thermoluminescence of sand grains around a South-Texas roll type deposit. U.S. Dept. Interior Geol. Surv. Open File Report 77-640, 14 pages.

- STUART-SMITH, P.G. and FERGUSON, J. 1978: The Oenpelli Dolerite - a Precambrian continental tholeiitic suite from the Northern Territory, Australia. *BMR J. Aust. Geol. Geophy.*, 3, p.125-133.
- STUART-SMITH, P.G., WILLS, K., CRICK, I.H. and NEEDHAM, R.S. 1980: Evolution of the Pine Creek Geosyncline. *In* Proc. of the I.U.S. on the Pine Creek Geosyncline. IAEA. p.23-38.
- SUN, S.S., NESBITT, R.W. and SHARASKIN, A.Y. 1979: Geochemical characteristics of mid-ocean ridge basalts. *Earth Planet. Sci. Lett.* 44, p.119-138.(*)
- SWEET, I.P. and SLATER, P.J. 1975: Precambrian Geology of the Westmoreland Region, Northern Australia. Part 1-Regional Setting and Cover Rocks. *BMR Geol. Geophy. Aust.*, Record 1975/88.
- TAYLOR, G.H. and ROWNTREE, J.C. 1980: The symposium - Retrospect and discussion. *In* Proc. of the I.U.S. on the Pine Creek Geosyncline. IAEA. p.751-758.
- TAYLOR, S.R. 1965: The application of trace element data to problems in petrology. *Phys. Chem. Earth* 6, p.133-213.
- TAYLOR, S.R. 1968: Geochemistry of Andesites. *In* Origins and Distributions of the Elements. Pergamon, London. Ed. L.H. Ahrens. p.559-583.(*)
- TILSLEY, J.E. 1980: Continental weathering and development of palaeo-surface related uranium deposits: Some genetic considerations. *In* Proc. of the I.U.S. on the Pine Creek Geosyncline. IAEA. p.721-732.
- TILSLEY, J.E. 1981: Genetic considerations relating to some uranium ore deposits: Part 2. Models for uranium ores in sandstones and carbonaceous pelites. *Geosci. Canada* 8, (1), p.3-7.
- TOWNSEND, P.D., and KELLY, J.C. 1973: Colour centres and imperfections in insulators and semiconductors. Sussex University Press. 261 pages.
- TUREKIAN, K.K. and WEDEPOHL, K.H. 1961: Distribution of the elements in some major units at the earth's crust. *Bull. Geol. Soc. Am.* 72, p.175-192.(*)
- VAZ, J.E. 1980: Effects of natural radioactivity on the thermoluminescence of apatite crystals at Cerro del Mercado, Mexico. *Mod. Geol.* 7, (3), p.171-176.
- VAN DER WEIJDEN, C.H., ARTHUR, R.C. and LANGMUIR, D. 1976: Sorption of uranyl by hematite: Theoretical and geochemical implications. *Geol. Soc. Am. Abstracts with Program*, 1976. Annual Meeting, Denver, Colorado.

- WEBB, A. 1973: Carpentaria age determination project. AMDEL Report AN2/1/0-1814/73. (Unpubl.)
- WEBB, A. 1975: Geochronology of 22 rock samples from the Nicholson Granite Complex. AMDEL Report AN2/1/0-2850/75. (Unpubl.)
- WEBER, F. and BONHOMME, M. 1975: Donnees radiochronologiques nouvelles sur le Francevillien et son environnement. In The Oklo Phenomenon, Proceedings of a symposium, Libreville, IAEA. p. 17-36.
- WEIL, J.A. 1984: A review of electron spin spectroscopy and its application to the study of paramagnetic defects in crystalline quartz. *Phy. Chem. Minerals* 10, 149-165.
- WILSON, I.H. 1978: Volcanism on a Proterozoic continental margin in north-western Queensland. *Precamb. Research* 7, p.205-235.
- WINTLE, A.G. and HUNTLEY, D.J. 1980: Thermoluminescence dating of ocean sediments. *Can. J. Earth Sci.* 17, (3), p.348-360.
- WOOD, D.A., TARNEY, J., VARET, J., SAUNDERS, A.D., BOUGAULT, H., JORON, J.L., TREVIL, M. and CANN, J.R. 1979: Geochemistry of basalts drilled in the North Atlantic by IPOD Leg 49: Implications for mantle heterogeneity. *Earth Planet. Sci. Lett.* 42, p.77-97.(*)
- WRIGHT, P.M., WEIL, J.A., BUCH, T. and ANDERSON, J.H. 1963: Titanium colour centres in rose quartz. *Nature* 197, p.246-248.
- YOKATO, R. 1968: Thermoluminescence of quartz and fused quartz coloured by x-ray radiation. *Phys. Rev.* 91, p.1013-1014.
- YPMA, P.J.M. and HOCHMAN, M.B.M. 1987: A thermoluminescence study of the role of a Middle Proterozoic unconformity in controlling uranium mineralisation, as shown at Eyre Peninsula, South Australia. *Bull. Mineral.* 110, p.173-186.
- YPMA, P.J.M. and FUZIKAWA, K. 1980: Fluid inclusion and oxygen isotope studies of the Nabarlek and Jabiluka deposits, Northern Territory, Australia. In Proc. of the I.U.S. on the Pine Creek Geosyncline. IAEA. p.375-398.
- ZELLER, E.J. 1968: Geological age determination by thermoluminescence. In Thermoluminescence of Geological Materials. Ed. D.J.McDougall. Academic Press. p.311-326.
- ZIMMERMAN, J. 1971: The radiation induced increase of the 100°C thermoluminescence sensitivity of fired quartz. *J. Phys. C Solid St. Physics*, 4, p.3,265-3,276.

APPENDIX 1

Binocular microscope descriptions
for Westmoreland samples.

APPENDIX 1: Location and tabulated description of samples.

Key : Quartz

wr	=	well rounded quartz grain
r	=	rounded quartz grain
sr	=	subrounded " "
sa	=	subangular " "
a	=	angular " "
H	=	Hematite
Ch.	=	Chlorite
C	=	Clay
S	=	Silicification
M	=	Uranium mineralization
✓	=	present
x	=	absent
c.g.	=	coarse grained
m.g.	=	medium grained
f.g.	=	fine grained
p.s.	=	poorly sorted
w.s.	=	well sorted
R.F.	=	Rock fragments
Cong.	=	Conglomeratic.

A
APPENDIX 1: Location and description of samples

Sample	Location	Quartz					H	Ch.	C	S	M	Comments
		wr	r	sr	sa	a						
UMD76/4	32m	Junnagunna					x	x	x	x	x	f.g. with c.g. bands.
UMD76/5	32m	"			✓					x		f.g.
"	39m	"			✓	✓				x		m.g.
"	45m	"	✓							x		
"	53m	"			✓				✓	x		f.g.
"	60m	"			✓	✓			✓	x		
UMD76/6	30m	"			✓	✓				x		
"	44.8m	"			✓	✓				x		
"	60m	"			✓					x		
UMD76/7	17m	"			✓	✓	✓			x	x	
"	25m	"			✓	✓	x			x	x	m.g.
"	49m	"				✓	x		✓	x		
"	57m	"			✓	✓	x		✓	x		m.g.
UMD76/8	20m	"			✓	✓				x		
"	44m	"			✓					✓		
"	70m	"			✓	✓				x		
UMD76/15	40m	"							✓	✓	x	p.s., m.g.
"	86m	"					✓	x	x	x	✓	m.g., p.s.
UMD76/16	14m	"			✓		✓		✓	✓		
"	21m	"			✓		x		✓	x		m.g.
"	30m	"			✓	✓	x		✓	x		
"	40m	"			✓	✓				x		
UMD76/17	34m	"			✓	✓	x		✓	x		f-m.g.
"	46m	"			✓		x		✓	x		f.g.
"	58m	"				✓	x		✓	x		f-m.g.
"	71m	"			✓	✓	x		✓	x		
"	84m	✓	"		✓	✓	x		✓	x		
UMD76/18	21m	"			✓	✓	✓			x	x	f-m.g.
"	36m	"				✓	✓			x	x	f.g.
"	41m	"			✓		✓			x	x	m.g.
"	66m	"								x		
"	81m	✓	"		✓					x		f-m.g.
UMD77/19	40m	"			✓		x		✓	x		f.g.
"	55m	"			✓	✓	x			x		f-m.g.
"	70m	"			✓	✓	x		✓	x		
"	85m	"								x		

APPENDIX 1: (cont'd)

Sample	Location	Quartz					H	Ch.	C	S	M	Comments
		wr	r	sr	sa	a						
UMD78/59	70.5m	Junnagunna	✓				✓		x	x	f-m.g.	
"	85.5m	"		✓	✓		x		✓	x		
"	88.8m	✓	✓				✓			✓		
"	98.5m	"			✓		✓		✓	x	f.g.	
UMD78/60	19m	"			✓					✓		
"	42m	"	✓	✓			x	x	x	✓	m.g., qtz. clasts.	
"	65m	"				✓	✓	x	x	✓	recrystallized, cherty.	
"	79m	"								x		
"	91.2m	"		✓	✓		✓	✓	x	x	recrystallized, cherty.	
"	124m	"		✓			✓	✓	✓	x	c.g., p.s.	
"	150m	"			✓	✓	✓	✓	✓	x	Ptw ₃ rd.qtz clasts.	
UMD78/64	59.7m	"					x	x	x	✓	p.s., m.g. recrystallized.	
"	100m	✓					x	x	x	✓	f.g., w.s.	
UMD78/69	26m	"					✓	x	x	✓	f.g.	
"	38m	"					✓	x	x	✓	m.g.	
"	50m	"					✓	x	✓	✓	vugs, minor recryst.	
"	61m	"					✓	✓	x	✓	vugs.	
UMD78/71	25m	"		✓			✓	x	x	✓	f.g.	
"	51m	"		✓	✓		x	x	✓	✓	f.g.	
"	70m	✓				✓	x	x	✓	x		
UMD78/72	30m	"					x	✓	x	✓	f.g.	
"	40m	"					✓	✓	x	✓	f-m.g.	
"	65m	"			✓		x	x	x	✓	m.g.	
"	80m	"					x	x	✓	✓	vugs, m.g., qtz clasts.	
"	110m	✓					✓	x	✓	x	f.g.	
UMD78/74	28m	"					✓	x	x	✓	very hematitic.	
"	49.7m	"					x	x	✓	x	well sorted.	
"	65m	"								x		
"	70m	"		✓		✓	✓	✓	✓	x	vugs.	
"	112m	✓					x	x	✓	x	R.F. and clasts vugs, limonite.	
UMD78/77	25.2m	"		✓			✓		x	✓	f.g.	
"	40m	"		✓						x	f.g.	
"	60m	"			✓		x		✓	x	f.g.	
"	80m	"		✓			x		✓	x	f.g.	
"	100m	✓		✓			✓		✓	x	m.g.	
UMD78/79	30m	"		✓	✓		✓	✓	✓	✓	f.g.	

APPENDIX 1: (cont'd)

Sample	Location	Quartz					H	Ch.	C	S	M	Comments
		wr	r	sr	sa	a						
UMD78/79	70m	Junnagunna	✓				✓	x	✓	✓	x	
"	80m	"			✓	✓			✓	x		f-m.g.
"	103m	"					✓	x	x	✓	x	w.s. recrystallized.
"	104m	"									x	
"	108m	"			✓		✓			✓	x	
"	110m	"				✓	✓	x	✓	✓	x	vugs and vein quartz.
"	111m	"		✓			✓			✓	x	f.g.
"	118m	✓	"		✓	✓	✓			x	x	
UMD78/81	30.5m	"			✓		x	x			x	
"	40m	"			✓	✓	x	x			x	f.g.
"	50m	"									x	
"	60m	"			✓					✓	x	
"	70m	"									x	
UMD78/82	28m	"	✓				x		✓	✓		p.s.
"	39m	"			✓	✓	x			✓	x	
"	51m	"				✓	x			✓	x	f.g.
"	62m	"				✓					x	f-m.g.
"	74m	"		✓			x			✓	x	f-m.g.
UMD78/83	35.5m	"					✓	✓	✓	✓	x	vuggy; volcanic fragments.
"	36m	"									x	
"	44m	"					✓	x	x	✓	x	f-m.g. Graded bedding.
"	53m	"					✓	x	x	✓	x	m.g. rd qtz clasts.
"	55m	"									x	
"	61m	"					✓	x	x	✓	x	m.g. dark qtz clasts.
"	70m	"									x	
"	70m	"					x	x		x	x	f.g. with c.g; p.s. band.
UMD78/84	32m	"					✓	x			x	f.g.-c.g.
"	54m	"					✓	x			x	p.s.
"	76m	"					✓	x			x	f.g., p.s.-c.g. p.s.
"	98m	"					✓	✓		x	x	p.s., occ.veinlets of qtz.
"	120m	✓	"				✓	✓			x	tuff.
UMD78/85	31.5m	"			✓					✓	x	m.g., w.s.
"	41m	"									x	
"	50m	"			✓						x	
"	60.1m	"			✓	✓				✓	x	
"	70.2m	✓	"			✓					x	f.g.
UMD78/86	30m	"					x	✓	x	x	x	vugs with vein quartz.

APPENDIX 1: (cont'd)

Sample	Location	Quartz					H	Ch.	C	S	M	Comments
		wr	r	sr	sa	a						
UMD78/86	60m	Junnagunna								x	Conglomeratic; R.F. and clasts.	
"	100m	"				✓	x	x	x	x	As above.	
UMD78/87	27m	"			✓					x	f.g.	
"	32m	"	✓			✓				x x		
"	37m	"			✓					x	f.g.	
"	43m	"			✓					x	f.g.	
"	44m	"			✓	✓	x		✓	x	m.g.	
UMD78/88	17m	"			✓	✓			✓	x		
"	25m	"			✓		x		✓	x	f-m.g.	
"	33m	"	✓				x		✓	x	f-m.g.	
"	41m	"			✓		x		✓	x	m.g.	
"	49m	"			✓	✓	✓			x x		
UMD78/89	10m	"	✓	✓		✓				x	m.g.	
"	30.1m	"				✓	x	x	✓	x	f-m.g.; w.s.	
"	50m	"			✓		x	x		x		
"	70.1m	"				✓	✓	x	✓	x	f.g.; w.s.	
UMD78/90	16m	"			✓	✓			✓	x		
"	24m	"			✓					x	m.g.	
"	32m	"			✓		x		✓	x	f-m.g.	
"	40m	"			✓	✓				x		
"	49m	"				✓	✓			x x	m.g.	
UMD78/91	8m	"			✓		✓			x x	m.g.	
"	18m	"			✓	✓	x		✓	x	m.g.	
"	28m	"				✓	x		✓	x		
"	38m	"				✓	x		✓	x		
"	49m	"			✓		✓		✓	x		
UMD78/92	27.8m	"			✓					x		
"	35m	"				✓				x		
"	70m	"			✓	✓				x		
"	106m	"			✓	✓				x		
UMD79/100	26m	"				✓	✓	x	x	✓	✓	m.g. Recrystallized.
"	44m	"			✓		✓	✓		x x	tuff.	
"	62m	"			✓	✓	✓	x		x x	m.g.	
"	78m	"			✓	✓	x	x	✓	x x	c.g. Qtz. clasts.	
"	94.5m	"				✓	✓	✓	x	✓	x x	Ptw ₃
UMD79/101	33.9m	"			✓		x	x		✓	✓	m-f.g.
"	52m	"				✓	✓	x	x	✓	x x	c.g. Acid volc. clasts.

APPENDIX 1: (cont'd)

Sample	Location	Quartz					H	Ch.	C	S	M	Comments
		wr	r	sr	sa	a						
UMD79/101	70m Junnagunna	✓					x	x	✓	x	x	
"	88m ✓ "	✓					✓	✓	✓	x	x	f.g. (tuff).
"	109m "			✓			✓	x	✓	x	x	qtz clasts. Conglom.
UMD79/102	28m "		✓				✓	x		x	x	m.g.
"	33m "		✓				✓	x	x	✓	x	m.g. recrystallized.
"	39m "			✓			x	x	✓	x		m.g.
"	44m "			✓			✓	x	✓	x		m.g.
"	50m "		✓	✓			✓	x	✓	✓	x	m.g.
UMD79/103	30m "		✓	✓			✓		✓	x		m.g.
"	48m "			✓							x	f-m.g.
"	66m "			✓			x		✓	x		f.g.
"	84m ✓ "			✓	✓		x	x		x	x	
"	100m "			✓	✓		✓			x	x	f-m.g.
UMD79/106	30m "		✓				x	✓	✓	x	x	f.g.
"	50m "		✓				✓	x	✓	✓	x	m.g.
"	70m "			✓			x	x	✓	✓	x	c.g.
"	90m "		✓	✓			✓	x	x	✓	x	m-c.g. Rd. clasts.
"	108m "			✓			✓	x	x	✓	x	Ptw ₃
UMD79/107	30m "			✓			✓	x	x	✓	✓	m.g.
"	50m "			✓			✓	x	✓	✓	x	f-m.g.
"	70m "			✓	✓		✓	x	✓	✓	x	m-c.g.
"	90m ✓ "			✓	✓		x	x	x	✓	x	m-c.g. milky qtz. clasts.
"	110m "			✓			✓	✓			x	Ptw ₃
UMD79/108	45m "			✓	✓		x	x	✓	✓		m.g.
"	65m "			✓	✓		x	x	x	✓		m.g.
"	85m "		✓		✓		x	x	x	x		m.g.
"	110m "			✓			✓	✓	x	✓	x	m.g.
"	130m ✓ "		✓	✓			x	✓		x	x	m.g.
UMD79/110	15.1m "			✓	✓		x	x	x	✓	x	m.g.
"	28.2m "		✓				✓	x	✓	✓	x	m.g.
"	47.6m "		✓				✓	x		x	✓	f.g.
"	60.1m "		✓				x	x	✓	✓	x	vugs, m-c.g.
"	75m ✓ "			✓			x	x	✓	✓	x	m.g.
UMD79/112	23m "			✓			✓	✓			x	f.g.
"	43m "			✓	✓		x	x	x	x		m.g.; R.F.
"	63m "			✓			x	x	✓	x	x	m.g.; p.s. clasts.

APPENDIX 1: (cont'd)

Sample	Location	Quartz					H	Ch.	C	S	M	Comments
		wr	r	sr	sa	a						
UMD79/112	83m ✓	Junnagunna			✓		x	x	✓	x	x	m.g.
"	102m	"				✓	x	✓	x	x		acid volc. clasts.
UMD79/114	25m	"									x	
"	50m	"									x	
"	70m	"									x	
"	95m	"									x	
"	107m ✓	"									x	
UMD79/116	40m	"			✓	✓	x	x	x	x	x	m.g.
"	50m	"					x	x	x	✓	x	m.g. recrystallized.
"	60m	"		✓			x	x	✓	✓	x	m.g.
"	69.5m	"			✓	✓	x	x	✓	✓	x	m.g.
"	77.5m ✓	"			✓		x	x	✓	x	x	f.g.
UMD79/117	29.5m	"				✓	✓	x	x	✓	x	m.g. recrystallized.
"	34m	"				✓	x	x	✓	✓	x	m.g. "
"	39m	"				✓	x	x	✓	✓	x	m.g.
"	44m	"			✓	✓	✓	x	x	✓	x	qtz. clasts.
"	49m	"		✓			✓	x	x	✓	x	m.g.
UMD79/119	26m	"			✓	✓	✓	x	x	✓	x	recrystallized.
"	31m	"			✓	✓	✓	x	x	✓	x	"
"	37m	"				✓	✓	x	x	x	✓	R.F. m.g.
"	43m	"			✓		✓	x	x	✓	x	f-m.g.; p.s.
"	49m	"		✓			✓	x	x	✓	x	m.g.; p.s.
UMD79/123	25m	"				✓	x	x			x	f-m.g.
"	45m	"									x	
"	60m	"				✓					x	f.g.
"	80m	"			✓	✓					x	
"	100m	"			✓		x	x		✓	x	m.g.
"	120m ✓	"			✓					✓	x	m.g.
UMD79/124	30m	"					✓	x		✓	x	m.g.; vugs.
"	48m	"					x	x		✓	x	f-m.g.
"	66m	"					✓	x	✓	✓	x	f.g.
"	84m	"					✓	x	✓	x	x	f.g., dark clasts.
"	100m ✓	"					✓	x	✓	x	x	"
UMD79/125	25m	"				✓					✓	f.g.
"	32m	"		✓							x	f.g.
"	38m	"			✓	✓					x	m.g.

APPENDIX 1: (cont'd)

Sample	Location	Quartz					H Ch. C S M	Comments	
		wr	r	sr	sa	a			
UMD79/125	44m	Junnagunna		✓				✓ x	f.g.
"	50m	"			✓	✓		x x	m.g.
UMD79/126	27m	"				✓	x	x ✓	f-m.g.
"	33m	"					x x	✓ ✓ x	Limonite, f-m.g.
"	39m	"					x x	x ✓ x	p.s; f.g.-c.g.
"	45m	"					x x	x ✓ x	"
"	50m	"					✓ x	x ✓ x	"
UMD79/127	26.1m	"		✓	✓			✓ ✓	m.g.
"	32m	"		✓				✓ x	f-m.g.
"	38m	"			✓			✓ x	f-m.g.
"	44.1m	"			✓			x	f-m.g.
"	50.1m	"		✓	✓	✓		x	f-m.g.
UMD79/133	25m	"		✓	✓	✓		✓ ✓	f.g.
"	37m	"		✓	✓	x		✓ x	
"	39.1m	"		✓	✓			x	m.g.
"	46.2m	"		✓	✓			x	f.g.
"	50m	"		✓		✓		✓ x	
UMD79/134	38m	"		✓				x	
"	43m	"		✓				x	f-m.g.
"	48m	"		✓	✓			x	
"	52m	"		✓	✓			✓ x	
UMD79/135	16m	"		✓	✓			x	f-m.g.
"	24m	"		✓				x	
"	32m	"		✓	✓	x	x	x	
"	40m	"		✓		✓		x x	
"	48m	"		✓	✓	✓		x x	
UMD79/137	26.5m	"			✓	✓	x	x ✓ x	Recrystallized.
"	30m	"		✓		✓	x	x ✓ ✓	m.g.
"	36m	"		✓		x	x	✓ ✓ x	m.g.
"	43m	"			✓	x	x	✓ ✓ x	m.g.
"	50m	"		✓	✓	x	x	✓ ✓ x	m.g. rd.dark qtz.clasts.
UMD79/138	40.5m	"		✓		✓		✓ x	
"	45.1m	"		✓	✓			x	
"	50.2m	"						x	
"	55.6m	"			✓			x	m.g.
"	60m	"		✓	✓			x	f.g.

APPENDIX 1: (cont'd)

Sample	Location	Quartz					H	Ch.	C	S	M	Comments
		wr	r	sr	sa	a						
UMD79/139	34m Junnagunna	✓					✓	✓		x x	f.g.	
"	38m "		✓	✓			x	x	✓	✓ x	m.g.; p.s.	
"	42m "	✓					✓	✓	✓	✓ x	f.g.	
"	46m "		✓	✓			x	✓	x	✓ x	m.g.	
"	50m "		✓	✓			x	✓	✓	✓ x		
UMD79/140	20m "		✓	✓			✓	x	x	✓ x	f-m.g. Recrystallized.	
"	28m "		✓	✓			x	✓	✓	✓ x	m.g.	
"	36m "		✓	✓			x	x		✓ x	f-m.g.	
"	43m "		✓	✓			x	x		✓ x	f-m.g.	
"	50m "		✓	✓			✓	x	✓	✓ x	m.g.	
UMD79/143	11m "	✓					✓	x	x	x x	Limonitic-m.g.	
"	17.9m "		✓	✓			x	x	✓	x x	f-m.g.	
"	25m "		✓	✓			✓	x	✓	✓ x	f.g.	
"	32m "		✓	✓			x	✓	✓	✓ x	f-m.g.	
"	40m "		✓	✓			x	✓	✓	✓ x	f-m.g.	
UMD79/144	5m "			✓			✓	x	✓	✓ x	Limonite-m.g.; w.s.	
"	11m "		✓	✓			x	x	✓	✓ x	f.g.	
"	17m "		✓				x	x	✓	✓ x	m.g.; m.s.	
"	23m "			✓			x	x	✓	✓ x	"	
"	29m "	✓					x	x	✓	✓ x	large rd.qtz. clasts.	
UMD79/145	7m "		✓				x	x	x	✓ x	f-m.g.	
"	14m "			✓			x	x	✓	x x	m.g.	
"	21m "		✓				x	x	x	✓ x	m.g.	
"	28.5m "			✓	✓		✓	✓	✓	x x	f.g. (Tuff)	
"	30m "						x	✓		x x	f.g.	
UMD79/146	10m "		✓				✓			x ✓		
"	18m "			✓	✓					x		
"	24m "			✓	✓					✓ x		
"	32m "			✓	✓					x		
"	40m "		✓	✓			x			✓ x	f.g.	
UMD78/60	12m "						✓	✓	x	✓ x	Recrystallized.	
"	13m "						✓	✓	x	✓ x	"	
"	14m "						✓	✓	x	✓ x	"	
"	15m "			✓	✓		✓	✓	x	✓ x	" , limonite.	
"	18m "			✓	✓		✓	✓	x	✓ x	Recrystallized, m.g.	

Sample	Location	Quartz					H	Ch.	C	S	M	Comments
		wr	r	sr	sa	a						
UMD78/60	20m Junnagunna	✓					✓	x	✓	✓	Recrystallized, m.g.	
"	21m "	✓					x	x	✓	x	" m.g. Boxworks.	
"	22m "	✓	✓	✓	✓		x	x	✓	x	Less recrystln. f-m.g.	
"	23m "	✓					x	x	✓	x	" "	
"	24m "	✓					x	✓	✓	x	" "	
"	25m "	✓					x	✓	✓	x	" "	
"	26m "	✓					x	x	✓	x	m.g. "	
"	27m "		✓	✓			✓	x	✓	✓	x	No recryst'n. m.g.
"	28m "		✓		✓		✓	x	x	✓	x	Recrystallized.
"	29m "		✓		✓		✓	x	x	✓	x	m.g.
"	30m "		✓				✓	x	x	✓	x	m.g.
"	31m "		✓	✓			✓	x	x	✓	x	m.g.
"	32m "		✓	✓			✓	x	x	✓	x	m.g.
"	33m "			✓			x	x	x	✓	x	m.g.
"	34m "				✓		x	x	x	✓	x	Recrystallized. Qtz veins.
"	35m "	✓	✓				x	x	✓	✓	x	m.g.; p.s. Clasts.
"	36m "		✓		✓		x	x	✓	✓	x	" " "
"	37m "		✓		✓		x	x	✓	✓	x	" "
"	38m "		✓		✓		x	x	✓	✓	x	" "
"	39m "		✓		✓		x	x	✓	✓	x	Many dark qtz. clasts.
"	40m "		✓		✓		x	x	✓	✓	x	" " " "
"	41m "		✓		✓		x	x	✓	✓	x	Larger clasts.
"	43m "		✓		✓		x	✓	✓	✓	x	Clear qtz. clasts.
"	44m "		✓		✓		x	✓		✓	x	m.g.
"	45m "			✓	✓	✓	✓	✓		✓	x	Partial recryst'n.
"	46m "		✓		✓		x	x	✓	✓	x	Minor recryst'n. Clasts.
"	47m "			✓			x	x		✓	x	f.g. Recrystallized.
"	48m "			✓		✓	x	x	✓	✓	x	"Acid dyke" appearance.
"	49m "			✓	✓	✓	x	x	✓	✓	x	Hematite in veinlets.
"	50m "			✓	✓		x	x	x	✓	x	Vugs with limonite + pyrite.
"	51m "			✓			x	x	x	✓	x	As above - purple qtz. crystals.
"	52m "		✓	✓			x	x	✓	✓	x	Recrystallized.
"	53m "			✓	✓		x	x	x	✓	x	As 51m. Recrystallized.
"	54m "			✓	✓		✓	x	x	✓	x	Recrystallized.
"	55m "		✓		✓	✓	x	x	✓	✓	x	Less recryst'n.
"	56m "			✓	✓	✓	x	x	x	✓	x	" " . Small euhedral qtz.
"	57m "		✓	✓					✓	x	m.g. No Te crystallization.	

Sample	Location	Quartz					H	Ch.	C	S	M	Comments
		wr	r	sr	sa	a						
UMD78/60	58m	Junnagunna		✓	✓	✓	✓	x	✓	x	m.g. Qtz veinlets.	
"	59m	"		✓	✓	✓	✓	x	✓	x	m.g. Minor recrystn.	
"	60m	"		✓	✓		✓	x	✓	x	Qtz + hematite veinlets.	
"	61m	"		✓	✓		✓	x	x	✓	Euhedral hematitic Qtz.	
"	62m	"		✓		✓	x	✓	x	✓	Qtz. veins.	
"	63m	"		✓		✓	✓	x	x	✓		
"	64m	"		✓		✓	✓	x	x	✓	Recrystallized, cherty.	
"	66m	"		✓	✓		✓	x	x	✓	Breccia with limonitic vugs.	
"	67m	"		✓	✓		x	x	x	✓	Breccia.	
"	68m	"			✓	✓	✓	✓	x	✓	Veins of Qtz, hem. vugs.	
"	69m	"		✓	✓		x	x	x	✓	As 67m.	
"	70m	"		✓	✓		✓	✓	x	x	Partial recrystn.	
"	71m	"		✓		✓	✓	x	x	✓	" "	
"	72m	"		✓	✓		x	x	x	✓	Fault Qtz.	
"	73m	"		✓	✓		✓	✓	x	✓	Qtz. veins.	
"	74m	"		✓	✓		✓	x	x	✓	Partial recrystn.	
"	75m	"		✓	✓		✓	x	x	✓	" "	
"	76m	"		✓			✓	✓	x	✓	" "	
"	77m	"			✓	✓	✓	x	x	✓	Hematite matrix.	
"	78m	"			✓	✓	✓	✓	x	x	" "	
"	79m	"			✓	✓	✓	✓	x	x	Veins of Qtz/hem/U ₃ O ₈ ?	
"	80m	"		✓		✓	x	✓	x	✓	m.g.	
"	81m	"		✓	✓		x	x	x	✓	Qtz. clasts.	
"	82m	"			✓	✓	x	x	x	✓	Cherty, recrystallized.	
"	83m	"		✓		✓	x	x	x	✓	Limonitic.	
"	84m	"		✓		✓	x	x	✓	✓	Vuggy.	
"	85m	"		✓	✓		✓	✓	x	✓	Pyrite.	
"	86m	"		✓	✓		✓	✓	✓	✓	Vuggy.	
"	87m	"			✓	✓	✓	x	x	✓	Recryst. Qtz/hem.clasts	
"	88m	"			✓	✓	x	x	x	✓	m.g.	
"	89m	"			✓	✓	✓	✓	✓	✓		
"	90m	"			✓	✓		x	x	✓	Partial recrystn.	
"	91m	"		✓	✓		x	x	✓	✓	p.s. m-c.g.conglom.	
"	92m	"		✓		✓	✓	x	x	✓		
"	93m	"		✓		✓	✓	x	x	✓	Hematite veins.	

Sample	Location	Quartz					H	Ch.	C	S	M	Comments
		wr	r	sr	sa	a						
UMD78/60	94m	Junnagunna	✓	✓		✓	✓	x	✓	x	Recrystallized.	
"	95m	"		✓	✓	x	x	x	✓	x	m-c.g.	
"	96m	"	✓	✓		x	x	x	✓	x	m.g. Little recrystn.	
"	97m	"	✓	✓		✓	✓	x	✓	x	m.g.	
"	98m	"	✓	✓		x	x	x	✓	x	Recrystallized.	
"	99m	"	✓	✓		x	✓	x	✓	x	"	
"	100m	"	✓	✓		✓	✓	x	✓	x	" f.g.-c.g.	
"	101m	"		✓	✓	✓	x	x	✓	x	Limonitic vein.	
"	102m	"	✓	✓		x	x	x	✓	x		
"	103m	"	✓	✓		x	x	x	✓	x	Massive qtz. vein.	
"	104m	"	✓	✓		x	x	x	✓	x	Euhedral qtz vein.	
"	105m	"		✓	✓	✓	✓	x	✓	x	qtz. veins.	
"	106m	"	✓	✓		x	x	✓	✓	x	Darker qtz. clasts.	
"	107m	"		✓	✓	x	x	✓	✓	x	Minor recrystn.	
"	108m	"		✓	✓	x	x	✓	✓	x	"	
"	109m	"		✓	✓	x	x	✓	✓	x	m.g.	
"	110m	"		✓	✓	✓	x	x	✓	x	euhedral qtz. veins.	
"	111m	"	✓	✓		✓	x	✓	✓	x	Minor recrystaln.	
"	112m	"	✓	✓		x	x	✓	✓	x	p.s., m.g.	
"	113m	"	✓	✓		x	x	x	✓	x	m.g. Larger clasts.	
"	114m	"		✓	✓	x	✓	✓	✓	x		
"	115m	"		✓	✓	x	✓	✓	✓	x	More clay.	
"	116m	"		✓	✓	✓	✓	✓	✓	x		
"	117m	"	✓			✓	✓	✓	✓	x	qtz. veins	
"	118m	"	✓	✓		✓	x	✓	✓	x	f.g.-m.g. Patchy silicifn	
"	119m	"	✓	✓		x	x	✓	✓	x	p.s., m.g.	
"	120m	"	✓			✓	✓	✓	✓	x	Larger clear grains.	
"	121m	"	✓			x	✓	✓	x	x	Crumbly-non silicified.	
"	122m	"	✓		✓	✓	x	✓	✓	x	m.g.	
"	123m	"	✓			x	✓	✓	✓	✓	tuffaceous?	
"	125m	"		✓	✓	✓	x		✓	x		
"	126m	"		✓	✓	x	✓	✓	✓	x	f.g.	
"	127m	"		✓	✓	✓	✓	✓	✓	x	hematite veinlets.	
"	128m	"	✓			✓	✓	✓	✓	x		
"	129m	"	✓			✓	✓	✓	✓	x	Tuffaceous? f.g.	
"	130m	"	✓		✓	✓	x		✓	x		

Sample	Location	Quartz					H	Ch.	C	S	M	Comments
		wr	r	sr	sa	a						
UMD78/60	131m	Junnagunna		✓	✓	✓	x		✓	x	Euhedral hem.qtz cryst.	
"	132m	"		✓	✓	✓	x	✓	✓	x	Conglomerate.	
"	133m	"	✓		✓	x	x	✓	✓	x	m.g.	
"	134m	"	✓		✓	✓	x	✓	✓	x	hem. on joint plane.	
"	135m	"			✓	✓	x	✓	✓	x	m.-c.g.	
"	136m	"	✓			✓	x	✓	✓	x	"	
"	137m	"			✓	✓	✓	x	✓	✓	x	c.g.
"	138m	"		✓		✓	x	✓	x	x		
"	139m	"	✓			✓	x	✓	x	x	Tuff?	
"	140m	"	✓		✓	x	✓	✓	✓	x	Volcanic fragments.	
"	141m	"			✓	✓	✓	✓	x		f.g.	
"	142m	"			✓	✓	x	✓	x		m-c.g. Some large clasts	
"	143m	"			✓	✓	x	✓	x		" " " "	
"	144m	"	✓		✓	✓	x	✓	x		" Bimodal.	
"	145m	"	✓		✓	✓	x	✓	x		"	
"	146m	"			✓	✓	✓	x	✓	x	Euhedral qtz. crystals in veins.	
"	147m	"			✓	✓	✓	x	x	✓	x	c-m.g.
"	148m	"	✓			✓	x	✓	✓	x	c-m.g.	
"	149m	"	✓			✓	x	✓	✓	x	more clay.	
"	151m	"	✓		✓	✓	✓	✓	x	x	Feldspar grains. Crumbly	
"	152m	"	✓		✓	✓	✓	✓	x	x	" " "	
"	153m	"	✓	✓		✓	✓	✓	x	x	" " "	
"	154m	"	✓	✓		✓	✓	✓	x	x	More clay, less feldspar	
UMD78/77	23m	"		✓	✓	✓	x	x	✓	x	m.g.	
"	24m	"		✓	✓	✓	x	x	✓	✓	m.g.	
"	26m	"		✓	✓	x	x	x	✓	✓	m.g.	
"	27m	"		✓	✓	✓	x	✓	✓	x	m.g.	
"	28m	"		✓	✓	✓	x	✓	✓	x	m.g.	
"	29m	"	✓	✓		x	✓	✓	x	x	micaceous.	
"	30m	"		✓	✓	✓	✓	x	✓	✓	x	veinlet of dark quartz.
"	31m	"		✓	✓	✓	x	✓	✓	x	m.g.	
"	32m	"		✓	✓	✓	x	✓	✓	✓	some vugs.	
"	33m	"		✓	✓	✓	x	✓	✓	x	less silicified, no vugs	
"	34m	"		✓	✓	x	x	✓	✓	✓	m.g.	
"	35m	"		✓	✓	✓	x	✓	✓	✓		

APPENDIX 1: (cont'd)

Sample	Location	Quartz					H Ch.	C S M	Comments			
		wr	r	sr	sa	a						
UMD78/77	36m	Junnagunna	✓		✓		✓	x	✓	✓	✓	patchy silicifn, mic.
"	37m	"	✓		✓		✓	✓	✓	✓	✓	m.g.
"	38m	"	✓		✓		✓	x		✓	✓	f-m.g.
"	39m	"		✓	✓		✓	x	✓	✓	x	m.g., p.s.
"	41m	"			✓	✓	✓	x	✓	✓	x	dark qtz. color, m.g.
"	42m	"			✓	✓	✓	x	✓	✓	x	" vugs with hematite.
"	43m	"			✓	✓	✓	x	✓	✓	x	m.g. black hem. patches.
"	44m	"			✓	✓	✓	x	✓	✓	x	" " " "
"	45m	"			✓	✓	✓	x	✓	✓	x	c.g. " " "
"	46m	"			✓	✓	✓	✓	✓	x	x	f-m.g. Red hem. streaks.
"	47m	"		✓	✓		x	x	✓	x	x	f-m.g. Occasional mica.
"	48m	"		✓	✓		x	x	✓	x	x	m.g.
"	49m	"			✓	✓	x	x	✓	x	x	f.g.
"	50m	"			✓	✓	✓	x	✓	✓	x	Very faint silicifn.
"	51m	"			✓	✓	x	x	✓	✓	x	" " "
"	52m	"	✓		✓		x	x	✓	✓	x	Occasional mica.
"	53m	"			✓	✓	x	x	✓	✓	x	m.g.; p.s.; Occ. R.F.
"	54m	"			✓	✓	x	x	✓	✓	x	" " " "
"	55m	"			✓	✓	x	x	✓	✓	x	" " " "
"	56m	"			✓		✓	x	✓	✓	x	" " " "
"	57m	"		✓	✓		x	x	✓	✓	x	f.g. " "
"	58m	"		✓	✓		x	x	✓	x	x	f.g. Larger R.F. & clasts
"	59m	"			✓	✓	x	x	✓	x	x	" " "
"	61m	"				✓	x	x	✓	✓	x	m.g.
"	62m	"				✓	x	x	✓	✓	x	f-c.g. R.F. Mica.
"	63m	"				✓	✓	x	x	✓	✓	R.F.
"	64m	"			✓		x	x	✓	x	x	Very clayey.
"	65m	"			✓	✓	x	x	✓	✓	x	Patchy silicification.
"	66m	"			✓	✓	x	x	✓	✓	x	" . Some R.F.
"	67m	"			✓	✓	✓	x	✓	✓	x	m.g.; R.F.
"	68m	"			✓		✓	x	✓	x	x	f-m.g.
"	69m	"			✓		✓	x	✓	x	x	"
"	70m	"			✓		✓	x	✓	x	x	"
"	71m	"			✓	✓	x	x	✓	x	x	m-c.g. Occ. R.F.
"	72m	"			✓	✓	x	x	✓	x	x	" "
"	73m	"			✓		x	x	✓	x	x	f-m.g. Occ. dark qtz. gr.

Sample	Location	Quartz					H	Ch.	C	S	M	Comments
		wr	r	sr	sa	a						
UMD78/77	74m	Junnagunna		✓	✓		x	x	✓	x	x	Very p.s. Lge qtz clasts.
"	75m	"		✓			x	x	✓	x	x	m.g. p.s. " " "
"	76m	"		✓			✓	x	✓	x	x	Black hem. bands.
"	77m	"		✓			✓	x	✓	x	x	p.s; m.g.
"	78m	"		✓	✓		✓	x	✓	x	x	" " vugs.
"	79m	"		✓	✓		x	x	✓	x	x	Silt band. m.g; p.s.
"	81m	"		✓	✓		x	x	✓	x	x	Silt patches.
"	82m	"	✓	✓			✓	x	✓	x	x	f.g. Black hem. patches.
"	83m	"	✓	✓			✓	x	✓	x	x	" " " "
"	84m	"	✓	✓			✓	x	✓	x	x	" " " "
"	85m	"	✓	✓			✓	x	✓	✓	x	Less clay.
"	86m	"		✓	✓		✓	x	✓	✓	x	Darker rounded grains.
"	87m	"		✓	✓		✓	x	✓	✓	x	" " "
"	88m	"		✓	✓		x	x	✓	x	x	Large clasts & R.F.
"	89m	"		✓	✓		x	x	✓	x	x	" " " "
"	90m	"		✓	✓		x	x	✓	x	x	" " " "
"	91m	"		✓	✓		x	x	✓	x	x	" patches of silt.
"	92m	"		✓	✓		x	x	✓	x	x	Larger clasts.
"	93m	"		✓	✓		x	x	✓	x	x	" " and R.F.
"	94m	"		✓	✓		x	x	✓	x	x	m.g.; p.s.
"	95m	"		✓	✓		x	x	✓	x	x	f.g.
"	96m	"		✓	✓		x	x	✓	x	x	Larger rounded clear grns.
"	97m	"		✓	✓		x	x	✓	x	x	" " " "
"	98m	"		✓	✓		x	x	✓	x	x	" with green clay.
"	99m	"		✓	✓		✓	x	✓	x	x	f.g.
"	101m	"			✓		✓	x	✓	x	x	f.g. & m.g. Micaceous tuff.
"	102m	"			✓		x	x	✓	x	x	m.g.
"	103m	"	✓	✓			x	x	✓	x	x	m.g. Occ.R.F.
"	104m	"	✓	✓			✓	x	✓	x	x	Igneous rock clasts.
"	105m	"	✓	✓			✓	✓	✓	x	x	Mottled altered appearance.
"	106m	"	✓	✓			✓	✓		x	x	Ptw ₃
"	107m	"	✓	✓			✓	✓		x	x	Ptw ₃ -hem. in matrix.
UMD76/14	11m	Redtree					✓	x		x	✓	Vuggy, larger pebbles.
"	15m	"									x	
"	29.9m	"					x	x	✓	✓	x	m.g.; w.s.

Sample		Location	Quartz					H	Ch.	C	S	M	Comments
			wr	r	sr	sa	a						
UMD77/21	15.6m	Garee Lens		✓	✓		✓	✓		x	✓	m.g; p.s. Larger pebbles.	
"	40m	"		✓	✓		✓	x	✓	x	✓		
"	60m	"		✓	✓		x	x		x	✓	Vuggy	
"	83m	"		✓			✓	✓		x	x	Ptw ₃ . Clasts rimmed by ch.	
UMD77/22	10m	"		✓	✓		x	x		x	x	Minor vugs.	
"	24.7m	"		✓			✓	x	x	✓	✓	Vuggy, recrystallized.	
"	37.7m	"		✓	✓		✓	x		x	✓	Band of pitchblende.	
"	69.5m	"		✓			x	x	✓	✓	x	m.g. Some vugs.	
UMD77/23	15.5m	Redtree		✓			x	x	✓	✓	x	Vugs with euhedral qtz.	
"	30.5m	"		✓			x	x	✓	x	x	Mud/shale band, c.g.	
"	59.2m	"		✓	✓						x		
UMD77/24	30m	"		✓	✓		x	x	✓	x	x	m-c.g. Vuggy.	
"	45m	"		✓	✓		x	x	✓	✓	x	Vugs, clasts.	
"	61.2m	"		✓			x	✓	✓	x	x	m.g.	
N7	300'	Jack Lens		✓			x	x	x	✓	✓	Vugs.	
"	336'	"					✓	x	x	✓	✓	Vugs, limonite.	
N26	357'	Redtree		✓			x	✓	✓	x	✓	Bimodal f.g. and c.g.	
"	446'	"					✓	x	x	✓	x	Ptw ₃ . Altered feldspars.	
"	552'	"		✓			✓	x	x	x	x	Ptw ₃ .	
N43A	162'	Jack Lens		✓	✓		✓	x	x	✓	x	w.s. f.g.	
"	306'	"		✓			✓	x	✓	x	x	Ptw ₃ . Acid volc. clasts.	
"	446'	"			✓		✓	x	✓	x	x	very very hematitic.	
N74	10'	"		✓			✓	x	x	x	x	m-f.g. Banded hematite.	
"	110'	"		✓			✓	x	x	x	✓	m.g. vuggy, secondary min	
"	185'	"					✓	x	✓	✓	x	Vugs with hematite, m.g.	
"	387'	"		✓			✓	x	x	✓	x	Vuggy, f.g.	
"	512'	"					✓	✓	x		x	Ptw ₃ . Acid volc. clasts.	
N123	198'	Redtree	✓	✓			✓	x	✓	✓	x	m-c.g.	
"	288'	"		✓			✓	x	✓	x	✓	Vuggy, m.g.	
"	447'	"			✓		✓	✓		✓	x	Ptw ₃ ?	
"	593'	"		✓	✓		✓	x		✓	x	Ptw ₃ . Acid volc. clasts.	
N128	65'	"			✓		x	x	✓	x	x	Some mica.	
"	240'	"					✓	✓		✓	x	Conglomeratic.	
"	362'	"					✓	x		✓	x	Volcanic clasts. Hem. matrix.	
"	560'	"					✓	x		✓	x	Altered feldspars in clasts. Ptw ₃ .	
N129	100'	"		✓			✓	x	✓	x	x	Much clay.	

APPENDIX 1: (cont'd)

Sample	Location	Quartz					H	Ch.	C	S	M	Comments	
		wr	r	sr	sa	a							
N129	168'	Redtree				✓	✓	x	x	✓	✓	m.g.	
"	260'	"	✓				x	x	✓	✓	x	m.g. Vugs, R.F.	
"	454'	"	✓	✓			✓	✓	x	✓	x	Ptw ₃ ? Acid volc. clasts	
N130	200'	"	✓	✓			✓	x	✓	✓	x	Many vugs.	
"	250'	"					✓	x	x	✓	✓	Recrystallized.	
"	594'	"					✓	✓	x	✓	x	Ptw ₃	
NE1	104'	"	✓				x	x	✓	✓	x	m.g.	
"	243'	"		✓	✓		✓	x	x	✓	x	f-m.g. Recrystallized.	
"	325'	"		✓			✓	✓	✓	✓	x	Between 2 volcanics.	
"	496'	"					✓	✓			x	f.g. pinkish "dyke-like"	
"	497'	"					✓	✓			x	Breccia.	
NE10	55'	"	✓				✓	x	x	✓	x	x	Vugs with qtz and limonite.
"	160'	"		✓	✓		x	✓	✓	✓	x		Dark and cherty qtz.
"	254'	"	✓	✓			✓	x	✓	✓	x		Vugs with qtz. and hem.
"	385'	"	✓				✓	✓	x	x	x		Ptw ₃ . Altered feldspars.
NE11	140'	"					✓	x	✓	x	x		Euhedral qtz and mic.hem.
"	294'	"					✓	x	x	✓	✓		Vuggy, hematitic.
"	421'	"		✓			✓	x	x	✓	x		Ptw ₃ . Evidence of HT alteration?
NE23	138'	"					✓	✓	✓	✓	x		Acid volc. clasts.
"	274'	"		✓	✓						x		Bottom contact of dyke.
"	346'	"					✓	✓	✓	✓	x		More clasts.
"	520'	"					✓	x	x	✓	x		Ptw ₃ . Recrystallised.
UMD76/9	10m	Huarabagoo					x	x	✓	x	x		Vuggy, limonitic.
"	29.6m	"					✓	✓	✓	x	x		Vuggy, qtz. clasts.
77/27	14.2m	"	✓				✓	x	✓	✓	x		c.g. Recryst.qtz.clasts.
"	44.6m	"		✓			✓	x	✓	x	x		f.g. Banded hem.
"	59.8m	"		✓			✓	x	✓	✓	x		m-c.g. vug qtz.
77/29	14m	"	✓				✓	x	✓	✓	x		Large clasts.
"	22.7m	"	✓	✓			✓	x	✓	x	x		Vugs, dark qtz.
"	41m	"	✓				✓	x	✓	✓	x		Conglomeratic.
"	59.5m	"	✓				✓	x	✓	✓	x		Acid volc. clasts.
78/99	29m	Huar-Junn.		✓	✓		✓	✓	✓	x	x		m.g.
"	37m	"		✓	✓		x	x	x	✓	x		Rounded clear qtz.clasts.
"	46.5m	"		✓			✓	x	✓	x	x		f.g. layers.
79/130	32m	"	✓	✓			✓	x		x	x		m.g. micaceous.
"	40m	"		✓	✓		x	x	✓	x	x		m.g.
"	50m	"		✓			x	✓	✓	x	x		m.g.

APPENDIX 1: (cont'd)

Sample	Location	Quartz					H	Ch.	C	S	M	Comments
		wr	r	sr	sa	a						
UMD79/136	14m Juar-Junn.		✓	✓		x	x	x	✓	x	m.g.	
"	32.3m "		✓	✓		x	✓	x	✓	x	p.s., m.g. R.F.	
"	50.4m "		✓	✓		✓	x	✓	x	x	f.g.	
NE18	156' Huarabagoo	✓				✓	x	✓	x	x	m.g. crumbly.	
"	302' "					✓	x	x	✓	✓	m-c.g. recrystallized	
"	448' "			✓		x	x	x	✓	x	Recrystallized-cherty	
"	624' "		✓		✓	✓	x	✓	✓	x	Ptw ₃	
H15	60' "		✓	✓		✓	x	x	✓	x	Small vugs	
"	312' "		✓	✓		x	x	x	✓	✓	m.g.	
"	465' "		✓	✓		x	✓	✓	✓	x	Conglomeratic volc.clasts.	
H25	100' "				✓	✓	x	✓	✓	x	Some recrystd.qtz.clasts.	
"	142' "		✓	✓		✓	x	x	✓	x	Some vein qtz.	
"	239' "		✓	✓		✓	x	✓	✓	✓	m.g.	
"	287' "	✓	✓			✓	✓	✓	x	x	f.g. layers.	
H31	103' "			✓		✓	x	✓	✓	x	m.g.	
"	197' "		✓			✓	✓	x	x	x	Occ. R.F.	
"	330' "		✓	✓		✓	x	✓	✓	x	Banded hem.	
"	500' "			✓		x	✓	x	x	x	Ptw ₃ . Large cherty clasts.	
H66	85' "			✓		x	x	x	✓	x	Many qtz. veins.	
"	149' "			✓		✓	✓	x	✓	✓	Near basic volcs.	
"	306' "		✓	✓		✓	x	✓	✓	x	c.g. Acid volc.clasts.	
UMD77/34	5m Longpocket		✓	✓						x		
"	21m "			✓		x	x	x	✓	x	Euhedral qtz.development.	
"	34.8m "		✓							x		
"	42m "		✓	✓		x	x	x	✓	x	Acid volc. clasts.	
"	59.9m "		✓	✓						x		
"	65.6m "			✓		✓	x	✓	✓	x	Ptw ₃	
77/38	22m "		✓			✓	x	x	✓	✓	f.g.	
"	50m "		✓	✓		x		✓	x	x	c.g.	
"	75m "			✓		✓	x	x	✓	x	Ptw ₃	
77/43	22m "		✓			✓	x	✓	✓	x	f.g., w.s.	
"	45m "			✓		✓	x	x	x	x	v.f.g. micaceous.	
"	65m "			✓		x	x	✓	✓	x	qtz. clasts.	
77/44	19.7m "					✓	✓	x	x	x	Tuff	
"	40m "					✓	x	x	✓	✓	m.g., w.s.	
"	60m "					✓	x	x	✓	x	Recrystallized.	
77/45	13.6m "					x	x	x	✓	✓	f.g., w.s.	

APPENDIX 1: (cont'd)

Sample	Location	Quartz					H	Ch.	C	S	M	Comments	
		wr	r	sr	sa	a							
77/45	67.3m	Longpocket			✓	✓	✓	x	✓	✓	x	Sulphides.	
77/46	20.3m	"	✓								x	x	Micaceous. Tuff.
"	42.9m	"		✓	✓		x	x	x	✓	x		v.f.g.
"	67.7m	"				✓	✓	x	x	✓	x		Ptw ₃ .
77/48	10m	"	✓			✓	x	x	✓	✓	x		Vuggy
"	41.8m	"		✓			✓	x	x	✓	✓		Below sill contact.
"	62m	"					✓	x	x	✓	x		Ptw ₃ .
77/49	30.4m	"		✓	✓		✓	x	✓	✓	x		m.g.
"	39.1m	"		✓	✓		x	x	x	✓	x		Cross-bedding.
"	62.5m	"				✓	✓	x	x	x	x		Ptw ₃ .
77/52	10m	"	✓				✓	x	✓	✓	x		f.g.
"	21m	"		✓		✓	✓	x	x	✓	x		Hem. layering.
"	38.3m	"		✓	✓		✓	x	x	✓	x		Vuggy
"	57m	"	✓				✓	x	x	x	x		Tuffaceous.
77/57	21m	"					x	x	x	✓	x		Graded bedding.
"	40.4m	"		✓			x	x	✓	✓	x		c.g.
"	60.6m	"				✓	✓	x	x	✓	x		Ptw ₃ .
78/66	30.5m	"					✓	x	x	x	✓		p.s. Clasts.
"	52m	"		✓	✓		✓	✓	x	✓	x		m.g.
"	56m	"					✓	x	✓	✓	x		Ptw ₃ .
78/70	8.9m	"					✓	✓	x	✓	x		Just below sill contact.
"	48.5m	"					x	x	x	✓	✓		m.g., w.s.
"	81m	"					x	✓	✓	✓	x		Ptw ₃ .
78/80	24.3m	"					✓	x	x	✓	✓		m.g., w.s.
"	33m	"					x	✓	✓	x	x		f-m.g. with larger clast
"	80m	"					✓	✓	x	x	x		Ptw ₃ .
79/118	8m	Golara		✓			x	x	x	✓	x		m.g.
"	17m	"		✓	✓		✓	x	x	✓	x		Vuggy.
"	24m	"				✓	✓	x	x	✓	✓		Recrystallized.
"	31m	"				✓	✓	x	x	x	x		m.g. with silty layers.
"	48.5m	"		✓	✓		x	✓	✓	x	x		m.g.
"	55.5m	"				✓		✓	✓	✓	x		Clay balls.
UMP/8/8	8-10m	Longpocket									x		Percussion sample.
"	18-20m	"									x		" "
78/9	12-14m	"									x		" "
78/14	10-12m	"									x		" "
"	16-18m	"									✓		" "

APPENDIX 1: (cont'd)

Sample	Location	Quartz					H	Ch.	C	S	M	Comments
		wr	r	sr	sa	a						
UMD77/53	10m	Red Hill			✓		✓	x	x	✓	x	Recrystallized.
"	30.5m	"			✓		x	✓	✓	x	x	Shale bands.
"	50.7m	"			✓	✓	x	x	✓	x	x	m.g. Very clayey.
SUD76/1	42m	"					✓	x	x	✓	x	Recrystallized.
"	80.3m	"					✓	x	x	✓	x	" Qtz. clasts.
"	130m	"					✓	✓		x	x	Ptw ₃ .
SUD76/2	30m	"					x	x	x	✓	x	Recrystallized.
"	60m	"					✓	x	✓	x	x	Volc. clasts.
"	90m	"			✓		x	x		x	x	f-m.g., p.s.
77/6	17.3m	"			✓		✓	x	✓	✓	x	f-m.g. Vuggy.
"	40m	"			✓	✓	x	✓	✓	x	x	Tuff.
"	61.8m	"			✓		x	x	x	✓	x	Ptw ₃ .
77/11	16m	"					✓	x	x	✓	x	f.g., w.s.
"	40m	"			x	x	x	x	x	x	x	p.s.; m.g.
"	59m	"					x	✓	x	✓	x	Ptw ₃ .
77/12	8m	"					✓	x	x	✓	x	Recrystallized. Vugs.
"	38m	"					✓	✓	x	✓	x	f.g., w.s.
"	51.7m	"					x	✓	x	✓	x	m.g., p.s.
78/15A	20.3m	"					x	x	✓	x	x	f.g. micaceous.
"	56.6m	"			✓	✓	✓	x	x	✓	x	Near fault.
"	58.3m	"					✓	x	x	x	✓	Qtz filled fault.
"	80.9m	"					✓	x	x	x	x	Altered feld. conglom.
78/22	20m	"					✓	x	✓	x	x	f.g.
"	50.7m	"			✓		x	x	✓	x	x	R.F. crumbly.
"	80m	"				✓	✓	x	x	✓	x	v.f.g. shale.
78/28	28.4m	"					✓	x	x	✓	✓	m.g., w.s.
"	55m	"					✓	✓	x	✓	x	tuffaceous.
"	78m	"					✓	x	✓	x	x	Ptw ₃ ?
SUD78/16	19.8m	Lilypond			✓						x	
"	39.9m	"			✓	✓					x	
"	60.1m	"				✓					x	
78/17	19.8m	"					✓	x	x	x	x	f.g. Recrystallized.
"	39.7m	"					✓	x	✓	x	x	Volc. fragments.
"	60.6m	"					✓	x	✓	x	x	m.g. partial recrystall;
78/24	20m	"					✓	x	x	x	x	Occ. vugs. f-m.g.
"	40m	"					✓	x	x	x	x	m.g. vuggy.
"	63.8m	"					x	✓	✓	✓	x	Recrystallized. Vuggy.

Sample	Location	Quartz					H	Ch.	C	S	M	Comments	
		wr	r	sr	sa	a							
SUD78/25	18.9m	Lilypond					✓	x	x	x	x	f.g., w.s.	
"	39.8m	"					x	x	x	x	x		
"	65m	"					✓	x	x	✓	x	Ptw ₃ cherty.	
78/26	13m	"					x	x	✓	x	x	f.g., w.s.	
"	30m	"				✓	✓	x	x	✓	x	Hem. in vugs.	
"	49.9m	"					✓	x	✓	x	x	Hem.shale patches & band.	
"	72m	"					✓	x	x	✓	x	Ptw ₃ .	
UWD76/6	35.8m	Flying Fox				✓	x	x	x	✓	x	Recrystallized.	
"	65m	Anticline				✓	x	x	✓	✓	x	p.s., m.g.	
"	91m	"					✓	✓	✓		x	Ptw ₃ .	
76/8	23.8m	"					✓	✓	x	x	✓	x	hem. clasts.
"	45m	"				✓	✓	✓	x	x	x	x	m.g.
"	64m	"				✓	✓	✓	✓	x	x	x	Micaceous tuff.
79/11	46m	"				✓	✓	✓	x	x	✓	x	m.g.
"	66m	"				✓	✓	✓	x	x	✓	x	m.g.
79/12	22.2m	"				✓	✓	✓	x	x	✓	x	Recrystallized.
"	35m	"				✓	✓	✓	x	✓	✓	x	m.g.
"	50m	"				✓	✓	✓	x	x	✓	x	vugs, euhedral qtz.
79/13	30m	"				✓	✓	✓			x	x	Tuff.
"	44.5m	"				✓		x	✓		x	x	m.g.
"	60m	"				✓	✓	✓	x	✓	x	x	Occ. large round clasts.
79/14	30m	"				✓	✓	x		x	x		Micaceous hem.
"	43.5m	"				✓	✓	✓	✓	✓	x	x	m.g.
"	60m	"				✓	✓	✓	x	✓	✓	x	m.g.
UMD79/121	6m	Jinjaree Valley				✓	✓	x	x	✓	x		Recrystallized.
"	7m	"	"			✓	x	✓	x	✓	x		"
"	23m	"	"			✓	✓	✓	x	✓	x		"
"	40m	"	"			✓	✓	x	✓	✓	x		f.g.
79/122	3m	"	"			✓	x	x	✓	x	x		Matrix supported.
"	11.5m	"	"			✓	x	x	x	✓	x		Vugs, vein qtz.
"	15m	"	"			✓	✓	x	✓	✓	x	x	Shale/vuggy ss.
"	30m	"	"				✓	✓	x	✓	✓	x	Layered
"	50m	"	"			✓	✓	✓	✓	✓	x	x	Limonite, dark clasts.
SUD79/29	10m	"	"			✓	✓	x	x	✓	x		f.g. limonite.
"	42m	"	"			✓	x	✓	✓	x	x		
"	69.5m	"	"			✓	✓		✓	x	x		tuff
"	76.7m	"	"			✓	x	x	x	✓	x		Acid volc.clasts.

APPENDIX 1: (cont'd)

Sample	Location	Quartz					H Ch. C S M	comments
		wr	r	sr	sa	a		
SUD79/29	77.1m	Jinjaree Valley			✓	✓	x x x	Ptw ₃ .
79/30	11m	"			✓	✓	x x ✓ x	Boxworks, vugs, limonite.
"	25m	"		✓	✓	✓	x ✓ x x	f.g. with clasts.
"	38.5m	"		✓	✓	✓	x ✓ ✓ x	Partial recrystalln. clasts.
79/31	20m	"		✓	✓	x	✓ ✓ x	Thin qtz.veinlets.
"	40.3m	"		✓	x	✓	x ✓ x	m.g.
"	58m	"		✓	x	x	✓ ✓ x	m-c.g., p.s.
"	63m	"		✓	✓	x	x ✓ x	Specular hem.
"	77.5m	"		✓	✓	x	x x	Occ. lge dark clasts
79/32	26.5m	"			✓	✓	x x ✓ x	Black, recrystall'd.
"	32m	"		✓	✓	x	x x x	Vugs, brecc.limonite
"	45m	"			✓	x	✓ ✓ x x	m.g.
SUD79/33	61.4m	Airstrip		✓	✓	✓	x x ✓ x	Recrystallized.
"	70m	"			✓	x	x x ✓ x	Partial recrystall'n
"	80m	"			✓	x	✓ x ✓ x	p.s., f-c.g.
79/34	132m	"						
"			✓	✓	✓	✓	x x	Tuff.
"	137m	"			✓	✓	x x ✓ x	Partial recrystalln.
"	141.2m	"			✓	✓	✓ x ✓ x	" qtz.veinlet.
UMD79/104	20m	Cliffdale		✓	✓	x	x ✓ x	Recrystallized.
"	52m	Fault sth of		✓	✓	x	✓ x x	Tuff.
"	82.5m	Junnagunna	✓	✓	✓	x	✓ ✓ x	Mottled, m.g..
79/105	20m	"		✓	✓	x	✓ ✓ x	Recrystallized.
"	35m	"		✓	✓	x	✓ x x	f-m.g.
"	50m	"	✓		✓		x x	Tuff.
"	69m	"		✓	✓	x	x ✓ x x	Euhedral qtz.on joint.
"	79m	"		✓	✓	x	✓ x x	Rounded qtz clasts.
"	81m	"		✓	✓	✓	✓ x x	f.g. with clasts.
UMD79/109	26m	Anomaly 22		✓	✓	✓	x x	Occ. mica & R.F.
"	35m	"		✓	✓	x	✓ ✓ x	m.g.
"	49m	"		✓	✓	✓	✓ x x	m.g.

Appendix 1 (cont'd)

Sample	Location	Quartz					H	Ch.	C	S	M	Comments
		wr	r	sr	sa	a						
T1	Traverse			✓			✓	x	x	✓	x	m.g.
T2	9645N			✓			✓	x	x	x	x	m.g.
T3	"			✓			✓	x	x	x	x	m.g.
T4	"			✓			✓	x	x	✓	x	m.g.
T5	"			✓			✓	✓	✓	x	x	m.g. Matrix supported.
T6	"				✓		✓	x	✓	x	x	m.g. Qtz cobbles.
T7	"			✓	✓		✓	x	✓	x	x	Matrix supported.
T8	"			✓	✓		✓	x	x	x	x	m.g.
T9	"			✓			✓	x	✓	x	x	m.g.
T10	"			✓			✓	x	✓	x	x	m.g. Matrix supported.
T11	NE dyke margin			✓	✓		✓	x	✓	x	x	m.g. Darker qtz.
T12	Traverse 9645N			✓			✓	x	✓	x	x	m.g.
T13	"				✓		✓	x	✓	✓	x	limonite.
T14	"			✓	✓		✓	x	x	✓	x	m.g.
T15	"					✓	✓	x	✓	x	x	c.g. with clasts.
T16	"			✓	✓		✓	x	✓	x	x	" " "
T17	"			✓			✓	x	x	✓	x	Occ. green grains.
T18	"			✓			✓	x	✓	x	x	
T19	"			✓	✓		✓	x	✓	x	x	Very crumbly.
T20	"					✓	✓	x	x	✓	x	A cobble, Camp Ridgeway.

APPENDIX 2

Tabulated thermoluminescence glow peak intensities
and glow peak temperatures for Westmoreland samples.

APPENDIX 2: TL data for samplesKey

76/4 32m refers to diamond drill hole UMD76/4 at a depth of 32 metres.
 S79/34 132m " " " " " SUD79/34 at a depth of 132 metres.
 P8 8-10m " " percussion drill hole UMD78/8 at a depth of 8-10 metres.
 N123 198' " " diamond drill hole N123 at a depth of 198 feet.
 NE1 104' " " " " " NE at a depth of 104 feet.
 H15 60' " " " " " H15 at a depth of 60 feet.
 WD6 36m " " " " " UWD76/6 at a depth of 36 metres.

*indicates that data has been obtained under different experimental conditions than those for the bulk of samples measured.

Inclination of non-vertical drill holes. (Magnetic bearing/inclination)

Jack/Garee Lens	Huarabagoo	Junnagunna
N7 (264/33)	NE18 (140/45)	UMD78/60 (040/45)
N26 (135/40)	H15 (181/26)	
N74 (135/40)	H25 (135/72)	
N123 (315/38)	H31 (314/40)	
N128 (315/40)	H66 (135/58)	
N129 (135/50)		
N130 (315/33)		
NE1 (135/45)		
NE10 (135/60)		
NE11 (148/60)		
NE23 (140/56)		

Sample	wt(mg)	Glow peak temperature (°C)					Glow peak intensity				
UMD76/4 32m	14.81	160	215	245	335		11.8	15.8	14.8	8.4	
76/5 32m	14.40	152	206	271	349		590	729	660	764	
" 39m	15.69	140	200	251	333		287	446	478	446	
" 45m	12.35	168	213	254	356		607	830	648	344	
" 53m	14.46	168	218	249	336		622	899	640	311	
" 60m	18.04	171	208	261	324		430	554	471	277	
76/6 30m	16.66	225	285	375			915	810	780		
" 44.8m	19.70	191	243	288	380		660	787	711	508	
" 60m	19.65	181	255	380			662	1,043	534		
76/7 17m	13.15	152	229	264	357		570	989	837	513	
" 25m	9.30	148	204	229	264	358	484	699	753	753	699
" 49m	15.95	157	188	273	322		815	1,003	2,571	831	
" 57m	15.60	153	181	240	264	358	513	593	705	641	401
76/8 20m	19.70	130	162	238	320		635	812	863	964	
" 44m	15.30	155	190	272	340		490	523	719	915	
" 70m	19.54	183	273	372			806	998	729		
76/15 40m	20.65	180	250	335			12.1	14.0	10.1		
" 86m	16.36	155	195	235	280	330	5.5	7.8	8.4	9.8	14.0
76/16 14m	16.21	141	177	268	329		185	231	401	432	
" 21m	20.41	142	208	263	330		269	318	404	441	
" 30m	18.76	145	174	281	334		213	213	320	453	
" 40m	14.40	152	193	277	327		208	243	365	399	
76/17 34m	14.35	139	180	236	261	335	383	453	523	557	470
" 46m	22.63	158	212	226	258	369	409	508	508	431	265
" 58m	12.25	176	222	248	356		551	694	612	367	
" 71m	18.45	201	230	264	358		434	420	420	298	
" 84m	17.89	175	201	230	243	360	503	559	559	503	266
76/18 21m	12.45	140	212	263	337		341	212	263	337	
" 36m	13.30	142	166	227	251	339	376	451	602	564	376
" 41m	15.60	145	189	262	337		353	353	481	321	
" 66m	10.20	147	169	235	261	360	417	466	564	539	368
" 81m	7.75	151	198	225	265	367	581	774	774	710	355
77/19 40m	16.94	140	191	266	328		457	649	649	767	
" 55m	23.25	181	221	273	350		634	774	634	344	
" 70m	14.48	170	239	276	342		501	639	622	397	
" 85m	17.30	163	206	254	353		578	665	578	405	
" 106m	20.52	161	213	272	353		414	536	487	341	
77/20 30m	14.50	151	195	262	329		397	569	552	603	
" 45m	16.25	145	206	276	345		354	554	615	692	

Sample	wt(mg)	Glow peak temperature(°C)					Glow peak intensity				
UMD77/20 60m	13.01	156	199	250	344		576	730	653	423	
" 80m	17.71	156	210	269	357		325	508	452	282	
" 111m	23.20	177	231	264	377		517	636	539	345	
77/32 25m	17.63	140	195	259	333		411	567	695	794	
" 36m	16.40	164	205	219	249	340	686	976	976	808	320
" 47m	8.95	148	190	231	272	348	475	642	698	615	559
" 58m	15.95	164	213	274	363		502	627	533	376	
" 70m	11.25	147	183	233	265	368	356	444	467	533	444
77/35 24m	14.83	137	192	267	333		388	489	624	944	
" 35m	17.25	150	200	267	344		406	522	537	348	
" 46m	15.79	154	212	277	360		380	507	522	380	
" 57m	14.46	145	210	262	336		346	501	501	380	
" 69m	12.62	148	192	262	365		416	555	495	396	
77/39 18m	6.35	196	223	348			787	787	472		
" 22m	17.63	140	198	245	257	337	425	652	780	780	681
" 30m	12.86	152	198	231	253	353	428	700	739	680	311
" 50m	15.25	183	225	258	338		689	1,066	789	393	
" 70m	15.99	164	206	263	302	358	1,376	1,501	2,502	1,110	469
77/40 15m	12.88	164	206	232	279	369	524	699	718	582	427
" 25m	11.75	152	204	240	269	345	681	809	851	809	723
" 40m	14.80	134	209	262	347		338	574	541	405	
" 54m	14.50	142	172	237	266	354	345	431	569	534	345
" 69m	14.55	144	201	271	379		378	481	481	344	
77/42 30m	12.23	146	179	268	339		450	491	1,083	1,002	
" 40m	17.10	173	221	268	344		599	746	614	336	
" 60m	17.00	163	210	266	368		441	529	544	382	
" 75m	17.55	150	203	271	373		313	556	527	399	
" 88m	15.47	157	207	270	351		323	372	549	388	
" 98m	10.21	143	194	273	338		416	490	612	686	
78/58 20m	17.85	150	195	262	343		532	616	812	756	
" 44m	16.62	145	240	315			361	481	933		
78/59 30m	14.00	170	215	280	380		607	768	786	536	
" 50.5m	18.00	169	224	256	337		472	639	556	389	
" 60m	17.10	204	260	355			934	877	643		
" 61.6m	16.65	170	235	255	363		435	541	480	240	
" 70.5m	16.14	193	229	258	370		496	465	449	325	
" 85.5m	15.67	143	266	335			255	415	383		
" 88.8m	14.81	144	180	265	315		473	405	692	912	
" 98.5m	13.63	151	264	337			330	587	404		
78/60 19m	-	187	238	272	385		10.5	14	11	6	*

Sample	wt(mg)	Glow peak temperature (°C)					Glow peak intensity				
UMD78/60 42m	16.60	148	176	209	247	264	331	451	482	482	467
" "	"	372					301				
" 65m	13.30	143	235	356			113	207	338		
" 79m	20.55	155	196	262	342		754	895	1,114	652	
" 91.2m	16.30	167	201	220	263	351	491	583	552	491	261
" 124m	17.50	139	173	255	333		343	400	514	314	
" 150m	19.04	148	169	244	264	331	210	249	263	249	131
78/64 60m	16.89	205	265	360			13.6	12.4	8.9	*	
" 100m	21.21	165	225	250	340		8.2	8.9	9.2	6.4	*
78/69 26m	22.05	142	206	240	267	334	374	601	669	669	703
" "	"	352					658				
" 38m	21.16	152	193	226	255	354	402	567	579	520	331
" 50m	14.98	164	196	247	334	360	484	567	501	401	367
" 61m	18.09	141	158	182	254	338	387	442	442	484	415
" "	"	352					387				
78/71 25m	19.89	161	220	266	344		528	754	855	779	
" 51m	20.10	230	280	365			1,095	896	498		
" 70m	20.30	218	275	378			1,281	1,034	665		
78/72 30m	20.59	138	200	244	262	339	376	607	680	680	680
" "	"	361					631				
" 40m	15.37	138	196	258	328	350	390	553	586	683	520
" 65m	16.15	142	197	225	262	349	372	480	480	433	341
" 80m	17.77	139	170	199	272	355	295	366	394	408	422
" "	"	376					338				
" 110m	20.21	131	188	249	332		198	247	272	173	
88/74 28m	10.30	150	185	260	320		6.3	7.0	10.5	10.7	*
" 49.7m	12.89	170	235	315			13.2	15.1	17.0	*	
" 65m	23.40	138	206	264	340		444	735	829	889	
" 70m	15.19	180	255	325			8.2	9.9	12.5	*	
" 112m	17.58	185	260	365			10.8	14.8	8.5	*	
78/77 25m	21.74	144	179	262	336		149	184	195	460	
" 40m	21.05	148	173	276	338		226	238	321	249	
" 60m	13.20	162	198	233	274	373	455	530	530	511	360
" 80m	15.66	192	235	266	352		463	479	463	399	
" 100m	21.00	140	188	232	256	330	202	250	286	298	298
78/79 30m	16.26	140	195	254	335		707	1,046	1,107	923	
" 70m	18.25	175	202	265	368		603	712	548	411	
" 80m	13.61	168	203	234	263	367	533	661	680	551	441
" 103m	10.64	153	199	219	254	350	587	752	799	705	446
" 104m	14.05	160	255	345			20.3	23.1	6.4	*	

Sample	wt (mg)	Glow peak temperature (°C)						Glow peak intensity				
UMD78/79	108m	13.20	144	214	234	261	362	341	455	473	473	303
"	110m	19.60	175	217	270	(321)		2,211	1,960	3,467		
"	111m	14.84	165	202	258	356		337	337	320	202	
"	118m	10.63	157	200	264	308	373	3,340	2,305	6,397	1,223	470
78/81	30m	14.75	149	196	244	339		373	475	492	373	
"	40m	18.66	152	201	244	358		482	643	536	348	
"	50m	22.27	155	209	261	367		449	718	573	404	
"	60m	16.69	148	173	195	226	246	539	614	689	659	569
"	"	"	353					359				
"	70m	6.71	147	206	272	364		484	745	633	447	
78/82	28m	12.45	137	197	240	269	335	522	723	843	884	1,145
"	39m	15.11	150	187	207	274	357	364	463	496	496	397
"	51m	17.05	176	200	234	280	350	440	499	469	455	367
"	62m	18.05	167	197	229	268	342	402	457	457	416	305
"	74m	17.85	184	209	264	373		448	504	392	280	
78/83	35m	23.40	185	245	300	355		17.1	21.4	22.9	27.1	*
"	36m	16.75	142	184	228	276	346	373	537	657	672	776
"	"	"	380					642				
"	44m	13.65	160	223	258	357		476	659	586	366	
"	53m	18.35	149	196	203	269	358	381	545	559	490	327
"	"	"	379					300				
"	55m	19.16	167	230	284	370		587	861	757	496	
"	61m	15.83	140	200	224	244	334	379	553	553	505	332
"	70m	20.15	150	226	282	355		447	720	620	471	
"	70m	18.76	145	173	216	252	360	400	493	506	480	373
78/84	32m	19.34	150	193	248	348	366	957	1,034	1,448	543	478
"	54m	19.97	141	199	225	249	347	401	576	576	551	401
"	"	"	362					351				
"	76m	15.90	141	186	259	339	361	362	503	503	440	425
"	98m	12.89	137	161	199	259	340	310	368	368	465	427
"	"	"	368					388				
"	120m	15.87	139	172	244	269	346	252	315	331	347	378
"	"	"	365					347				
78/85	32m	13.45	152	220	234	268	349	446	669	706	651	558
"	41m	11.66	154	219	237	272	349	472	665	665	600	407
"	50m	15.31	144	198	225	260	343	359	523	555	539	392
"	60m	12.85	176	221	261	332		623	700	661	350	
"	70m	12.50	180	227	257	389		560	640	560	320	
78/86	30m	14.65	225	265	350			15.7	14.3	8.5	*	
"	60m	13.32	215	270	360			14.3	11.3	7.1	*	
"	100m	16.55	160	225	340			27.2	14.5	9.0	*	

Sample		wt(mg)	Glow peak temperature (°C)					Glow peak intensity				
UMD78/87	27m	22.85	146	164	231	283	338	186	197	241	284	438
"	32m	18.79	167	216	273	345		506	692	585	386	
"	37m	19.40	179	204	262	339		348	387	348	258	
"	43m	12.80	160	205	249	340		430	566	449	313	
"	44m	10.10	179	209	262	320		644	743	668	396	
78/88	17m	-	153	209	257	352		6.25	9.75	9	6	*
"	25m	13.21	185	222	250	328		568	643	568	341	
"	33m	15.84	198	224	264	348		568	631	552	284	
"	41m	19.65	174	232	259	347		407	509	445	229	
"	49m	13.17	155	179	262			9,871	7,897	23,235		
78/89	10m	19.30	150	209	251	352		285	492	505	376	
"	30.1m	24.44	185	265	350			5.9	10.8	6.1	*	
"	50m	13.91	161	227	272	368		539	647	629	252	
"	70.1m	21.90	205	260	365			12.3	9.8	6.4	*	
78/90	16m	19.35	151	170	202	259	338	271	323	388	401	426
"	24m	17.40	174	218	272	350		460	575	460	316	
"	32m	-	171	223	261	343		9.5	12	10	6	*
"	40m	20.05	181	214	223	254	339	599	798	823	648	349
"	49m	20.40	173	231	266	341		380	576	515	270	
78/91	8m	19.70	139	264	336			228	355	457		
"	18m	18.03	148	172	243	260	343	347	361	471	458	277
"	28m	15.11	149	180	236	268	344	414	480	761	794	430
"	38m	16.06	151	199	241	259	341	389	436	451	467	311
"	49m	18.47	142	166	230	259	339	379	406	487	501	311
78/92	28m	19.90	165	245	330			452	754	427		
"	35m	11.30	176	249	350			796	1,106	664		
"	70m	21.73	200	281	373			529	690	437		
"	106m	19.70	158	179	275	354		406	419	558	355	
79/100	26m	18.10	143	195	260	340		276	345	414	345	
"	44m	18.66	168	233	264	354		429	496	482	362	
"	62m	21.31	143	189	268	363		399	587	540	469	
"	78m	19.06	150	199	269	382		433	656	525	420	
"	94.5m	20.65	177	277	350			194	242	145		
79/101	34m	18.31	171	238	263	352		669	560	546	573	
"	52m	14.16	170	195	262	326		918	918	600	282	
"	70m	17.60	174	227	260	340		682	909	682	313	
"	88m	15.05	176	205	261	339		532	565	565	465	
"	109m	15.60	164	200	273	321		513	449	1,410	256	
79/102	28m	15.85	194	229	277	253		394	473	442	410	
"	33m	12.15	198	222	361			617	658	288		
"	39m	12.76	203	221	261	355		666	725	588	294	

Sample	wt(mg)	Glow peak temperature(°C)					Glow peak intensity					
UMD79/102	44m	15.93	162	223	254	360		565	879	628	282	
"	50m	17.25	179	204	221	264	357	464	522	551	435	232
79/103	30m	17.30	181	225	271	353		347	434	361	173	
"	48m	18.35	170	223	262	346		395	463	422	218	
"	66m	12.68	135	192	260	353		394	513	591	552	
"	84m	18.55	145	161	252	361		418	458	485	270	
"	100m	19.50	169	266	344			346	410	256		
79/106	30m	18.46	151	198	233	262	342	352	460	488	474	379
"	50m	20.10	210	232	261	362		448	448	398	261	
"	70m	18.50	157	188	238	265	386	378	432	446	432	324
"	90m	16.16	203	224	264	357		511	495	433	325	
"	108m	18.37	165	210	272	319		653	544	953	395	
79/107	30m	19.15	144	182	269	334		313	405	548	783	
"	50m	17.20	143	200	265	344		334	378	494	378	
"	70m	20.35	153	192	263	349		491	860	516	479	
"	90m	24.95	165	233	270	359		471	471	441	261	
"	110m	20.85	170	210	268	325		1,007	1,079	2,134	719	
79/108	45m	16.10	167	193	255	349		466	528	621	466	
"	65m	21.54	160	200	264	364		371	464	499	325	
"	85m	18.88	146	186	259	338		238	291	503	450	
"	110m	15.35	173	204	251	344		586	619	717	407	
"	130m	24.98	144	196	269	338		360	460	550	440	
79/110	15m	25.90	146	232	279	362		627	772	656	405	
	28.2m	27.75	158	221	284	367		450	505	649	568	
"	47.6m	22.30	167	213	270	290	362	404	415	504	538	762
"	60.1m	23.80	194	228	276	385		756	809	767	462	
"	75m	25.35	158	213	287	362		552	710	671	392	
79/112	23m	17.50	138	197	275	334		229	300	371	657	
"	43m	18.55	170	188	231	256	367	445	499	431	404	270
"	63m	16.45	184	215	250	346		441	502	426	304	
"	83m	17.59	169	196	229	263	356	441	512	455	398	242
"	102m	16.10	154	209	264	310		9,193	6,956	19,875	3,975	
79/114	25m	18.65	144	210	260	336		335	483	550	590	
"	50m	12.94	172	230	268	346		560	618	580	348	
"	70m	14.91	166	187	219	255	340	469	520	537	453	201
"	95m	12.65	191	249	365			593	494	375		
"	107m	16.15	170	198	261	362		356	356	372	294	
79/116	40m	19.40	138	198	261	333		258	361	399	541	
"	50m	11.64	139	201	264	339		258	408	430	473	
"	60m	16.24	157	201	224	260	364	431	554	585	446	323

Sample		wt(mg)	Glow peak temperature (°C)					Glow peak intensity				
UMD79/116	69.5m	12.18	203	234	266	356		534	493	452	246	
"	77.5m	18.55	146	211	278	359		243	364	404	431	
79/117	30m	21.23	178	217	257	340		294	341	294	224	
"	34m	18.74	221	256	344			480	374	267		
"	39m	15.70	158	218	264	353		382	541	446	271	
"	44m	17.52	166	218	267	342		400	514	371	200	
"	49m	26.00	160	211	256	369		423	577	442	231	
79/119	26m	18.69	189	229	269	303	368	589	883	749	722	495
"	31m	-	203	226	249	341		6	7	6	3.5	*
"	37m	22.77	164	215	266	345		439	659	483	264	
"	43m	24.94	170	228	264	345		501	682	531	281	
"	49m	19.29	172	218	256	332		518	752	570	259	
79/123	25m	19.25	151	173	249	268	335	377	468	675	675	364
"	45m	13.20	152	235	263	334		379	549	473	303	
"	60m	14.39	141	181	223	272	332	452	521	678	573	851
"	80m	18.55	143	183	272	334		350	404	539	755	
"	100m	12.20	188	226	262	361		1,332	820	779	492	
"	120m	17.65	160	193	277	365	375	510	751	637	737	737
79/124	30m	24.99	141	196	234	266	333	340	470	470	430	420
"	"	"	353					390				
"	48m	17.44	168	223	252	337	356	459	659	559	315	287
"	66m	17.74	163	200	256	338	354	479	564	423	225	225
"	84m	19.70	161	185	220	261	358	609	622	596	508	228
"	100m	17.85	160	189	231	261	341	476	532	560	504	336
"	"	"	369					280				
79/125	25m	18.22	143	216	234	266	345	370	549	576	576	521
"	32m	18.18	156	201	223	264	348	605	729	743	715	523
"	38m	19.20	170	224	248	337		495	677	599	286	
"	44m	12.33	150	200	233	265	336	446	527	568	527	406
"	50m	14.75	179	213	261	347		475	610	475	288	
79/126	27m	24.44	138	191	226	267	338	266	368	409	440	481
"	"	"	359					389				
"	33m	26.55	159	198	229	261	332	377	452	452	377	264
"	"	"	356					245				
"	39m	22.85	173	195	225	264	359	438	481	481	438	241
"	"	"	378					219				
"	45m	21.94	153	207	259	367	384	319	410	422	251	228
"	50m	19.96	162	205	249	273	370	426	551	501	451	288
79/127	26m	19.05	150	225	267	355		367	669	604	525	
"	32m	11.50	146	229	265	353		370	717	609	391	
"	38m	16.45	152	214	234	267	345	456	653	653	547	334

Sample		wt(mg)	Glow peak temperature (°C)				Glow peak intensity					
UMD79/127	44m	15.65	153	217	257	347		591	942	703	319	
"	50m	14.90	154	215	268	341		453	705	520	336	
79/133	25m	19.97	160	198	259	345		300	401	351	351	
"	37m	21.15	160	203	260	352		307	426	378	437	
"	39.1m	15.60	178	227	258	339		577	833	641	272	
"	46.2m	13.03	159	203	268	342		460	537	576	595	
"	50m	15.90	175	204	254	329		503	645	503	314	
79/134	38m	19.35	140	195	271	337		310	426	517	801	
"	43m	12.40	169	200	231	260	341	444	565	585	544	363
"	48m	13.90	214	257	351			683	576	324		
"	52m	17.54	165	216	257	345		570	941	684	342	
79/135	16m	17.15	159	247	258	359		379	583	569	437	
"	24m	19.84	221	242	365			478	491	290		
"	32m	19.10	191	227	249	338		576	589	510	262	
"	40m	21.02	140	188	269	332		238	262	333	392	
"	48m	18.60	142	196	263	338		296	376	349	323	
79/137	27m	15.44	142	192	270	337		194	259	340	372	
"	30m	18.15	140	188	242	273	336	413	468	606	579	702
"	36m	19.25	149	182	197	241	360	312	403	416	416	260
"	43m	20.30	200	234	272	347		468	493	443	271	
"	50m	20.05	166	229	268	370		349	449	374	237	
79/138	41m	14.95	140	199	270	343		268	334	468	602	
"	45.1m	15.55	138	191	258	342		402	579	595	531	
"	50.2m	17.08	215	225	260	354		468	556	439	234	
"	55.6m	16.37	154	194	245	341		367	504	489	275	
"	60m	18.15	146	206	233	256	349	358	496	551	523	275
79/139	34m	23.90	174	213	231	262	362	314	418	439	335	209
"	38m	21.69	166	195	226	259	365	507	588	588	461	219
"	42m	20.53	176	221	256	346		365	475	390	207	
"	46m	19.89	172	225	348			440	490	277		
"	50m	16.15	185	209	264	380		449	495	433	279	
79/140	20m	15.75	144	198	264	337		254	429	460	508	
"	28m	18.51	144	230	336			1,688	594	405		
"	36m	20.90	181	210	252	272	359	431	467	467	455	383
"	43m	18.20	214	246	358			659	246	358		
"	50m	20.00	174	212	251	274	353	425	488	475	450	325
79/143	11m	20.73	202	227	260	349		386	410	374	205	
"	17.9m	18.97	209	242	345			527	501	290		
"	25m	20.69	142	194	262	333		205	266	338	314	
"	32m	17.95	148	185	254	344		292	348	446	334	

Sample	wt(mg)	Glow peak temperature(°C)						Glow peak intensity				
UMD79/143	40m	17.80	184	245	270	319		351	449	421	225	
79/144	5m	19.30	154	176	261	351		285	311	415	246	
"	11m	16.00	148	269	345			297	375	391		
"	17m	19.61	142	169	243	258	361	280	357	459	459	306
"	23m	16.75	142	216	250	341		328	448	478	299	
"	29m	19.03	168	195	262	347		552	604	578	342	
79/145	7m	20.45	141	168	244	266	333	269	318	367	367	342
"	14m	19.15	223	245	359			496	470	235		
"	21m	18.51	212	262	353			432	351	243		
"	28.5m	16.69	171	189	262	341		389	449	389	419	
"	30m	19.75	149	202	264	342		228	291	367	418	
79/146	10m	22.24	140	241	278	352		247	337	360	629	
"	18m	18.84	190	223	278	394		491	584	451	265	
"	24m	19.10	178	221	260	359		557	681	510	262	
"	32m	19.35	216	266	361			491	452	323		
"	40m	19.90	206	262	353			452	427	327		
78/60	12m	12.60	140	188	260	320	352	595	921	1,040	944	754
"	13m	11.80	158	214	254	358		1,017	1,559	1,093	695	
"	14m	19.71	163	215	244	344		649	817	700	416	
"	15m	26.50	182	227	264	354		494	600	626	264	
"	18m	18.30	138	228	259	318		454	798	847	1,180	
"	20m	16.79	200	250	360			2,341	1,918	1,221		
"	21m	20.74	197	224	260	345		1,408	1,350	1,321	993	
"	22m	17.10	168	204	241	354		1,310	1,667	1,637	1,094	
"	23m	19.76	162	200	228	258	364	1,118	1,635	1,533	1,447	1,123
"	24m	26.16	214	242	262	382		1,662	1,667	1,563	1,151	
"	25m	21.13	211	242	266	358		1,406	1,496	1,391	984	
"	26m	22.19	200	234	254	367		1,821	2,055	1,893	1,334	
"	27m	17.24?	136	196	246	267	346	626	1,189	1,323	1,235	1,079
"	28m	23.55	136	186	259	324		399	531	781	896	
"	29m	13.60	136	188	262	332		603	728	919	1,287	
"	30m	-	137	188	234	254	327	8.4	13.5	18.1	16.8	19.3*
"	31m	17.50	148	193	256	346		617	903	1,154	1,034	
"	32m	19.43	150	207	270	341		592	937	1,132	1,076	
"	33m	17.00	198	240	265	344		1,141	1,376	1,376	1,065	
"	34m	15.52	198	229	266	357		1,070	1,153	1,121	722	
"	35m	8.83	184	237	259	330		1,416	1,427	1,359	1,212	
"	36m	18.69	189	220	246	338		1,332	1,380	1,268	647	
"	37m	10.70	158	200	226	257	344	1,009	1,234	1,234	1,196	785
"	38m	24.80	146	204	266	354		540	915	988	823	

Sample	wt(mg)	Glow peak temperature(°C)						Glow peak intensity				
UMD78/60	39m	19.75	156	208	264	346		562	759	957	653	
"	40m	21.66	206	266	360			882	979	586		
"	41m	20.55	172	222	254	352		925	1,075	1,051	715	
"	43m	15.20	193	264	340			368	368	592		
"	44m	22.95	204	250	362			1,007	1,098	584		
"	48m	8.45	194	225	253	352		1,538	1,598	1,503	911	
"	46m	21.33	200	234	259	338		980	989	942	525	
"	47m	22.00	168	194	232	258	340	855	1,055	1,123	1,068	550
"	48m	18.60	200	232	253	342		704	785	785	462	
"	49m	18.67	202	256	342			852	1,018	745		
"	50m	17.50	210	266	344			749	1,051	600		
"	51m	14.84	204	238	266	317		1,637	2,109	1,765	1,004	
"	52m	13.53	202	250	340			953	1,168	658		
"	53m	17.25	194	260	340			991	1,096	771		
"	54m	22.30	189	208	230	271	360	996	1,094	1,000	848	507
"	55m	24.40	178	208	229	256	356	828	1,012	992	889	471
"	56m	18.20	192	212	240	263	332	659	703	786	747	516
"	57m	23.41	195	230	256	333		756	803	859	632	
"	58m	10.05?	188	238	256	334		1,263	1,413	1,383	876	
"	59m	10.11+	194	214	250	355		1,840	1,949	1,949	1,187	
"	60m	10.96	208	244	270	347		1,186	1,359	1,296	1,031	
"	61m	12.76	178	230	258	327		1,199	1,693	1,505	807	
"	62m	17.84	180	192	220	250	321	1,205	1,379	1,485	1,289	589
"	63m	15.36	192	218	232	254	318	1,348	1,426	1,419	1,302	645
"	64m	20.63	138	196	234	266	352	417	543	645	674	1,236
"	66m	15.78	204	257	319	339		1,090	2,725	1,584	1,578	
"	67m	20.80	199	237	263	344		447	558	529	438	
"	68m	16.69	190	235	256	336		725	905	857	473	
"	69m	26.99	223	257	270	330		508	682	697	433	
"	70m	18.35	194	247	306			975	1,417	638		
"	71m	17.13	174	196	238	260	340	555	648	765	800	485
"	72m	21.50	182	195	253	327		660	712	898	540	
"	73m	17.35	208	262	278	341	364	888	1,037	928	611	548
"	74m	21.74	210	243	268	327	356	837	938	865	543	483
"	75m	20.98	196	262	340			524	839	724		
"	76m	23.15	154	201	278	332		229	389	652	916	
"	77m	17.29	199	268	336			850	1,243	920		
"	78m	16.90	155	198	258	332		692	1,041	1,296	793	
"	80m	19.65	152	186	250	337		712	1,064	1,160	646	
"	81m	19.50	195	259	341	365		1,056	1,159	723	728	
"	82m	14.60	142	228	250	263	331	548	959	1,000	952	815

Sample	wt (mg)	Glow peak temperature (°C)						Glow peak intensity				
UMD78/60 83m	17.72	200	250	265	340			1,078	1,174	1,174	615	
" 84m	15.30	208	270	344	360			869	1,033	673	660	
" 85m	23.28	149	188	256	340	360		434	760	803	511	485
" 86m	15.35	171	190	259	334			1,094	1,231	1,537	899	
" 87m	25.72	196	232	260	330	368		1,011	1,100	1,120	642	622
" 88m	21.80	198	228	260	340	376		1,248	1,335	1,202	679	674
" 89m	23.25	184	223	251	339	1,187		1,269	1,191	581		
" 90m	23.95	200	228	246	346	366		1,223	1,236	1,165	622	630
" 91m	18.01	194	228	261	355			3.40	3.35	3.20	2.80	*
" 92m	24.47	196	224	249	348	365		1,132	1,189	1,124	588	588
" 93m	25.36	205	238	273	368			935	962	907	524	
" 94m	-	177	200	266	340	370		16.7	18.9	23.6	15.6	14.0*
" 95m	21.85	172	205	268	372			1,011	1,309	1,057	632	
" 96m	-	204	222	268	364			27.1	27.4	22.8	12.7	*
" 97m	21.49	202	234	263	370			1,084	1,154	1,135	670	
" 98m	15.91	208	230	268	364			1,364	1,433	1,326	691	
" 99m	21.94	191	236	270	370			1,076	1,180	1,130	665	
" 100m	22.01	200	232	264	368			1,027	1,059	977	554	
" 101m	14.62	164	198	220	254	341		1,033	1,252	1,245	1,142	616
" 102m	17.70	202	230	260	361			1,085	1,040	983	661	
" 103m	17.75	193	237	263	378			1,079	1,114	1,015	676	
" 104m	16.26	180	223	244	272	345		1,039	1,181	1,218	1,070	677
" "	16.26	364						664				
" 105m	22.04	203	238	260	354			1,107	1,112	1,084	631	
" 106m	16.61	210	237	266	361			1,222	1,198	1,090	632	
" 107m	17.49	193	224	253	335	362		1,149	1,155	1,184	743	749
" 108m	20.70	170	194	219	259	342		1,068	1,261	1,285	1,140	594
" "	20.70	372						609				
" 109m	10.95	158	196	218	256	352		1,406	1,918	1,945	1,626	785
" 110m	12.87	198	238	265	340	365		1,041	1,049	862	699	692
" 111m	17.95	176	200	234	274	348		969	1,114	1,159	1,070	657
" "	17.95	376						663				
" 112m	11.95	176	200	264	354	377		1,130	1,264	1,247	745	770
" 113m	15.85	172	202	266	354	378		921	1,066	1,155	694	700
" 114m	18.60	174	192	239	267	366		887	959	1,048	1,183	629
" 115m	7.72	176	189	258	362			1,308	1,360	1,425	972	
" 116m	14.13	196	224	240	260	331		764	821	878	934	609
" "	14.13	360						602				
" 117m	15.15	192	236	264	346			891	990	997	726	
" 118m	12.50	170	201	235	267	339		1,016	1,128	1,296	1,240	896
" "	12.50	366						808				

Sample		wt(mg)	Glow peak temperature(°C)					Glow peak intensity				
UMD78/60	119m	17.78	168	199	222	265	350	939	1,153	1,288	1,069	591
"	"	17.78	368					579				
"	120m	20.29	156	197	227	259	343	694	951	991	1,020	626
"	"	20.29	371					660				
"	121m	17.80	158	186	226	262	326	713	865	1,045	1,107	1,084
"	"	17.80	349					961				
"	122m	15.40	209	246	268	364		896	968	981	792	
"	123m	20.34	180	192	234	262	340	855	949	1,052	1,121	841
"	"	20.34	364					846				
"	125m	22.65	200	226	264	347	370	852	901	993	698	680
"	126m	17.00	139	179	240	270	332	341	547	706	765	1,418
"	127m	17.38	184	236	274	333		639	823	932	967	
"	128m	23.29	140	179	274	334	343	223	348	648	790	803
"	129m	23.56	184	237	282	339		390	577	671	1,167	
"	130m	18.55	144	189	237	265	334	388	712	933	997	981
"	131m	17.52	190	270	338			788	1,050	896		
"	132m	20.60	202	262	331	346		578	752	714	684	
"	133m	13.48	201	274	336	353		675	1,053	912	883	
"	134m	15.60	202	236	264	338	356	814	1,038	1,090	923	871
"	135m	17.65	197	261	335	365		884	1,088	793	714	
"	136m	17.30	194	263	338			1,023	1,462	1,063		
"	137m	20.54	182	252	357			1,047	1,164	696		
"	138m	15.15	182	204	266	360		574	601	713	614	
"	139m	20.05	207	238	265	329	350	698	833	888	823	908
"	140m	13.65	201	228	258	330		989	1,004	960	777	
"	141m	18.35	158	204	254	321		403	545	1,074	757	
"	142m	20.05	176	202	238	260	325	818	793	758	768	429
"	143m	-	170	231	260	336		12.6	14.8	15.6	7.8	*
"	144m	14.61	171	193	236	258	332	1,081	1,150	1,225	1,205	609
"	"	14.61	372					500				
"	145m	13.10	166	227	262	324	364	641	771	794	489	435
"	146m	16.10	167	202	246	266	341	787	943	1,074	968	443
"	147m	14.60	202	233	267	359		979	973	952	425	
"	148m	19.85	170	203	233	278	340	625	695	730	640	383
"	149m	16.72	172	204	228	256	332	526	532	628	748	449
"	151m	21.45	154	214	261	325	358	541	601	681	569	466
"	152m	19.76	181	242	270	343		526	683	774	405	
"	153m	17.19	165	204	264	330		448	524	634	460	
"	154m	14.59	168	222	265	334		528	651	781	535	

Sample	wt(mg)	Glow peak temperature ($^{\circ}\text{C}$)					Glow peak intensity				
UMD78/77 23m	-	177	222	284	333		12.8	18.0	21.1	32.5	*
" 24m	15.23	168	212	268	319		519	657	978	1,654	
" 26m	19.76	150	180	220	268	332	273	364	496	703	1,315
" 27m	18.61	208	266	344			1,064	1,290	1,295		
" 28m	19.27	199	251	332	357		1,235	1,604	1,629	1,437	
" 29m	20.29	192	234	269	342		655	941	1,173	1,341	
" 30m	14.65	200	236	268	344		1,058	1,208	1,229	1,222	
" 31m	18.65	204	272	343			697	987	917		
" 32m	19.21	203	272	350			864	937	770		
" 33m	17.80	172	204	234	274	338	506	640	781	1,028	1,213
" 34m	19.60	195	268	338			663	954	883		
" 35m	9.09?	176	223	262	323		605	847	990	1,419	
" 36m	16.83	142	190	265	324		321	469	761	1,337	
" 37m	17.23	139	170	217	268	317	272	308	400	696	1,288
" 38m	18.30	148	192	276	330		366	481	760	1,098	
" 39m	13.19	133	184	254	318		569	644	955	963	
" 41m	14.76	138	177	254	320		610	705	982	799	
" 42m	26.34	150	195	258	336		649	786	915	645	
" 43m	13.40	132	172	253	328		731	925	1,187	948	
" 44m	10.91	137	184	254	332	351	862	1,155	1,338	1,054	990
" 45m	15.70	138	190	246	336		694	1,115	1,166	866	
" 46m	15.65	154	192	260	352		665	907	1,118	907	
" 47m	15.55	140	212	274	348	378	624	1,016	1,170	1,061	1,025
" 48m	9.84	136	190	253	347		793	1,179	1,280	965	
" 49m	13.88	134	190	247	328	360	829	1,254	1,383	1,268	1,102
" 50m	20.00	138	164	223	243	328	725	965	1,340	1,235	820
" 51m	17.20	138	164	193	222	254	1,035	1,331	1,535	1,581	1,500
" "	17.20	332					1,029				
" 52m	16.93	140	232	259	343	362	644	1,105	1,087	939	856
" 53m	16.88	150	191	234	258	360	883	1,250	1,440	1,363	995
" 54m	20.73	162	238	260	359		950	1,433	1,336	921	
" 55m	16.49	136	227	260	343		740	1,219	1,255	1,055	
" 56m	16.81	141	188	246	338		648	904	1,005	797	
" 57m	15.54	143	194	264	340		779	1,042	1,236	1,075	
" 58m	12.05	160	204	264	359		778	913	1,120	1,046	
" 59m	20.70	143	195	255	360		691	967	1,000	715	
" 61m	14.44	145	184	236	257	346	734	928	1,004	983	755
" 62m	14.35	145	190	264	359		746	941	864	718	
" 63m	7.55	130	185	245	346		993	1,510	1,497	1,205	
" 64m	10.25	128	188	261	348		790	1,366	1,259	1,102	
" 65m	15.02	135	200	264	342		573	866	985	999	

Sample	wt(mg)	Glow peak temperature($^{\circ}$ C)						Glow peak intensity				
UMD78/77 66m	9.64	187	265	345	368		1,027	1,100	871	902		
" 67m	10.05	204	263	353			1,294	1,214	866			
" 68m	17.93	140	199	262	358		669	1,071	1,009	747		
" 69m	10.85	142	203	249	360		922	1,272	1,134	894		
" 70m	18.29	149	192	264	346		662	826	908	847		
" 71m	15.03	166	192	239	274	368	1,204	1,417	1,417	1,557	951	
" 72m	16.74	168	203	236	259	356	1,004	1,081	1,135	1,135	902	
" 73m	22.73	170	226	262	364		1,087	1,245	1,166	919		
" 74m	12.90	143	190	258	361		791	1,101	1,023	814		
" 75m	15.82	134	178	224	256	336	948	1,212	1,226	1,258	999	
" 76m	22.80	146	194	258	350		785	1,013	1,026	934		
" 77m	18.42	138	168	198	270	360	852	1,048	1,118	1,178	1,075	
" 78m	14.54	156	196	222	252	338	1,190	1,355	1,396	1,369	1,107	
" 79m	13.36	149	192	232	270	370	928	1,145	1,108	1,108	891	
" 81m	10.40	178	224	258	340		1,375	1,375	1,298	923		
" 82m	17.85	164	184	218	253	352	1,087	1,165	1,115	1,148	997	
" 83m	20.53	150	199	262	354		701	979	955	838		
" 84m	22.66	146	191	246	346		852	1,249	1,143	869		
" 85m	22.49	166	224	266	368		1,152	1,383	1,174	711		
" 86m	22.26	172	198	263	359		1,056	1,155	1,038	813		
" 87m	20.20	146	188	254	333	358	738	1,040	1,010	822	837	
" 88m	21.39	140	188	262	346		711	930	949	893		
" 89m	13.75	137	182	248	345		836	1,309	1,200	975		
" 90m	18.18	146	199	258	340	363	770	979	1,056	765	803	
" 91m	15.54+	144	186	254	340		965	1,223	1,216	933		
" 92m	19.20	155	187	221	254	340	1,021	1,292	1,266	1,203	859	
" 93m	20.20	146	195	260	353		757	1,000	1,040	926		
" 94m	23.00	146	199	264	351		804	1,165	1,117	965		
" 95m	22.05	161	202	232	265	357	785	957	934	961	785	
" 96m	15.07	153	190	247	349		995	1,175	1,088	849		
" 97m	15.05	128	177	253	328	346	678	990	1,063	824	831	
" 98m	19.14	165	191	232	259	356	831	925	852	883	664	
" 99m	18.85	142	165	192	236	264	541	637	690	759	859	
" "	18.85	346					753					
" 101m	19.27	136	184	252	328		607	758	981	721		
" 102m	23.95	150	188	259	342		610	764	977	701		
" 103m	29.75	157	191	256	358		578	686	760	608		
" 104m	24.31	166	206	266	305	370	1,407	1,670	3,254	1,341	691	
" 105m	22.10	139	194	266	344		557	647	769	665		
" 106m	17.18	161	224	260	321		1,030	1,519	1,874	774		
" 107m	21.02	152	251	305	336		1,066	1,513	595	466		

Sample	wt(mg)	Glow peak temperature (°C)					Glow peak intensity				
UMD76/14 11m	11.45	215	255	345			18.3	18.3	12.2	*	
" 15m	14.82	205	245	330			19.5	17.5	11.5	*	
" 29.9m	18.85	170	215	250	340		14.0	17.5	15.9	10.0	*
72/21 16m	19.46	180	265	335			6.4	8.7	11.3	*	
" 40m	17.76	153	204	272	348		704	676	985	1,070	
" 60m	21.90	164	210	284	360		639	651	913	982	
" 83m	14.22	165	264	330			1,547	1,723	721		
77/22 10m	-	150	196	275	346		12.0	13.3	16.5	23.8	*
" 24.7m	20.70	159	194	244	346		217	229	254	821	
" 37.7m	24.75	154	185	255	342		323	283	354	859	
" 69.5m	25.60	143	191	264	364		674	781	820	605	
77/23 16m	16.66	230	272	338			930	750	450		
" 30.5m	17.00	175	220	280	360		559	647	765	706	
" 59.2m	22.11	225	280	370			724	659	430		
77/24 30m	13.72	140	196	255	330		784	911	1,130	1,203	
" 45m	8.55	168	185	285	354		643	731	1,111	1,199	
" 61.2m	25.40	150	183	249	371		630	709	591	433	
N7 300'	22.70	166	214	267	300	358	584	925	881	859	1,344
" 336'	16.25	140	180	255	315		18.5	17.2	33.5	41.8	*
N26 357'	24.55	159	200	261	291	359	387	407	591	652	876
" 446'	22.79	205	252	386			439	450	340		
" 552'	20.14	152	191	261	367		397	497	645	497	
N43A 162'	23.10	177	208	272	380		779	823	823	541	
" 306'	27.86	145	196	240	258	365	305	395	449	431	377
" 446'	16.10	187	256	370			1,087	1,196	1,056		
N74 10'	20.75	151	185	276	339		373	349	578	867	
" 110'	26.28	174	231	353			656	400	732		
" 185'	15.87	195	250	365			32.1	34.6	24.2	*	
" 387'	23.55	151	179	280	329		297	276	510	679	
" 512'	-	180	260	345			155	145	80	*	
N123 198'	17.35	170	221	250	270	390	461	576	576	490	317
" 288'	18.30	169	206	260	352		410	355	410	984	
" 447'	13.55	225	265	325			5,314	2,878	2,140	*	
" 593'	24.39	204	326	347			1,025	1,271	1,169		
N128 65'	20.25	216	234	266	364		679	716	704	531	
" 240'	18.41	190	250	360			32.0	31.0	16.8	*	
" 362'	16.95	180	255	325			44.2	31.8	38.3	*	
" 560'	17.03	150	185	250	350		15.8	22.3	26.1	24.0	*
N129 100'	18.63	180	205	260	330		38.1	39.7	35.7	37.6	*
" 168'	19.51	159	229	289	389		846	1,384	1,179	1,333	
" 260'	19.25	176	227	270	368		792	987	909	610	

Sample		wt(mg)	Glow peak temperature (°C)				Glow peak intensity					
N129	454'	18.15	179	210	256	368		331	441	592	413	
N130	200'	19.45	170	195	274	365		463	566	643	437	
"	250'	-	155	250	330			200	300	770	*	
"	594'	21.30	150	190	255	350		9.1	15.7	21.4	17.8	*
NE1	104'	16.69	190	285	370			599	809	689		
"	243'	18.40	159	190	285	335		408	408	652	652	
"	325'	17.96	206	264	371			5,290	2,116	2,227		
"	496'	19.10	145	197	241	343		366	471	890	497	
"	497'	17.15	151	180	258	358		364	350	423	379	
NE10	55'	25.40	156	215	281	376		492	551	709	551	
"	160'	18.10	153	185	227	280	325	414	483	552	746	953
"	254'	18.41	210	254	367			1,141	1,141	801		
"	385'	25.55	160	205	240	280	396	352	479	470	460	391
NE11	140'	23.59	180	275	335			26.5	35.2	23.5	*	
"	294'	15.50	150	255	330			13.2	20.6	42.2	*	
"	421'	16.20	210	270	400			694	602	463		
NE23	138'	17.41	190	240	335			36.2	37.3	24.4	*	
	274'	26.75	151	171	268	331		383	393	542	467	
	346'	21.05	210	275	365			26.8	27.5	18.5	*	
	520'	19.07	185	260	350			14.1	19.1	10.2	*	
76/9	10m	21.35	185	230	330			16.8	17.3	8.0	*	
"	29.6m	17.81	210	265	350			11.8	15.4	7.2	*	
77/27	14m	26.45	156	183	261	350		491	529	624	501	
"	44.6m	22.47	183	226	290	350		401	490	478	423	
"	59.8m	14.42	179	225	280	375		936	1,248	867	555	
79/29	14m	23.99	155	205	240	269	348	375	459	417	459	333
"	22.7m	23.51	165	207	282	355		425	468	510	351	
"	41m	26.70	185	251	271	362		637	730	712	468	
"	59.5m	23.90	190	217	274	354		649	711	711	513	
78/99	29m	21.61	140	190	266	344		472	625	870	1,023	
"	37m	22.42	164	203	237	344		937	1,173	1,097	620	
"	46.5m	26.48	149	186	222	249	334	551	691	785	819	483
79/130	32m	28.00	170	206	240	274	354	500	650	600	590	425
"	40m	14.14	171	206	259	344		750	900	825	375	
"	50m	19.13	152	182	210	222	340	850	1,000	975	900	450
79/136	14m	15.45	171	202	230	273	364	977	1,191	1,288	984	563
"	32.3m	9.45	166	232	282	364		1,069	1,534	1,344	836	
"	50.4m	-	139	200	222	264	342	14.0	22.6	20.5	16.5	13.0*
NE18	156'	17.00	174	242	294	373		618	868	794	544	
"	302'	17.45	140	250	310			9.7	20.0	39.5	*	

Sample		wt (mg)	Glow peak temperature(°C)					Glow peak intensity				
NE18	448'	17.20	175	204	268	384		494	640	596	436	
"	624'	17.20	145	174	254	367		233	262	407	233	
H15	60'	23.25	184	245	365			409	538	387		
"	312'	25.30	155	235	275	359		889	1,779	1,423	1,739	
"	465'	17.85	199	261	354			686	714	504		
H25	100'	28.00	146	194	241	266	334	796	1,057	1,314	1,304	804
"	100'	28.00	356					811				
"	142'	21.90	140	182	230	266	337	626	703	744	831	781
"	239'	23.40	133	171	259	312	358	603	838	983	1,248	953
"	287'	21.15	167	194	258	340	368	832	870	894	719	723
H31	103'	25.20	165	212	254	362		869	1,091	901	548	
"	197'	29.24	136	168	195	262	358	646	828	927	1,043	766
"	330'	23.85	164	258	330			918	1,409	914		
"	500'	19.56	176	212	244	328		1,329	1,278	1,253	828	
H66	85'	15.65	151	186	277	361		415	431	591	447	
	149'	17.95	151	178	194	275	325	474	390	362	724	724
	306'	18.79	227	275	371			718	772	399		
77/34	5m	19.46	160	195	276	354		411	450	565	591	
"	21m	18.85	184	270	366			743	743	517		
"	34.8m	21.25	196	255	365			753	682	459		
"	42m	25.47	200	238	255	393		609	510	491	353	
"	59.9m	17.90	195	260	373			782	726	489		
"	65.6m	24.00	161	181	263	376		448	563	542	292	
77/38	22m	17.75	150	192	278	350		296	324	479	676	
"	50m	22.75	189	272	373			571	626	418		
"	75m	18.95	153	205	281	355		580	950	620	369	
77/43	22m	22.10	201	254	346			498	509	283		
"	45m	20.18	170	281	374			3,271	3,568	396		
"	65m	24.75	173	264	376			646	657	364		
77/44	19.7m	13.74	180	240	320			12.4	15.6	13.6	*	
"	40m	18.29	175	240	325			2.7	4.1	10.9	*	
"	60m	17.30	180	245	335			8.9	9.8	8.9	*	
77/45	13.6m	12.08	200	265	365			25.4	24.4	16.5	*	
"	67.3m	16.00	185	273	355			500	500	375		
77/46	20.3m	14.40	156	209	260	354		660	781	833	712	
"	42.9m	18.37	194	274	378			517	512	408		
"	67.7m	13.94	210	250	390			224	267	416		
77/48	10m	20.58	149	176	206	269	355	486	534	534	680	559
"	41.8m	16.59	138	170	257	320		377	347	512	693	

Sample		wt (mg)	Glow peak temperature (°C)					Glow peak intensity				
77/48	62m	15.17	180	270	350			26.0	20.8	16.5	*	
77/49	30.4m	20.75	148	201	261	355		410	578	578	530	
"	39.1m	19.39	150	200	268	346		464	516	683	619	
"	62.5m	21.40	185	271	396			666	584	339		
77/52	10m	17.70	218	276	389			621	621	424		
"	21m	17.17	165	197	283	348		437	393	612	1,077	
"	38.3m	17.55	168	201	296	349		427	456	627	598	
"	57m	14.80	174	210	271	350		574	574	676	709	
77/57	21m	19.03	205	265	360			21.2	19.7	12.3	*	
"	40.4m	17.39	191	200	270	380		748	748	748	575	
"	60.6m	24.45	165	267	306	380		1,104	1,247	593	307	
78/66	30m	12.35	145	180	250	325		15.8	20.2	31.2	31.2	*
"	52m	17.30	193	264	367			607	564	376		
"	56m	15.64	180	265	355			22.4	19.2	11.8	*	
78/70	8.9m	23.21	205	275	360			13.8	15.5	14.4	*	
"	48.5m	19.75	205	285	360			19.2	25.3	22.5	*	
"	81m	13.14	200	265	370			27.0	22.8	14.1	*	
78/80	24.2m	18.75	150	195	265	330		12.3	12.3	20.2	23.5	*
"	33m	20.00	200	250	345			20.5	22.2	16.0	*	
"	80m	17.02	180	260	355			16.7	17.9	7.0	*	
79/118	8m	22.76	160	199	219	243	358	1,125	1,340	1,375	1,129	593
"	17m	20.82	138	186	256	325	348	576	663	850	850	749
"	24m	21.90	138	176	224	271	326	667	982	995	1,018	813
"	"	21.90	375					630				
"	31m	24.85	149	181	234	290	328	419	523	616	732	913
"	"	24.85	369					793				
"	48.5m	26.67	178	260	342	373		645	720	450	446	
"	55.5m	13.95	180	258	374			760	839	538		
P8	8-10m	20.38	138	172	250	268	330	2.5	2.7	2.95	2.85	2.6
"	"	20.38	357					2.7	*			
"	18-20m	23.35	133	162	221	250	332	3.1	3.5	3.8	3.7	2.7
"	"	23.35	356					2.7	*			
P9	12-14m	27.09	142	184	231	258	333	2.0	2.2	2.3	2.5	3.3*
P14	10-12m	22.90	141	198	234	266	334	2.7	3.1	3.2	2.9	2.0
"	"	22.90	362					1.9	*			
"	16-18m	20.39	133	165	256	323		2.2	2.3	2.7	2.2	*
77/53	10m	22.57	155	215	245	261	360	332	421	432	432	399
"	30.5m	20.05	165	263	340			599	461	324		
"	50.7m	15.03	205	276	393			832	832	566		

Sample	wt(mg)	Glow peak temperature (°C)					Glow peak intensity					
S76/1	42m	19.55	180	225	270	355		23.0	30.2	22.5	12.3	*
	80.3m	17.10	195	255	355			12.8	10.5	6.7	*	
	130m	14.84	175	250	340			7.4	9.1	5.4	*	
S76/2	30m	17.90	205	260	375			24.0	22.5	14.5	*	
"	60m	18.30	190	260	350			17.5	19.4	15.8	*	
"	90m	15.92	170	250	350			25.1	31.4	16.0	*	
S77/6	17m	16.08	155	209	255	354		498	606	622	466	
"	40m	12.51	155	174	263	364		500	560	620	480	
"	61.8m	17.30	163	190	269	372		434	535	549	376	
S77/11	16m	16.85	190	240	340			21.4	21.4	14.8	*	
"	40m	20.89	195	265	375			18.7	18.4	11.5	*	
"	59m	14.05	180	260	355			23.1	24.2	10.7	*	
S77/12	8m	20.48	154	185	277	343		293	317	366	366	
"	38m	18.05	195	261	375			416	388	208		
"	51.7m	18.55	175	240	345			10.5	11.3	6.2	*	
S78/15A	20m	14.95	145	245	338			535	736	518		
"	56.6m	19.53	155	190	268	355		435	422	384	525	
"	58.3m	14.95	145	220				100	268			
"	80.9m	17.44	185	275	374			430	487	229		
S78/22	20m	24.10	220	270	370			23.6	17.8	11.8		
"	50.7m	23.29	182	258	368			558	526	301		
"	80m	16.99	160	266	310			1,978	1,978	765		
S78/28	28m	16.86	160	195	270	335		11.8	13.9	16.0	29.6	*
"	55m	19.21	200	270	360			19.3	22.6	22.9	*	
"	78m	12.20	195	275	370			23.3	24.2	18.0		
S78/16	20m	22.74	149	199	253	347		330	418	407	297	
"	39.9m	20.85	189	260	382			492	432	264		
"	60.1m	21.00	159	196	263	379		345	429	476	310	
S78/17	20m	16.20	150	185	250	340		478	617	648	386	
"	39.7m	16.60	185	260	365			28.0	27.4	14.7	*	
"	60.6m	19.95	183	250	360			551	602	388		
S78/24	20m	17.86	205	250	340			23.8	22.4	13.7	*	
"	40m	19.45	185	255	360			22.4	24.9	14.9	*	
"	63.8m	20.00	205	275	380			23.2	23.0	14.0	*	
S78/25	19m	12.92	175	230	270	365		10.4	12.0	11.6	7.3	*
"	39.8m	16.59	180	260	365			13.3	15.0	8.4	*	
"	65m	14.21	165	265				21.1	19.3	*		
S78/26	13m	16.60	210	255	335			32.5	25.9	12.6	*	
"	30m	21.30	189	261	373			634	563	364		
"	49.9m	24.20	185	265	345			13.8	21.0	16.1	*	
"	72m	14.11	180	275	355			19.1	35.1	19.8	*	

Sample		wt(mg)	Glow peak temperature (°C)				Glow peak intensity					
WD6	36m	23.05	172	212	244	354		1,410	1,813	1,388	620	
"	65m	21.25	159	214	244	329		828	1,026	946	621	
"	91m	19.70	161	208	257	364		1,066	1,371	1,030	650	
WD8	24m	17.60	165	229	256	336		932	1,653	1,460	852	
"	45m	20.89	178	214	256	354		843	1,197	814	431	
"	64m	21.90	165	202	278	346		489	589	630	680	
WD11	46m	29.99	136	184	246	343		604	977	857	654	
"	66m	25.05	160	194	240	333		842	1,042	770	387	
WD12	22m	26.30	172	202	240	347	376	764	939	833	392	380
"	35m	21.91	169	204	239	334	353	949	1,196	936	388	370
"	50m	27.30	169	220	255	349		678	912	740	399	
WD13	30m	22.85	148	194	261	323		521	696	713	919	
"	44.5m	21.21	143	189	244	267	341	523	707	731	669	443
"	"	21.21	377					401				
"	60m	16.38	162	204	250	326	356	836	922	775	409	433
WD14	30m	29.30	139	205	233	262	339	509	997	925	870	676
"	"	29.30	365					635				
"	43.5m	22.60	161	198	223	256	336	695	827	832	761	504
"	"	22.60	364					460				
"	60m	22.10	148	187	218	251	340	620	828	842	814	516
79/121	6m	18.11	182	219	244	349		718	729	729	475	
	7m	19.79	192	227	262	364		980	970	834	551	
	23m	11.77	187	221	272	372		663	646	603	510	
	40m	22.25	182	231	260	338	356	683	602	544	364	364
79/122	3m	24.28	202	223	261	370		803	774	577	457	
"	11.5m	23.20	198	247	342			780	1,276	487		
"	15m	25.40	147	200	263	352		421	594	598	594	
"	30m	19.70	172	249	353			777	766	553		
"	50m	24.00	130	208	261	352		608	883	767	579	
S79/29	10m	20.38	176	214	252	361		662	785	672	476	
"	42m	17.67	150	199	228	270	359	566	753	702	662	515
"	"	17.67	384					521				
"	69.5m	10.50	156	262	351			448	619	381		
"	76.7m	28.65	157	184	222	253	354	614	625	586	583	422
"	77.1m	23.94	143	184	260	356		485	589	660	464	
S79/30	11m	15.15	149	173	230	258	344	455	607	667	634	469
"	25m	18.32	185	247	353			688	666	486		
"	38.5m	17.09	186	250	352			878	761	527		
S79/31	20m	24.45	181	215	250	277	392	528	646	618	540	368
"	40.3m	21.98	185	228	270	356	384	896	1,083	924	537	541
"	58m	21.14	170	198	230	264	374	1,055	1,145	1,202	1,093	620

Sample	wt(mg)	Glow peak temperature(°C)						Glow peak intensity				
S79/31 63m	21.15	140	206	268	338		478	671	747	856		
" 77.5m	15.96	165	249	348			1,065	1,003	764			
S79/32 27m	13.60+	156	191	212	258	337	2,522	2,250	2,169	1,287	699	
" 32m	23.70	132	189	254	309		367	494	527	523		
" 45m	10.66	168	197	230	258	356	1,238	1,379	1,351	1,032	769	
S79/33 61m	19.80	169	229	252	346	374	899	1,409	1,313	672	631	
" 70m	16.13	198	230	247	363		1,358	1,426	1,290	608		
" 80m	14.55+	158	196	231	269	349	832	1,031	1,093	983	612	
S79/34 132m	18.16m	137	170	200	268	341	430	507	573	556	749	
" 137m	20.02	168	225	256	306	350	1,379	1,893	1,728	849	654	
" 141.2m	15.80	171	209	276	365		848	1,095	861	494		
79/104 20m	15.00	168	202	251	274	354	533	700	720	687	540	
52m	27.72	182	235	329			411	408	400			
82.5m	22.41	140	187	258	376		415	611	598	437		
79/105 20m	20.36	176	224	264	340		599	722	609	378		
" 35m	23.07	160	197	235	259	354	559	607	594	559	338	
" 50m	14.36	190	213	250	274	341	940	1,072	975	836	585	
" 69m	17.65	136	165	251	277	341	510	623	635	538	397	
" "	17.65	389					408					
" 79m	19.86m	138	174	231	259	354	453	554	589	645	433	
" "	19.86m	384					403					
" 81m	19.75	136	184	242	347		486	633	618	435		
79/109 26m	17.35	194	254	327	342		1,095	876	744	749		
" 35m	27.88m	158	215	256	336	358	882	1,349	1,019	574	538	
" 49m	24.11	168	217	254	338	367	983	1,282	1,107	684	651	
T1	20.10	182	219	258	361		986	1,318	1,025	576		
T2	21.65	167	212	263	340		722	1,089	722	483		
T3	16.69	149	198	241	324		557	850	685	441		
T4	20.20	162	204	238	340		691	895	713	425		
T5	24.20	161	220	259	354		547	726	621	383		
T6	28.89	158	205	241	342		624	757	682	379		
T7	27.70	162	229	272	359		691	1,048	879	673		
T8	22.35	161	191	240	326	353	699	897	688	589	584	
T9	26.49	204	251	338			1,280	1,073	720			
T10	23.45	198	228	260	348		948	1,004	902	654		
T11	23.22	194	244	332			668	719	694			
T12	28.45	175	237	258	278	327	774	1,080	1,093	963	693	
T13	18.47	168	205	252	336		911	1,050	917	603		
T14	25.63	162	214	257	338		754	1,028	932	658		

Sample	wt(mg)	Glow peak temperature ($^{\circ}$ C)					Glow peak intensity				
T15	23.99	197	231	264	345		1,100	1,220	1,095	770	
T16	26.05	200	230	256	344		1,027	1,099	1,018	566	
T17	19.05	156	202	228	260	366	639	742	924	867	588
T18	26.74	171	249	270	360		927	1,409	1,183	847	
T19	22.55	186	232	252	340		726	752	737	529	
T20	25.85	125	289	374			81	994	3,737		
D1	25.44	134	266				806	3,494			
C6	22.85	163	199	273			1,833	2,276	1,225		
A2	21.40	158	238	261	342		537	1,734	1,710	1,159	
A1	20.90	165	234	263	288	360	756	2,234	2,292	2,196	1,124
C7	19.24	152	196	258	378		509	904	603	567	
V4	13.16	220	258				1,968	973			
SK2	19.05	170	237	320			1,538	10,173	14,383		
B1	19.27	166	230	301			794	1,806	763		
R1	17.20	136	212	240	304	320	878	994	1,093	1,465	1,337
H1	28.55	160	186	239	340		161	186	221	592	
S1	21.59	186	233	360			259	347	116		
Ptw ₂	21.75	166	236	338	384		368	395	244	221	
C4	18.83	162	198	271			2,066	2,544	1,514		
C3	18.51	170	224	278	356		692	918	648	389	
C2	24.15	158	230	330			692	1,391	1,048		
C1	16.16	136	308				2,351	6,188			
V2	21.60	174	225	266	370		1,000	1,157	833	491	

APPENDIX 3

Microscope descriptions of selected thin and polished sections.

APPENDIX 3: Microscopic descriptions of selected thin sections and polished sections.

- 549/202 Location: UMD78/66 26-28m, Outcamp Sill.
 Classification: Altered basaltic sill.
- Minerals: Plagioclase 50% Well preserved rectangular laths varying from small to large (2mm x 0.5mm). These show no preferred orientation due to crystal settling, growth etc. and are frequently replaced by clay, chlorite and sericite. No distinctive twinning is observed.
- Mesostasis 45%. The plagioclase laths are enclosed in an originally glassy mesostasis which has now been completely replaced by kaolinite, illite and chlorite with minor quartz also being present.
- Clinopyroxene. Isolated phenocrysts are randomly scattered throughout the rock and are completely replaced by chlorite.
- Opagues 4%. Abundant small skeletal opaques are scattered through the section frequently occurring in association with altered plagioclase laths. This may be a result of the exsolution of small rod-like needles of magnetite which are contained within clouded plagioclase (Heinrich 1965, p.356).
- Texture and comments: Although totally altered relict shapes give an indication of the original texture of the specimen. No flow banding or outstanding phenocryst phases are present and the rock is composed of randomly oriented plagioclase laths with isolated clinopyroxene phenocrysts in an originally glassy mesostasis.
- 549/203 Location: UMD78/80 20m, Siegal Volcanics.
 Classification: Altered basalt
- Minerals: Plagioclase 65% Randomly oriented intersecting generally lath shaped grains which are altered mainly to a light green chlorite rather than to sericite or clay. Chloritization is patchy, often occurring in the centre of laths. Finer darker brown chlorite is gradually replacing the light green variety.
- Mesostasis 25% Orange brown replacement minerals of the mesostasis are illite and sericite. Minor light green and dark brown chlorite also occurs. Rod like opaques and anhedral grains are randomly scattered through the matrix.
- Clinopyroxene 5% Large subrounded phenocrysts which occur scattered through the slide. These are replaced by chlorite and quartz.
- Opagues 3%. These occur in two forms: (1) anhedral randomly scattered grains, (2) skeletal exsolved structures often associated with plagioclase. Many inclusions are parallel, perhaps exsolving along cleavage directions.
- Texture and comments: 549/203 is texturally similar to 549/202 with the addition of more clinopyroxene phenocrysts and minor opaque filled veinlets.
- 549/204 Location: N123 438', Redtree dyke.
 Classification: Altered dolerite.
- Minerals: Plagioclase 50%. These laths are generally better preserved than those in the altered extrusives and twinning is obvious in larger grains. Grain size varies from small to very large (5m.m x 2m.m). Smaller grains are completely replaced by chlorite, larger grains less so but are partially replaced by sericite. The replacive

chlorite is itself included by many small opaques.

Mesostasis 45%. Totally sericitized with abundant small opaque inclusions.

Opaques 5%. These are mainly granular, subhedral to euhedral and are far more abundant than in the basaltic equivalents. Micro-veinlets of opaques are also present.

Texture and comments: The random orientation of plagioclase laths and broken nature of same is consistent with the intrusion of a partially consolidated and fractionated magma as was suggested in section 1.8 along geochemical lines. The presence of very large relatively unaltered plagioclase laths may indicate that some crystal settling had also occurred.

Thin veinlets of reddish oxidized opaques (with minor quartz) are a late-stage secondary feature.

549/206 Location: NE23 280'

Classification: Altered doleritic dyke.

Minerals: Plagioclase 40%. Small clusters of broken laths replaced by chlorite and clay. The laths are smaller than in other specimens which indicates a more rapid cooling.

Mesostasis 55%. A totally altered orange brown "matrix" of sericite and clay has replaced original glass, chlorite ± clinopyroxene in the mesostasis. Many patches of secondary quartz are also present.

Opaques 2%. Relict shapes of broken grains indicate that these were originally magnetite and/or ilmenite which have been altered to leucoxene. No skeletal opaques are present.

Texture and comments: Many small altered plagioclase laths randomly oriented in a sericitized altered mesostasis. The whole sample has also been silicified as well as deuterically altered as evidenced by many quartz growths which occur in all minerals as well as the presence of numerous quartz veins cutting the section.

Quench textures still observable in the mesostasis indicate rapid cooling of the sample.

549/207 Location: H15 195'

Classification: Altered dolerite dyke.

Minerals: Plagioclase 35%. Altered clusters of randomly altered laths altered to mainly chlorite and sericite. Some larger laths which show minor silicification also occur.

Mesostasis 60%. The dominant component of the section being similarly altered as other samples, i.e. to an orange-brown sericite/clay mixture. Small needle-like opaques in one distinct orientation and one minor orientation also occur within the mesostasis perhaps reflecting original mineral or cleavage orientations.

Opaques 2%. Dominantly as broken grains though they also occur as needle-like inclusions mentioned above. They have been altered to leucoxene.

Texture and comments: Very similar to 549/206 though with a larger mesostasis proportion. This reflects inherent compositional differences between samples.

- 549/208 Location: UMD77/49 34-37m. Outcamp Sill
 Classification: Altered basalt.
- Minerals: Plagioclase 55%. Medium to large randomly oriented laths. Many are well preserved though many are also broken. Intersecting laths indicate a period of differentiation prior to intrusion. Replacement minerals are quartz and a light green chlorite.
- Mesostasis 40%. Although totally altered it does not have the characteristic orange-brown alteration color obvious in some previous samples. Alteration is mainly a dark green-light brown indicative of chlorite with some clay. This chlorite appears different to that replacing plagioclase.
- Clinopyroxene 2-3%. These are totally altered to chlorite and occur as phenocrysts defined by intersecting and broken plagioclase laths. Trace of any phenocrysts originally in the mesostasis has been obliterated.
- Opagues 2%. These are subhedral and broken occurring (1) as large randomly scattered grains, and (2) as very small grains associated with plagioclase laths.
- Texture and comments: Texturally this sample is similar to others of the Siegal Volcanics or Outcamp Sill. The difference in alteration characteristics points to different types of alteration processes having occurred in samples, i.e. a silicic alteration in some samples, a low temperature deuteric alteration leading to sericite and clay formation in others, and a third type of slightly higher temperature(?) leading to chlorite formation as in this sample. The presence of clay in the mesostasis indicates that even this process was relatively low temperature rather than hydrothermal.
- 549/209 Location: UMD77/48 34.5-41m. Outcamp Sill.
 Classification: Intersection of two phases of altered basalt.
- Minerals: Plagioclase Phase A 20% Phase B 50%. Phase A contains randomly scattered small to medium grained laths which upon approaching the contact take on a preferred orientation parallel to the contact. Alteration of the laths is mainly silicic and to a lesser extent chloritic. Phase B contains more abundant medium grained laths which have been similarly altered. These occur in a random orientation even at the contact.
- Mesostasis. Phase A 70%, Phase B 25-30%. Phase A mesostasis is a fine grained isotropic glass indicative of rapid cooling. Phase B is similar but less common. Radiating quench textures are present in the mesostasis of phase B near the contact but disappear away from it.
- Clinopyroxene. Phase A 10% Phase B 20%. In phase A these are small randomly oriented phenocrysts often occurring close to the contact. They have been replaced by a pale green chlorite. Phase B clinopyroxene phenocrysts are larger and more abundant occurring randomly scattered throughout the sample. These also are chloritized.
- Opagues. Phase A 2%, Phase B 2-3%. Opagues are slightly more abundant in phase B. In both phases they are fine grained subhedral grains and needle-like inclusions in other minerals or are randomly scattered through the mesostasis.

- Texture and comments: Phase B is typical hypidiomorphic textured basalt. Phase A which is composed mainly of glass appears to have been the later intrusion which has then crystallized very quickly. A very sharp contact with thin chilled margin exists between the two with no intrusion of one into the other. The significance of this section is that it indicates that extrusion/intrusion occurred in a number of pulses rather than as one isolated event.
- 549/214 Location: UMD78/83 29m. Siegal Volcanics.
Classification: Altered vesicular basalt.
- Minerals: Plagioclase 35%. Small randomly oriented sericitized laths.
Mesostasis 30%. Similar to most other samples. Alteration is chloritic.
Vugs 30%. These are medium to very large (5mm x 5mm) and are rounded. They are not obvious in any other previous samples. A zoning is apparent across the vesicles with layers of different colored (light to dark green) chlorite lining their edges and the centre being filled with quartz. Minor opaques are also concentrated in the central portion of some vugs.
Opaques 2%. These occur in similar forms to other samples.
Clinopyroxene 3%. Clinopyroxene phenocrysts are randomly scattered through the section and have been replaced by light green chlorite. They are frequently included by small opaques.
- Texture and comments: The sample is texturally similar to others in the Siegal Volcanics apart from the presence of vugs. This is taken from five metres above the contact with the underlying Westmoreland Conglomerate. The vugs may therefore represent either an original feature of the basalt having been gas-filled bubbles, or may have resulted from weathering if this marked the top of one flow before extrusion of others.
- 549/219 Location: Airstrip.
Classification: Quartz veined volcanic?
This entire sample is a mass of orange-brown sericite and clay with minor remnant plagioclase laths. No original relict textures to classify major minerals or volcanic type are present. Large quartz patches may represent infilled inherent vesicles though these lack the chlorite lining of 549/214.
Alteration is of two types: 1) the sericitic clay alteration which has obliterated original textures and 2) a widespread silicification manifest in quartz replacement of many minerals.
- 549/236 Location: UMD79/123 54-55m. Redtree dyke.
Classification: Altered dolerite dyke.
- Minerals: Plagioclase 35%. Randomly oriented well shaped and broken laths which are totally replaced by sericite and minor chlorite such that even the characteristic twinning is absent.
Mesostasis 45-50%. An orange-brown sericite-clay mixture forming the alteration of the original glassy component.
Clinopyroxene 15%. Randomly scattered chloritized phenocrysts in the mesostasis and cutting plagioclase laths.
Opaques 5%. Subhedral to euhedral grains altered to leucoxene.
- Texture and comments: Although similar to other samples in this basic suite, this particular sample is, overall, finer grained than others. Alteration has been of the sericite-chlorite-clay type with minor secondary quartz veinlets also present.

- 549/237 Location: SUD79/34 95m. Siegal Volcanics.
 Classification: Altered vesicular basalt.
- Minerals: Plagioclase 20%. Small broken laths completely replaced by quartz and sericite. They are randomly scattered and oriented.
Mesostasis 40%. An orange-brown clay and dominantly sericite replacement of the original presumed glassy mesostasis has occurred. Relict shapes with this groundmass are not observed. Hematite staining also occurs.
Clinopyroxene 20%. Large broken and common phenocrysts scattered throughout the slide. These are chloritized and frequently contain small quartz inclusions.
Vesicles 20%. In contrast to previous samples these large vesicles had a quartz rim and are totally filled with a light green chlorite. Occasionally a quartz mosaic is present at the centre of the vug. No opaque inclusions occur within or at the edge of these.
Opagues. These are very minor in contrast to the abundance in other slides and are very small anhedral grains associated with plagioclase and the groundmass.
- Texture and comments: Alteration precludes positive textural classification other than as described above. The sample is taken from near the contact of the Westmoreland Conglomerate (implying an early extrusion) and is covered by 95m of overburden which may both account for the presence of the large clinopyroxene proportions.
- 549/238 Location: SUD79/34 122m. Siegal Volcanics.
 Classification: Altered basalt.
- Minerals: Plagioclase 40%. Although altered and sericitized twinning is still obvious in the broken randomly oriented plagioclase laths. Composition of the laths is A_{65} placing them in the labradorite field. The laths are small to medium and occasionally intersect the extremely broken clinopyroxene grains.
Mesostasis 30%. Very similar to other samples though the replacive mineral is dominantly a darkish chlorite rather than a clay.
Clinopyroxene 25%. These phenocrysts occur in two forms: (1) Large broken grains frequently overlying or crosscutting plagioclase laths, and (2) as small anhedral highly pleochroic grains scattered throughout the section. Both types but particularly the former are replaced by chlorite.
Opagues 5%. The abundant opagues also occur in two forms: (1) as small anhedral to subhedral scattered grains, and (2) as long needle like inclusions occurring in groups with a distinct preferred orientation which mimics that of the plagioclase laths in that area.
- Texture and comments: Similar to 549/237 apart from a larger percentage of clinopyroxene. This sample is taken from adjacent to the Westmoreland Conglomerate contact and hence represents the first extrusion so could be expected to have a higher clinopyroxene content than other samples.
- 549/246 Location: SUD79/34 131.2m.
 Classification: Tuff.
- Minerals: Quartz 40%. These are small angular and rounded grains, many of which are an original component of the rock, others of which represent contamination from the surrounding sandstone. Grains are not in contact but are supported by the groundmass.

Groundmass 60%. A very fine grained "matrix" of quartz, feldspar and mica with some fine opaques. Accessory apatite needles are also present. Much of the more mafic portion of the groundmass has been replaced by a light green chlorite. Minor hematite staining is also present.

Texture and comments: Although no shards are observable the high proportion of mica and chlorite seems to suggest a pyroclastic tuffaceous origin for this sample. The very fine grain size and angular nature of much of the quartz is also indicative of such an origin.

549/248 Location: L18 495. Black Hill dyke.

Classification: Altered dolerite.

Minerals: Plagioclase 30%. Randomly oriented small-medium well shaped laths which have been totally altered to a dark green chlorite.

Clinopyroxene 30%. Originally large very broken and shattered phenocrysts also totally replaced by a lighter green chlorite containing minute opaque inclusions.

Mesostasis 40%. A chloritized and partially silicified replacement of the presumed originally glassy matrix.

Opagues. These occur in two forms: (1) large anhedral broken grains with a faint purple tinged-leucoxene after ilmenite, and (2) small black grains and stringers associated with plagioclase grains.

Comments: The distinctive features of this sample are: (1) the alteration type which is completely chloritic rather than sericitic and (2) the high clinopyroxene content which is more typical of a basaltic member of the volcanic suite rather than of a dolerite dyke.

549/252 Location: L20 551'. Black Hill dyke.

Classification: Contact between two dolerite dykes.

These dykes are composed of the same minerals as the other mentioned sections (plagioclase, clinopyroxene, mesostasis, opaques) though the proportions vary in both phases of the dyke.

The first phase is a finer grained dolerite composed of abundant plagioclase and clinopyroxene and opaques in a glassy mesostasis has suffered a chloritic and silicic alteration, and also has minor hematite staining.

The second phase which appears to intrude the first is a coarser grained totally altered conglomeration of sericitized plagioclase laths and large broken clinopyroxene grains in an orange-brown clayey sericitized matrix. Iron oxide staining is prevalent and in many cases stringers of iron oxides appear to define a preferred orientation replacing or staining plagioclase laths.

549/254 Location: Kratos Camp.

Classification: Basalt.

Minerals: Clinopyroxene 15%. Large partially broken phenocrysts set in a glassy groundmass. Alteration is not complete and is present as a partial chlorite replacement. Unaltered grains have high order interference colors and a distinct cleavage trace is also apparent (cleavage angle 84°).

Plagioclase 10%. Grey partially sericitized laths randomly oriented and frequently associated with and cutting clinopyroxene phenocrysts.

Glass 75%. Very fine grained glassy groundmass which has been chloritized and sericitized and also has hematite staining. Radiating quench textures are very common.

Texture and comments: The high proportion of glass and numerous quench features indicate that the sample cooled very quickly after intrusion. Given its fresh relatively unaltered appearance it may represent the last stage of volcanic intrusion.

549/220 Location: UMD78/74 49.7 Junnagunna

Classification: Sandstone.

The sample has been taken from well below the Siegal Volcanic contact and occurs in an unmineralized sandstone area. This sandstone is very poorly sorted with grain size ranging from small to large. Grains of quartz are subangular to subrounded and do not show any kind of preferential banding or layering. Initial porosity must have been very high as is indicated by the poor sorting and also by the fact that many grains are matrix supported. Where grains are in contact they are usually only in pairs; no triple points are observed. The long grain contacts where grains do touch indicate that some pressure solution has occurred.

The matrix is a mixture of secondary quartz and clay much of which has been sericitized. Occasional dark green chlorite patches and light red hematite stains are also found.

Rock fragments, mainly acid volcanics and altered feldspars are small and abundant. Metamorphic quartz is rare.

Minerals: Quartz - 80%
Rock fragments - 8%
Opagues - 1%
Chlorite - 1%
Matrix - 10%

549/211 Location: SUD77/12 8.5m Red Hill.

Classification: Sandstone

This sample is taken from just beneath the Siegal Volcanics and contains 10 ppm U. It is composed of a number of interlocking subrounded quartz grains with frequent tangential and long grain boundaries. This implies some degree of pressure solution between grains has occurred. Many pore spaces are filled with secondary silica and initial porosity was high. A high proportion of rock fragments are present which are mainly volcanic quartz and probable altered feldspar. The clay content of the sample is low indicating textural maturity.

Quartz is of two types: 1) large-coarse subrounded grains with undulose extinction with or without subgrain boundaries, and 2) small-medium angular agglomerations of composite very small grains. This may represent quartz from the Murphy Metamorphics and is very much in the minority. A third type somewhere between these two is also present in minor amounts.

Minerals: Quartz - 80%
Rock fragments - 10%
Opagues - 2% mainly interstitial. Some may be pitchblende, others hematite.
Clay/Interstitial cement - 8%.

549/221 Location: UMD 76/6 56.8m Huarabagoo.

Classification: Sandstone.

This sample is similar to 549/220. It is a matrix supported chloritic sandstone with an original high porosity. It is poorly sorted and grain size of quartz varies from small to large. Some grains are in contact and triple points are observed. Dominant grain boundaries are tangential and long.

The quartz is subrounded and has mainly straight extinction with minor undulose extinction. Very rare metamorphic quartz is present.

The matrix is a mixture of clay (altered feldspar), sericite and minor chlorite. Anhedronal opaques are also present and are often associated with chlorite.

Minerals: Quartz - 75-80%
 Rock fragments - 7%
 Chlorite - 2%
 Opaques - 1%
 Matrix/Cement - 10-15%

549/222 Location: UMD78/64 46.3m Junnagunna.

Classification: Sandstone from a shear zone.

This sandstone is poorly sorted. Grain size varies from small to very large and shape from subangular to subrounded. Texturally it is very similar to 549/220 and 221 with a groundmass consisting of clay and sericite which has been partially silicified. Overall initial porosity is very high.

Where this sample differs from the previous two is in the chlorite content, which is interstitial though not detrital, and approaches 5%.

Few opaques are observed and rock fragments and metamorphically derived quartz are also rare.

Minerals: Quartz - 75%
 Matrix - 20%
 Chlorite - 5%
 Opaques/Rock fragments - <1%

549/240 Location: NE18, 302', Redtree-Huarabagoo.

Classification: Sandstone.

This sandstone sample is taken from one foot below an area mineralized with a grade of 0.07% U_3O_8 . No major mineralization is present within this sample as indicated by the lack of opaques. The cut-off between mineralized and non-mineralized areas is thus quite sharp.

The sandstone is poorly to moderately sorted with medium-large subangular grains. Quartz grains have tangential to long boundaries indicating some pressure solution. Undulose extinction and sub-grain boundaries in many samples also indicates some pressure.

Metamorphic quartz, while not abundant is present.

Initial porosity was medium and the matrix is now composed of a partially silicified mixture of sericite and/or clay.

Minerals: Quartz - 85%
 Matrix - 10%
 Chlorite - 5%
 Opaques - <1%

549/241

Location: N130 250'. East of Jack Lens

Classification: Mineralized sandstone (1.91% U_3O_8)

The sample is composed of very coarse rounded to well rounded quartz grains with long grain boundaries where in contact. These are in a matrix of dark green chlorite and hematite with some opaques. One very large opaque acid volcanic clast is present.

The quartz grains have undulose extinction and the majority are split and infilled by a chlorite/hematite mix indicating that this is a later feature. Metamorphic quartz is rare.

Pitchblende is also present as sooty colloform coatings, anhedral interstitial grains and minor veinlets.

Minerals: Quartz ~72-75%
 Chloritic/Hematitic Matrix - 15%
 Pitchblende - 2%
 Other opaques - <1%
 Rock fragments - 10%

80/24.25

Location: UMD78/80 24.25m, Longpocket.

Classification: Mineralized Sandstone (0.072% U_3O_8)

Subhedral medium sized subangular quartz crystals in a partially interlocking mosaic indicating some degree of recrystallization. Initial porosity was lower than in previous samples, probably of the order of 5% to 10%.

Subgrain boundary development and minor veinlets in the quartz grains indicate some degree of stress or pressure.

Rock fragments composed mainly of altered feldspars are quite abundant and frequently are broken down to form part of the matrix.

The matrix is composed mainly of clay indicating textural sub-maturity. Pitchblende occurs as anhedral grains interstitial to quartz grains and also as coatings on the rims of grains.

Minerals: Quartz - 85%
 Matrix - 5%
 Rock fragments - 8%
 Opaques - 2%

U92/27.8

Location: UMD78/92, 27.8m Junnagunna.

Classification: Sandstone.

A very poorly sorted sandstone with grain size varying from fine to very coarse. Some recrystallization has taken place as evidenced by triple point boundaries, long grain contacts and development of smaller grains within larger. Many of the smaller grains are enclosed in a clayey sericite matrix.

Rock fragments which appear to be broken down and altered feldspars are common as are interstitial opaques which occur as anhedral grains and stringers.

Despite the poor sorting porosity is low.

Minerals: Quartz - 85%
 Matrix - 5%
 Rock fragments - 7%
 Opaques - 3%

U24/25

Location: UMD77/24 25m. Redtree.

Classification: Sandstone.

Major recrystallization has occurred in this sandstone. This is evident from the many triple points and sub-grain formation. Grain size varies from small to coarse and generally the coarser grains show most recrystallization. Metamorphically derived quartz which is distinguishable from other quartz types is also present, though is not abundant.

Rock fragments which are mainly acid volcanic fragments also occur.

In some cases the breakdown of feldspar from such fragments has resulted in the formation of clay and sericite which constitutes a poor local matrix to some grains. In other cases such fragments are wholly enclosed with individual quartz grains.

Opagues are not common and usually occur interstitially or as rims of small grains or dusty inclusions.

Minerals: Quartz - 90%
 Rock fragments - 5%
 Opagues - 2%
 Matrix - 3%

80/80

Location: UMD78/80 80m. Longpocket.

Classification: Sandstone/Conglomerate.

The sample is taken from 1.5 metres above the Ptw_3 contact. It is very poorly sorted with grain size ranging from fine to coarse. Some individual grains have been recrystallized - others have not. The sample is conglomeratic in nature and has a very extensive sericitized matrix which has resulted from the breakdown of a large initial acid volcanic clast/feldspar component.

Some of the large grains are composite with inclusions of smaller optically discontinuous quartz grains and opagues (probably ilmenite/magnetite). Muscovite is also present as an inclusion.

The important point about this sample is the very large inherent volcanic fragment component which typifies Ptw_3 and near- Ptw_3 samples.

Minerals: Quartz - 70%
 Matrix - formed by breakdown of volcanic component.
 Rock fragments/Volcanic fragments etc. - 30%
 Opagues - Hematite, magnetite, ilmenite, less than 1%.

U89/104

Location: UMD78/89 104m. Junnagunna-Huarabagoo.

Classification: Sandstone

This sample is taken from just above Ptw_3 and is composed a small subangular to subrounded grains in a sericitic matrix. It is well sorted. Only minor recrystallization has occurred as many grains are not in contact with each other. This indicates that this is a juvenile and texturally immature sediment.

The subangular nature of grains, small size, good sorting and nature of the matrix indicates that part of this sample may have a tuffaceous origin though no direct evidence of this such as shards or chloritic banding are observed.

Opagues are rare generally occurring as broken anhedral interstitial grains.

Minerals: Quartz - 85%
 Matrix - 15%
 Rock fragments + opagues <1%.

U6/30 Location: UMD76/6 30m. Junnagunna

Classification: Sandstone.

Medium to large subrounded to well rounded interlocking grains make up this sandstone which has been considerably recrystallized resulting in loss of initial porosity and matrix material. Many subgrain boundaries within grains, long grain boundaries and triple points are observed. The recrystallization may have been the result of the extrusion of the Siegal Volcanics which are two metres above this sample.

Metamorphic quartz consisting of totally recrystallized angular elongated grains with polygonal sub-grain boundaries is also present. Rock fragments which are mainly altered acid volcanics and broken down feldspars are common reflecting the provenance area of the sandstone, i.e. Cliffdale Volcanics.

Minerals: Quartz - 85%
Rock fragments - 15%
Opagues - less than 1%.

S22/20 Location: SUD78/22 20m. Red Hill.

Classification: Chloritic Sandstone.

Well rounded medium to large grains in a matrix of chlorite and sericite. Grains are not always in contact (though many are) but are supported by the enclosing matrix. Some silicification has also occurred as indicated by overgrowths on many grains.

Extinction in grains varies from straight to slightly undulose though overgrowths are optically discontinuous. Some grains of metamorphically derived quartz have been totally recrystallized and have very undulose extinction. Such grains also have a preferred orientation direction of extinction, elongation and sub-grain development.

Many rock fragments are present which are often strongly chloritized. These are probably remnants of acid volcanic fragments.

Opagues are also common, varying from small to very large and are interstitial.

Minerals: Quartz - 80%
Matrix - 10%
Rock fragments - 8%
Opagues - 2%

83/35.5 Location: UMD78/83 35.5m. Junnagunna.

Classification: Sandstone.

A partially recrystallized mosaic of subrounded medium-large quartz grains with long grain boundaries but only rare to absent triple points. A weak though pervasive hematite chloritic matrix exists which partially supports many grains.

Rock fragments and metamorphic quartz are present, the former is quite abundant. Small muscovite inclusions in quartz are also observed.

Opagues are generally coarse grained, broken and hematized, or occur as trails of dusty inclusions in quartz grains.

Minerals: Quartz - 75-80%
Matrix - 10 to 12%
Rock fragments - 10%
Opagues - 2%

549/213

Location: SUD78/28

Classification: Silicified sandstone

A poorly sorted combination of large polygonal recrystallized angular quartz grains with very small polygonal recrystallized quartz. "Normal" sandstone grains and textures are also present, i.e. well sorted small to medium matrix supported grains. The matrix is composed of chlorite sericite and clay which again may represent broken or altered feldspars. Minor rock fragments and opaques are also present.

The sample has been taken from a silicified fault zone and hence probably represents a "normal" sandstone which has been greatly silicified.

Minerals: Quartz - 60%
 Silicification - 20%
 Matrix - 20%
 Rock fragments - <1%
 Opaques - <1%

549/210

Location: SUD76/1 8.7-9.7m. West of Sue.

Classification: Recrystallized silicified sandstone

This sample is taken from an area in the Siegal Volcanics supposedly mapped as an andesite with quartz veining. In reality it is a completely recrystallized silicified microcrystalline sandstone with occasional patches of recrystallized rock fragments and banding of opaques - mainly hematite and limonite.

549/211

Location: SUD78/15A 34.1m North of Sue.

Classification: Tuff.

Very fine grained subangular to subrounded quartz grains in a sericitic and coarse grained muscovite knot matrix. The quartz grains have an undulose extinction and are often in direct contact with each other indicating a degree of pressure solution or stress.

The sample is best classified as a tuff in view of the fine grained nature, quartz type, muscovite knots and "stringers" of fine grained muscovite.

Opaques are large anhedral and abundant.

Minerals: Quartz - 70%
 Matrix (sericite) - 20%
 Muscovite knots - 5%
 Opaques - 5%

549/216

Location: UMD76/15 111.6m. Huarabagoo.

Classification: Recrystallized chloritic silicified sandstone

Although logged as a dyke this rock is petrologically very similar to 549/210. It is composed of a completely recrystallized small polygonal quartz mosaic usually very fine though coarse in patches. Triple points, long grain boundaries and undulose extinction are common.

In coarser patches a light green chlorite is also found. This has also taken part in the recrystallization process as evidenced by its stringer wispy nature and hence is probably either an original constituent of the rock, or formed at an early diagenetic time.

Opaques occur as large broken anhedral grains or as rims around some of the microcrystalline recrystallized quartz indicating that opaque minerals were also partially redistributed during recrystallization.

549/223

Location: SUD78/15A 58m. North of Sue.

Classification: Partially recrystallized sandstone.

Although taken from within a fault the sample consists of an extremely coarse grained partially recrystallized sandstone with a very large acid volcanic clast.

The quartz in the sandstone ranges from small polygonal recrystallized mosaics to large subangular to subrounded matrix supported grains with some long and tangential grain boundaries indicating the beginning of recrystallization.

The matrix is composed of clay, chlorite and sericite.

The large acid volcanic clast is reddish in color (hematite stained and very silicic). It is comprised of microcrystalline polygonal quartz mosaics though vague relic shapes of some original grains are still observed. Some rectangular partially silicified grains may represent original feldspars.

Opaques are not common in the sandstone though are fairly frequent interstitial minerals in the acid volcanic clast.

Minerals:	Quartz	- 70%
	Matrix	- 10%
	Acid volcanic clast	- 20%
	Opaques	- <1%

Polished section descriptions

- 549/214 Location: UMD78/83 28.95-29.45m. Siegal Volcanics.
- The only mineral which is identifiable under reflected light is a magnetite-like mineral. These are abundant and interstitial to the ferro-magnesium silicates and plagioclase. They are subhedral showing some euhedral relic shapes. Optically these grains are anisotropic and may have been altered to hematite or perhaps even ilmenite. They often have small cores of greyish magnetite (under ordinary light) which are tinged red under cross polars reflecting abundant hematite staining.
- 549/22, 37.7 Location: UMD77/22 37.7m Garee Lens (0.143% U_3O_8)
- Large well rounded quartz grains comprise the bulk of the section. Ore minerals are interstitial to these. The major metallic mineral is hematite which fill these interstices and vugs in an irregular random manner. Grains are very fine and appear to be a later feature perhaps related to mineralization rather than being a primary feature. Pitchblende occurs with hematite as large grey masses with frequent gangue inclusions.
- 549/213 Location: SUD78/28 28m(?) Red Hill Fault.
- The section is comprised of two distinct parts - one is a pink fine-grained completely recrystallized sandstone, the other is a white vein quartz which has intruded the former.
- No sulphides or uranium minerals are associated with either quartz type or with the contact. Minor leucoxene grains (after magnetite?) are present within the recrystallized sandstone though none are found in the vein or fault quartz.
- 549/S6,17 Location: SUD77/6 17m. Sue. Non-mineralised sandstone.
- The sample is a medium-grained recrystallized sandstone. Although sulphides have been reported in drill logs, none are obvious under the microscope. Individual grain shapes are largely destroyed by the recrystallization and silicification. No sulphides, iron oxides or uranium oxides are present.
- UMD78/60 64.75m Fault quartz from the Cliffdale Fault.
- The sample is composed of a white-buff vein or fault quartz. No inclusions of metallic minerals are obvious within this lithotype. Veins and stringers have cut this quartz and may have been associated with fault activity.
- These are composed of a pyrite magnetite mixture though appear to have been originally totally pyrite which has subsequently partial oxidized to magnetite.
- Narrow stringers are totally altered to magnetite whereas thicker ones still retain pyritic edges and cores. These have also contained pyrite crystals as very large euhedral relic shapes are observed. Such crystals may have been zoned as lines of inclusions parallel to grain edges are observed (see plate A4.1). Some pyrite cores are surrounded by an isotropic mineral which is unidentifiable.

549/220

Location: UMD78/74 49.7m. Hematitic unmineralized sandstone.

This sandstone has been silicified (though not recrystallized) and has also been extensively hematized. Hematite covers a half of the section though is a secondary solution introduced feature rather than primary interstitial grains. It occurs as a micaceous coating on grains.

Within the hematitic portion of the sample small pyrite and magnetite crystals occur interstitially to quartz grains. They are not found within the "clean" sandstone which suggests that they may be related to the influx of hematite.

549/528, 28

Location: SUD78/28 28m. Red Hill Fault. Minor mineralization.

Large well rounded grains with large interstitial pores comprise the bulk of this sample. Minor silicification has occurred yet porosity is still high.

Stringers of hematite occur in the interstices. In many cases these appear to have exsolved from a pre-existing mineral - probably magnetite as the stringers and fibres mimic relic grain shape. Silicification has post dated hematite formation as silica is found between the hematite fibres.

No uranium minerals are observed.

549/49, 30.4

Location: UMD77/49 30.4m. Sulphide veinlet above Outcamp Sill.

This sample taken from just above the Outcamp Sill is a partially silicified sandstone. Interstitial spaces still exist as do many vugs. Within the pore space are sulphide grains and veinlets - mainly pyrite with minor sphalerite \pm covellite. The vugs are devoid of minerals though do contain an oxidized sulphide remanent, perhaps a thin coating of marcasite.

The sulphides are post-lithification as they also occur as stringers and veinlets running along grain boundaries. These are probably related to intrusion of the basic sill - perhaps due to Fe^{2+} migration or degassing of S_2 .

Very minor pitchblende is associated with some pyrite, generally at the sulphide grain boundaries or as inclusions indicating that formation of uranium ore post dated introduction of sulphides.

549/52, 40

Location: UMD77/52 40m.

The quartz type and silicification is the same in this sample as in those above. Interstitial spaces are filled with oriented hematite needles which also cut across grains and occur within cracks in the grains. This suggests that hematite introduction has been post-lithification and as such may be related to extrusion of the Siegal Volcanics which lie three metres above the specimen.

549/U79, 70

Location: UMD78/79 70m.

This sample is a loosely compacted sandstone with high porosity composed of poorly sorted well-rounded quartz grains. Silicification is present but minor. Many grains show slight serration of edges which may be the result of partial silicification or abrasion.

Small hematite grains occur within the interstices. These are inherent features of the rock rather than secondary. They are generally subhedral to euhedral. No other metallic minerals are present.

APPENDIX 4

Major and trace element geochemical tables for the Siegal
Volcanics, dykes and tuffs at Westmoreland, with a discussion
of their geochemistry and comparison to other similarly aged
basaltic rock suites in Northern Australia.

Geochemistry of the Siegal Volcanics, dolerite dykes
and assorted tuffs.

Location of geochemical samples

<u>Siegal Volcanics</u>			<u>Tuffs</u>		
549/202	UMD78/66	26-28m	549/239	UMD78/77	67m
" 203	UMD78/80	20m	" 243	L18	499'
" 208	UMD77/49	34m-37m	" 245	SUD79/34	132m
" 209A	UMD77/48	34.5m-41m	" S8	UMD77/43	44.2m
" 209B	UMD77/48	34.5m-41m	" J33	UMD78/82	37.5m
" 214	UMD78/83	29m	" J42	UMD77/40	25.6m
" 217	UMP78/8	22-24m			
" 237	SUD79/34	95m			
" 238	SUD79/34	122m			
" 249	SUD79/32	20m			
" 250	SUD79/33	30m			
" 253	Kratos Camp				
" 254	" "				
" 012	UMD78/61				
" 028	UMD78/67	27.6m			
" F1	WD5	43.4m			
" F3	WD9	94.8m			
	<u>Dykes</u>				
549/204	N123	438'			
" 205	NE1	274'			
" 206	NE23	280'			
" 207	H15	195'			
" 230	N128	283'			
" 236	UMD79/123	54-55m			
" 248	L18	495'			
" 252	L20	551'			
" H2	UMD79/108	99.5-103m			
" HE12	HE12	48m			
" J29	UMD76/15	104m			
" N11	N74	343'			

N.B. All samples with an alpha-numeric listing, e.g. 012, N11, F1 etc. were re-analysed from materials collected by R.A. Manning. Her permission to do is gratefully acknowledged.

GeochemistrySiegal Volcanics

	202	203	208	209A	209B	214	217	237	238	249
SiO ₂	49.69	47.48	41.78	46.70	48.89	58.96	50.27	50.86	51.70	52.53
Al ₂ O ₃	18.38	14.09	16.98	13.46	13.25	11.05	13.51	13.46	11.95	12.74
Fe ₂ O ₃ ^t	9.79	15.64	17.97	16.07	14.87	10.42	12.18	11.04	11.42	12.40
MnO	0.05	0.08	0.07	0.21	0.20	0.15	0.19	0.14	0.17	0.10
MgO	7.66	11.39	11.72	6.46	5.20	10.02	7.92	10.88	8.72	11.94
CaO	0.55	0.41	0.51	6.88	8.14	2.21	3.17	0.60	7.26	0.09
Na ₂ O	0.06	0.19	0.05	2.05	2.09	0.23	0.77	0.67	1.57	0.05
K ₂ O	3.76	2.65	1.26	1.81	1.52	1.10	1.59	4.24	1.97	0.70
TiO ₂	2.96	2.29	2.63	2.17	2.09	1.33	2.20	1.47	1.39	1.47
P ₂ O ₅	0.34	0.28	0.33	0.28	0.26	0.14	0.29	0.16	0.13	0.15
LOI	5.88	6.05	7.26	3.28	2.78	5.34	7.37	5.51	3.59	7.31
Total	99.11	100.56	100.58	99.37	99.30	100.95	99.46	99.03	99.86	99.48
Rb	177	60	34.1	57	53	37.9	53	73	68	16.9
Sr	5.9	9	3.0	102	112	10.3	34.7	100	141	4.1
Ba	33	283	45	461	378	53	156	-	-	-
Ce	26	52	50	48	50	132	42	41	45	-
Nd	19	34	39	32	29	74	31	10	25	-
Zr	277	212	242	197	188	125	202	151	134	145
Nb	19.8	15.4	16.9	14.4	12.8	8.8	13.9	10.7	9.4	9.7
Ni	-	60	153	-	-	140	57	-	-	-
V	591	446	539	401	378	279	417	267	277	287
Sc	47	38	44	33	30	23	35	-	-	-
Y	63	46.3	62	48.3	45.6	24.6	49.5	27.4	24.2	29.7
Cr	177	142	163	125	116	-	130	-	-	-

N.B. Total iron measured as Fe₂O₃

	Siegal Volcanics							Dykes			
	250	253	254	012	028	F1	F3	204	205	206	207
SiO ₂	54.03	48.65	52.68	42.08	49.15	51.48	50.53	52.99	46.71	61.42	58.11
Al ₂ O ₃	12.30	14.43	14.08	15.42	15.61	12.21	12.10	15.71	17.50	15.98	15.39
Fe ₂ O ₃ ^t	10.31	13.81	11.39	17.16	14.37	10.21	10.13	13.53	13.62	5.47	8.64
MnO	0.25	0.10	0.20	0.13	0.17	0.06	0.15	0.09	0.07	0.04	0.03
MgO	8.84	10.21	5.92	13.17	8.71	15.77	13.19	6.48	8.19	3.35	3.15
CaO	1.66	0.38	4.76	0.54	0.51	0.19	1.66	0.46	0.58	0.36	0.42
Na ₂ O	1.94	0.08	3.13	0.04	0.04	0.03	0.04	0.15	0.07	0.10	0.12
K ₂ O	3.04	5.10	4.20	0.36	1.46	0.16	0.66	3.13	4.84	8.43	8.88
TiO ₂	1.30	1.40	1.55	2.56	2.49	1.45	1.44	2.26	2.89	2.11	2.50
P ₂ O ₅	0.13	0.18	0.16	0.31	0.29	0.13	0.14	0.27	0.41	0.25	0.31
LOI	5.89	5.47	2.46	7.50	5.85	7.37	9.33	5.40	5.71	2.67	2.60
Total	99.69	99.82	100.54	99.27	98.63	99.06	99.37	100.47	100.57	100.18	100.15
Rb	69	97	111	11.8	47.2	4.7	27.6	104	69	143	135
Sr	69	13.7	126	3.6	6.5	3.0	6.4	10.1	39.3	18.5	5.0
Ba	-	-	-	19	33	16	18	559	248	501	260
Ce	46	28	54	60	30	41	42	-	74	39	32
Nd	24	17	32	43	22	25	25	-	41	19	19
Zr	132	144	165	227	235	138	135	226	260	240	233
Nb	9.1	9.6	12.1	16.4	16.0	8.2	9.7	15.1	18.6	16.7	16.8
Ni	-	-	-	101	81	186	170	52	-	45	221
V	271	303	276	499	503	294	299	406	577	454	470
Sc	-	-	-	43	40	25	25	35	44	38	39
Y	25.3	26.5	28.3	57	51	24.3	25.3	44.7	56	42.3	40.4
Cr	-	133	136	160	158	700	631	-	174	-	147

	D y k e s								T u f f s	
	230	236	248	252	H2	HEI2	J29	N11	239	243
SiO ₂	59.38	51.93	47.61	63.32	46.97	60.84	67.33	50.88	67.14	61.57
Al ₂ O ₃	19.14	16.17	14.31	16.53	14.89	16.34	13.88	13.67	20.10	18.66
Fe ₂ O ₃ ^t	4.44	13.20	16.79	3.99	13.81	3.60	5.24	14.63	1.24	4.14
MnO	0.04	0.07	0.07	0.01	0.07	0.02	0.05	0.22	0.02	0.02
MgO	1.87	6.96	10.06	1.83	11.50	2.55	4.06	4.80	0.52	2.87
CaO	0.78	0.49	0.48	0.57	0.61	0.48	0.19	6.38	0.13	0.73
Na ₂ O	0.10	0.07	0.06	0.09	0.05	0.13	0.08	2.12	0.61	0.16
K ₂ O	5.61	2.93	0.68	6.64	0.67	9.85	3.22	2.52	5.24	4.65
TiO ₂	3.57	2.75	2.44	2.60	2.79	2.51	1.07	2.04	1.11	2.83
P ₂ O ₅	0.50	0.32	0.28	0.37	0.42	0.30	0.11	0.26	0.04	0.38
LOI	4.03	5.24	6.82	3.13	6.91	2.39	3.87	2.26	3.17	4.06
Total	99.45	100.12	99.61	99.07	98.71	99.00	99.09	99.79	99.32	100.09
Rb	180	64	22	243	29.3	140	133	91	176	182
Sr	13.9	12.3	9.6	12	6.9	15.1	7.1	165	58	32.4
Ba	145	-	-	-	28	313	72	452	-	-
Ce	-	49	46	25	40	52	41	61	128	83
Nd	-	28	31	22	25	29	26	33	47	46
Zr	345	256	226	275	257	257	246	205	258	267
Nb	25.3	18.0	16.1	19.6	18.7	18.1	14.1	13.7	26.2	19.2
Ni	73	-	-	-	-	16	37	49	-	-
V	1,303	546	490	570	478	490	207	309	-	573
Sc	40	-	-	-	39	44	20	27	-	-
Y	76	48.3	49.1	60	54	52	39.4	45.4	19.3	61
Cr	-	-	-	-	138	157	82	96	-	170

	T u f f s			
	245	S8	J33	J42
SiO ₂	66.66	61.15	63.05	47.90
Al ₂ O ₃	16.91	22.77	22.15	28.53
Fe ₂ O ₃ ^t	3.03	1.85	1.69	3.64
MnO	0.00	0.00	0.01	0.02
MgO	1.86	0.64	0.85	2.18
CaO	0.41	0.13	0.32	0.34
Na ₂ O	0.08	0.14	0.77	0.28
K ₂ O	5.56	6.84	5.33	8.60
TiO ₂	1.21	1.21	0.99	1.41
P ₂ O ₅	0.22	0.11	0.17	0.25
LOI	3.69	3.56	3.51	5.20
Total	99.63	98.38	98.84	98.36
Rb	241	241	216	439
Sr	16.8	303	82	82
Ba	-	-	154	461
Ce	78	185	159	185
Nd	43	76	70	84
Zr	324	634	566	356
Nb	19.2	33.7	25.5	30.7
Ni	-	-	40	43
V	196	-	45	191
Sc	-	-	12	25
Y	32.7	9.1	40.6	48.6
Cr	-	-	-	156

A4.1 Geochemistry of the Siegal Volcanics, dykes and tuffs

A geochemical study of basic volcanics at Westmoreland (the extrusive Siegal Volcanics, intrusive Redtree dolerite dyke and minor interbedded tuffs and tuffaceous shales, has been undertaken in order to establish any petrogenetic relationship existing between the three and to determine the origin of the parental magma giving rise to the Siegal Volcanics. A comparison of other similarly aged basic suites in Northern Australia is also included to highlight any similarities or differences. Such a study is also of value to clarify the nature of these rocks (i.e. basalt, andesite, dacite, continental, oceanic etc.) which indicates their suitability as uranium suppliers.

Data consisting of whole rock analyses and trace element concentrations for 35 samples is contained in Appendix 4 and indicates that the extrusive rocks are best classified as basalts.

A4.1.1 Major element geochemistry

The major element geochemistry is summarised in the variation diagrams contained in figure 4.5, where major element oxides are plotted against SiO_2 content. In most cases, a linear fractionation trend from basalts to dolerites is observed indicating a genetic link. A linear relationship is observed between SiO_2 and Al_2O_3 , K_2O and inverse relationship with Fe_2O_3^t . P_2O_5 and TiO_2 remain constant throughout the SiO_2 range and a large scattering of data points for other elements obscures any trends.

Minerals exerting a control on fractionation are likely to be plagioclase (Al_2O_3), clinopyroxene (MnO), clinopyroxene/chlorite (Fe_2O_3 , MgO) and magnetite/ilmenite (TiO_2). The generally linear to slightly increasing trend of P_2O_5 with fractionation indicates only minor control. Apatite is the most common mineral to exert a control on P_2O_5 , though none was observed in thin sections.

The basalts and dolerites are strongly enriched in K_2O (up to 10%), and severely depleted in CaO and Na_2O (though fresher samples contain up to 8% CaO and 3% Na_2O). Such strong enrichments and depletions are due to alteration effects rather than primary magmatic effects.

From these, it can be seen that the Siegal Volcanics approximate the composition of the average basalt of Turekian and Wedepohl (1961) (ignoring those elements redistributed by alteration), being slightly depleted in TiO_2 and slightly enriched in MgO .

In general, the major element variation diagrams are linear, indicating a differentiation process from the basalts to the more siliceous dolerites. If both are derived from the same magma, as it seems is so, then the intruded dolerites (younger than the basalts) represent the end product of differentiation and may well originate from the residue left after extrusion of the basalts.

The tuffs are enriched in Al_2O_3 (up to 28-53%), K_2O and are depleted in Fe_2O_3 , MgO , Na_2O and CaO . Their lack of geochemical co-linearity with the basic rocks in figure 4.5, indicates that they are not obviously related to the magmatic differentiation of the basalts and dolerites.

A4.1.2 Trace element geochemistry

The trace element geochemistry of these rocks is expressed in the variation diagrams contained in figure 4.6. A linear relationship exists between SiO_2 and Rb, Zr, Y, V; an inverse relationship with Sc and a constant relationship with Ca and Cr. No trend is observed for Sr, Ba and Ni.

Minerals exerting a control during the fractionation process are likely to be clinopyroxene ($Kd_{Ce} = 0.04-0.25$ for basalts and andesites, Frey et al. 1977, Gill, 1978; $Kd_Y = 0.20$, Frey et al. op. cit; $Kd_{Sc} = 2$, Gill, op. cit. and an early control on Cr) plagioclase ($Kd_{Ce} = 0.12$ for basalts and andesites, Arth, 1976) and magnetite/ilmenite ($Kd_V = 24-63$, Gill, op. cit; Ni and a later control on Cr).

The basic rocks are enriched in Rb and to a lesser extent Ba also, far above other tholeiites, whether oceanic (Melson and Thompson, 1971) or continental (Condie et al. 1969). Conversely they are severely depleted in Sr. These enrichments and depletions echo those observed for K_2O , CaO and Na_2O and are related to alteration effects rather than primary magmatic effects.

Of those elements that have remained immobile during alteration, the Siegal Volcanics are therefore enriched in Zr, Y and V and are approximately the same in other elemental concentrations, as the average basalt of Turekian and Wedpohl (1961). The general differentiation process from basalt to dolerite observed in major element variation diagrams, is also observed in trace element variations. As observed in the major element geochemistry, the tuffaceous material does not follow the same differentiation trends as the basic rocks and so is unlikely to be related to the magma generation and extrusion/intrusion of the basalts and dolerites.

The recognition of the basic (as opposed to intermediate or acid) nature of these volcanics indicates that they have little potential as a source of significant uranium.

A4.1.3 Alteration of the basic rocks

Alteration has resulted in the extreme depletion of Na_2O , CaO and Sr, and the enrichment of K_2O , Rb and Ba. Petrographically, the result is seen as a severe sericitization of plagioclase laths and an alteration of much of the chlorite, clinopyroxene mesostasis to kaolinite and illite.

Knutson et al. (1979), who worked on the Settlement Creek Volcanics (these occur at the top of the Tawallah Group) at the Redbanks copper deposit, 50 kilometres west of Westmoreland, considered that alteration was the result of potash metasomatism closely associated with magmatic carbonate

complexes at high crustal levels. They postulated that the breccia pipes hosting the copper deposits were formed by explosively released fluids following a pressure build-up in a carbonated potassium-rich trachytic magma 2-3 km below surface. A second alternative which they considered was one of diagenetic alteration, resulting from reactions between widespread tuffaceous material and saline groundwaters, however the former was preferred, due to the close spatial association of the potassium metasomatism with the breccia pipes.

In the Westmoreland region no evidence of explosive trachytic carbonated magmas in the forms of breccia pipes, primary carbonate ocelli or otherwise is observed, thus rendering a magmatic potassium metasomatising event unlikely. It is likely, however, that the original melt forming the Siegal Volcanics was enriched in potassium though not to the presently observed extent.

Extreme K_2O enrichment over Na_2O has also been noted by Scott (1966) in Tertiary ash flow sheets in Nevada, which occurred soon after extrusion during initial cooling of the volcanic pile. The enrichment was attributed to an ion exchange reaction in which a permeating potassium-rich aqueous solution causes exchange of K^+ for Na^+ in the plagioclase lattice resulting in sericitized plagioclase laths. Such plagioclase characterizes the Siegal Volcanics and Redtree dolerites.

The source of the potassium-rich solution may be related to the diagenesis, breakdown and devitrification of the underlying basement Cliffdale Volcanics and their clasts in the Westmoreland Conglomerate. These are potassium-rich acid lavas in which breakdown of orthoclase and minor biotite would release potassium for transport in aqueous solution.

A4.2 Tectonic setting of the Siegal Volcanics

Because of the considerable alteration in many samples which has resulted in the redistribution of elements such as K_2O , Na_2O , CaO , Ba , Rb , Sr and to a lesser extent MgO also, the use of these elements may not be appropriate in determining the tectonic setting of the Siegal Volcanics. In cases where the usage of one or more of these elements is employed, then only results from the freshest samples are taken. Recent authors (Pearce and Cann, 1973; Pearce et al. 1975; Floyd and Winchester, 1975, and others) have found that discriminatory diagrams of certain of the immobile elements are useful in assessing the tectonic setting of Tertiary basic igneous rocks, and an application to Northern Australia Proterozoic basic igneous rocks has also had considerable success among numerous workers summarized by Rossiter and Ferguson (1980).

Figure 4.7 is a plot of the alkalinity nature of the Siegal Volcanics after Irving and Barager (1971). The majority of samples fall

in the sub-alkaline field indicating the tholeiitic nature of the samples. Figures 4.8-4.10 distinguish between the oceanic, continental, alkalic and tholeiitic nature of the basic suite. On the whole and despite some overlap, figures 4.8 and 4.10 indicate the non-oceanic or continental affinities of the Siegal Volcanics and the dolerites, and figure 4.9 has a spread of data which is mainly concentrated in the calc alkali basalt field.

Considering this as well as the observed association of the Siegal Volcanics with shallow water sediments (sandstone layers, one 200m thick, are found within the Siegal Volcanics) then these are best described as belonging to the continental tholeiitic basalt association.

McDougall (1962) indicated that continental tholeiites are characterized by increasing V and TiO_2 contents with iron enrichment. Figure 4.11 shows such plots which do generally indicate a trend of increasing V and TiO_2 with Fe_2O_3 , despite some abnormally high values for dykes in the low Fe_2O_3 range. Most of these dykes contain uranium mineralization or are very near to mineralized areas. The abnormal V and TiO_2 values can thus be explained given the association of uranium mineralization with V and the presence of brannerite in the mineralized dykes.

Further evidence of the continental nature of the volcanics can be gained from their high incompatible element concentration, particularly Zr which averages 150 ppm-200 ppm in the Siegal Volcanics and 250 ppm in the dolerites vs 100 ppm for oceanic tholeiites (Melson and Thompson, 1971) and from the K/Rb ratio of 270 (average of eight freshest samples) which is similar to the Ferrar Dolerite in Antarctica (Gunn, 1966) and the Karoo basalts of South Africa (Compston, et al. 1968).

Both basalts and dolerites conform to the continental tholeiitic trend and in view of their progressive differentiation sequences observed in figures 4.5 and 4.6, can be confidently said to be petrogenetically related. This is further confirmed by incompatible trace element variation diagrams presented in figure 4.12 where linear trends are also apparent. A possible petrogenetic model may begin with the extrusion of a slightly fractionated magma after differentiation in the upper crust forming the Siegal Volcanics, followed by intrusion of the residue of more highly fractionated magma as the dolerite dyke suite.

In view of the geochemical and petrological similarities of the basalts and dolerites, it appears that the original magma underwent only minor fractionation in the upper crust settling mainly plagioclase with some ilmenite/magnetite \pm apatite \pm clinopyroxene + minor zircon. This more fractionated portion gave rise to the dolerite dykes with the basaltic suite

being comprised of plagioclase, clinopyroxene, chlorite \pm magnetite/ilmenite \pm apatite.

A4.3

Origin of the melt

The remaining question to be considered concerns the origin of the tholeiitic melt prior to fractionation and emplacement. As only limited fractionation has taken place a weighted average of basalts (7) and a dolerite may approximate this original melt. The approximation is contained in Table 4.4.

Incompatible trace element ratios compared with chondritic ratios (equivalent to mantle) may also prove helpful. Four such ratios averaged from the freshest samples are observed in Table 4.5. Chondritic ratios are after Nesbitt and Sun (1976). These ratios indicate that the melt forming the Siegal Volcanics was enriched in Zr and Nb and to a lesser extent in Y also.

If one follows the now often used procedure of assuming that elements such as Zr and Ti are indicative of the MREE components and Y of the HREE components then an approximate REE pattern can be determined for the Siegal Volcanic primary melt. Relative positions of the indicator elements are after Sun et al. (1979) and Wood et al. (1979). The approximate REE pattern is found in figure 4.13 and indicates that these basalts are strongly enriched in LREE and moderately so in HREE.

Similar REE patterns for basalts have been obtained by Frey et al. (1977), who considers that these were formed by relatively high degrees of partial melting of a pyrolite mantle ($\geq 20\%$ P.M.) with olivine and pyroxene being retained. This type of process is also indicated for continental tholeiites by Carmichael et al. (1974), who consider that such parental magmas are formed by olivine and orthopyroxene separation at intracrustal levels. Such mechanism if applied to the Siegal Volcanics explains its LREE enriched nature as these elements will be concentrated in the first melts produced. The depleted nature of the HREE relative to LREE indicates that a mineral such as garnet or amphibole which would control HREE, must have been retained in the residue during mantle derivation of the primary magma. The LREE enriched magma would then rise to shallow crustal levels where minor differentiation occurred and was then erupted as a sequence of thick basalt flows followed by intrusion of the fractionated portion of the melt as the suite of dolerites.

A4.4

 Comparison with other similarly aged North-Australian basaltic suites.

It is proposed in this section to briefly compare the Siegal Volcanics and Redtree Dolerite with other Middle Proterozoic basaltic/

doleritic suites in Northern Australia in order to observe any significant similarities or differences. Figure 4.14 is a chondrite normalized REE substitution plot comparing the Siegal Volcanics with the Oenpelli Dolerite and Zamu Dolerite in the Pine Creek Geosyncline of the Northern Territory, and the Eastern Creek Volcanics of the Mt. Isa Orogenic Domain. The two Northern Territory doleritic suites are both continental tholeiites produced by olivine-orthopyroxene and olivine-plagioclase separation respectively (Stuart-Smith and Ferguson 1978; Ferguson and Needham, 1978). The Eastern Creek Volcanics are also continental tholeiites (Glickson, 1976) overlying the calc-alkaline volcanics of the Tewinga Group (Wilson, 1978).

The data indicates that all sequences are strongly enriched in LREE and less so in HREE. This, coupled with their similar ages suggests that all may have originated from a similar source, either having undergone different degrees of partial melting or differentiation before emplacement. Giles and Teale (1979a) have employed a ratio method of overcoming the effects of variable differentiation when comparing different basaltic suites. They have used the ratios of incompatible elements, e.g. Ce/Y, Nd/Y etc. since the increase in elemental concentration with differentiation implies that their ratios should remain constant. These ratios can then be chondrite normalized to indicate enrichment or depletion relative to the primary mantle value. Figure 4.15 contains the data. It suggests that the Siegal Volcanics and Eastern Creek Volcanics are very similar and likely to be related to the same tectonic processes. The Zamu Dolerite and Oenpelli Dolerite are distinctly enriched in LREE and HREE relative to the Siegal Volcanics and Eastern Creek Volcanics though are similar in MREE. This implies that these two groupings have been derived from subtly different sources.

Varying degrees of partial melting for both groups would not simply explain the differences as the MREE portion of the Northern Territory dolerites is not similarly enriched as are the LREE and HREE portions. The difference rather suggests that both groups had a different residuum after initiation of melting with the residue of the Oenpelli and Zamu Dolerites containing less apatite and garnet/amphibole than the residue of the Siegal and Eastern Creek Volcanics thus enriching the melt of the former group in LREE and HREE.

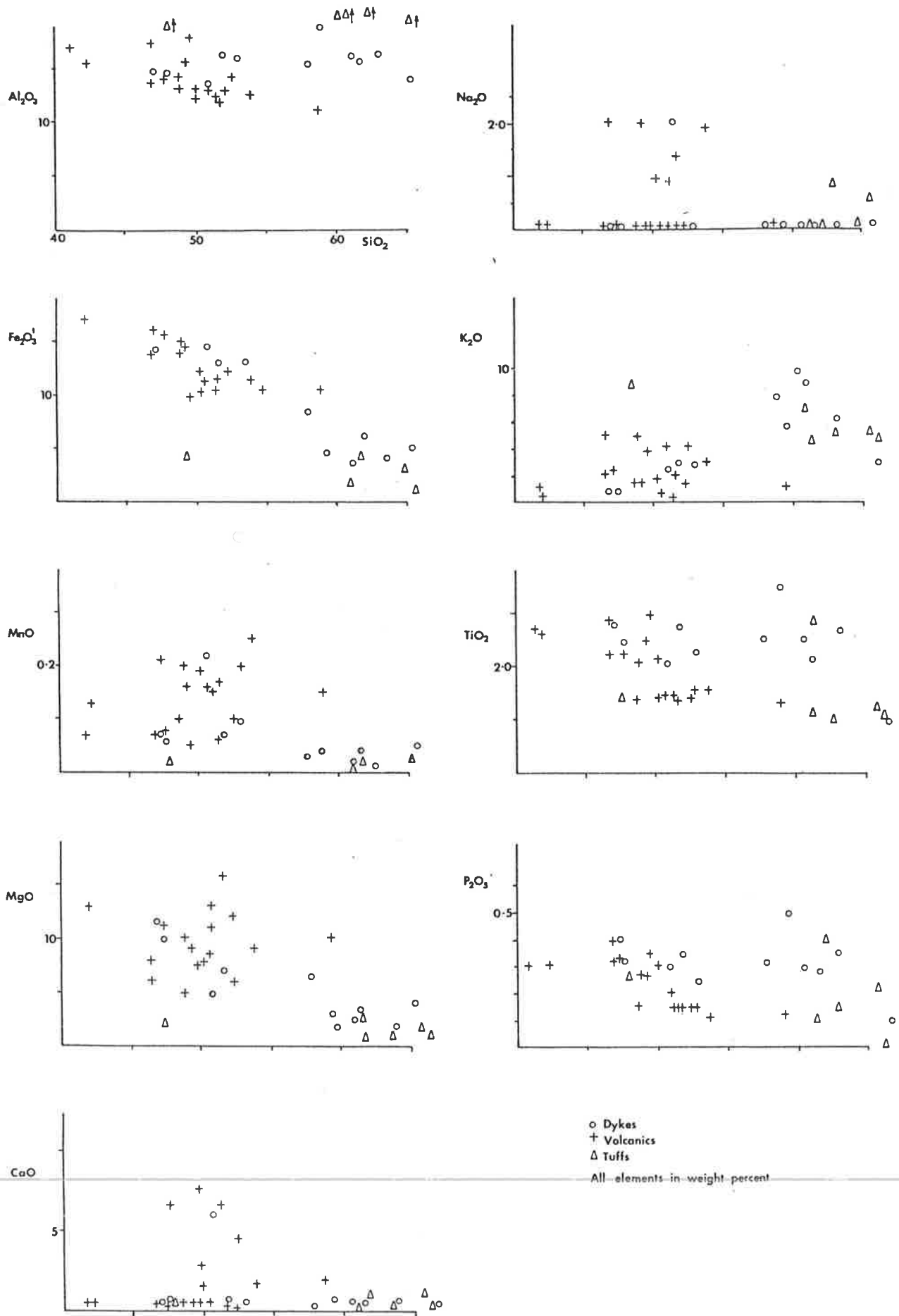


Figure 4.5 Major element variation diagrams vs SiO_2 for the Siegal Volcanics, dykes and tuffs.

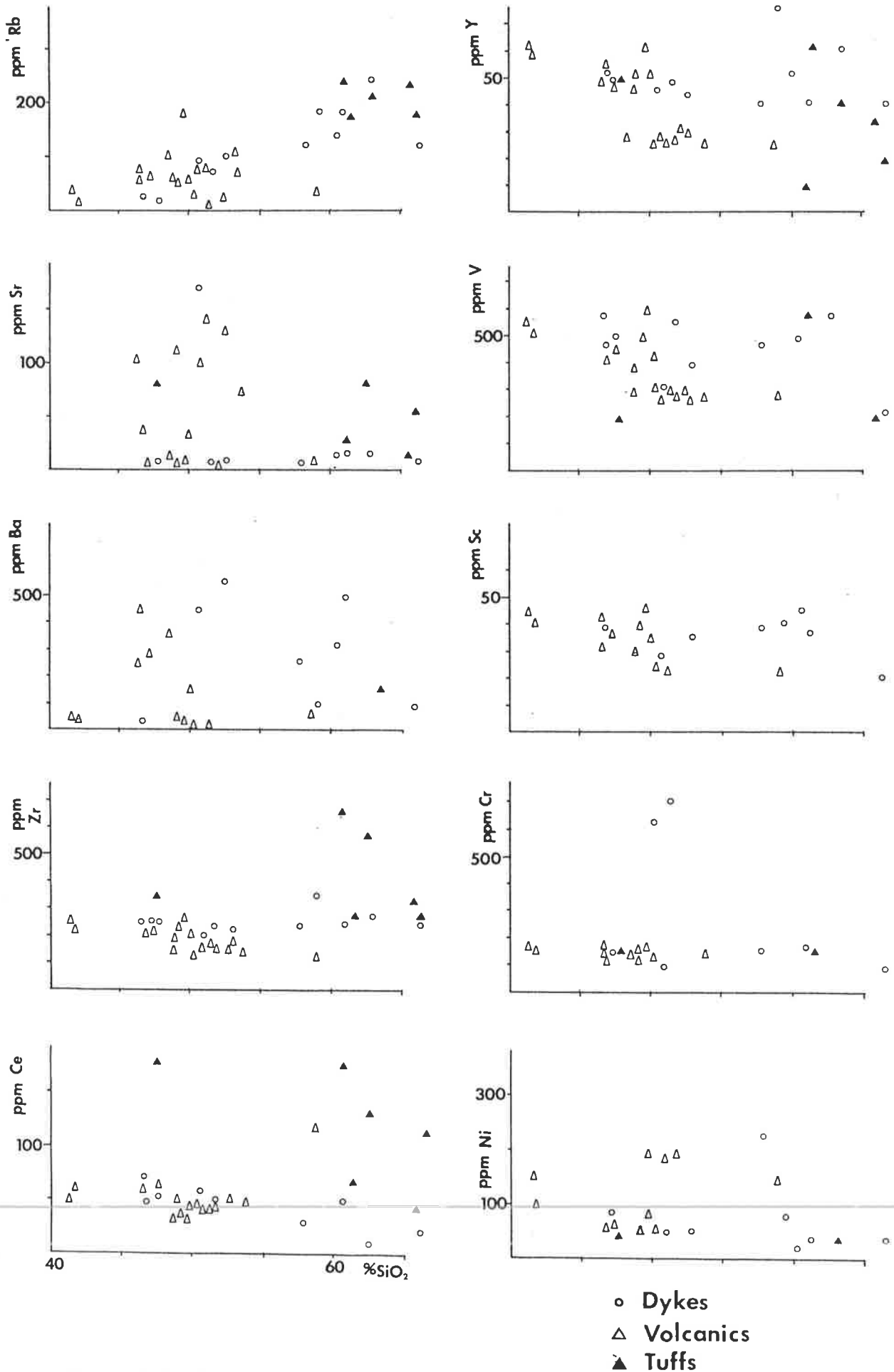


Figure 4.6 Trace element variation diagrams vs SiO₂ for the Siegal Volcanics, dykes and tuffs.

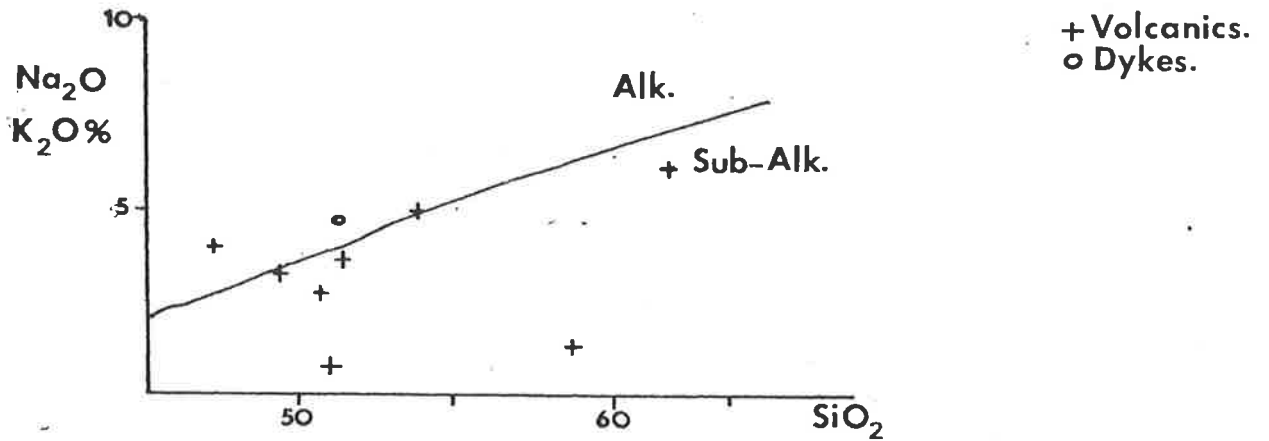


Figure 4.7 Alkalinity diagram for the Westmoreland basic rocks (after Irving and Baranger, 1971).

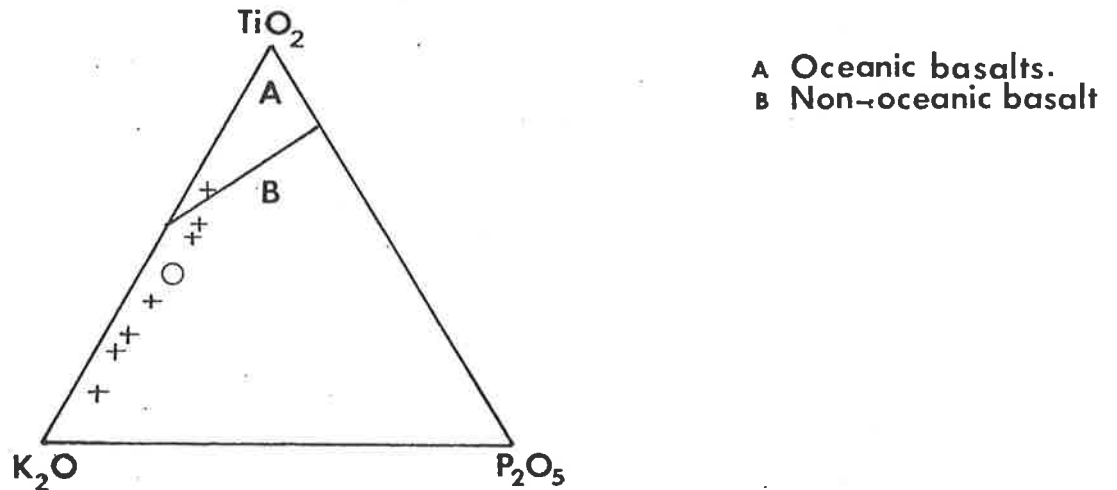


Figure 4.8 Discriminatory diagram for oceanic and non-oceanic basalts (after Pearce et al. 1975).

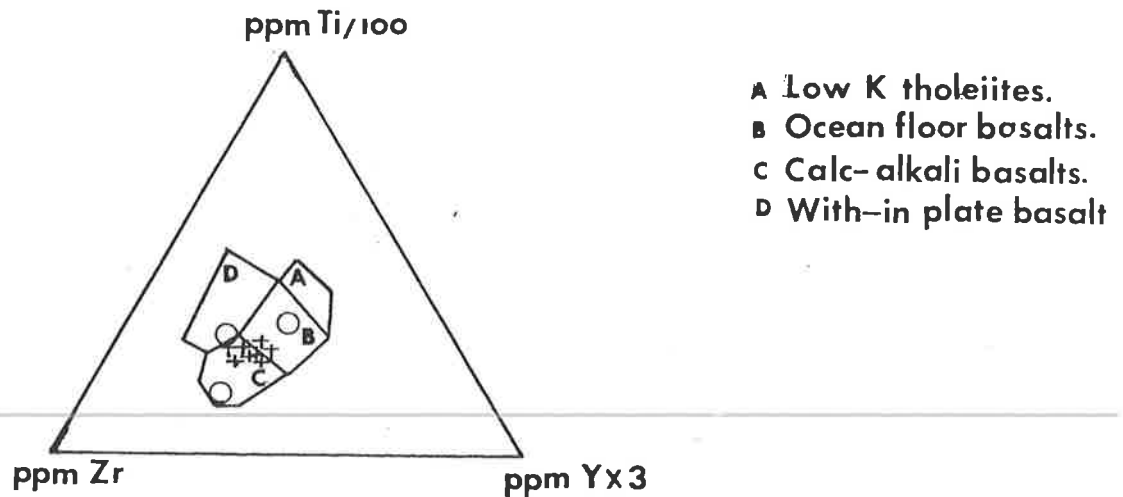


Figure 4.9 Trace element determination of tectonic setting (after Pearce and Cann, 1973).

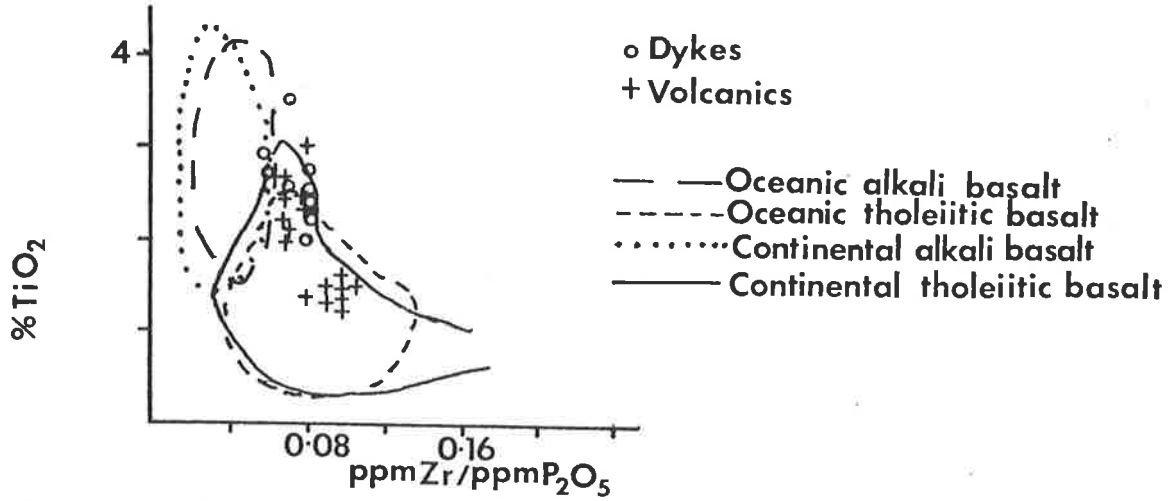


Figure 4.10 Basaltic tectonic settings (after Floyd and Winchester, 1975).

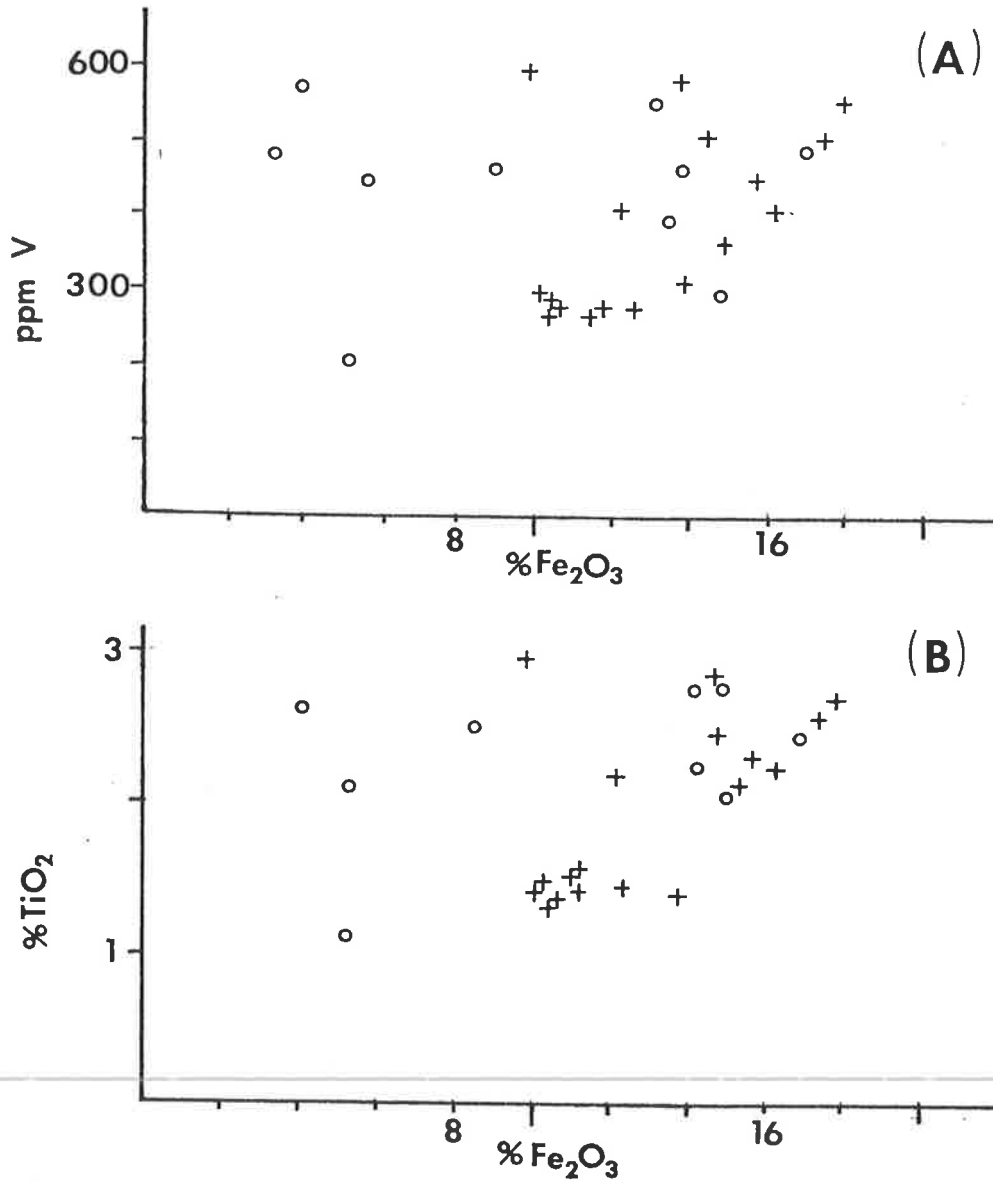


Figure 4.11 Percentage of Fe₂O₃ vs (a) ppm V and (b) percentage TiO₂ (after McDougall, 1962).

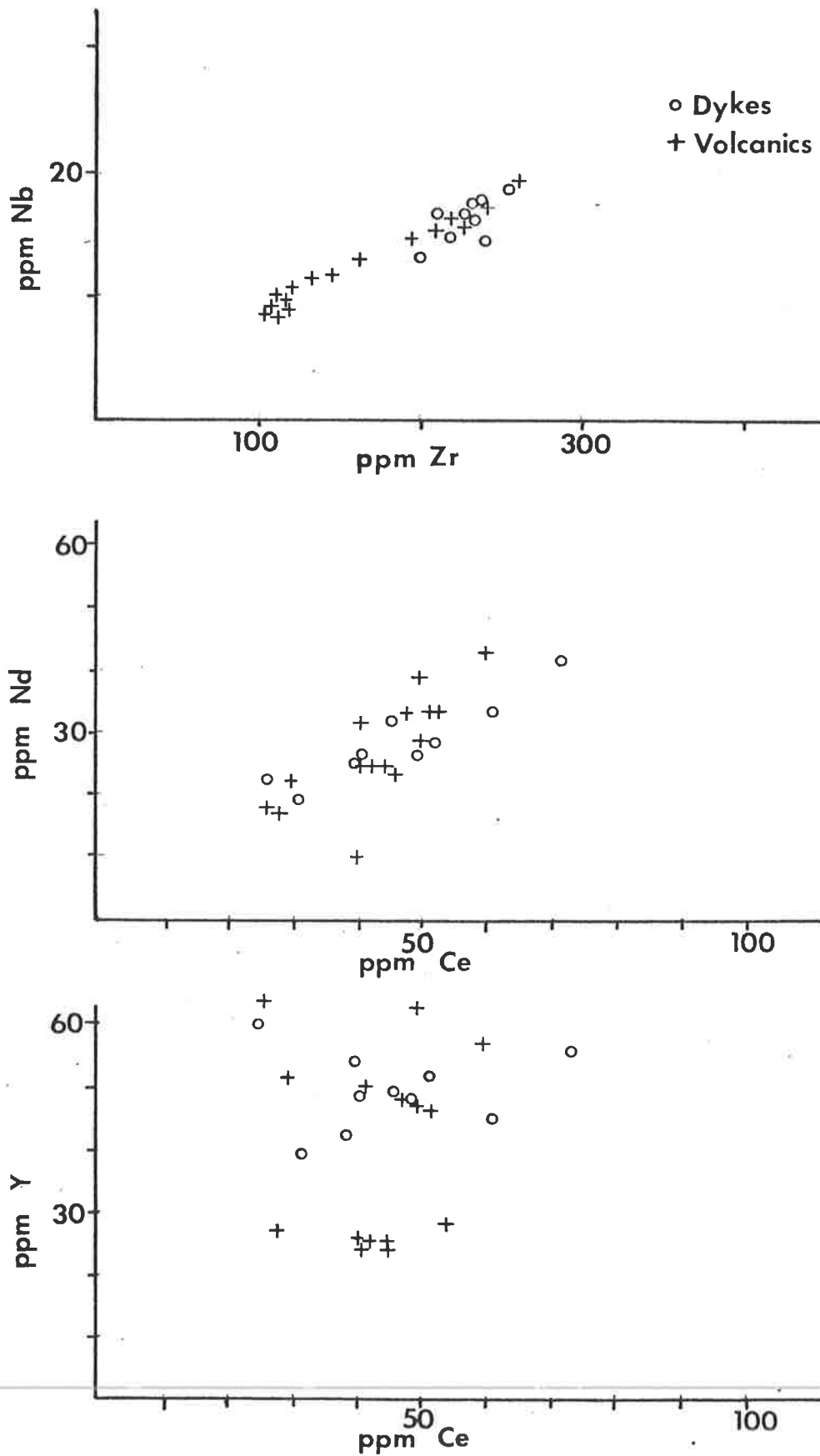


Figure 4.12 Variation diagrams of selected incompatible trace elements: Zr vs Nb; Ce vs Nd and Ce vs Y.

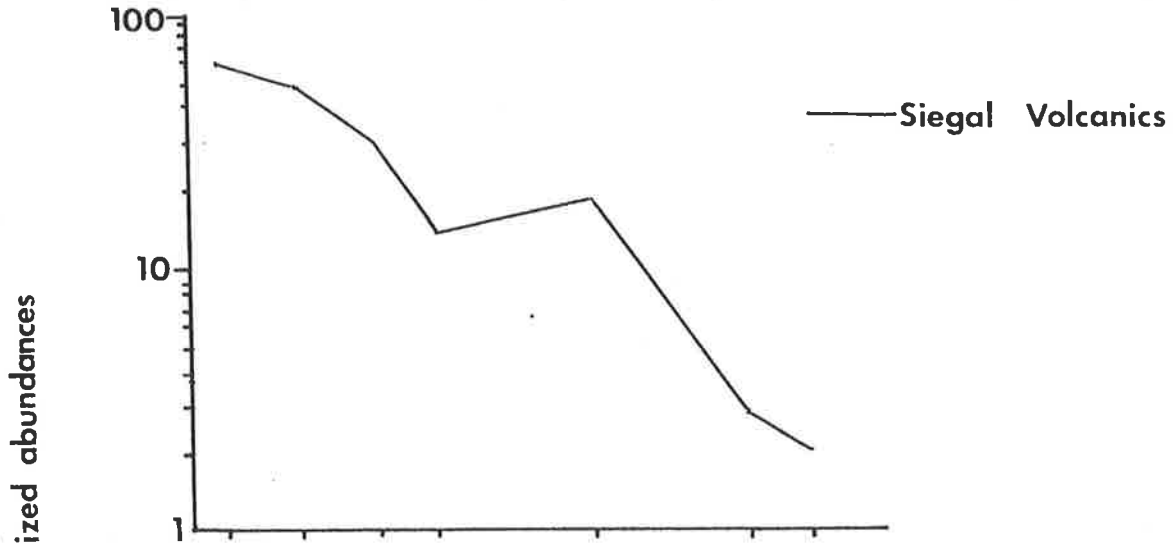


Figure 4.13 Chondrite normalized rare earth element plot for the Siegal Volcanics.

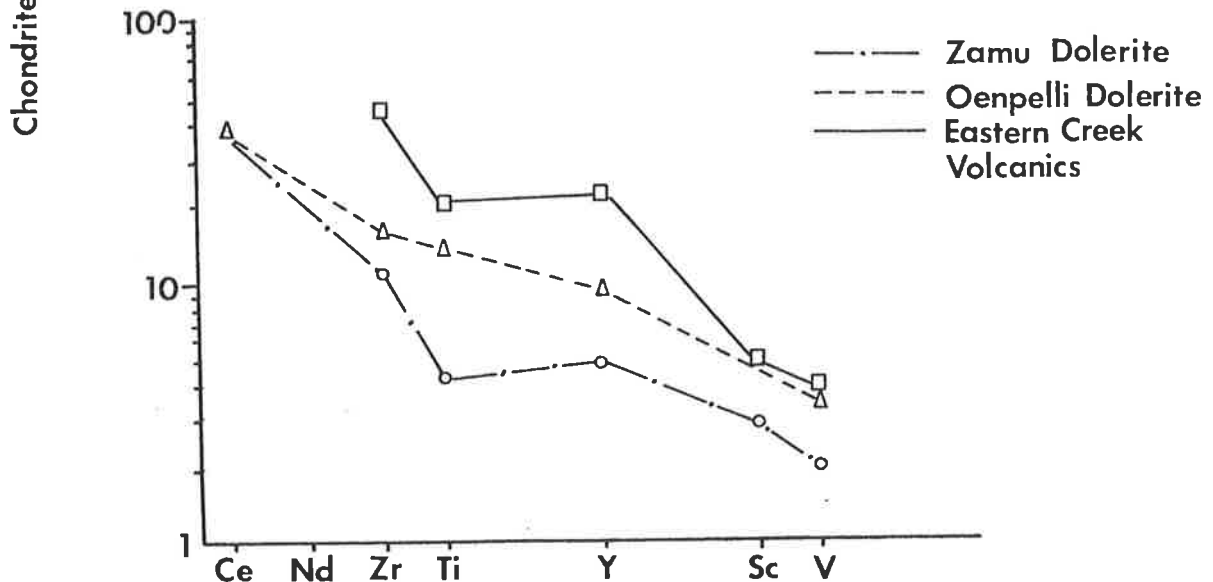


Figure 4.14 Chondrite normalized rare earth element plot for other North Australian Proterozoic basaltic suites.

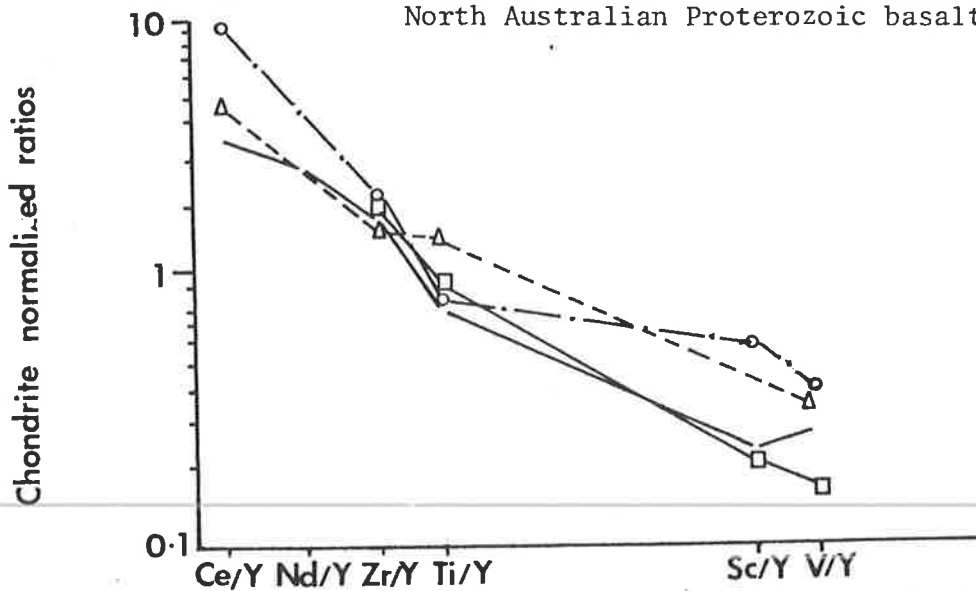


Figure 4.15 Chondrite normalized rare earth element ratios for the Siegal Volcanics and other North Australian Proterozoic basaltic suites.

Ratio	Siegal Volcanics	Chondrite
Ti/Zr	51.0	100-110
Ti/Y	237.1	256
Zr/Y	4.65	2.5
Zr/Nb	14.3	16

Table 4.5: Incompatible trace element ratios for the Siegal Volcanics compared with chondritic ratios.

SiO ₂	50.71
Al ₂ O ₃	13.04
Fe ₂ O ₃ ^t	12.63
MnO	0.20
MgO	7.63
CaO	4.99
Na ₂ O	1.71
K ₂ O	2.16
TiO ₂	1.77
P ₂ O ₅	0.21
LOI	4.62
Total	<u>99.67</u>
Rb	66
Sr	95
¹ Ba	293
Ce	49
Nd	29
Zr	170
Nb	11.9
¹ Ni	78
V	329
¹ Sc	30
Y	36
¹ Cr	121

¹Average of 5 samples.

Table 4.4: Weighted geochemical average of the eight freshest samples of seven basalts and one dolerite.

THERMOLUMINESCENCE AS A TOOL IN URANIUM EXPLORATION

M.B.M. HOCHMAN and P.J.M. YPMA

Department of Economic Geology, University of Adelaide, P.O. Box 498, Adelaide SA 5001 (Australia)

(Received May 25, 1983; revised and accepted February 22, 1984)

ABSTRACT

Hochman, M.B.M. and Ypma, P.J.M., 1984. Thermoluminescence as a tool in uranium exploration. *J. Geochem. Explor.*, 22: 313–331.

Fundamental principles of thermoluminescence (TL) and the special role of TL in uranium exploration techniques are given in this paper with examples from Australia illustrating its application.

TL can be used in two ways in uranium exploration. The first usage stems from the property of minerals capable of TL, to act as dosimeters accounting for charging of available traps by ionizing radiation. The second usage relates to ionizing radiation interfering with the crystal structure of the host mineral and thereby changing the capability for TL. Studies at the Beverley and Westmoreland uranium deposits utilize this second property.

At Beverley a continuous drop in TL intensity is observed upon approaching the orebody with TL intensity at a minimum within the orebody. Recognition of ore type TL glow curves and sensitized (or marginal) TL glow curves within the area surrounding the orebody have enlarged the exploration target beyond that of the orebody and its associated radiometric halo.

Traverses examining the variations in glow peak intensities, ratios and temperatures across the Junnagunna orebody at Westmoreland show that the glow peak intensity of the high-temperature glow peak increases, that of the low-temperature peak fluctuates though generally decreases, the high temperature/low-temperature glow peak ratio increases upon approaching the orebody. The high-temperature glow peak temperature is at a minimum within the orebody. Similar variations detected nearby may indicate further potential exploration sites.

An example from an unmineralized area at Bremer River has indicated a lack of widespread radiation sensitization indicating the unsuitability of the area for economic uranium accumulation.

INTRODUCTION

Thermoluminescence (TL) describes the emission of light caused by thermal activation of trapped excess electrons and their corresponding electron deficient sites (holes). Activation may lead to a recombination of electron and hole and the resultant emission of a quantum of light.

The phenomenon of TL has been known in physics since 1663 when

Robert Boyle remarked of a certain Mr. Clayton's diamond that it "being rubb'd upon my cloaths ... did in the dark manifestly shine like rotten wood, or the scales of whittings, or other putrified fish ... much fainter than the light of a glowworm ... " (quoted in Aitken, 1965). Little work was done in the intervening 300 years till that of Randall and Wilkins (1945), since which time much research has been devoted to the understanding of the physical processes involved, and the application of TL to dating, palaeoclimate determination and mineral exploration. A summary of these and other applications may be found in McDougall (1968).

This paper deals with examples of the application of thermoluminescence to uranium exploration.

BASIC PRINCIPLES OF THERMOLUMINESCENCE

Ionizing radiation entering a crystal is capable of dislodging electrons from their atomic positions thus creating free electrons and holes (sites which have lost an electron). Most electrons and holes recombine almost immediately but in non-conducting minerals a small percentage of the holes and excess electrons may be trapped on lattice defects and impurities.

In quartz, the mineral most widely used in TL investigations of uranium deposits, a well known hole trap is a silicon site in which Al^{3+} has been substituted for Si^{4+} . Electrons can also be trapped, usually on vacant oxygen sites where an O^{2-} charge is missing. Initially the number of hole traps in quartz may be expected to be larger than the number of electron traps, but as the number of holes and electrons eventually trapped must be equal, the electron trapping mechanism becomes the predominant factor affecting the resultant strength of the TL signal.

These trapped charges can be released by thermal activation which facilitates recombination of holes and electrons. If recombination occurs at a specific site it may result in the emission of a quantum of visible light. This light can be measured and recorded as a glow peak. As electrons and holes may be trapped on a variety of sites with different crystal field energy, different amounts of thermal activation will be required to release them, and so over a range of temperature a number of glow peaks are recorded which constitute a glow curve. In this study, measurements of quartz gave three major glow peaks at approximately 190°C – 260°C – 350°C with subordinate peaks at 150°C and 220°C .

Further details regarding the theory of TL particularly related to quartz may be found in Kaul et al. (1972), Fuller and Levy (1977), Durrani et al. (1977a, b) and David et al. (1977).

The intensity and shape of the quartz glow curve depends on a number of factors such as lattice vacancies and impurities capable of acting as traps and on their respective crystal field energies, trap densities and charge occupancies. The charge occupancy rate is a function of ionizing radiation. As the charge occupancy affects the strength of the TL signal, TL has been used

as a dosimeter. However as radiation may also affect trap densities a permanent variation in both intensity and shape of the glow curve may be the result. This property, i.e. quartz "remembering" exposure to past radiation may be utilized in uranium exploration (Levy, 1978).

EFFECT OF RADIATION ON QUARTZ TL GLOW CURVE

Figure 1a shows a typical glow curve for quartz which has not been subject to more than small amounts of radiation. It shows three major glow peaks with the low temperature (LT) and middle temperature (MT) peaks being most prominent. For radiation doses less than 5×10^5 rads the shape of the glow curve remains essentially the same although the intensity of the peaks will increase as the dose increases. At a cumulative dose of approximately 5×10^5 rads the process of sensitization begins. This describes the stage where the quartz lattice itself is affected leading to changes in the shape of the glow curve. Further details regarding the exact dose and physical processes involved may be found in the references cited above.

Figure 1b shows the sensitization stage after exposure to radiation doses above 5×10^5 rads. The LT peak has increased in intensity such that it obscures the other peaks. Apparently doses up to 10^8 rads improve the efficiency of the electron-hole entrapment process probably by the creation of more electron traps to restore the imbalance between hole (abundant) and electron traps (Zimmerman, 1971; Kaul et al., 1972; Shekhmametev, 1973; Durrani et al., 1977a, Levy, 1978). The net gain in electron traps results in an increase in the efficiency of the electron-hole pair entrapment and recombination process by a factor of 20–100 and is expressed by an increase of the intensity of the LT peak.

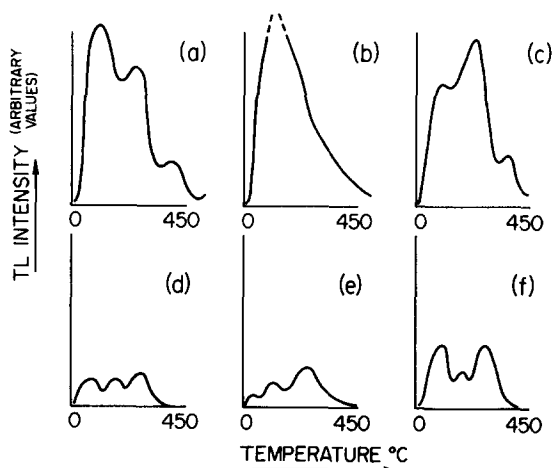


Fig. 1. Variation in thermoluminescence intensity and glow curve shape with increasing radiation. (a) represents the case of little radiation sensitization and (c) represents the onset of major radiation damage. Further details are given in the text.

At some stage the number of electron traps will equal the number of hole traps and further radiation beyond this will cause the number of hole traps to become the limiting factor in the entrapment and recombination process. Levy (1978) put this optimal ratio as the result of 2×10^8 rads. Exceeding this radiation dose causes a sharp drop in TL intensity seen in Fig. 1c — decreasing to two or three percent of the previous intensity. This stage will naturally occur at different radiation doses for different glow peaks and is classed as the stage at which major radiation damage has occurred to the quartz lattice. Figure 1d illustrates the case where the MT peak has also surpassed its optimal ratio.

Further radiation exposure to the quartz crystal results in a continual decay in the LT and MT peaks whilst the high temperature peak (HT = 350°C) continues to increase. This is represented in Fig. 1e which is the glow curve most commonly observed from the host quartz of mineralized uranium samples.

Radiation damaged quartz may recover by annealing of the crystal which will first be visible for the LT and MT peaks such that they may start to increase in intensity though to nowhere near their original level. This annealing effect is represented in Fig. 1f. Such occurrences are rare and geologically correspond to thermal influences since major radiation damage occurred.

GEOLOGICAL APPLICATION OF TL AND PREVIOUS USAGE

TL can be used in two ways in geological studies. The first relates to the charging or filling of available traps by ionizing radiation. As the radiation dose is increased the TL intensity also increases. In this usage TL plays the role of a dosimeter — measuring the amount of incident radiation. This is the principle applied in TL dating, in particular in archaeology and in general to all sediments which have been exposed (bleached) by UV light from the sun. For TL to be effective the present radioactive element concentrations and their corresponding radiation dose rates must be known. TL can be used to measure total radiation dose and hence an age can be calculated.

The second type of application follows from the changes in the number of available traps caused by the ionizing radiation as explained in the preceding section. These changes, expressed in the range of glow curves in Fig. 1, reflect the total dose to which the quartz sample has been subjected, that is the past and present dose, and herein lies the advantage of TL in uranium exploration over conventional techniques such as geochemistry, soil radon surveys, alpha metering, radiometrics etc. These latter techniques rely on detection of the uranium or its daughter products close to mineralization. However, because TL is a measure of past as well as present radiation dose it does not rely on proximity to mineralization in order to detect radiation sensitization or damage to the host quartz lattice. In the case of progressive cumulative deposits such as Tertiary roll front type deposits, TL has the capability of tracing radiation effects over a distance of kilometres from the present ore position. The usefulness of such a technique in present arid and

deeply weathered environments is immediately obvious as past radiation effects should still be discernable, while the actual cause of the TL anomalies has been completely removed from the surface or sample.

There have been some previous attempts to use TL in uranium exploration. Spirakis et al. (1977) used TL to track the front of a South Texas roll front type deposit. The geology of such deposits is given in Goldhaber et al. (1978) and Reynolds and Goldhaber (1978). Spirakis et al. (1977) used the increase in intensity of the low-temperature glow peaks (100–310°C) towards mineralization as a means of monitoring roll front positions in the Miocene Catahoula Sandstone. They found: (a) a total increased TL response in areas through which the roll front must have passed; and (b) an increase in the ratio of low-temperature to high-temperature (315–410°C) glow peaks in areas which contain a higher proportion of immobile uranium, such as the front of ore zones. Their study thus used TL purely as a dosimeter showing all samples still in the sensitization stage with no major radiation damage.

Charlet et al. (1978) conducted a TL study on the Bleton anomaly near Mons (Belgium) where a series of Viséan-Namurian strata containing a radioactive bed were covered by Tertiary sands. Their study was concentrated on the Tertiary sand and succeeded in detecting several low anomalies (eU: 100 ppm at most) in the underlying strata which had not previously been detected by scintillometer techniques. They concluded that TL could be used in exploration for uranium mineralization buried at too great a depth to be detected by scintillometer techniques.

EXPERIMENTAL PROCEDURE

Samples of rock, drill core, percussion chips or unconsolidated sands are all suitable. After crushing, samples are sieved to extract the -30 +50# fraction. This fraction is washed to remove dust, dried and passed through a Frantz electromagnetic separator (utilizing the diamagnetic properties of quartz) to separate quartz. Samples are then assessed under a binocular microscope to ensure that impurities are absent and to record the quartz type, i.e., clear, white, milky, iron-stained, smoky, etc.

As natural TL measurements are meaningless on samples which have been exposed to UV rays from sunlight (UV rays will bleach the TL), artificial TL must be induced. This involves the filling of the lattice defects described earlier by exposing the sample to a radiation dose less than that required to induce sensitization. Quartz samples are placed in gelatine capsules, covered in aluminium foil to shield them from further sunlight, and irradiated by ^{60}Co gamma rays to a total test dose of 5×10^5 rads. Samples are then left for 24–72 hours to allow phosphorescence to decay and are measured on standard TL measuring equipment in an atmosphere of flowing high-purity nitrogen to avoid chemiluminescence.

Reproduceability of samples from the same core is $\pm 10\%$ for glow peak intensity and $\pm 5\%$ for glow peak temperatures. Reproduceability of ratios

of glow peak intensities is $\pm 5\%$. The subject of fluctuations is considered in the discussion of results.

Effect of thorium and potassium

The effects of potassium (1 ppm contributes 0.112 rads/year) and thorium (1 ppm contributes 0.079 rads/year) are negligible compared with uranium (1 ppm contributes 0.312 rads/year) in the vicinity of a major uranium deposit).

RESULTS

Beverley, South Australia

The Beverley uranium deposit occurs in a sedimentary sequence of Miocene age about 10 km east of the metamorphic Mt. Painter Block which is of Proterozoic age (Fig. 2). The deposit has no radiometric surface expression of any kind and was discovered by drilling. The exploration model was based on the premise that uplift of the uraniferous Mt. Painter Block established a hydraulic head driving uranium-bearing solutions into the sedimentary pediment of the Lake Frome embayment. An account of the regional geology of the Beverley area is given by Haynes (1976) and Callen (1976).

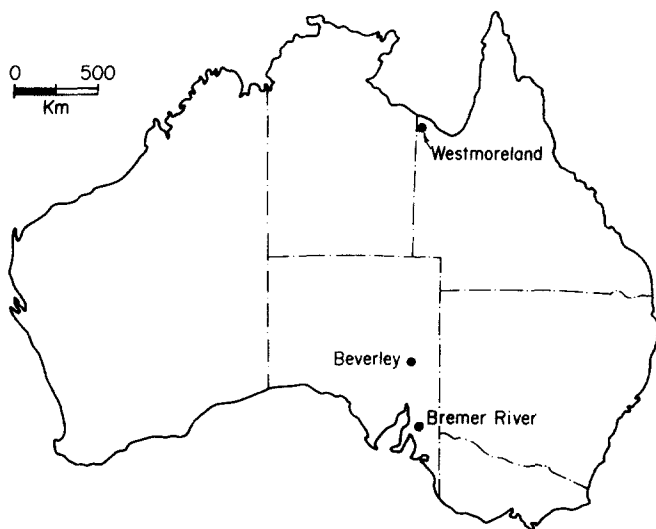


Fig. 2. Locality map of the Beverley and Westmoreland Uranium Deposits and the Bremer River prospect.

Drilling started close to the Mt. Painter area and proceeded eastward along creek beds, under the assumption that Tertiary channels had similar locations. This led to the discovery of a series of north-south-trending sand-

stone lenses containing uraninite which constitute the Beverley orebody. The ores are contained in the lower part of an arenaceous formation resting on finer grained carbonaceous shales and siltstones.

Samples for a TL study were collected from a series of drillholes extending away from the Mt. Painter basement towards the Beverley orebody, and from other holes around the orebody. Locations of holes sampled are contained in Fig. 3. Note that holes with the same prefix, 39, 39A, 39A56W etc. indicate holes drilled close to hole 39 in Fig. 3. Three samples were collected from each hole — one from the arenaceous formation hosting the mineralization and one each from the intervals 10 m above and 10 m below this unit.

The data fit into three categories: (1) background (upstream of the orebody); (2) marginal, and (3) ore-type TL values. Figures 3 and 4 indicate a gradual increase in radiation sensitization through holes 32, 31 etc. (7 km from the orebody) to holes 26, 48 etc. (at a distance of 3 km from the orebody) and major radiation damage in 46, 33A, 42 (at a distance of 1–1.5 km from the orebody).

The degree of radiation damage — notwithstanding the young age of the

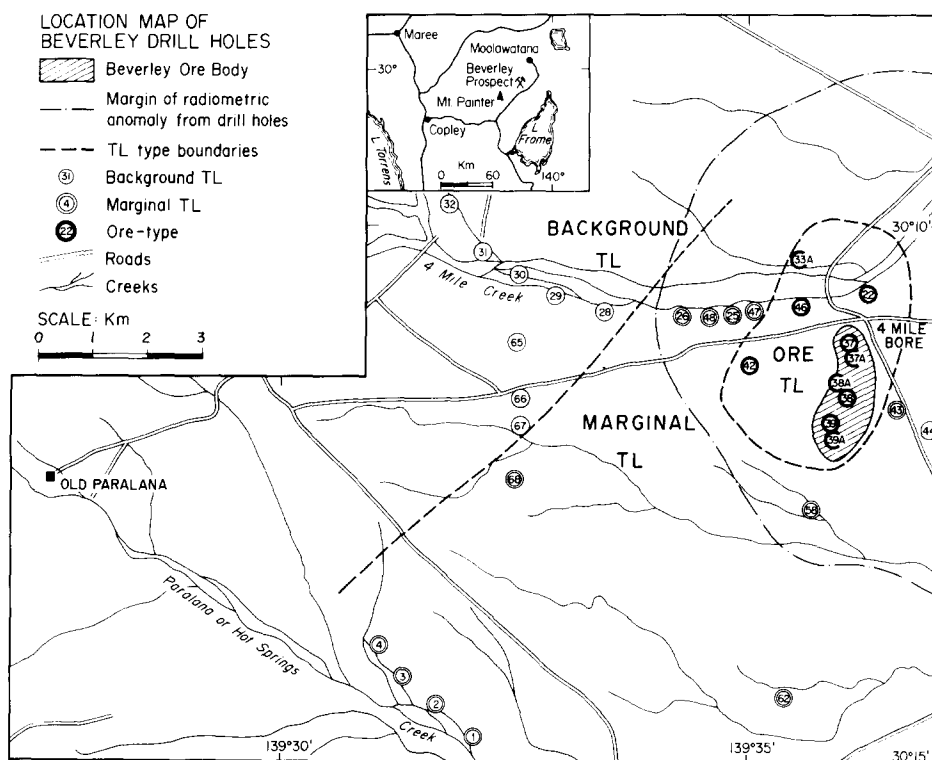


Fig. 3. Location of the Beverley drill holes showing TL and radiometric haloes. Note the much larger marginal TL halo compared to radiometric halo and ore type TL zone as compared to the orebody.

deposit — suggests that the marginal TL type is due to actual uranium mineralization which has been displaced downstream by oxidizing uranium-bearing solutions. The uranium content expected in such solutions (100–1000 ppb) is too low to have produced the radiation damage observed.

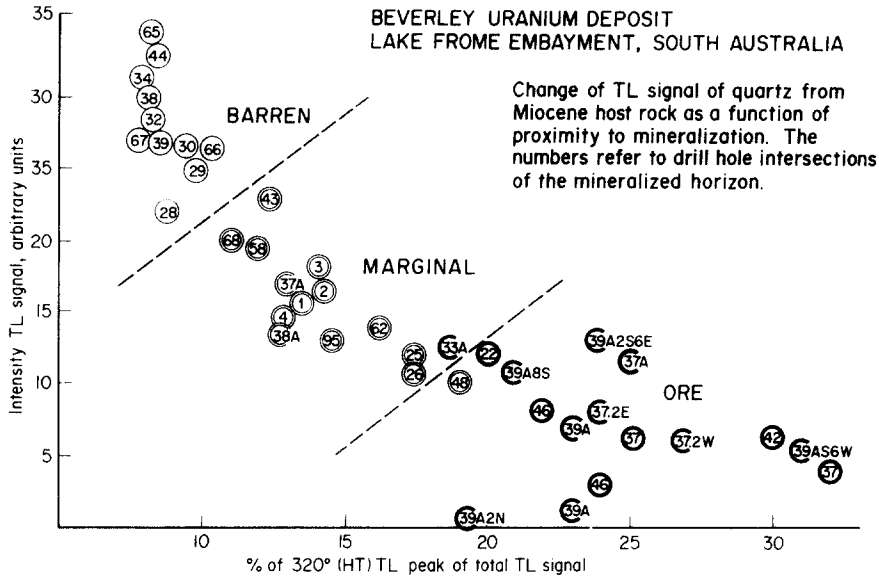


Fig. 4. Variation in TL signal of quartz as a function of proximity to mineralization at Beverley.

Samples 10 m above and 10 m below the mineralized horizon indicated a lack of radiation damage, which means that uranium precipitation was confined to a layered zone of limited thickness. Uranium only occurs in underlying and overlying rocks in the vicinity of the main orebodies.

A significant point is that some holes show mineralized TL glow curves (42, 22, 46, 33A) but contain no uranium mineralization. Recognition of “mineralized” TL glow curves in non-mineralized areas surrounding the orebody has effectively enlarged the target zone above that of geochemistry. Note that in Fig. 3 this zone of “mineralized” ore-type TL is four to five times larger than the actual orebody.

Recognition of the existence of a marginal TL zone incorporating holes 1, 2, 3, 4, 62, 58 and 68, as well as non-mineralized holes on the same drainage channel as the orebody, has enlarged the secondary target zone far beyond that of the radiometric halo.

Holes 1, 2, 3 and 4 were drilled in a separate drainage channel to the south of the Beverley orebody. These are all non-mineralized but exhibit marginal TL. TL measurements at this stage of exploration would have indicated the absence of increasing sensitization patterns within this particular drainage

channel, yet with the recognition that they exhibited marginal TL, may have facilitated an earlier discovery of the orebody.

Westmoreland, Queensland

The Westmoreland uranium deposits are situated approximately 400 km north-northwest of Mt. Isa (Fig. 2) and occur in the Middle Proterozoic Westmoreland Conglomerate, the lowermost unit of the Tawallah Group which is, itself, the lowermost member of the McArthur Basin sedimentary succession (Plumb and Derrick, 1975).

The main ore mineral is pitchblende with secondary carnotite and meta-torbernite at the surface. The orebodies comprise a series of horizontal lenses and vertical pods adjacent to northeast-trending dolerite dykes and underlying the basaltic Siegal Volcanics. Further details of mineralization are contained in Hills and Thakur (1975).

The analysis of more than 600 samples of the host rock and of different quartz types found in basement or in veins was undertaken.

The most noticeable feature of samples measured was that all had suffered major radiation damage and hence had a reduced TL intensity. The large variation in TL intensity observed upon approaching Tertiary uranium deposits was therefore absent. The small variations still present, however, corresponded to variations in glow curves contained in Fig. 1, d and e.

Traverses across the largest of the orebodies — the Junnagunna prospect (Fuchs and Schindlmayer, 1981) — examined variations in (a) TL intensity of the LT and HT glow peaks, (b) HT/LT glow peak ratios and (c) temperature of the HT glow peak. Drill hole locations used in the traverses are given in Fig. 5.

Peak intensity and glow peak ratio traverses

Figure 6 A–G shows the variations in peak intensities and ratios across the Junnagunna orebody for samples taken within 10 m of the Westmoreland Conglomerate/Siegal Volcanics contact. Although there is no linear correlation between peak intensity and grade of mineralization there is a positive correlation in some instances between the peak intensity and the geographical ore position (regardless of grade). For example in Fig. 6F the LT peak doubles in intensity away from ore. A smaller increase in LT peak intensity is also observed away from minor mineralization found in hole 146 (Fig. 6I), however, the opposite trend is observed in Fig. 6G with LT peak intensity decreasing away from ore. In other traverses the LT peak intensity is variable and no distinct trends are present.

The HT peak intensity is generally at a maximum within the mineralized zones and decreases away from mineralization, e.g. Fig. 6C, G and I and, to a lesser extent, Fig. 6F.

No absolute LT or HT peak intensity is characteristic of mineralization, e.g. a HT peak intensity of 600–700 in Fig. 6F corresponds to a grade of

0.22% U_3O_8 , whereas a HT peak intensity of 700–800 in Fig. 6A occurs in a non-mineralized zone. This suggests that absolute peak intensity is of doubtful value as an indicator of proximity to mineralization in Proterozoic uranium deposits where there is likely to have been much mobilization and redistribution of mineralization.

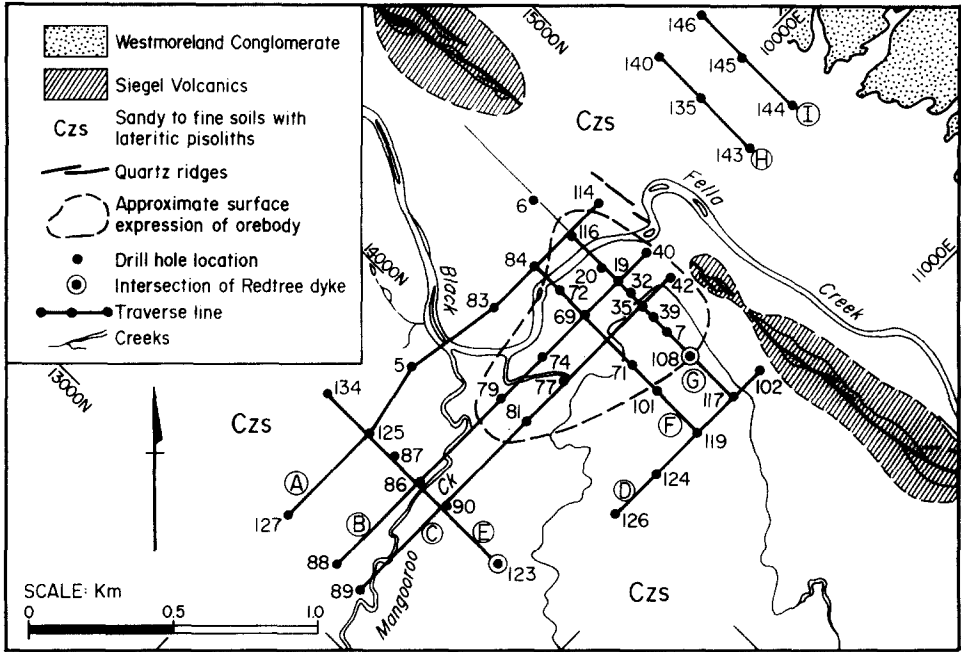


Fig. 5. Drill hole locations at Junnagunna. Dark lines represent traverse lines used in the following figure.

The HT/LT peak ratio in Fig. 6 increases upon approaching the main orebody (Fig. 6B, C, F and G) or minor mineralization (Fig. 6I). In these traverses a HT/LT peak ratio of greater than 1.4 indicates proximity to the orebody. Many presently non-mineralized samples have a HT/LT peak ratio of greater than 1.0 indicating that they have suffered radiation damage almost to the same extent as presently mineralized samples. This suggests that these too may have been mineralized at some stage in the past, that is they are areas formerly occupied by mineralization.

Interpretations of these techniques in this instance are as follows:

(1) Once a sample has crossed the radiation damage threshold, further incident radiation should cause the LT glow peak to decrease and the HT glow peak to increase. This is expected when approaching mineralized zones.

(2) Local fluctuations and some non-linearity can be expected as TL measures positions of both past and present ore, and for this reason, no correlation is expected between present ore grade and TL intensity.

(3) Further fluctuations can be caused by the variable concentration of

hole and electron traps in different samples and by a variable ionization effect caused by short range alpha-particles.

Despite such local fluctuations overall trends should still be present. Figure 6 shows that these local fluctuations affect the LT traps more than the HT traps and therefore LT peak intensity alone is not a reliable guide of proximity to this particular type of mineralization. The HT peak intensity is

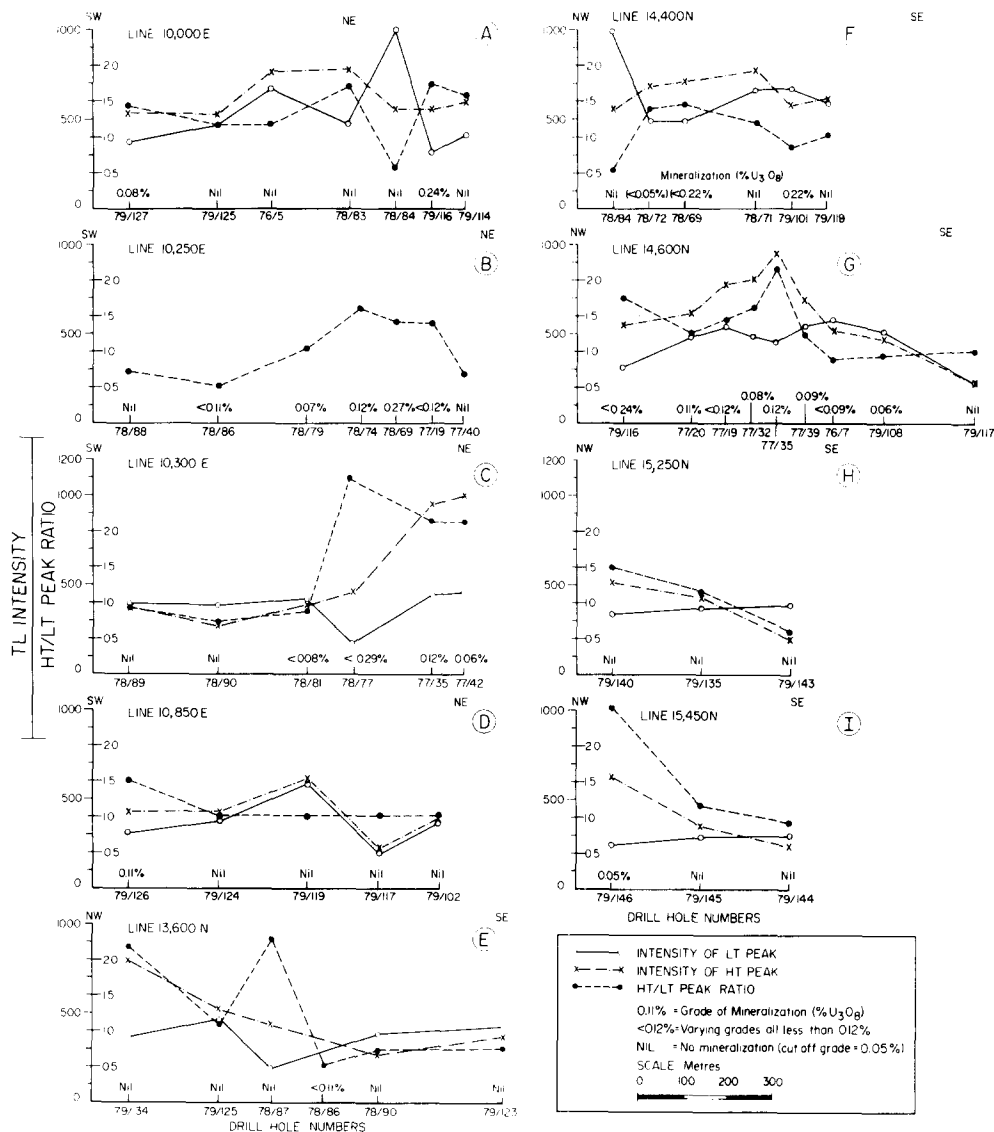


Fig. 6. Traverses showing variation in TL intensity and glow peak ratio across the Junnagunna orebody.

less susceptible to local fluctuation and may be of localized use within known orebodies.

Ratio of glow peaks

As the LT glow peak decreases and the HT glow peak increases the HT/LT glow peak ratio should also increase. This ratio has generally been observed to be a reliable indicator of increasing radiation sensitization and damage because many fluctuations mentioned above will be cancelled out.

Analysis of these three parameters, particularly the latter two, could prove useful within a known uraniferous area to identify, in areas distant from the orebody, increasing sensitization trends which are similar to those observed upon approaching the orebody. Such trends can be used to suggest sites for extensions to the orebody or even new orebodies (Fig. 6E and Fig. 6H, I).

Figure 6H and I show two parallel northwest-southeast trending traverses away from the proposed extension of the Redtree dyke (assumed to be close to holes 143 and 144 and having a north-easterly trend). Both traverses indicate increasing sensitization to the northwest with HT/LT peak ratios greater than 1.4 in holes 146 and 140, and intersection of minor mineralization in hole 146. This trend is similar to that observed upon approaching the main Junnagunna orebody and is consistent with the idea of increasing proximity to further mineralization.

Similarly increasing sensitization to the northwest is shown in Fig. 6E towards a locality near which minor mineralization had previously been detected. Results of follow-up work on these sensitization trends are not yet known.

Glow peak temperature traverses

A shift in the temperature of individual glow peaks which is present in or near ore samples could also be used as a potential indicator of proximity to mineralization. This shift is most noticeable in the 350°C glow peak (HT) and Fig. 7 shows the variation of this parameter across three of the previously selected traverses. Results are promising with Fig. 7A indicating all non-mineralized samples having a HT glow peak temperature greater than 365°C, whilst for two of the three mineralized samples the equivalent temperature is less than 340°C. Figure 7B indicates a wide spread of HT glow peak temperatures (328–352°C) in ore though they are generally less than 340°C. The temperature is lowest in the central part of the orebody. Figure 7C again shows all mineralized samples as having a HT glow peak temperature of less than 340°C as does one non-mineralized sample.

In general (13 out of 15 samples) the 350°C glow peak of mineralized samples shows a shift towards a lower temperature of less than 340°C. As this is related to total radiation damage it will not vary according to the time of ore formation; that is some recently formed ore samples may not show a low temperature shift. Conversely some presently non-mineralized samples may show a low temperature shift indicating that at some past stage uranium

was present. The non-mineralized samples from hole 90 in Fig. 7C and hole 117 in Fig. 7B may represent such cases. No previous workers in this field have noticed this phenomenon associated with sandstone-hosted uranium deposits though Levy et al. (1977) noticed a similar feature in carbonate hosted lead-zinc deposits. Physical reasons for this phenomenon will be discussed in Ypma et al. (in prep.). Further details regarding use of TL at Westmoreland in uranium exploration and genesis of the deposits will be given elsewhere (Hochman and Ypma, in prep.).

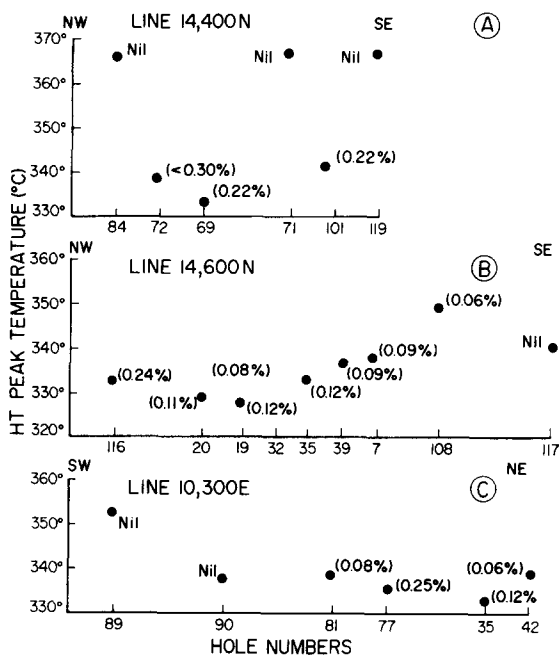


Fig. 7. Traverses showing variations in glow peak temperature across the Junnagunna orebody. Corresponding U_3O_8 values are given in parentheses.

Bremer River, South Australia

A study was conducted in the Bremer River Basin in South Australia. Samples were collected from the Oligocene–Eocene “Continental Group”, a sequence of carbonaceous sands and clays overlain by the Early–Middle Oligocene Ettrick Formation, the Miocene Mannum Formation and the Late Pliocene Parilla Sands. The “Continental Group” is underlain by Cambrian quartzites and micaceous schists of the Kanmantoo Group which constitute basement. The Tertiary sedimentary units increase in thickness to the southeast away from the basement.

No uranium mineralization is known in this area and the TL study was undertaken to determine: (a) whether any particular stratigraphic horizon

appeared more prospective than others and (b) whether any area within the drilled portion of the basin showed the effects of having or having had high uranium concentrations.

Since many samples were in the sensitization stage of TL (many glow curves as in Fig 1 c), the major methods employed involved studying variations in the intensity of the LT glow peak and in the HT/LT glow peak ratio along a line of drill holes extending away from the basement — holes 80HRM 12 to 80HRM 4. Since at this stage of radiation sensitization the LT glow peak will be decreasing more rapidly than the HT glow peak is increasing, increasing sensitization should be reflected by a decrease in the LT glow peak intensity and an increase in the HT/LT glow peak ratio. Locations of the holes are given in Fig. 8 and selected results are portrayed in Fig. 9.

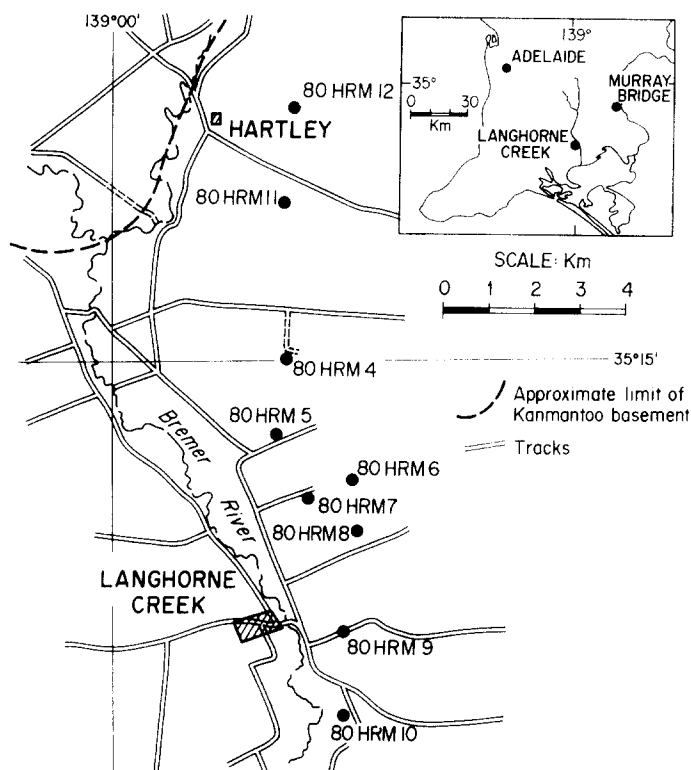


Fig. 8. Location of drill holes at Bremer River.

Figure 9A shows results obtained for the stratigraphic interval up to six metres below the base of the Mannum Formation (a limestone). There is little systematic variation in either of the TL parameters implying that no significant uranium concentrations have been present or mobilized through this stratigraphic interval.

Figure 9B shows results for a fluvialite channel sequence within the "Continental Group". These indicate that the LT glow peak intensity is least and the HT/LT glow peak ratio at a maximum in holes 80HRM 12 and 11 implying greatest sensitization (and in the case of 80HRM 12 radiation damage) in this region. These holes are adjacent to the basement and intersected the thinnest limestone cover and thinnest fluvialite channel sands.

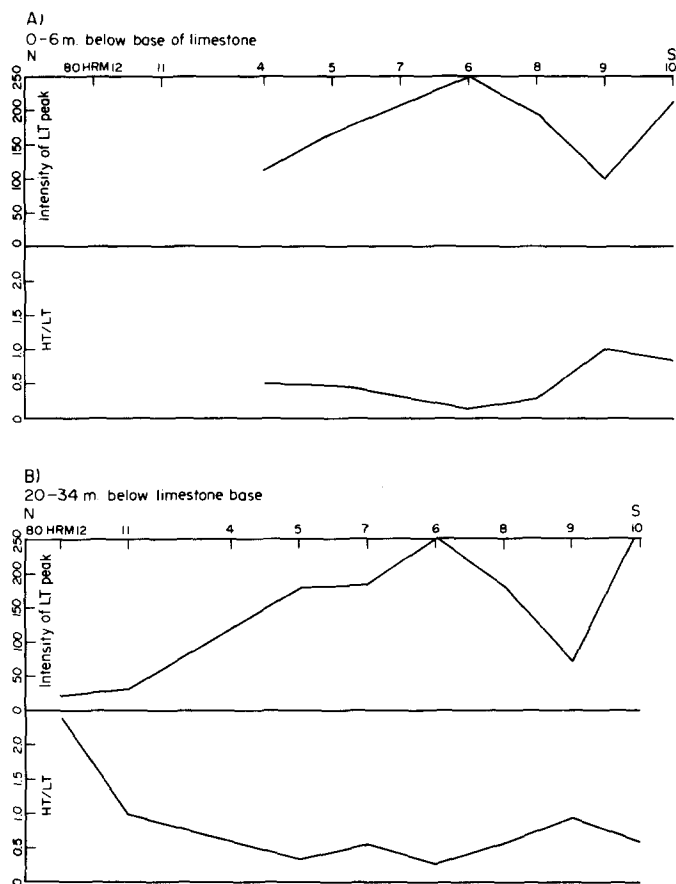


Fig. 9. Variation in TL intensity and glow peak ratio at Bremer River.

Apart from the anomalies in 80HRM 12 and 11 the rest of the fluvialite channel sands showed no more sensitization than any other stratigraphic interval sampled in the "Continental Group".

A possible explanation for the isolated anomalies in 80HRM 12 and 11 is the local concentration of uranium leached from the basement into adjacent sediments. At this locality the host sediments are very thin and as there is no widespread sensitization in other sampled portions of the basin, the potential for economic uranium accumulation is considered remote.

CONCLUSIONS

(1) TL has detected an eastward trend of increasing radiation sensitization in the Frome embayment. This is thought to be due to an eastward moving mobile orefront.

The zone of "ore type" TL around the Beverley orebody is four to five times larger than the orebody itself and the zone of marginal TL is also larger than the radiometric halo. Thus identification of TL haloes around this type of orebody will increase recognition of target zones.

(2) Traverses examining LT glow peak and HT glow peak intensities across the Proterozoic Junnagunna orebody at Westmoreland have not shown unambiguous variations associated with ore. HT/LT glow peak ratios are better indicators of proximity to ore as they increase towards the orebody. Similar variations detected nearby are consistent with the theory of increasing proximity to further mineralization.

(3) The presence or absence of widespread radiation sensitization (as at Beverley, Westmoreland and Bremer River) may facilitate an understanding of past and present uranium behaviour in any given region.

ACKNOWLEDGEMENTS

The authors wish to acknowledge Mrs. Joan Brumby for typing this manuscript and Ms. Sharon Proferes for the drafting. Our thanks are also extended to CRA Exploration and Urangesellschaft Australia for supplying samples for the Bremer River and Westmoreland studies, respectively.

REFERENCES

- Aitken, M.J., 1965. Thermoluminescence. *Sci. J.*, 1(4): 32–38.
- Callen, R.A., 1976. Lake Frome area — regional geology, Tertiary stratigraphy and uranium localization. In: C.L. Knight (Editor), *Economic Geology of Australia and Papua New Guinea*, 1. Metals. Australas Inst. Min. Metall. Monogr., 5: 803–808.
- Charlet, J.M., Dupuis, Ch. and Quinif, Y., 1978. Mise en évidence par la thermoluminescence (TL) des sables landeniens d'anomalies radiométriques nouvelles dans la coupe du canal de Blaton. *Ann. Soc. Géol. Belg.*, 101: 337–349.
- David, M., Sunta, C.M. and Ganguly, A.K., 1977. Thermoluminescence of quartz: Part 1 — Glow curve and spectral characteristics. *Indian J. Pure Appl. Phys.*, 15: 201–204.
- Durrani, S.A., Khazal, K.A.R., McKeever, S.W.S. and Riley, R.J., 1977a. Studies of changes in the thermoluminescence sensitivity in quartz induced by proton and gamma radiation. *Radiat. Eff.*, 33: 237–244.
- Durrani, S.A., Groom, P.J., Khazal, K.A.R. and McKeever, S.W.S., 1977b. The dependence of thermoluminescence sensitivity upon the temperature of radiation in quartz. *J. Phys. D*, 10: 1351–1361.
- Fuchs, H.D. and Schindlmayer, W.E., 1981. The Westmoreland uranium deposit, Queensland, Australia. In: *Uranium Exploration Case Histories*. IAEA, Vienna, pp. 59–73.
- Fuller, G.E. and Levy, P.W., 1977. Thermoluminescence of natural quartz. *Bull. Am. Phys. Soc.*, 23: 324–325.

- Goldhaber, M.B., Reynolds, R.L. and Rye, R.O., 1978. Origin of a South Texas Roll-type uranium deposit: 2, Petrology and sulphur isotope studies. *Econ. Geol.*, 73: 1690–1705.
- Haynes, R.W., 1976. Beverley sedimentary uranium orebody. Frome Embayment, S.A. In: C.L. Knight (Editor), *Economic Geology of Australia and Papua New Guinea*. 1. Metals. Australas Inst. Min. Metall., Monogr., 5: 808–813.
- Hills, J.H. and Thakur, V.K., 1976. Westmoreland uranium deposits. In: C.L. Knight (Editor), *Geology of Australia and Papua New Guinea*. 1. Metals. Australas Inst. Min. Metall., Monogr., 5: 343–347.
- Hochman, M.B.M. and Ypma, P.J.M., in prep. Thermoluminescence applied to uranium exploration and genesis of the Westmoreland uranium deposits, Northwest Queensland.
- Kaul, I.K., Ganguli, D.K. and Hess, B.H.F., 1972. Influencing parameters in thermoluminescence of quartz. *Mod. Geol.*, 3: 201–207.
- Levy, P.W., 1978. Thermoluminescence studies having application to geology and archaeometry. Brookhaven National Laboratory Report No. BNL24606, 21 pp.
- Levy, P.W., Holmes, R.J., Ypma, P.J., Chen, C.C. and Swiderski, H.S., 1977. New thermoluminescence techniques for mineral exploration. In: *Nuclear Techniques and Mineral Resources 1977*. IAEA, Vienna, pp. 523–538.
- McDougall, D.J., 1968. Natural thermoluminescence of igneous rocks and associated ore deposits. In: D.J. McDougall (Editor), *Thermoluminescence of Geological Materials*. Academic Press, New York, N.Y., pp. 527–544.
- Plumb, K.A. and Derrick, G.M., 1975. Geology of the Proterozoic rocks of the Kimberley to Mt. Isa region. In: C.L. Knight (Editor), *Economic Geology of Australia and Papua New Guinea*. 1. Metals. Australas. Inst. Min. Metall., Monogr., 5: 217–252.
- Randall, J.T. and Wilkins, M.H.F., 1945. Phosphorescence and electron traps. I. The study of trap distributions. *Proc. R. Soc.*, A184: 366–389.
- Reynolds, R.L. and Goldhaber, M.B., 1978. Origin of a South Texas Roll-type uranium deposit: 1, alteration of iron-titanium oxide minerals. *Econ. Geol.*, 73: 1671–1689.
- Shekhmametev, R.I., 1973. Effect of radiation from radioactive material on natural quartz thermoluminescence. *Opt. Spektrosk.*, 34: 505–509.
- Spirakis, C.S., Goldhaber, M.B. and Reynolds, R.L., 1977. Thermoluminescence of sand grains around a South Texas Roll-type deposit. U.S. Dept. Interior, Geol. Surv. Openfile Rep. 77-640, 14 pp.
- Ypma, P.J.M., Hochman, M.B.M. and Levy, P.W., in prep. Thermoluminescence of the host rock of the Beverley uranium deposit, Lake Frome, South Australia.
- Zimmerman, J., 1971. The radiation induced increase of the 100°C thermoluminescence sensitivity of fired quartz. *J. Phys. C*, 4: 3265–3276.

Hochman, M. B. M., & Ypma, P. J. M. (1984, August). Thermoluminescence applied to uranium exploration and genesis of the Westmoreland uranium deposits - implications for the Northern Territory. In *Annual conference of the Australasian Institute of Mining and Metallurgy*. (p. 215-224). Darwin, Australia.

NOTE:

This publication is included in the print copy
of the thesis held in the University of Adelaide Library.

The Accretionary Migration of Uranium in Tertiary Sandstones – Thermoluminescence Evidence from the Beverley Deposit, South Australia

M.B.M. HOCHMAN and P.J.M. YPMA

Department of Geology and Geophysics, University of Adelaide, G.P.O. Box 498, Adelaide, S.A. 5001 (Australia)

(Accepted for publication November 4, 1986)

ABSTRACT

Hochman, M.B.M. and Ypma, P.J.M., 1987. The accretionary migration of uranium in Tertiary sandstones - Thermoluminescence evidence from the Beverley deposit, South Australia. In: B. Poty and M. Pagel (Editors), *Concentration Mechanisms of Uranium in Geological Environment - A Conference Report*. Uranium, 3: 245-259.

The Beverley uranium deposit occurs in Tertiary sandstones in the Lake Frome Embayment, South Australia, ~30 km to the east of the Middle Proterozoic Mt. Painter granitic and metamorphic basement.

Artificial thermoluminescence (TL) studies have been undertaken on the sandstone host rocks to the Beverley deposit. These have shown a progressive increase in radiation effects through a line of drill holes extending ~8 km towards the deposit. Three TL zones are recognized: (1) a background TL zone with few radiation effects; (2) a marginal TL zone showing the onset of radiation sensitization; and (3) an ore-type TL zone showing radiation damage. The ability of TL to detect cumulative radiation effects, i.e. past as well as present exposure to U, has been utilized to show that the marginal TL type is due to hostrock exposure to protore rather than uraniferous solutions.

The increase in radiation effects towards the Beverley deposit are indicative of an increasing U concentration, i.e. an accretionary movement of U. Beyond the orebody radiation effects quickly drop away to background levels.

Samples analyzed from strata 10 m above and below the protore transport horizon have less radiation effects than the protore horizon, indicating semi-confined transport.

Recognition of the degree of cumulative radiation damage is also a very reliable indicator of proximity to mineralization.

1. INTRODUCTION

Sandstone-hosted uranium deposits (commonly of Tertiary age) have been well studied and constitute a major present source of U. These deposits are well known in the western U.S.A. and in Africa, and in recent years a growing number have been found in Australia. These include Beverley (Haynes, 1976), Honeymoon (Brunt, 1978), those of the Billeroo Channel (Ellis, 1980) and

those of the Narlaby Palaeochannel (Binks and Hooper, 1984). All of these occur in the state of South Australia, being in reasonably close proximity to different Middle Proterozoic granites and metamorphic complexes.

The genesis of sandstone-hosted U deposits has been in general, well studied – particularly those of the western U.S.A. It is generally agreed that such deposits form by precipitation of U from oxidizing groundwaters upon encountering reduced environments which may contain pyrite, carbonaceous materials or other reductants. As such orebodies usually represent an addition of <1% to the host rock (Rackley, 1976) there are few mineralogical effects noticeable on the host rock other than addition of some epigenetic minerals. Rackley (1976) consequently suggests that the means of recognition of alteration within such a geochemical cell deserves more research.

Although it is generally agreed that U is transported in oxidizing groundwaters down a hydrodynamic gradient within a semi-confined aquifer, there has been comparatively little work done, demonstrating the accretionary migration or “snowballing” of uranium protore movement. Previous works of this kind include the equilibrium/disequilibrium studies of Rosholt (1961), Robinson and Rosholt (1961) and more recently Ludwig et al. (1982).

This study uses a new technique, thermoluminescence (TL), as a measure of cumulative radiation effects and radiation damage to indicate the increasing uranium protore concentration with development of the geochemical cell. Exploration advantages of TL, given that it measures cumulative rather than instantaneous radiation effects, are also discussed.

2. PRINCIPLES OF THERMOLUMINESCENCE APPLIED TO URANIUM GEOLOGY STUDIES

Thermoluminescence (TL) describes the emission of light when a previously irradiated crystal is heated. This irradiation may be either by exposure to naturally occurring radioactive minerals in the field (natural TL) or by exposure to artificial radioactive sources in the laboratory, for example ^{60}Co gamma rays (artificial TL).

When ionizing radiation, and gamma radiation in particular, enters a crystal, it is capable of dislodging electrons from their atomic positions. This results in formation of free electrons and electronic holes (sites which have lost an electron). Although most electrons and holes recombine immediately a small percentage will be trapped on substitutional and structural defects.

Quartz is the mineral most commonly used in TL investigations of U deposits, being both widespread and resistant to weathering and moderate thermal effects (up to 300–400°C). In quartz, holes may be trapped on Al^{3+} sites and electrons on vacant oxygen sites, though Ge^{4+} centres have also been recently suggested (McKeever et al., 1984).

These charges, once trapped, can be released by heating the crystal. Once

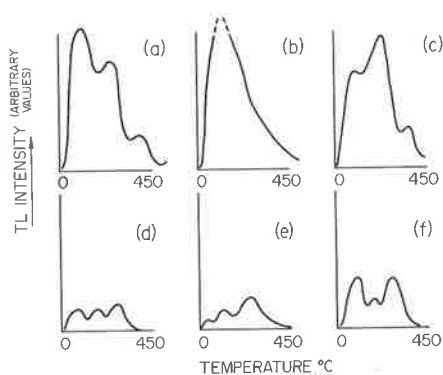


Fig. 1. Variation in the quartz TL glow curve with increasing radiation. (a) and (b) represent the least amounts of cumulative radiation exposure and (e) and (f) the most. Note a progressive increase and decrease in the intensity of firstly the low-temperature glow peak and then the middle-temperature glow peak with increasing radiation. Details are given in the text.

released the holes and electrons will recombine which may produce a pulse of light if recombination occurs at a colour centre. This light emission is measured with a photomultiplier and recorded as a glow peak. As release of trapped charges occurs over a range of temperatures, a number of glow peaks results which constitute a glow curve.

TL glow curves of quartz from the Beverley region gave three glow peaks at approximately 150°, 220° and 320° C. Illustrations of various glow curves are contained in Figs. 1 and 7-9.

The intensity and shape of the TL glow curve depend on a number of factors including the number and type of defect centres capable of acting as traps and their occupancy rate. This latter factor is largely a function of ionizing radiation and as charge occupancy rate affects the strength of the TL signal, TL has been used as a dosimeter. This is the operative principle behind natural TL measurements and studies of this sort on U deposits have been accomplished by Spirakis et al. (1977), Charlet et al. (1978) and Dhana Raju et al. (1984).

However, radiation itself can also affect trap densities and results in a permanent variation in both intensity and shape of the quartz TL glow curve. It is this characteristic that is most useful in uranium geology exploration and genesis studies, as the changes in TL glow curve shape and intensity are a permanent measure of past as well as present radiation effects.

2.1. Variations in quartz thermoluminescence glow curve with increasing radiation

The variations in the quartz TL glow curve as a result of exposure to increasing radiation are portrayed in Fig. 1. A full explanation of the theory behind

these variations is contained in Hochman and Ypma (1984a,); however, a brief explanation is included here for clarity and continuity of argument.

Fig. 1a shows a glow curve which has been exposed to only small amounts of radiation. The low-temperature glow peak (LT) is dominant though other peaks may have a higher profile depending on the trap types present. Fig. 1b illustrates a glow curve after exposure above the sensitization radiation dose. This dose has been put at $\sim 5 \cdot 10^5$ rad by Levy (1978). It marks the dose at which the quartz lattice itself begins to be changed by the ionizing radiation and results in a vast increase in the intensity of the LT glow peak such that it completely overshadows the middle-temperature (MT) and high-temperature (HT) glow peaks. An increase up to two orders of magnitude above background is not uncommon. The physical reason for this increase may be in the creation of more electron traps (Durrani et al., 1977a, b; Levy, 1978).

This stage of sensitization lasts up to $\sim 2 \cdot 10^8$ rad gamma radiation after which further radiation results in a decrease in the LT peak, whilst the MT and HT glow peaks continue to increase. This stage is portrayed in Fig. 1c. Levy (1983) mathematically describes this decrease (and the subsequent MT glow peak decrease) in terms of second-order and interactive kinetics. Put simply, this means that instead of first-order kinetics where all trapped charges recombine after release (due to heating), that some charges may be retrapped, possibly in different energy trapping levels. These retrapped charges may then be released at higher temperatures and thus contribute to the luminescence of higher-temperature glow peaks. This results in an enhancement of the higher-temperature glow peaks and consequent decrease in intensity of lower-temperature glow peaks.

Such phenomena occur at different radiation doses and thus the MT glow peak will also begin to decrease as is represented in Fig. 1d. Eventually only the HT glow peak will continue to increase as in Fig. 1e. This stage is indicative of very high radiation doses and in our experience has been found most commonly associated with mineralized U samples.

Further radiation may result in the heat-enhanced recovery of the LT glow peak by annealing (Fig. 1f), though such cases are geologically rare. Durrani et al. (1975) also report a stage of no TL emission at all associated with the reactor zones at the Oklo U deposit in Gabon, Africa.

It should be stressed here that these glow curves are a measurement of the cumulative radiation dose suffered by the quartz, i.e. past as well as present radiation dose, and thus make it possible to say whether U has been present in the geological past in a given geological or geographical area. Trends of increasing radiation effects thus contribute to a knowledge of U movement and hence a prediction of where U may presently be found.

2.2. Experimental procedure

Quartz was extracted from drill core and cuttings by means of crushing and sieving. Samples were then washed to remove any dirt, dried and passed through

a Frantz[®] isodynamic electromagnetic separator to remove any impurities. As natural TL measurements are meaningless on samples which have been exposed to ultra-violet rays from sunlight (which will bleach the TL), artificial TL was induced by exposing samples to a total dose of $5 \cdot 10^5$ rad ⁶⁰Co gamma radiation. This artificial radiation dose is the optimum dose to recharge all available lattice traps. Samples were left for 24–72 hr. to allow phosphorescence to decay and were then measured on standard TL equipment in an atmosphere of flowing high-purity nitrogen (to avoid chemiluminescence). Glow curves were recorded on a Hewlett-Packard[®] integrating recorder 5580A.

3. PREVIOUS USE OF THERMOLUMINESCENCE IN URANIUM GEOLOGY

Most previous usages of TL in uranium geology have used natural TL as a dosimeter to detect the presence of U mineralization. These include the studies of Spirakis et al. (1977) on a South Texas roll front who found an increase in total TL approaching mineralization; Charlet et al. (1978) who found that natural TL could be used to detect buried low-level mineralization which was otherwise undetectable by other radiometric techniques; and Dhana Raju et al. (1984) who noted the increase in natural TL along a drill section upon approaching shear zones containing U.

While natural TL may be used as a dosimeter to gain meaningful information relating to present U position, artificial TL has even more advantages. These relate to the detection of cumulative radiation effects over geological history to indicate sites of past U concentration as well as present. It is this application that is utilized at the Beverley deposit in this study to show the accumulating radiation effects approaching the Beverley orebody.

4. GEOLOGY OF THE BEVERLEY REGION

The Beverley U deposit occurs in the Tertiary Frome Embayment to the east of the Mount Painter Block, north of the Olary Ranges and west of the Barrier Ranges – all of Middle Proterozoic age. Fig. 2 shows the geographical location of the Beverley deposit related to these two Middle Proterozoic inliers. Callen (1975) describes the Frome Embayment as a lobe in the extensive Great Arterian Basin of northern Australia formed during Early Jurassic times. Its present aspect is the result of Late Tertiary and Quaternary tectonic events.

Spatially, the Beverley U deposit is closest to the Mt. Painter basement – a complex consisting of altered sediments (the Radium Creek metamorphics), a suite of “older granites” dated as Carpentarian (1600 Myr. ago), Late Proterozoic sediments and basic volcanics, and a suite of younger granites intruded during the Ordovician. Both suites of granites have higher than background radioactive element contents. Blight (1977) reports U contents up to 22 ppm for some of the granitoids of the “younger granite” suite.

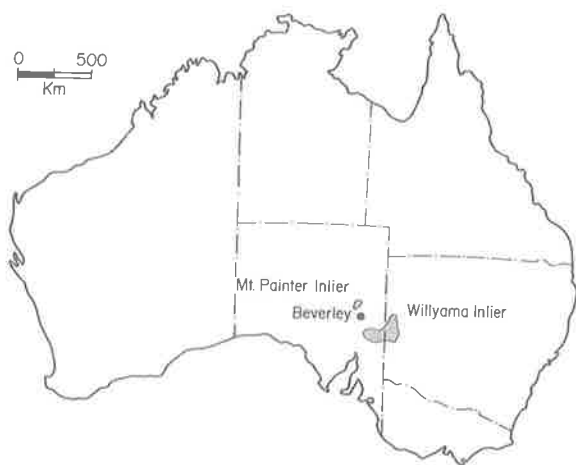


Fig. 2. Location of the Beverley uranium deposit in relation to the Middle Proterozoic Mount Painter and Willyama Inliers.

Within the Frome Embayment, Precambrian basement is overlain by folded Cambrian redbeds and limestones, Jurassic fluvial sediments, transgressive marine Cretaceous beds and later by regressive non-marine units. Callen (1976) has broadly divided the overlying Tertiary into two units: (1) the Palaeocene–Eocene Eyre Formation; and (2) Oligocene–Miocene sands, silts, carbonaceous and non-carbonaceous clays and some carbonates. U occurrences are known within Palaeocene medium- to coarse-grained sands, Eocene medium- to coarse-grained sands and silts to fine-grained sands, and in Miocene medium- to coarse-grained sands, carbonaceous in part with occasional pebbles.

Within the Beverley region, U mineralization occurs in sand lenses within fine unconsolidated argillaceous sediments of Miocene age overlying thin carbonaceous clays. These unconformably overlie Cretaceous shales and sandstones which directly overlie the Precambrian basement. The Miocene sediments are overlain by possible Pleistocene argillaceous and occasional clastic sediments with some boulder beds.

The orebody consists of very finely divided uraninite adsorbed on clay within a series of north–south-trending sands at an oxidation–reduction interface with the underlying carbonaceous clays (Haynes, 1976). U values occasionally extend into the underlying carbonaceous clays. Total reserves are estimated at 15,800 t* U_3O_8 at a recoverable grade of 0.24% U_3O_8 . Haynes (1976) reports that although the Beverley deposit contains many similarities to the western U.S.A. U deposits it also contains notable differences, i.e. the lack of Mo, Cu,

*1 t = 1 metric tonne = 10^3 kg.

V and Th, and the lack of abundant pyrite in the host sands. Further details concerning local geology are contained in Haynes (1976) and of the Mount Painter Complex in Youles (1976).

5. RESULTS

Samples were collected from 33 drill holes extending eastwards from the Mt. Painter basement to the orebody. Three samples were collected from each hole, generally one from the ore horizon, one from 10 m above it and one from 10 m below. Approximately 100 samples were measured in total. Results for the ore horizon are plotted in Figs. 3 and 4, for samples above the ore horizon in Fig. 5 and below the ore horizon in Fig. 6. Drill hole locations are contained in Fig. 3.

Figs. 3 and 4 indicate a progressive increase in radiation effects in the ore horizon upon approaching the orebody with data fitting into three main categories:

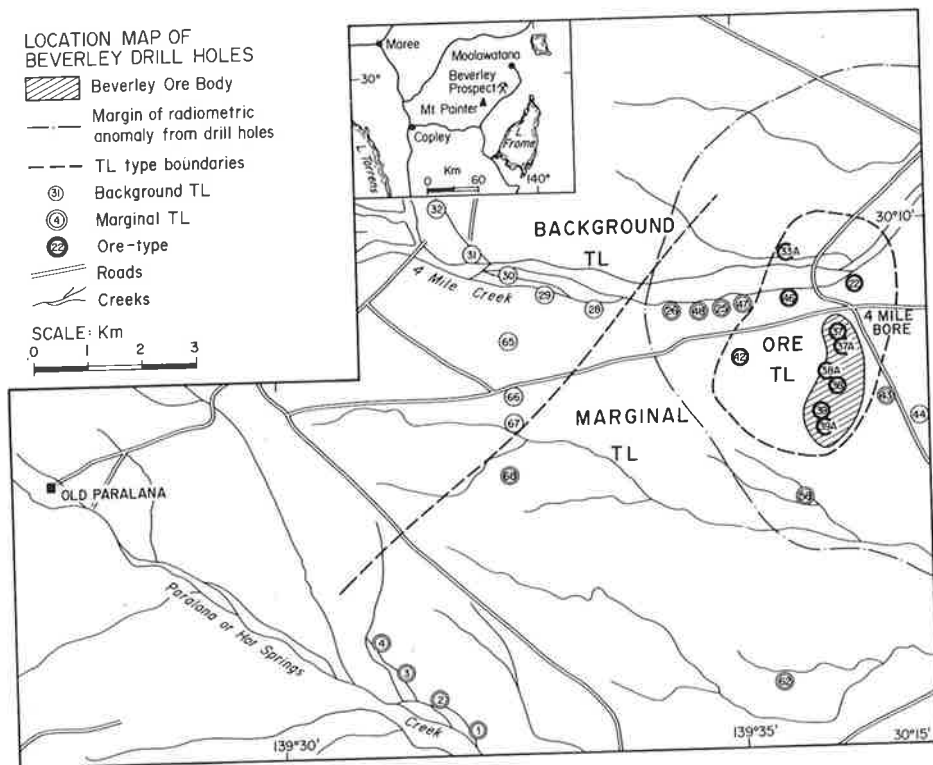


Fig. 3. Location of the Beverley drill holes showing TL and radiometric halos. Note the much larger marginal TL halo compared to the radiometric halo and ore-type TL zone as compared to the orebody.

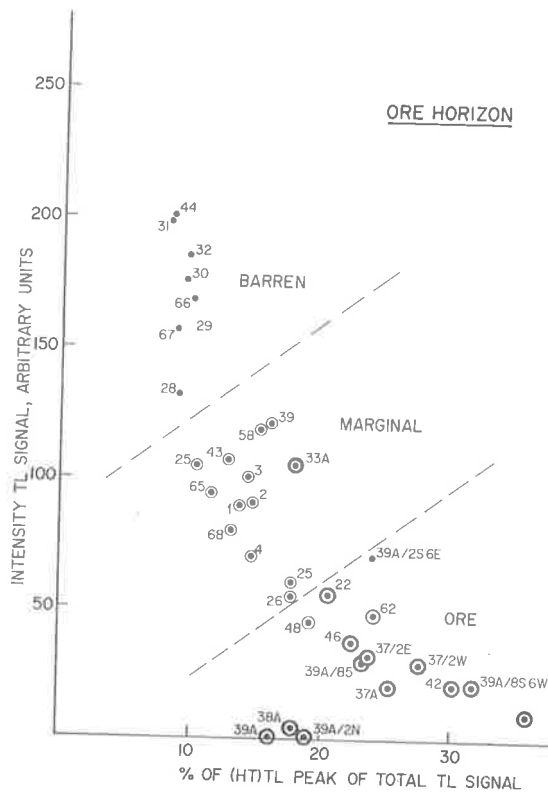


Fig. 4. Variation in the TL signal of quartz within the protore transport horizon as a function of proximity to mineralization at Beverley.

(a) Background TL (up-stream of the orebody). Samples in this group have very little radiation effects. A typical glow curve is illustrated in Fig. 7 which can be compared with the experimentally derived Fig. 1b; i.e. a large LT glow peak which obscures the MT and HT glow peaks. Such a glow curve is the common one for unsensitized sands in the Lake Frome Embayment.

(b) Marginal TL (further downstream though not in close proximity to the orebody and occupying a very large territory in Fig. 3). TL glow curves in this group are generally similar to those in Fig. 1c and d. A typical glow curve in the marginal TL group is shown in Fig. 8 with a reduced LT and MT glow peak intensity. Proportionately the LT glow peak has decreased more than the MT glow peak.

(c) Ore-type TL (within proximity to the orebody). These glow curves are similar to those in Fig. 1d and e – more particularly Fig. 1e. A typical glow curve from this category at Beverley is contained in Fig. 9. It shows even more reduction in the LT and MT glow peaks with a corresponding increase in the HT glow peak.

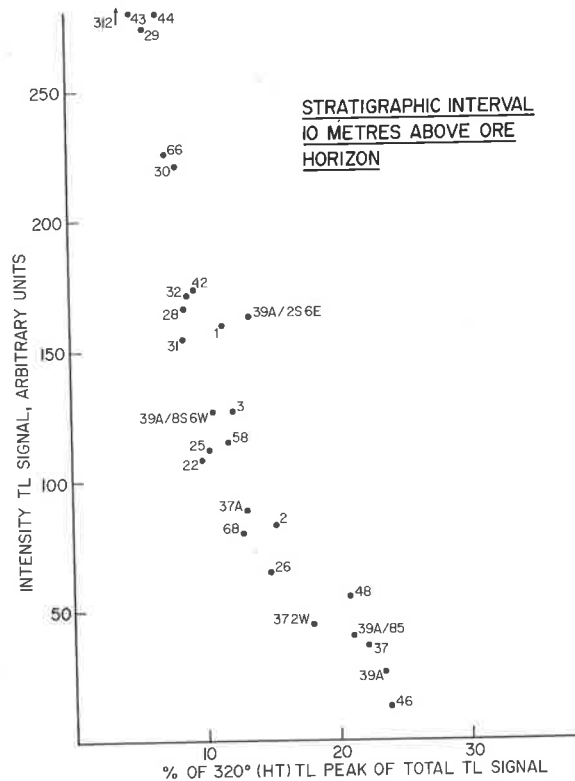


Fig. 5. Variation in the TL signal of quartz from an interval 10 m above the protore transport horizon at Beverley.

Samples taken from the stratigraphic interval, 10 m above the ore horizon show a similar trend of increasing radiation effects towards Beverley, though the overall radiation effects are less than for the ore horizon. This is illustrated in that samples from any given drill hole, in this interval show less radiation effects than their corresponding samples from the ore horizon. This is particularly noticeable from some samples within the orebody where these samples, 10 m above the ore horizon, plot in the marginal, rather than ore-type TL categories, e.g. 39A/2S6E and 39A/8S6W.

Samples taken from 10 m below the ore horizon show even less radiation effects again. A progressive increase in radiation effects is still discernible along this horizon with samples from particular drill holes again showing less sensitization than their corresponding samples from the ore horizon. A particularly notable point is the lack of samples with ore-type TL characteristics even from within the orebody (apart from holes 39A and 37).

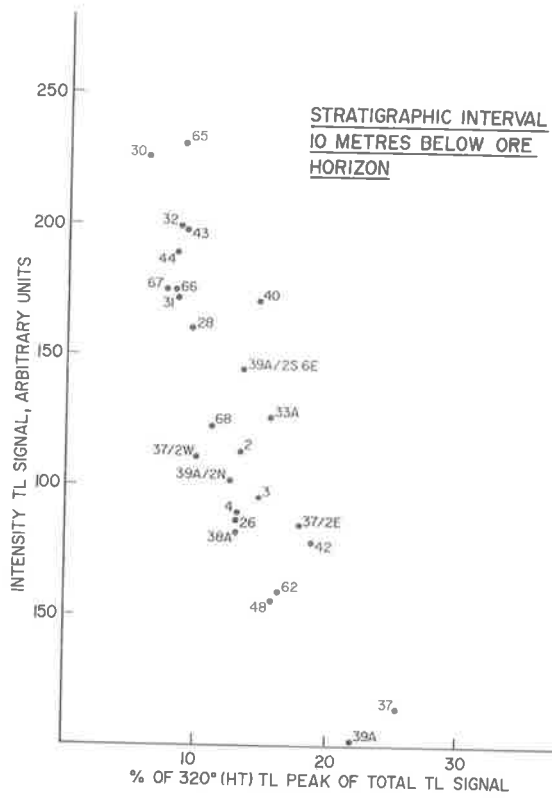


Fig. 6. Variation in the TL signal of quartz from an interval 10 m below the protore transport horizon at Beverley.

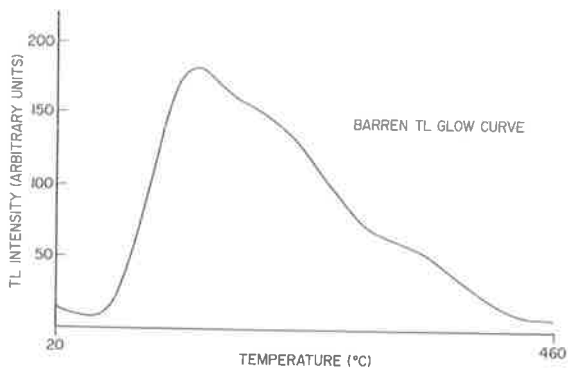


Fig. 7. Typical glow curve for quartz from the background TL zone. The low-temperature glow peak overshadows the others. The sample is from the protore transport horizon in hole 32.

6. DISCUSSION

The degree of radiation damage when considering: (1) the threshold effect

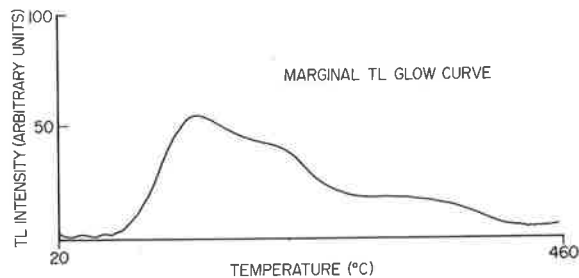


Fig. 8. Typical glow curve for quartz from the marginal TL zone. The low- and middle-temperature glow peaks have begun to decrease in intensity. The sample is from the protore transport horizon in hole 26.

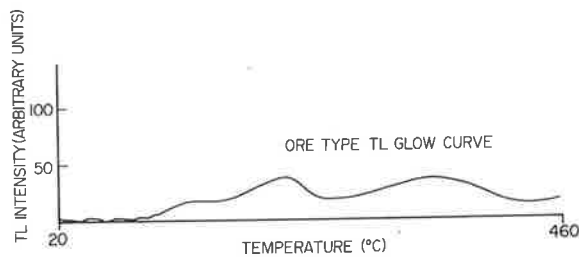


Fig. 9. Typical glow curve for quartz from the ore-type TL zone. Only the high-temperature glow peak continues to increase. The sample is from the protore transport horizon in hole 37.

of U needed to initiate radiation effects; and (2) the young age of the deposit suggests that the marginal TL type is due to actual U mineralization (i.e. protore) which has been displaced downdip by oxidizing U-bearing solutions. The U content expected in such solutions (100–1000 ppb) is too low to have produced the radiation damage observed.

Studies by Hayslip and Renault (1976) found that under geological conditions (as opposed to laboratory conditions) a threshold of 10 ppm U was needed to initiate TL in the HT glow peak. This suggests that the marginal TL type is due to U concentrations > 10 ppm. The fact that many, if not most, of the drill holes in this region currently contain < 10 ppm U indicates that the U has moved, and illustrates the usefulness of the TL technique in measuring past as well as present radiation effects.

As the radiation damage is due to displacement of uranium protore, then the progressive increase in the radiation effects observed over a distance of 8 km eastwards towards the orebody is consistent with the accretionary or “snowballing” concentration of U during transport. In fact these results actually suggest such a concentration mechanism for U. If the period of time for which the U has remained in each spot during transport is approximately constant then the increase in radiation effects can only be due to increasing concentrations of U. That is, as TL measures cumulative radiation effects –

(time) \times (concentration) – then if time has been approximately the same for each point in the migratory pathway, then concentration of U must be increasing in order to explain the increasing radiation damage observed.

That such an increase in radiation effects is not merely a function of proximity to mineralization is obvious by the rapid return to background TL, or non-radiation damaged levels, beyond the orebody. For example, hole 43 ~ 500 m east of the orebody (downdip) has only marginal TL, and hole 44 ~ 1000 m east of the orebody has background TL. Holes a similar distance west of the orebody (updip), e.g. 42 and 46, show far more radiation damage.

The lesser radiation effects in horizons 10 m above and below the ore horizon – in some cases even within the ore body – indicate that transport and accretionary movement has been more or less confined to one stratigraphic horizon. This indicates that during a U exploration programme it may be just as necessary to identify the correct stratigraphy for U transport as it is to identify the correct geographical region.

6.1. Source of uranium

TL may also be used to give some evidence regarding the source of U for the Beverley deposit.

For Tertiary sandstone-type deposits in general, three principal ideas exist regarding U sources:

- (a) leaching of U from a granitic hinterland at some time after sediment deposition (Harshman, 1972);
- (b) leaching of U from within the original host sandstone or arkose (Shockey et al., 1968); and
- (c) derivation from devitrified or leached volcanic debris, tuffs and flows within or overlying the host rock (Davis, 1969). Many authors including the above acknowledge that combinations of the above possibilities may occur and that different mechanisms and sources are applicable for different deposits.

In the case of the Beverley deposit the possibility of leaching of an interbedded volcanic source can be ruled out because of the absence of such volcanic interbeds. Further, Callen (1976) reports clay mineralogy as montmorillonite rather than tuffaceous bentonite as is commonly found in the United States deposits. No volcanic quartz or glass shards have been found.

It is also unlikely that the U has been derived from within the sandstone as the sandstone layers are thin and could not have supplied the necessary volume of U. Further to this, the TL data for samples 10 m above and below the host unit, and also from the host unit itself downdip of the orebody, all indicated the non-sensitized nature of the sandstone and hence its low inherent U content.

Modern groundwater draining the Mt. Painter granitic basement is rich in U and the dating of U within the basement indicates mobilization within the last 1 Myr. (Callen, 1976). Further to this as mentioned previously, granites

of the Mt. Painter Complex are also presently enriched in U. When accompanied with the TL data indicating the progressive increase in radiation effects eastwards away from the Mt. Painter basement, it seems likely that U has been derived by leaching from the uraniumiferous Mt. Painter basement rocks in the case of the Beverley example.

6.2. Use of TL in uranium exploration

Recognition of the degree of cumulative radiation damage within the accreting ore front also has important implications in exploration for such deposits.

The Beverley orebody has no surface geochemical or radiometric anomaly. The radiometric anomaly indicated in Fig. 3 is subsurface. Comparison of the marginal TL zone incorporating holes 1-4, 62, 58 and 68 as well as non-mineralized holes along Four Mile Creek, has enlarged the secondary target zone far beyond that of the radiometric halo - it may possibly even be too large. However, even within the marginal TL zone holes closer to the ore zone (though still 3 km distant) such as 26, 48 and 25 show greater radiation effects than holes further away within this halo such as 58, 68 and 62.

Within the marginal TL zone is the ore-type TL halo where all glow curves essentially conform to Fig. 1d-e. A significant point is that some holes within this zone (42, 22, 46, 33A) contain no U mineralization yet still have TL glow curves as expected for mineralized samples. Thus recognition of such TL glow curves despite discouraging geochemical results would have indicated not only the presence of U mineralization but also proximity to such mineralization. From Fig. 3 it can also be noted that this zone of "mineralized" ore-type TL is four to five times larger than the orebody itself and thus has enlarged the primary target zone.

Even the recognition of an increase in radiation effects along a palaeochannel may indicate firstly the presence of a mobile ore front, and secondly the relative position of the front itself.

Further uses of TL in uranium exploration at Beverley and elsewhere are contained in Hochman and Ypma (1984a, b).

7. CONCLUSIONS

(1) TL has detected a trend of increasing radiation effects in the Lake Frome Embayment, South Australia. This trend is traceable over a distance of 8 km eastwards away from the Mt. Painter basement to the Beverley orebody.

TL data fit into three main categories: (1) background TL, indicative of little radiation effects; (2) marginal TL, indicative of some greater radiation effects; and (3) ore-type TL, indicative of the presence of U mineralization.

(2) The degree of radiation effects in the marginal TL zone is greater than

that caused by uraniferous solutions and is indicative of protore movement, being caused by concentrations of a minimum of 10 ppm U.

(3) The progressive increase in radiation effects towards Beverley and sudden drop once past the orebody are indicative of increasing concentrations of U during transport.

(4) Lesser radiation effects in stratigraphic horizons 10 m above and below the ore-carrying horizon, imply that transport and accretion occurred in a confined or semi-confined aquifer.

(5) Recognition of ore-type TL glow curves has enlarged the primary target zone some four to five times beyond the orebody. The marginal TL halo is still larger again, being vastly greater in extent than the subsurface radiometric halo.

ACKNOWLEDGEMENTS

The authors' sincere thanks go to Miss Bronwyn Hosking for her expert typing and Mrs. Sharon Proferes for her skillful drafting. One of us (M.B.M.H.) received a University of Adelaide Postgraduate Grant during the course of this study. Financial assistance was also provided under ARGS grant E79/15698.

REFERENCES

- Binks, P.J. and Hooper, G.J., 1984. Uranium in Tertiary paleochannels "West Coast Area", South Australia. *Proc. Australas. Inst. Min. Metall.*, No. 289, pp. 271-275.
- Blight, P.G., 1977. Uraniferous metamorphics and "younger" granites of the Paralana area, Mount Painter Province, South Australia: A petrographical and geochemical study. B.Sc. (Hons.) Thesis, University of Adelaide, Adelaide, S.A. (unpublished).
- Brunt, A.D., 1978. Uranium in Tertiary stream channels, Lake Frome area, South Australia. *Proc. Australas. Inst. Min. Metall.*, No. 226, pp. 79-90.
- Callen, R.A., 1976. Lake Frome area - regional geology. Tertiary stratigraphy and uranium localization. In: G.L. Knight (Editor), *Economic Geology of Australia and Papua New Guinea*, Vol. 1. Metals. *Australas. Inst. Min. Metall.*, Monogr. No. 5, pp. 803-808.
- Charlet, J.M., Dupuis, Ch. and Quinif, Y., 1978. Mise en évidence par la thermoluminescence (TL) des sables landeniens d'anomalies radiométriques nouvelles dans la coupe du canal de Blaton. *Ann. Soc. Géol. Belg.*, 101: 337-349.
- Davis, J.F., 1969. Uranium deposits of the Powder River Basin. *Univ. Wyo. Contrib. Geol.*, 8(2, Part 1): 131-141.
- Dhana Raju, R., Venkataraman, B. and Anantharaman, K.B., 1984. Natural thermoluminescence of whole-rock samples as an aid in uranium exploration: A case study from Singhbhum Shear Zone, Bihar, India. *Uranium*, 1(3): 279-287.
- Durrani, S.A., Khazal, K.A.R., Malik, S.R., Fremlin, J.H. and Hendry, G.L., 1975. Thermoluminescence and fission track studies of the Oklo fossil reactor materials. In: *The Oklo Phenomenon - Proceedings of a Symposium*, Libreville. I.A.E.A. (Int. At. Energy Agency), Vienna, pp. 207-220.
- Durrani, S.A., Groom, P.J., Khazal, K.A.R. and McKeever, S.W.S., 1977a. The dependence of

- thermoluminescence sensitivity upon the temperature of radiation in quartz. *J. Phys. D, Appl. Phys.*, 10: 1351-1361.
- Durrani, S.A., Khazal, K.A.R., McKeever, S.W.S. and Riley, R.J., 1977b. Studies of changes in the thermoluminescence sensitivity in quartz induced by proton and gamma radiation. *Radiat. Effects*, 33: 237-244.
- Ellis, G.K., 1980. Distribution and genesis of sedimentary uranium near Curnamona, Lake Frome region, South Australia. *Am. Assoc. Pet. Geol. Bull.*, 64(10): 1643-1657.
- Harshman, E.N., 1972. Geology and uranium deposits, Shirley Basin area. Wyoming. U.S. Geol. Surv., Prof. Pap. No. 745, 82 pp.
- Haynes, R.W., 1976. Beverley sedimentary uranium orebody, Frome Embayment, S.A. In: C.L. Knight (Editor), *Economic Geology of Australia and Papua New Guinea, Vol. 1. Metals. Australas. Inst. Min. Metall., Monogr. No. 5*, pp. 343-347.
- Hayslip, D.L. and Renault, J.R., 1976. Potential of quartz thermoluminescence in uranium exploration. *Abstr., 29th Annu. Meet. Rocky Mnt. Sect., Geol. Soc. Am., Albuquerque, N.M.*, p. 590.
- Hochman, M.B.M. and Ypma, P.J.M., 1984a. Thermoluminescence applied to uranium exploration and genesis of the Westmoreland uranium deposits - Implications for the Northern Territory. *Aust. Inst. Min. Metall. Annu. Conf. Vol., Darwin, N.T.*, 1984, pp. 215-224.
- Hochman, M.B.M. and Ypma, P.J.M., 1984b. Thermoluminescence as a tool in uranium exploration. *J. Geochem. Explor.*, 22(1-3): 315-331.
- Levy, P.W., 1978. Thermoluminescence studies having application to geology and archaeometry. *Brookhaven Natl. Lab. Rep. No. BNL 24606*, 21 pp.
- Levy, P.W., 1983. Characteristics of thermoluminescence glow curves for minerals exhibiting more than one glow peak. *PACT (Proc. Annu. Conf. Thermoluminescence)*, 9: 109-122.
- Ludwig, K.R., Goldhaber, M.B., Reynolds, R.L. and Simmons, K.R., 1982. Uranium-lead isochron age and preliminary sulphur isotope systematics of the Felder uranium deposit, South Texas. *Econ. Geol.*, 77: 557-563.
- McKeever, S.W.S., Chen, C.Y. and Halliburton, L.A., 1984. Point defects and the pre-dose effect in natural quartz. 4th Specialist Seminar on TL and E.S.R. Dating. *Max Planck Inst. Kernphysik, Heidelberg*, 1984. *Abstr. No. 7*.
- Rackley, R.I., 1976. Origin of Western-States type uranium mineralization. In: K.H. Wolf (Editor), *Handbook of Strata-bound and Stratiform Ore Deposits*. Elsevier, Amsterdam, pp. 89-156.
- Robinson, C.S. and Rosholt, Jr., J.N., 1961. Uranium migration and geochemistry of uranium deposits in sandstone above, at and below the water table, Part II. *Econ. Geol.*, 56: 1404-1420.
- Rosholt, Jr., J.N., 1961. Uranium migration and geochemistry of uranium deposits in sandstone above, at and below the water table, Part I. *Econ. Geol.*, 56: 1392-1403.
- Shockey, P.N., Rackley, R.I. and Dahill, M.P., 1968. Source beds and solution fronts. *Remarks Wyo. Meet. Sect. AIME (Am. Inst. Min. Metall. Eng.)*, Feb. 27, 1968, 7 pp.
- Spirakis, C.S., Goldhaber, M.B. and Reynolds, R.L., 1977. Thermoluminescence of sand grains around a South Texas roll-type deposit. *U.S. Geol. Surv., Open-file Rep. 77-640*, 14 pp.
- Youles, I.P., 1976. Mount Painter uranium deposits. In: C.L. Knight (Editor), *Economic Geology of Australia and Papua New Guinea, Vol. 1. Metals. Australas. Inst. Min. Metall., Monogr. No. 5*, pp. 505-508.

CHANGES IN THE ARTIFICIAL THERMOLUMINESCENCE GLOW CURVES OF QUARTZ ASSOCIATED WITH URANIUM DEPOSITS

M. B. M. HOCHMAN and P. J. M. YPMA*

Department of Geology and Geophysics, The University of Adelaide, South Australia 5000, Australia

(Received 1 August 1987; in final form 14 December 1987)

Abstract—Previous laboratory-based studies have shown that quartz TL glow curves change in intensity and shape in response to large radiation doses. Initially, low temperature peaks are sensitized (which results in an increase in intensity) though at gamma doses of greater than 10^5 – 10^6 kGy desensitization occurs.

This study has examined the change in artificial TL in quartz at various distances from a uranium deposit. Such quartz has been subjected to varying palaeoradiation doses in a natural uranium rich environment. Quartz from an uranium rich environment shows that the 130°C glow peak is the dominant glow peak in “background” radiation environments, though this peak decreases with increasing palaeoradiation dose. At doses greater than 10^5 – 10^6 kGy the 350°C glow peak is the dominant glow peak in these quartz samples.

An increase in E'_1 centre concentration also occurs from the least radiation affected sample to the most radiation affected sample. These results suggest that artificial TL is useful in uranium exploration.

1. INTRODUCTION

ALTHOUGH quartz is used extensively in thermoluminescence (TL) dating, the mechanism of TL production in quartz is not fully understood. Many studies have contributed to a partial knowledge of the effects of radiation, heat and trace element type and concentration on quartz TL. McKeever (1985) references many such studies.

Most previous studies have utilized single crystal hydrothermal quartz; such quartz, while having the basic quartz structure, has characteristics attributable to a different growth process which is likely to make it quite different from the growth process that applies to almost all quartz in the geological environment (i.e. igneous or metamorphic processes).

This study utilizes quartz from a geological environment where many variables (e.g. quartz type provenance and hence internal chemistry, and thermal effects), are expected to be very similar. Thus the TL glow curves obtained from these quartz samples should be primarily a function of differences in radiation environment, particularly if the samples were obtained at varying distances from a uranium ore deposit. Such studies provide information on the TL of quartz subject to doses far larger than those expected in archaeometric studies.

The application of these studies to uranium exploration are described by Hochman and Ypma (1984, 1987) and Ypma and Hochman (1987).

2. PREVIOUS WORK

It is well known that large experimental doses of radiation change the intensity and shape of quartz TL glow curves. Ichikawa (1968) exposed samples of clear crystal Brazilian quartz to varying amount of gamma radiation up to 9.2×10^6 rad (92 kGy). Some of his relevant data is reproduced in Fig. 1 which shows the variation in glow peak intensities and overall glow curve shape with radiation. A significant point about this data is that overall TL intensity continues to increase with increasing radiation, but at higher doses (Fig. 1(c)) the low temperature peak (Ichikawa's B1 peak) begins to decrease. The 180°C glow peak (B1) reaches maximum intensity after exposure to 5.7×10^6 rad (57 kGy). Similarly, the 260°C peak (Ichikawa's C peak) reaches maximum intensity at 8.0×10^6 rad (80 kGy) and then decreases with higher doses. The higher temperature D peak (350°C) continues to increase throughout the experiment. The change in intensity of various glow peaks thus contributes to a change in overall glow curve shape, and hence also glow peak ratios.

Similar results were found by Durrani *et al.* (1977) who found that both TL intensity and sensitivity (the subsequent response to a test dose) increased over three orders of magnitude in natural clear Brazilian quartz exposed to gamma radiation doses between 10^5 and 10^7 rad (1–100 kGy). Their data is shown in Fig. 2.

*Also at School of Mining Engineering and Petroleum Technology, Delft University of Technology, Delft, The Netherlands.

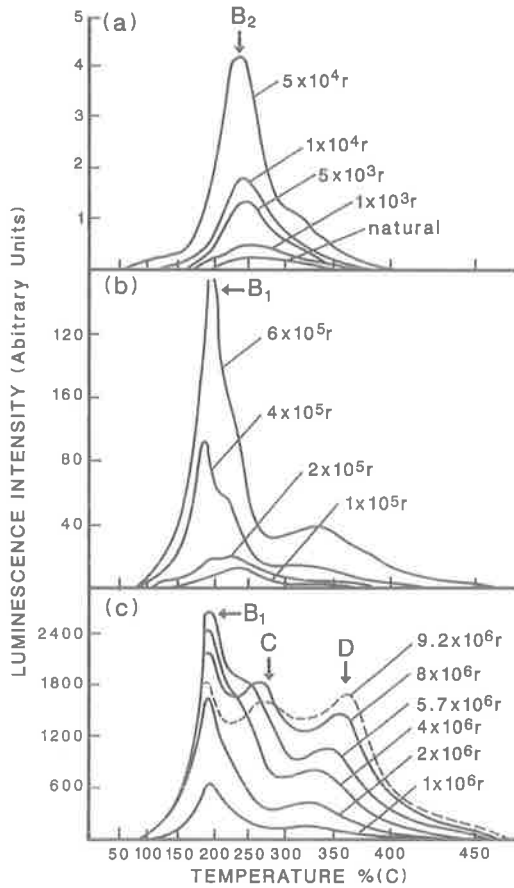


FIG. 1. Change in Brazilian quartz TL glow curve with increasing gamma radiation (after Ichikawa, 1968).

In order to examine the effect of even larger radiation doses on the TL of quartz, Durrani *et al.* (1977) used proton irradiation to obtain doses up to 5×10^{11} rad (5×10^5 kGy). This data is shown in Fig. 3 where the TL response (defined as the area under the glow curve from 240 to 480°C) and TL sensitivity are plotted against proton dose. These curves show an initial TL growth with increasing dose up to approximately 10^7 rad (100 kGy), a zone of level TL response, followed by a sharp decrease in both TL response and TL sensitivity at approximately 10^9 rad (10^4 kGy). A further decrease in TL occurs at doses greater than 10^{11} rad (10^5 kGy).

Such a response to radiation indicates that one has to be cautious with the interpretation of total area alone, e.g. the TL response is the same at 10^6 rad (10 kGy) as at approximately 10^{10} rad (10^5 kGy), yet the shape of the glow curve changes drastically in this range. This is illustrated in Fig. 4, where (a) is the glow curve for a quartz slice irradiated with a dose of 10^7 rad (100 kGy) 10 MeV protons and (b) the glow curve after 2×10^{10} rad (2×10^5 kGy) 10 MeV protons. The former shows four glow peaks with the two lower temperature peaks having largest intensity. The latter shows only one glow peak remaining, the high temperature peak at approximately 350°. Durrani *et al.* (1977) also noted that proton irradiation was much less efficient at producing TL as opposed to gamma radiation and they used this information in explaining their subsequent model for sensitization in quartz.

One of the most useful single observations regarding the use of TL in uranium exploration is that of

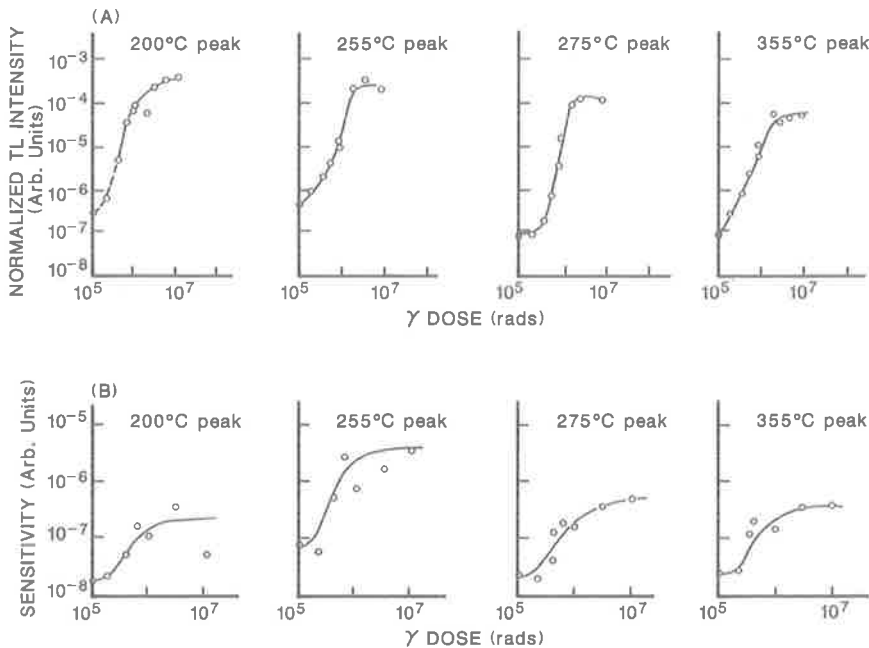


FIG. 2. Change in (a) TL intensity and (b) TL sensitivity of the 200°C, 255°C, 275°C and 355°C glow peaks of Brazilian quartz in response to increasing gamma radiation doses (after Durrani *et al.*, 1977). Sensitivity is defined as the increase in the response following a test dose.

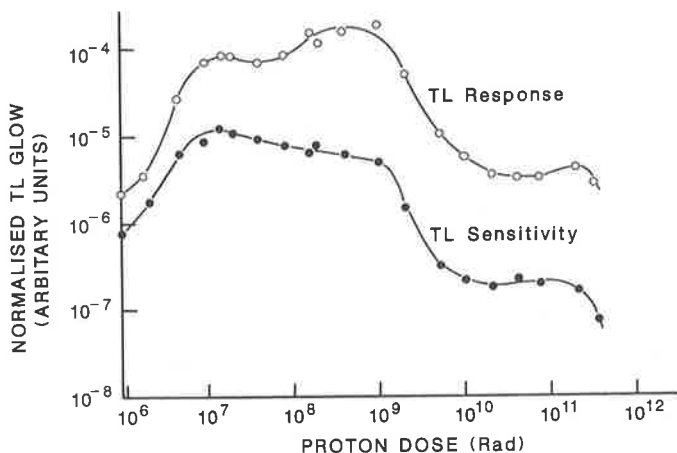


FIG. 3. Changes in the TL response and TL sensitivity following 10 MeV proton irradiation. Note the decrease in both parameters at 10^9 rad and again at 10^{11} rad (after Durrani *et al.*, 1977).

Levy (1979), the quartz “remembers” exposure to previous large irradiations. The earlier quoted works by Ichikawa (1968) and Durrani *et al.* (1977) showed that increasing radiation doses resulted in sensitization phenomena and a change in glow curve shape. However, these changes were noted as a result of total (sensitization) doses and not as the result of

test doses after thermal untrapping of the total dose. Under normal burial conditions in the geological environment, a significant proportion of naturally accumulated trapped charges will be thermally untrapped and thus a mechanism to re-read this large naturally accumulated dose would obviously be helpful in uranium exploration. Levy’s (1979) work shows that this can be done and his results are contained in Fig. 5. This figure shows that when the sensitizing dose exceeds 5×10^5 rads (5 kGy) that the TL response to the second test dose is noticeably larger than that obtained for the first test dose, i.e. that quartz “remembers” exposure to the large previous sensitizing dose.

In summary, therefore, the significant points of previous studies on the effects of large radiation doses on quartz TL are: (a) that the peak intensities, and the glow curve shape change with increasing radiation doses from an initial large low temperature peak at “low” doses to a dominant high temperature peak at high doses, (b) that overall TL intensity decreases at doses in excess of approximately 10^8 rad (10^3 kGy) and (c) that quartz contains a memory for previous exposure to radiation above 5×10^5 rad (5 kGy).

3. RESULTS

3.1. Sample selection

The radiation induced changes in TL glow curves of quartz in a geological environment have been examined by selecting samples from various positions within a roll-front type uranium deposit. Roll-front uranium deposits are very common in the western United States and in South Australia. They commonly occur in Tertiary sandstones and are formed by precipitation of uranium at an oxidation-reduction interface occurring where the oxidizing uranium bearing solution encounters a suitable reducing material. For example uranium in oxidizing groundwater is carried in the U^{6+} state and is reduced to

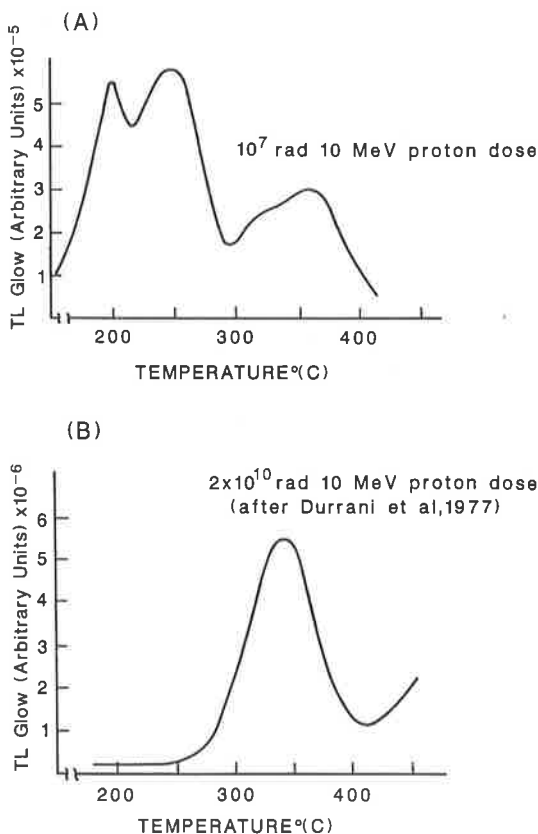


FIG. 4. The TL glow curve for Brazilian quartz after a proton dose of (a) 10^7 rad and (b) 2×10^{10} rad. Note that in (b) only the high temperature glow peak (350°C) remains. (Figure after Durrani *et al.*, 1977).

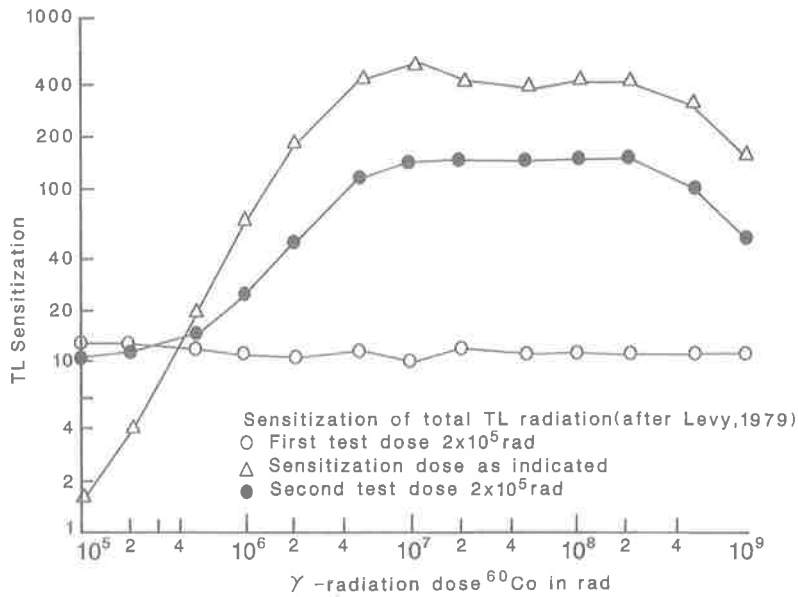


FIG. 5. Sensitization of TL in Brazilian quartz showing the quartz "remembers" exposure to previous radiation (after Levy, 1979).

the U^{4+} state upon encountering pyrite, organic materials or other reducing agents. The precipitated uraninite or pitchblende can be redissolved by a later influx of oxidizing groundwater, reprecipitated, redissolved, etc.

In this way, the uranium ore migrates from one position to another, downdip in the sandstone unit. The flow of oxidizing (often uraniferous) groundwater and the configuration of channels

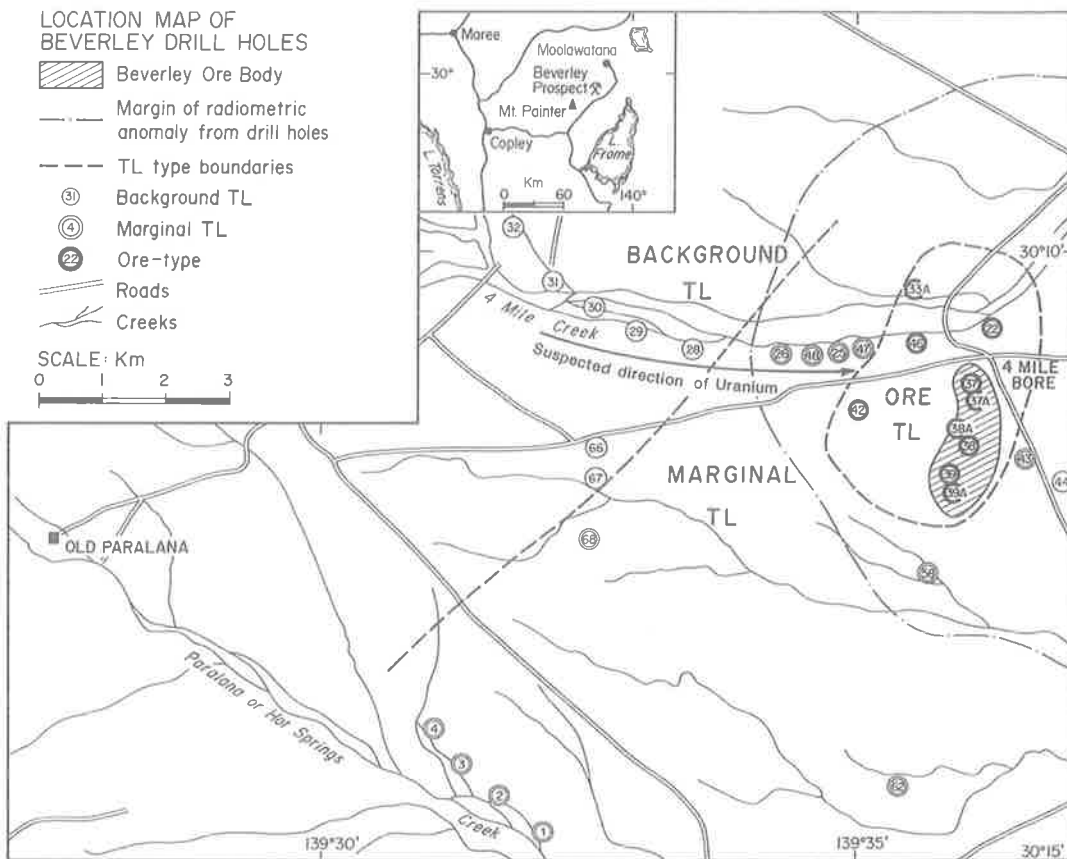


FIG. 6. Location of the Beverley uranium deposit in South Australia showing sampled drill hole locations and suspected direction of uranium movement.

control the direction of migration. An important point for this study is that as the uranium ore migrates it accretes, i.e. the volume (and concentration) of uranium increases. Both the migratory nature and accretionary behaviour of uranium under these conditions have been demonstrated by the lead-isotope studies of Rosholt (1961), Robinson and Rosholt (1961) and Ludwig *et al.* (1982). More information about roll-front type deposits can be found in Rackley (1976).

Four typical samples were selected from a number of analyzed drill-holes at different locations within the roll-front system at the Beverley uranium deposit, South Australia. The location of the sampling sites, relative to the ore body, is shown in Fig. 6. Also shown is the expected direction of migration (from geological evidence). Further information about TL studies on the Beverley deposit is contained in

Hochman and Ypma (1987). The general geology is as described by Callen (1976) and Haynes (1976).

These four samples should show differing radiation effects, due to their differing positions in the roll-front system: for example, the sample from hole 32 should have had the least exposure to radiation, the sample from hole 26 should show greater radiation effects, the sample from hole 42 even larger effects and, finally the sample from hole 37, within the present orebody, should show the largest radiation effects of the four chosen.

At this stage it is important to show that the effect of other factors which may influence the TL of quartz do not obviate the palaeodose effects. This is necessary to demonstrate that the observed TL glow curve changes are, in all probability, related to variations in radiation (or palaeoradiation) dose. To begin, it must be emphasized that all samples are from the same geological location and even the same stratigraphic horizon: thus all samples should have the same provenance (source rock), i.e. they are derived from the same source rock and should have a very similar initial internal chemistry.

Similarly, all samples were taken from depths between 123 metres and 135 metres below the surface and, therefore, any variations in thermal effects due to depth should be minimal.

Quartz was extracted from these drill hole samples using procedures described in Hochman and Ypma (1984), the experimental techniques are also as described in Hochman and Ypma (1984) and Ypma and Hochman (1987). No precautions were taken to shield samples from direct sunlight after drilling and thus natural TL should be insignificant compared to the artificially induced TL. A standard test dose of 5 kGy ^{60}Co gamma irradiation was applied to the samples. After irradiation they were wrapped in aluminium foil and stored for 24 h, to allow phosphorescence and low temperature TL peaks to decay. A dose of 5 kGy was used. This dose should fill the maximum number of empty lattice traps without inducing sensitization (from results of Levy, 1979; see Fig. 5).

After storing for 24 h, each TL sample was measured in an atmosphere of flowing high purity nitrogen. TL measurements were made with commercially available apparatus from Littlemore Scientific Company; an ND2 filter was used to reduce the red light from the heating strip.

3.2. TL glow curves

Glow curves obtained with four samples from different locations are contained in Fig. 7.

Figure 7(a) shows the glow curve for sample 32, which should have received the lowest radiation dose. This curve is dominated by a large peak at 130°C which obscures other higher temperature peaks.

Figure 7(b) contains the glow curve for sample 26 where the cumulative palaeoradiation is expected to be higher than that for the previous sample. The

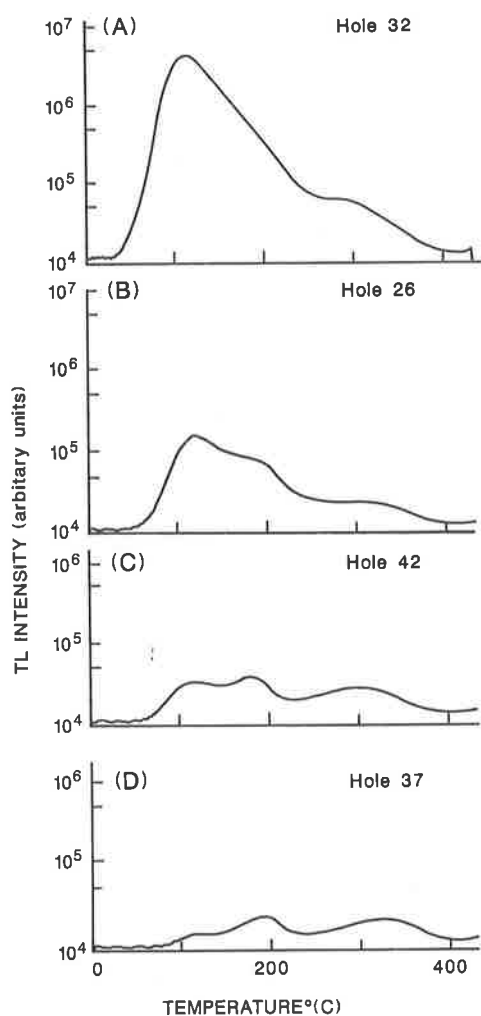


Fig. 7. TL glow for quartz from the same stratigraphic horizon taken from four drill holes along the suspected uranium transport horizon. Note the diminution in 130°C glow peak intensity and change in overall glow peak shape. Further details are contained in the text.

130°C glow peak has been reduced in intensity and, whereas it is still the dominant peak, another peak, at 180°C, is nearly as large.

Figure 7(c) illustrates the next stage in the cumulative palaeoradiation process. In this curve the 180°C glow peak is now higher than the 130°C glow peak, which continues to decrease as the dose is increased.

A TL glow curve for the sample from the current ore zone is shown in Fig. 7(d) where both the 130°C and 180°C glow peaks are greatly reduced and a high temperature peak with a maximum at 350°C is of equal intensity to the 180°C peak.

This last glow curve represents the stage of maximum radiation effects observed with samples from the Beverley uranium deposit: the lower temperature peaks are even more reduced and the 350°C glow peak higher in samples from several (other) older and/or higher grade uranium deposits. In those cases, the glow curves resemble those in Fig. 5(b) which were obtained in the laboratory based experiments of Durrani *et al.* (1977).

Once again, considering the similarities in quartz type and geological history, it is reasonable to conclude that the observed glow curve changes shown in Fig. 7(a)–(d) result from their radiation history.

In general, therefore, these results conform to the previously quoted laboratory experiments: (a) there is a decrease in overall TL intensity with radiation doses exceeding an optimal sensitization. (This decrease occurred at doses greater than approximately 100–1,000 kGy in the laboratory experiments). (b) The high temperature glow peak is proportionately increased relative to lower temperature glow peaks as radiation dose increases.

It is also interesting to note that Fairchild *et al.* (1978) found similar changes in the TL of LiF. This occurred in the radiation range 800 to 3×10^7 rad (8 Gy–300 kGy). The LiF results show a gradual decrease in lower temperature peak intensities and an enhancement of higher temperature peak intensities as the dose increased through this range. Similar sensitization and subsequent desensitization is likely to occur in a number of minerals.

3.3. Sensitization and desensitization in quartz

Although the sensitization of the 110°C glow peak in quartz has been comparatively widely studied, little work has been reported on the observation, let alone interpretation, of the sensitization and desensitization of the higher temperature glow peaks in quartz. The earlier quoted works of Ichikawa (1968), Durrani *et al.* (1977) and Levy (1979) are exceptions to this statement as is the work of David *et al.* (1978) and Shekhmametev (1973).

Durrani *et al.* (1977) proposed a trap creation model to explain both the sensitization and the desensitization observed in quartz. Their explanation was based on changes in the concentration of Al/alkali trapping centres and electron traps. It also

assumed that Al/alkali centres acted as luminescent centres in quartz. They postulated that an initial oversupply of hole traps made the electron trap concentration the critical factor in determining the amount of luminescence. If radiation created more electron traps, the increased number of traps would facilitate increased luminescence, i.e. sensitization. As radiation proceeded and the number of electron traps created increased, the concentration of electron traps would exceed that of hole traps and luminescent centres and, thus, the luminescent intensity would reach a saturation and eventually decline, i.e. desensitization would occur. A reduction in the number of luminescence centres was also suggested at high radiation doses: this was attributed to the blocking of quartz c-axis channelways by interstitial oxygen. This blocking inhibited the alkali ion mobility needed to restore Al/alkali centers functioning as potential hole traps.

By itself the current work adds little to this or other models. However, samples from the Beverley ore deposit have been subject to electron paramagnetic resonance studies (see Ypma, Chatagnon and Hochman, in preparation) to determine the E' centre concentration. This centre is generally believed to be a bridging oxygen which has trapped an electron (see McKeever, 1985). These samples were from drill holes 32, 30, 28, 48, 37 and 39 shown in Fig. 6. The results show an increase in E'_1 centre concentration over an order of magnitude (from a value of 73 in hole 30 to 1913 in hole 39).

Since E'_1 centres are associated with oxygen vacancies these results indicate an increase in oxygen vacancy concentration associated with increasing radiation exposure. If oxygen vacancies do function as electron traps, then the effect of radiation is to create more electron traps. Such an observation would lend support to Durrani *et al.*'s (1977) model by indicating that large radiation doses from the natural geological environment do create more electron traps.

4. CONCLUSIONS

In conclusion, this study can be regarded as a demonstration that the changes in the quartz TL glow curves by laboratory radiation also occur in the geological environment. Whilst the study may add little to an understanding of sensitization and desensitization phenomena in quartz, it does show:

(a) that results obtained with hydrothermal crystal quartz can be duplicated in pyrogenic natural quartz;

(b) that the TL signal increase, induced by additional laboratory irradiations, does have a direct application in uranium exploration—rather than remaining merely a “potential” tool (cf. McKeever, 1985, p. 322);

(c) the change in quartz glow curve shape induced by laboratory irradiation also occurs in quartz from naturally occurring uraniumiferous geological systems;

(d) the observed trend in such a system is that lower temperature glow peaks (in particular the 130°C glow peak) are reduced in intensity, and that the higher temperature glow peaks (the 350°C glow peak) are less reduced in intensity and even increase in intensity as the palaeodose increases; and

(e) that when coupled with EPR results, these TL data suggest that an increasing (palaeo) radiation dose increases the oxygen vacancy concentration.

REFERENCES

- Callen R. A. (1976) Lake Frome area-regional geology. Tertiary stratigraphy and uranium localization. In *Economic Geology of Australia and Papua New Guinea* (Edited by Knight G. L.), Vol. 1, pp. 803–808. Australian Inst. Min. Metall., Monogr. No. 5.
- David M., Sunta C. M., Bapat V. N. and Ganguly A. K. (1978) Thermoluminescence of quartz—Part III: sensitization by a pre-gamma exposure. *Ind. J. Pur appl. Phys* **16**, 423–427.
- Durrani S. A., Khazal K. A. R., McKeever S. W. S. and Riley R. J. (1977) Studies of changes in the thermoluminescence sensitivity in quartz induced by proton and gamma radiation. *Radiat. Effects* **33**, 237–244.
- Fairchild R. G., Mattern P. L., Lengweiler K. and Levy P. W. (1978) Thermoluminescence of LiF TLD-100 dosimeter crystals; glow curve kinetics. *J. appl. Phys.* **49**, 4523–4533.
- Haynes R. W. (1976) Beverley sedimentary uranium ore-body, Frome Embayment, S. A. In *Economic Geology of Australia and Papua New Guinea* (Edited by Knight G. L.), Vol 1, pp 343–347. Australian Inst. Min. Metall., Monogr. No. 5.
- Hochman M. B. M. and Ypma P. J. M. (1984) Thermoluminescence as a tool in uranium exploration. *J. Geochem. Explor.* **22**, 315–331.
- Hochman M. B. M. and Ypma P. J. M. (1987) The accretionary migration of uranium in Tertiary sandstones—thermoluminescence evidence from the Beverley deposit, South Australia. *Uranium* **3**, 245–259.
- Ichikawa Y. (1968) Thermoluminescence of natural quartz irradiated by gamma rays. *Jap. J. appl. Phys.* **7**, 220–226.
- Levy P. W. (1979) Thermoluminescence studies having applications to geology and archaeology. *PACT J. Eur. Study Gr. Phys. Chem. Math. Techn. appl. Archaeol.* **3**, 466–480.
- Ludwig K. R., Goldhaber M. B., Reynolds R. L. and Simmons K. R. (1982) Uranium—lead isochron age and preliminary sulphur isotope systematics of the Felder uranium deposit, South Texas. *Econ. Geol.* **77**, 557–563.
- McKeever S. W. S. (1984) Thermoluminescence in quartz and silica. *Radiat. Protect. Dos.* **8**, 81–89.
- McKeever S. W. S. (1985) *Thermoluminescence of Solids*. Cambridge University Press, Cambridge, U.K.
- Rackley R. I. (1976) Origin of Western-States type uranium mineralization. In *Handbook of Stratabound and Stratiform Ore Deposits* (Edited by Wolf K. H.), pp. 89–156. Elsevier, Amsterdam.
- Robinson C. S. and Rosholt J. N., Jr (1961) Uranium migration and geochemistry of uranium deposits in sandstone above, at and below the water table, Part II. *Econ. Geol.* **56**, 1404–1420.
- Rosholt J. N., Jr (1961) Uranium migration and geochemistry of uranium deposits in sandstone above, at and below the water table, Part I. *Econ. Geol.* **56**, 1392–1403.
- Shekmametev R. I. (1973) Effect of radiation from radioactive material on natural quartz thermoluminescence. *Opt. Spektrosk.* **34**, 505–509.
- Ypma P. J. M. and Hochman M. B. M. (1987) A thermoluminescence study of the role of a Middle Proterozoic unconformity in controlling uranium mineralization, as shown at Eyre Peninsula, South Australia. *Bull. Franc. Mineral.* **110**, 173–186.

Ypma, P. J., & Hochman, M. B. M. (1987). A thermoluminescence study of the rôle of a middle proterozoic unconformity in controlling uranium mineralization, as shown at Eyre peninsula, South Australia. *Bulletin de Mineralogie*, 110(2-3), 173-186.

NOTE:

This publication is included in the print copy
of the thesis held in the University of Adelaide Library.